Improving Efficiency by Using Continuous Flow to Enable Cycles: Pseudo-Catalysis, Catalysis and Kinetics

By

Ryan Sullivan

A thesis submitted to the
University of Ottawa
in partial fulfillment of the requirements
for the Degree of
Doctor of Philosophy
in
Chemistry

Department of Chemistry and Biomolecular Sciences
Faculty of Science
University of Ottawa

ABSTRACT

Improving Efficiency by Using Continuous Flow to Enable Cycles: Pseudo-Catalysis, Catalysis and Kinetics

Ryan Sullivan
University of Ottawa, 2020

Advisor:
Stephen Newman

This thesis is centered around the use of flow chemistry to enable cycles in order to increase reaction or process efficiency. Chapter two describes the development of a pseudo-catalytic cycle in space; a strategy to achieve formal sub-stoichiometric loading of a chiral auxiliary. By telescoping auxiliary attachment, asymmetric transformation and auxiliary cleavage into one continuous flow process, coupled with separation of product and recovery of auxiliary, the reuse of the auxiliary can be automated by returning the recovered auxiliary back to the start of the process to achieve 'turn-over.' An asymmetric hydrogenation mediated by Oppolzer's sultam is used to demonstrate this concept.

In order to achieve cycles such as the one discussed in Chapter two, the ability to telescope reactions in flow is paramount. However, solid handling challenges are frequent when transitioning to flow, leading to limitations in potential solvents or conditions in order to achieve homogeneity. This complicates the ability to telescope reactions, and to address this challenge the work in Chapter three focuses on the development of a general and simple solution to negate precipitation problems arising from precipitation of base·HX salts, a frequent reaction by-product of common reactions. By using bases that form low- to moderate-melting salts upon protonation, precipitation is precluded while reactions are performed above the melting point of the base·HX salt. This is shown to be applicable for a wide variety of substitution reactions and allow facile reaction telescoping.

Chapter four focus on overcoming severe scope limitations in palladium catalyzed transformations that result when rapid background reactions deplete the nucleophilic coupling partner faster than catalyst turnover. This work starts with real-time MS investigations to investigate why slow addition of Grignard or organolithium nucleophiles facilitates substantial

scope expansion in Kumada-Corriu or Murahashi cross-couplings, and then uses the information gleaned from these studies to significantly expand the accessible scope of palladium catalyzed aryl halide–diazo cross-coupling, through controlled addition of the diazo reagent at a rate that approximates aryl halide oxidative addition, in combination with on-demand flow synthesis of non-stabilized diazo reagents.

Chapter five focuses on improving efficiency in the collection of kinetic data in flow, by developing a reaction cycling reactor. Conversion over time data is obtained by passing a discrete reaction slug back-and-forth between two residence coils, with analysis performed each time the solution passes from one coil to the other. In contrast to a traditional steady state flow system, which requires >5 × the total reaction time to collect data, this reactor design collects all the data during a single reaction. Multiple reactions can also be monitored at the same time by performing multiple reactions as sequential slugs in the reactor. The reactor is demonstrated by application to a wide variety of transformations and different methods of kinetic analysis.

Dedicated to my friend and colleague Saeed K. Kashani who died on Ukrainian Airlines flight PS752. May his generaous nature, optimistic personality and dedicated work ethic be an inspiration to others.

Table of Contents

List of Figures

List of Schemes

List of Charts

List of Tables

List of Abbreviations

ACS	American Chemical Society
API	Active Pharmaceutical Ingredient
Ar	aryl
atm	atmospheres
ATR	attenuated total reflectance
b.p.	boiling point
BASIL	Biphasic Acid Scavenging using Ionic Liquids
Bn	benzyl
boc	*tert*-butyloxycarbonyl
BPR	back pressure regulator
br	broad
BuIm	1-butylimidazole
Bz	benzoyl
calcd	calculated
CCRI	Centre for Catalysis Research and Innovation
conc.	concentrated
const.	constant
Cy	cyclohexyl
d	doublet
DBU	1,8-diazabicyclo[5.4.0]undec-7-ene
DCM	dichloromethane
d.e.	diastereomeric excess
DFT	density functional theory
DMAP	4-dimethylaminopyrindine
DMF	*N*,*N*-dimethylformamide
DMP	Dess-Martin periodinane
DoE	design of experiments

d.r.	diastereomeric ratio
E_a	activation energy
ECP	effective core potential
E_{DZ}	energy calculated using a double zeta basis set
ee	enantiomeric excess
eq.	equivalents
e.r.	enantiomeric ratio
ESI-MS	electrospray ionization mass spectrometry
Et	ethyl
Et_2O	diethyl ether
EtOAc	ethyl acetate
EtOH	ethanol
E_{TZ}	energy calculated using a triple zeta basis set
E_{zpe}	zero point energy
FID	flame ionization detection
g	grams
G2	second generation
GC	gas chromatography
GC/MS	gas chromatography with mass spectrometer detector
GC-FID	gas chromatography with flame ionization detector
h	hours
het	heterocycle
HPLC	high performance liquid chromatography
I.D.	inner diameter
IBX	2-iodoxybenzoic acid
i-Pr	isopropyl
i-Pr_2NH	diisopropylamine
i-PrI	isopropyl iodide
i-PrMgCl	isopropylmagnesium chloride

i-PrOH	isopropanol
IR	infrared
istd	internal standard
kg	kilograms
k_{obs}	observed rate constant
L	litres
L/L	liquid-liquid
L-DOPA	L-3,4-dihydroxyphenylalanine
m/z	mass to charge ratio
M	molar
MCP	modular circular polarimeter
Me	methyl
MeOH	methanol
MIm	1-methylimidazole
min	minutes
MIRC	Michael-initiated ring closure
mL	millilitres
mm	millimeter
mM	millimolar
mmol	millimole
mol	mole
mol%	mole percent
mp	melting point
MS	mass spectrometry
NMP	*N*-methylpyrolidinone
NMR	nuclear magnetic resonance
NSERC	National Science and Engineering Research Council
O.D.	outer diameter
OAc	acetate

OMe	methoxy
PBR	packed bed reactor
Pd/C	palladium on carbon
PEEK	polyether ether ketone
PFA	perfluoroalkoxy alkane
Ph	phenyl
PhBr	bromobenzene
PhCl	chlorobenzene
PhI	iodobenzene
PhLi	phenyllithium
PhMgBr	phenylmagnesium bromide
PhMgCl	phenylmagnesium chloride
precat.	precatalyst
PTC	phase transfer catalyzed or phase transfer catalyst
PTFE	polytetrafluoroethylene
q	quartet
quant.	quantitative
r.t.	room temperature
RPKA	Reaction Progress Kinetic Analysis
rxn	reaction
SHOP	Shell Higher Olefins Process
SS	stainless steel
t	triplet
t/a	tonne per annum
TBSCl	*tert*-butyl silyl chloride
t-Bu	*tert*-butyl
t-BuOH	*tert*-butanol
t-BuSH	*tert*-butylthiol
TDI	turnover determining intermediate

TDTS	turnover determining transition state
THF	tetrahydrofuran
TMS	trimethylsilyl
TOF	turnover frequency
TON	turnover number
TosOH	4-toluenesulfonic acid
t_{res}	residence time
Ts	tosyl = 4-toluenesulfonyl
µL	microlitre
µm	micrometer
µmol	micromole
VTNA	Variable Time Normalization Analysis
w.r.t	with respect to
X_C	chiral auxiliary

List of Flow Schematic Symbols


pump


syringe pump

mixer (tee or cross)


reactor coil

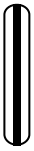
packed bed reactor

reactor with active mixing

back-pressure regulator


gravity liquid-liquid separator

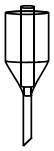
membrane-based liquid-liquid separator

Acknowledgements

This thesis work was possible thanks to scholarships from the Natural Sciences and Engineering Research Council of Canada, the province of Ontario, and the University of Ottawa. Additional funding, equipment and necessary materials were provided by the NSERC Discovery Grant program, the Canada Research Chairs Program and the Canadian Foundation for Innovation. I would like to thank my advisor Stephen Newman for his guidance and assistance during my studies, as well as the other members of my advisory committee, Deryn Fogg and André Beauchemin. Thank you also to the support staff at the University, particularly in the NMR facility, the machine and electronics shops and within the chemistry department. Thank you also to Debasis Mallik (CCRI flow chemistry facility), and Peter Zhang (Vici Valco) for programming the drivers used to control the sampling valves discussed in Chapter five. I am also very grateful for the camaraderie and support of my fellow graduate students and to my parents for their continuing support and encouragement. Most importantly, thank to my wife Elnaz and son Adrian for the constant joy and support they have provided to me during my studies.

Statement of Contributions

All work in this thesis is original and was performed by me unless otherwise noted below and in footnotes within the respective chapters. The work discussed in Chapters two and five was conducted independently. The work discussed in Chapter three was the result of collaboration with my colleague Saeed K. Kashani. Work on the acylation and S_NAr reactions was performed by Saeed. Work on S_N2 reactions and telescoped synthesis of Lidocaine were my contributions. The work discussed in Chapter four was part of a collaboration with my colleagues XiYe (Kaylie) Hua, Jeanne Masson-Makdissi and Garrett Freure. Kaylie and Jeanne developed the synthetic procedures for the Kumada-Corriu coupling which are discussed as part of the chapter introduction and assisted with the real-time ESI-MS mechanistic investigation detailed in the first part of the chapter by preparing the starting materials used for the experiments. Garrett performed the investigations into the cross-coupling of stabilized ethyl 2-diazopropanoate with aryl chlorides under my supervision. All other work within this chapter were my contributions.

Claims to Original Research

List of Publications

Parts of this thesis have been published in scientific reports:

5. Sullivan, R. J.; Newman, S. G. Reaction cycling for kinetic analysis in flow. *J. Org. Chem*, **2020**, ASAP, doi: 10.1021/acs.joc.0c00216.
4. Sullivan, R. J.; Freure, G. P. R.; Newman, S. G. Overcoming scope limitations in cross-coupling reactions of diazo nucleophiles by manipulating catalyst speciation and using flow diazo generation. *ACS Catal*., **2019**, *9*, 5623–5630.
3. K. Kashani, S.; Sullivan, R. J.; Andersen, M.; Newman, S. G. Overcoming solid handling issues in continuous flow substitution reactions through ionic liquid formation. *Green Chem.* **2018**, *20*, 1748–1753.
2. Sullivan, R. J.; Newman, S. G. Chiral auxiliary recycling in continuous flow: automated recovery and reuse of Oppolzer's sultam. *Chem. Sci.* **2018**, *9*, 2130–2134.
1. Hua, X.; Masson-Makdissi, J.; Sullivan, R. J.; Newman, S. G. Inherent vs. apparent chemoselectivity in the Kumada–Corriu cross-coupling reaction. *Org. Lett.* **2016**, *18*, 5312−5315.

List of Presentations

Parts of this thesis have been presented in conference proceedings and technical meetings:

6. Sullivan R. J.; Hua, X.Y.; Freure, G. P. R. ; Masson-Makdissi, J. ; Newman, S. G. Using flow chemistry to 'turn on' catalytic cycles. CCRI technical meeting, University of Ottawa, Feb 13, 2020.
5. Sullivan, R. J.; Newman, S. G. Efficient kinetics in flow: Sequential sampling from a cycling reaction slug. 30th QOMSBOC held at the University of Ottawa, Nov 08-10, 2019.
4. Sullivan, R. J.; Freure, G. P. R.; Newman, S. G. Palladium catalyzed cross-coupling of flow-generated, non-stabilized diazo compounds with aryl bromides and chlorides. 102nd Canadian Chemistry Conference and Exhibition held in Quebec City, June 3–7, 2019.
3. Sullivan, R. J.; Newman, S. G. Automating chiral auxiliary recycling in flow. 28th QOMSBOC held at McGill University, Nov 17–19, 2017.
2. Sullivan, R. J.; Newman, S. G. Automating chiral auxiliary recycling. 100th Canadian Chemistry Conference and Exhibition held in Toronto, May 28–June 1, 2017.
1. Sullivan, R. J.; Newman, S. G. Automating chiral auxiliary recycling. 27th QOMSBOC held at University of Waterloo, Nov 11–13, 2016.

Chapter 1 Introduction

1.1 Continuous flow chemistry for improving reaction efficiency

In conventional batch chemistry reactions are performed by combining reagents in an appropriate vessel — most commonly a round bottom flask — under suitable conditions. In contrast, continuous flow chemistry is performed by pumping solutions/mixtures of reagents through a reactor vessel equipped with an inlet and outlet — in an academic context typically a coil of small diameter tubing (e.g., PFA, PEEK, stainless steel, etc.) but numerous reactor designs are available for different purposes — and reactions proceed as the material moves through the reactor.[1] Reaction 'time' is tied to residence time inside the reactor, which is in turn a direct consequence of the flow rate of materials and volume of the reactor vessel. Continuous flow chemistry is the norm in the bulk chemical industry due to the sheer volume of material produced. However, despite numerous potential benefits from operating in continuous flow, batch methods largely predominate at academic, pharmaceutical and fine chemical scales.

In the last couple decades however, interest in continuous flow chemistry within academia and pharma has increased immensely in recognition of the benefits achievable in flow.[1] These potential benefits include improved heat and mass transfer, access to wider temperature and pressure windows, safer use of high energy intermediates, facile recovery and reuse of heterogeneous catalysts, and the ability to telescope multi-step syntheses. As a result, the application of continuous flow chemistry to improve reaction efficiency and decrease environmental impact is becoming increasingly common.[2]

1.1.1 Improved heat and mass transfer

The improvement in heat and mass transfer realized with continuous flow systems stems primarily from the decreased reactor dimensions that facilitate rapid mixing and efficient heat transfer due to small diffusion path lengths and large surface area to volume ratios.[1,3] In combination with the tight control over residence times achievable in a flow system, this can provide greatly improved selectivity and yield for very fast and exothermic reactions. The largest impact in this area has been the seminal contributions from the Yoshida group in the development of flash chemistry.[4] The most common application has been for the selective formation of (unstable) organometallic reagents at non-cryogenic temperatures.

For example, double functionalization of *ortho*-dibromobenzene (**1.1**) was achieved using a flow reactor by sequential lithium-halogen exchange/electrophile trapping reaction sequences (Scheme 1.1), whereas in a batch setup the degradation of *ortho*-bromophenyllithium to benzyne cannot be prevented.[5] Furthermore, the second lithium-halogen exchange and electrophile quench can be performed at 0 °C, whereas in batch cryogenic temperatures are generally required to control the reaction exotherms and prevent organolithium decomposition and other side reactions for this family of transformations.[6] Numerous examples within academia have been demonstrated,[4] and flash chemistry has begun to see use in the pharmaceutical industry for organolithium and Grignard reagent formation and utilization.[7] Efficient heat transfer also, in principle, allows reactions to be performed at higher concentrations due to efficient control of exotherms. However, the need to avoid precipitation usually prevents the use of high concentrations from being realized in practise. These concepts and limitations will be revisited in Chapter 3.

Scheme 1.1. Flash chemistry enabled double functionalization of *ortho*-dibromobenzene using sequential lithium–halogen exchange/ electrophile trapping reactions.

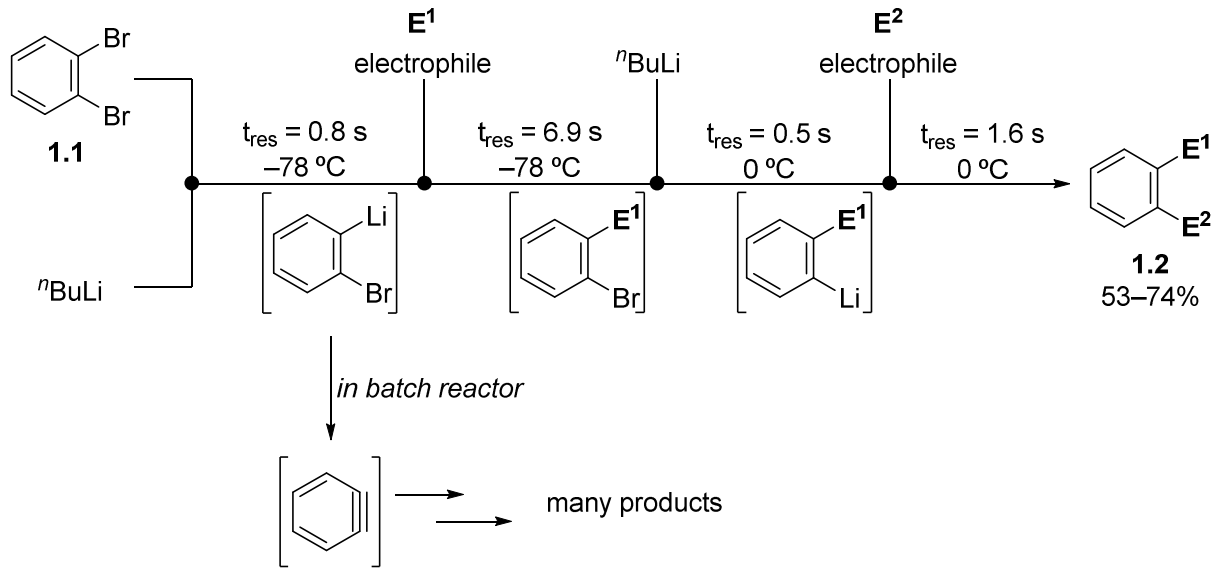

1.1.2 Access to wider temperature and pressure windows

The application of pressure in a continuous flow system is trivial, not requiring expensive, specialized equipment or substantial infrastructure investment as is the case for batch chemistry. Pressure in a flow system is achieved through application of a back-pressure regulator at the exit

stream of the reactor, with the upper limit defined by either the material strength of the reactor components or ability of pump(s) to deliver material against the set pressure. For example, a flow reactor comprising HPLC pumps and stainless steel tubing can accommodate pressures of 200 bar at 350 °C.[8] As a consequence, reactions can be easily conducted in flow at temperatures above the atmospheric boiling point of the solvent, giving access to accelerated reaction kinetics. Furthermore, reactions conducted at (highly) elevated temperature allow not just acceleration of known chemistry, but also access to chemistries that are not possible in batch.[1,2f,8,9] For example, thermal deprotection of *N*-boc-protected amines **1.3** was achieved at neutral *p*H in flow by using reaction temperatures of 300 °C, a transformation not realizable under batch conditions (Scheme 1.2).[10] Numerous other novel transformations have been achieved using high-temperature, high-pressure flow conditions and the reader is directed to reviews available on the subject.[1,8,9]

Scheme 1.2. A thermal boc deprotection developed by Bogdan and coworkers.

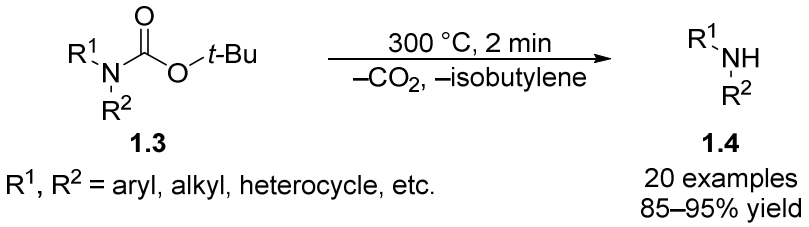

Use of high pressure is also beneficial for gas-liquid reactions by increasing the solubility of the gaseous reactant in the liquid phase. For example, hydrogenation reactions frequently occur under biphasic (gas-liquid) or triphasic (gas-liquid-solid) conditions, with mass transport between H_2 and the catalyst typically rate limiting. The application of pressure and efficient agitation is often therefore essential to achieve desired reaction rates due to the low solubility of hydrogen in most organic solvents.[2f] Consequently, conducting a large-scale batch hydrogenation not only requires the use of expensive, specialized high-pressure equipment, but also introduces considerable safety risks due to the need for a pressurized headspace of highly flammable hydrogen gas. In a flow system however, not only is the equipment cost to manufacture a reactor much lower,[11] but there is also no large headspace present, so safety risks are minimized. Furthermore due to the ease of application of high pressures and small reactor dimensions mass transport between hydrogen gas and the liquid phase or solid catalyst is greatly enhanced.[2f]

As a result, continuous flow hydrogenations are increasingly popular within academic,[12] medicinal chemistry,[13] and process chemistry[14] groups. Both heterogeneous (vide infra, section 1.1.4) and homogeneous catalyzed reactions are common. For example, researchers at Eli Lilly developed a continuous flow, homogeneously catalyzed asymmetric hydrogenation of enone **1.5** to ketone **1.6** in the process route towards LY500307 (**1.7**, Scheme 1.3), achieving ~13 kg/day throughput with a 73 L plug flow tubular reactor (Figure 1.1).[14a] The flow process was essential to allow scale up since high pressures of hydrogen (70 bar) were required to reach complete conversion of this challenging, tetrasubstituted enone, and large scale autoclaves capable of handling this pressure were not available in the researchers' manufacturing area, with prohibitive capital expense deterring acquisition. The benefits of trivial access to high pressure to accelerate hydrogenation reactions will be important in Chapter 2.

Scheme 1.3. Flow asymmetric hydrogenation for the scale up of ketone **1.6**.

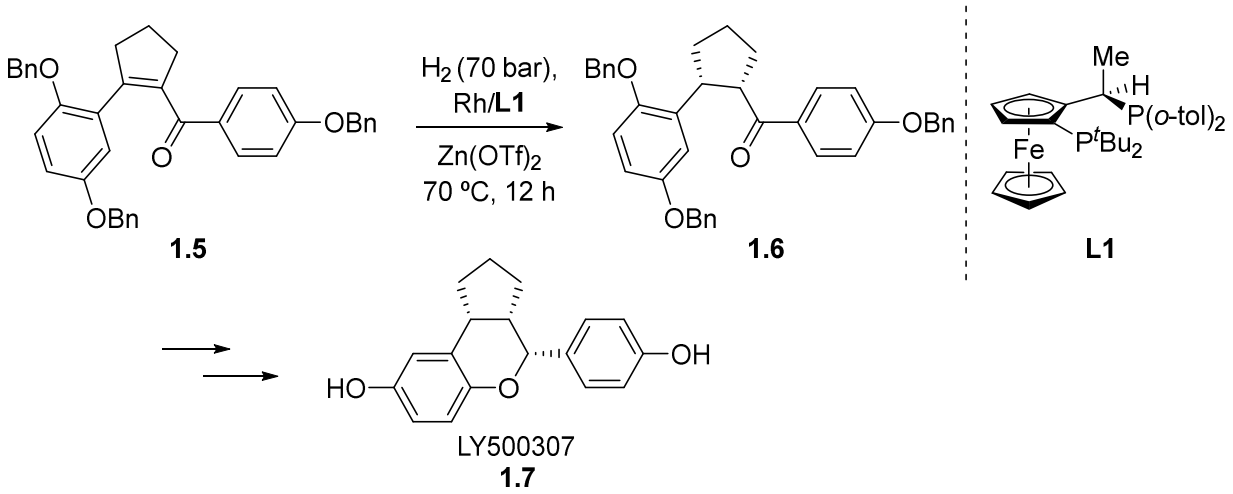

1.1.3 Safe use of high-energy intermediates

In section 1.1.2 the use of continuous flow reactors to minimize risk by removing the necessity for a large, pressurized headspace of flammable hydrogen was highlighted. Flow systems can also minimize safety concerns for other hazardous chemistries as well. Implementation of a flow process allows many of the safety risks associated with the use of high energy compounds to be addressed. Not only does the high heat transport achieved in flow allow tight control over reaction exotherms, minimizing the risk of reaction run-away, but the smaller dimensions of a flow

Figure 1.1. 73 L plug flow reactor used at Eli Lilly for the continuous flow hydrogenation of enone **1.5**. Image reproduced from ref 14a with permission from ACS publications.[15]

reactor also mean smaller quantities of high energy species are present at any given time. By combining flow generation with immediate quench of the reactive species into one process, further safety concerns can be mitigated through removal of need to stock large quantities of the hazardous chemical, and minimizing exposure risk since physical manipulations (e.g., loading or work up and isolation) are not required. This makes it possible to consider atom economical synthetic routes that would traditionally be discarded because of safety concerns in batch scale up.

For example, diazo compounds are very versatile reagents that enable a wide variety of interesting transformations, typically with high atom efficiency.[16] Nonetheless, the health and safety concerns due to high toxicity and tendency to decompose explosively have traditionally precluded application of diazo compounds at scale.[17] Furthermore, the necessity for a stabilizing electron withdrawing group alpha to the diazo functionality places severe limitations on the types of diazo compounds that are accessible even at small scale. Continuous flow processes for the safe synthesis and immediate consumption of diazo compounds are brokering a renaissance of diazo chemistry, demonstrating assess to a wide variety of diversely functionalized diazo compounds,[18] including at industrially relevant scales.[17] For example, recent work by the groups of Ley[19] and Charette[20] has demonstrated the ability safely synthesize non-stabilized diazo compounds (**1.9**) by on-demand oxidation of hydrazones (**1.8**) in flow, and apply these diverse reagents in atom economical syntheses of a variety of densely functionalized compounds, including diverse pyrazolines and pyrazolidines (**1.10**), esters (**1.11**), cyclopropanes (**1.12**), allenes (**1.13**), and

secondary or tertiary alkanes (**1.14**) (Scheme 1.4). The ability to safely access diazo compounds using continuous flow will be important in Chapter 4.

Scheme 1.4. On-demand flow synthesis of non-stabilized diazo compound by oxidation of hydrazones for the synthesis of varied chemical products.

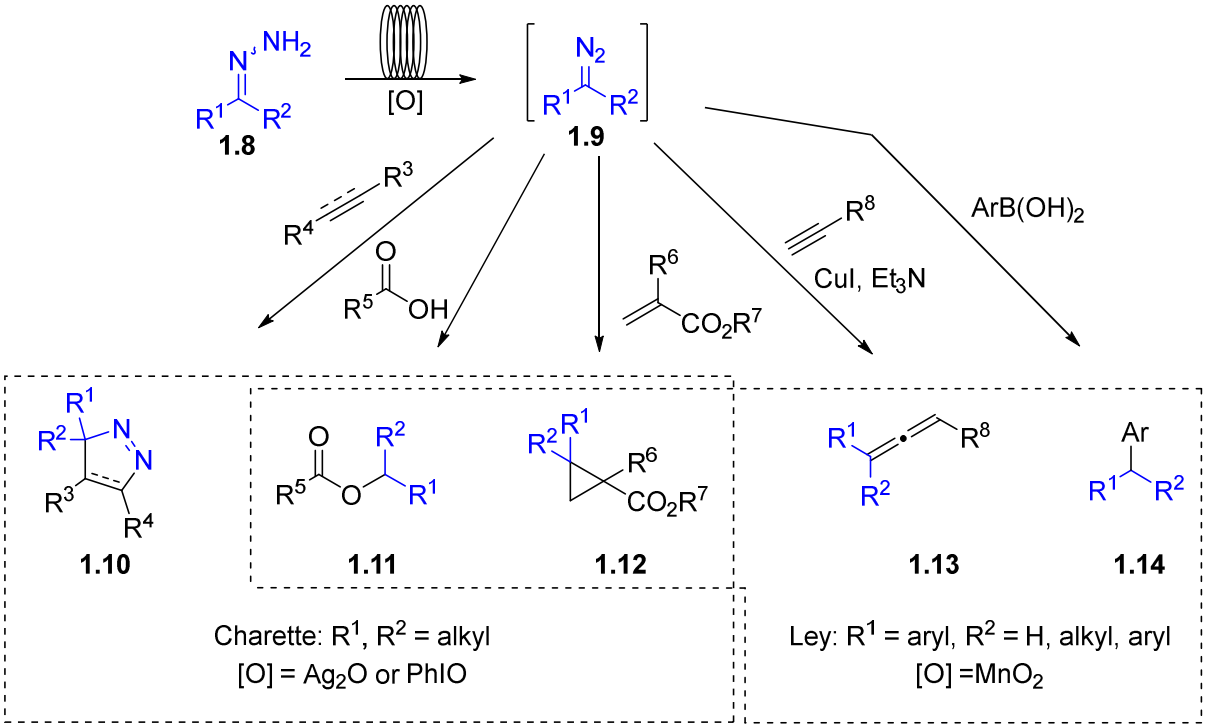

1.1.4 Efficient application of heterogeneous catalysts

In most cases converting a reaction to continuous flow can facilitate process intensification due to improved heat and mass transfer, allowing higher concentrations and shorter reaction times to be used. For heterogeneously catalyzed processes however, the potential benefits of operating in continuous flow are much greater. This is for two reasons. First, a heterogeneously catalyzed process is necessarily operative in different phases (e.g., solid-liquid, solid-gas or solid-liquid-gas) and as such mass transport plays a large role in the reaction kinetics. The smaller dimensions of continuous flow reactors greatly improve mass transport, accelerating heterogeneously catalyzed reactions as already mentioned (vide supra, section 1.1.2). Second, and perhaps more significant, the effective catalyst loading in a flow process is substantially higher than in a batch case. This is a consequence of reactor design.

To perform a heterogeneously catalyzed reaction in flow one typically uses either a packed bed or fluidized bed reactor. A packed bed reactor is filled with catalyst particles and capped with porous frits on either end. Reaction fluids are pumped through the bed, travelling through the void spaces (Figure 1.2A). A fluidized bed reactor is quite similar but is only partially filled with catalyst and the reaction fluids are pumped in from the bottom at a sufficiently high flow rate to agitate the solid catalyst particles, 'fluidizing' the bed (Figure 1.2B). In both cases, the entirety of the heterogeneous catalyst but only a very small portion of the reaction solution is present at any given time. This results in super-stoichiometric effective catalyst loadings, greatly increasing reaction rates.

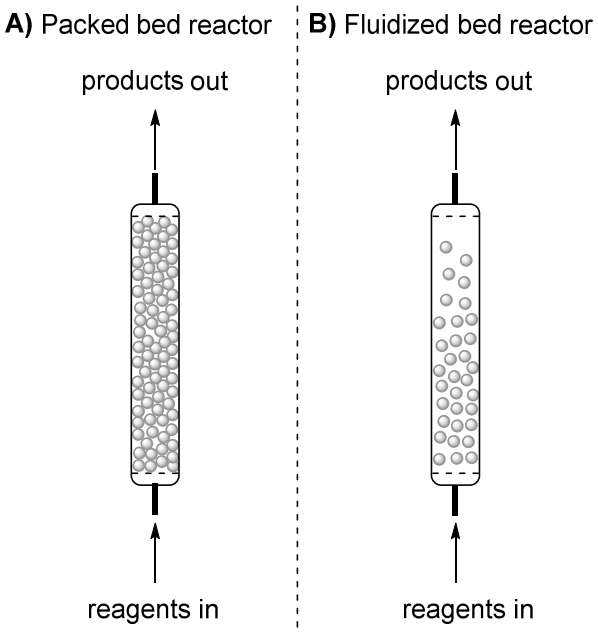

Figure 1.2. Simplified schematic of a packed bed (A) vs. fluidized bed (B) reactor.

An example from our laboratories highlights the rate acceleration achievable. A collaborator in industry was pursuing a synthetic route that included a nitro reduction step of a functionalized aromatic nitroarene **1.15** (Scheme 1.5A). In batch the reaction was slow, requiring 22 h at room temperature, while attempts to accelerate the reaction by applying more forcing conditions led to erosion of product selectivity due to over reduction of the aryl halide groups. By converting to a continuous flow process using a packed bed reactor the contact time necessary between the reaction solution and the catalyst could be drastically decreased. Furthermore, due to the ability to

tightly control the contact time, use of elevated temperatures was feasible without leading to overreduction, allowing a further decrease in necessary contact time with the catalyst to only ~3 min (Scheme 1.5B).[21] Given the drastic decrease in reaction time possible it is therefore unsurprising that performing heterogeneously catalyzed reductions in continuous flow has attracted considerable interest in the pharmaceutical and agrichemical industries.[22] Efficient use of heterogenous catalysts and packed beds of reagents will be important in both Chapters 2 and 4.

Scheme 1.5. Nitro reduction of an industrially relevant intermediate was greatly accelerated by converting from a batch to flow hydrogenation.

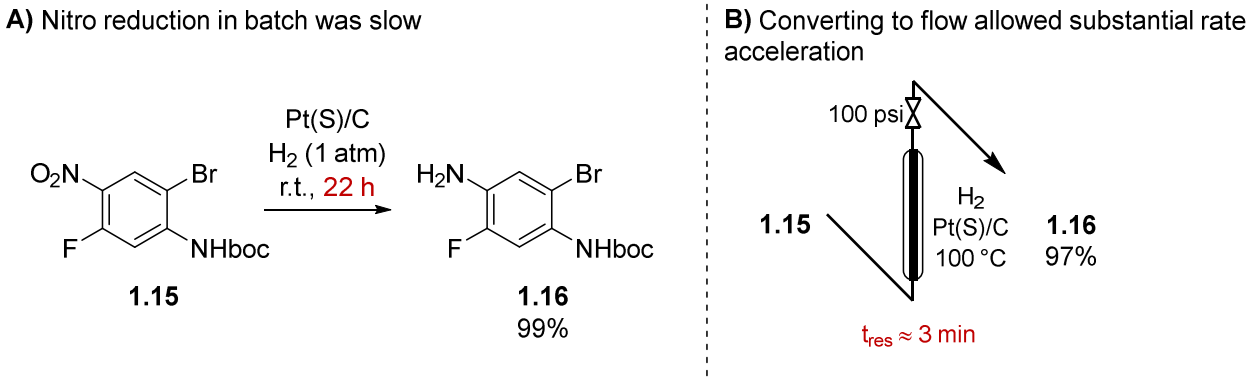

1.1.5 Telescoped multi-step reaction sequences

Synthesis of complex, functionalized molecules typically requires multi-step reaction sequences. Non-quantitative yields and losses during purification and isolation at each step quickly add up to give low overall yields from start to finish. In addition, the isolation and purification of numerous intermediates makes the process labor intensive. Consequently, development of synthetic routes that are shorter and require fewer intermediate isolations are major goals during process scale up and total synthesis to improve efficiency. One approach to cut down on intermediate isolations is to use the crude reaction mixture from one reaction directly as the starting material for the next reaction by performing reactions back-to-back in continuous flow.[23] This 'telescoping' of reactions into a single process can improve the efficiency and decrease the manual labor involved in a multi-step synthesis.

For example, Jamison and coworkers reported a telescoped seven-step synthesis of Linezolid (**1.26**), a last-line-of-defense antibiotic for multi-drug resistant gram-positive bacteria (Scheme

1.6).[24] The conversion to a telescoped continuous flow process allowed shortening the reaction time from start to finish to 27 min, achieving an overall 73% yield of **1.26** compared to >60 h and 50% overall yield obtained in the optimized batch process.[25] With such substantial improvements possible, it is no surprise that a major research focus in the pharmaceutical industry has been investigating feasibility of telescoping continuous flow syntheses of APIs.[26] The ability to telescope reactions plays a crucial role in Chapters 2 and 4, and is also featured in Chapter 3.

1.2 Implementing cycles to improve efficiency

1.2.1 Cycles by reagent design: Catalytic cycles

While use of continuous flow chemistry can be an excellent way to improve reaction efficiency by facilitating process intensification and/or accessing shorter synthetic routes, it is by no means the only approach available. The construction of closed cycles is another powerful strategy used to improve efficiency and reduce waste. The most common context of this approach is the development of catalysts that interact with reagent(s), enable a desired transformation, and re-emerge unaltered after releasing product(s). This allows the catalyst to subsequently engage with a new set of reagents, generate additional product, etc. until all reagents are consumed, or the catalyst dies through a non-productive pathway. This type of closed cycle is operative in *time*; the catalyst remains in the same place (e.g., the flask) but continuously 'travels' through the cycle as time passes, affecting multiple net transformations (Scheme 1.7).

While an incredibly elegant and powerful solution to enable numerous important reactions, development of new catalytic transformations is not trivial. A functioning catalytic cycle requires numerous elementary reaction steps to operate in a carefully balanced harmony under a single set of reaction conditions, in competition with a myriad of unproductive side reactions and catalyst decomposition pathways.[27] As a result, it is very common that small changes to reaction components or conditions result in large changes in reaction outcome. The most frustrating consequence of this is the high tendency to encounter scope limitations when applying reported catalytic methods to highly functionalized substrates. For example, the Buchwald-Hartwig amination is an intensely studied, well developed, and well understood catalytic reaction to form a new carbon–nitrogen bond, and yet a 55% failure rate is reported for Buchwald-Hartwig

Scheme 1.6. Telescoped seven step continuous flow synthesis of Linezolid reported by Jamison and coworkers.

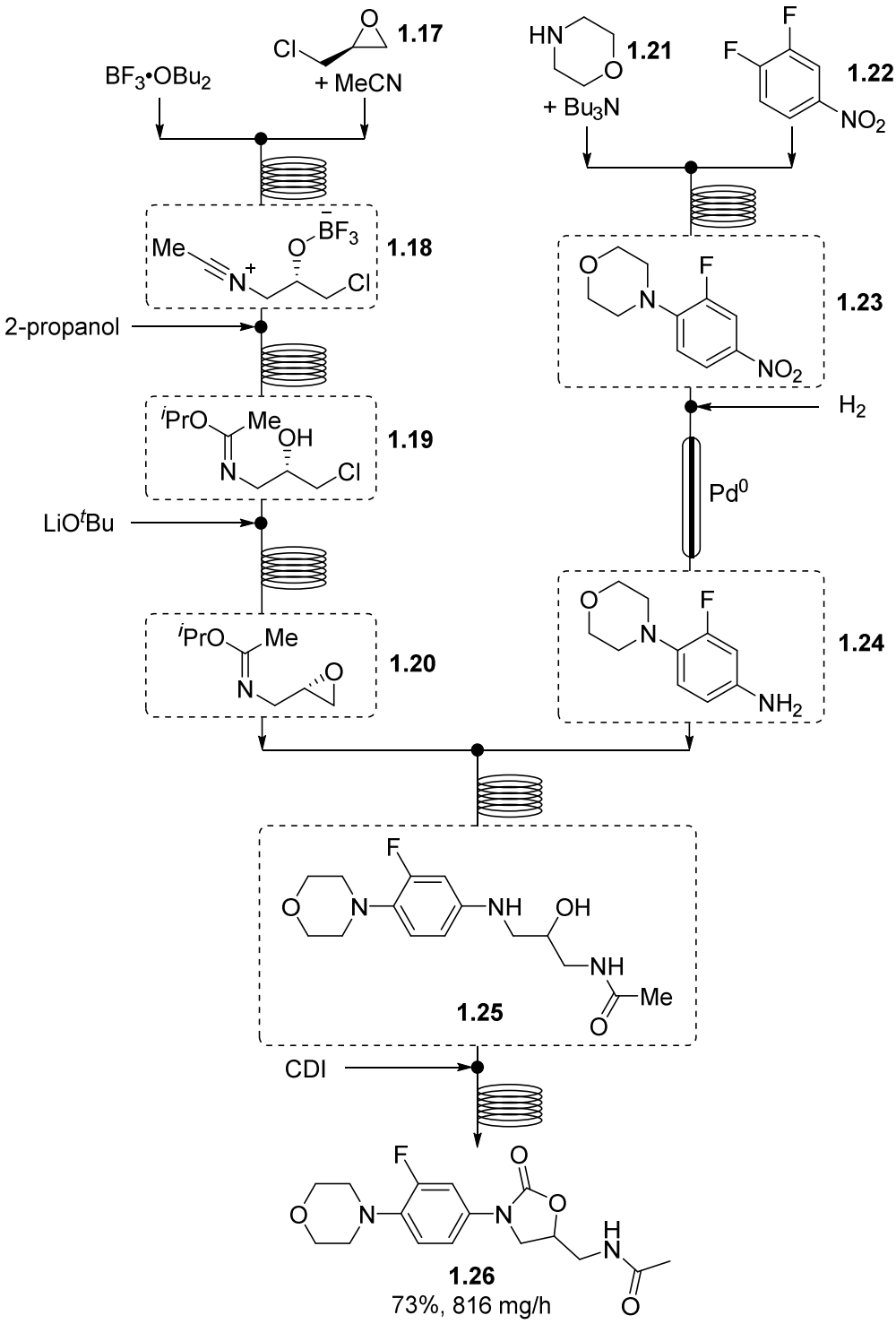

Scheme 1.7. A generic catalytic cycle — *a cycle in time.*

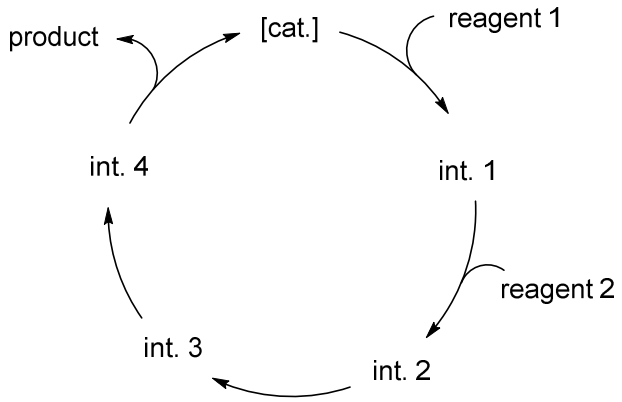

aminations on densely functionalized drug intermediates in the pharmaceutical industry.[28] As a result, there is a constant need for research to overcome scope limitations in existing catalytic reactions through the identification of new catalysts, alternate reaction conditions and novel transformations.

1.2.2 Cycles by reactor design: Recycle loops

While catalysis is perhaps the most obvious and elegant example, it is not the only instance where cycles are used to increase efficiency in chemical processes. The continuous recycling of unreacted reagents in industrial processes operated at partial conversion is also a case where implementation of cycles is used to maximize efficiency and minimize waste. In this case however, the cycles are operative in *space*; material is physically moved in a circular path, returning unreacted material exiting a process back to the beginning, while products are continuously removed.

Implementation of cycles in space is common at the bulk chemical scale, where chemical processes operate continuously. For example, in catalytic hydrocracking operations heavy fractions of crude oil are treated with H_2 over catalyst beds to facilitate the production of lighter naphtha fractions. Upon exiting the reaction zone, the material is a mixture of various hydrocarbons ranging from low boiling (light fractions) to high boiling (heavy fractions). The problem of low selectivity during the cracking is overcome by incorporating a closed recycle loop to recover and retreat the fractions that are heavier than desired. After separation of the various product cuts by distillation, the heaviest fractions of material are *sent back to the reaction zone* for

re-cracking via a recycle loop to increase the production of the desired, lighter products (Figure 1.3).[29]

Another example of a very important chemical process that utilizes a cycle in space is the Haber-Bosch process to produce ammonia. In this case the reaction suffers from low conversion due to the equilibrium favoring the reactant N_2 and H_2 gasses rather than the product. The disadvantaged thermodynamics are overcome by accepting low conversion and using looped reactor designs to continuously recover and recycle the unreacted N_2 and H_2 (Figure 1.4).[30]

1.3 Using continuous flow to enable cycles

1.3.1 Implementing cycles in space to turnover stoichiometric reagents

It is only possible to implement cycles in space such as those discussed above if operating a continuous process. However, since most new chemical transformations are developed using traditional batch approaches (e.g., in round-bottom flasks), implementing looped reactor designs is not generally considered when faced with problems in synthetic organic chemistry. The development of new catalysts or catalytic transformations on the other hand is a frequently targeted

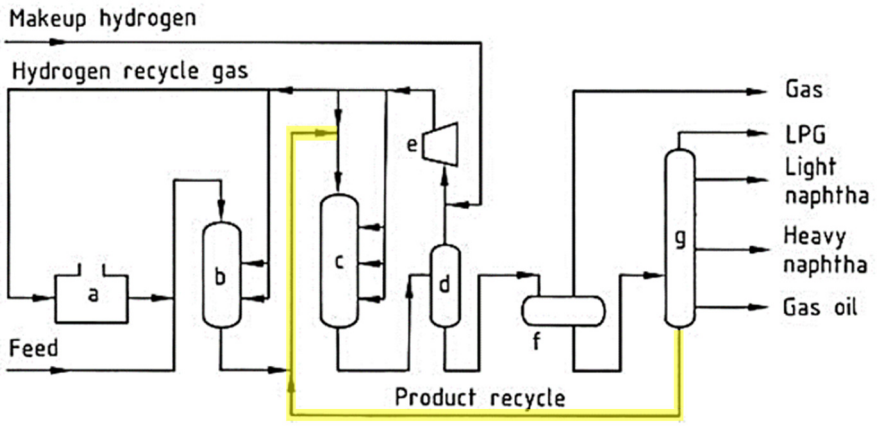

Figure 1.3. Schematic of a two-stage catalytic hydrocracking operation: a) hydrogen heater; b) first-stage reactor (hydrotreating); c) second-stage reactor (hydrocracking); d) high-pressure separator; e) hydrogen compressor; f) low-pressure separator; g) fractionator with *recycle* of highest boiling fractions back to hydrocracker for subsequent re-treatment — *a cycle in space*. Image adapted from ref 29 with permission for J. Wiley and Sons.

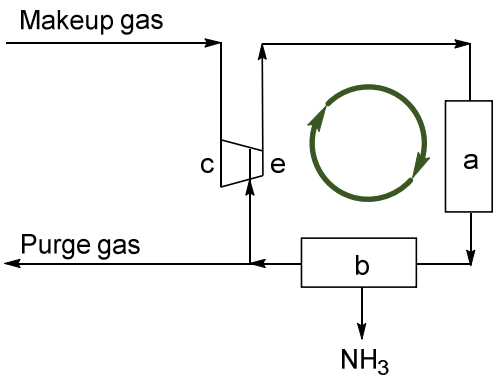

Figure 1.4. Schematic of a typical Haber-Bosch process loop: a) ammonia converter with heat exchangers; b) ammonia recovery by chilling and condensation; c) synthesis gas compressor; d) recycle compressor. Unreacted H_2 and N_2 gasses are continuously recycled back to the reaction zone — *a cycle in space*. Image adapted from ref 30 with permission from J. Wiley and Sons.

solution to develop new reactions and improve efficiency. Furthermore, implementation of catalytic processes rather than using stoichiometric reagents is one of the twelve principles of Green Chemistry to reduce environmental impact by limiting waste production and resource consumption.[31] We considered that since catalysis is implementation of a cycle operating in time, implementing a cycle operating in space using recycle loops in continuous flow could, in principle, achieve comparable benefits. We hypothesized that designing a cycling reactor to 'turnover' a stoichiometric reagent could realize the same benefits as developing a new catalyst (Figure 1.5).

This concept is in part inspired by the recovery and reuse of homogenous catalysts in continuous flow systems, which has been well documented using strategies such as scavenging columns, liquid-liquid biphasic reaction conditions and organic solvent nanofiltration.[32] Furthermore, at the industrial scale, liquid-liquid biphasic conditions to recover and reuse homogeneous catalysts in continuous processes are used at the 10^5 t/a scale in, for example, the Ruhr Chemie/Rhône-Poulenc process for hydroformylation of propene to butanal[33] and the Shell Higher Olefin Processes (SHOP) for ethylene oligomerization.[34] However, while continuous recovery and reuse of homogenous catalysts is clearly beneficial from a cost perspective, through a conceptual lens the consequence of implementing a cycle in space to facilitate catalyst reuse is simply to increase turnover number (TON) of a reagent that already exhibits turnover. We

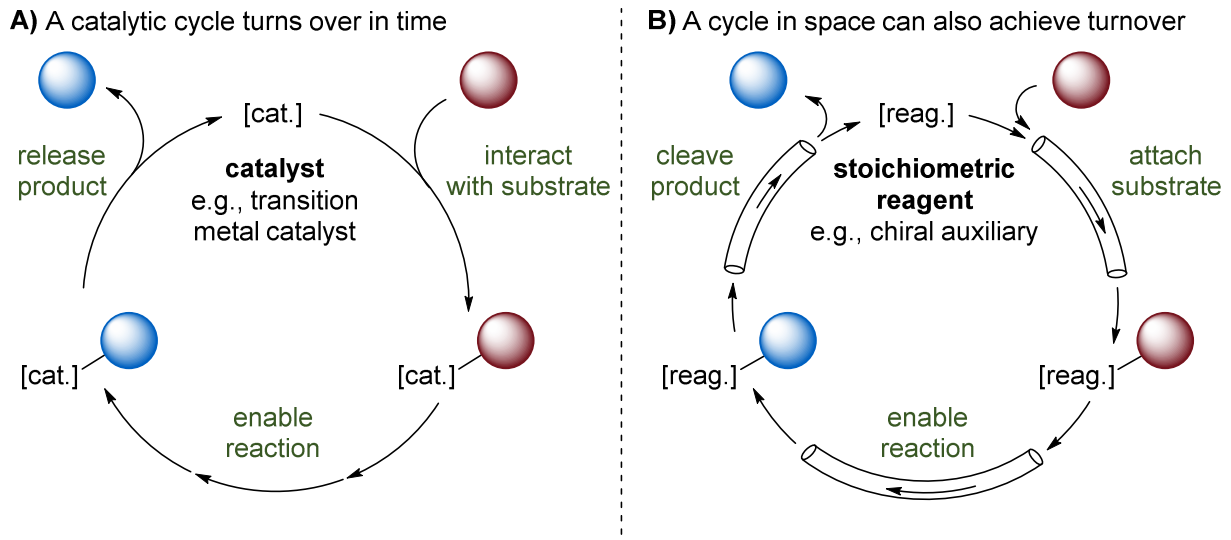

Figure 1.5. A) A catalyst turns over in time to improve reaction efficiency. B) Facilitating reagent turnover by designing a continuous process with recycle loop is hypothesized to realize the same efficiency benefits in direct analogy to a catalytic cycle, but operative in space.

envisioned that more challenging problems could be overcome by using flow chemistry to implement closed cycles and these ideas are explored in Chapters 2 and 5.

1.3.2 Using controlled reagent addition to facilitate catalytic cycles

Catalytic transformations are incredibly powerful but the complexity of balancing multiple productive elementary steps in competition with numerous undesired side reactions often results in scope limitations. Possible reasons for reaction failure include the catalyst suffering from competitive inhibition, off-cycle sequestration or decomposition.[27a] However, there are other situations where the reason for reaction failure lies not with the catalyst become inactive, but rather with one or more of the substrates decomposing before engaging in the desired, catalyzed pathway. Specifically, when one or more substrates undergo uncatalyzed background reactions, the ability to obtain a high yield or selectivity of the desired product depends on the relative rates of these catalyzed (desired) versus uncatalyzed (undesired) pathways. This is most commonly appreciated in the context of enantioselective catalysis, where the presence of uncatalyzed, and therefore non-enantioselective, background reactions erode product ee but not necessarily yield.[35] In order to achieve high enantioselectivity it is necessary to have negligible background reaction on the time scale of the catalyzed transformation.

This concept is not limited to asymmetric catalysis but is also encountered in cases of reagent incompatibility, where substrates can react directly via uncatalyzed background reactions.[36] In these cases, the background reactions result in low yields of the desired product. Similar strategies can be employed in either case to vary the relative rates of desired (catalyzed) versus undesired (background) reactions. For example, inclusion of additives or screening of solvents are common approaches to optimize yield and selectivity. Nonetheless, the most effective solution is often to develop a better catalyst with faster turnover (Scheme 1.8). In this way the reactive substrate is consumed by the desired pathway before having the chance to undergo unwanted background reactions.

Scheme 1.8. Substrate scope failures resulting from competing side reactions that deplete one of the substrates can be overcome by accelerating the desired chemistry (development of a faster catalyst, conventional) or slowing of the undesired side reactions via slow addition of the substrate (proposed).

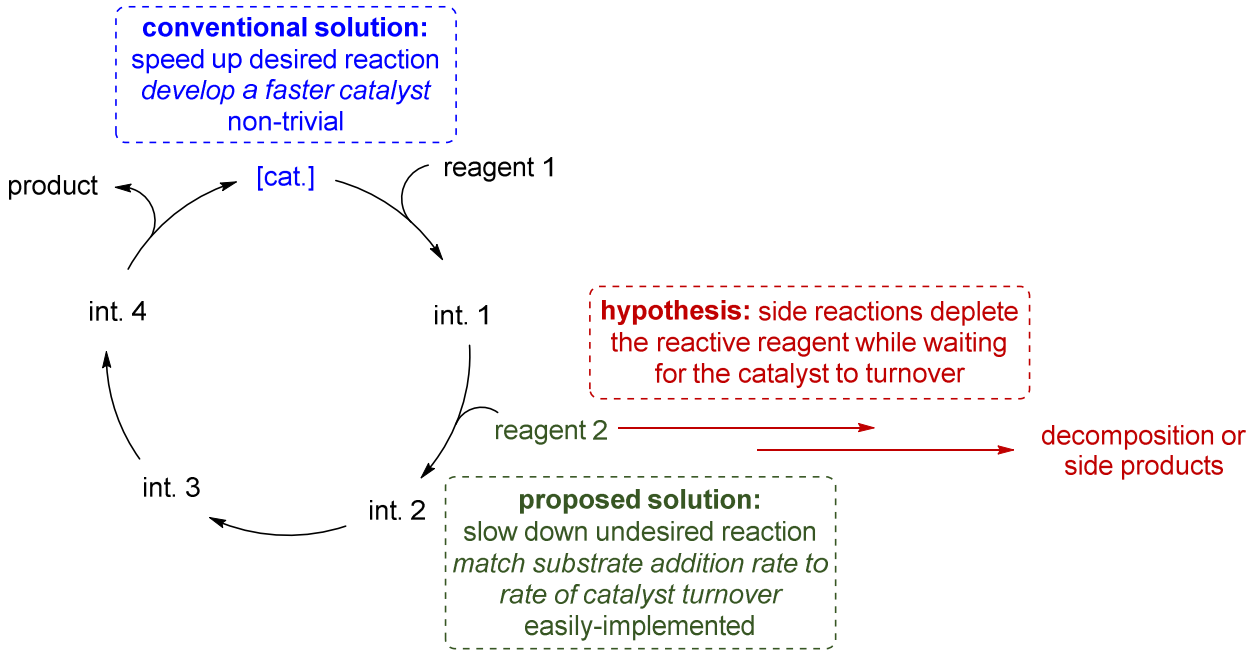

However, while this is elegant and seemingly straightforward, development of new catalysts is a laborious experimental exercise. While rational design can play a role,[37] often brute force screening and serendipity are the driving forces in new catalyst discovery.[27b] We hypothesized that as an alternative to accelerating catalyst turnover, slow addition of the substrate prone to

background reactivity could be used to slow the undesired reaction(s). This follows from the hypothesis that background reactions occur while waiting for the catalyst to turnover. If the troublesome substrate is added slower than the catalyst turns over, the substrate won't need to wait for the catalyst because the catalyst will already be present as the correct intermediate on the catalytic cycle, ready to consume the reagent as it is added. Slow addition of reagents is common in catalytic reactions using reactive organometallic substrates,[38] but mechanistic reasoning is seldom given, and to our knowledge the strategy of matching addition rate of a reagent to catalyst turnover had not been previously described. This hypothesis will be further elaborated on the introduction to Chapter 4, where these concepts will be central to the work discussed.

1.4 Research goals

The motivation of this thesis is to explore these two unconventional strategies to enable 'turn-over' — designing continuous flow reactors/processes that incorporate 'cycling' and matching reagent addition rate to rate of catalyst turnover enable catalytic transformations. The ability to telescope reactions, safely access high-energy intermediates, and accelerate chemical transformations by leveraging the other benefits of continuous flow discussed in Section 1.1 will be central to realize these goals.

Chapter 2 explores the hypothesis that design of a telescoped continuous flow process incorporating a recycle loop can achieve formal 'catalytic' loading of a stoichiometric reagent. An asymmetric hydrogenation mediated by Oppolzer's sultam is used for this proof of concept work, which is accomplished by telescoping the three reactions of auxiliary attachment, hydrogenation, and auxiliary cleavage into an efficient continuous flow process with incorporation of recovery and reuse of the auxiliary to achieve 'turn-over'.

Chapter 3 focuses on enabling reactions to be conducted in continuous flow, a prerequisite to implementing strategies such as continuous recycling of reagents described in Chapter 2. Solid handling in flow is a great challenge, particularly problematic for substitution reactions that generate stoichiometric acid by-products, therefore requiring quenching with a base and producing insoluble base·HX salts. It was hypothesized that this problem could be overcome by selecting organic bases for which the base·HX salt is molten at the reaction temperature, and this strategy is demonstrated to be easily implemented for acylation, S_NAr, S_N2, and silylation reactions.

Chapter 4 explores the second hypothesis, that matching reagent addition rate to rate of catalyst turnover can enable catalytic reactions that would otherwise fail due to competing background reactivity. Mechanistic understanding to provide support for the hypothesis is gleaned from real-time ESI-MS monitoring to track relevant intermediates on the catalytic cycle as a function of organometallic reagent addition rate for Kumada-Corriu and Murahashi cross-coupling reactions enabled by Grignard or organolithium slow addition respectively. The strategy is then extended to substantially broaden the scope of palladium catalyzed cross-coupling of aryl halides and diazo reagents, in combination with on-demand continuous flow synthesis of non-stabilized diazo compounds.

Lastly, Chapter 5 returns to the idea of cycling materials in space. This time cycling of an entire reaction solution is targeted to efficiently obtain conversion over time data using continuous flow equipment. Sequential analysis as a reaction progresses is challenging in continuous flow because reaction 'time' is coupled with movement in space. It was hypothesized that if a reaction solution could be moved in a cyclical path, it would be possible to perform analysis once each 'loop', and therefore efficiently obtain conversion over time data. A reactor that accomplishes this goal is developed and demonstrated for the kinetic analysis of a variety of reactions using various methods of kinetic analysis.

1.5 References

[1] Plutschack, M. B.; Pieber, B.; Gilmore, K.; Seeberger, P. H. The hitchhiker's guide to flow chemistry. *Chem. Rev.* **2017**, *117*, 11796−11893.

[2] a) Webb, D.; Jamison, T. F. Continuous flow multi-step organic synthesis. *Chem. Sci.* **2010**, *1*, 675−680; b) Yoshida, J.-i.; Kim, H.; Nagaki, A. Green and sustainable chemical synthesis using flow microreactors. *ChemSusChem* **2011**, *4*, 331−340; c) Wiles, C.; Watts, P. Continuous flow reactors: A perspective. *Green Chem.* **2012**, *14*, 38−54; d) Ley, S. V. On being green: Can flow chemistry help? *Chem. Rec.* **2012**, *12*, 378−390; e) Newman, S. G.; Jensen, K. F. The role of flow in green chemistry and engineering. *Green Chem.* **2013**, *15*, 1456−1472; f) Gutmann, B.; Cantillo, D.; Kappe, C. O. Continuous-flow technology — A tool for the safe manufacturing of active pharmaceutical ingredients. *Angew. Chem. Int. Ed.* **2015**, *54*, 6688−6728.

[3] a) Capretto, L.; Cheng, W.; Hill, M.; Zhang, X. Micromixing within microfluidic devices. In *Microfluidics: Technologies and applications*; Lin, B. C., Ed. 2011; Vol. 304, p 27–68; b) Schwolow, S.; Hollmann, J.; Schenkel, B.; Röder, T. Application-oriented analysis of mixing performance in microreactors. *Org. Process Res. Dev.* **2012**, *16*, 1513–1522; c) Born, S.; O'Neal, E.; Jensen, K. F. 9.03 Organic synthesis in small scale continuous flow: Flow chemistry. In *Comprehensive Organic Synthesis II*; 2 ed; Knochel, P., Ed.; Elsevier: Amsterdam, 2014, p 54–93; d) Gobert, S. R. L.; Kuhn, S.; Braeken, L.; Thomassen, L. C. J. Characterization of milli- and microflow reactors: Mixing efficiency and residence time distribution. *Org. Process Res. Dev.* **2017**, *21*, 531−542; e) Reckamp, J. M.; Bindels, A.; Duffield, S.; Liu, Y. C.; Bradford, E.; Ricci, E.; Susanne, F.; Rutter, A. Mixing performance evaluation for commercially available micromixers using Villermaux–Dushman reaction scheme with the interaction by exchange with the mean model. *Org. Process Res. Dev.* **2017**, *21*, 816−820.

[4] a) Yoshida, J. i.; Nagaki, A.; Yamada, T. Flash chemistry: Fast chemical synthesis by using microreactors. *Chem. Eur. J.* **2008**, *14*, 7450−7459; b) Yoshida, J. I. Flash chemistry: Flow microreactor synthesis based on high-resolution reaction time control. *Chem. Rec.* **2010**, *10*, 332−341; c) Yoshida, J.-i.; Takahashi, Y.; Nagaki, A. Flash chemistry: Flow chemistry that cannot be done in batch. *Chem. Commun.* **2013**, *49*, 9896−9904; d) Yoshida, J.-i. *Basics of Flow Microreactor Synthesis*; Springer Japan: Tokyo, 2015.

[5] Usutani, H.; Tomida, Y.; Nagaki, A.; Okamoto, H.; Nokami, T.; Yoshida, J.-i. Generation and reactions of *o*-bromophenyllithium without benzyne formation using a microreactor. *J. Am. Chem. Soc.* **2007**, *129*, 3046−3047.

[6] Leroux, F.; Schlosser, M.; Zohar, E.; Marek, I. The preparation of organolithium reagents and intermediates. In *Patai's Chemistry of Functional Groups, Online*; John Wiley & Sons, Ltd. 2009, doi: 10.1002/9780470682531.pat0305.

[7] a) Schwalbe, T.; Autze, V.; Hohmann, M.; Stirner, W. Novel Innovation systems for a cellular approach to continuous process chemistry from discovery to market. *Org. Process Res. Dev.* **2004**, *8*, 440−454; b) Hafner, A.; Filipponi, P.; Piccioni, L.; Meisenbach, M.; Schenkel, B.; Venturoni, F.; Sedelmeier, J. A simple scale-up strategy for organolithium chemistry in flow mode: From feasibility to kilogram quantities. *Org. Process Res. Dev.* **2016**, *20*, 1833−1837; c) Li, H.; Sheeran, J. W.; Clausen, A. M.; Fang, Y. Q.; Bio, M. M.; Bader, S. Flow asymmetric propargylation: Development of continuous processes for the preparation of a chiral β-amino alcohol. *Angew. Chem. Int. Ed.* **2017**, *56*, 9425−9429; d) Hughes, D. L. Applications of flow chemistry in drug development: Highlights of recent patent literature.

Org. Process Res. Dev. **2018**, *22*, 13-20; e) Usutani, H.; Cork, D. G. Effective utilization of flow chemistry: Use of unstable intermediates, inhibition of side reactions, and scale-up for boronic acid synthesis. *Org. Process Res. Dev.* **2018**, *22*, 741−746.

[8] Razzaq, T.; Kappe, C. O. Continuous flow organic synthesis under high-temperature/pressure conditions. *Chem. Asian J.* **2010**, *5*, 1274–1289.

[9] a) Damm, M.; Glasnov, T. N.; Kappe, C. O. Translating high-temperature microwave chemistry to scalable continuous flow processes. *Org. Process Res. Dev.* **2010**, *14*, 215−224; b) Adeyemi, A.; Bergman, J.; Brånalt, J.; Sävmarker, J.; Larhed, M. Continuous flow synthesis under high-temperature/high-pressure conditions using a resistively heated flow reactor. *Org. Process Res. Dev.* **2017**, *21*, 947−955; c) Sullivan, R. J.; Newman, S. G. Flow-assisted synthesis of heterocycles at high temperatures. In *Flow Chemistry for the Synthesis of Heterocycle*; Topics in Heterocyclic Chemistry, v. 56; Sharma, U., Van der Eycken, E., Eds.; Springer: Berlin, Heidelberg, 2018, p 161−186.

[10] a) May, S. A.; Johnson, M. D.; Braden, T. M.; Calvin, J. R.; Haeberle, B. D.; Jines, A. R.; Miller, R. D.; Plocharczyk, E. F.; Rener, G. A.; Richey, R. N.; Schmid, C. R.; Vaid, R. K.; Yu, H. Rapid development and scale-up of a 1H-4-substituted imidazole intermediate enabled by chemistry in continuous plug flow reactors. *Org. Process Res. Dev.* **2012**, *16*, 982−1002; b) Bogdan, A. R.; Charaschanya, M.; Dombrowski, A. W.; Wang, Y.; Djuric, S. W. High-temperature boc deprotection in flow and its application in multistep reaction sequences. *Org. Lett.* **2016**, *18*, 1732−1735.

[11] Johnson, M. D.; May, S. A.; Haeberle, B.; Lambertus, G. R.; Pulley, S. R.; Stout, J. R. Design and comparison of tubular and pipes-in-series continuous reactors for direct asymmetric reductive amination. *Org. Process Res. Dev.* **2016**, *20*, 1305−1320.

[12] Irfan, M.; Glasnov, T. N.; Kappe, C. O. Heterogeneous catalytic hydrogenation reactions in continuous-flow reactors. *ChemSusChem* **2011**, *4*, 300–316.

[13] a) Cossar, P. J.; Hizartzidis, L.; Simone, M. I.; McCluskey, A.; Gordon, C. P. The expanding utility of continuous flow hydrogenation. *Org. Biomol. Chem.* **2015**, *13*, 7119−7130; b) Russell, C. C.; Baker, J. R.; Cossar, P. J.; McCluckey, A. Recent developments in the use of flow hydrogenation in the field of medicinal chemistry. In *New Advances in Hydrogenation Processes*; Ravanchi, M. R., Ed.; IntechOpen: 2017, doi: 10.5772/65518.

[14] a) Johnson, M. D.; May, S. A.; Calvin, J. R.; Remacle, J.; Stout, J. R.; Diseroad, W. D.; Zaborenko, N.; Haeberle, B. D.; Sun, W.-M.; Miller, M. T.; Brennan, J. Development and scale-up of a continuous,

high-pressure, asymmetric hydrogenation reaction, workup, and isolation. *Org. Process Res. Dev.* **2012**, *16*, 1017−1038; b) Ouchi, T.; Battilocchio, C.; Hawkins, J. M.; Ley, S. V. Process intensification for the continuous flow hydrogenation of ethyl nicotinate. *Org. Process Res. Dev.* **2014**, *18*, 1560−1566; c) Chen, J.; Przyuski, K.; Roemmele, R.; Bakale, R. P. Improved continuous flow processing: Benzimidazole ring formation via catalytic hydrogenation of an aromatic nitro compound. *Org. Process Res. Dev.* **2014**, *18*, 1427−1433; d) Cantillo, D.; Damm, M.; Dallinger, D.; Bauser, M.; Berger, M.; Kappe, C. O. Sequential nitration/hydrogenation protocol for the synthesis of triaminophloroglucinol: Safe generation and use of an explosive intermediate under continuous-flow conditions. *Org. Process Res. Dev.* **2014**, *18*, 1360−1366; e) Loos, P.; Alex, H.; Hassfeld, J.; Lovis, K.; Platzek, J.; Steinfeldt, N.; Hübner, S. Selective hydrogenation of halogenated nitroaromatics to haloanilines in batch and flow. *Org. Process Res. Dev.* **2016**, *20*, 452-464; f) May, S. A.; Johnson, M. D.; Buser, J. Y.; Campbell, A. N.; Frank, S. A.; Haeberle, B. D.; Hoffman, P. C.; Lambertus, G. R.; McFarland, A. D.; Moher, E. D.; White, T. D.; Hurley, D. D.; Corrigan, A. P.; Gowran, O.; Kerrigan, N. G.; Kissane, M. G.; Lynch, R. R.; Sheehan, P.; Spencer, R. D.; Pulley, S. R.; Stout, J. R. Development and manufacturing GMP scale-up of a continuous Ir-catalyzed homogeneous reductive amination reaction. *Org. Process Res. Dev.* **2016**, *20*, 1870−1898; g) Amara, Z.; Poliakoff, M.; Duque, R.; Geier, D.; Franciò, G.; Gordon, C. M.; Meadows, R. E.; Woodward, R.; Leitner, W. Enabling the scale-up of a key asymmetric hydrogenation step in the synthesis of an API using continuous flow solid-supported catalysis. *Org. Process Res. Dev.* **2016**, *20*, 1321−1327; h) Cantillo, D.; Wolf, B.; Goetz, R.; Kappe, C. O. Continuous flow synthesis of a key 1,4-benzoxazinone intermediate via a nitration/hydrogenation/cyclization sequence. *Org. Process Res. Dev.* **2017**, *21*, 125-132; i) Said, M. B.; Baramov, T.; Herrmann, T.; Gottfried, M.; Hassfeld, J.; Roggan, S. Continuous selective hydrogenation of Refametinib iodo-nitroaniline key intermediate DIM-NA over Raney cobalt catalyst at kg/day scale with online UV–visible conversion control. *Org. Process Res. Dev.* **2017**, *21*, 705−714; j) Gulotty, R. J.; Rish, S.; Boyd, A.; Mitchell, L.; Plageman, S.; McGill, C.; Keller, J.; Starnes, J.; Stadalsky, J.; Garrison, G. Run parameters for a continuous hydrogenation process using ACMC-Pd to replace commercial batch reactor processes. *Org. Process Res. Dev.* **2018**, *22*, 1622−1627; k) Touge, T.; Kuwana, M.; Komatsuki, Y.; Tanaka, S.; Nara, H.; Matsumura, K.; Sayo, N.; Kashibuchi, Y.; Saito, T. Development of asymmetric transfer hydrogenation with a bifunctional oxo-tethered ruthenium catalyst in flow for the synthesis of a Ceramide (d-erythro-CER[NDS]). *Org. Process Res. Dev.* **2019**, *23*, 452–461.

[15] Future permissions for reproduction should be direct to ACS publications. The original image is available from ref 14a at the following link: https://pubs.acs.org/doi/full/10.1021/acs.oprd.6b00148.

[16] a) Ye, T.; McKervey, M. A. Organic synthesis with α-diazo carbonyl compounds. *Chem. Rev.* **1994**, *94*, 1091−1160; b) Zollinger, H. *Diazo Chemistry I: Aromatic and Heteroaromatic Compounds*, Wiley: Weinheim, 1995; c) Zollinger, H. *Diazo Chemistry II: Aliphatic, Inorganic and Organometallic Compounds*, Wiley: Weinheim, 1995; d) Doyle, M. P.; McKervey, M. A.; Ye, T. *Modern Catalytic Methods for Organic Synthesis with Diazo Compounds: From Cyclopropanes to Ylides*; Wiley: New York, 1998; e) Ford, A.; Miel, H.; Ring, A.; Slattery, C. N.; Maguire, A. R.; McKervey, M. A. Modern organic synthesis with α-diazocarbonyl compounds. *Chem. Rev.* **2015**, *115*, 9981−10080.

[17] a) Movsisyan, M.; Delbeke, E. I. P.; Berton, J. K. E. T.; Battilocchio, C.; Ley, S. V.; Stevens, C. V. Taming hazardous chemistry by continuous flow technology. *Chem. Soc. Rev.* **2016**, *45*, 4892−4928; b) Struempel, M.; Ondruschka, B.; Daute, R.; Stark, A. Making diazomethane accessible for R&D and industry: Generation and direct conversion in a continuous micro-reactor set-up. *Green Chem.* **2008**, *10*, 41−43.

[18] a) Müller, S. T. R.; Wirth, T. Diazo compounds in continuous-flow technology. *ChemSusChem* **2015**, *8*, 245−250; b) Deadman, B. J.; Collins, S. G.; Maguire, A. R. Taming hazardous chemistry in flow: The continuous processing of diazo and diazonium compounds. *Chem. Eur. J.* **2015**, *21*, 2298−2308.

[19] a) Tran, D. N.; Battilocchio, C.; Lou, S.-B.; Hawkins, J. M.; Ley, S. V. Flow chemistry as a discovery tool to access sp2–sp3 cross-coupling reactions via diazo compounds. *Chem. Sci.* **2015**, *6*, 1120−1125; b) Roda, N. M.; Tran, D. N.; Battilocchio, C.; Labes, R.; Ingham, R. J.; Hawkins, J. M.; Ley, S. V. Cyclopropanation using flow-generated diazo compounds. *Org. Biomol. Chem.* **2015**, *13*, 2550–2554; c) Poh, J.-S.; Tran, D. N.; Battilocchio, C.; Hawkins, J. M.; Ley, S. V. A versatile room-temperature route to di- and trisubstituted allenes using flow-generated diazo compounds. *Angew. Chem. Int. Ed.* **2015**, *54*, 7920–7923; d) Poh, J.-S.; Makai, S.; von Keutz, T.; Tran, D. N.; Battilocchio, C.; Pasau, P.; Ley, S. V. Rapid asymmetric synthesis of disubstituted allenes by coupling of flow-generated diazo compounds and propargylated amines. *Angew. Chem. Int. Ed.* **2017**, *56*, 1864–1868.

[20] a) Rullière, P.; Benoit, G.; Allouche, E. M. D.; Charette, A. B. Safe and facile access to non-stabilized diazoalkanes using continuous flow technology. *Angew. Chem. Int. Ed.* **2018**, *57*, 5777−5782; b) Allouche, E. M. D.; Charette, A. B. Non-stabilized diazoalkane synthesis via the oxidation of free hydrazones by iodosylbenzene and application in in situ MIRC cyclopropanation. *Chem. Sci.* **2019**, *10*, 3802−3806.

[21] Sullivan, R. J.; Newman, S. G. unpublished results.

[22] a) Ouchi, T.; Battilocchio, C.; Hawkins, J. M.; Ley, S. V. Process intensification for the continuous flow hydrogenation of ethyl nicotinate. *Org. Process Res. Dev.* **2014**, *18*, 1560−1566; b) Cantillo, D.; Damm, M.; Dallinger, D.; Bauser, M.; Berger, M.; Kappe, C. O. Sequential nitration/hydrogenation protocol for the synthesis of triaminophloroglucinol: Safe generation and use of an explosive intermediate under continuous-flow conditions. *Org. Process Res. Dev.* **2014**, *18*, 1360−1366; c) Chen, J.; Przyuski, K.; Roemmele, R.; Bakale, R. P. Improved continuous flow processing: Benzimidazole ring formation via catalytic hydrogenation of an aromatic nitro compound. *Org. Process Res. Dev.* **2014**, *18*, 1427−1433; d) Amara, Z.; Poliakoff, M.; Duque, R.; Geier, D.; Franciò, G.; Gordon, C. M.; Meadows, R. E.; Woodward, R.; Leitner, W. Enabling the scale-up of a key asymmetric hydrogenation step in the synthesis of an API using continuous flow solid-supported catalysis. *Org. Process Res. Dev.* **2016**, *20*, 1321−1327; e) Loos, P.; Alex, H.; Hassfeld, J.; Lovis, K.; Platzek, J.; Steinfeldt, N.; Hübner, S. Selective hydrogenation of halogenated nitroaromatics to haloanilines in batch and flow. *Org. Process Res. Dev.* **2016**, *20*, 452–464; f) Cantillo, D.; Wolf, B.; Goetz, R.; Kappe, C. O. Continuous flow synthesis of a key 1,4-benzoxazinone intermediate via a nitration/hydrogenation/cyclization sequence. *Org. Process Res. Dev.* **2017**, *21*, 125–132; g) Said, M. B.; Baramov, T.; Herrmann, T.; Gottfried, M.; Hassfeld, J.; Roggan, S. Continuous selective hydrogenation of Refametinib iodo-nitroaniline key intermediate DIM-NA over Raney Cobalt catalyst at kg/day scale with online UV–visible conversion control. *Org. Process Res. Dev.* **2017**, *21*, 705−714; h) Gulotty, R. J.; Rish, S.; Boyd, A.; Mitchell, L.; Plageman, S.; McGill, C.; Keller, J.; Starnes, J.; Stadalsky, J.; Garrison, G. Run parameters for a continuous hydrogenation process using ACMC-Pd to replace commercial batch reactor processes. *Org. Process Res. Dev.* **2018**, *22*, 1622−1627.

[23] a) Webb, D.; Jamison, T. F. Continuous flow multi-step organic synthesis. *Chem. Sci.* **2010**, *1*, 675−680; b) Wegner, J.; Ceylan, S.; Kirschning, A. Flow chemistry - A key enabling technology for (multistep) organic synthesis. *Adv. Synth. Catal.* **2012**, *354*, 17–57.

[24] Russell, M. G.; Jamison, T. F. Seven-step continuous flow synthesis of Linezolid without intermediate purification. *Angew. Chem. Int. Ed.* **2019**, *58*, 7678−7681.

[25] Perrault, W. R.; Pearlman, B. A.; Godrej, D. B.; Jeganathan, A.; Yamagata, K.; Chen, J. J.; Lu, C. V.; Herrinton, P. M.; Gadwood, R. C.; Chan, L.; Lyster, M. A.; Maloney, M. T.; Moeslein, J. A.; Greene, M. L.; Barbachyn, M. R. The synthesis of *N*-aryl-5(S)-aminomethyl-2-oxazolidinone antibacterials and derivatives in one step from aryl carbamates. *Org. Process Res. Dev.* **2003**, *7*, 533−546.

[26] a) Bogdan, A. R.; Dombrowski, A. W. Emerging trends in flow chemistry and applications to the pharmaceutical industry. *J. Med. Chem.* **2019**, *62*, 6422−6468; b) Mascia, S.; Heider, P. L.; Zhang, H.;

Lakerveld, R.; Benyahia, B.; Barton, P. I.; Braatz, R. D.; Cooney, C. L.; Evans, J. M. B.; Jamison, T. F.; Jensen, K. F.; Myerson, A. S.; Trout, B. L. End-to-end continuous manufacturing of pharmaceuticals: Integrated synthesis, purification, and final dosage formation. *Angew. Chem. Int. Ed.* **2013**, *52*, 12359–12363; c) Adamo, A.; Beingessner, R. L.; Behnam, M.; Chen, J.; Jamison, T. F.; Jensen, K. F.; Monbaliu, J.-C. M.; Myerson, A. S.; Revalor, E. M.; Snead, D. R.; Stelzer, T.; Weeranoppanant, N.; Wong, S. Y.; Zhang, P. On-demand continuous-flow production of pharmaceuticals in a compact, reconfigurable system. *Science* **2016**, *352*, 61–67.

[27] a) Crabtree, R. H. Deactivation in homogeneous transition metal catalysis: Causes, avoidance, and cure. *Chem. Rev.* **2015**, *115*, 127–150; b) Isbrandt, E. S.; Sullivan, R. J.; Newman, S. G. High throughput strategies for the discovery and optimization of catalytic reactions. *Angew. Chem. Int. Ed.* **2019**, *58*, 7180–7191.

[28] Santanilla, A. B.; Regalado, E. L.; Pereira, T.; Shevlin, M.; Bateman, K.; Campeau, L.-C.; Schneeweis, J.; Berritt, S.; Shi, Z.-C.; Nantermet, P.; Liu, Y.; Helmy, R.; Welch, C. J.; Vachal, P.; Davies, I. W.; Cernak, T.; Dreher, S. D. Nanomole-scale high-throughput chemistry for the synthesis of complex molecules. *Science* **2015**, *347*, 49–53.

[29] Alfke, G.; Irion, W. W.; Neuwirth, O. S. Oil refining. In *Ullmann's Encyclopedia of Industrial Chemistry*; Wiley-VCH Verlag GmbH & Co. KGaA: Weinheim, 2007.

[30] Appl, M. Ammonia, 2. Production processes. In *Ullmann's Encyclopedia of Industrial Chemistry*; Wiley-VCH Verlag GmbH & Co. KGaA: Weinheim, 2011.

[31] Anastas, P.; Eghbali, N. Green chemistry: Principles and practice. *Chem. Soc. Rev.* **2010**, *39*, 301–312.

[32] Vural Gursel, I.; Noel, T.; Wang, Q.; Hessel, V. Separation/recycling methods for homogeneous transition metal catalysts in continuous flow. *Green Chem.* **2015**, *17*, 2012–2026.

[33] Kohlpaintner, C. W.; Fischer, R. W.; Cornils, B. Aqueous biphasic catalysis: Ruhrchemie/Rhône-Poulenc oxo process. *Appl. Catal., A* **2001**, *221*, 219–225.

[34] Keim, W. Oligomerization of ethylene to α-olefins: Discovery and development of the Shell Higher Olefin Process (SHOP). *Angew. Chem. Int. Ed.* **2013**, *52*, 12492–12496.

[35] For a few recent examples where uncatalyzed background reactivity erodes enantioselectivity see: a) Stache, E. E.; Rovis, T.; Doyle, A. G. Dual nickel- and photoredox-catalyzed enantioselective desymmetrization of cyclic *meso*-anhydrides. *Angew. Chem. Int. Ed.* **2017**, *56*, 3679–3683; b) Yamashita,

Y.; Yasukawa, T.; Yoo, W.-J.; Kitanosono, T.; Kobayashi, S. Catalytic enantioselective aldol reactions. *Chem. Soc. Rev.* **2018**, *47*, 4388–4480; c) Zhang, X.; Liu, X.; Zhang, J.; Zhang, D.; Lin, L.; Feng, X. Enantioselective [3 + 2] cycloaddition and rearrangement of thiazolium salts to synthesize thiazole and 1,4-thiazine derivatives. *Org. Chem. Front.* **2018**, *5*, 2126–2131.

[36] For example, aggressive organometallic cross-coupling nucleophiles such as Grignard reagents can react directly via nucleophilic attack with electrophilic functional groups, and therefore cross-coupling electrophiles are generally considered incompatible in reactions such as Kumada-Corriu cross-coupling if they bear other electrophilic functional groups. See: Knappke, C. E. I.; Jacobi von Wangelin, A. 35 years of palladium-catalyzed cross-coupling with Grignard reagents: How far have we come? *Chem. Soc. Rev.* **2011**, *40*, 4948–4962.

[37] For example: a) Sullivan, R. J.; Kim, J.; Hoyt, C.; Silks Iii, L. A.; Schlaf, M. Ruthenium-8-quinolinethiolate-phenylterpyridine versus ruthenium-bipyridine-phenyl-terpyridine complexes as homogeneous water and high temperature stable hydrogenation catalysts for biomass-derived substrates. *Polyhedron* **2016**, *108*, 104–114; b) Olsen, E. P. K.; Arrechea, P. L.; Buchwald, S. L. Mechanistic insight leads to a ligand which facilitates the palladium-catalyzed formation of 2-(hetero)arylaminooxazoles and 4-(hetero)arylaminothiazoles. *Angew. Chem. Int. Ed.* **2017**, *56*, 10569–10572; c) Thomas, A. A.; Speck, K.; Kevlishvili, I.; Lu, Z.; Liu, P.; Buchwald, S. L. Mechanistically guided design of ligands that significantly improve the efficiency of CuH-catalyzed hydroamination reactions. *J. Am. Chem. Soc.* **2018**, *140*, 13976–13984.

[38] For example: a) Cardellicchio, C.; Fiandanese, V.; Marchese, G.; Ronzini, L. Functionalized ketones by iron mediated reaction of grignard reagents with acyl chlorides. *Tetrahedron Lett.* **1987**, *28*, 2053–2056; b) Sundermeier, M.; Zapf, A.; Beller, M. A convenient procedure for the palladium-catalyzed cyanation of aryl halides. *Angew. Chem. Int. Ed.* **2003**, *42*, 1661–1664; c) Nakamura, M.; Matsuo, K.; Ito, S.; Nakamura, E. Iron-catalyzed cross-coupling of primary and secondary alkyl halides with aryl Grignard reagents. *J. Am. Chem. Soc.* **2004**, *126*, 3686–3687; d) Guérinot, A.; Reymond, S.; Cossy, J. Iron-catalyzed cross-coupling of alkyl halides with alkenyl Grignard reagents. *Angew. Chem. Int. Ed.* **2007**, *46*, 6521–6524; e) Manolikakes, G.; Muñoz Hernandez, C.; Schade, M. A.; Metzger, A.; Knochel, P. Palladium- and nickel-catalyzed cross-couplings of unsaturated halides bearing relatively acidic protons with organozinc reagents. *J. Org. Chem.* **2008**, *73*, 8422–8436; f) Giannerini, M.; Fañanás-Mastral, M.; Feringa, B. L. Direct catalytic cross-coupling of organolithium compounds. *Nat. Chem.* **2013**, *5*, 667–672; g) Hornillos, V.; Giannerini, M.; Vila, C.; Fañanás-Mastral, M.; Feringa, B. L. Catalytic direct cross-coupling of organolithium

compounds with aryl chlorides. *Org. Lett.* **2013**, *15*, 5114–5117; h) Jin, M.; Adak, L.; Nakamura, M. Iron-catalyzed enantioselective cross-coupling reactions of α-chloroesters with aryl Grignard reagents. *J. Am. Chem. Soc.* **2015**, *137*, 7128−7134.

Chapter 2 Creating a Pseudo-Catalytic Cycle in Space: Automated Recycling and Reuse of Oppolzer's sultam[a]

2.1 Introduction

Accessing enantiopure molecules remains one of the toughest challenges in synthetic organic chemistry. There are three general approaches to achieve this goal. The first option is to use the chiral pool, i.e., select as a starting material a chiral molecule that is readily available from nature in enantio-pure form (e.g., amino acids, sugars, or terpenes).[1] This can be the most cost-effective strategy if a short synthetic route can be envisioned to produce the desired product from one of the small handful of chiral pool molecules available cheaply on commercial scale. This strategy is convenient if the product closely resembles an available chiral pool starting material, and when applicable is a very powerful technique that maintains current industrial relevance.[2]

The second option is to use a chiral auxiliary, i.e., an enantiopure, chiral molecule that is covalently attached to a substrate to impact diastereoselective control during a subsequent asymmetric transformation (Scheme 2.1). This is a very powerful strategy for a wide array of transformations but is generally seen as wasteful because chiral auxiliaries are necessarily stoichiometric reagents, and their use adds additional reaction steps to the synthetic route for the required auxiliary attachment and cleavage. Nonetheless, chiral auxiliaries remain a core tool for asymmetric synthesis due to their ability to enable predictable, robust, highly stereoselective transformations, in many instances for reactions where catalytic methods do not exist or are inefficient,[3] and continue to be used in the pharmaceutical industry for large scale synthesis of APIs.[4]

The third option is to use a chiral catalyst, i.e., address the shortcomings of the chiral auxiliary strategy though implementation of a closed cycle (Scheme 2.2). The reaction steps used in the auxiliary mediated approach (auxiliary attachment, diastereoselective transformation, auxiliary cleavage) become the elementary steps of a catalytic cycle operating under a single set of conditions, requiring transient rather than covalent interactions between the enantiopure reagent

[a] Parts of this chapter have appeared in print: Sullivan, R. J.; Newman, S. G. Chiral auxiliary recycling in continuous flow: Automated recovery and reuse of Oppolzer's sultam. *Chem. Sci.* **2018**, *9*, 2130–2134. Excerpts from the results section and Figure 2.1 have been adapted from Sullivan, R. J.; Newman, S. G. *Chem. Sci.* **2018**, *9*, 2130–2134. – published by the Royal Society of Chemistry, under a Creative Commons 4.0 license.

(i.e., the catalyst) and substrate. This elegant approach is generally seen as less wasteful and is therefore the preferred strategy.

Scheme 2.1. A) Common chiral auxiliaries. B) The three reaction steps needed for a generic chiral auxiliary mediated transformation: auxiliary attachment, diastereoselective reaction to set a new stereocenter, and auxiliary cleavage. C) An industrial example: Evan's auxiliary mediated aldol reactions used in the large-scale synthesis of (+)-Discodermolide by Novartis.[5]

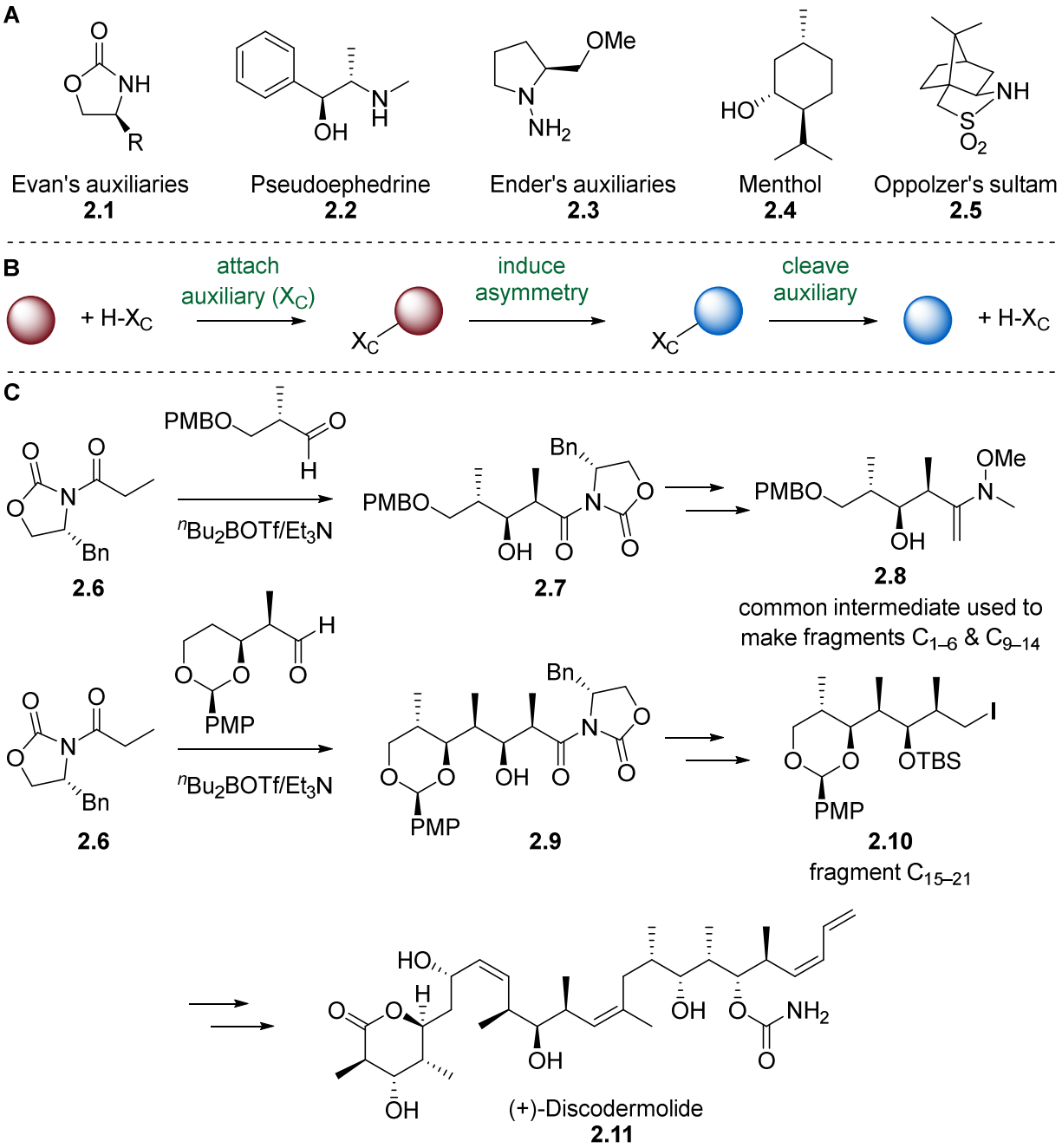

Scheme 2.2. A) A generic catalytic cycle. B) An industrial example: Knowles asymmetric hydrogenation for the synthesis of L-Dopa (the first industrial chiral catalytic process; recognized with part of the 2001 Nobel Prize shared between Knowles (asymmetric hydrogenation) Sharpless (asymmetric oxidation) and Noyori (asymmetric hydrogenation).[6]

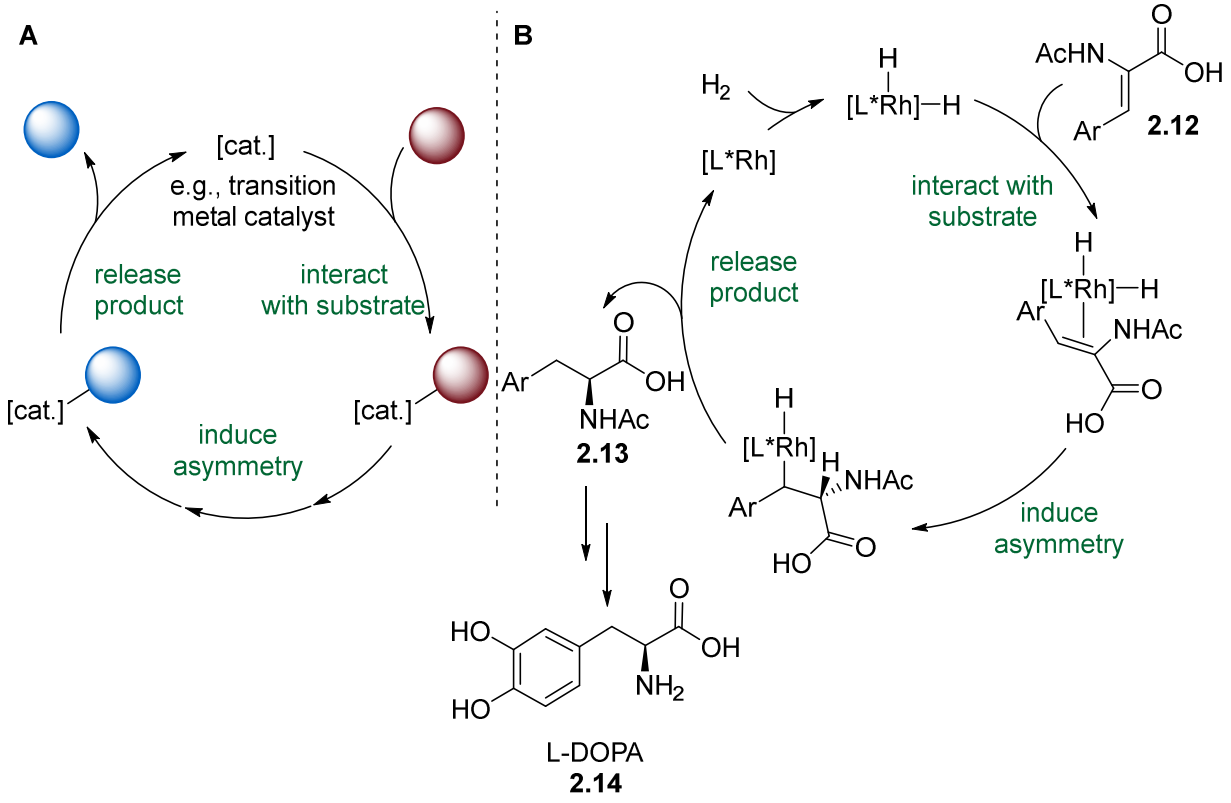

We envisioned that implementation of a catalytic cycle operating in time was not the only way to address the inefficiencies of using a chiral auxiliary mediated approach. With the central hypothesis that implementing any type of cycle would realize the same benefits, we envisioned creating a pseudo-catalytic cycle in space by using continuous flow chemistry (Scheme 2.3A). This necessitated telescoping the three reaction steps of auxiliary attachment, diastereoselective transformation, and auxiliary cleavage into one continuous flow process and incorporating automated recovery and recycling of the auxiliary to facilitate 'turnover.' An Oppolzer's sultam (camphorsultam, **2.5**) mediated hydrogenation (Scheme 2.3B) was selected to demonstrate this concept.

Scheme 2.3. A) A flow-enabled pseudo catalytic cycle in space. In contrast to the conventional catalytic cycle, wherein a series of reaction steps are separated by time, the pseudo-catalytic cycle can be realized because a series of continuous reaction steps are separated by space. B) The envisioned pseudo-catalytic cycle in space for an Oppolzer's sultam mediated hydrogenation.

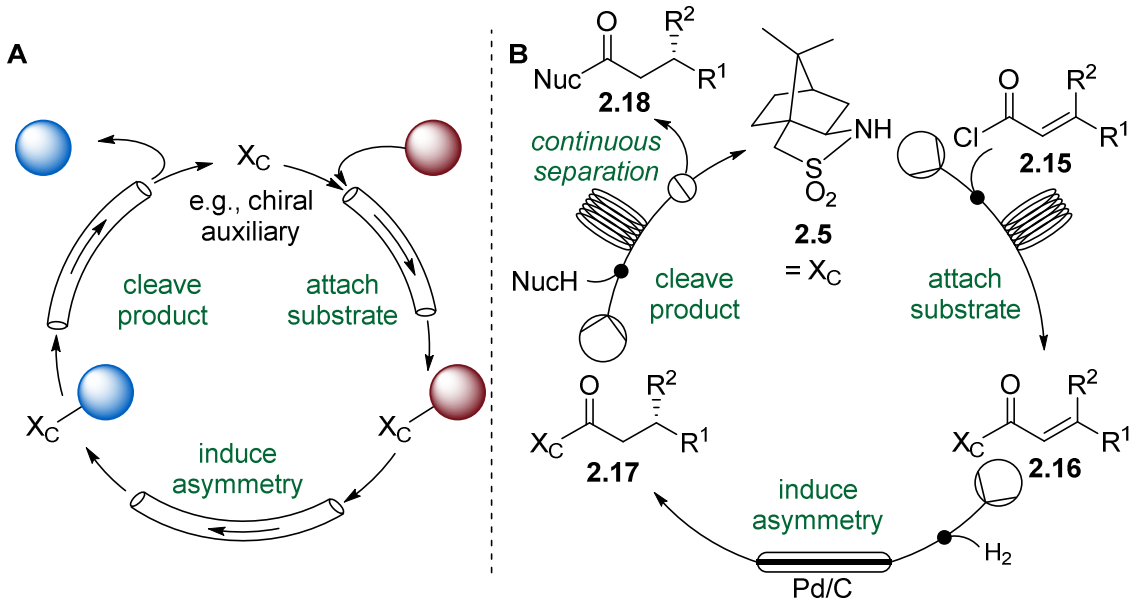

2.1.1 Oppolzer's sultam (Camphorsultam)

Camphorsultam (**2.5**) is a very versatile auxiliary, exerting high diastereo-control in a wide variety of transformations ranging from alkylation to cycloaddition to oxidation state manipulation.[7] It is inexpensive, available commercially as both enantiomers, and there is good precedent for recovery of the auxiliary after a variety of cleavage protocols.[8] This last condition is essential for implementation of our proposed pseudo-catalytic cycle, but is not always a common feature of popular auxiliaries, with many suffering racemization or destruction during cleavage except under specifically tailored conditions.[9] This is an artifact of historical research efforts focused mainly on achieving high diastereoselective control, crystallinity of products (to facilitate recrystallization), and the ability to cleave auxiliaries under mild conditions, since these features are the most crucial for broad synthetic utility. Emphasis is generally placed on auxiliary recovery more during process design if applying auxiliary chemistry at large scale, with modification of cleavage conditions, if necessary, to prevent auxiliary destruction.[10]

2.1.1.1 Camphorsultam mediated nucleophilic attack with the auxiliary installed on the nucleophile

2.1.1.1.1 Alkylation and related chemistry

The use of camphorsultam to control face selectivity of an electrophile's approach to a sulfonimide enolate is a very selective method to set a new alpha stereocenter. This has been applied to alkylation and allylation of **2.19** using alkyl and allyl halides respectively on route to enantiopure carboxylic acids **2.21** or alcohols **2.22** following either hydrolysis or reductive cleavage of the auxiliary (Scheme 2.4),[11] including at kilogram scale[12] and extensively in the total synthesis of natural and biologically active products.[13] Alpha-alkylation mediated by camphorsultam has also been applied to the synthesis of unnatural and isotopically labelled amino acids **2.23** (Scheme 2.5) and other biologically active molecules.[14]

Scheme 2.4. Camphorsultam mediated diastereoselective alkylation.

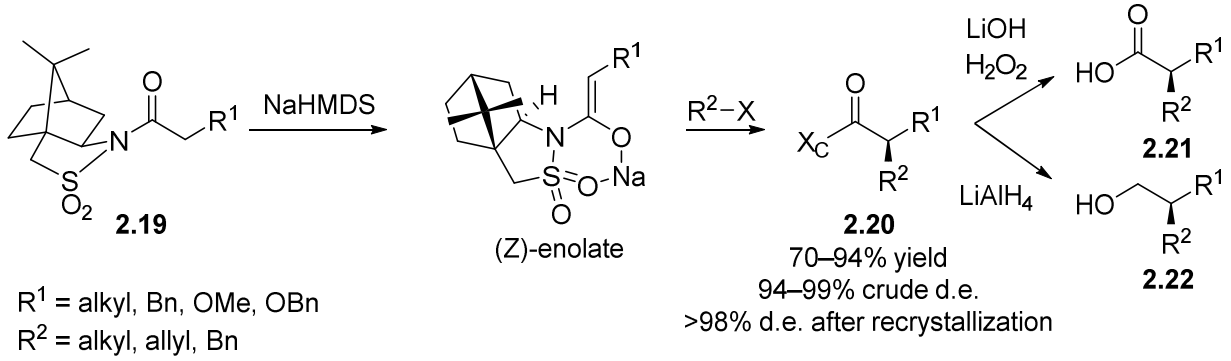

Scheme 2.5. Synthesis of enantiopure amino acids using a camphorsultam mediated alkylation to set the alpha stereocenter.

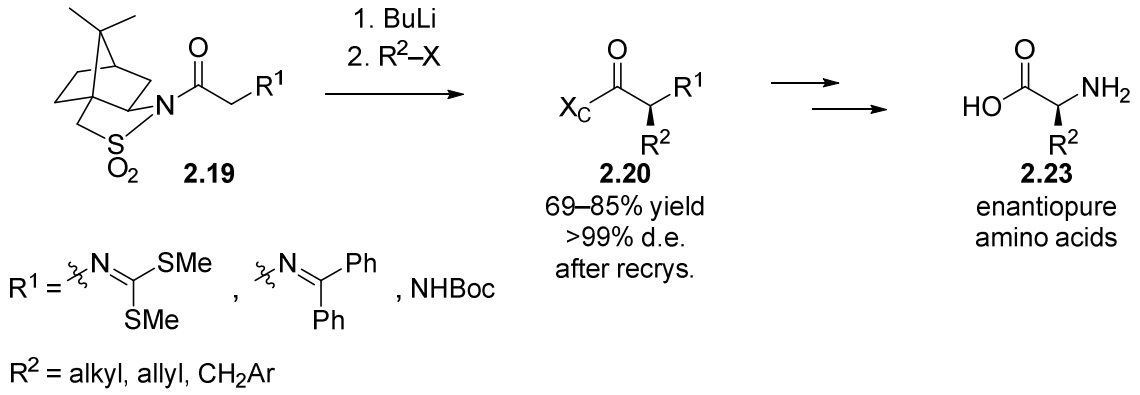

2.1.1.1.2 Aldol and related chemistry

Camphorsultam is a highly effective chiral auxiliary for stereoselective aldol reactions, with complimentary product selectivity (either syn or anti) achievable through selection of various tailored reaction conditions (Scheme 2.6).[15] As a result camphorsultam mediated aldol chemistry has been extensively used in stereoselective total syntheses of natural products and molecules of biological interest.[16] The extension of this strategy to control of stereocenter formation at the beta position has also been demonstrated with the use of zinc enolates in the Dreiding-Schmidt reaction to produce lactones **2.28** (Scheme 2.7).[17]

Scheme 2.6. Complimentary selectivity in camphorsultam mediated aldol reactions through selection of Lewis acids.

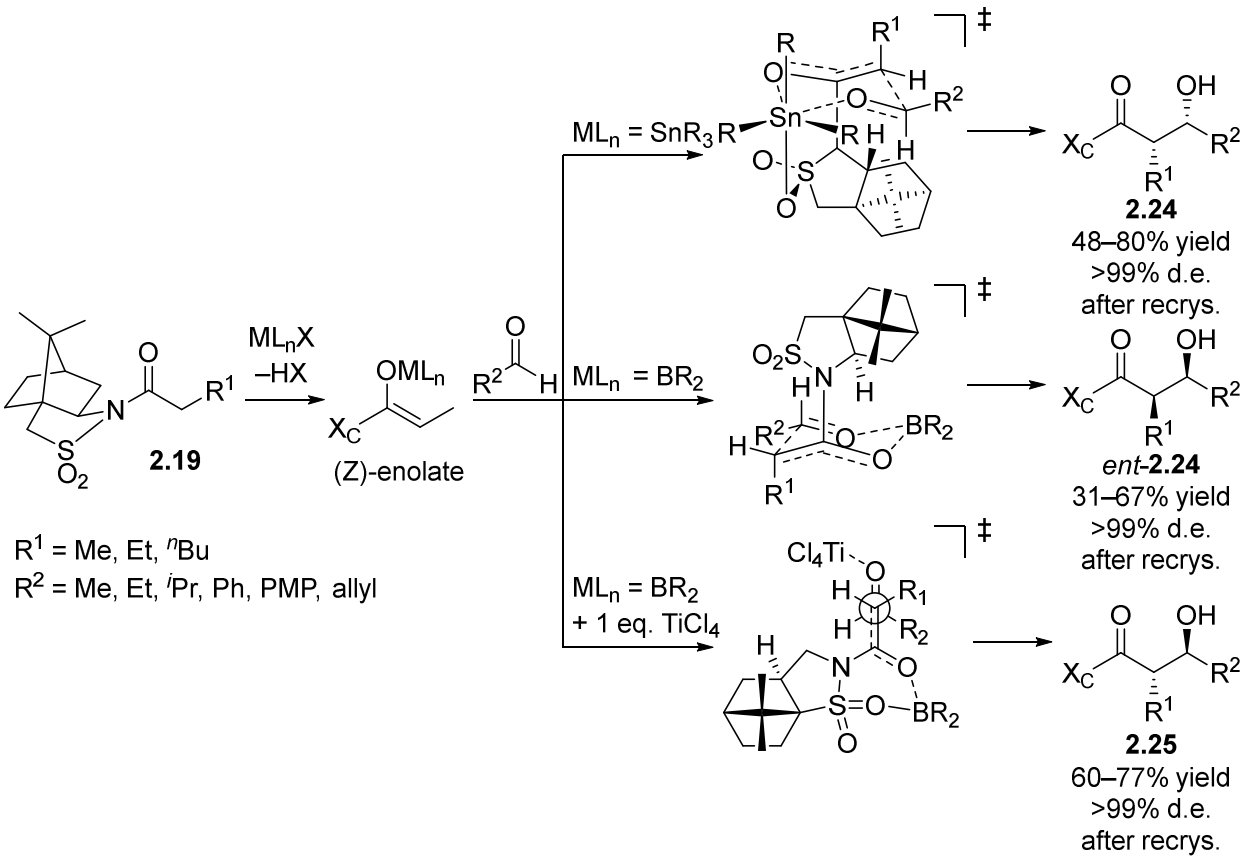

Scheme 2.7. Camphorsultam mediated Dreiding-Schmidt reaction.

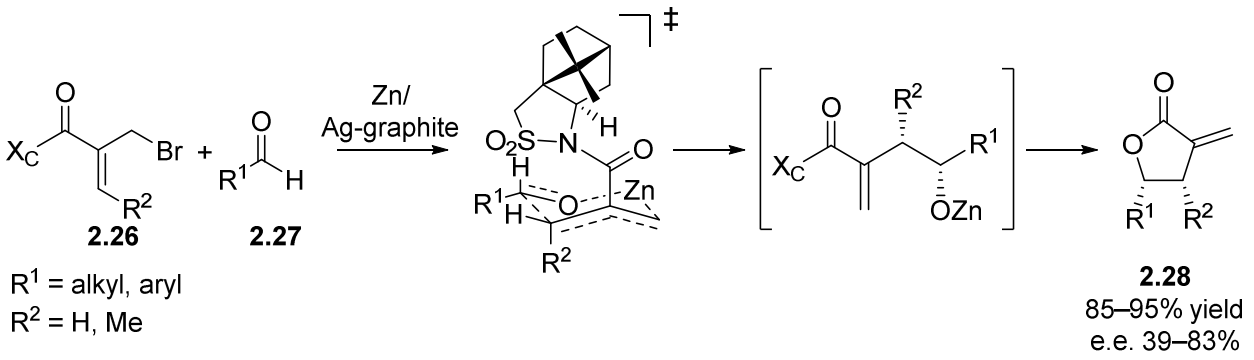

2.1.1.1.3 Amination, hydroxylation and related chemistry

Alpha amination[18] and hydroxylation[19] have also been achieved with high stereoselectivity using the camphorsultam auxiliary, providing an alterative route to unnatural amino acids **2.23** (Scheme 2.8) or enantiomerically pure α-hydroxy carbonyl compounds **2.30** (Scheme 2.9). Camphorsultam mediated aza-Darzens reactions have also been reported with excellent diastereoselectivity for the synthesis of aziridines **2.32** (Scheme 2.10).[20]

Scheme 2.8. Synthesis of enantiopure amino acids using a camphorsultam mediated amination to set the alpha stereocenter.

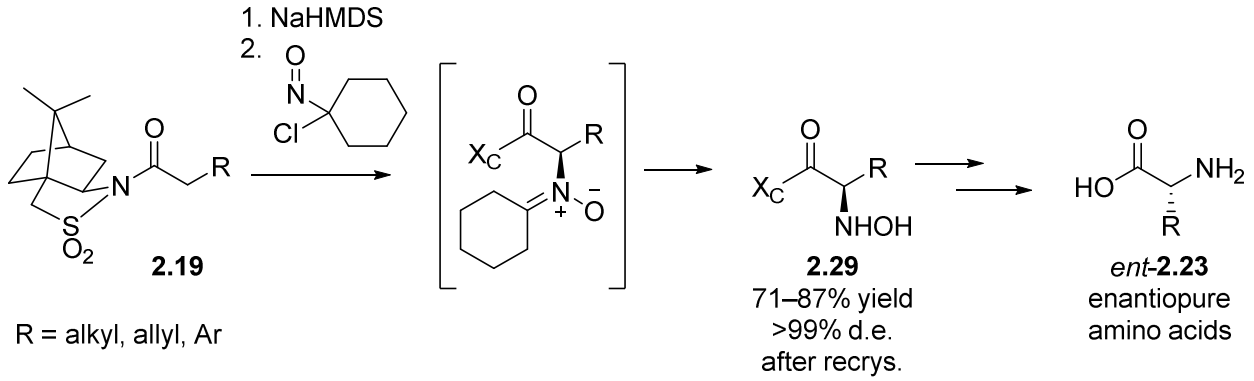

Scheme 2.9. Diastereoselective α-hydroxylation using a camphorsultam mediated strategy.

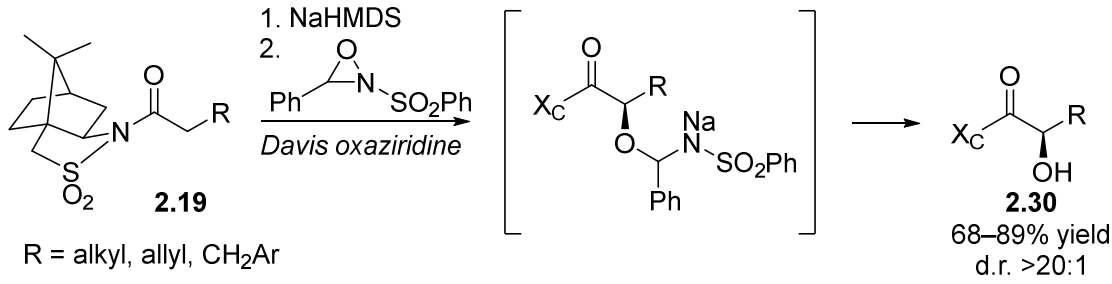

Scheme 2.10. Stereoselective aza-Darzens reaction mediated by camphorsultam.

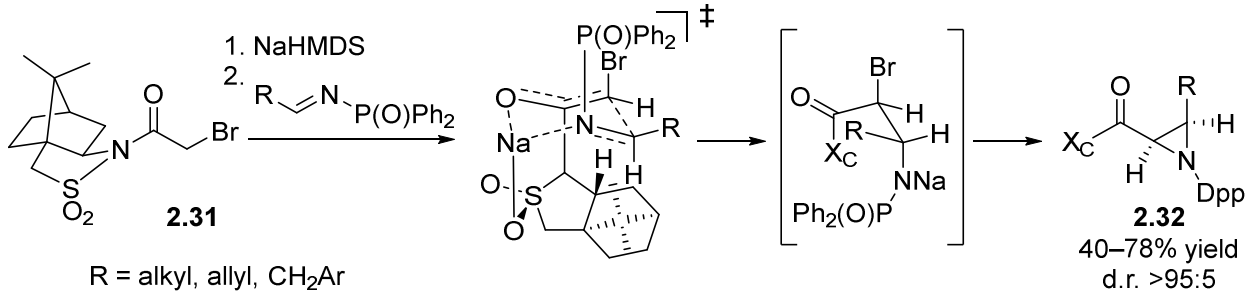

2.1.1.2 Camphorsultam mediated nucleophilic attack with the auxiliary installed on the electrophile

2.1.1.2.1 Nucleophile attack at the alpha position

The same principles that control facial approach of an electrophile towards a camphorsultam derived sulfonimide enolate can also control nucleophile approach to a camphorsultam derived α-keto sulfonimide **2.33** or **2.38**, or α-imine sulfonimide **2.36**. This strategy has been demonstrated for allylation (Scheme 2.11),[21] alkoxylation (Scheme 2.12),[22] nitroaldol (Henry) reactions (Scheme 2.13),[23] and Friedel-Crafts chemistry (Scheme 2.14).[24]

Scheme 2.11. Allylation of α-keto *N*-acyl camphorsulfonimides.

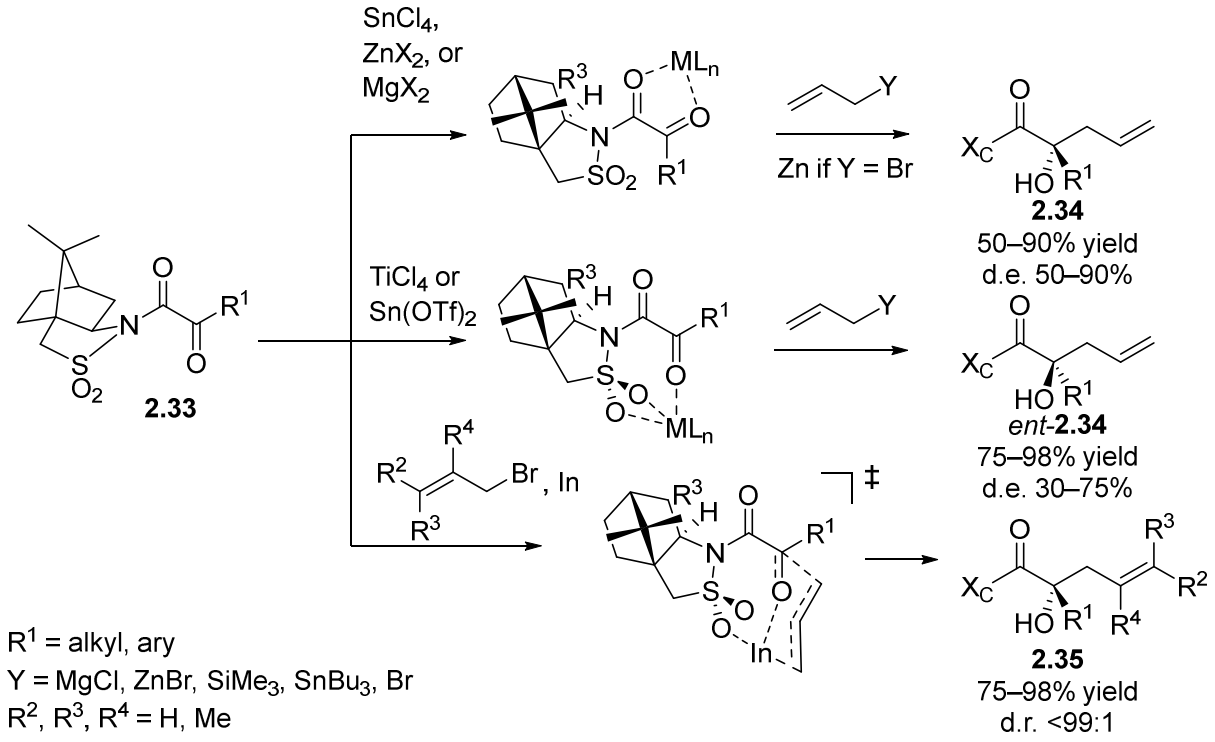

Scheme 2.12. Hydroxylation of α-imine *N*-acyl camphorsulfonimides.

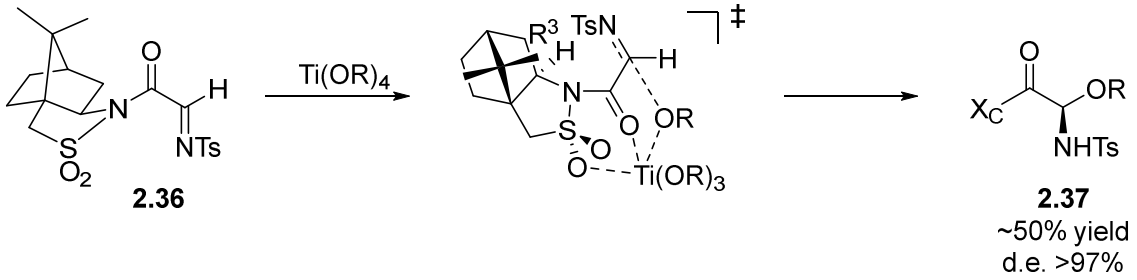

Scheme 2.13. Camphorsultam mediated Henry reactions.

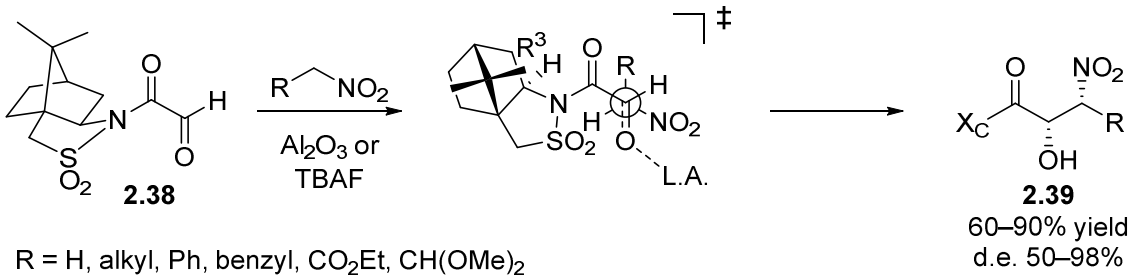

Scheme 2.14. Camphorsultam mediated Friedel-Crafts chemistry.

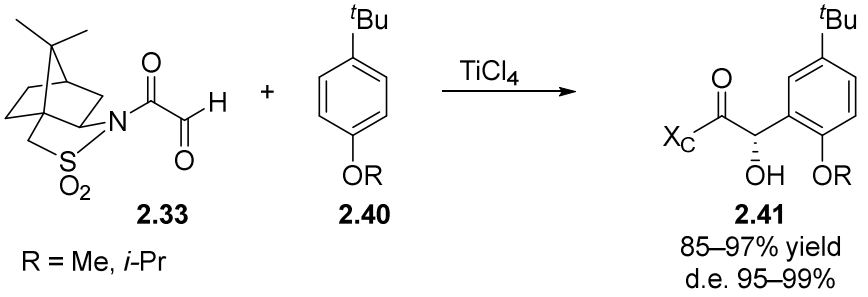

S_N2 type nucleophilic substitution on α-bromo sulfonimides **2.42** has also been reported, with dynamic kinetic resolution from a mixture of starting diastereomers possible if using the sterically hindered nucleophile **2.43** (Scheme 2.15).[25] S_N2' type nucleophilic substitutions have also been developed starting from γ-bromo-α,β-unsaturated camphorsultam sulfonimides **2.45** (Scheme 2.16).[26]

Scheme 2.15. Camphorsultam mediated dynamic kinetic resolution during S_N2 of α-bromo substrates.

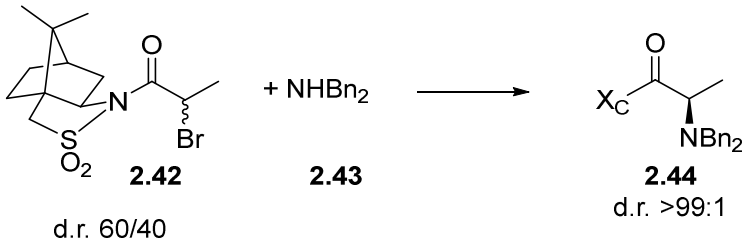

Scheme 2.16. Camphorsultam mediated S_N2' reaction of γ-bromo-α,β-unsaturated substrates.

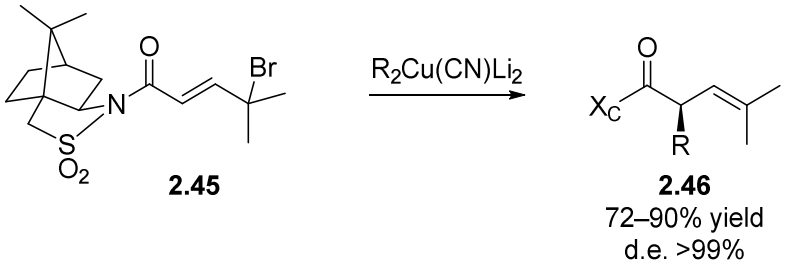

1,2-Hydride reduction of the α-carbonyl to form diastereomerically enriched α-hydroxy products **2.47** and *ent*-**2.47** has also been reported with either (*R*) or (*S*) configuration for the

product accessible from the same auxiliary enantiomer by selection of appropriate reducing agent (Scheme 2.17).[27]

Scheme 2.17. Camphorsultam mediated 1,2-hydride reduction of α-carbonyl sulfonimide substrates.

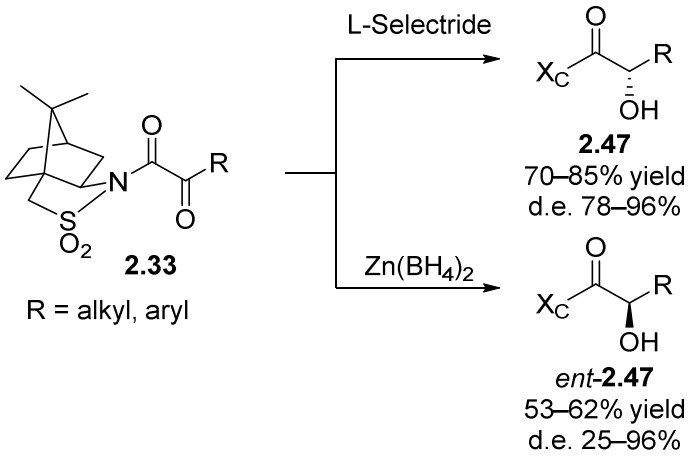

2.1.1.2.2 Nucleophile attack at the beta position

Analogous control of nucleophile approach at the beta position is also possible using camphorsultam to mediate Michael additions to compounds **2.48** or **2.50**.[28] Two contiguous stereocenters can be created at both the alpha and beta positions by quench of the resulting enolate following nucleophile attack with an alkylating agent (Scheme 2.18A) or by stereoselective protonation if the enolate is already substituted at the alpha position (Scheme 2.18B). Interestingly, both strategies result in the same final stereochemistry for the products due to divergent formation of either (*Z*)- or (*E*)-enolates depending on the substitution of the alpha position in the Michael acceptor. These practical approaches to set new beta-stereocenters and have found use in a variety of syntheses of natural and medicinal products.[29] This strategy has also been extended to include 1,4-addition of sulfur nucleophiles (Scheme 2.19) [30] and Michael initiated ring formation (MIRC) reactions (Scheme 2.20 and 2.21).[31]

Scheme 2.18. Camphorsultam mediated Michael addition. A) When there is no substituent at the alpha position of the unsaturated sultamamide a (*Z*)-enolate forms as the intermediate after nucleophilic attack. B) When the alpha position of the unsaturated sultamamide is substituted by with an R group an (*E*)-enolate forms after nucleophilic attack due to torsion of the π system from steric interactions between R^2 and the auxiliary.

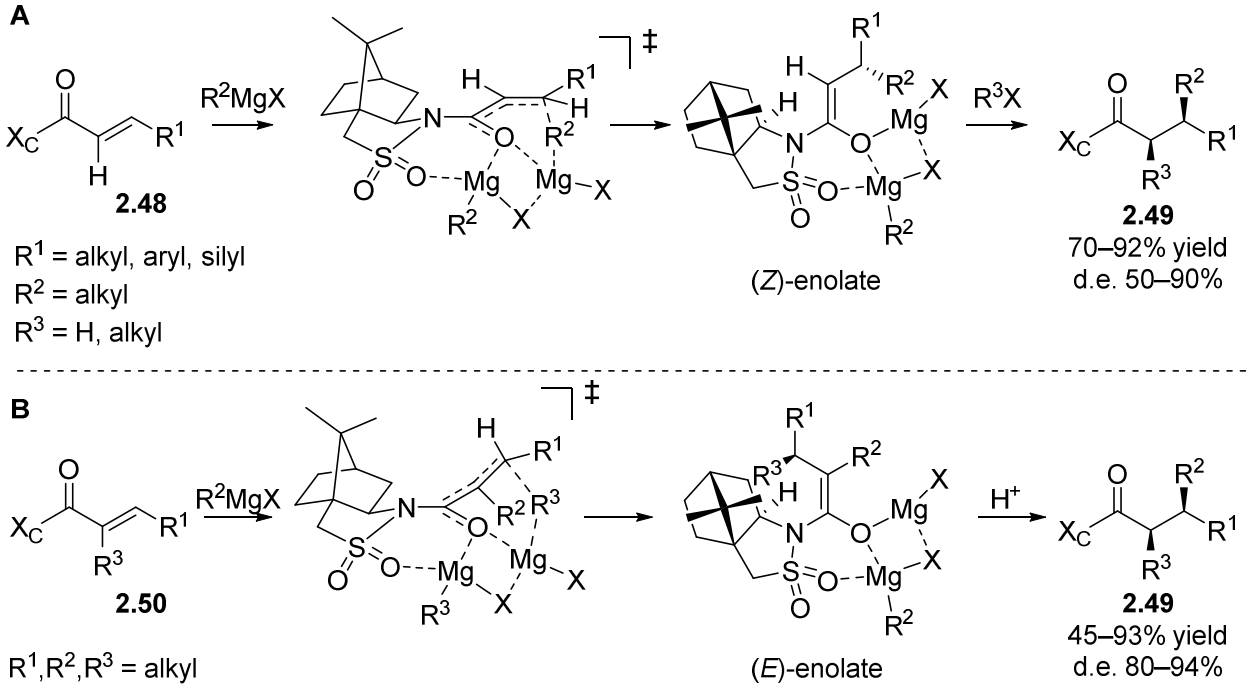

Scheme 2.19. Camphorsultam mediated 1,4-addition of thiols or thiolates.

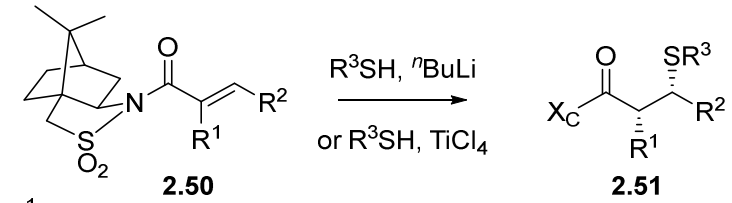

Scheme 2.20. Camphorsultam mediated, rhodium catalyzed 1,4-addition with subsequent cyclization of the rhodium enolate.

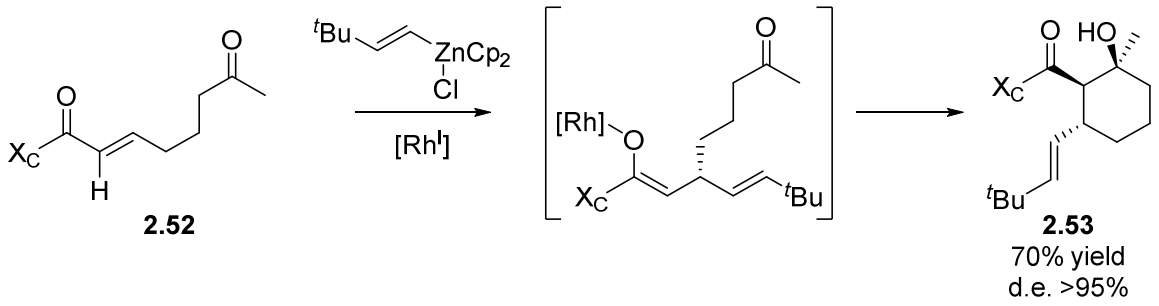

Scheme 2.21. Camphorsultam mediated MIRC cyclopropanation.

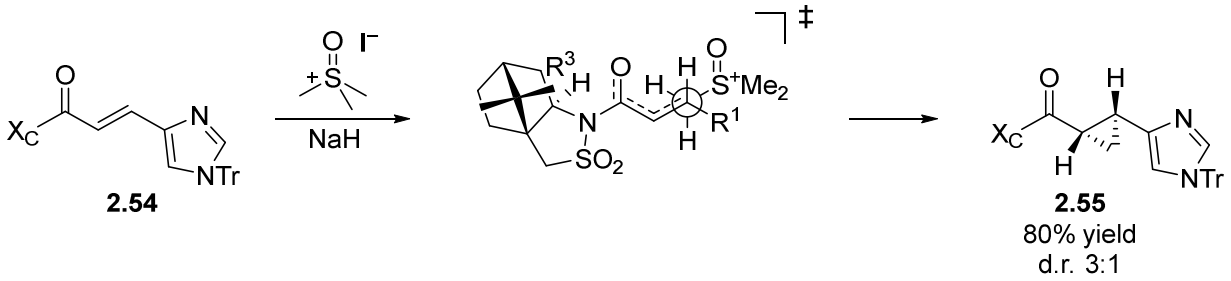

Similar stereo-control is also achieved in 1,4-hydride reduction chemistry of **2.16** (Scheme 2.22)[32] and this strategy has been used in the total synthesis of various natural and biologically active products.[33]

Scheme 2.22. Camphorsultam mediated 1,4-hydride reduction.

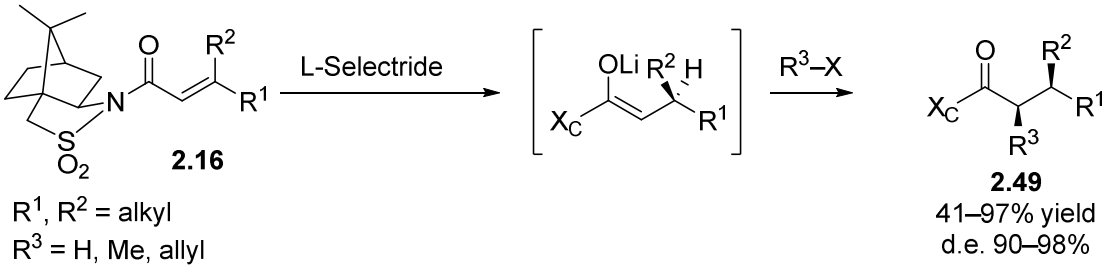

2.1.1.2.3 Nucleophilic attack at the sulfonimide carbonyl

It was also demonstrated that camphorsultam can be used to control stereoselectivity during nucleophile attack on the carbonyl group of compound **2.56**, forming a new alpha stereocenter by controlling the approach geometry of the nucleophile for the synthesis of β-amino acids **2.59** (Scheme 2.23).[34]

Scheme 2.23. Camphorsultam mediated nucleophilic attack at the sulfonimide carbonyl on route to β-amino acids.

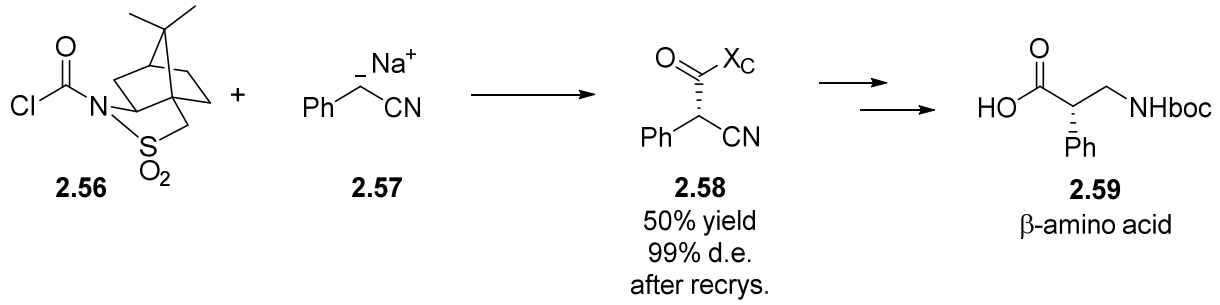

2.56 **2.57** **2.58** 50% yield 99% d.e. after recrys. **2.59** β-amino acid

2.1.1.3 Camphorsultam mediated radical chemistry

In continuing conceptual analogy, camphorsultam has been applied as an effective auxiliary to control stereocenter formation at the alpha carbon in various radical addition and cyclization reactions. The auxiliary has been installed on both the initially generated radical (Scheme 2.24) and radical acceptor (Scheme 2.25) with similar success.[35] Due to effective stereo-control, camphorsultam mediated radical methods have been applied in the synthesis of various natural and bioactive products.[36]

2.1.1.4 Camphorsultam mediated cycloaddition and related chemistry

2.1.1.4.1 [4 + 2] and [3 + 2] cycloaddition

Camphorsultam derived sulfonimides **2.48**, **2.38**, **2.36** and **2.85** are also excellent substrates in Diels-Alder (Scheme 2.26)[37] and hetero Diels-Alder reactions (Scheme 2.27).[38] The same principles that controlled diastereoselectivity in Michael addition chemistry (vide supra) exert stereo-control in cycloaddition chemistry with high selectivity as well, and this strategy has therefore been used in various total syntheses of natural and bioactive products.[39,40]

Scheme 2.24. Camphorsultam mediated radical chemistry with the auxiliary installed on the radical precursor. A) Allylation. B) Addition to furan or *N*-methylpyrrole. C) Cyclization.

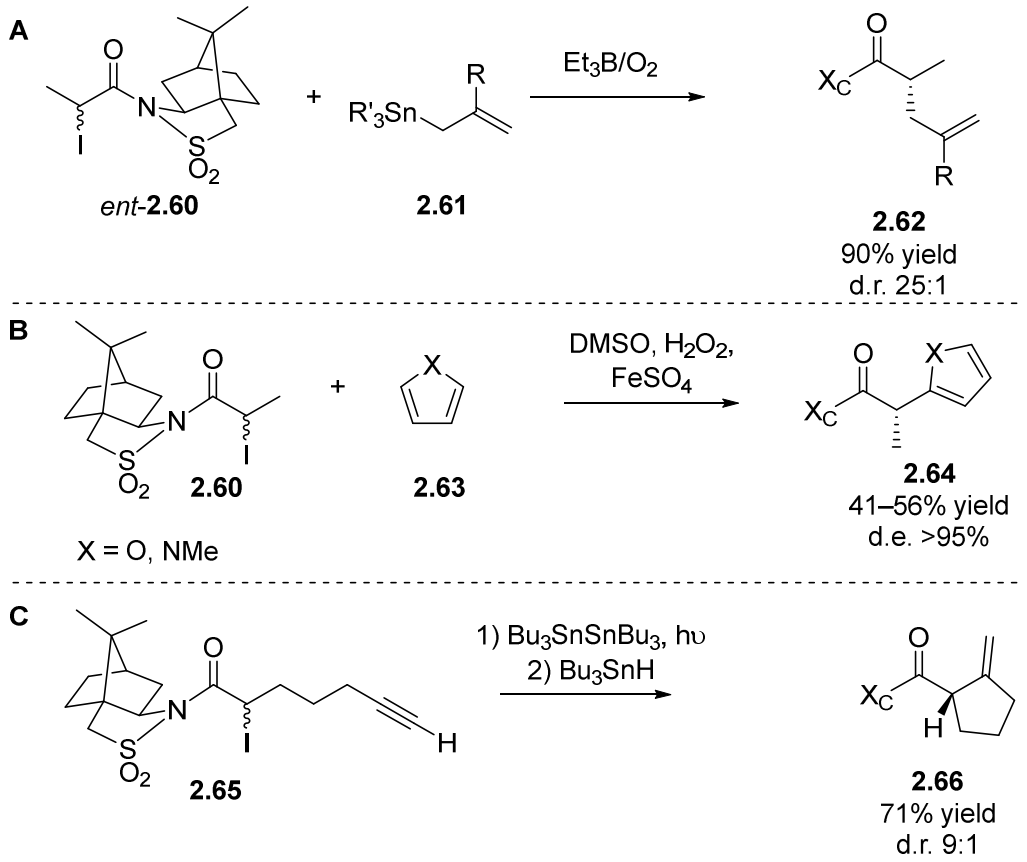

Camphorsultam sulfonimides **2.48** and **2.67** are also suitable dipolarophiles for highly stereoselective [3 + 2] cycloaddition reactions with nitrile oxides **2.89** (Scheme 2.28A),[41] azomethine ylides **2.94** (Scheme 2.28B),[42] and nitrones or silyl nitronates **2.96** (Scheme 2.28C),[43] and have consequently been used in numerous stereoselective synthesis of valuable products.[44]

2.1.1.4.2 Alder-ene reaction

The Alder-ene reaction proceeds through a conceptually analogous transition state as a [3 + 2] cycloaddition, but with the replacement of one π-bond by a σ X–H bond. In this class of conceptually related reactions camphorsultam is again an effective auxiliary to control diastereoselectivity by installation on either the eneophile **2.38** (Scheme 2.29A)[45] or ene reagent **2.100** (Scheme 2.29B).[46]

Scheme 2.25. Camphorsultam mediated radical addition chemistry with the auxiliary installed on the radical acceptor. A) Sequential radical addition, allylation. B) Radical addition for the generation of novel synthetic amino acids. C) Radical iodoperfluoroalkylation on route to fluorinate amino acids.

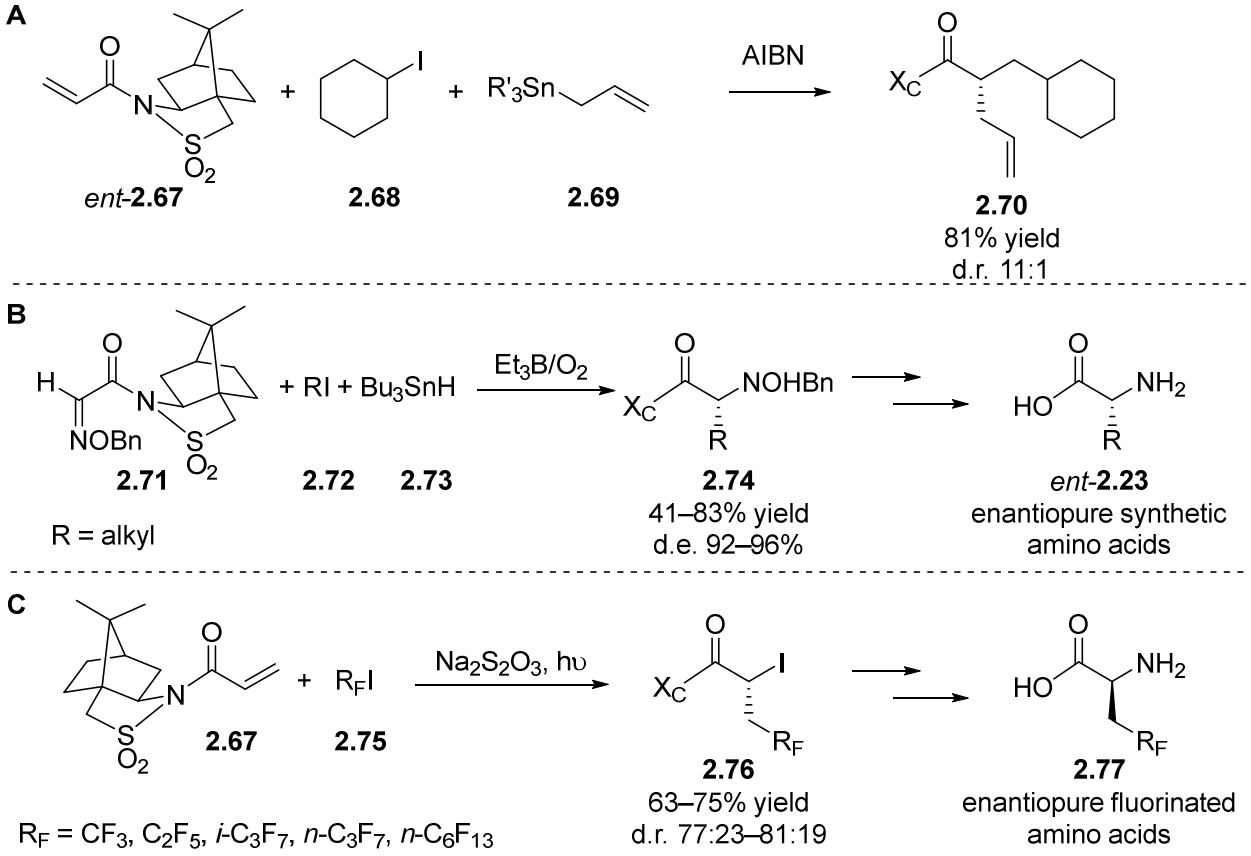

Scheme 2.26. Camphorsultam mediated Diels-Alder reactions.

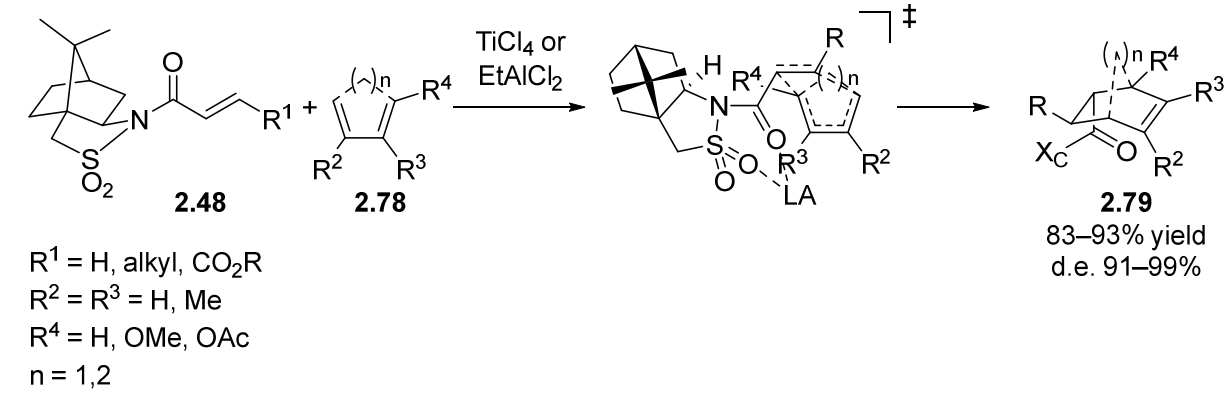

Scheme 2.27. Camphorsultam mediated hetero Diels-Alder reactions with ketone (A), imine (B) and nitroso (C) substrates.

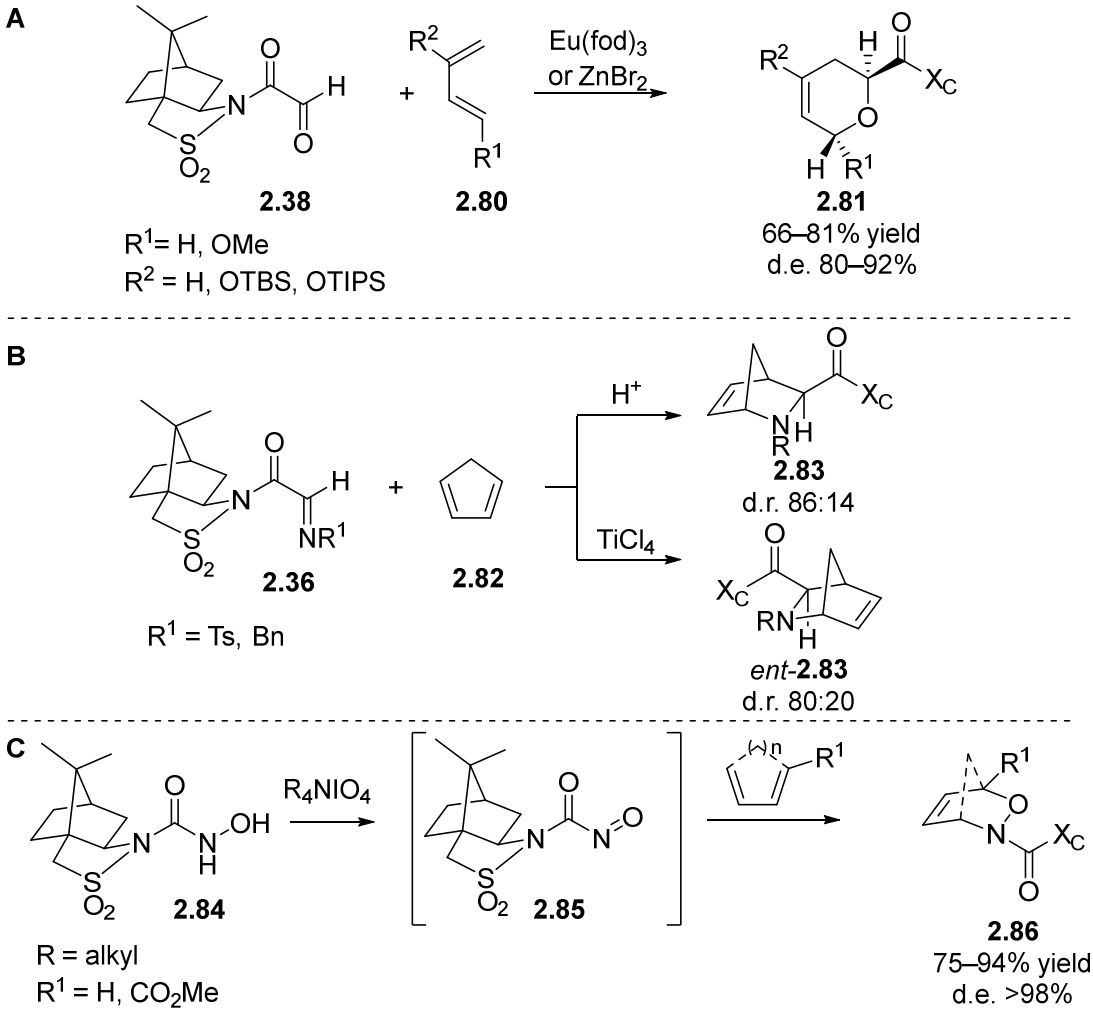

2.1.1.4.3 Epoxidation, cyclopropanation and dihydroxylation

Camphorsultam can also be used to provide good to excellent facial selectivity for epoxidation (Scheme 2.30)[47] and cyclopropanation reactions (Scheme 2.31).[48] Because of the high diastereoselectivity achieved with a wide range of tolerated aromatic and heterocycle substituents in camphorsultam mediated cyclopropanation, this strategy has been employed in multiple stereoselective syntheses of biologically active molecules.[49] Good facial selectivity in *syn*-dihydroxylation using OsO_4 or RuO_4 can also be achieved using camphorsultam as an auxiliary to provide α,β-diols (Scheme 2.32).[50]

Scheme 2.28. Camphorsultam mediated [3 + 2] cycloadditions. A) With nitrile oxides. B) With azomethine ylides. C) With nitrones or silyl nitronates.

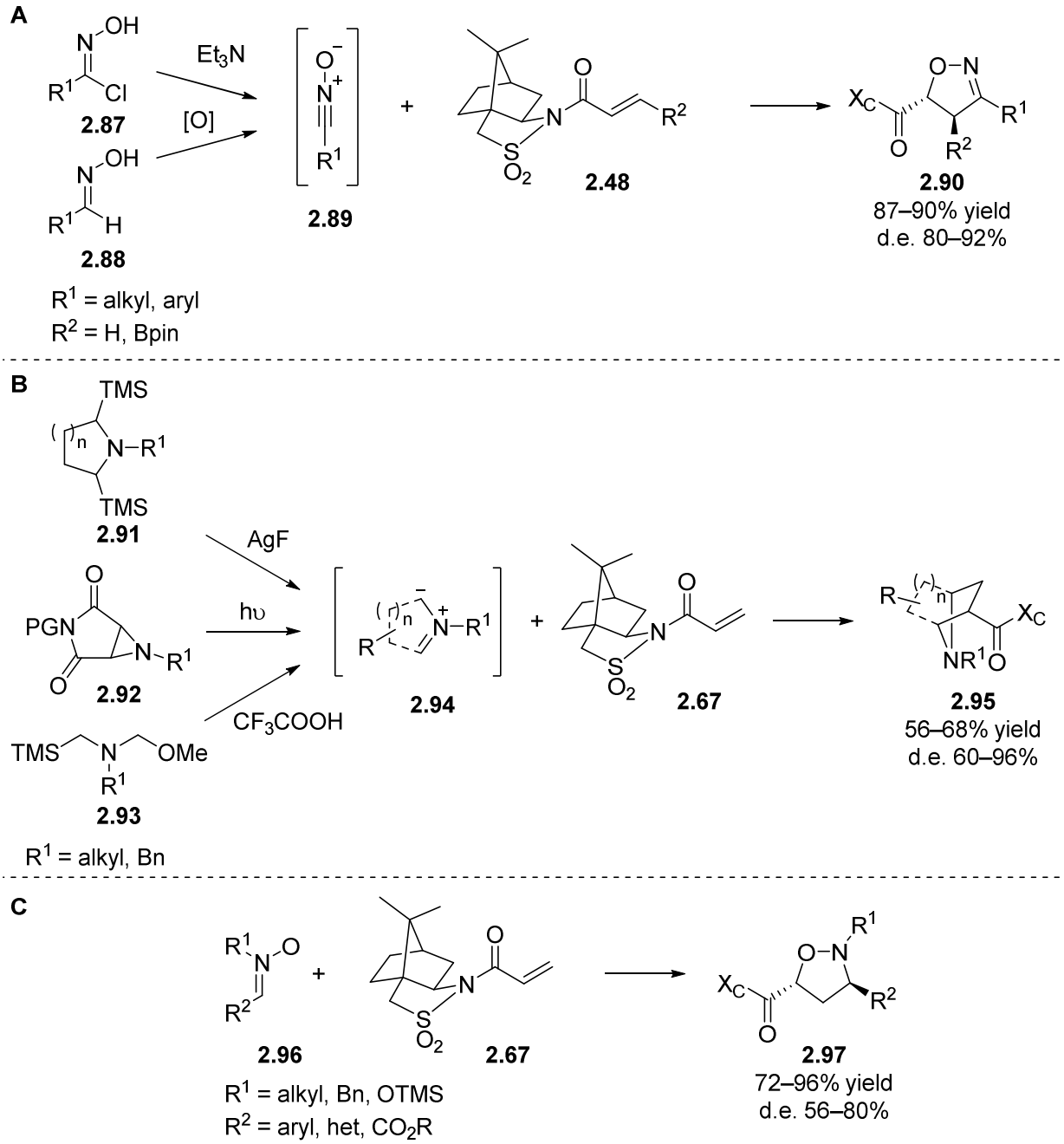

Scheme 2.29. Camphorsultam mediated Alder-ene reactions. A) Auxiliary on the enophile. B) Auxiliary on the ene reagent.

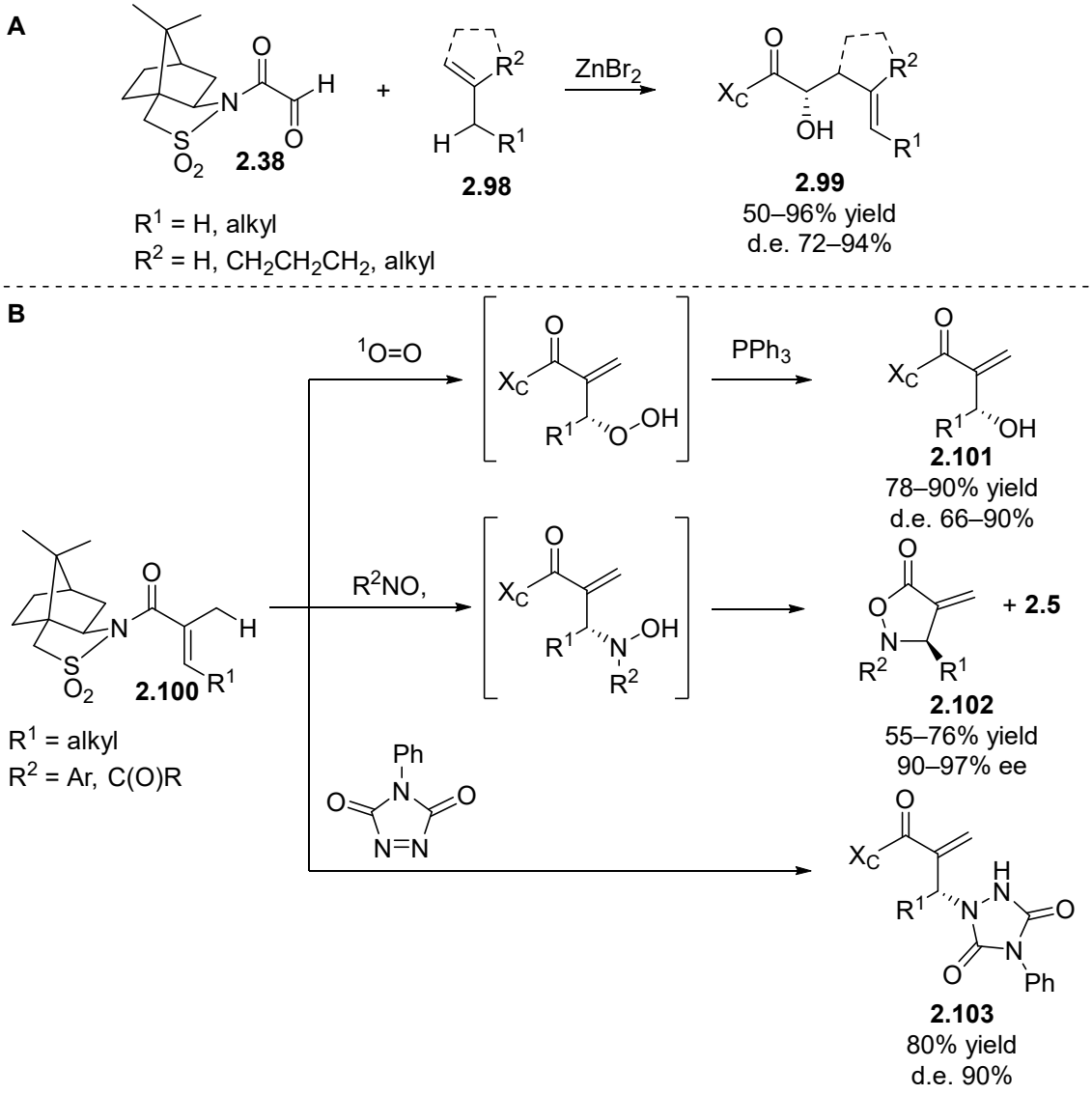

2.1.1.5 Camphorsultam mediated halohydrin reactions

Halohydrin reactions mediated by camphorsultam have also been developed. A desymmetrizing transformation leading to γ-lactone products with concomitant loss of the auxiliary was reported by Shibuya and coworkers from substrate **2.111** (Scheme 2.33A),[51] and a bromohydrin reaction of α-β unsaturated camphorsultam sulfonimides **2.50** was developed by Hajra and coworkers (Scheme 2.33B).[52]

Scheme 2.30. Camphorsultam mediated epoxidation.

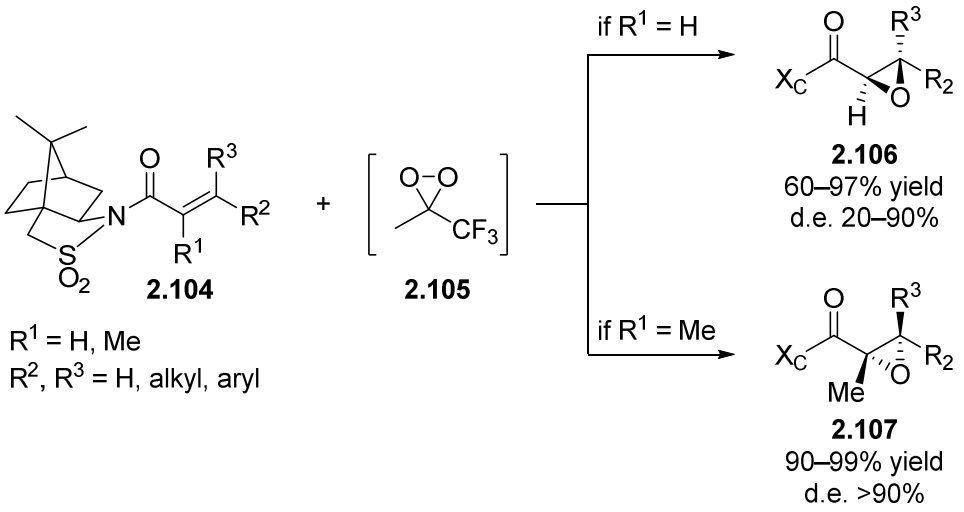

Scheme 2.31. Camphorsultam mediated cyclopropanation.

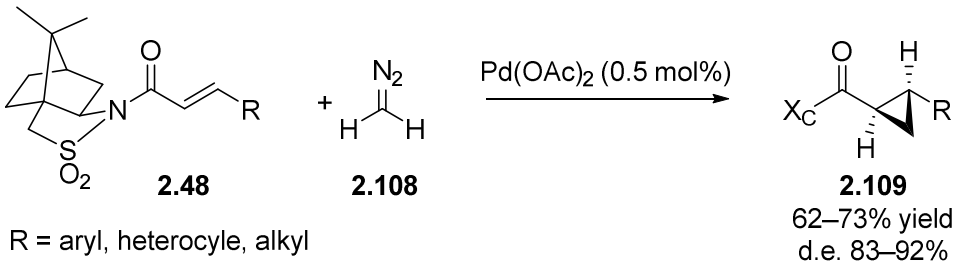

Scheme 2.32. Camphorsultam mediated dihydroxylation.

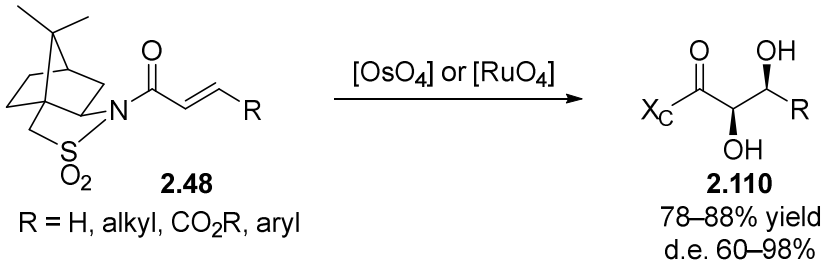

Scheme 2.33. Camphorsultam mediated halohydrin reactions. A) Iodolactonization. B) $Yb(OTf)_3$ catalyzed bromohydrin and iodohydrin chemistry.

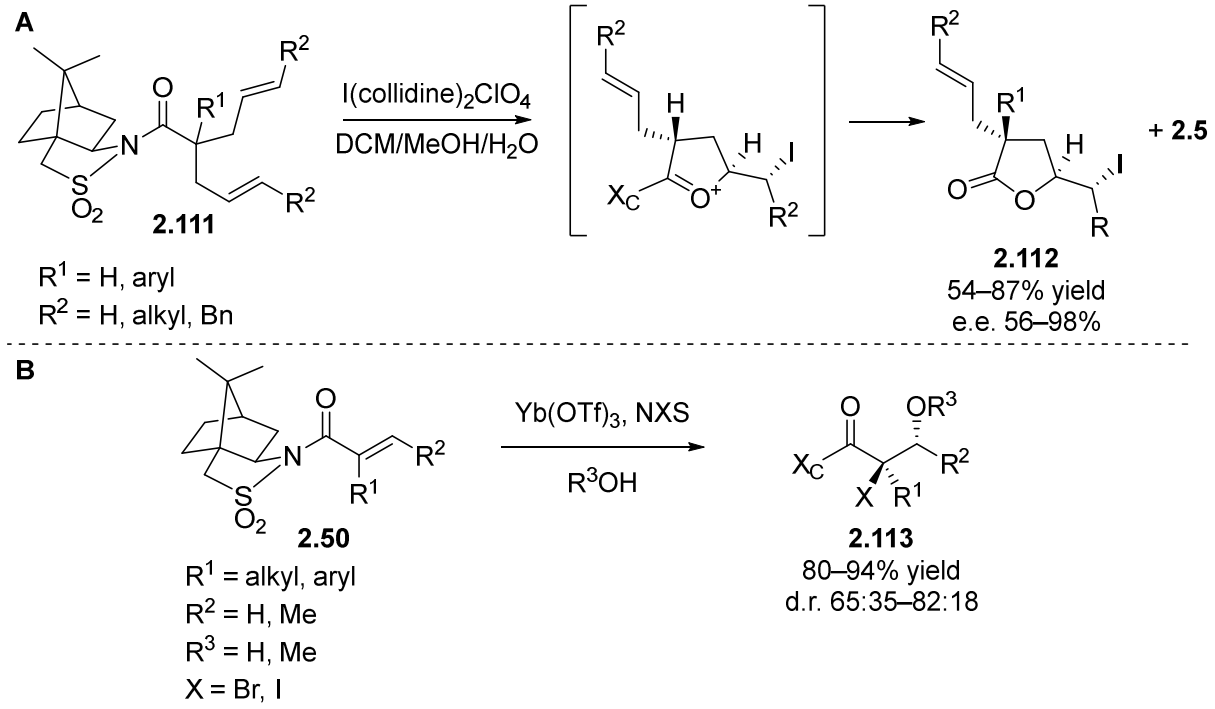

2.1.1.6 Camphorsultam mediated oxidative cyclization

Use of the camphorsultam auxiliary to control diastereoselectivity during oxidative cyclization reactions to form tetrahydrofuran[53] rings **2.115**, **2.116**, or **2.18** and tetrahydropyran[54] rings **2.120** from 1,5- or 1,6-dienes **2.114**, **2.117** and **2.119** respectively has been reported with good stereo-control and simultaneous formation of up to 4 new stereocenters and is therefore a powerful technique that has been used in the total synthesis of various THF containing natural products.[55] Absolute configuration of the formed chiral centres is dependent on both the auxiliary enantiomer and the geometry of the double bonds in the diene (Scheme 2.34).

Scheme 2.34. Camphorsultam mediated oxidative cyclizations. A) from *cis*-substituted 1,5-diene. B) from *trans*- substituted 1,5-diene. C) from geminal substituted 1,5-diene. D) from *trans*-substituted 1,6-diene.

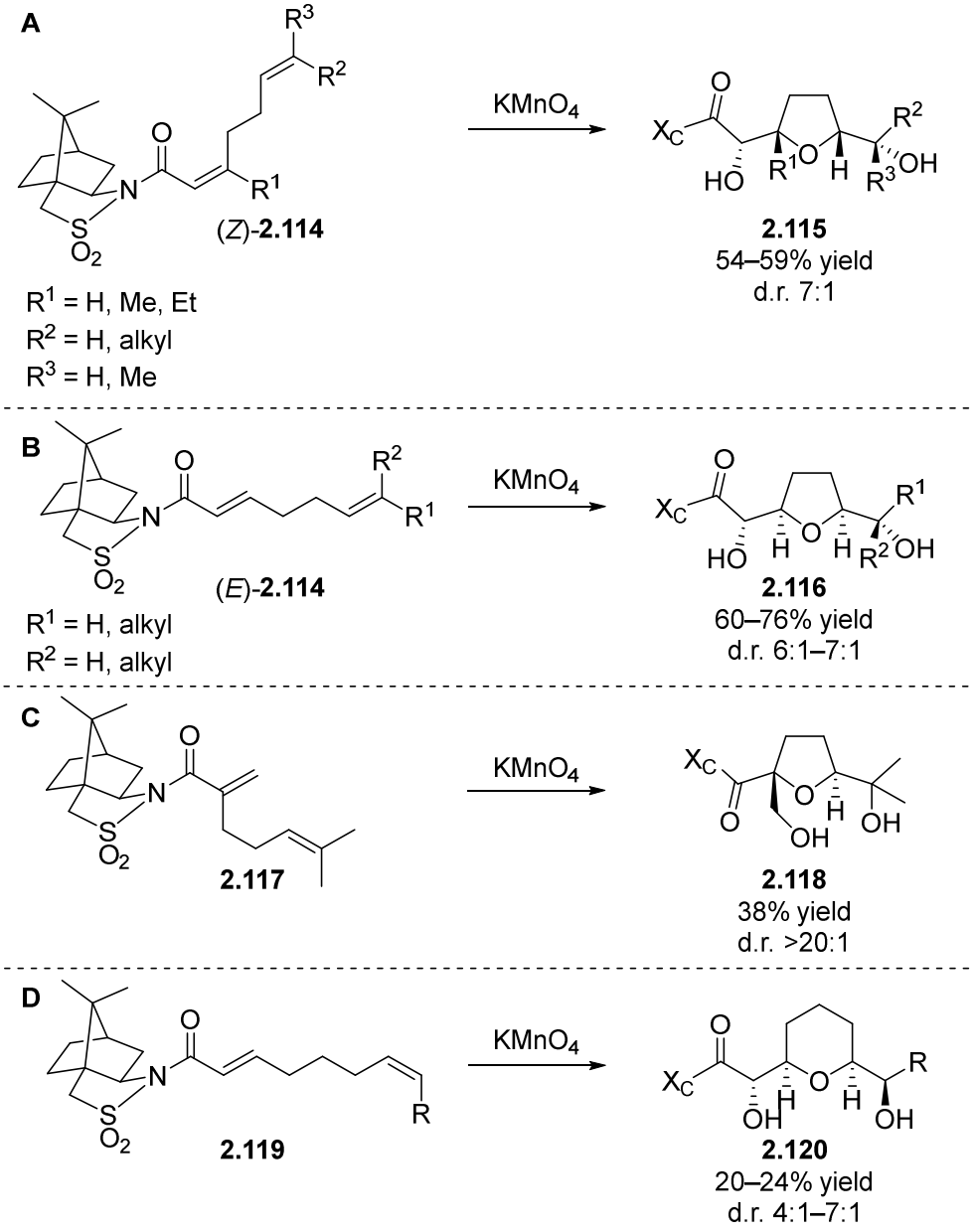

2.1.1.7 Camphorsultam mediated hydrogenation

Another highly selective transformation mediated by camphorsultam is the asymmetric hydrogenation of β,β-dialkyl substituted, α,β-unsaturated sulfonimides **2.16** (Scheme 2.35), [56] and it is this transformation that was targeted for investigation of the pseudo-catalytic cycle in space

concept. This camphorsultam mediated asymmetric hydrogenation sets a new chiral center at the β-position for substrates that are surprisingly challenging to hydrogenate with high ee using asymmetric hydrogenation catalysts (vide infra) and has consequently been used in the synthesis of multiple biologically active molecules.[57]

Scheme 2.35. Camphorsultam mediated hydrogenation.

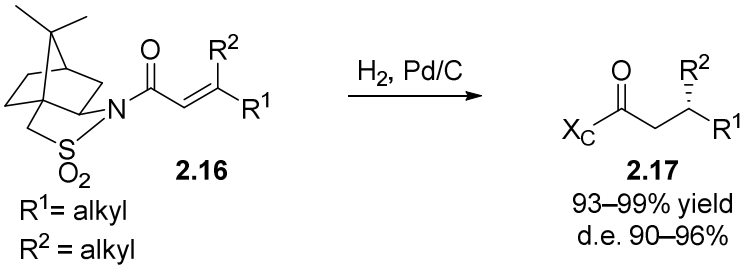

2.1.2 Catalytic methods to reduce β,β-dialkyl-α-β-unsaturated carbonyl substrates

As highlighted above, the strong preference for use of catalysts over chiral auxiliaries has led to an enormous amount of research devoted to the development of new catalysts. Nonetheless, there still exist many auxiliary mediated transformations for which alternate catalytic methods are not yet clearly superior, and the camphorsultam mediated hydrogenation discussed above (Scheme 2.35) is one such transformation. Catalytic hydrogenations or 1,4-hydride reductions to enact the equivalent net transformation have been developed but suffer from lower enantioselectivities and/or limited substrate scopes in comparison to the auxiliary mediated transformation.

2.1.2.1 Catalytic asymmetric hydrogenation

Development of homogeneous catalysts for enantioselective hydrogenation of olefins has been an active area of research ever since the seminal contributions from Knowles,[6] and these have overshadowed use of auxiliary mediated methods for hydrogenations.[58] However, while numerous asymmetric hydrogenation catalysts have been developed that achieve high enantioselectivity for hydrogenation of α,β-unsaturated substrates functionalized with aryl rings or heteroatoms at the α or β positions, for simple β,β-dialkyl substrates achieving high ee is surprisingly challenging, whereas selectivity is typically excellent when using the auxiliary mediated approach (Scheme 2.35).[59]

Early work towards enantioselective hydrogenation of these challenging substrates was performed by Valentine Jr. and coworkers.[60] Using a rhodium catalyst with a chiral phosphine ligand derived from menthol (**L1**), a modest 79% ee in the hydrogenation of **2.121** was achieved (Scheme 2.36).

Scheme 2.36. Asymmetric hydrogenation developed by Valentine Jr. and coworkers.

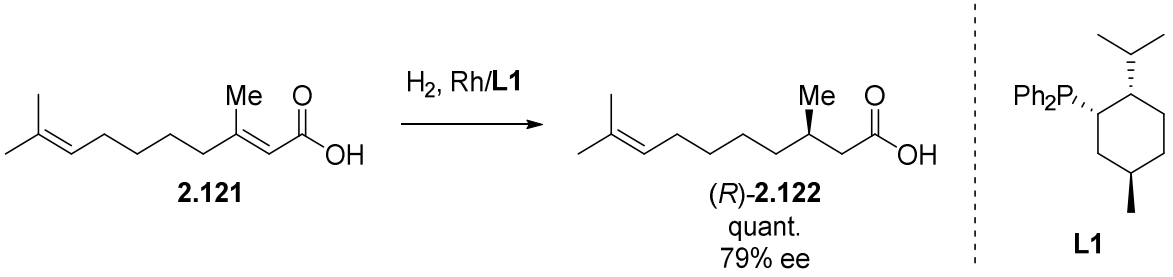

Substantial progress in asymmetric induction was made by the Noyori group with the development of the BINAP ligands, with 87% ee now achievable (Scheme 2.37) in the hydrogenation of **2.123** using a ruthenium catalyst ligated by **L2**.[61]

Scheme 2.37. Asymmetric hydrogenation reported by Noyori and coworkers.

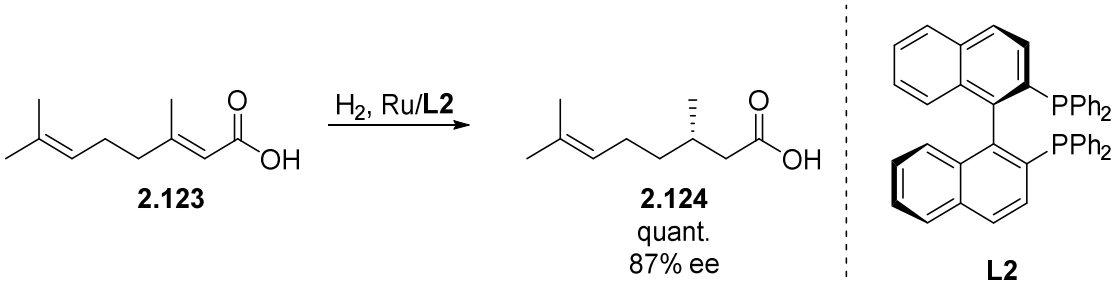

Subsequent work has focussed on the development of increasingly sophisticated ligands. The Pfaltz group developed iridium precatalyst **2.127** with bidentate P-N ligands that achieved very high, 97% ee for the hydrogenation of aryl substituted compounds such as **2.125a** and 90% ee for dialkyl substituted compound **2.125b** (Scheme 2.38).[62] Further ligand development and screening lead to ee's in the mid 90's for the first time with these challenging substrates using precatalysts **2.130** and **2.131 (**Table 2.1).[63] However, application of these precatalysts to a different α,β-dialkyl

substituted substrate **2.132** resulted in a drastically lower enantioselectivity (Scheme 2.39) highlighting the lack of robustness towards substrate modification.

Scheme 2.38. Asymmetric hydrogenation developed by Pfaltz and coworkers.

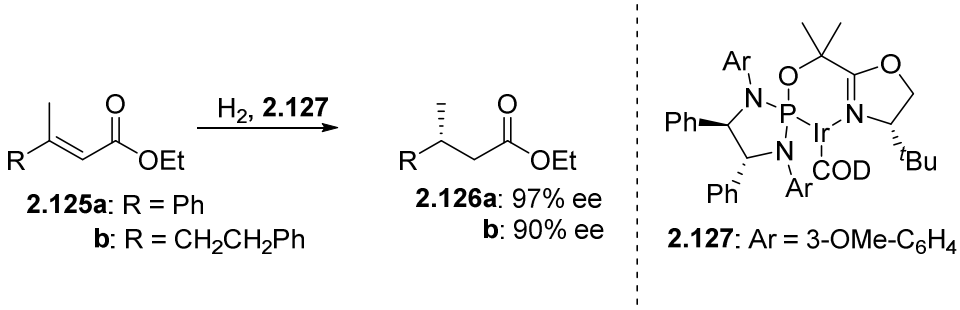

Table 2.1. Subsequent generation Pfaltz catalysts for asymmetric hydrogenation of challenging β,β-dialkyl substrates.

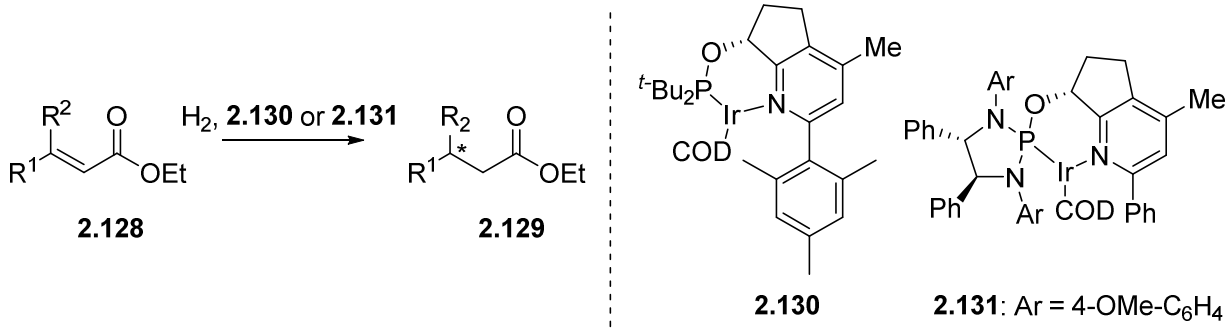

Entry	compound	R^1	R^2	catalyst	ee (%)	configuration
1	**2.128a**	CH_2CH_2Ph	Me	**2.130**	94	*R*
2	**2.128a**	CH_2CH_2Ph	Me	**2.130**	93	*S*
3	**2.128b**	Me	CH_2CH_2Ph	**2.130**	96	(–)
4	**2.128b**	Me	CH_2CH_2Ph	*ent*-**2.131**	91	(–)

Scheme 2.39. Hydrogenation of a different α,β-dialkyl substrate using precatalysts **2.130** and **2.131**.

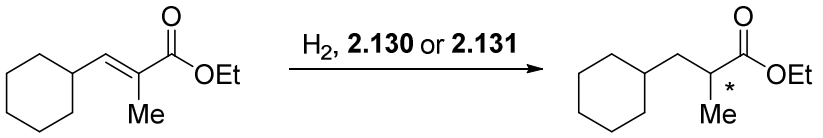

2.132 **2.133**

for **2.130**: 45% ee (+)
for **2.131**: 32% ee (+)

Burgess and coworkers reported high stereoselectivity for the hydrogenation of β,β-dialkyl substituted α,β-unsaturated esters **2.134** bearing a (protected) hydroxyl group at the γ-position (Scheme 2.40), but the presence of this oxygen atom was essential for high enantioselectivity.[64] For compound **2.137** where the protected γ-hydroxyl group was on a chiral centre, a match/mismatch effect could also be observed (Scheme 2.41).[65] The authors subsequently attempted to develop improved bidentate phosphite ligands by dimerization of binol substituted, quinine derived phosphites but the highest enantioselectivity achieved was only 75% ee using ligand **L3** (Scheme 2.42).[66]

Scheme 2.40. Diastereoselective hydrogenation developed by Burgess and coworkers.

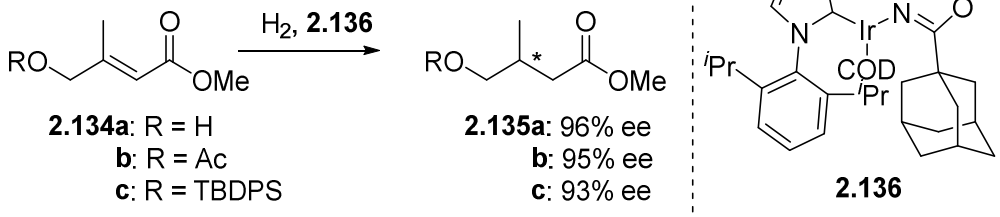

2.134a: R = H
b: R = Ac
c: R = TBDPS

2.135a: 96% ee
b: 95% ee
c: 93% ee

2.136

Adam and coworkers at Hoffman-La Roche developed an asymmetric hydrogenation of the α,β-unsaturated lactone **2.139** using a ruthenium catalyst ligated by **L4** (Scheme 2.43).[67] This catalyst system was identified by screening 22 different chiral, bidentate ligands with Ru, Rh and Ir metals for the desired transformation, and the reaction was successfully scaled up to kg scale.

Scheme 2.41. Diastereoselective hydrogenation with match/mismatch effect developed by Burgess and coworkers.

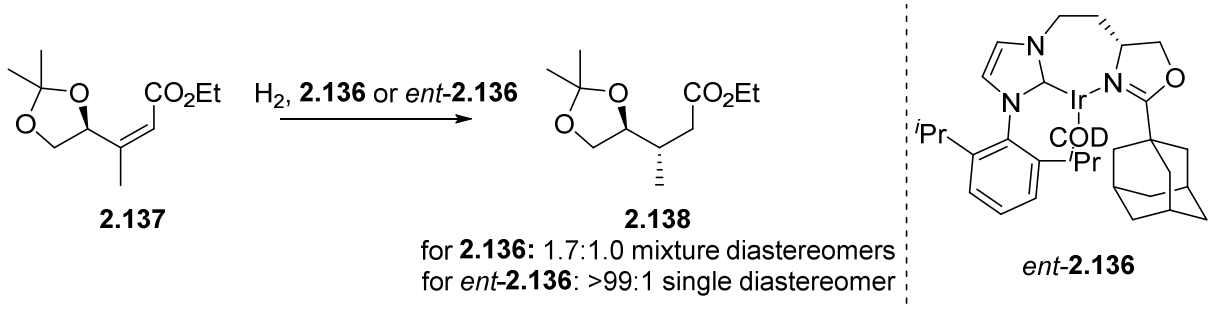

Scheme 2.42. Attempts to improve enantioselectivity with quinine derived bidentate phosphite ligands.

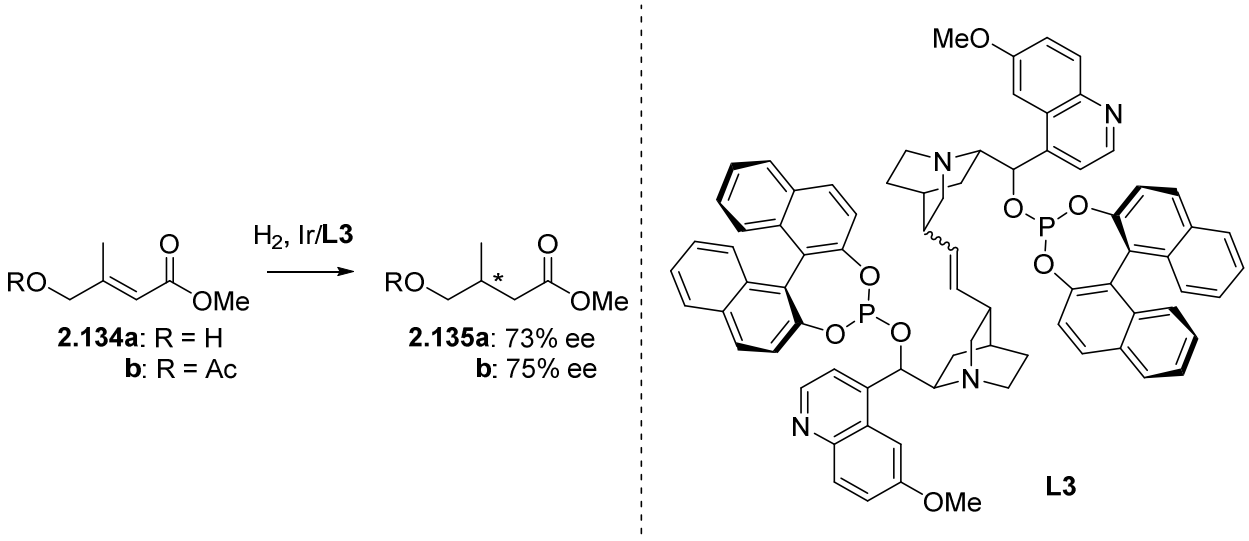

Scheme 2.43. Enantioselective hydrogenation reported by Adam and coworkers.

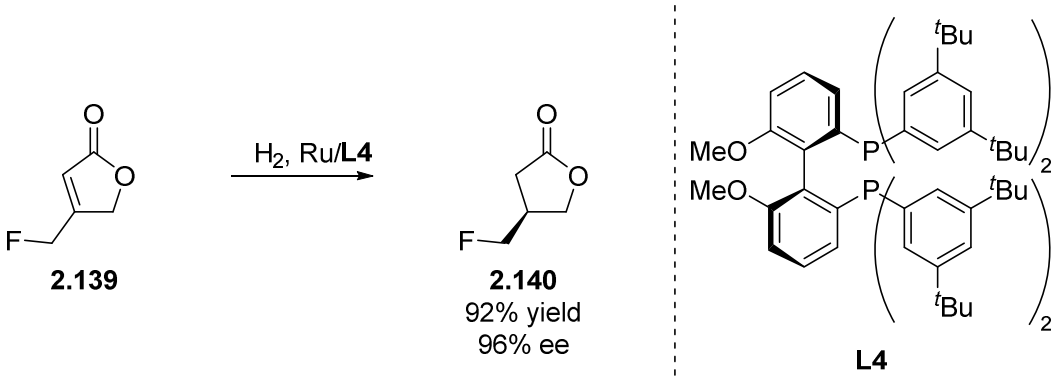

The Andersson group reported the first hydrogenation of α,β-unsaturated esters **2.128** with good enantioselectivity for multiple fully saturated, β,β-dialkyl substrates (Table 2.2).[68] Even so, the enantioselectivities achieved for β,β-dialkyl substrates were only in the high 80s to low 90s, while for aryl, alkyl substrates ~98% ee was achieved (entries 1,4), again highlighting the greater difficulty to achieve high selectivity in catalytic hydrogenation of substrates with fully saturated β,β-dialkyl substituents.

Table 2.2. Select scope examples from the enantioselective hydrogenation developed by Andersson and coworkers.

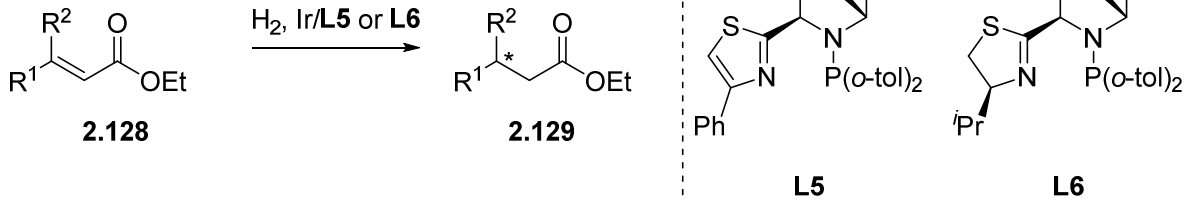

Entry	compound	R^1	R^2	ligand	ee (%)	configuration
1	**2.128c**	Ph	Me	**L5**	98	(*R*)-(–)
2	**2.128d**	CH_2(*t*-Bu)	Me	**L5**	87	(+)
3	**2.128e**	Cy	Me	**L5**	87	(*R*)-(–)
4	**2.128f**	Me	Ph	**L6**	98	(*S*)-(+)
5	**2.128g**	Me	CH_2(*t*-Bu)	**L6**	87	(–)
6	**2.128h**	Me	Cy	**L6**	93	(*S*)-(+)

Lastly, a rhodium-catalyzed asymmetric hydrogenation of β-substituted ε-caprolactams **2.141** was recently reported by Zhang and coworkers that could tolerate a benzyl group at the β-position, but again enantioselectivity was lower than for substrates with a β-aryl group (Scheme 2.44).[69]

Scheme 2.44. Enantioselective hydrogenation of α,β-unsaturated ε-caprolactams developed by Zhang and coworkers.

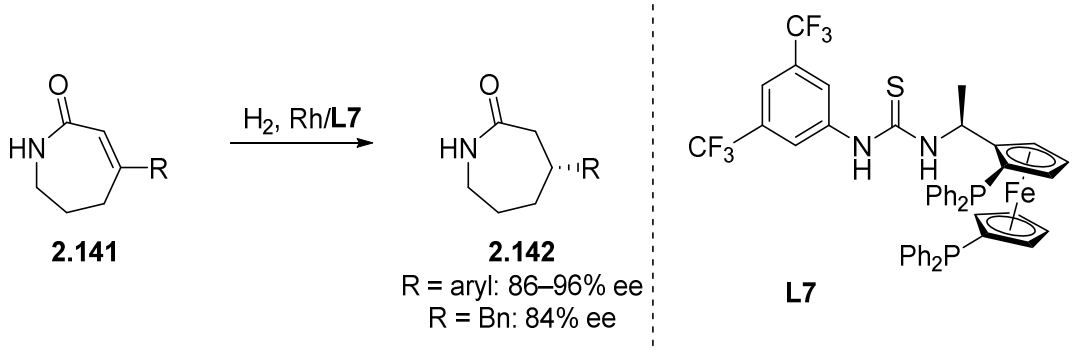

While the progress has been substantial in this area, none of the catalytic systems developed to date has realized the generality and high selectivity of the chiral auxiliary mediated transformation when the two β-substituents are simple alkanes (Section 2.1.1.7).

2.1.2.2 Catalytic asymmetric 1,4-hydride reduction

Enantioselective 1,4-hydride reduction is an alternative strategy to reduce α,β-unsaturated carbonyl compounds. In their seminal work, the Pfaltz group reported highly enantioselective 1,4-hydride reduction using a cobalt catalyst ligated by a semi-corrin ligand **L8** and $NaBH_4$ as the stoichiometric reducing agent (Scheme 2.45).[70] Unlike the catalytic hydrogenations discussed in section 2.1.2.1, these catalytic 1,4-reductions are not adversely affected when both β substituents are alkyl groups, however the atom economy is poorer due to generation of stoichiometric waste from the terminal reducing agent.

Scheme 2.45. Asymmetric 1,4-hydride reduction developed by Pfaltz and coworkers.

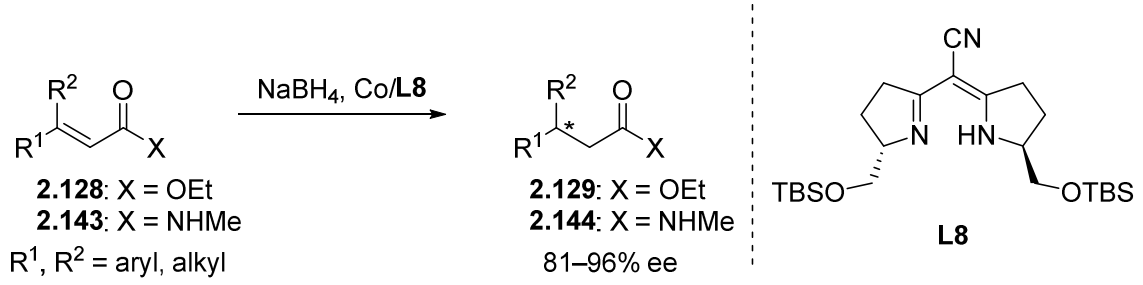

Subsequent contributions from the Buchwald group significantly advanced this chemistry by replacing $NaBH_4$ with polymethylhydroxosilane (PMHS) as the terminal reducing agent through the use of a copper catalyst and BINAP type ligand **L9** (Scheme 2.46).[71] The same catalyst system was also applicable for the asymmetric reduction of α,β-unsaturated lactones and lactams as well.[72]

Scheme 2.46. Asymmetric 1,4-hydride reduction developed by Buchwald and coworkers.

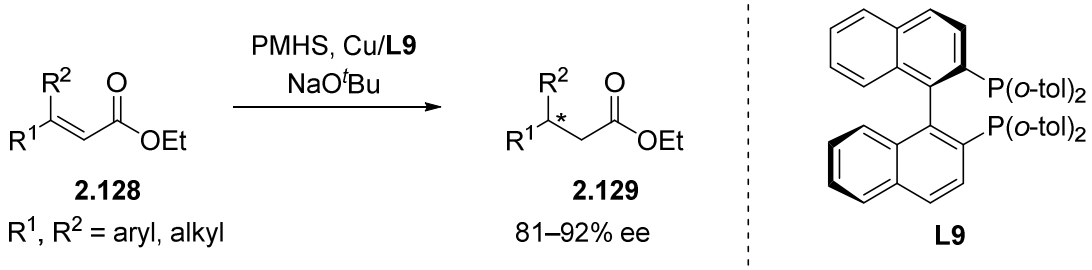

Enantioselectivities were improved by the Lipshutz group with the use of a copper catalyst ligated by a JosiPhos type ligand **L10** (Scheme 2.47).[73] Nishiyama and coworkers developed a rhodium(bisoxazolinylphenyl) pre-catalyst **2.147** that achieved similar enantioselectivity using $(EtO)_2MeSiH$ as the terminal reducing agent (Scheme 2.48).[74] Lastly, the Reiser and Kitamura groups also recently re-investigated cobalt catalysts with $NaBH_4$ as the terminal reductant and achieved ee's in the high 90's with the azabis(oxazoline) ligand **L11** or pre-catalyst **2.148** (Scheme 2.49).[75] The Co/**L11** catalyst was also capable of affecting the reduction of α,β-unsaturated amides **2.143**.

Scheme 2.47. Asymmetric 1,4-hydride reduction developed by Lipshutz and coworkers.

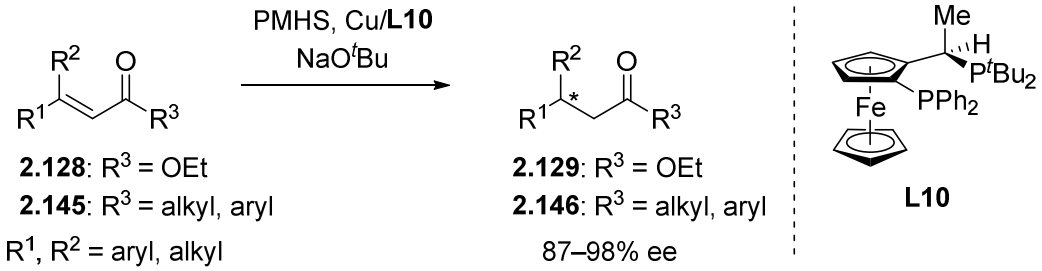

Scheme 2.48. asymmetric 1,4-hydride reduction developed by Nishiyama and coworkers.

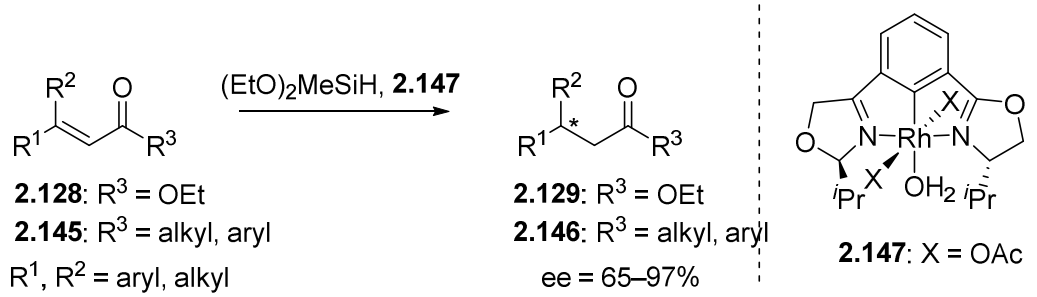

Scheme 2.49. Asymmetric 1,4-hydride reductions developed by the Reiser and Kitamura groups.

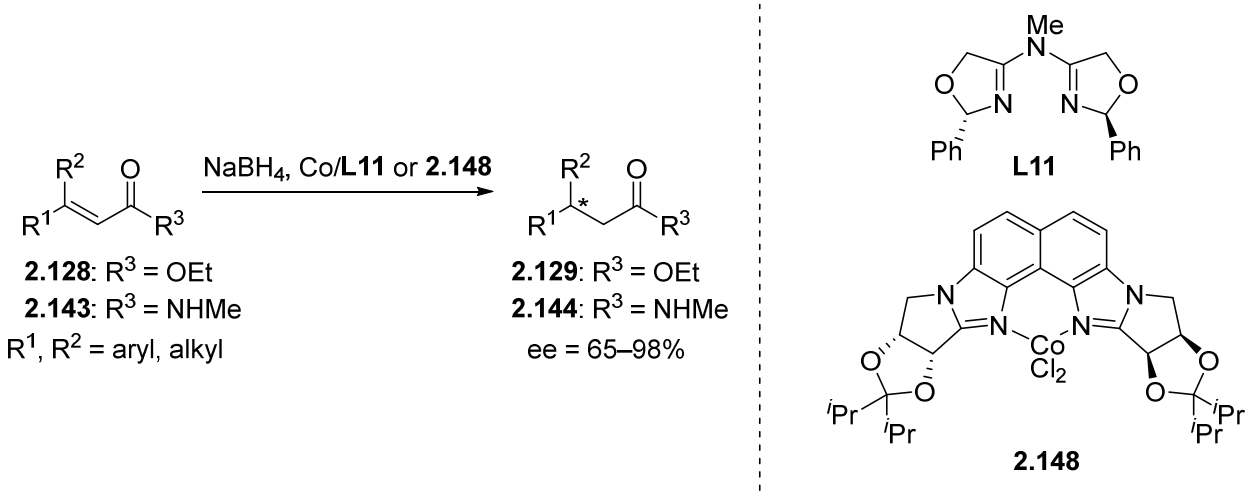

While the enantioselectivity achieved in the asymmetric 1,4-hydride reduction chemistry has been excellent, heterogeneously catalyzed hydrogenation is generally preferred in industry over stoichiometric reduction due to higher atom economy, no stoichiometric waste, and improved product isolation (i.e., filter off catalyst, evaporate solvent).[76] As such, the camphorsultam mediated process (Section 2.1.1.7), which achieves comparable stereoselectivity, would be desirable based on these considerations if the downsides of using a chiral auxiliary were addressed.[77]

2.2 Results and Discussion

At the outset of the investigation, challenges preventing direct translation of the established literature protocol into a telescoped flow process were identified (Scheme 2.50). First, the literature procedure used a different solvent for each of the three reactions. Second, purification options are more limited in flow and use of continuous liquid/liquid extractions was desired for both inline purifications between steps and the eventual separation of the auxiliary and product at the end of the process (based on pK_a differences). Last, NaH was the base used for the reported sultam acylation reaction. This is incompatible with flow due to insolubility of both NaH and NaCl that precipitates during the reaction under the necessarily anhydrous conditions.

Scheme 2.50. Asymmetric hydrogenation developed by Oppolzer and coworkers.

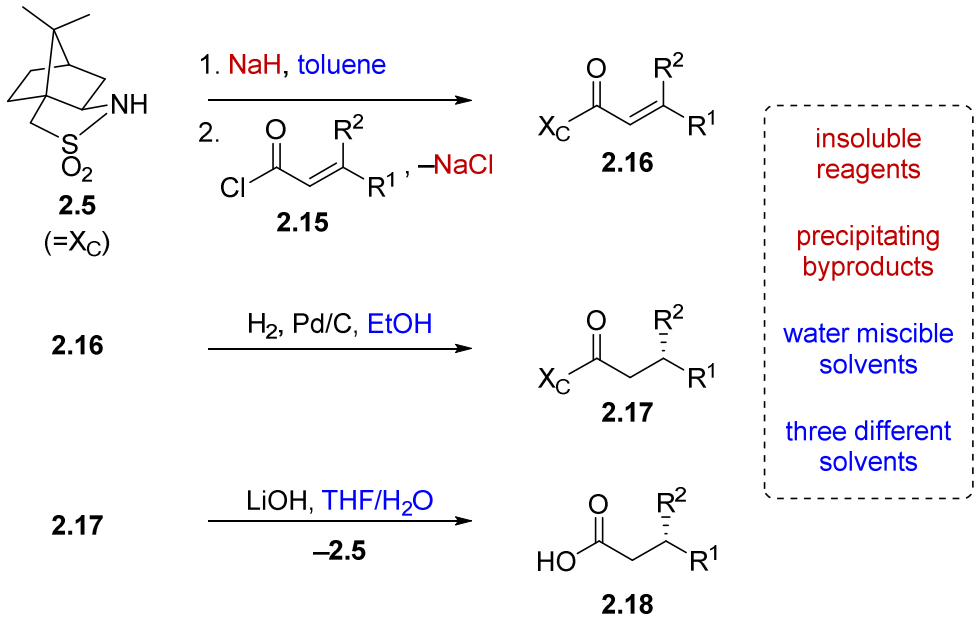

To address solvent-related challenges, it was decided to re-develop the three reactions in toluene, therefore removing the need for solvent switches between steps and introducing potential for liquid/liquid separations. Towards overcoming solid handling issues, flow-compatible reaction conditions were explored for the acylation step (Table 2.3). Substituting NaH with organic bases was unsatisfactory due to low conversions and precipitate formation (entry 2). Changing from acid chlorides to mixed anhydrides (entry 3) or activated esters (entry 4) was ineffective due to unachievable substrate synthesis and low reactivity respectively. Biphasic Schotten-Baumann

conditions were efficient with phase transfer catalysis (PTC) in batch (entry 5),[78] however only moderate and highly variable yields were obtained in slug flow (entry 6). Incorporation of active mixing in flow returned yields to near quantitative (entry 7).[79] A simple custom mixing unit was utilized composed of a hollowed syringe reactor with oscillating stir bars, inspired by a similar designed from Ley and coworkers, providing high mass transfer at low flow rates.[80] For the post-reaction liquid/liquid separation, membrane based separators proved incompatible with the high *p*H aqueous phase and therefore gravity-based separation was used (for details see Appendix I). Addition of 4% (w/w) NaCl to the 4% (w/w) NaOH aqueous phase was found to improve the separation.

Table 2.3. Design of a flow-compatible acylation process.

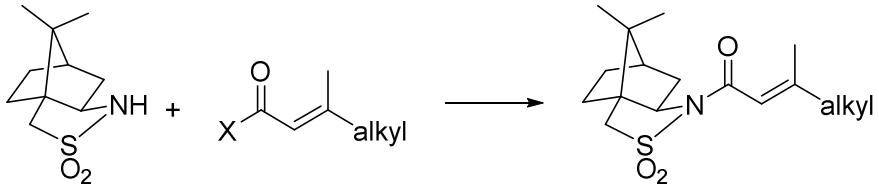

2.5 **2.15** **2.16**

Entry	x	Mode	Conditions	Result
1	Cl	batch	NaH[a]	Up to 84% (ref 56)
2	Cl	batch	organic bases	low conversion; solid formation
3	OPiv	n/a	n/a	not isolable substrate
4	OC_6F_5	batch	organic bases	low–moderate yields; competing decomp.
5	Cl	batch	PTC, vigorous stirring, 10 min[b]	>95%
6	Cl	flow	PTC, passive mixing, t_{res} = 10 min[c]	30–70%[d]
7	Cl	flow	PTC, active mixing, t_{res} = 4.3 min[e]	>95%

[a] Sultam first treated with NaH prior to addition of acid chloride in toluene. [b] 1 Mol% Aliquat 336 added as a phase transfer catalyst, toluene/4% $NaOH_{(aq)}$.[81] [c] 1 Mol% Aliquat 336 added as a phase transfer catalyst in a tubular plug flow reactor. [d] Yields varied with time due to poor mixing. [e] 1 Mol% Aliquat 336 added as phase transfer catalyst using active mixing units.

The hydrogenation was next investigated using a packed bed reactor (PBR) of Pd/C.[82] Full conversion ($t_{res} \approx 1$ min) was initially achieved but catalyst deactivation prevented long term operation. Hypothesizing that basic impurities were at fault,[83] a co-feed of 0.1% (v/v) aqueous acetic acid was incorporated in combination with an increase of the PBR temperature to 45 °C.[84] With these minor modifications, the acylation and hydrogenation reactions were successfully telescoped to yield 97% of hydrogenated substrate with no observable loss of catalytic activity over several hours of operation (Scheme 2.51). A 95:5 d.r. was obtained for product **2.17a**, consistent with the literature batch procedure that used EtOH as solvent with a 1.5 h reaction time. The process output could be carried through a modified Biotage Universal Phase Separator (Figure AI.4) to separate the excess hydrogen gas and aqueous co-feed, retaining the product in the organic phase.

Scheme 2.51. Hydrogenation of **2.16a** using a packed bed of Pd/C.

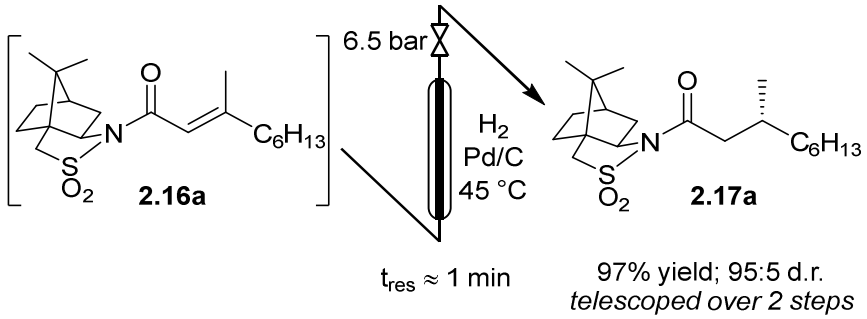

Auxiliary cleavage and separation from the product by selective deprotonation (carboxylic acid aq. p$K_a \approx 5$, sultam aq. p$K_a \approx 11.5$) and continuous liquid/liquid extraction was next examined (Table 2.4). Initial attempts to perform the hydrolysis using PTC appeared promising but were ultimately abandoned due to long reaction times and solid formation (entry 2). Introducing MeOH as a co-solvent to improve reaction homogeneity greatly improved reaction rates, but precipitate formation was still problematic (entry 3). Expecting that solubility problems stemmed from either salt formation or substrate/product decomposition, it was decided to target methanolysis instead of hydrolysis. Replacing KOH with NaOMe allowed milder conditions and shorter residence times without precipitate formation (entry 4). Further, this greatly simplified the product-auxiliary separation since the recovered auxiliary could be directly extracted from the organic phase. Overall yields of ~70% could now be achieved over the three telescoped steps and 4 single-stage

liquid/liquid extractions/separations, representing average yields/recoveries of ~95% over each of these 7 operations. A schematic of the full experimental set up is shown in Figure 2.1 and detailed descriptions are available in Appendix I (Figures AI.1–6). Total residence time from start to finish over all three stages was ~30 min, including processing time through all pumps and the liquid/ liquid separators used for in-line work up.

Table 2.4. Design of a flow-compatible auxiliary cleavage reaction.

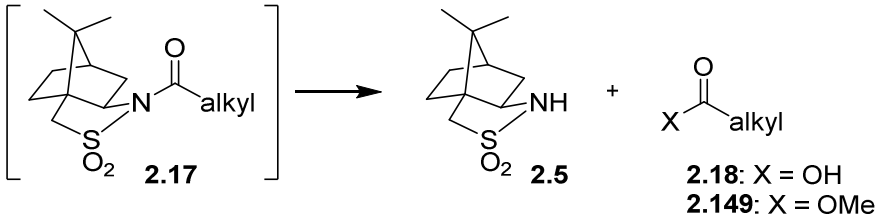

Entry	x	Mode	Conditions	Result
1	OH	batch	LiOH, 18 h	92% – quant. (ref 56) *aux. not recovered*
2	OH	batch	PTC, KOH[a]	Slow reaction; precipitate formation
3	OH	flow	KOH, MeOH, 90 °C, 9 min	Fast reaction; precipitate formation
4	OMe	flow	NaOMe, 50 °C, 4.5 min	~70% yield of Me ester[b] *Telescoped over 3 steps*

[a] 5 mol% 18-crown-6 and 5 mol% 2,5-dimethyl-2,5-hexanediol added as phase transfer catalysts in a tubular plug flow reactor.[85] [b] Yields and auxiliary recovery varied depending on nature of alkyl group. See Table 2.5.

To verify that the process was general for different β,β-disubstituted α,β-unsaturated acid chlorides, a selection of substrates was examined in the multi-stage flow reactor (Table 2.5, top). In each case, the separated product and auxiliary effluents were collected for a 3 h period at steady state. The final ester products were obtained with isolated yields of 67–72%. Diastereoselectivity over the hydrogenation ranged from 92:8 to 98:2. In comparison to the 3-step batch process, this represented similar to greatly improved yields (batch yields over 3 steps: 45–76%) with greatly reduced processing times (batch reaction times: 2.5 h for acylation, 1.5 h for hydrogenation, 18 h for hydrolysis[37b,56]) and equivalent diastereoselectivity. Moreover, due to the designed separation

of the auxiliary and product in the three-step flow process, the auxiliary could be directly recovered in 71–79% crude yield and recrystallized to >99% purity (48–56% yield), which enabled reuse of the material for each subsequent substrate scope example.

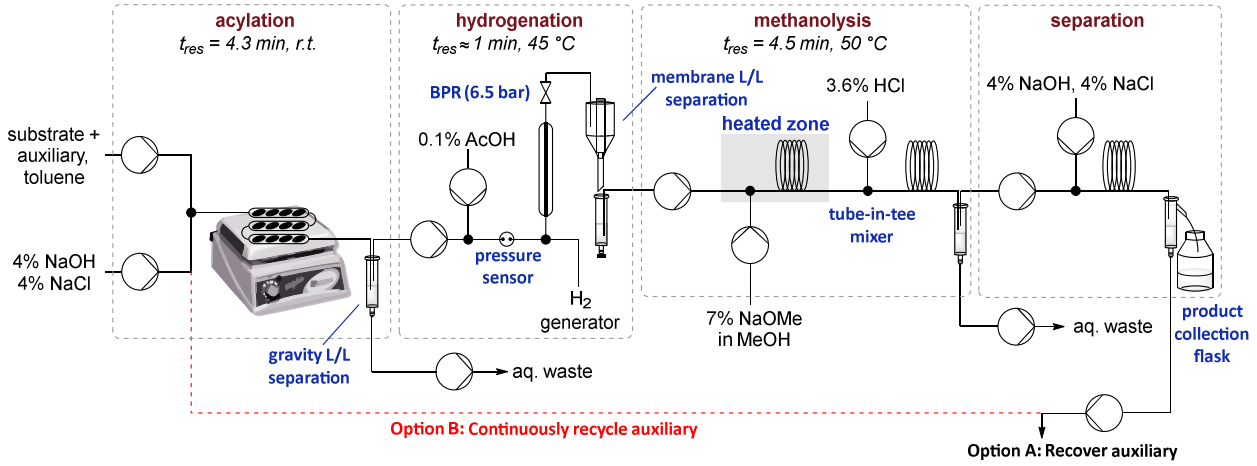

Figure 2.1. Schematic of flow reactor set up for the telescoped reaction sequence with or without automated recycling of the auxiliary. For auxiliary recovery experiments (Option A) 1.0 eq of auxiliary w.r.t. substrate. For recycle experiments (Option B) 0.35 eq. of auxiliary w.r.t. substrate. L/L = liquid/liquid, BPR = back pressure regulator.[a]

Focus was then turned towards automating the auxiliary recycling process (Fig. 2.1, dotted line). The same flow system was utilized with only two modifications. First, the amount of auxiliary in the substrate feed solution was decreased from 1 eq. to 0.35 eq. (the amount determined experimentally to be necessary to make up for lost auxiliary over the three transformations and four inline liquid/liquid extractions). Second, 0.65 eq. of auxiliary was dissolved in the 4% (w/w) NaOH, 4% (w/w) NaCl feed solution used for start-up, then after steady state was reached this feed was replaced by the extracted auxiliary stream exiting the process.

The same substrate scope was re-evaluated with this modified process, operating continuously for 4.5 hours (~8 auxiliary recycles; Table 2.5, bottom). In each case, transition to a recycling reactor went smoothly, with only slight losses in overall yield relative to the process without auxiliary recycling, due to inefficiencies of single-stage extractions and impurity carry-

[a] Adapted from Sullivan, R. J.; Newman, S. G. *Chem. Sci.* **2018**, *9*, 2130–2134 – published by the Royal Society of Chemistry under a Creative Commons 4.0 licence.

through with the recycle feed. Diastereomeric ratios remained constant over 4.5 h of steady state operation and were consistent with the d.r. values obtained in the previous experiments without auxiliary recycle.

Table 2.5. Substrate scope for auxiliary recovery and recycle experiments.

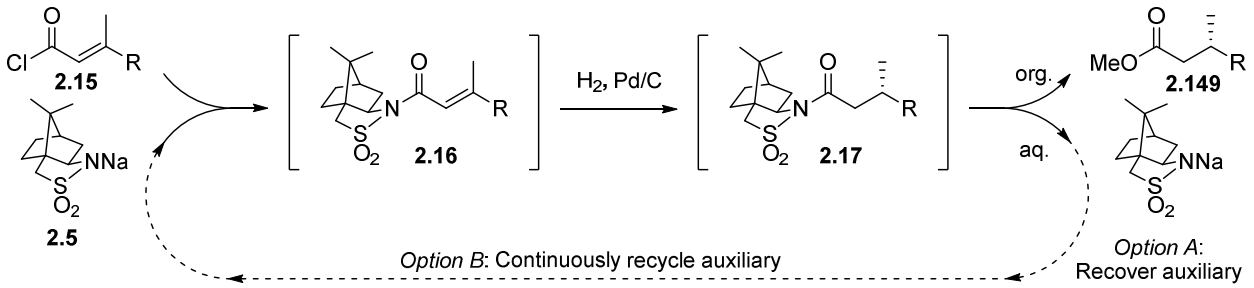

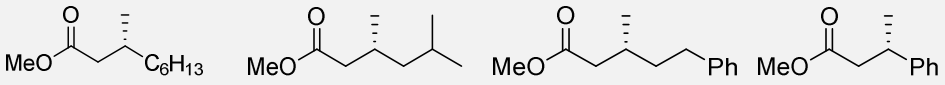

2.149a **2.149b** **2.149c** **2.149d**

A: auxiliary recovery experiments[a]				
Product yield (e.r.)	67% (95:5)	72% (98:2)	71% (93:7)	67% (92:8)
Recovered auxiliary[b]	79% (53%)	71% (54%)	73% (56%)	72% (48%)
B: auxiliary recycle experiments[c]				
Product yield (e.r.)	54%[d] (95:5)	48% (98:2)	57% (95:5)	68% (90:10)

[a] Product collected over 6 residence volumes (3 h; 3.6 mmol processed) at steady state. Isolated yields are reported. Enantiomeric ratios determined by monitoring *via* GC, the diastereomeric ratio of the intermediate after hydrogenation. See Fig AI.8–A11. [b] Crude yield (purified yield after recrystallization from hexanes). [c] Product collected over 9 residence volumes (4.5 h; 5.4 mmol processed) at steady state. Isolated yields are reported. [d] 94% purity; contaminated with aldehyde by-product.

2.3 Conclusions

In summary, a continuous flow system was developed to enable the auxiliary-mediated asymmetric hydrogenation of conjugated olefins to occur in a single telescoped process. The chiral auxiliary and chiral ester product were continuously separated, allowing the auxiliary to be recovered and subsequently reused. Alternatively, the auxiliary re-use could be automated in real

time by sending the auxiliary recovery feed from the last reaction step back to the first reaction step inlet, creating a recycle loop. Average yields/recoveries ranged from 90–95% per reaction or in-line purification step, with a processing time of approximately 30 minutes per pass, giving a substantial improvement in efficiency while maintaining similar control in stereochemistry as compared to the batch procedure. To our knowledge, this represents the first example of a telescoped chiral auxiliary-mediated process incorporating automated reuse of the auxiliary, achieving formal sub-stoichiometric auxiliary loading with respect to the process while maintaining fully stoichiometric auxiliary in each reaction by using a 'pseudo-catalytic cycle in space' concept.

2.4 Experimental

2.4.1 General experimental details

Unless otherwise noted reagents were used as received. Palladium on carbon was purchased from Strem, (10% palladium on activated carbon, reduced, dry powder, product 46-1900). All other chemicals were obtained from either Sigma Aldrich or Combi-Blocks. Aliquat 336 was absorbed onto silica gel, dry loaded onto a 40×100 mm silica column, eluted with DCM→95:5 DCM:MeOH, and evaporated prior to use.

^{1}H NMR and ^{13}C NMR were recorded on a Bruker AVANCE 400 MHz spectrometer and referenced to residual solvent signals. Melting point ranges were determined on a Canlab GallenKamp Melting Point Apparatus. GC yields for optimization studies were obtained via a 5-point calibration curve using FID analysis on an Agilent Technologies 7890B GC with 30 m × 0.25 mm HP-5 column. Accurate mass data was obtained using GC-EI-MS from an Agilent 5977A GC/MS using MassWorks 4.0 software from CERNO bioscience.[86] HPLC chromatograms were collected using an Agilent 1200 HPLC equipped with a 30 cm Chiralcel OD-H column. Optical rotations were recorded on an Anton Paar MCP 500 polarimeter with a 10.00 mm path length at 20 °C and 589 nm wavelength.

2.4.2 Details of flow reactor setup

A schematic of the reactor setup is shown in Figure 2.2 and a photo of the setup in the fume hood is provided in Appendix I (Figure AI.7). All pump feed tubes were either 1/16" O.D., 1.0

mm I.D. PFA or 1/8" O.D., 1/16" I.D. PFA. All tubes in the hydrogenation stage between the pump and the BPR were 1/16" O.D., 0.75 mm I.D. 316 Stainless steel (SS). All other tubing was 1/16" O.D., 0.5 mm I.D. PFA unless otherwise stated. PEEK fittings and tee mixers were used for all PFA and PEEK tubing as well as for stainless steel coil C1. 316 Stainless steel fittings and tees were used for all stainless-steel tubes in the hydrogenation stage. PEEK fittings and parts were purchased from UpChurch Scientific. Stainless steel fittings and parts were purchased from VICI Valco or Swagelok. Further details about the individual components of the flow reactor are provided in Appendix I.

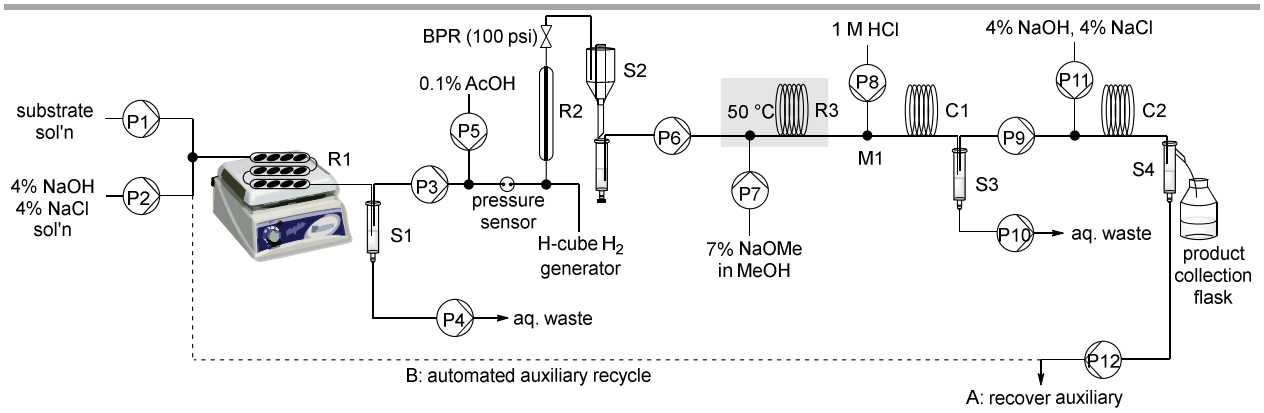

Figure 2.2. Schematic of complete flow reactor set up.

P1 – SyrDos 2 continuous syringe pump equipped with 0.5 mL glass syringes. 200 µL/min.

A: 0.1 M acid chloride, 0.1 M sultam, 0.001 M Aliquat 336 in toluene.

B: 0.1 M acid chloride, 0.035 M sultam, 0.001 M Aliquat 336 in toluene.

P2 – New Era NE-300 syringe pump equipped with either 60 or 25 mL luer-lock HSW norm-ject syringe. 150 µL/min.

A: 4% NaOH, 4% NaCl.

B: 4% NaOH, 4% NaCl with 0.87 M sultam for start-up only; replaced by the recovered auxiliary stream from P12 after reaching steady state.

P3 – ThalesNano micro HPLC pump, adjusted to maintain constant volume of organic phase in gravity phase separator.

P4 – ThalesNano micro HPLC pump, adjusted to maintain constant volume of aqueous phase in gravity phase separator.

P5 – ThalesNano micro HPLC pump. 50 µL/min.

P6 – Vapourtec V3 pump with red tubing, adjusted to match flow rate of organic phase exiting Biotage universal phase separator.

P7 – Chemyx fusion 200 syringe pump equipped with 25 mL stainless steel syringe (Harvard). 23.0 µL/min.

P8 – SyrDos 2 continuous syringe pump equipped with 2.5 mL glass syringes. 200 µL/min.

P9 – Global FIA milliGAT pump, adjusted to maintain constant volume of organic phase in gravity phase separator.

P10 – Vapourtec V3 pump with red tubing, adjusted to maintain constant aqueous volume in gravity phase separator.

P11 – SyrDos 2 continuous syringe pump equipped with 1.0 mL glass syringes. 150 μL/min.

P12 – Vapourtec V3 pump with red tubing, adjusted to maintain constant aqueous volume in gravity phase separator.

R1 – continuous stirred tubular reactors 3 × 0.5 mL. See section AI.1.1 in Appendix I.

R2 – packed bed reactor, 1/4" O.D., 3 mm I.D. × 30 cm length packed with a mixture of 3 g 150–212 μm glass beads and 110 mg 10% Pd/C. See section AI.1.4 in Appendix I.

R3 – 1.0 mL, 1/16" O.D., 0.75 mm I.D. PEEK tube.

C1 – 1.0 mL, 1/8" O.D., 2 mm I.D. 316 SS tube.

C2 – 200 μL, 1/16" O.D., 0.5 mm I.D. PFA tube.

M1 – tube-in-tee mixer, see section AI.1.5 in Appendix U.

S1, S3, S4 – Gravity liquid-liquid separators – see section AI.1.2 in Appendix I.

S2 – Modified Biotage Universal Phase Separator – see section AI.1.3 in Appendix I.

2.4.3 Procedure for the synthesis of substrates

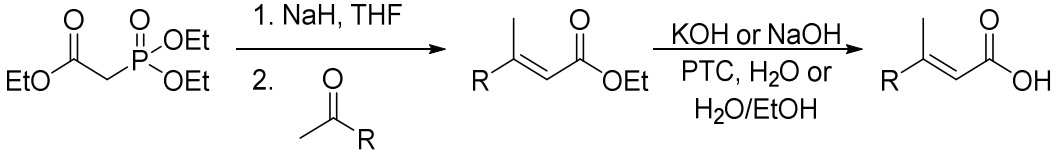

General procedure for synthesis of (*E*)-α-β-unsaturated acids. Based on the report by Seto and coworkers,[87] NaH (60% in mineral oil, 5.0 g, 125 mmol) was suspended in anhydrous THF (90 mL) under Ar and cooled to 0 ºC. Triethyl phosphonoacetate (30 g, 132 mmol) was added dropwise under Ar at 0 ºC. After the addition was complete the flask was allowed to warm to r.t. and stirred for 15 min until gas evolution ceased. Ketone (125 mmol) in THF (20 mL) was added dropwise. The resulting solution was stirred under Ar for 16 h. Water (100 mL) was added and the phases were separated. The aqueous phase was extracted with 2 × 50 mL Et_2O and all organic phases were combined and dried over Na_2SO_4 then concentrated to yield crude ethyl ester as a mixture of ~3:1 (*E*):(*Z*) isomers. The crude esters were hydrolyzed and purified by varying conditions to yield pure *(E)*-α-β-unsaturated carboxylic acid.

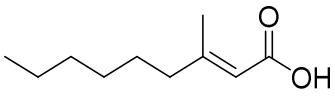

(E)-3-Methylnon-2-enoic acid: Prepared according to the general procedure and hydrolyzed by refluxing in 1 M NaOH (189 mL, 189 mmol) with 18-crown-6 (348 mg, 1.3 mmol) and 2,5-

dimethyl-2,5-hexanediol (187 mg, 1.3 mmol) until the oil layer was gone (ca. 16 h). The mixture was cooled to room temperature, washed with 25 mL hexanes and the *p*H was adjusted to <1 with conc. HCl resulting in formation of a separate organic phase. The product was extracted with 3 × 25 mL hexanes, the combined organic extracts dried over Na_2SO_4 and the solvent evaporated to yield 18.97 g (88%) of ~3:1 (*E*):(*Z*)-3-methyl-2-nonenoic acid as a colourless oil. Repeated recrystallization from MeOH at -78 °C[87] yielded 5.42 g (25%) of >99% (*E*)-3-methylnon-2-enoic acid as a white powder that melted to a colourless oil at room temperature. Characterization data was in agreement with the literature.[88] ^{1}H NMR (400 MHz, $CDCl_3$): δ 12.17 (br s, 1H), 5.68 (sext, *J* = 1.2 Hz, 1H), 2.16 (t, *J* = 1.2 Hz, 3H), 2.15 (t, *J* = 7.5 Hz, 2H), 1.48 (pent, *J* = 7.3 Hz, 2H), 1.28 (m, 6H), 0.89 (T, *J* = 7.0 Hz, 3H). ^{13}C{^{1}H} NMR (100 MHz, $CDCl_3$): δ 172.7, 163.8, 115.2, 41.4, 31.7, 29.0, 27.5, 22.7, 19.2, 14.2.

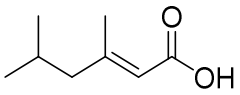

(E)-3,5-Dimethylhex-2-enoic acid: Prepared according to the general procedure and hydrolyzed by refluxing in 1 M NaOH (188 mL, 188 mmol), with 18-crown-6 (334 mg, 1.3 mmol) and 2,5-dimethyl-2,5-hexanediol (183 mg, 1.3 mmol) until the oil layer was gone (ca. 16 h). The mixture was cooled to room temperature, washed with 25 mL hexanes and the *p*H was adjusted to <1 with conc. HCl resulting in the formation of a separate organic phase. The product was extracted with 3 × 25 mL hexanes, the combined organic extracts dried over Na_2SO_4 and the solvent evaporated to yield 14.67 g (81%) of ~3:1 (*E*):(*Z*)-3,5-dimethylhex-2-enoic acid as a colourless oil. Repeated recrystallization from 4:1 MeOH:H_2O at -78 °C[87] yielded 2.21 g (12%) of >99% (*E*)-3-methyl-2-nonenoic acid as white needles. Characterization data was in agreement with the literature.[89] ^{1}H NMR (400 MHz, $CDCl_3$): δ 12.10 (br s, 1H), 5.67 (s, 1H), 2.15 (s, 3H), 2.03 (d, *J* = 7.2 Hz, 2H), 1.88 (septet, *J* = 6.8 Hz, 1H), 0.89 (d, *J* = 6.6 Hz, 6H). ^{13}C{^{1}H} NMR (100 MHz, $CDCl_3$): δ 172.5, 162.7, 116.4, 50.9, 26.5, 22.5, 19.1.

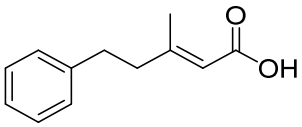

(E)-3-Methyl-5-phenylpent-2-enoic acid: Prepared according to the general procedure and hydrolyzed by addition of EtOH (100 mL), water (200 mL) and NaOH (65 g, 10 eq.)[90] and stirring

the resulting biphasic mixture rapidly at room temperature for 5 h until a single phase was achieved. The solution was then washed with 50 mL of 1:1 hexanes:EtOAc followed by 25 mL of hexanes. The *p*H was adjusted to <1 with conc. HCl resulting in the formation of a separate organic phase that was collected. The aq. phase was extracted with 50 mL 1:1 hexanes:EtOAc then 25 mL hexanes and all organic phases were combined and dried over Na_2SO_4. The solvent was evaporated to yield an oil. EtOAc (100 mL) was added followed by cyclohexylamine (15.3 g, 154 mmol) with rapid stirring, resulting in a thick white slurry of 3-methyl-5-phenyl-2-pentenoic acid·cyclohexylamine salt that was recrystallized twice from EtOAc[91] to remove the *z* isomer. The resulting white solid was then added to 3 M HCl (100 mL) and the free acid was extracted with 2×25 mL DCM. The combined extracts were dried over Na_2SO_4 and the solvent evaporated yielding a colourless oil. Boiling hexanes (80 mL) were added resulting in a fine suspension that was hot filtered and cooled to –20 °C yielding colourless crystals of the desired product in 97% purity. Recrystallizing a second time from hexanes yielded white needles of pure (*E*)-3-methyl-5-phenylpent-2-enoic acid. Yield 8.75 g (37%). Characterization data was in agreement with the literature.[88] ^{1}H NMR (400 MHz, $CDCl_3$): δ 11.98 (s, br, 1H), 7.31 (m, 2H), 7.20 (m, 3H), 5.72 (q, *J* = 1.2 Hz, 1H), 2.81 (dd, *J* = 9.4, 6.7 Hz, 2H), 2.49 (dd, *J* = 9.3, 6.2 Hz, 2H), 2.23 (d, *J* = 1.2 Hz, 3H). ^{13}C{^{1}H} NMR (100 MHz, $CDCl_3$): δ 172.3, 162.3, 141.0, 128.6, 128.4, 126.3, 115.7, 43.1, 34.0, 19.4.

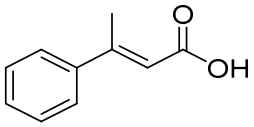

(E)-3-Phenylbut-2-enoic acid: Prepared as reported by Yamada and coworkers.[92] Cs_2CO_3 (26.07 g, 80 mmol), DBU (3.00 g, 20 mmol) and triethylphosphonoacetate (22.41 g, 100 mmol) were combined. Acetophenone (12.00 g, 100 mmol) was added and the slurry stirred at 40 °C for 3 days under Ar. The reaction was then quenched with H_2O (100 mL) and extracted with 3×25 mL hexanes and the combined organic extracts were dried over Na_2SO_4. The solvent was removed *in vacuo* yielding 19.34 g of a mixture of the desired product and acetophenone. To the crude mixture was added KOH (8.4 g, 150 mmol) and MeOH (100 mL) and the solution was refluxed overnight. The MeOH was then evaporated and H_2O (100 mL) and EtOAc (50 mL) were added. The mixture was agitated then allowed to settle. The organic phase was discarded and the aqueous phase was washed with 25 mL hexanes. The aqueous phase was then acidified to *p*H <1 with conc. HCl

resulting in formation of a separate organic phase. The product was extracted with 50 mL 1:1 EtOAc:hexanes then 2 × 25 mL hexanes. The combined extracts were dried over Na_2SO_4 and evaporated *in vacuo*. The crude yellow powder was recrystallized from hexanes yielding white needles of pure (*E*)-3-phenylbut-2-enoic acid. Yield 5.41 g (33%). Characterization data was in agreement with the literature.[89] ^{1}H NMR (400 MHz, $CDCl_3$): δ 12.02 (br s, 1H), 7.51 (m, 2H), 7.40 (m, 3H), 6.19 (q, *J* = 1.3 Hz, 1H), 2.62 (d, *J* = 1.3 Hz, 3H). $^{13}C\{^1H\}$ NMR (100 MHz, $CDCl_3$): δ 172.6, 158.7, 142.2, 129.5, 128.7, 126.6, 116.6, 18.5.

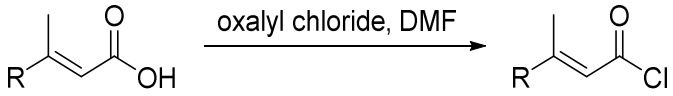

General procedure for synthesis of (*E*)- α-β-unsaturated acid chlorides. Et_2O (2.5 mL), DMF (7 μL, 0.1 mmol) and oxalyl chloride (1.7 mL, 20 mmol) were combined under Ar and the flask placed in a room temperature water bath. *(E)*-α-β-unsaturated acid (10 mmol), dissolved in Et_2O (7.5 mL), was added in small portions over the course of 30 min to the stirred oxalyl chloride solution. The mixture was stirred one additional hour after the addition was complete, then the Et_2O and excess oxalyl chloride were removed *in vacuo*.

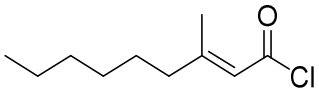

(E)-3-Methylnon-2-enoic acid chloride (**2.15a**): Prepared according to the general procedure. Purified by Kugelrohr distillation at 95 °C under high vacuum. Yield 1.81 g (96%) 99.2:0.8 (*E*):(*Z*) (relative GC-FID area count). The colourless oil was stored at –20 °C in a N_2 atmosphere glovebox. ^{1}H NMR (400 MHz, $CDCl_3$): δ 6.02 (sext, *J* = 1.2 Hz, 1H), 2.19 (td, *J* = 7.6, 1.0 Hz, 2H), 2.13 (d, *J* = 1.2 Hz, 3H), 1.49 (pent, *J* = 7.6 Hz, 2H), 1.29 (m, 6H), 0.88 (t, *J* = 7.0 Hz, 3H). $^{13}C\{^1H\}$ NMR (100 MHz, $CDCl_3$): δ 168.2, 163.9, 122.1, 41.1, 31.7, 29.0, 27.4, 22.6, 20.5, 14.2.

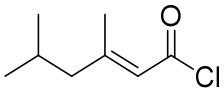

(E)-3,5-Dimethylhex-2-enoic acid chloride (**2.15b**): Prepared according to the general procedure. Purified by Kugelrohr distillation at 56 °C under high vacuum. Yield 1.51 g (92%) 99.5:0.5 (*E*):(*Z*) (relative GC-FID area count). The colourless oil was stored at –20 °C in a N_2 atmosphere glovebox. Characterization data was in agreement with the literature.[93] ^{1}H NMR (400 MHz, $CDCl_3$): δ 6.01

(sext, J = 1.1 Hz, 1H), 2.12 (d, J = 1.2 Hz, 3H), 2.06 (d, J = 7.1 Hz, 2H), 1.90 (nonet, J = 6.6 Hz, 1H), 0.91 (d, J = 6.6 Hz, 6H). $^{13}C\{^{1}H\}$ NMR (100 MHz, $CDCl_3$): δ 167.1, 163.8, 123.2, 50.4, 26.8, 22.5, 20.4.

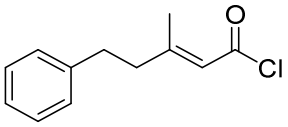

(E)-3-Methyl-5-phenylpent-2-enoic acid chloride (**2.15c**): Prepared according to the general procedure. The crude acid chloride was stored at –20 °C in a N_2 atmosphere glovebox overnight and then used without further purification the following day. Yield 1.84 g (88%) >99.5:0.5 (*E*):(*Z*) (relative GC-FID area count). ^{1}H NMR (400 MHz, $CDCl_3$): δ 7.31 (t, J = 7.5 Hz, 2H), 7.23 (t, J = 7.3 Hz, 1H), 7.17 (d, J = 6.8 Hz, 2H), 6.03 (q, J = 1.2 Hz, 1H), 2.82 (dd, J = 9.1, 6.7 Hz, 2H), 2.52 (dd, J = 9.4, 6.4 Hz, 2H), 2.18, (d, J = 1.2 Hz, 3H). $^{13}C\{^{1}H\}$ NMR (100 MHz, $CDCl_3$): δ 166.3, 164.0, 140.2, 128.8, 128.4, 126.6, 122.7, 42.7, 33.8, 20.6.

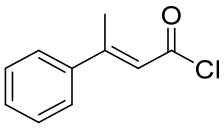

(E)-3-Phenylbut-2-enoic acid chloride (**2.15d**): Prepared according to the general procedure except 22 mL of Et_2O was necessary to dissolve the acid and addition was over 60 min. Purified by Kugelrohr distillation at 103 °C under high vacuum. Yield 1.66 g (98 %) 99:1 (*E*):(*Z*) (relative GC-FID area count). The bright yellow oil was stored at –20 °C in a N_2 atmosphere glovebox. Characterization data was in agreement with the literature.[93] ^{1}H NMR (400 MHz, $CDCl_3$): δ 7.52 (m, 2H), 7.44 (m, 3H), 6.48 (q, J = 1.2 Hz, 1H), 2.56 (d, J = 1.2 Hz, 3H). $^{13}C\{^{1}H\}$ NMR (100 MHz, $CDCl_3$): 164.2, 161.4, 140.3, 130.7, 128.9, 126.8, 122.7, 19.4.

2.4.4 Experimental details from optimization of reaction steps for flow

2.4.4.1 Acylation optimization from Table 2.3

DBU, Et_3N, DBU/DMAP and Et_3N/DMAP were screened as organic bases in small scale batch experiments with 3,3-dimethylacrylic acid chloride and camphorsultam. Low to moderate yields were obtained and precipitate formation was observed, suggesting conversion to flow may be problematic.

3,3-Dimethylacrylic acid pivalate ester could be prepared in ~80% purity by reaction of 3,3-dimethylacrylic acid and pivaloyl chloride. Isolation in higher purity was unachievable due to interconversion with the two symmetrical anhydrides during both synthesis and distillation.

3,3-Dimethylacylic acid pentafluorophenol ester was prepared by DCC coupling between 3,3-dimethylacrylic acid and pentafluorophenol. Screening of DBU, DBU/DMAP, Et_3N, Et_3N/ DMAP, morpholine, morpholine/DMAP, tetramethylguanidine, tetramethylguanidine/DMAP in a 2.00 mL tubular plug flow reactor at various temperatures exhibited low to moderate yields and substrate decomposition.

PTC with passive mixing: 0.1 M (*E*)-3-methylnon-2-enoic acid chloride with 0.001M Aliquat 336 (1 mol%)[81], 0.01 M hexadecane (istd) and 0.1 M camphorsultam in toluene were pumped at 200 µL/min and mixed in a PEEK T-mixer with 4% (w/w) NaOH pumped at either 150 or 200 µL/min and then passed through a 4.00 mL 1/16" O.D., 1.0 mm I.D. PFA coil. Yield varied with time due to poor mixing, ranging from poor to moderate as monitored by off-line GC-FID analysis.

PTC with active mixing: 0.1 M (*E*)-3-methylnon-2-enoic acid chloride with 0.001M Aliquat 336 (1 mol%), 0.01 M hexadecane (istd) and 0.1 M camphorsultam in toluene were pumped at 200 µL/min and mixed in a PEEK T-mixer with 4% NaOH with or without 4% NaCl at 150 or 200 µL/min then passed through the active mixer reactor (Figure AI.1.1). Yields were near quantitative as monitored by off-line GC analysis.

2.4.4.2 Hydrogenation in PBR from Scheme 2.51

Start-up as per the description in section 2.4.5.1 general procedures for process start-up but with only the acylation and hydrogenation stages telescoped together. 97:3 (*E*):(*Z*)-3-methylnon-2-enoic acid chloride was used as the substrate. The effluent was collected for 1 h 50 min then evaporated and the residue chromatographed (silica gel, 3:1 hexanes:Et_2O) to yield 790 mg (97%) hydrogenated product, d.r.: 90:10.

2.4.4.3 Methanolysis optimization from Table 2.4

Various phase transfer catalysts were screened in batch. The combination of 18-crown-6 and 2,5-dimethyl-2,5-hexanediol[85] with 55% (w/w) KOH $_{(aq)}$ and 0.1 M substrate in toluene was

effective but when transitioning into flow precipitate formation and slow reaction rates were problematic.

Delivering instead KOH in MeOH (30% w/w, 18 μL/min, 5 eq.) and mixing with 0.1 M substrate in toluene (200 μL/min) in a PEEK T-mixer then passing through a residence coil of either 1.0 or 2.0 mL volume of either 1/16" O.D., 1.0 mm I.D. PFA or 1/16" O.D., 0.75 mm I.D. PEEK at various temperatures led to identification of conditions (90 °C, 9 min in 2.0 mL, 0.75 mm I.D. PEEK) that achieved complete consumption of starting material but precipitate formed in the tubing resulting in variable yields and would likely lead to eventual clogging.

Delivering NaOMe instead of KOH in MeOH greatly improve the reaction rate and homogeneity. Screening the NaOMe concentration (from 25% to 7% w/w), equivalents of NaOMe (from 1.25 to 2.0 eq.), and residence coil (0.5, 1.0 or 2.0 mL volume of 1/16" O.D., 0.75 mm I.D. PEEK) led to identification of conditions (50 °C, 4.5 min in 1.0 mL, 1/16" O.D., 0.75 mm I.D. coil) that gave consistent high yields for both the methyl ester and recovered auxiliary without precipitation and could be telescoped into the full process without issues. Full details of telescoped reactions in section 2.4.5.

2.4.5 Procedure for telescoped flow synthesis of chiral materials

2.4.5.1 General procedure for process start-up

The system was assembled as described in Section 2.4.2. The packed bed reactor was heated to 45 °C and conditioned by wetting with toluene (400 μL/min) then eluting with the biphasic mixture of toluene (400 μL/min) and 0.1% acetic acid (100 μL/min) until the *p*H of the aqueous phase exiting the PBR was <2. The flow rates were then decreased to the process flow rates (200 μL/min toluene, 50 μL/min 0.1% AcOH) and the H-cube H_2 production was turned on. The packed bed was then conditioned with these parameters for 30 min while the acylation phase was reaching steady state, before the toluene feed was changed to the process feed. The resulting pressure drop over the conditioned packed bed reactor was typically ~30 bar.

The process was started consecutively in phases beginning with the acylation reaction and allowing each phase to reach steady state (discarding the first ~three residence volumes) before diverting effluent to in-line phase separators S1–S4. After filling the phase separator, the next phase was commenced. Times to steady state: acylation: 14 min; hydrogenation: 15 min;

methanolysis and acid wash: 25 min; auxiliary extraction: 10 min, plus 10 min for each in-line phase separator ≈ 2 h total for start-up. Each gravity liquid/liquid phase separator was maintained with ~1 mL of organic phase and ~0.25 mL of aqueous phase. The flow rate of pumps internal to the flow path (i.e., withdrawing from phase separators) were adjusted to maintain a constant volume in the separator (i.e., flow in = flow out for each liquid phase). Diastereoselectivity of the hydrogenation reaction was monitored off-line by withdrawing a ~25 μL aliquot from the post-hydrogenation organic phase and submitting to GC analysis every 30 min (see Appendix I, Section AI.4).

2.4.5.2 Telescoped process with auxiliary recovery

The acid chloride, auxiliary and PTC were all combined in the organic solution and 4% (w/w) NaOH, 4% (w/w) NaCl was used as the aqueous solution for the PTC acylation. No background camphorsultam sulfonimide formation in the stock solution was observed over the timeframe of the experiment (~6 h).

The acid chloride solutions were prepared by combining *(E)*-α-β-unsaturated acid chloride **2.15** (6.0 mmol), toluene (~5 mL), Aliquat 336 (24 mg, 60 μmol) and camphorsultam **2.5** (1.29 g, 6.0 mmol), then making up the solution to 60.00 mL with toluene.

After steady state was reached for the entire process, collection of the product and recovered auxiliary streams commenced. Effluents were collected for 3 h, then all pumps were stopped. The product phase effluent was evaporated and the methyl ester was purified by chromatography (20×150 mm silica; pentane→5% Et_2O in pentane eluent).

The recovered auxiliary phase effluent was acidified to *p*H<1 with conc. HCl and then extracted with 2×15 mL DCM. The combined organic extracts were dried over Na_2SO_4 and evaporated to yield the crude auxiliary. Recrystallization from hexanes gave white needles of pure camphorsultam.

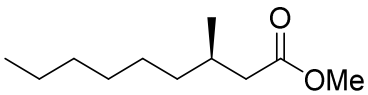

(*R*)-3-Methylnonanoic acid methyl ester (**2.149a**): Yield: 447 mg (67%). Characterization data was in agreement with the literature.[94] ^{1}H NMR (400 MHz, $CDCl_3$): δ 3.64 (s, 3H), 2.28 (dd, *J* = 14.7, 6.0 Hz, 1H), 2.08 (dd, *J* = 14.7, 8.2 Hz, 1H), 1.92 (m, 1H), 1.24 (m, 10H), 0.90 (d, *J* = 6.7

Hz, 3H), 0.86 (t, J = 6.6 Hz, 3H). $^{13}C\{^{1}H\}$ NMR (100 MHz, $CDCl_3$): δ 173.9, 51.4, 41.8, 36.8, 32.0, 30.5, 29.5, 27.0, 22.7, 19.8, 14.2. $[\alpha]_D^{20}$ = +3.8 ° (c = 1.03, CH_2Cl_2) [lit.[94] $[\alpha]_D^{25}$ = +5.9 ° (c = 4.70, $CHCl_3$)]. Crude sultam recovery: 79%; recrystallized: 410 mg, 53%. Enantiomeric ratio was taken from diastereomeric ratio data: 95 (*R*): 5 (*S*).

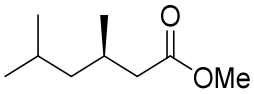

(*R*)-3,5-Dimethylhexanoic acid methyl ester (**2.149b**): Yield: 410 mg (72%). ^{1}H NMR (400 MHz, $CDCl_3$): δ 3.66 (s, 3H), 2.27 (dd, J = 14.2, 5.3 Hz, 1H), 2.08 (dd, J = 14.2, 8.3, 1H), 2.01 (octet, J = 6.2 Hz, 1H), 1.61 (nonet, J = 6.6 Hz, 1H), 1.08 (m, 2H), 0.90 (d, J = 6.4 Hz, 3H), 0.86 (t, J = 6.5 Hz, 6H). $^{13}C\{^{1}H\}$ NMR (100 MHz, $CDCl_3$): δ 173.9, 51.6, 46.4, 42.1, 28.2, 25.3, 23.3, 22.2, 19.9. $[\alpha]_D^{20}$ = +4.5 ° (c = 1.05, CH_2Cl_2). Accurate mass *m/z* = 158.1268, spectral accuracy 98%, calc: 158.1301. Crude sultam recovery: 71%; recrystallized: 420 mg, 54%. Enantiomeric ratio was taken from diastereomeric ratio data: 98 (*R*): 2 (*S*).

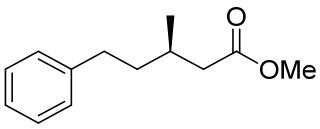

(*R*)-3-Methyl-5-phenlybutanoic acid methyl ester (**2.149c**): Yield: 528 mg (71%). Characterization data was in agreement with literature.[95] ^{1}H NMR (400 MHz, $CDCl_3$): δ 7.28 (m, 2H), 7.18 (m, 3H), 3.67 (s, 3H), 2.62 (m, 2H), 2.36 (dd, J = 14.7, 6.0 Hz, 1H), 2.18 (dd, J = 14.8, 8.0 Hz, 1H), 2.02 (oct, J = 6.5 Hz, 1H), 1.67 (m, 1H), 1.53 (m, 1H), 1.01 (d, 6.6 Hz, 3H). $^{13}C\{^{1}H\}$ NMR (100 MHz, $CDCl_3$): δ 173.6, 142.4, 128.45, 128.42, 125.8, 51.5, 41.6, 38.6, 33.4, 30.2, 19.8. $[\alpha]_D^{20}$ = +14.7 ° (c = 1.05, CH_2Cl_2) [lit.[96] $[\alpha]_D^{25}$ = +18.5 ° (c = 0.88, CH_2Cl_2)]. Enantiomeric ratio was confirmed by chiral HPLC using a 30 cm Chiralcel OD-H column, 0.5 mL/min 99.7% hexanes/0.3% *i*-PrOH, retention times 49.3 min (minor) and 60.3 min (major):[95] 93.4 (*R*): 6.6 (*S*); in agreement with diastereomeric ratio data (93:7). Crude sultam recovery: 73%; recrystallized: 435 mg, 56%.

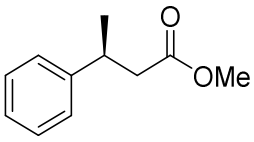

(*S*)-3-Phenylbutanoic acid methyl ester (**2.149d**): Yield: 431 mg (67%). Characterization data was in agreement with literature.[97] ^{1}H NMR (400 MHz, $CDCl_3$): δ 7.31 (m, 2H), 7.21 (m, 3H), 3.63 (s, 3H), 3.29 (hextet, J = 7.3 Hz, 1H), 2.60 (ABX pattern, J = 15.2, 8.2, 6.9 Hz, 2H), 1.3 (d, J = 7.6 Hz, 3H). ^{13}C{^{1}H} NMR (100 MHz, $CDCl_3$): δ 172.9, 145.8, 128.6, 126.8, 126.5, 51.6, 42.8, 36.5, 21.9. $[\alpha]_D^{20}$ = +23.5 ° (c = 0.99, CH_2Cl_2) [lit.[97] $[\alpha]_D^{20}$ = +7.3 ° (c = 1.36, $CHCl_3$, ee = 44%)]. Crude sultam recovery: 72%; recrystallized: 358 mg, 46%. Enantiomeric ratio was taken from diastereomeric ratio data: 92 (*S*): 8 (*R*).

2.4.5.3 Telescoped process with auxiliary recycling

For auxiliary recycle experiments the acid chloride, 35% auxiliary make up and PTC were combined in the organic solution and the other 65% of auxiliary was dissolved in a solution of 4% NaOH, 4% NaCl used for the acylation during start-up.

The acid chloride solutions were prepared by combining *(E)*-α-β-unsaturated acid chloride **2.15** (7.5 mmol), toluene (~5 mL), Aliquat 336 (30 mg, 75 μmol) and camphorsultam **2.5** (0.56 g, 2.6 mmol), then making up the solution to 75.00 mL with toluene.

The auxiliary in 4% NaOH, 4% NaCl solution used for start-up was prepared by taking camphorsultam **2.5** (0.46 g, 2.2 mmol) and making up to 25.00 mL with 4% NaOH, 4% NaCl.

After steady state was reached for the entire process as in the single pass experiments, collection of the product stream was commenced and the recovered auxiliary stream was connected to the acylation phase, completing the recycle loop. Product containing effluent was collected for 4.5 h, then all pumps were stopped. The effluent was evaporated and the methyl ester purified by chromatography (20×150 mm silica, pentane→5% Et_2O in pentane eluent).

(*R*)-3-Methylnonanoic acid methyl ester (**2.149a**): Yield: 548 mg (54%), contaminated with ~33 mg (6% by mass) rac-3-methylnonanal impurity. The aldehyde impurity was removed by treating the product with Brady's reagent (2,4-dinitrophenylhydrazine, 100 mg, 0.5 mmol) in MeOH (10 mL) with 1 drop H_2SO_4 at 40 °C for 20 min and then separation of the formed hydrazone from the methyl ester by chromatography (20 × 150 mm silica gel column, pentane→5% Et_2O in pentane

eluent) giving the methyl ester as a pale yellow oil. Kugelrohr distillation at 80 °C, high vacuum yielded the pure methyl ester product as a colourless oil, 444 mg (44%). Enantiomeric ratio taken from diastereomeric ratio data: 95 (*R*): 5 (*S*).

(*R*)-3,5-Dimethylhexanoic acid methyl ester (**2.149b**): Yield: 411 mg (48%). Enantiomeric ratio taken from diastereomeric ratio data: 98 (*R*): 2 (*S*).

(*R*)-3-Methyl-5-phenlybutanoic acid methyl ester (**2.149c**): Yield: 640 mg (57%). Enantiomeric ratio taken from diastereomeric ratio data: 95 (*R*): 5 (*S*).

(*S*)-3-Phenylbutanoic acid methyl ester (2.149d): Yield: 658 mg (68%). Enantiomeric ratio taken from diastereomeric ratio data: 90 (*S*): 10 (*R*).

2.5 References

[1] a) Brill, Z. G.; Condakes, M. L.; Ting, C. P.; Maimone, T. J. Navigating the chiral pool in the total synthesis of complex terpene natural products. *Chem. Rev.* **2017**, *117*, 11753−11795; b) Dalpozzo, R. The chiral pool in the Pictet–Spengler reaction for the synthesis of β-carbolines. *Molecules* **2016**, *21*, 699−716; c) Casiraghi, G.; Zanardi, F.; Rassu, G.; Spanu, P. Stereoselective approaches to bioactive carbohydrates and alkaloids — With a focus on recent syntheses drawing from the chiral pool. *Chem. Rev.* **1995**, *95*, 1677−1716.

[2] a) Fujieda, H.; Maeda, K.; Kato, N. Efficient and scalable synthesis of glucokinase activator with a chiral thiophenyl-pyrrolidine scaffold. *Org. Process Res. Dev.* **2019**, *23*, 69−77. b) Anderson, K. R.; Atkinson, S. L. G.; Fujiwara, T.; Giles, M. E.; Matsumoto, T.; Merifield, E.; Singleton, J. T.; Saito, T.; Sotoguchi, T.; Tornos, J. A.; Way, E. L. Routes for the synthesis of (2S)-2-methyltetrahydropyran-4-one from simple optically pure building blocks. *Org. Process Res. Dev.* **2010**, *14*, 58−71.

[3] a) Farina, V.; Reeves, J. T.; Senanayake, C. H.; Song, J. J. Asymmetric synthesis of active pharmaceutical ingredients. *Chem. Rev.*, **2006**, *106*, 2734−2793; b) Gnas, Y.; Glorius, F. Chiral auxiliaries — Principles and recent applications. *Synthesis*, **2006**, 1899−1930.

[4] a) Roth, G. P.; Landi, J. J.; Salvagno, A. M.; Müller-Bötticher, H. Optimization and Scale-Up of an Asymmetric Route to the LTB4 Inhibitor Ontazolast. *Org. Process Res. Dev.* **1997**, *1*, 331−338; b) Reichard, G. A.; Spitler, J.; Mergelsberg, I.; Miller, A.; Wong, G.; Raghavan, R.; Jenkins, J.; Gan, T.; McPhail, A. T. The asymmetric synthesis of (3R)-N-methyl-2-oxo-[1,4′-bipiperidine]-3-acetamide in

quantity. *Tetrahedron: Asymmetry* **2002**, *13*, 939–943; c) Loiseleur, O.; Koch, G.; Wagner, T. A practical building block for the synthesis of discodermolide. *Org. Process Res. Dev.* **2004**, *8*, 597–602; d) Song, J. J.; Xu, J.; Tan, Z.; Reeves, J. T.; Grinberg, N.; Lee, H.; Kuzmich, K.; Feng, X.; Yee, N. K.; Senanayake, C. H. Development of an Asymmetric Acetate Aldol Reaction with a Trifluoromethyl Ketone. *Org. Process Res. Dev.* **2007**, *11*, 534–538; e) Li, B.-F.; Hughes, R. M.; Le, J.; McGee, K.; Gallagher, D. J.; Gross, R. S.; Provencal, D.; Reddy, J. P.; Wang, P.; Zegelman, L.; Zhao, Y.; Zook, S. E. Efficient Synthesis of (2S,3S)-2-Ethyl-3-methylvaleramide Using (1S,2S)-Pseudoephedrine as a Chiral Auxiliary. *Org. Process Res. Dev.* **2009**, *13*, 463-467; f) Chang, S.; Halperin, S.; Moore, J.; Britton, R. Principles, concepts and strategies of stereoselective synthesis. In *Stereoselective Synthesis of Drugs and Natural Products*. Andrushko, V.; Andrushko, N. Eds.; Wiley: Hoboken, 2013, p 3–44.

[5] a) Mickel, S. J.; Sedelmeier, G. H.; Niederer, D.; Daeffler, R.; Osmani, A.; Schreiner, K.; Seeger-Weibel, M.; Bérod, B.; Schaer, K.; Gamboni, R.; Chen, S.; Chen, W.; Jagoe, C. T.; Kinder, F. R.; Loo, M.; Prasad, K.; Repič, O.; Shieh, W.-C.; Wang, R.-M.; Waykole, L.; Xu, D. D.; Xue, S. Large-scale synthesis of the anti-cancer marine natural product (+)-Discodermolide. Part 1: Synthetic strategy and preparation of a common precursor. *Org. Process Res. Dev.* **2004**, *8*, 92–100; b) Mickel, S. J.; Sedelmeier, G. H.; Niederer, D.; Schuerch, F.; Koch, G.; Kuesters, E.; Daeffler, R.; Osmani, A.; Seeger-Weibel, M.; Schmid, E.; Hirni, A.; Schaer, K.; Gamboni, R.; Bach, A.; Chen, S.; Chen, W.; Geng, P.; Jagoe, C. T.; Kinder, F. R.; Lee, G. T.; McKenna, J.; Ramsey, T. M.; Repič, O.; Rogers, L.; Shieh, W.-C.; Wang, R.-M.; Waykole, L. Large-scale synthesis of the anti-cancer marine natural product (+)-Discodermolide. Part 3: Synthesis of fragment c15-21. *Org. Process Res. Dev.* **2004**, *8*, 107–112.

[6] a) Knowles, W. S.; Sabacky, M. J. Catalytic asymmetric hydrogenation employing a soluble, optically active, rhodium complex. *Chem. Commun. (London)* **1968**, 1445-1446; b) Knowles, W. S.; Sabacky, M. J.; Vineyard, B. D. L-Dopa and intermediates. US Patent 4005127A, 1977.

[7] a) Oppolzer, W. Camphor derivatives as chiral auxiliaries in asymmetric synthesis. *Tetrahedron* **1987**, *43*, 1969–2004; b) Kim, B. H.; Curran, D. P. Asymmetric thermal reactions with Oppolzer's camphor sultam. *Tetrahedron* **1993**, *49*, 293–318; c) Heravi, M. M.; Zadsirjan, V. Recent advances in the application of the Oppolzer camphorsultam as a chiral auxiliary. *Tetrahedron: Asymmetry* **2014**, *25*, 1061–1090.

[8] a) Oppolzer, W.; Lienard, P. Non-destructive cleavage of N-acylsultams under neutral conditions: Preparation of enantiomerically, pure fmoc-protected α-amino acids. *Helv. Chim. Acta* **1992**, *75*, 2572–2582; b) Miyata, O.; Fujiwara, Y.; Nishiguchi, A.; Honda, H.; Shinada, T.; Ninomiya, I.; Naito, T. An efficient method for removal of chiral auxiliaries, camphorsultam and 4-isopropyl-2-oxazolidinone.

Synlett **1994**, *1994*, 637–638; c) Oppolzer, W.; Darcel, C.; Rochet, P.; Rosset, S.; De Brabander, J. Non-destructive removal of the bornanesultam auxiliary in α-substituted *N*-acylbornane-10,2-sultanis under mild conditions: An efficient synthesis of enantiomerically pure ketones and aldehydes. *Helv. Chim. Acta* **1997**, *80*, 1319–1337; d) Hasegawa, T.; Yamamoto, H. A practical removal method of camphorsultam. *Synlett* **1998**, *1998*, 882–884.

[9] For example, Evan's oxazolidinones often suffer destruction during cleavage, but specific $NaBH_4$ reduction conditions have been developed to facilitate auxiliary recovery, for a review see: Heravi, M. M.; Zadsirjan, V.; Farajpour, B. Applications of oxazolidinones as chiral auxiliaries in the asymmetric alkylation reaction applied to total synthesis. *RSC Adv.* **2016**, *6*, 30498–30551.

[10] a) Chang, H.; Zhou, L.; McCargar, R. D.; Mahmud, T.; Hirst, I. A convenient practical method for the preparation of (−)-(1S,2S)-5-norbornene-2-carboxylic acid, incorporating efficient recovery of the chiral auxiliary D-pantolactone. *Org. Process Res. Dev.* **1999**, *3*, 289–291; b) Gibson, F. S.; Singh, A. K.; Soumeillant, M. C.; Manchand, P. S.; Humora, M.; Kronenthal, D. R. A practical synthesis of L-valyl-pyrrolidine-(2R)-boronic acid: Efficient recycling of the costly chiral auxiliary (+)-pinanediol. *Org. Process Res. Dev.* **2002**, *6*, 814–816.

[11] a) Oppolzer, W.; Moretti, R.; Thomi, S. Asymmetric alkylation of *N*-acylsultams: A general route to enantiomerically pure, crystalline C(α,α)-disubstituted carboxylic acid derivatives. *Tetrahedron Lett.* **1989**, *30*, 5603–5606.

[12] Hasegawa, T.; Kawanaka, T.; Kasamatsu, E.; Iguchi, Y.; Yonekawa, Y.; Okamoto, M.; Ohta, C.; Hashimoto, S.; Ohuchida, S. Process development of ONO-2506: A therapeutic agent for stroke and Alzheimer's disease. *Org. Process Res. Dev.* **2003**, *7*, 168–171.

[13] a) Batchelor, M. J.; Gillespie, R. J.; Golec, J. M. C.; Hedgecock, C. J. R.; Jones, S. D.; Murdoch, R. Total syntheses of close analogues of the immunosuppressant FK506. *Tetrahedron* **1994**, *50*, 809–826; b) Oppolzer, W.; Rosset, S.; De Brabander, J. Asymmetric synthesis of ibuprofen via diastereoselective alkylation of a homochiral N-acylbornanesultam. *Tetrahedron Lett.* **1997**, *38*, 1539–1540; c) Nicolaou, K. C.; He, Y.; Vourloumis, D.; Vallberg, H.; Roschangar, F.; Sarabia, F.; Ninkovic, S.; Yang, Z.; Trujillo, J. I. The olefin metathesis approach to epothilone A and its analogues. *J. Am. Chem. Soc.* **1997**, *119*, 7960–7973; d) Bijoy, P.; Avery, M. A. Synthetic studies directed towards epothilone A: Enantioselective synthesis of a C7 - C15 carboxaldehyde segment. *Tetrahedron Lett.* **1998**, *39*, 209–212; e) Brundish, D.; Bull, A.; Donovan, V.; Fullerton, J. D.; Garman, S. M.; Hayler, J. F.; Janus, D.; Kane, P. D.; McDonnell, M.; Smith, G. P.; Wakeford, R.; Walker, C. V.; Howarth, G.; Hoyle, W.; Allen, M. C.; Ambler, J.; Butler,

K.; Talbot, M. D. Design and synthesis of thrombin inhibitors: Analogues of MD-805 with reduced stereogenicity and improved potency. *J. Med. Chem.* **1999**, *42*, 4584–4603; f) Mori, K.; Tashiro, T.; Sano, S. Enantioselective synthesis of (1S,3S,7R)-3-methyl-α-himachalene, the sex pheromone of the sandfly Lutzomyia longipalpis from Jacobina, Brazil. *Tetrahedron Lett.* **2000**, *41*, 5243–5247; g) Alvarez-Ibarra, C.; Csákÿ, A. G.; Gómez de la Oliva, C.; Rodríguez, E. Conformationally restricted glutamic acid derivatives: asymmetric synthesis of 4-substituted 4,5-dihydro-3(2H)-pyridazinones. *Tetrahedron Lett.* **2001**, *42*, 2129-2131; h) Fürstner, A.; Mathes, C.; Grela, K. Concise total syntheses of epothilone A and C based on alkyne metathesis. *Chem. Commun.* **2001**, 1057–1059; i) Hindupur, R. M.; Panicker, B.; Valluri, M.; Avery, M. A. Total synthesis of epothilone A. *Tetrahedron Lett.* **2001**, *42*, 7341–7344; j) Fürstner, A.; Mathes, C.; Lehmann, C. W. Alkyne metathesis: Development of a novel molybdenum-based catalyst system and its application to the total synthesis of epothilone A and C. *Chem. Eur. J.* **2001**, *7*, 5299–5317; k) Boulet, S. L.; Paquette, L. A. Toward a total synthesis of Okilactomycin. 2. A metathesis-based approach to the heavily functionalized cyclohexane ring. *Synthesis* **2002**, *2002*, 0895–0900; l) Liu, J.; Yang, Y.; Ji, R. An effective and convenient method for the preparation of KAD-1229. *Helv. Chim. Acta* **2004**, *87*, 1935–1939; m) Jung, J.-C.; Kache, R.; Vines, K. K.; Zheng, Y.-S.; Bijoy, P.; Valluri, M.; Avery, M. A. Total syntheses of Epothilones B and D. *J. Org. Chem.* **2004**, *69*, 9269–9284; n) Cossy, J.; Tsuchiya, T.; Reymond, S.; Kreuzer, T.; Colobert, F.; Markó, I. E. Convergent synthesis of the C18-C30 fragment of Amphidinol 3. *Synlett* **2009**, *2009*, 2706–2710; o) Yamaki, Y.; Shigenaga, A.; Li, J.; Shimohigashi, Y.; Otaka, A. Synthesis of amide-type fluoroalkene dipeptide isosteres by an intramolecular redox reaction. *J. Org. Chem.* **2009**, *74*, 3278–3285; p) Manaviazar, S.; Hale, K. J.; LeFranc, A. Enantioselective formal total synthesis of the Dendrobatidae frog toxin, (+)-pumiliotoxin B, via O-directed alkyne free radical hydrostannation. *Tetrahedron Lett.* **2011**, *52*, 2080–2084; q) Shklyaruck, D.; Matiushenkov, E. Stereoselective synthesis of (3S,5S,6S)-tetrahydro-6-isopropyl-3,5-dimethylpyran-2-one; a C5-epimer of a component of a natural sex pheromone of the wasp *Macrocentrus grandii*, the larval parasitoid of the European corn borer *Ostrinia nubilalis*. *Tetrahedron-Asymmetry* **2011**, *22*, 1448–1454; r) Lu, W.-C.; Cao, X.-F.; Hu, M.; Li, F.; Yu, G.-A.; Liu, S.-H. A highly enantioselective access to chiral 1-(beta-arylalkyl)-1H-1,2,4-triazole derivatives as potential agricultural bactericides. *Chemistry & Biodiversity* **2011**, *8*, 1497–1511; s) Yang, X.-d.; Dong, C.-m.; Chen, J.; Ding, Y.-h.; Liu, Q.; Ma, X.-y.; Zhang, Q.; Chen, Y. Total synthesis of Tubulysin U and Its C-4 epimer. *Chem. Asian J.* **2013**, *8*, 1213–1222; t) Cooksey, J. P. Synthesis of a C1–C11 fragment of Zincophorin using planar chiral, neutral π-allyl iron complexes. *Org. Biomol. Chem.* **2013**, *11*, 5117–5126; u) Rival, N.; Hanquet, G.; Bensoussan, C.; Reymond, S.; Cossy, J.;

Colobert, F. Diastereoselective synthesis of the C14–C29 fragment of amphidinol 3. *Org. Biomol. Chem.* **2013**, *11*, 6829−6840; v) Raghavan, S.; Samanta, P. K. Stereoselective synthesis of the C3–C12 subunit of laulimalide. *Tetrahedron Lett.* **2014**, *55*, 913−915; w) Marx, L. B.; Burton, J. W. A total synthesis of Salinosporamide A. *Chem. Eur. J.* **2018**, *24*, 6747−6754; x) Lindner, F.; Friedrich, S.; Hahn, F. Total synthesis of complex biosynthetic late-stage intermediates and bioconversion by a tailoring enzyme from Jerangolid biosynthesis. *J. Org. Chem.* **2018**, *83*, 14091−14101.

[14] a) Oppolzer, W.; Moretti, R.; Thomi, S. Asymmetric alkylations of a sultam-derived glycinate equivalent: Practical preparation of enantiomerically pure α-amino acids. *Tetrahedron Lett.* **1989**, *30*, 6009-6010; b) Josien, H.; Chassaing, G. Asymmetric synthesis of the diastereoisomers of L-1-indanylglycine and L-1-benz[f]indanylglycine, χ1,χ2-constrained side-chain derivatives of L-phenylalanine and L-2-naphthylalanine. *Tetrahedron: Asymmetry* **1992**, *3*, 1351−1354; c) Oppolzer, W.; Moretti, R.; Zhou, C. Y. Asymmetric alkylations of a Sultam-derived glycine equivalent — Practical preparation of enantiomerically pure alpha-amino-acids. *Helv. Chim. Acta* **1994**, *77*, 2363–2380; d) Lankiewicz, L.; Nyassé, B.; Fransson, B.; Grehn, L.; Ragnarsson, U. Synthesis of amino acid derivatives substituted in the backbone with stable isotopes for application in peptide synthesis. *J. Chem. Soc., Perkin Trans. 1* **1994**, 2503−2510; e) Liu, W.-Q.; Roques, B. P.; Garbay-Jaureguiberry, C. Enantioselective synthesis of *N*-fmoc protected di-tert-butyl 4-phosphonomethyl-L-phenylalanine: A hydrolytically stable analogue of O-phosphotyrosine. *Tetrahedron: Asymmetry* **1995**, *6*, 647−650; f) Voigt, K.; Stolle, A.; Salaün, J.; Meijere, A. d. Enantiopure α-allyl-α-amino acids by Pd-catalyzed allylation of a camphorsultam modified glycine equivalent. *Synlett* **1995**, *1995*, 226–228; g) Ayoub, M.; Chassaing, G.; Loffet, A.; Lavielle, S. Diastereoselective alkylation of sultam-derived amino acid aldimines preparation of Cα-methylated amino acids. *Tetrahedron Lett.* **1995**, *36*, 4069–4072; h) Sjöberg, S.; Hawthorne, M. F.; Wilmouth, S.; Lindström, P. Asymmetric synthesis of carboranyl amino acids with potential use in BNCT. *Chem. Eur. J.* **1995**, *1*, 430−435; i) Martin, A.; Chassaing, G.; Vanhove, A. Stereoselective synthesis of L-[1-13C], L-[2-13C] and L-[15N] amino acids. *Isot. Environ. Health S.* **1996**, *32*, 15−19; j) Elemes, Y.; Ragnarsson, U. Synthesis of enantiopure α-deuteriated boc-L-amino acids. *J. Chem. Soc., Perkin Trans. 1* **1996**, 537−540; k) Warshawsky, A. M.; Flynn, G. A.; Koehl, J. R.; Mehdi, S.; Vaz, R. J. The synthesis of aminobenzazepinones as anti-phenylalanine dipeptide mimics and their use in nep inhibition. *Bioorg. Med. Chem. Lett.* **1996**, *6*, 957−962; l) Blommaert, A. G. S.; Dhôtel, H.; Ducos, B.; Durieux, C.; Goudreau, N.; Bado, A.; Garbay, C.; Roques, B. P. Structure-based design of new constrained cyclic agonists of the cholecystokinin CCK-B receptor. *J. Med. Chem.* **1997**, *40*, 647−658; m) Dong, C. Z.; Rocquigny, H.;

RÉMy, E.; Mellac, S.; FourniÉ-Zaluski, M. C.; Roques, B. P. Synthesis and biological activities of fluorescent acridine-containing HIV-1 nucleocapsid proteins for investigation of nucleic acid-NCp7 interactions. *J. Pept. Res.* **1997**, *50*, 269–278; n) Bennett, F. A.; Barlow, D. J.; Dodoo, A. N. O.; Hider, R. C.; Lansley, A. B.; Lawrence, M. J.; Marriott, C.; Bansal, S. S. L-(6,7-dimethoxy-4-coumaryl) alanine: An intrinsic probe for the labelling of peptides. *Tetrahedron Lett.* **1997**, *38*, 7449–7452; o) Liu, W.-Q.; Roques, B. P.; Garbay, C. Synthesis of L-2,3,5,6-tetrafluoro-4-(phosphonomethyl) phenylalanine, a novel non-hydrolyzable phosphotyrosine mimetic and L-4-(phosphonodifluoromethyl)phenylalanine. *Tetrahedron Lett.* **1997**, *38*, 1389–1392; p) López, A.; Pleixats, R. Highly diastereoselective monoalkylation and Michael addition of *N*-(diphenylmethylene)glycinesultam under solid–liquid phase-transfer catalysis conditions using potassium carbonate as base. *Tetrahedron: Asymmetry* **1998**, *9*, 1967–1977; q) Karoyan, P.; Sagan, S.; Clodic, G.; Lavielle, S.; Chassaing, G. Asymmetric synthesis of boc-N-methyl-p-benzoyl-phenylalanine. Preparation of a photoreactive antagonist of Substance P. *Bioorg. Med. Chem. Lett.* **1998**, *8*, 1369–1374; r) Lodwig, S. N.; Unkefer, C. J. Stereoselective synthesis of stable isotope-labeled L-α-amino acids: Enantioselective synthesis of 13C-, 15N-labeled L-proline using Oppolzer's glycine template. *J. Labelled Compd. Radiopharm.* **1998**, *41*, 983–991; s) Koltai, E.; Alexin, A.; Rutkai, G.; Tóth-sarudy, É. Synthesis of optically pure (D)-phenyl[3-14C]alanine. *J. Labelled Compd. Radiopharm.* **1998**, *41*, 977–982; t) Bennett, F. A.; Barlow, D. J.; Dodoo, A. N. O.; Hider, R. C.; Lansley, A. B.; Lawrence, M. J.; Marriott, C.; Bansal, S. S. Synthesis and properties of (6,7-dimethoxy-4-coumaryl)alanine: A fluorescent peptide label. *Anal. Biochem.* **1999**, *270*, 15–23; u) Isaac, M.; Slassi, A.; Da Silva, K.; Xin, T. Synthesis of chiral and geometrically defined 5,5-diaryl-2-amino-4-pentenoates: novel amino acid derivatives. *Tetrahedron Lett.* **2001**, *42*, 2957–2960; v)Deng, W.-P.; Wong, K. A.; Kirk, K. Convenient syntheses of 2-, 5- and 6-fluoro- and 2,6-difluoro-L-DOPA. *Tetrahedron: Asymmetry* **2002**, *13*, 1135–1140; w) Dourlat, J.; Valentin, B.; Liu, W.-Q.; Garbay, C. New syntheses of tetrazolylmethylphenylalanine and O-malonyltyrosine as pTyr mimetics for the design of STAT3 dimerization inhibitors. *Bioorg. Med. Chem. Lett.* **2007**, *17*, 3943–3946.

[15] a) Oppolzer, W.; Blagg, J.; Rodriguez, I.; Walther, E. Bornane sultam-directed asymmetric synthesis of crystalline, enantiomerically pure syn aldols. *J. Am. Chem. Soc.* **1990**, *112*, 2767–2772; b) Oppolzer, W.; Starkemann, C.; Rodriguez, I.; Bernardinelli, G. Enantiomerically pure, crystalline 'anti'-aldols from N-acylbornanesultams: aldolization and structure of intermediate t-butyldimethylsilyl-N,O-ketene acetal. *Tetrahedron Lett.* **1991**, *32*, 61–64; c) Oppolzer, W.; Lienard, P. Efficient asymmetric synthesis of anti-aldols from bornanesultam derived boryl enolates. *Tetrahedron Lett.* **1993**, *34*, 4321–4324; d) Iseki, K.;

Oishi, S.; Kobayashi, Y. Diastereo-face selectivity in the aldol reaction of boryl enolate derived from Oppolzer's sultam. *Chem. Pharm. Bull.* **1996**, *44*, 2003–2008; e) Bond, S.; Perlmutter, P. *N*-Acetylbornane-10,2-sultam: A useful, enantiomerically pure acetate synthon for asymmetric aldol reactions. *J. Org. Chem.* **1997**, *62*, 6397–6400; f) Fraser, B. H.; Gelman, D. M.; Perlmutter, P.; Vounatsos, F. Diethylboron triflate-promoted anti aldol additions of Oppolzer's sultam. *Tetrahedron: Asymmetry* **2006**, *17*, 1152–1155.

[16] a) Oppolzer, W.; De Brabander, J.; Walther, E.; Bernardinelli, G. Asymmetric synthesis of (−)-denticulatins A and B via group-selective aldolization of a meso dialdehyde with a chiral N-propionylsultam. *Tetrahedron Lett.* **1995**, *36*, 4413–4416; b) Oppolzer, W.; Walther, E.; Balado, C. P.; Brabander, J. D. Enantioselective synthesis of the Prelog-Djerassi lactonic acid via group-selective aldolization/desymmetrization of a meso dialdehyde with a chiral N-propionylsultam. *Tetrahedron Lett.* **1997**, *38*, 809–812; c) De Brabander, J.; Rosset, S.; Bernardinelli, G. Towards a Synthesis of Epothilone A: Rapid Assembly of the C1-C6 and C7-C12 Fragments. *Synlett* **1997**, *1997*, 824–826; d) Fraser, B.; Perlmutter, P. A nucleophilic addition ring closure [NARC]-based synthesis of (+)-nonactic acid. *J. Chem.Soc., Perkin Trans. 1* **2002**, 2896–2899; e) Nguyen, G.; Perlmutter, P.; Rose, M. L.; Vounatsos, F. A new nucleophilic addition/ring-closure sequence. Enantioselective synthesis of 3-deoxy-8-oxatropanes. *Org. Lett.* **2004**, *6*, 893–895; f) Archibald, S. C.; Barden, D. J.; Bazin, J. F. Y.; Fleming, I.; Foster, C. F.; Mandal, A. K.; Mandal, A. K.; Parker, D.; Takaki, K.; Ware, A. C.; Williams, A. R. B.; Zwicky, A. B. Stereocontrol in organic synthesis using silicon-containing compounds. Studies directed towards the synthesis of ebelactone A. *Org. Biomol. Chem.* **2004**, *2*, 1051–1064; g) García-Fortanet, J.; Murga, J.; Carda, M.; Marco, J. A. stereoselective synthesis of the cytotoxic macrolide FD-891. *Org. Lett.* **2006**, *8*, 2695–2698; h) Nishii, T.; Inai, M.; Kaku, H.; Horikawa, M.; Tsunoda, T. A practical total synthesis of (+)-Antimycin A9. *J. Antibiot.* **2007**, *60*, 65–72; i) García-Fortanet, J.; Murga, J.; Carda, M.; Marco, J. A.; Matesanz, R.; Díaz, J. F.; Barasoain, I. The total synthesis and biological properties of the cytotoxic macrolide FD-891 and its non-natural (Z)-C12 isomer. *Chem. Eur. J.* **2007**, *13*, 5060–5074; j) Ciampini, M.; Perlmutter, P.; Watson, K. Enantioselective synthesis of a potential key intermediate for the total synthesis of fumagillin. *Tetrahedron: Asymmetry* **2007**, *18*, 243–250; k) Prabhakar, P.; Rajaram, S.; Venkateswarlu, Y. Asymmetric synthesis of a sex pheromone (3S,5R,6S)-3,5-dimethyl-6-isopropyl-3,4,5,6-tetrahydropyran-2-one. *Tetrahedron: Asymmetry* **2009**, *20*, 1806–1808; l) Inai, M.; Nishii, T.; Tanaka, A.; Kaku, H.; Horikawa, M.; Tsunoda, T. Total synthesis of the (+)-Antimycin A family. *Eur. J. Org. Chem.* **2011**, *2011*, 2719–2729; m) Prabhakar, P.; Ramesh, D.; Rajaram, S.; Reddy, D. K.;

Venkateswarlu, Y. Asymmetric synthesis of Simplactones A and B. *Helv. Chim. Acta* **2011**, *94*, 1481−1487; n) Srihari, P.; Hari Krishna, N.; Sridhar, Y.; Krishnam Raju, A.; Kamal, A. An expedient total synthesis of Mupirocin H. *RSC Adv.* **2014**, *4*, 37629−37636; o) Li, M.; Han, P.; Mao, Z.-Y.; Zhou, W.; Si, C.-M.; Xiong, J.; Wei, B.-G.; Hu, J.-F. Studies toward asymmetric synthesis of hoiamides A and B. *Tetrahedron Lett.* **2016**, *57*, 5620−5623; p) Tian, Y.; Wang, J.; Liu, W.; Yuan, X.; Tang, Y.; Li, J.; Chen, Y.; Zhang, W. Stereodivergent total synthesis of Br-nannocystins underpinning the polyketide (10R,11S) configuration as a key determinant of potency. *J. Mol. Struct.* **2019**, *1181*, 568−578.

[17] Csuk, R.; Schröder, C.; Hutter, S.; Mohr, K. Enantioselective Dreiding-Schmidt reactions: Asymmetric synthesis and analysis of α-methylene-γ-butyrolactones. *Tetrahedron: Asymmetry* **1997**, *8*, 1411−1429.

[18] a) Oppolzer, W.; Tamura, O. Asymmetric synthesis of α-amino acids and α-*N*-hydroxyamino acids via electrophilic amination of bornanesultam-derived enolates with 1-chloro-1-nitrosocyclohexane. *Tetrahedron Lett.* **1990**, *31*, 991−994; b) Oppolzer, W.; Tamura, O.; Deerberg, J. Asymmetric synthesis of α-amino acids and α-*N*-hydroxyamino acids from *N*-acylbornane-10,2-sultams: 1-Chloro-1-nitrosocyclohexane as a practical [NH_2^+] equivalent. *Helv. Chim. Acta* **1992**, *75*, 1965−1978; c) Oppolzer, W.; Merifield, E. Synthesis of (−)-Pinidine via asymmetric, electrophilic enolate hydroxyamination/nitrone reduction. *Helv. Chim. Acta* **1993**, *76*, 957−962; d) Trojnar, J.; Chmielewski, M. Practical synthesis of (+)-Alloisoleucine. *Synth. Commun.* **2000**, *30*, 2245−2252.

[19] Zhang, L.; Zhu, L.; Yang, J.; Luo, J.; Hong, R. Stereoselective α-hydroxylation of amides using Oppolzer's sultam as chiral auxiliary. *J. Org. Chem.* **2016**, *81*, 3890−3900.

[20] a) Sweeney, J. B.; Cantrill, A. A.; McLaren, A. B.; Thobhani, S. Asymmetric aziridine synthesis by aza-Darzens reaction of N-diphenylphosphinylimines with chiral enolates. Part 1: Formation of cis-aziridines. *Tetrahedron* **2006**, *62*, 3681−3693; b) Sweeney, J. B.; Cantrill, A. A.; Drew, M. G. B.; McLaren, A. B.; Thobhani, S. Asymmetric aziridine synthesis by aza-Darzens reaction of N-diphenylphosphinylimines with chiral enolates. Part 2: Inversion of diastereoselectivity. *Tetrahedron* **2006**, *62*, 3694−3703.

[21] a) Kiegiel, K.; Jurczak, J. Diastereoselective addition of allylic reagents to chiral α-ketoimides derived from Oppolzer's sultam. *Tetrahedron Lett.* **1999**, *40*, 1009−1012; b) Kulkarni, N. A.; Wang, S.-G.; Lee, L.-C.; Tsai, H. R.; Venkatesham, U.; Chen, K. Highly diastereoselective allylation and reduction of chiral camphor-derived α-ketoamides. *Tetrahedron: Asymmetry* **2006**, *17*, 336−346; c) Shin, J. A.; Cha, J.

H.; Pae, A. N.; Choi, K. I.; Koh, H. Y.; Kang, H.-Y.; Cho, Y. S. Indium-mediated diastereoselective allylation reactions: preparation of tert-α-hydroxy acids. *Tetrahedron Lett.* **2001**, *42*, 5489–5492.

[22] Kulesza, A.; Mieczkowski, A.; Romański, J.; Jurczak, J. Asymmetric addition of titanium and sodium alkoxides to chiral imines. *Tetrahedron: Asymmetry* **2003**, *14*, 1161–1166.

[23] a) Kudyba, I.; Raczko, J.; Jurczak, J. Highly diastereoselective nitroaldol reactions with chiral derivatives of glyoxylic acid. *Tetrahedron Lett.* **2003**, *44*, 8681–8683; b) Kudyba, I.; Raczko, J.; Urbańczyk-Lipkowska, Z.; Jurczak, J. Highly diastereoselective Henry reaction of nitro compounds with chiral derivatives of glyoxylic acid. *Tetrahedron* **2004**, *60*, 4807–4820.

[24] Bauer, T.; Gajewiak, J. Diastereoselective synthesis of 2-alkoxy-5-tert-butylmandelic acid. *Synthesis* **2004**, *2004*, 20–22.

[25] a) Ward, R. S.; Pelter, A.; Goubet, D.; Pritchard, M. C. Diastereoselective synthesis of α-bromoamides leading to diastereomerically enriched α-amino-, α-hydroxy- and α-thiocarboxylic acid derivatives. *Tetrahedron: Asymmetry* **1995**, *6*, 93–96; b) Ward, B. R. S.; Pelter, A.; Goubet, D.; Pritchard, M. C. Diastereoselective synthesis of α-bromo amides leading to diastereomerically enriched α-amino-, α-hydroxy- and α-thiocarboxylic acid derivatives. *Tetrahedron: Asymmetry* **1995**, *6*, 469-498.

[26] Girard, C.; Mandville, G.; Bloch, R. Regioselective SN′ allylic substitution versus 1,4-addition: Asymmetric induction with Oppolzer's chiral sultam. *Tetrahedron: Asymmetry* **1993**, *4*, 613–616.

[27] Kiegiel, J.; Papis, A.; Jurczak, J. Asymmetric reduction of *N*-methylglyoxyloyl- and *N*-phenylglyoxyloyl-(2R)-bornane-10,2-sultam. *Tetrahedron: Asymmetry* **1999**, *10*, 535–541.

[28] a) Oppolzer, W.; Mills, R. J.; Pachinger, W.; Stevenson, T. Preparation of enantiomerically pure β-silylcarboxyl derivatives by asymmetric 1,4-addition to *N*-enoyl-sultams. Preliminary communication. *Helv. Chim. Acta* **1986**, *69*, 1542–1545; b) Oppolzer, W.; Poli, G.; Kingma, A. J.; Starkemann, C.; Bernardinelli, G. Asymmetric induction at C(β) and C(α) of *N*-enoylsultams by organomagnesium 1,4-addition/enolate trapping. *Helv. Chim. Acta* **1987**, *70*, 2201–2214; c) Oppolzer, W.; Kingma, A. J.; Poli, G. Asymmetric 1,4-additions of Gilman reagents to alpha,beta-disubstituted (*E*)-enoylsultams/enolate protonations. *Tetrahedron* **1989**, *45*, 479-488; d) Reid, G. P.; Brear, K. W.; Robins, D. J. Diastereoselective conjugate addition of Grignard reagents to a homochiral fumaramide derived from Oppolzer's sultam. *Tetrahedron: Asymmetry* **2004**, *15*, 793–801; e) Cao, X.; Liu, F.; Lu, W.; Chen, G.; Yu, G.-A.; Liu, S. H. Regio- and diastereoselective conjugate addition of Grignard reagents to aryl substituted α,β-unsaturated carbonyl compounds derived from Oppolzer's sultam. *Tetrahedron* **2008**, *64*, 5629–5636; f) Piątek, A. M.;

Sadowska, A.; Chapuis, C.; Jurczak, J. Diastereoselective alkyl Grignard 1,4-additions to para-substituted (2R)-*N*-cinnamoylbornane-10,2-sultam eerivatives: Influence of *N*-atom pyramidalization. *Helv. Chim. Acta* **2011**, *94*, 2141−2167; g) Piątek, A.; Chapuis, C. Grignard 1,4-additions to para-substituted (2R)-*N*-cinnamoylbornane-10,2-sultam derivatives: Revised configuration for the N,OAc-keteneacetal formation in the presence of Cu(I). *Helv. Chim. Acta* **2016**, *99*, 573−582.

[29] a) Oppolzer, W.; Schneider, P. Enantioselective synthesis of β-Necrodol and of 1-Epi-β-necrodol via asymmetric 1,4-addition and magnesium-ene cyclization. Preliminary communication. *Helv. Chim. Acta* **1986**, *69*, 1817−1820; b) Brantley, S. E.; Molinski, T. F. Synthetic studies of trichloroleucine marine natural products. Michael addition of $LiCCl_3$ to *N*-crotonylcamphor sultam. *Org. Lett.* **1999**, *1*, 2165−2167; c) Huang, J. X.; Li, Y.; Ma, X. Q.; Zhou, Z. Q. Study on synthesis of the sex pheromone of peach leafminer moth. *Chinese J. Org. Chem.* **1999**, *19*, 528−532; d) Harding, J. R.; Hughes, R. A.; Kelly, N. M.; Sutherland, A.; Willis, C. L. Syntheses of isotopically labelled L-α-amino acids with an asymmetric centre at C-3. *J. Chem. Soc., Perkin Trans. 1* **2000**, 3406−3416; e) Fletcher, M. D.; Harding, J. R.; Hughes, R. A.; Kelly, N. M.; Schmalz, H.; Sutherland, A.; Willis, C. L. Three approaches to the synthesis of L-leucine selectively labelled with carbon-13 or deuterium in either diastereotopic methyl group. *J. Chem. Soc., Perkin Trans. 1* **2000**, 43−51; f) Liang, B.; Carroll, P. J.; Joullié, M. M. Progress toward the total synthesis of Callipeltin A (I): Asymmetric synthesis of (3S,4R)-3,4-dimethylglutamine. *Org. Lett.* **2000**, *2*, 4157−4160; g) Liddle, J.; Huffman, J. W. Enantioselective synthesis of 11-hydroxy-(1′S,2′R)-dimethylheptyl-Δ8-THC, a very potent CB1 agonist. *Tetrahedron* **2001**, *57*, 7607−7612; h) Amat, M.; Coll, M. D.; Llor, N.; Escolano, C.; Molins, E.; Miravitlles, C.; Bosch, J. Asymmetric synthesis of tetracyclic substructures of Strychnos indole alkaloids. *Tetrahedron: Asymmetry* **2003**, *14*, 1691−1699; i) Seki, C.; Hirama, M.; Sato, T.; Takeda, S.; Kohari, Y.; Ishigaki, M. O.; Yokoi, K.; Nakana, H.; Uwai, K.; Takano, N.; Umemura, K.; Matsuyama, H. One step synthesis of optically active diazoabicyclo[3.3.0]octanones or diazabicyclo[4.3.0]nonanones by asymmetric conjugate addition of cyclic hydrazine. *Heterocycles* **2012**, *85*, 1045−1052; j) Sang, F.; Feng, P.; Chen, J.; Ding, Y.; Duan, X.; Zhai, J.; Ma, X.; Zhang, B.; Zhang, Q.; Lin, J.; Chen, Y. Epothilone D and its 9-methyl analogues: Combinatorial syntheses, conformation, and biological activities. *Eur. J. Med. Chem.* **2013**, *68*, 321−332.

[30] a) Wu, M.-J.; Wu, C.-C.; Tseng, T.-C.; Pridgen, L. N. Asymmetric conjugate addition of thiols to chiral beta-substituted *N*-enoylsultams. *J. Org. Chem.* **1994**, *59*, 7188-7189; b) Wu, S. L.; Huang, F. K.; Uang, B. J.; Tsai, W. J.; Liang, J. J. Antiferroelectric liquid crystals derived from a new optically active (R)-3-ethylmercapto-2-methylpropionic acid. *Liq. Cryst.* **1995**, *18*, 715-721.

[31] a) Khan, M. A.; Yates, S. L.; Tedford, C. E.; Kirschbaum, K.; Phillips, J. G. Diastereoselective synthesis of *trans*-2-(1-triphenylmethyl-1H-imidazol-4-yl)cyclopropanecarboxylic acids: Key intermediates for the preparation of potent and chiral histamine H3 receptor agents. *Bioorg. Med. Chem. Lett.* **1997**, *7*, 3017–3022; b) Kakuuchi, A.; Taguchi, T.; Hanzawa, Y. Rhodium-catalyzed 1,4-addition of alkenylzirconocene chlorides to electron deficient alkenes. *Tetrahedron* **2004**, *60*, 1293−1299; b) Hanzawa, Y.; Takebe, Y.; Saito, A.; Kakuuchi, A.; Fukaya, H. Rh(I)-catalyzed conjugate addition of alkenylzirconocene chloride: Stereoselective formation of carbocycles through cascade reaction. *Tetrahedron Lett.* **2007**, *48*, 6471−6474; c) Aires-de-Sousa, J.; Prabhakar, S.; Lobo, A. M.; Rosa, A. M.; Gomes, M. J. S.; Corvo, M. C.; Williams, D. J.; White, A. J. P. Asymmetric synthesis of N-aryl aziridines. *Tetrahedron: Asymmetry* **2002**, *12*, 3349−3365.

[32] Oppolzer, W.; Poli, G. Asymmetric induction at C(beta) and C(alpha) of n-enoyl Sultams by 1,4-hydride addition enolate trapping. *Tetrahedron Lett.* **1986**, *27*, 4717–4720.

[33] a) Palomo, C.; Aizpurua, J. M.; Gracenea, J. J. Diastereoselective conjugate reduction and enolate rrapping with glyoxylate imines. A concise approach to β-lactams that involves a ternary combination of components. *J. Org. Chem.* **1999**, *64*, 1693−1698; b) Baltrusch, A. W.; Bracher, F. Enantioselective Synthesis of 6-nor-Fluvirucinin B1. *Synlett* **2002**, *2002*, 1724−1726; c) Gaich, T.; Mulzer, J. Synthesis of epothilones via a silicon-tethered RCM reaction. *Org. Lett.* **2005**, *7*, 1311−1313; d) Pichlmair, S.; Marques, M. M. B.; Green, M. P.; Martin, H. J.; Mulzer, J. A novel approach toward the synthesis of Kendomycin: Selective synthesis of a C-aryl glycoside as a single atropisomer. *Org. Lett.* **2003**, *5*, 4657−4659; e) Takao, K.-i.; Saegusa, H.; Tsujita, T.; Washizawa, T.; Tadano, K.-i. Synthetic studies of Pestalotiopsin A: Asymmetric synthesis of the 2-oxabicyclo[3.2.0]heptane substructure. *Tetrahedron Lett.* **2005**, *46*, 5815−5818.

[34] Ponsinet, R.; Chassaing, G.; Lavielle, S. Asymmetric synthesis of boc-β2-homophenylglycine. *Tetrahedron: Asymmetry* **1998**, *9*, 865−871.

[35] a) Curran, D. P.; Shen, W.; Zhang, J.; Heffner, T. A. Asymmetric radical addition, cyclization, and annulation reactions with Oppolzer's camphor sultam. *J. Am. Chem. Soc.* **1990**, *112*, 6738−6740; b) Curran, D. P.; Geib, S. J.; Lin, C.-H. Group selective radical cyclizations with Oppolzer's camphor sultam. *Tetrahedron: Asymmetry* **1994**, *5*, 199−202; c) Baciocchi, E.; Muraglia, E.; Villani, C. Stereoselective heteroaromatic homolytic substitution with carbon radicals derived from Oppolzer's Camphorsultam. *Synlett* **1994**, *1994*, 821−822; Miyabe, H.; Ushiro, C.; Ueda, M.; Yamakawa, K.; Naito, T. Asymmetric

synthesis of α-amino acids based on carbon radical addition to glyoxylic oxime ether. *J. Org. Chem.* **2000**, *65*, 176–185.

[36] a) Rummakko, P.; Brunow, G.; Orlandi, M.; Rindone, B. Asymmetric biomimetic oxidations of phenols: Enantioselective synthesis of (+)- and (-)-Dehydrodiconiferyl Alcohol. *Synlett* **1999**, *1999*, 333–335; b) Bragnier, N.; Guillot, R.; Scherrmann, M.-C. Diastereoselective addition of sugar radicals to camphorsultam glyoxilic oxime ether: A route toward C-glycosylthreonine and allothreonine. *Org. Biomol. Chem.* **2009**, *7*, 3918–3921; c) Yajima, T.; Yamaguchi, K.; Hirokane, R.; Nogami, E. Photoinduced radical hydroperfluoroalkylation and the synthesis of fluorinated amino acids and peptides. *J. Fluorine Chem.* **2013**, *150*, 1–7; d) Fujino, H.; Nagatomo, M.; Paudel, A.; Panthee, S.; Hamamoto, H.; Sekimizu, K.; Inoue, M. Unified total synthesis of polyoxins J, L, and fluorinated analogues on the basis of decarbonylative radical coupling reactions. *Angew. Chem. Int. Ed.* **2017**, *56*, 11865–11869.

[37] a) Oppolzer, W.; Chapuis, C.; Bernardinelli, G. Camphor-derived *N*-acryloyl and *N*-crotonoyl sultams: Practical activated dienophiles in asymmetric Diels-Alder reactions. Preliminary communication. *Helv. Chim. Acta* **1984**, *67*, 1397-1401; b) Oppolzer, W.; Dupuis, D. Asymmetric intramolecular Diels-Alder reactions of *N*-acyl-camphor-sultam trienes. *Tetrahedron Lett.* **1985**, *26*, 5437–5440; c) Oppolzer, W.; Rodriguez, I.; Blagg, J.; Bernardinelli, G. Asymmetric Diels-Alder reactions: X-Ray crystal-structure analysis of [*N*-((*E*)-but-2-enoyl)bornane-10,2-sultam]tetrachlorotitanium. *Helv. Chim. Acta* **1989**, *72*, 123–130; d) Pindur, U.; Lutz, G.; Fischer, G.; Schollmeyer, D.; Massa, W.; Schröder, L. Cycloadditions of vinylindoles with chiral carbodienophiles: The first asymmetric Diels-Alder reactions in the vinylhetarane series. *Tetrahedron* **1993**, *49*, 2863–2872; e) Chapius, C.; Rzepecki, P.; Bauer, T.; Jurczak, J. Complete π-Facial Stereoselectivity in the TiCl4-Mediated [4 + 2] Cycloaddition of cyclopentadiene to N,N′-fumaroyldi[(2R)-bornane-10,2-sultam]. *Helv. Chim. Acta* **1995**, *78*, 145–150; f) Bauer, T.; Chapuis, C.; Kucharska, A.; Rzepecki, P.; Jurczak, J. Influence of Lewis Acids on the [4 + 2] Cycloaddition of N,N′-Fumaroylbis[(2R)-bornane-10,2-sultam] to cyclopentadiene and application to various dienes. *Helv. Chim. Acta* **1998**, *81*, 324–329; g) Achmatowicz, M.; Chapuis, C.; Rzepecki, P.; Jurczak, J. Stereoselectivity in the TiCl4-catalyzed [4+2] cycloaddition of cyclopentadiene to (2R)-bornane-10,2-sultam derivatives of fumaric acid monoesters. *Helv. Chim. Acta* **1999**, *82*, 182–190.

[38] a) Bauer, T.; Chapuis, C.; Kozak, J.; Jurczak, J. Asymmetric Diels-Alder reaction of 1-methoxybuta-1,3-diene with (2R)-*N*-glyoxyloylbornane-10,2-sultam. *Helv. Chim. Acta* **1989**, *72*, 482–486; b) Gouverneur, V.; Dive, G.; Ghosez, L. Asymmetric Diels-Alder reactions of a nitroso compound derived

from D-bornane-10,2-sultam. *Tetrahedron: Asymmetry* **1991**, *2*, 1173−1176; c) Jurczak, J.; Jeżewski, A. The asymmetric cyclocondensation reaction of 1-methoxy-3-silyloxybuta-1,3-dienes with *N*-glyoxyloyl-(2R)-bornane-10,2-sultam. *Tetrahedron: Asymmetry* **1996**, *7*, 1413−1418; d) Bauer, T.; Szymański, S.; Jeżewski, A.; Gluziński, P.; Jurczak, J. Asymmetric [4+2] cycloaddition of cyclopentadiene to *N*′-tosylimine of *N*-glyoxyloyl-(2R)-bornane-10,2-sultam. *Tetrahedron: Asymmetry* **1997**, *8*, 2619−2625; e) Gouverneur, V.; McCarthy, S. J.; Mineur, C.; Belotti, D.; Dive, G.; Ghosez, L. New acylnitroso compounds for the asymmetric oxyamination of dienes. *Tetrahedron* **1998**, *54*, 10537−10554; f) Szymanski, S.; Chapuis, C.; Jurczak, J. Diastereoselectivity in the hetero 4+2 cycloaddition of cyclopentadiene to *N*-benzyliminoacetyl derivatives of (2R)-bornane-10,2-sultam and other chiral secondary alcohols. *Tetrahedron-Asymmetry* **2001**, *12*, 1939–1945; g) Kosior, M.; Malinowska, M.; Jóźwik, J.; Caille, J.-C.; Jurczak, J. Highly diastereoselective hetero-Diels–Alder reaction of buta-1,3-diene with *N*-glyoxyloyl-(2R)-bornane-10,2-sultam: An efficient synthesis of homochiral (S)-3-[2-{(methylsulfonyl)oxy}ethoxy]-4-(triphenylmethoxy)-1-butanol methanesulfonate. *Tetrahedron: Asymmetry* **2003**, *14*, 239–244; h) Kosior, M.; Asztemborska, M.; Jurczak, J. Diastereoselective reaction of buta-1,3-diene with chiral derivatives of glyoxylic acid: Effective route to optically pure 2-substituted 3,6-dihydro-2H-pyrans. *Synthesis* **2004**, *2004*, 87–91.

[39] a) Vandewalle, M.; Van der Eycken, J.; Oppolzer, W.; Vullioud, C. Iridoids: Enantioselective synthesis of Loganin via an asymmetric Diels-Alder reaction. *Tetrahedron* **1986**, *42*, 4035–4043; b) Oppolzer, W.; Dupuis, D.; Poli, G.; Raynham, T. M.; Bernardinelli, G. Enantioselective synthesis and absolute configuration of (−)-pulo'upone by asymmetric intramolecular Diels-Alder reaction. *Tetrahedron Lett.* **1988**, *29*, 5885−5888; c) Smith, A. B.; Hale, K. J.; Laakso, L. M.; Chen, K.; Riéra, A. FK-506 synthetic studies. 3. An efficient asymmetric synthesis of the C(24)–C(34) fragment of FK-506, FR-900520, and FR-900523. *Tetrahedron Lett.* **1989**, *30*, 6963−6966; d) Mayor, S. C.; Pfizenmayer, A. J.; Cordova, R.; Li, W.-R.; Joullié, M. M. Synthetic studies of a constrained ring Didemnin analog. *Tetrahedron: Asymmetry* **1994**, *5*, 519−522; e) Mayer, S. C.; Pfizenmayer, A. J.; Joullié, M. M. Synthetic routes to a constrained ring analog of Didemnin B. *J. Org. Chem.* **1996**, *61*, 1655−1664; f) Xiao, D.; Vera, M. D.; Liang, B.; Joullié, M. M. Total synthesis of a conformationally constrained Didemnin B analog. *J. Org. Chem.* **2001**, *66*, 2734–2742; g) Roush, W. R.; Limberakis, C.; Kunz, R. K.; Barda, D. A. Diastereoselective synthesis of the endo- and exo-spirotetronate subunits of the Quartromicins. The first enantioselective Diels−Alder reaction of an acyclic (Z)-1,3-diene. *Org. Lett.* **2002**, *4*, 1543−1546; h) Roush, W. R.; Barda, D. A.; Limberakis, C.; Kunz, R. K. Studies on the synthesis of the Quartromicins: Partial stereochemical assignment of Quartromicins

A3 and D3 and diastereoselective synthesis of the endo- and exo-spirotetronate subunits. *Tetrahedron* **2002**, *58*, 6433–6454; i) Klun, J. A.; Khrimian, A.; Margaryan, A.; Kramer, M.; Debboun, M. Synthesis and repellent efficacy of a new chiral piperidine analog: Comparison with Deet and Bayrepel activity in human-volunteer laboratory assays against *Aedes aegypti* and *Anopheles stephensi*. *J.Med. Entomol.* **2003**, *40*, 293–299; j) Khrimian, A.; Margaryan, A. K.; Schmidt, W. F. An improved synthesis of ethyl cis-5-iodo-trans-2-methylcyclohexanecarboxylate, a potent attractant for the Mediterranean fruit fly. *Tetrahedron* **2003**, *59*, 5475–5480; k) Hirama, M.; Kato, Y.; Seki, C.; Nakano, H.; Takeshita, M.; Oshikiri, N.; Iyoda, M.; Matsuyama, H. An efficient synthesis of chiral isoquinuclidines by Diels–Alder reaction using Lewis acid catalyst. *Tetrahedron* **2010**, *66*, 7618–7624; l) Robins, J. G.; Kim, K. J.; Chinn, A. J.; Woo, J. S.; Scheerer, J. R. Intermolecular Diels–Alder cycloaddition for the construction of bicyclo[2.2.2]diazaoctane structures: Formal synthesis of Brevianamide B and Premalbrancheamide. *J. Org. Chem.* **2016**, *81*, 2293–2301; m) Wang, Y.; Leng, L.; Liu, Y.; Dai, G.; Xue, F.; Chen, Z.; Meng, J.; Wen, G.; Xiao, Y.; Liu, X.-Y.; Qin, Y. Asymmetric synthesis of an advanced tetracyclic framework of (+)-Sarain A. *Org. Lett.* **2018**, *20*, 6701–6704.

[40] a) Bauer, T.; Jeżewski, A.; Jurczak, J. The stereocontrolled synthesis of methyl 2,6-*N*,*N*-diacetyl-D-purpurosaminide C. *Tetrahedron: Asymmetry* **1996**, *7*, 1405–1412; b) Bauer, T.; Chapuis, C.; Jeżewski, A.; Kozak, J.; Jurczak, J. Stereochemical course of the [4+2] cycloaddition of 1-methoxybuta-1,3-diene to *N*-glyoxyloyl-(2R)-bornane-10,2-sultam. The formal synthesis of Compactin and Mevinolin. *Tetrahedron: Asymmetry* **1996**, *7*, 1391–1404; c) Johnson, S. C.; Crasto, C.; Hecht, S. M. Facial selectivity in the cycloaddition of heterodienes to carbohydrate cyclic ketene acetals. A novel synthesis of disaccharide derivatives. *Chem. Commun.* **1998**, 1019–1020; d) Cabanal-Duvillard, I.; Berrien, J.-F.; Ghosez, L.; Husson, H.-P.; Royer, J. A Formal asymmetric synthesis of (−)-Epibatidine using a highly diastereoselective hetero Diels–Alder reaction 1. *Tetrahedron* **2000**, *56*, 3763–3769; e) Cabanal-Duvillard, I.; Berrien, J.-F.; Royer, J. An expeditious formal synthesis of (−)-Epibatidine. *Tetrahedron: Asymmetry* **2000**, *11*, 2525–2529; f) Bertilsson, S. K.; Ekegren, J. K.; Modin, S. A.; Andersson, P. G. The aza-Diels–Alder reaction protocol — A useful approach to chiral, sterically constrained α-amino acid derivatives. *Tetrahedron* **2001**, *57*, 6399–6406.

[41] a) Curran, D. P.; Kim, B. H.; Daugherty, J.; Heffner, T. A. The preparation of optically active δ2-isoxazolines. A model for asymmetric induction in the non Lewis acid catalyzed reactions of Oppolzer's chiral sultam. *Tetrahedron Lett.* **1988**, *29*, 3555–3558; b) Wallace, R. H.; Liu, J.; Zong, K. K.; Eddings, A. An efficient method for the preparation of optically active 4-hydroxy-Δ2-isoxazolines. *Tetrahedron Lett.*

1997, *38*, 6791–6794; c) Romanski, J.; Chapuis, C.; Jurczak, J. 1,3-Dipolar cycloadditions of a 2-oxoethanenitrile oxide derived from (2R)-bornane-10,2-sultam to electronically modified 4,4′-disubstituted stilbenes. *Helv. Chim. Acta* **2009**, *92*, 1056–1069; d) Romanski, J.; Nowak, P.; Maksymiuk, A.; Chapuis, C.; Jurczak, J. Diastereoselective 1,3-dipolar cycloadditions of both electronically modified phenyl-nitrile oxides and stilbenes. *RSC Adv.* **2013**, *3*, 23105–23118.

[42] a) Garner, P.; Ho, W. B. Stereoselective 1,3-dipolar cycloadditions of photochemically generated azomethine ylides to Oppolzer's chiral acryloyl sultam. An asymmetric approach to Quinocarcin. *J. Org. Chem.* **1990**, *55*, 3973–3975; b) Garner, P.; Ho, W. B.; Grandhee, S. K.; Youngs, W. J.; Kennedy, V. O. Development of an asymmetric approach to the 3,8-diazabicyclo[3.2.1]octane moiety of Quinocarcin via intramolecular 1,3-dipolar cycloadditions of photochemically generated azomethine ylides. *J. Org. Chem.* **1991**, *56*, 5893–5903; c) Pandey, G.; Laha, J. K.; Mohanakrishnan, A. K. [3+2]-Cycloaddition of nonstabilized azomethine ylides, part 9: A general approach for the construction of X-azabicyclo[m.2.1]alkanes in optically pure form by asymmetric 1,3-dipolar cycloaddition reactions. *Tetrahedron Lett.* **1999**, *40*, 6065–6068; d) Karlsson, S.; Högberg, H.-E. Synthesis of enantiomerically pure 4-substituted pyrrolidin-3-ols via asymmetric 1,3-dipolar cycloaddition. *Tetrahedron: Asymmetry* **2001**, *12*, 1977–1982.

[43] a) Kim, B. H.; Lee, J. Y. Asymmetric silyl nitronate cycloadditions with bornane-10,2-sultam derivatives. *Tetrahedron: Asymmetry* **1991**, *2*, 1359–1370; b) Kim, B. H.; Lee, J. Y.; Kim, K.; Whang, D. Asymmetric induction in silyl nitronate cycloadditions to Oppolzer's chiral sultam derivatives. *Tetrahedron: Asymmetry* **1991**, *2*, 27–30; c) Tejero, T.; Dondoni, A.; Rojo, I.; Merchán, F. L.; Merino, P. 1,3-Dipolar cycloaddition of C-(2-thiazolyl)nitrones to chiral acrylates. Synthesis of enantiopure α-amino-2-alkylthiazoles and 5-formylpyrrolidin-2-ones. *Tetrahedron* **1997**, *53*, 3301–3318.

[44] a) Curran, D. P.; Heffner, T. A. On the scope of asymmetric nitrile oxide cycloadditions with Oppolzer's chiral sultam. Total syntheses of (+)-hepialone, (–)-(1R,3R,5S)-1,3-dimethyl-2,9-dioxabicyclo[3.3.1]nonane, and (–)-(1S)-7,7-dimethyl-6,8-dioxabicyclo[3.2.1] octane. *J. Org. Chem.* **1990**, *55*, 4585–4595; b) Zhang, J.; Curran, D. P. Stereoselective synthesis of 1,2-diols by the cycloadditive strategy: Total synthesis of (±)-exo-Brevicomin and (±)-and (–)-Pestalotin. *J. Chem. Soc., Perkin Trans. 1* **1991**, 2627–2631; c) Kim, B. H.; Lee, J. Y. Enantioselective syntheses of (+)-methyl nonactate and (−)-methyl 8-epi-nonactate via asymmetric cycloadditive route. *Tetrahedron Lett.* **1992**, *33*, 2557–2560; d) Chung, Y. J.; Ryu, E. J.; Keum, G.; Byeang Hyean, K. Synthesis of 2-isoxazoline and α-hydroxy

ketomethylene dipeptide isosteres. *Biorg. Med. Chem.* **1996**, *4*, 209–225; e) Geffaut, T.; Bauer, U.; Airola, K.; Koskinen, A. M. P. Asymmetric 1,3-dipolar cycloaddition: Synthesis of *N*-protected (4S)-4-hydroxy L-glutamic acid diester. *Tetrahedron: Asymmetry* **1996**, *7*, 3099–3102; f) Merino, P.; Revuelta, J.; Tejero, T.; Chiacchio, U.; Rescifina, A.; Piperno, A.; Romeo, G. Enantioselective synthesis of 4-hydroxy-d-pyroglutamic acid derivatives by an asymmetric 1,3-dipolar cycloaddition. *Tetrahedron: Asymmetry* **2002**, *13*, 167–172; g) Kim, D.; Lee, J.; Shim, P. J.; Lim, J. I.; Doi, T.; Kim, S. Role of conformational effects on the regioselectivity of macrocyclic INOC reactions: Two new asymmetric total syntheses of (+)-Brefeldin A,1. *J. Org. Chem.* **2002**, *67*, 772–781; h) Tamura, O.; Kanoh, A.; Yamashita, M.; Ishibashi, H. Synthesis of (3′R,5′S)-3′-hydroxycotinine using 1,3-dipolar cycloaddition of a nitrone. *Tetrahedron* **2004**, *60*, 9997–10003; i) Kotian, P. L.; Lin, T. H.; El-Kattan, Y.; Chand, P. A practical large-scale synthesis of (3R,4R)-4-(hydroxymethyl)pyrrolidin-3-ol via asymmetric 1,3-dipolar cycloaddition. *Org. Process Res. Dev.* **2005**, *9*, 193–197; j) Jung, J. Y.; Ho Jung, S.; Koh, H. Y. Asymmetric synthesis of chiral piperazinylpropylisoxazoline ligands for dopamine receptors. *Eur. J. Med. Chem.* **2007**, *42*, 1044–1048; k) Yun, H.; Paek, S.-M.; Jung, J.-W.; Kim, N.-J.; Kim, S.-H.; Suh, Y.-G. First total syntheses of (−)-Macrosphelides J and K and elucidation of their absolute configuration. *Chem. Commun.* **2009**, 2463–2465; l) Romanski, J.; Nowak, P.; Chapuis, C.; Jurczak, J. Total synthesis of (5S)-dihydroyashabushiketol. *Tetrahedron: Asymmetry* **2011**, *22*, 787–790; m) Merino, P.; Greco, G.; Tejero, T.; Chiacchio, U.; Corsaro, A.; Pistarà, V.; Romeo, G. High-yield synthesis of pyrrolidinyl PNA monomers. *Tetrahedron Lett.* **2011**, *52*, 6003–6006; n) An, H.; Kim, S. H.; Kim, H.; Kim, K.; Sim, J.; Jang, J.; Paek, S. M.; Suh, Y. G.; Yun, H. Synthesis and synthesis-based structural elucidation of (–)-Macrosphelides J and K. *Heterocycles* **2015**, *91*, 970–988.

[45] a) Jeżewski, A.; Chajewska, K.; Wielogórski, Z.; Jurczak, J. The asymmetric ene reaction of N-glyoxyloyl-(2R)-bornane-10,2-sultam with 1-pentene and 1-hexene. *Tetrahedron: Asymmetry* **1997**, *8*, 1741–1749; b) Kwiatkowski, P.; Kwiatkowski, J.; Majer, J.; Jurczak, J. Synthesis of chiral 4-substituted 2-hydroxypent-4-enoic acid derivatives via diastereoselective ene reaction promoted by ZnBr2. *Tetrahedron: Asymmetry* **2007**, *18*, 215–223.

[46] a) Adam, W.; Degen, H.-G.; Krebs, O.; Saha-Möller, C. R. Efficient π-facial control in the ene reaction of nitrosoarene, triazolinedione, and singlet oxygen with tiglic amides of the bornane-derived sultam as chiral auxiliary: An economical synthesis of enantiomerically pure nitrogen- and oxygen-functionalized acrylic acid derivatives. *J. Am. Chem. Soc.* **2002**, *124*, 12938–12939; b) Frazier, C. P.; Engelking, J. R.; Read de Alaniz, J. Copper-catalyzed aerobic oxidation of hydroxamic acids leads to a

mild and versatile acylnitroso ene reaction. *J. Am. Chem. Soc.* **2011**, *133*, 10430-10433; c) Teo, Y. C.; Pan, Y.; Tan, C. H. Organic dye-photocatalyzed acylnitroso ene reaction. *ChemCatChem* **2013**, *5*, 235–240.

[47] a) Lee, W.-D.; Chiu, C.-C.; Hsu, H.-L.; Chen, K. On the scope of diastereoselective epoxidation of various chiral auxiliaries derived enones: The conformational analysis of camphor derived N- and O-enones. *Tetrahedron* **2004**, *60*, 6657–6664; b) Zhang, S.-J.; Chen, Y.-K.; Li, H.-M.; Huang, W.-Y.; Rogatchov, V.; Metz, P. Diastereoselective epoxidation of *N*-enoylsultams with different chiral sultams as auxiliaries. *Chin. J. Chem* . **2006**, *24*, 681–688; c) Hajra, S.; Bhowmick, M. Asymmetric epoxidation of cinnamic acid derivatives by *in situ* generated dioxiranes of chloroacetones: Scope and limitations. *Tetrahedron: Asymmetry* **2010**, *21*, 2223–2229.

[48] a) Vallgårda, J.; Hacksell, U. Stereoselective palladium-catalyzed cyclopropanation of α,β-unsaturated carboxylic acids derivatized with Oppolzer's sultam. *Tetrahedron Lett.* **1991**, *32*, 5625–5628; b) Vallgårda, J.; Appelberg, U.; Csoregh, I.; Hacksell, U. Stereoselectivity and generality of the palladium-catalysed cyclopropanation of [small alpha],[small beta]-unsaturated carboxylic acids derivatized with Oppolzer's sultam. *J. Chem. Soc., Perkin Trans. 1* **1994**, 461–470.

[49] a) Vangveravong, S.; Nichols, D. E. Stereoselective synthesis of trans-2-(indol-3-yl)cyclopropylamines: Rigid tryptamine analogs. *J. Org. Chem.* **1995**, *60*, 3409–3413; b) Vallgårda, J.; Appelberg, U.; Arvidsson, L.-E.; Hjorth, S.; Svensson, B. E.; Hacksell, U. *trans*-2-Aryl-*N*,*N*-dipropylcyclopropylamines: Synthesis and interactions with 5-HT1A receptors. *J. Med. Chem.* **1996**, *39*, 1485–1493; c) Sun, L.-Q.; Takaki, K.; Chen, J.; Bertenshaw, S.; Iben, L.; Mahle, C. D.; Ryan, E.; Wu, D.; Gao, Q.; Xu, C. (R)-2-(4-Phenylbutyl)dihydrobenzofuran derivatives as melatoninergic agents. *Bioorg. Med. Chem. Lett.* **2005**, *15*, 1345–1349; d) Springthorpe, B.; Bailey, A.; Barton, P.; Birkinshaw, T. N.; Bonnert, R. V.; Brown, R. C.; Chapman, D.; Dixon, J.; Guile, S. D.; Humphries, R. G.; Hunt, S. F.; Ince, F.; Ingall, A. H.; Kirk, I. P.; Leeson, P. D.; Leff, P.; Lewis, R. J.; Martin, B. P.; McGinnity, D. F.; Mortimore, M. P.; Paine, S. W.; Pairaudeau, G.; Patel, A.; Rigby, A. J.; Riley, R. J.; Teobald, B. J.; Tomlinson, W.; Webborn, P. J. H.; Willis, P. A. From ATP to AZD6140: The discovery of an orally active reversible P2Y12 receptor antagonist for the prevention of thrombosis. *Bioorg. Med. Chem. Lett.* **2007**, *17*, 6013–6018; e) Cheng, J.; McCorvy, J. D.; Giguere, P. M.; Zhu, H.; Kenakin, T.; Roth, B. L.; Kozikowski, A. P. Design and discovery of functionally selective serotonin 2C (5-HT2C) receptor agonists. *J. Med. Chem.* **2016**, *59*, 9866–9880.

[50] a) Oppolzer, W.; Barras, J.-P. Asymmetric dihydroxylations of β-substituted *N*-(α,β-enoyl)bornane-10,2-sultams. *Helv. Chim. Acta* **1987**, *70*, 1666–1675; b) Raczko, J.; Achmatowicz, M.; Jezewski, A.;

Chapuis, C.; Urbañczyk-Lipkowska, Z.; Jurczak, J. Asymmetric syn-dihydroxylation of β-substituted (2R)-*N*-(α,β-enoyl)bornane-10,2-sultams. *Helv. Chim. Acta* **1998**, *81*, 1264–1277; c) Lee, A. W. M.; Chan, W. H.; Yuen, W. H.; Xia, P. F.; Wong, W. Y. Ruthenium catalyzed asymmetric dihydroxylation with sultams as chiral auxiliaries. *Tetrahedron: Asymmetry* **1999**, *10*, 1421−1424; d) Raczko, J.; Achmatowicz, M.; Kwiatkowski, P.; Chapuis, C.; Urbanczyk-Lipkowska, Z.; Jurczak, J. Asymmetric syn-dihydroxylation of γ-substituted (2R)-N-(β,γ-enoyl)bornane-10,2-sultams. *Tetrahedron: Asymmetry* **2000**, *11*, 1027-1041.

[51] a) Yokomatsu, T.; Iwasawa, H.; Shibuya, S. Enantioselective halolactonisation of bis-γ,δ-unsaturated carboxylic acid derivatives: Use of a sultam and oxazolidine-2-ones as chiral auxiliary. *J. Chem. Soc., Chem. Commun.* **1992**, 728−729; b) Yokomatsu, T.; Iwasawa, H.; Shibuya, S. Highly enantioselective creation of quaternary carbons in a halolactonization of bis-γ,δ-unsaturated carboxylic imides derived from a camphorsultam: Enantioselective synthesis of (+)-mesembrine. *Tetrahedron Lett.* **1992**, *33*, 6999−7002.

[52] Hajra, S.; Bhowmick, M.; Karmakar, A. Lewis acid catalyzed asymmetric halohydrin reactions of chiral α,β-unsaturated carboxylic acid derivatives with *N*-halosuccinimide (NXS) as the halogen source. *Tetrahedron Lett.* **2005**, *46*, 3073−3077.

[53] a) Walba, D. M.; Przybyla, C. A.; Walker, C. B. Total synthesis of ionophores. 6. Asymmetric induction in the permanganate-promoted oxidative cyclization of 1,5-dienes. *J. Am. Chem. Soc.* **1990**, *112*, 5624−5625; b) Brown, R. C. D.; Bataille, C. J.; Hughes, R. M.; Kenney, A.; Luker, T. J. Permanganate oxidation of 1,5,9-trienes: Stereoselective synthesis of tetrahydrofuran-containing fragments. *J. Org. Chem.* **2002**, *67*, 8079−8085.

[54] Cecil, A. R. L.; Brown, R. C. D. Stereoselective synthesis of cis-2,6-bis-hydroxyalkyl-tetrahydropyrans by the permanganate promoted oxidative cyclisation of 1,6-dienes. *Tetrahedron Lett.* **2004**, *45*, 7269−7271.

[55] a) Brown, R. C. D.; Kocienski, P. J. A synthesis of Salinomycin. Part 1. Synthesis of key fragments. *Synlett* **1994**, *1994*, 415-417; b) Cecil, A. R. L.; Hu, Y.; Vicent, M. J.; Duncan, R.; Brown, R. C. D. Total synthesis and preliminary biological evaluation of *cis*-Solamin isomers. *J. Org. Chem.* **2004**, *69*, 3368−3374; c) Head, G. D.; Whittingham, W. G.; Brown, R. C. D. Synthesis of Membranacin. *Synlett* **2004**, *2004*, 1437−1439; d) Bhunnoo, R. A.; Hobbs, H.; Lainé, D. I.; Light, M. E.; Brown, R. C. D. Synthesis of the non-adjacent bis-THF core of cis-Sylvaticin using a double oxidative cyclisation. *Org. Biomol. Chem.* **2009**, *7*, 1017−1024l; e) Morris, C. L.; Hu, Y.; Head, G. D.; Brown, L. J.; Whittingham, W. G.; Brown, R. C. D. Oxidative cyclization reactions of trienes and dienynes: Total synthesis of Membrarollin. *J. Org.*

Chem. **2009**, *74*, 981−988; f) Sheikh, N. S.; Bataille, C. J.; Luker, T. J.; Brown, R. C. D. Enantioselective formal synthesis of Eurylene: Synthesis of the *cis*- and *trans*-THF fragments using oxidative cyclization. *Org. Lett.* **2010**, *12*, 2468-2471; g) Li, Y.; Cooksey, J. P.; Gao, Z.; Kocieński, P. J.; McAteer, S. M.; Snaddon, T. N. A Formal synthesis of Ionomycin featuring a permanganate-mediated oxidative cyclisation. *Synthesis* **2011**, *2011*, 104−108; h) Sheikh, N. S. Stereoselective synthesis of *trans*-THF rings using an oxidative cyclisation-radical deoxygenation sequence: Application to the formal synthesis of *trans*-(2R,5R)-linalool oxide. *RSC Adv.* **2015**, *5*, 3941−3953.

[56] Oppolzer, W.; Mills, R. J.; Reglier, M. Efficient asymmetric hydrogenations of camphor-sultam-imide-conjugated alkenes. *Tetrahedron Lett.* **1986**, *27*, 183−186.

[57] a) Otaka, A.; Mitsuyama, E.; Kinoshita, T.; Tamamura, H.; Fujii, N. Stereoselective synthesis of CF2-substituted phosphothreonine mimetics and their incorporation into peptides using newly developed deprotection procedures. *J. Org. Chem.* **2000**, *65*, 4888–4899; b) Otaka, A.; Mitsuyama, E.; Watanabe, J.; Watanabe, H.; Fujii, N. Synthesis of fluorine-containing bioisosteres corresponding to phosphoamino acids and dipeptide units. *J. Pept. Sci.* **2004**, *76*, 140−149; c) Jawaid, S.; Farrugia, L. J.; Robins, D. J. Asymmetric synthesis of 2-substituted butane-1,4-diols by hydrogenation of homochiral fumaramide derivatives. *Tetrahedron: Asymmetry* **2004**, *15*, 3979–3988; d) Pigza, J. A.; Quach, T.; Molinski, T. F. Oxazoline−oxazinone oxidative rearrangement. Divergent syntheses of (2S,3S)-4,4,4-trifluorovaline and (2S,4S)-5,5,5-trifluoroleucine. *J. Org. Chem.* **2009**, *74*, 5510−5515; e) Kumazaki, E.; Nagano, H. Stereoselective catalytic hydrogenation and conjugate reduction of 4-methyl itaconate derivatives bearing a chiral auxiliary. *Tetrahedron* **2013**, *69*, 3486–3494.

[58] For some representative reviews see: a) Zhou, Y.-G. Asymmetric hydrogenation of heteroaromatic compounds. *Acc. Chem. Res.* **2007**, *40*, 1357−1366; b) Wang, D.-S.; Chen, Q.-A.; Lu, S.-M.; Zhou, Y.-G. Asymmetric hydrogenation of heteroarenes and arenes. *Chem. Rev.* **2012**, *112*, 2557−2590; c) Etayo, P.; Vidal-Ferran, A. Rhodium-catalysed asymmetric hydrogenation as a valuable synthetic tool for the preparation of chiral drugs. *Chem. Soc. Rev.* **2013**, *42*, 728−754; d) Wang, D.; Astruc, D. The golden age of transfer hydrogenation. *Chem. Rev.* **2015**, *115*, 6621−6686; e) Zhang, Z.; Butt, N. A.; Zhang, W. Asymmetric hydrogenation of nonaromatic cyclic substrates. *Chem. Rev.* **2016**, *116*, 14769−14827.

[59] For example: a) Shang, J.; Han, Z.; Li, Y.; Wang, Z.; Ding, K. Highly enantioselective asymmetric hydrogenation of (*E*)-β,β-disubstituted α,β-unsaturated Weinreb amides catalyzed by Ir(i) complexes of SpinPhox ligands. *Chem. Commun.* **2012**, *48*, 5172−5174; b) Yan, Q.; Kong, D.; Zhao, W.; Zi, G.; Hou, G.

Enantioselective hydrogenation of β,β-disubstituted unsaturated carboxylic acids under base-free conditions. *J. Org. Chem.* **2016**, *81*, 2070−2077.

[60] Valentine, D.; Johnson, K. K.; Priester, W.; Sun, R. C.; Toth, K.; Saucy, G. Rhodium chiral monophosphine complex catalyzed hydrogenations of terpenic and .alpha.-(acylamino)-substituted acrylic acids. *J. Org. Chem.* **1980**, *45*, 3698−3703.

[61] Ohta, T.; Takaya, H.; Kitamura, M.; Nagai, K.; Noyori, R. Asymmetric hydrogenation of unsaturated carboxylic acids catalyzed by BINAP-ruthenium(II) complexes. *J. Org. Chem.* **1987**, *52*, 3174−3176.

[62] Schönleber, M.; Hilgraf, R.; Pfaltz, A. Chiral bis(N-arylamino)phosphine-oxazolines: Synthesis and application in asymmetric catalysis. *Adv. Synth. Catal.* **2008**, *350*, 2033−2038.

[63] a) Woodmansee, D. H.; Muller, M.-A.; Neuburger, M.; Pfaltz, A. Chiral pyridyl phosphinites with large aryl substituents as efficient ligands for the asymmetric iridium-catalyzed hydrogenation of difficult substrates. *Chem. Sci.* **2010**, *1*, 72−78l; b) Woodmansee, D. H.; Müller, M.-A.; Tröndlin, L.; Hörmann, E.; Pfaltz, A. Asymmetric hydrogenation of α,β-unsaturated carboxylic esters with chiral iridium N,P ligand complexes. *Chem. Eur. J.* **2012**, *18*, 13780−13786.

[64] Khumsubdee, S.; Fan, Y.; Burgess, K. A Comparison between oxazoline-imidazolinylidene, -imidazolylidine, -benzimidazolylidene hydrogenation catalysts. *J. Org. Chem.* **2013**, *78*, 9969−9974.

[65] Zhao, J.; Burgess, K. Aldol-type chirons from asymmetric hydrogenations of trisubstituted alkenes. *Org. Lett.* **2009**, *11*, 2053−2056.

[66] Khumsubdee, S.; Burgess, K. Metathesis for catalyst design: Metacatalysis. *Tetrahedron* **2014**, *70*, 1326−1335.

[67] Adam, J.-M.; Foricher, J.; Hanlon, S.; Lohri, B.; Moine, G.; Schmid, R.; Stahr, H.; Weber, M.; Wirz, B.; Zutter, U. Development of a scalable synthesis of (S)-3-sluoromethyl-γ-butyrolactone, building block for Carmegliptin's lactam moiety. *Org. Process Res. Dev.* **2011**, *15*, 515−526

[68] Li, J. Q.; Quan, X.; Andersson, P. G. Highly enantioselective iridium-catalyzed hydrogenation of α,β-unsaturated esters. *Chem. Eur. J.* **2012**, *18*, 10609−10616.

[69] Huang, Y.; Li, P.; Dong, X.-Q.; Zhang, X. Synthesis of chiral seven-membered β-substituted lactams via Rh-catalyzed asymmetric hydrogenation. *Org. Biomol. Chem.* **2018**, *16*, 8819−8823.

[70] a) Leutenegger, U.; Madin, A.; Pfaltz, A. Enantioselective reduction of α,β-unsaturated carboxylates with $NaBH_4$ and catalytic amounts of chiral cobalt semicorrin complexes. *Angew. Chem. Int. Ed.* **1989**, *28*, 60−61; b) von Matt, P.; Pfaltz, A. Enantioselective conjugate reduction of α,β-unsaturated carboxamides

with semicorrin cobalt catalysts. *Tetrahedron: Asymmetry* **1991**, *2*, 691−700; c) Misun, M.; Pfaltz, A. Enantioselective reduction of electrophilic C=C Bonds with sodium tetrahydroborate and 'semicorrin' cobalt catalysts. *Helv. Chim. Acta* **1996**, *79*, 961−972.

[71] Appella, D. H.; Moritani, Y.; Shintani, R.; Ferreira, E. M.; Buchwald, S. L. Asymmetric conjugate reduction of α,β-unsaturated esters using a chiral phosphine−copper catalyst. *J. Am. Chem. Soc.* **1999**, *121*, 9473−9474.

[72] Hughes, G.; Kimura, M.; Buchwald, S. L. Catalytic enantioselective conjugate reduction of lactones and lactams. *J. Am. Chem. Soc.* **2003**, *125*, 11253−11258.

[73] a) Lipshutz, B. H.; Servesko, J. M. CuH-catalyzed asymmetric conjugate reductions of acyclic enones. *Angew. Chem. Int. Ed.* **2003**, *42*, 4789−4792; b) Lipshutz, B. H.; Servesko, J. M.; Petersen, T. B.; Papa, P. P.; Lover, A. A. Asymmetric 1,4-reductions of hindered β-substituted cycloalkenones using catalytic SEGPHOS−ligated CuH. *Org. Lett.* **2004**, *6*, 1273−1275; c) Lipshutz, B. H.; Servesko, J. M.; Taft, B. R. Asymmetric 1,4-hydrosilylations of α,β-unsaturated esters. *J. Am. Chem. Soc.* **2004**, *126*, 8352−8353.

[74] a) Tsuchiya, Y.; Kanazawa, Y.; Shiomi, T.; Kobayashi, K.; Nishiyama, H. Asymmetric conjugate reduction of α,β-unsaturated esters with chiral rhodium(bisoxazolinylphenyl) catalysts. *Synlett* **2004**, *2004*, 2493−2496; b) Kanazawa, Y.; Tsuchiya, Y.; Kobayashi, K.; Shiomi, T.; Itoh, J. i.; Kikuchi, M.; Yamamoto, Y.; Nishiyama, H. Asymmetric conjugate reduction of α,β-unsaturated ketones and esters with chiral rhodium(2,6-bisoxazolinylphenyl) catalysts. *Chem. Eur. J.* **2006**, *12*, 63−71.

[75] a) Geiger, C.; Kreitmeier, P.; Reiser, O. Cobalt(II)-azabis(oxazoline)-catalyzed conjugate reduction of α,β-unsaturated carbonyl compounds. *Adv. Synth. Catal.* **2005**, *347*, 249−254; b) Shuto, Y.; Yamamura, T.; Tanaka, S.; Yoshimura, M.; Kitamura, M. Asymmetric $NaBH_4$ 1,4-reduction of C3-disubstituted 2-propenoates catalyzed by a diamidine cobalt complex. *ChemCatChem* **2015**, *7*, 1547−1550.

[76] Blaser, H. U.; Malan, C.; Pugin, B.; Spindler, F.; Steiner, H.; Studer, M. Selective hydrogenation for fine chemicals: Recent trends and new developments. *Adv. Synth. Catal.* **2003**, *345*, 103–151.

[77] Asymmetric conjugate addition is another viable route to access to β-chiral carboxylic acid derivatives. For a review see: Harutyunyan, S. R.; den Hartog, T.; Geurts, K.; Minnaard, A. J.; Feringa, B. L. Catalytic asymmetric conjugate addition and allylic alkylation with Grignard reagents. *Chem. Rev.* **2008**, *108*, 2824−2852.

[78] White, T. D.; Berglund, K. D.; Groh, J. M.; Johnson, M. D.; Miller, R. D.; Yates, M. H. Development of a continuous Schotten–Baumann route to an acyl sulfonamide. *Org. Process Res. Dev.* **2012**, *16*, 939−957.

[79] a) Hisamoto, H.; Saito, T.; Tokeshi, M.; Hibara, A.; Kitamori, T. Fast and high conversion phase-transfer synthesis exploiting the liquid-liquid interface formed in a microchannel chip. *Chem. Commun.* **2001**, *0*, 2662−2663; b) Ueno, M.; Hisamoto, H.; Kitamori, T.; Kobayashi, S. Phase-transfer alkylation reactions using microreactors. *Chem. Commun.* **2003**, 936−937; c) Jovanović, J.; Rebrov, E. V.; Nijhuis, T. A.; Hessel, V.; Schouten, J. C. Phase-transfer catalysis in segmented flow in a microchannel: Fluidic control of selectivity and productivity. *Ind. Eng. Chem. Res.* **2010**, *49*, 2681−2687.

[80] O'Brien, M.; Koos, P.; Browne, D. L.; Ley, S. V. A prototype continuous-flow liquid-liquid extraction system using open-source technology. *Org. Biomol. Chem.* **2012**, *10*, 7031−7036.

[81] Achard, D.; Grisoni, S.; Malleron, J. L.; Peyronel, J. F.; Tabart, M. Preparation of perhydroisoindoles as substance P antagonists. U.S. Patent 5463077, 1995.

[82] The commercially available H-Cube Mini from ThalesNano was used for this purpose, in combination with an in-house built PBR filled with Pd/C dispersed on glass beads to limit pressure drop (Figure AI.5). For a similar set up utilizing Pd/C dispersed in silica, see: Jensen, R. K.; Thykier, N.; Enevoldsen, M. V.; Lindhardt, A. T. A high mobility reactor unit for R&D continuous flow transfer hydrogenations. *Org. Process Res. Dev.* **2017**, *21*, 370–376.

[83] Degradation products from the tetraalkyl ammonium phase transfer catalyst or deprotonated auxiliary are plausible catalyst poisons.

[84] Elevating bed temperature was previously identified as crucial for extended catalyst life in packed beds of Pd/C, attributed to improvements in solvolytic cleaning of the catalyst surface. See: Knudsen, K. R.; Holden, J.; Ley, S. V.; Ladlow, M. Optimisation of conditions for *O*-benzyl and *N*-benzyloxycarbonyl protecting group removal using an automated flow hydrogenator. *Adv. Synth. Catal.* **2007**, *349*, 535−538.

[85] Dehmlow, E. V.; Thieser, R.; Sasson, Y.; Pross, E. The extraction of alkoxide anions by quaternary ammonium phase-transfer catalysis. *Tetrahedron* **1985**, *41*, 2927−2932.

[86] Wang, Y.; Gu, M. The concept of spectral accuracy for MS. *Anal. Chem.* **2010**, *82*, 7055−7062.

[87] Ogura, K.; Nishino, T.; Koyama, T.; Seto, S. Enzymic condensation of 3-methyl-2-alkenyl pyrophosphates with isopentenyl pyrophosphate. *J. Am. Chem. Soc.* **1970**, *92*, 6036−6041.

[88] Takimoto, M.; Hou, Z. Cu-catalyzed formal methylative and hydrogenative carboxylation of alkynes with carbon dioxide: Efficient synthesis of α,β-unsaturated carboxylic acids. *Chem. Eur. J.* **2013**, *19*, 11439–11445.

[89] Bellassoued, M.; Mouelhi, S.; Fromentin, P.; Gonzalez, A. Two-carbon homologation of ketones via sily ketene acetals: Synthesis of α,β-unsaturated acids and α-trimethylsilyl δ-ketoacids. *J. Organomet. Chem.* **2005**, *690*, 2172–2179.

[90] Yan, Q.; Kong, D.; Zhao, W.; Zi, G.; Hou, G. Enantioselective hydrogenation of β,β-disubstituted unsaturated carboxylic acids under base-free conditions. *J. Org. Chem.* **2016**, *81*, 2070–2077.

[91] Woodmansee, D. H.; Muller, M.-A.; Neuburger, M.; Pfaltz, A. Chiral pyridyl phosphinites with large aryl substituents as efficient ligands for the asymmetric iridium-catalyzed hydrogenation of difficult substrates. *Chem. Sci.* **2010**, *1*, 72–78.

[92] Ando, K.; Yamada, K. Highly *E*-selective solvent-free Horner-Wadsworth-Emmons reaction catalyzed by DBU. *Green Chem.* **2011**, *13*, 1143–1146.

[93] Tiseni, P. S.; Peters, R. Catalytic asymmetric formation of δ-lactones by [4+2] cycloaddition of zwitterionic dienolates generated from α,β-unsaturated acid chlorides. *Angew. Chem. Int. Ed.* **2007**, *46*, 5325–5328.

[94] Suzuki, T.; Ozaki, J.; Sugawara, R. Synthesis of optically active aggregation pheromone analogues of the red flour beetle, *Tribolium castaneum*. *Agric. Biol. Chem.* **1983**, *47*, 869–875.

[95] López, F.; Harutyunyan, S. R.; Meetsma, A.; Minnaard, A. J.; Feringa, B. L. Copper-catalyzed enantioselective conjugate addition of Grignard reagents to α,β-unsaturated esters. *Angew. Chem. Int. Ed.* **2005**, *44*, 2752–2756.

[96] Trost, B. M.; Masters, J. T.; Taft, B. R.; Lumb, J.-P. Asymmetric synthesis of chiral [small beta]-alkynyl carbonyl and sulfonyl derivatives via sequential palladium and copper catalysis. *Chem. Sci.* **2016**, *7*, 6217–6231.

[97] Hou, C.-J.; Guo, W.-L.; Hu, X.-P.; Deng, J.; Zheng, Z. Chiral ferrocenyl phosphine-phosphoramidite ligands for Cu-catalyzed asymmetric conjugate reduction of α,β-unsaturated esters. *Tetrahedron: Asymmetry* **2011**, *22*, 195–199.

Chapter 3 Enabling Substitution Reactions in Flow by Selecting Organic Bases that Form Protic Ionic Liquids[a,b]

3.1 Introduction

The extensive re-optimization required in Chapter 2 to adapt previously published batch reactions into a flow process — primarily required to avoid solid handling issues during the acylation and hydrolysis steps — brought to our attention how frequently major adaptation is required when transitioning from batch to flow simply to avoid solid formation. This is perhaps unsurprising considering most reactions are discovered and optimized in traditional flasks, where the limitations of batch are addressed but those of flow are not considered. The incompatibility of solids is arguably the most significant of these. Since most flow reactions often involve pumping homogeneous reactant streams through tubular reactors, even small amounts of solid can result in clogging, fouling, or failure of the various pumps, tubes and other reactor components.

As a result, prevention of solid formation must be addressed on a case-by-case basis for each reaction conducted, creating an economic and psychological barrier to widespread implementation of flow processes. Since continuous flow processing has been identified as one the most important areas of research to improve sustainability by leaders in the pharmaceutical and fine chemical industries,[1] a solution to address this barrier would be highly valuable.

3.1.1 Avoiding precipitation of base·HX salts

When considering the most important and frequently performed reactions in the pharmaceutical industry: acylations, arylations, and alkylations using acyl, aryl, and alkyl halides, respectively (Scheme 3.1) the severity and commonality of the solid handling problem becomes clear.[2] These reactions generally require scavenging of the by-product acid by a stoichiometric

[a] Parts of this chapter have appeared in print: K. Kashani, S.; Sullivan, R. J.; Andersen, M.; Newman, S. G. Overcoming solid handling issues in continuous flow substitution reactions through ionic liquid formation. *Green Chem.* **2018**, *20*, 1748–1753. Excerpts from the results section have been adapted from K. Kashani, S.; Sullivan, R. J.; Andersen, M.; Newman, S. G. *Green Chem.* **2018**, *20*, 1748–1753 with permission from the Royal Soceity of Chemistry.

[b] The work in this Chapter was started by S. K. Kashani with investigation of the ability to enable acylation reactions using acid chlorides and protic ionic liquid forming organic bases. After his initial results were promising we divided the subsequent work. S. K. Kashani demonstrate scope for acylation reactions and optimized and demonstrated scope for S_NAr reactions; I optimized and demonstrated scope for S_N2 reactions and demonstrated the ability to apply the strategy in telescoped multistep synthesis. Lastly, we each performed one silylation scope example.

base. While trivial in batch, this is frustratingly challenging in flow since inorganic bases are insoluble in most organic solvents, as are the conjugate acids of many organic bases (e.g., $Et_3N{\cdot}HCl$).

Scheme 3.1. Substitution reactions commonly lead to solid handling problems when converting to flow.

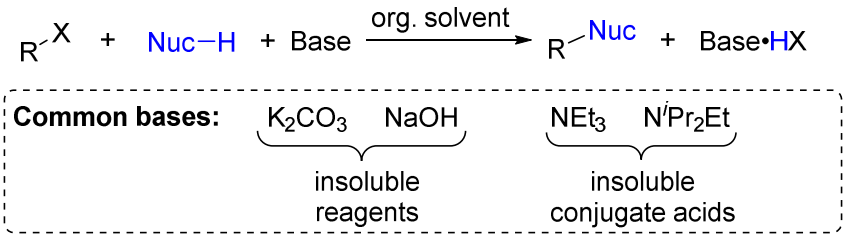

Many tailored solutions have been implemented to maintain homogeneity for desired reactions in flow. By far the most common approach is to modify the reaction solvent(s) and concentration. While conducting reactions in polar solvents (e.g., EtOH, NMP, DMF) or at dilute concentrations are often successful approaches to prevent precipitate formation, implementing these modifications undermines the very benefits that motivate conversion to flow in the first place. Specifically, the excellent heat and mass transfer achievable in flow can efficiently handle exotherms, allowing reactions to be run more concentrated,[3] and the ability to telescope multiple reaction steps together into one process reduces waste and increases efficiency.[4] Clearly, when prevention of precipitate formation requires a reaction to be performed more dilute, this is not achieving the desired benefits of flow processing.[5] Likewise, for the telescoping of multi-step reactions it is desirable to be able to use continuous liquid-liquid extractions for removal of impurities/by-products between steps, but this is not possible if a highly polar, and therefore water miscible, solvent is required to maintain reaction homogeneity.

3.1.2 Engineering solutions to prevent precipitation

An alternate approach to handle solids in a continuous process is to use an engineering solution, i.e., design a reactor capable of handling solid formation. Many examples of this have been presented, but successful implementation requires capital investment and engineering expertise, making these solutions less generally applicable to the average chemist. Use of sonication to prevent solids aggregation is the conceptually simplest approach,[6] but other strategies

including design of miniaturized continuous stirred tank reactors,[7] screw extrusion reactors,[8] or use of crystal seeding to prevent solids aggregation[9] have been reported.[10]

3.1.3 Preventing precipitation using ionic liquid acid scavengers

A simpler, more universal solution to efficiently enable substitution reactions in flow would be to use bases for which neither the free base nor conjugate acid is prone to precipitate formation. For instance, in the BASF BASIL process, 1-methylimidazole (MIm, **3.3**) is used as a base in the condensation of alcohols with chlorophosphines (Scheme 3.2).[11] 1-Methylimidazolium chloride (**3.5**), the conjugate acid, is a protic ionic liquid (pK_a = 7.1; mp = 70 °C)[12] that forms a discrete second liquid phase as the reaction progresses (Figure 3.1), avoiding solid-handling issues and enabling easy separation and recovery of all reaction components. Other salts with moderate melting points include tributylammonium chloride (**3.6**, pK_a = 10.9; mp = 60 °C)[13] and DBU hydrochloride (**3.7**, pK_a = 13.5; mp = 66 °C).[14]

Scheme 3.2. The BASF BASIL process.

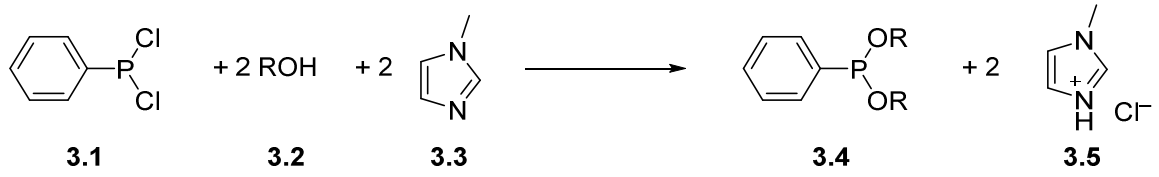

3.1 3.2 3.3 3.4 3.5

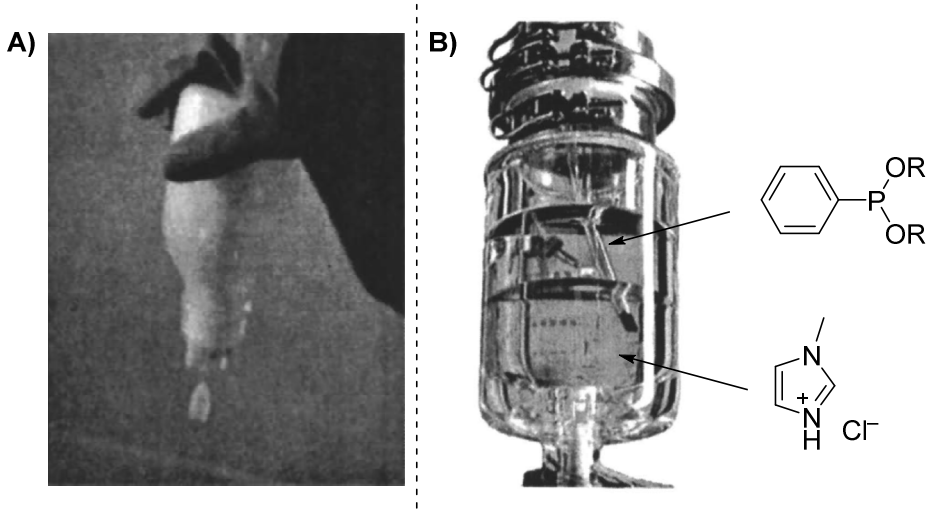

Figure 3.1. Reaction mixtures after synthesis of dialkoxyphenylphosphines. A) A thick slurry forms if using a tertiary amine as the acid scavenger. B) Two immiscible liquid phases form if using MIm as the acid scavenger. Reproduced from ref 11b with permission from ACS publications.

While protic ionic liquids have been explored as solvents or catalysts,[12c] the synthetic potential of forming these species as side products has not been widely recognized.[15] It was hypothesized that the BASF BASIL strategy could be generalized for a variety of important reactions that require acid scavenging in flow, without imposing limitations on the concentrations or solvents that could be used (Scheme 3.3).

Scheme 3.3. Flow substitution reactions enabled by ionic liquid forming acid scavengers.

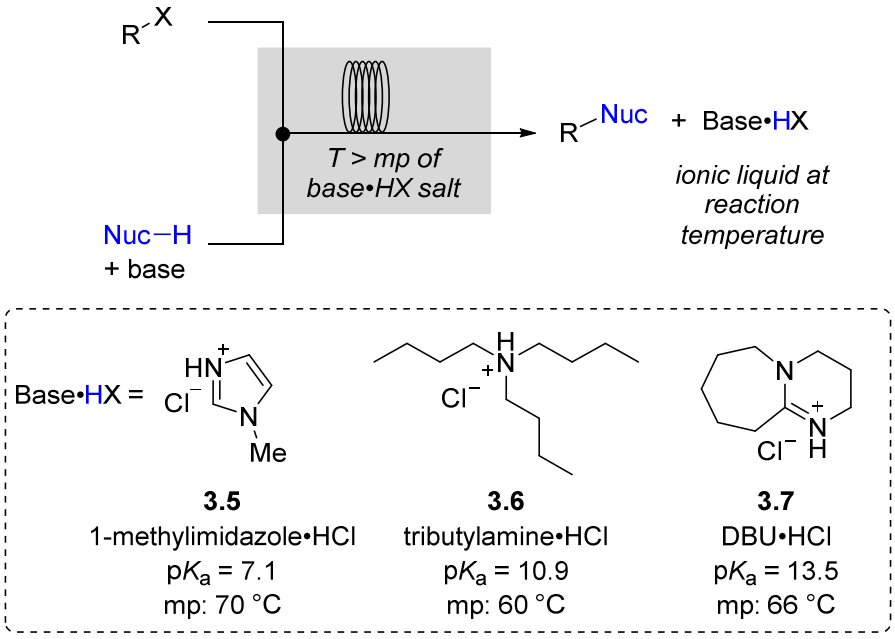

3.2 Results and Discussion

Initially the use of acid chlorides in continuous flow acylation chemistry with oxygen, nitrogen, and sulfur-centered nucleophiles was investigated. These seemingly trivial transformations can give significant precipitation problems when operating in continuous flow, a challenge further enhanced when operating under relatively concentrated conditions with non-polar solvents. Toluene was selected as the solvent and a range of concentrations was evaluated to examine the effectiveness of using an ionic liquid generating base.

The reaction of benzoyl chloride (**3.8**) and phenol (**3.9**) was used as a model reaction (Table 3.1). Performing a 0.5 M reaction at 90 °C in toluene using triethylamine (entry 1), *N*-methylmorpholine (entry 2) or *N*-methylpiperidine (entry 3) as the base led to rapid clogging of 1 mm I.D. tubing with precipitated conjugate acid. On the other hand, using 1-methylimidazole

(MIm, entry 4), tributylamine (entry 5), or DBU (entry 6) as the organic base allowed the reaction to proceed smoothly, giving high yields of ester **3.10**. In each case, phase separation of a new ionic liquid phase was observed in the PFA reactor coils before addition of water to prevent crystallization of the salt after exiting the heated reaction zone. Furthermore, performing the reaction at 2 M concentration, where the volume of the phase-separated ionic liquid generated was comparable to the organic phase, clearly demonstrated that this strategy does not impose concentration limitations because solubility of the protonated acid scavenger in the organic phase is not a requirement (entry 7).

Table 3.1. Influence of bases on clogging in the acylation of phenol.[a]

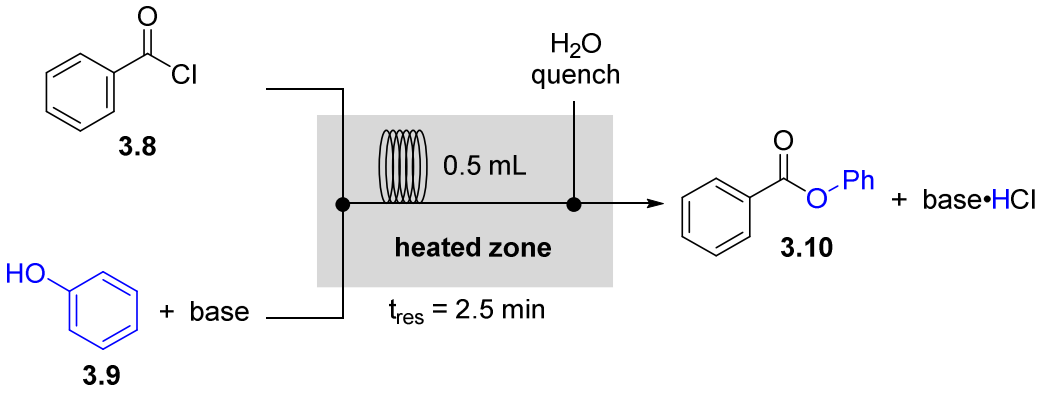

Entry	Base	Conc (M)	Temp (°C)	Yield (%)[b]
1	Et_3N	0.5	90	Clog
2	*N*-methylmorpholine	0.5	90	Clog
3	*N*-methylpiperidine	0.5	90	Clog
4	1-methylimidazole	0.5	90	95
5	Bu_3N	0.5	90	95
6	DBU	0.5	90	91
7	1-methylimidazole	2	90	99

[a] Reactions performed in a 0.5 mL PFA coil with 1.25 eq. of phenol and base with t_{res} = 2.5 min. See Experimental for full details. [b] Yield determined by ^{1}H NMR of the crude mixture of a sample collected at steady state.

The strategy of using MIm (**3.3**) as a base to enable continuous acylation reactions at high concentrations proved to be general (Table 3.2). By running reactions at 0.5 M in toluene with 1.25 equivalents of phenol and base, phenyl benzoate **3.10** could be isolated in 83% yield. The same conditions could be applied using an electron-deficient or electron-rich phenol derivative to

isolate **3.11** and **3.12**, respectively. Use of an aliphatic alcohol did not require re-optimization, enabling ester **3.13** to be prepared in 78% yield. Due to their moderate solubility in toluene at 0.5 M, anilides **3.14**–**3.17** were prepared in good yields using THF instead as the reaction solvent with the inclusion of a 40 psi back pressure regulator at the product outlet to prevent solvent boiling. Lastly, the preparation of amides via substitution of acid chlorides with aliphatic amines required use of DBU rather than MIm as the base. Since the pK_a of MIm is lower than typical amine nucleophiles, it is not sufficiently basic to use as a terminal base in these cases, and instead the secondary amines are protonated, leading to precipitation/clogging. DBU on the other hand is sufficiently basic (pK_a of conjugate acid = 13.5) to serve as the terminal base without competition from the amine nucleophiles, allowing amides **3.18** and **3.19** to be synthesized in 95% and 91% yield, respectively.

Other classes of substitution reactions were then targeted: arylations and alkylations via S_NAr and S_N2 mechanisms, respectively. These more challenging transformations are commonly run in polar, highly solubilizing solvents such as DMF and EtOH. However, solid-handling issues are still commonly encountered when trying to run these reactions in flow due to the low solubility of the base·HX salts, and highly tailored conditions are often used including dilute conditions, aqueous co-solvent, or exceptionally high temperatures (for solubility studies of Et_3N salts in polar aprotic solvents see Appendix II, Table AII.1).[16] To test if the use of the ionic-liquid forming acid scavengers MIm and DBU would be similarly effective at preventing clogging in S_NAr reactions, a series of experiments was carried out with a range of nucleophilic and electrophilic partners (Table 3.3). The reaction of aliphatic amines with (hetero)nitroarenes proceeded smoothly when using NMP as a solvent at 1 M concentration to form **3.20**–**3.22** in excellent yield in 5 minutes at 115 °C. As was the case for acylation reactions, use of DBU was necessary to prevent competing protonation and precipitation of the amine nucleophile. The high basicity of DBU also enabled the synthesis of ether **3.23** in 89% yield under similar conditions via deprotonation of the corresponding phenol nucleophile. In contrast, thioether **3.24** could be prepared using less expensive MIm as the base due to the lower pK_a of the thiophenol nucleophile.

Table 3.2. Continuous flow acylation reactions without clogging through use of MIm or DBU as ionic liquid-forming acid scavengers.[a]

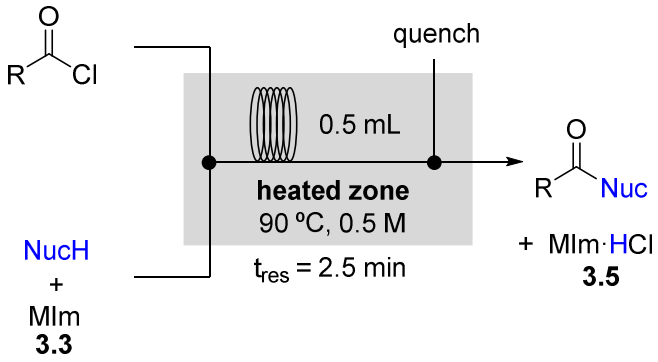

product	yield (%)	product	yield (%)	product	yield (%)
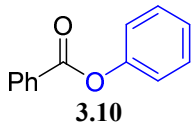 **3.10**	83	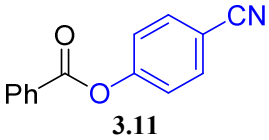 **3.11**	86	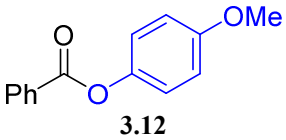 **3.12**	88
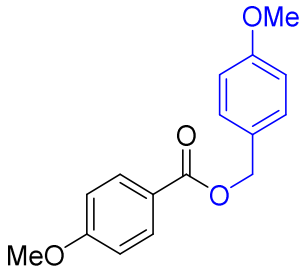 **3.13**	78	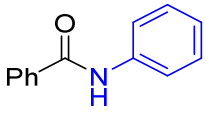 **3.14**	81	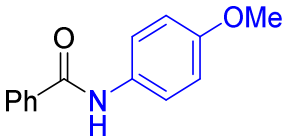 **3.15**	87
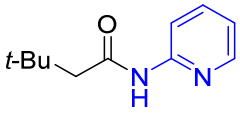 **3.16**	71	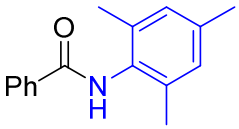 **3.17**	99	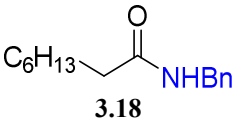 **3.18**	95[b]
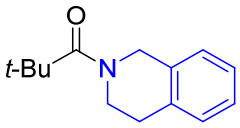 **3.19**	91[b]				

[a] Reactions performed in a 0.5 mL coil submerged in a 90 °C oil bath with 1.25 eq. of nucleophile and MIm as base. t_{res} = 2.5 min. Toluene was used as solvent for **3.10**–**3.13**. THF was used as solvent for **3.14-3.19**. Pure products were isolated by column chromatography or extraction (see Experimental) after collection of 1.25 mL at steady state. [b] DBU used as base.

Table 3.3. Continuous flow S_NAr reactions without clogging through use of DBU or MIm as ionic liquid-forming acid scavengers.[a]

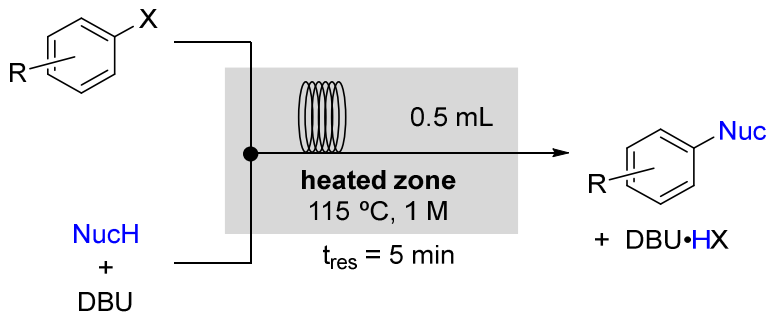

product	yield (%)	product	yield (%)	product	yield (%)
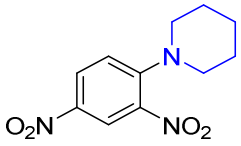 **3.20**, X = Cl	93	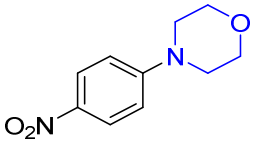 **3.21**, X = F	85	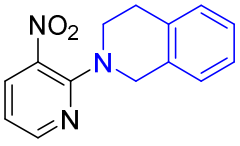 **3.22**, X = Cl	85
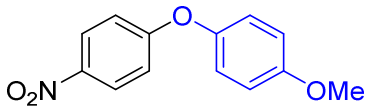 **3.23**, X = F	89[b]	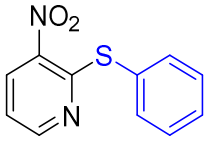 **3.24**, X = Cl	97[c]		

[a] Reactions performed in a 0.5 mL coil submerged in a 115 °C oil bath with 1.5 eq. of nucleophile and DBU as base. t_{res} = 5 min. NMP was used as solvent. Pure products were isolated by column chromatography after collection of 1.25 mL at steady state. [b] Reaction at 130 °C. t_{res} = 30 min. [c] Reaction performed in a 1 mL coil at 90 °C. t_{res} = 20 min at 0.5 M concentration with MIm as base.

A series of S_N2 reactions was next studied using Bu_3N as a general, inexpensive base (comparable in cost to Et_3N) that provides an ionic liquid conjugate acid upon protonation (Table 3.4). Without case-by-case optimization, *N*-methylaniline was alkylated using three different electrophiles with variation of the R substituent and the halide leaving group to form **3.25**–**3.27** in good yields, using only the minimal amount of solvent needed to make the electrophile starting material solutions (4 M in NMP) and dosing the nucleophile and base neat. The reaction of benzyl chloride with *N*-methylaniline could also be performed completely neat, providing 90% yield after work-up and purification, and giving 0.63 g (3.2 mmol) of product per hour through the 1 mL reactor coil. Use of thiophenol as a nucleophile was similarly straightforward, providing **3.28** in 83% yield. Lastly, the use of DBU again allowed the use of aliphatic amine nucleophiles, providing

access to alkylated products **3.29** and **3.30**. Notably, precipitate-free solutions were produced regardless of the leaving groups (F^-, Cl^-, Br^- and I^-) demonstrating the generality of this acid scavenging strategy. Furthermore, control reactions were performed using Et_3N as base in batch with otherwise identical conditions to the flow experiments. Precipitation was observed in each case, which would inevitably lead to clogging issues if performed in continuous flow.

Table 3.4. Continuous flow S_N2 reactions without clogging through use of Bu_3N or DBU as ionic liquid forming acid scavengers.[a]

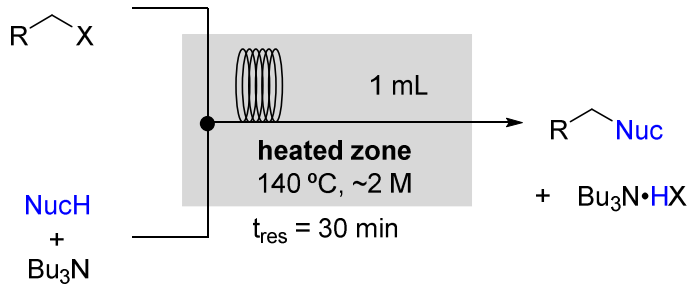

product	yield (%)	product	yield (%)	product	yield (%)
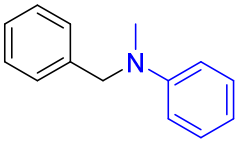 **3.25**, X = Cl	96 (90)[b]	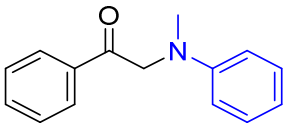 **3.26**, X = Br	78	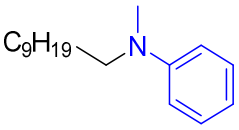 **3.27**, X = I	90
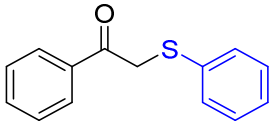 **3.28**, X = Br	83	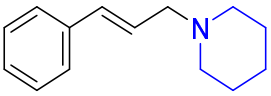 **3.29**, X = Cl	84[c]	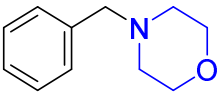 **3.30**, X = Cl	94[c]

[a] Reactions performed in a 1.0 mL coil submerged in a 140 °C oil bath with 1.25 eq. of electrophile and Bu_3N as base. t_{res} = 30 min. NMP was used as solvent. Pure products were isolated by column chromatography after collection of 2 mL at steady state. [b] Reaction performed neat. [c] DBU used as base.

Lastly, the protection of alcohols with TBSCl (**3.31**, Scheme 3.4) was investigated. These reactions are frequently carried out at mild temperatures in DCM using imidazole as both a base and nucleophilic catalyst,[17] resulting in precipitation of the imidazolium salt upon product formation. While the use of MIm at elevated temperatures may allow these reactions to proceed in flow without clogging issues, we instead chose to investigate 1-butylimidazole (**3.32**, BuIm). The corresponding HCl salt of this base melts at 29 °C,[12b,c] enabling the silylation reactions to be

studied at the mild temperatures common in the literature. Using 1.15 equivalents of **3.31** and 2 equivalents of **3.32**, silyl ethers **3.33** and **3.34** were prepared in excellent yield at 1 M concentration in DCM with a 5 minute residence time at 35 °C. Due to the higher cost of **3.32** compared to MIm, the ionic liquid by-product was isolated after the synthesis of **3.33** by collecting the phase separated conjugate acid, **3.32**·HCl, and treating with NaOH (**3.32**·HCl spontaneously phase separates from the DCM reaction mixture and remains as a second liquid phase at room temperature, see Figure 3.8 in the Experimental for a representative photograph). A 95% recovery was achieved after purification, demonstrating the recyclability of **3.32** if desired.

Scheme 3.4. Continuous flow silylation reactions without clogging through use of 1-butylimidazole as an ionic liquid forming acid scavenger.

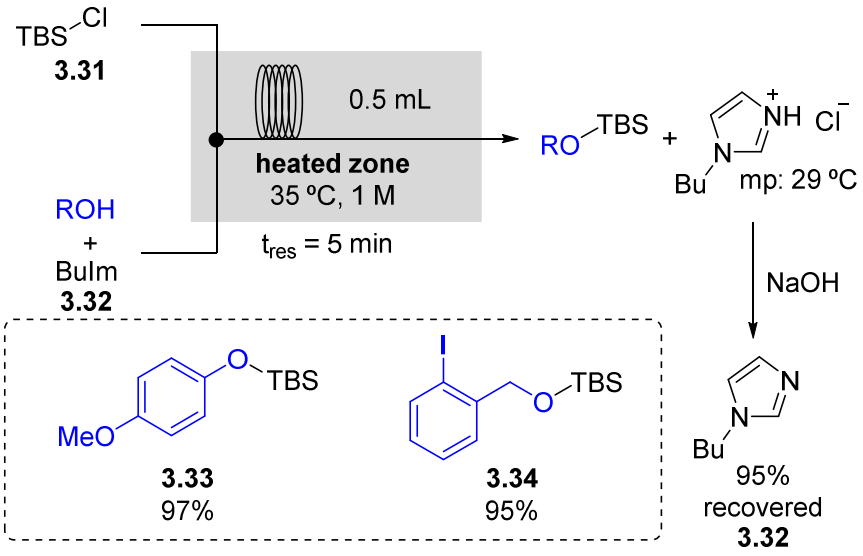

Towards demonstrating the simplicity with which the use of ionic liquid-forming acid scavengers can enable straightforward implementation of telescoped flow procedures, the synthesis of the local anaesthetic Lidocaine (**3.38**) was investigated. Previous flow routes towards this molecule required redevelopment of the literature conditions (i.e. toluene as solvent)[18] to use highly solubilizing $CHCl_3$/DMF[19] or NMP/MeOH/H_2O[20]. Using tributylamine as a base and toluene as solvent, 2-chloroacetylchloride (**3.35**) and 2,6-dimethylaniline (**3.36**) were mixed in a flow reactor at 90 °C, followed by addition of diethylamine (**3.37**) and DBU to give a 66% isolated yield of **3.38** (Scheme 3.5). At a 0.4 M concentration with a total residence time of 10.8 minutes

this allowed production of 0.37 g of **3.38** per hour in the 1.1 mL reactor coil, equivalent to a space time yield of 0.34 $kg \cdot h^{-1} \cdot L^{-1}$.

Scheme 3.5. Telescoped continuous flow synthesis of Lidocaine without clogging using Bu_3N and DBU as ionic liquid forming acid scavengers.

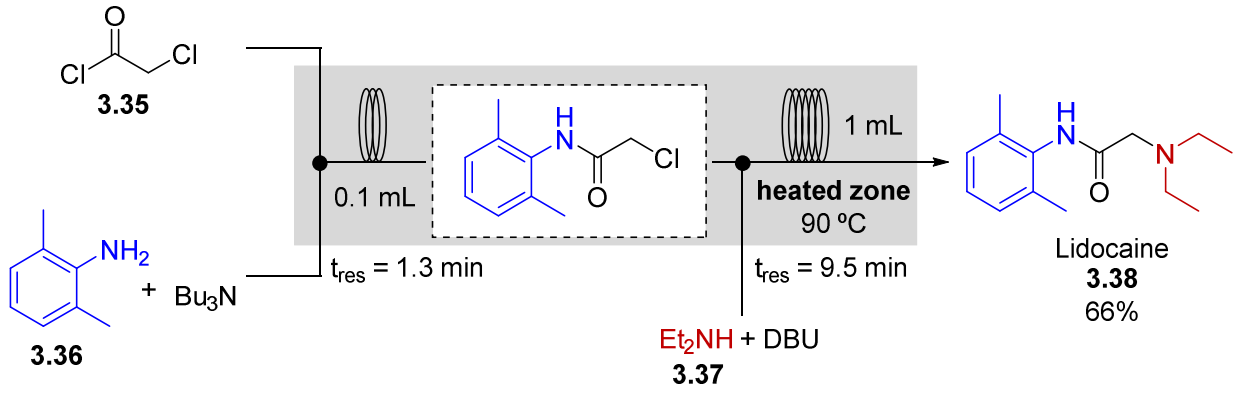

3.3 Conclusions

Despite the many advantages of running reactions continuously, the barriers associated with adapting batch procedures to flow hinders the adoption of this technology. The challenges associated with solid formation, particularly in reactions that require an acid scavenging base, are some of the most common and frustrating problems in flow chemistry. Through the rational selection of bases that form ionic liquids upon protonation, these solid-handling issues can be easily alleviated. In particular, 1-methylimidazole, tributylamine, DBU, and 1-butylimidazole enable precipitate-free reactions of acyl, aryl, alkyl, and silyl halide electrophiles using N, O, and S nucleophiles. These reactions give high yields with short reaction times. Furthermore, concentrations ranging from 0.5 M to neat are utilized, demonstrating that the improved efficiency theoretically possible with a flow process (due to effective heat and mass transfer) can be easily realized for reactions that generate stoichiometric base·HX by-products using this strategy. In the case where the base utilized is less accessible than a more traditional alternative (i.e., 1-butylimidazole), it was also demonstrated that direct recovery from the reaction mixture is trivial. Lastly, the ability to simplify implementation of telescoped processes for multistep syntheses was demonstrated by the synthesis of Lidocaine via sequential acylation and alkylation reactions.

3.4 Experimental

3.4.1 General experimental details

Unless otherwise indicated, reagents were obtained from Sigma Aldrich, Fisher Scientific or Combi-Blocks and used as received. 2-Bromoacetophenone was recrystallized from EtOH, 4-methoxyphenol was recrystallized from benzene, and cinnamyl chloride was distilled over K_2CO_3 prior to use.

^{1}H NMR and ^{13}C NMR were recorded on a Bruker AVANCE 400 MHz spectrometer and referenced to residual solvent signals. Yields for optimization studies were determined by NMR or GC analysis of the crude reaction mixture using 1,3,5-trimethoxybenzene as an internal standard. IR spectra were collected on a Thermo Scientific Nicolet 6700 FTIR equipped with a diamond ATR crystal (ThermoScientific) and are reported in terms of frequency of absorption (cm^{-1}). GC analysis were conducted on an Agilent Technologies 7890B GC with 30 m × 0.25 mm HP-5 column. Accurate mass data were obtained from an Agilent 5977A GC/MS using MassWorks 4.0 from CERNO bioscience.[21] Continuous flow experiments were performed using 1.0 mm inner diameter PFA tubing reactor coils heated in silicone oil baths and NewEra NE-300 syringe pumps equipped with 5 or 10 mL Hamilton Gastight glass syringes for reagents and 10 mL HSW norm-ject plastic syringes for quench streams when necessary. PEEK fittings, tee mixers and back-pressure regulators were purchased from UpChurch Scientific.

3.4.2 General procedures

Note: For flow reactions it is important to correctly prepare solutions of stated concentration, i.e., solute is weighed into a calibrated volumetric apparatus and filled to desired final solution volume with solvent. Assuming negligible volume of solute and simply adding the desired solution volume worth of solvent is an incorrect practise and results in substantial stoichiometry errors when dealing with concentrated solutions (e.g., adding 1.0 mL of solvent to 0.5 mmol of solute does not prepare a 0.5 M solution, but rather a substantially less concentrated solution depending on the solute).

General procedure A for acylation reactions to produce esters. Nucleophile (2.25 mmol) and base (2.25 mmol) were combined and made up to 2.00 ml with toluene to give a 1.125 M solution

and loaded into a 5 mL Hamilton Gastight syringe. Electrophile (2.25 mmol) was made up to 2.00 mL with toluene to make a 1.125 M solution and loaded into a second 5 mL Hamilton Gastight syringe. The continuous flow reactor depicted in Figure 3.2 was used with flow rates of 89 μL/min for electrophile solution and 111 μL/min for nucleophile solution to give a residence time of 2.5 min and a 1:1.25:1.25 ratio of electrophile:nucleophile:base (MIm) through a 0.5 mL reactor coil submerged in a 90 °C oil bath. To quench the reaction mixture at the end of the reactor, pump C was loaded with water with flow rate of 300 μL/min, and a 5 psi back pressure regulator was set at the end of the outlet line. The first 6 min (2.5 residence volumes) of effluent was discarded to reach steady state, then effluent was collected for 5 min. 1 M HCl (20 mL) was added to the collected effluent and the product was extracted with DCM (3 × 40 mL). The combined organic extracts were washed with 2 M NaOH (40 mL), dried over Na_2SO_4 and the solvent evaporated. The residue was chromatographed on silica gel to yield the pure product.

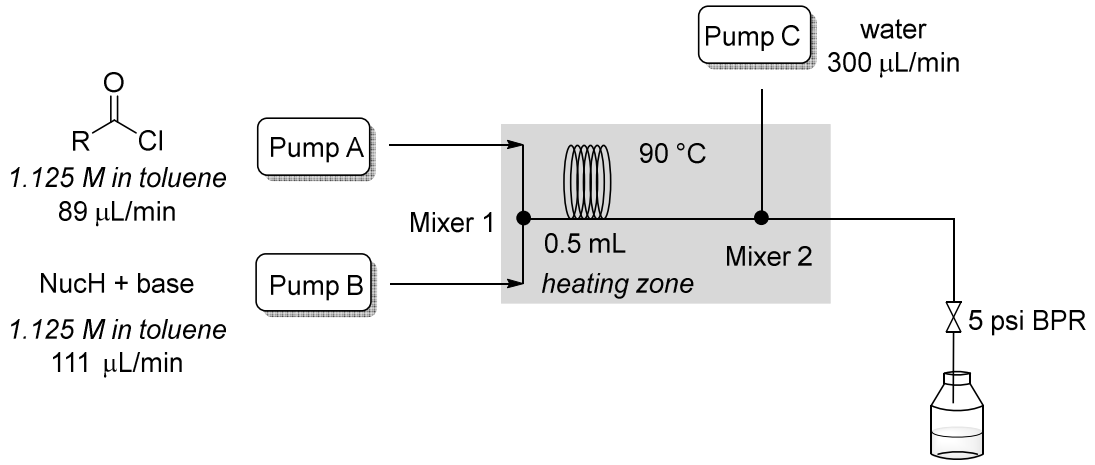

Figure 3.2. Schematic of flow reactor used for acylation reactions to produce esters.

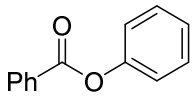

Phenyl benzoate (**3.10**):[a] General procedure A was followed with reaction of benzoyl chloride and phenol. Column chromatography (6:1 hexanes:EtOAc) yielded the pure product as a white solid (83 mg, 83% yield). Characterization data were in agreement with the literature.[22] ^{1}H NMR (400 MHz, $CDCl_3$) δ 8.22 (d, J = 6.9 Hz, 2 H), 7.65 (t, J = 8.2 Hz, 1H), 7.52 (t, J = 7.0 Hz, 2H), 7.44

[a] Prepared by S. K. Kashani

(t, J = 8.3 Hz, 2H), 7.32-7.18 (m, 3H). $^{13}C\{^{1}H\}$ NMR (100 MHz, $CDCl_3$) δ 165.3, 151.1, 133.7, 130.3, 129.7, 129.6, 128.7, 126.0, 121.9.

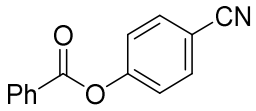

4-Cyanophenyl benzoate (**3.11**):[a] General procedure A was followed with reaction of benzoyl chloride and 4-cyanophenol. Column chromatography (3:1 hexanes:EtOAc) yielded the pure product as a white solid (96 mg, 86% yield). Characterization data were in agreement with the literature.[22] ^{1}H NMR (400 MHz, $CDCl_3$) δ 8.20 (d, J = 7.8 Hz, 2H), 7.75 (d, J = 9.1 Hz, 2H), 7.68 (t, J = 7.6 Hz, 1H), 7.54 (t, J = 7.9 Hz, 2H), 7.37 (d, J = 8.6 Hz, 2H). $^{13}C\{^{1}H\}$ NMR (100 MHz, $CDCl_3$) δ 164.4, 154.4, 134.3, 133.9, 130.4, 128.9, 128.8, 123.1, 118.4, 110.0.

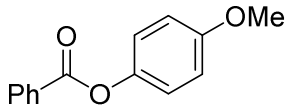

4-Methoxyphenyl benzoate (**3.12**):[a] General procedure A was followed with reaction of benzoyl chloride and 4-methoxyphenol. Column chromatography (3:1 hexanes:EtOAc) yielded the pure product as a white solid (100 mg, 88% yield). Characterization data were in agreement with the literature.[23] ^{1}H NMR (400 MHz, $CDCl_3$) δ 8.20 (d, J = 8.1 Hz, 2 H), 7.63 (t, J = 7.8 Hz, 1H), 7.51 (t, J = 7.8 Hz, 2H), 7.13 (d, J = 9.0 Hz, 2H), 6.94 (d, J = 9.9 Hz, 2H) 3.82 (s, 3H). $^{13}C\{^{1}H\}$ NMR (100 MHz, $CDCl_3$) δ 165.7, 157.5, 144.6, 133.6, 130.3, 129.8, 128.7, 122.6, 114.7, 55.7.

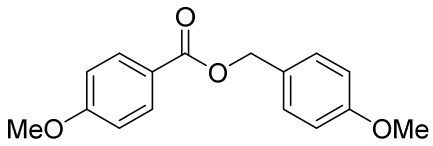

4-Methoxybenzyl 4-methoxybenzoate (**3.13**):[a] General procedure A was followed with reaction of 4-methoxybenzoyl chloride and 4-methoxybenzylalcohol. Column chromatography (10:1 hexanes:EtOAc) yielded the pure product as a colourless oil (107 mg, 78% yield). Characterization data were in agreement with the literature.[24] ^{1}H NMR (400 MHz, $CDCl_3$) δ 8.01 (d, J = 9.0 Hz, 2 H), 7.38 (d, J = 8.9 Hz, 2H), 7.94-6.87 (m, 4H), 5.27 (s, 2H), 3.84 (s, 3H), 3.81 (s, 3H). $^{13}C\{^{1}H\}$

[a] Prepared by S. K. Kashani

NMR (100 MHz, $CDCl_3$) δ 166.4, 163.5, 159.7, 131.8, 130.1, 128.5, 122.8, 114.1, 113.7, 66.4, 55.5, 55.4.

General procedure B for acylation reactions to produce amides. General procedure A was followed with three modifications. First, THF was used in the place of toluene for solution preparation. Second, an additional quench pump D, delivering 300 μL/min EtOAc was added as shown in Figure 3.3. Lastly, the back pressure was increased to 40 psi. The first 6 min (2.5 residence volumes) of effluent was discarded to reach steady state, then effluent was collected for 5 min. 1 M HCl (30 mL) was added to the collected effluent and the product was extracted with DCM (3 × 30 mL). The combined organic extracts were washed with 1 M NaOH (20 mL), dried over Na_2SO_4 and the solvent evaporated. The white solids obtained were washed with hexanes to yield pure products when applicable, otherwise chromatographed on silica gel to yield pure compound.

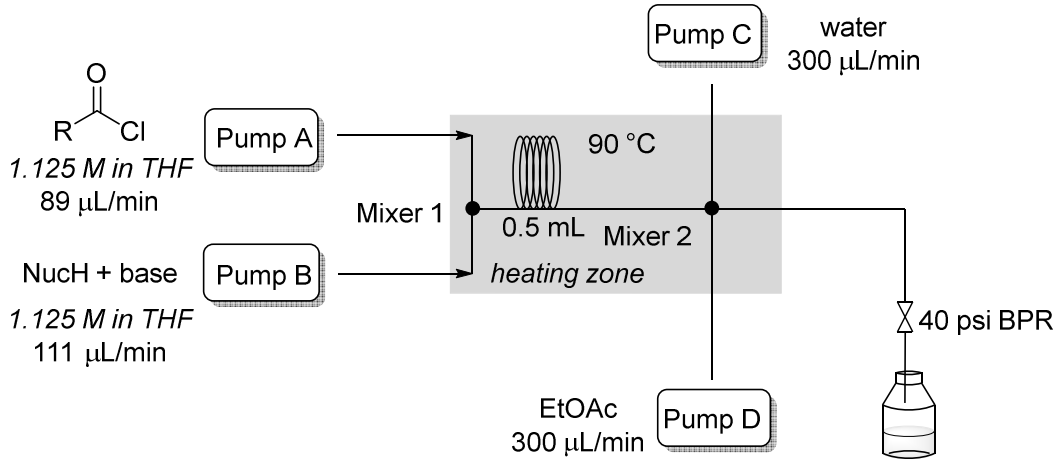

Figure 3.3. Schematic of flow reactor used for acylation reactions to produce amides.

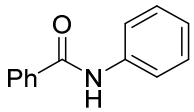

N-Phenylbenzamide (**3.14**):[a] General procedure B was followed with reaction of benzoyl chloride and aniline. Washing with hexanes yielded the pure product as a white solid (80 mg, 81% yield). Characterization data were in agreement with the literature.[25] ^1H NMR (400 MHz, $CDCl_3$) δ 7.88

[a] Prepared by S. K. Kashani

(d, J = 6.9 Hz, 2 H), 7.80 (br s, 1H), 7.64 (d, J = 7.6 Hz, 2H), 7.56 (t, J = 7.5 Hz, 1H), 7.50 (t, J = 7.6 Hz, 2H), 7.38 (t, J = 7.5 Hz, 2H), 7.16 (t, J = 7.3 Hz, 1H). $^{13}C\{^1H\}$ NMR (100 MHz, $CDCl_3$) δ 165.8, 138.1, 135.2, 131.9, 129.2, 128.9, 127.1, 124.7, 120.3.

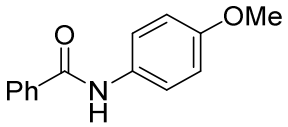

N-(4-Methoxyphenyl)benzamide (**3.15**):[a] General procedure B was followed with reaction of benzoyl chloride and 4-methoxyaniline. Washing with hexanes yielded the pure product as a white solid (99 mg, 87% yield). Characterization data were in agreement with the literature.[26] ^1H NMR (400 MHz, $CDCl_3$) δ 7.86 (d, J = 7.5 Hz, 2H), 7.75 (br s, 1H), 7.58-7.44 (m, 5H), 6.90 (d, J = 9.1 Hz, 2H), 3.82 (s, 3H). $^{13}C\{^1H\}$ NMR (100 MHz, $CDCl_3$) δ 165.8, 156.8, 135.2, 131.8, 131.1, 128.9, 127.1, 122.2, 114.4, 55.6.

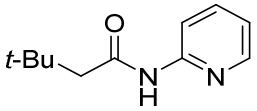

3,3-Dimethyl-N-(pyridin-2-yl)butanamide (**3.16**):[a] General procedure B was followed with reaction of 3,3-dimethylbutanoyl chloride and 2-aminopyridine. Column chromatography (3:1 hexanes:EtOAc) yielded the pure product as an off-white solid (68 mg, 71% yield). mp: 86–87 °C. ^1H NMR (400 MHz, $CDCl_3$) δ 8.53 (br s, 1H), 8.35-8.37 (m, 2H), 7.75-7.64 (m, 1H), 7.08-6.97 (m, 1H), 2.24 (s, 2H), 1.06 (s, 9H). $^{13}C\{^1H\}$ NMR (100 MHz, $CDCl_3$) δ 170.7, 151.7, 147.7, 138.6, 119.8, 114.3, 51.6. 31.4, 29.9. IR ν (cm^{-1}) 3243, 3074, 2952, 2861, 1658, 1590, 1576, 1523, 1474, 1456, 1428, 1395, 1361, 1328, 1306, 1285, 1233, 1146, 1134, 1095, 1051, 974, 952, 909, 878, 846, 805, 771, 737, 649, 618, 561. HRMS calc. for $C_{11}H_{16}N_2O$: 192.1019; found: 192.1106, spectral accuracy 99.3%.

[a] Prepared by S. K Kashani.

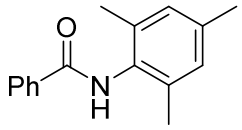

N-Mesitylbenzamide (**3.17**):[a] General procedure B was followed with and the modification that DCM was used in the place of EtOAc during the quench. The product was produced by reaction of benzoyl chloride and 2,4,6-trimethylaniline. Washing with hexanes yielded the pure product as a white solid (119 mg, 99% yield). Characterization data were in agreement with the literature.[27] ^{1}H NMR (400 MHz, CDCl3) δ 7.92 (d, *J* = 7.1 Hz, 2H), 7.58 (t, *J* = 6.4 Hz, 1H), 7.49 (t, *J* = 7.9 Hz, 2H), 7.35 (br s, 1H), 6.93 (s, 2H), 2.30 (s, 3H), 2.24 (s, 6H). 13C{1H} NMR (100 MHz, CDCl3) δ 166.2, 137.2, 135.4, 134.8, 131.8, 131.3, 129.1, 128.9, 127.3, 21.1, 18.5.

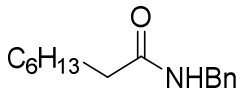

N-Benzyloctanamide (**3.18**):[a] General procedure B was followed with the modification that DCM was used in the place of EtOAc during the quench and DBU was used as base instead of MIm. The product was produced by reaction of octanoyl chloride and benzyl amine. Column chromatography (2:1 hexanes:EtOAc) yielded the pure product as a white solid (111 mg, 95% yield). Characterization data were in agreement with the literature.[28] ^{1}H NMR (400 MHz, $CDCl_3$) δ 7.36-7.24 (m, 5H), 5.72 (s, 1H), 4.44 (d, *J* = 5.6 Hz, 2H), 2.22 (t, *J* =7.4 Hz, 2H), 1.70-1.60 (m, 2H), 1.35-1.22 (m, 8H), 0.87 (t, *J* =6.7 Hz, 3H). ^{13}C{^{1}H} NMR (100 MHz, $CDCl_3$) δ 173.1, 138.6, 128.8, 128.0, 127.6, 43.7, 37.0, 31.8, 29.4, 29.1, 25.9, 22.7, 14.2.

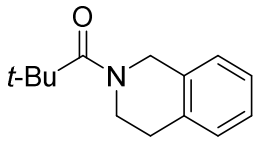

1-(3,4-Dihydroisoquinolin-2(1H)-yl)-2,2-dimethylpropan-1-one (**3.19**):[a] General procedure B was followed with the modification that DCM was used in the place of EtOAc during the quench and DBU was used as base instead of MIm. The product was produced by reaction of *tert*-butylacetyl chloride and 1,2,3,4-tetrahydroisoquinoline. Column chromatography (2:1 hexanes:EtOAc) yielded the pure product as a white solid (99 mg, 91% yield). Characterization data were in

[a] Prepared by S. K. Kashani

agreement with the literature.[29] ^{1}H NMR (400 MHz, $CDCl_3$) δ 7.23-7.07 (m, 4H), 4.75 (s, 2H), 3.85 (t, J = 5.9 Hz, 2H), 2.89 (t, J = 6.32 Hz, 2H), 1.32 (s, 9H). ^{13}C{^{1}H} NMR (100 MHz, $CDCl_3$) δ 176.8, 134.5, 133.7, 128.8, 126.6, 126.5, 126.4, 47.6, 43.5, 47.6, 43.5, 38.9, 29.1, 28.5.

General procedure C for S_NAr reactions with N nucleophiles. Nucleophile (9.0 mmol) and base (9 mmol) were combined and made up to 3.00 mL with NMP to make a 3.0 M solution and loaded into a 5 mL Hamilton Gastight syringe. Electrophile (6.0 mmol) was made up to 3.00 mL with NMP to make a 2.0 M solution and loaded into a second 5 mL Hamilton Gastight syringe. The continuous flow reactor depicted in Figure 3.4 was used with flow rates of 50 μL/min for both nucleophile and electrophile solutions, to give a residence time of 5 min and a 1:1.5:1.5 ratio of electrophile:nucleophile:base (DBU), through a 0.5 mL reactor submerged in a 115 °C oil bath. A 5 psi back pressure regulator provided back pressure for the system. The first 15 min (3 residence volumes) of effluent was discarded to reach steady state, then effluent was collected for 5 min. DCM (60 mL) was added to the collected effluent and the organic phase was washed with water (5 × 10 mL). The organic layer was dried over Na_2SO_4 and the solvent evaporated. The residue was chromatographed on silica gel to yield the pure product.

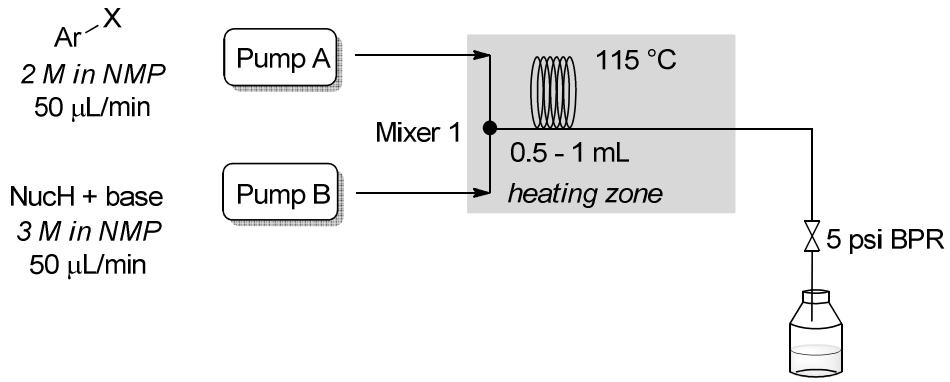

Figure 3.4. Schematic of flow reactor used for S_NAr reactions with N nucleophiles.

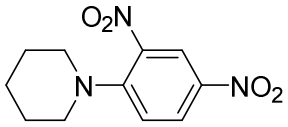

1-(2,4-Dinitrophenyl)piperidine (**3.20**):[a] General procedure C was followed with reaction of 2,4-dinitrochlorobenzene and piperidine. Column chromatography (3:1 hexanes:EtOAc) yielded the pure product as an orange solid (117 mg, 93% yield). Characterization data were in agreement with the literature.[30] ^{1}H NMR (400 MHz, $CDCl_3$): δ 8.68 (d, *J* = 2.8 Hz, 1H), 8.21 (dd, *J* =9.4, 2.7 Hz, 1H), 7.08 (d, *J* = 9.4 Hz, 1H), 3.28-3.22 (m, 4H), 1.77-1.67 (m, 6H). ^{13}C{^{1}H} NMR (100 MHz, $CDCl_3$): δ 149.9, 137.6, 128.2, 124.1, 119.2, 52.0, 25.6, 23.7.

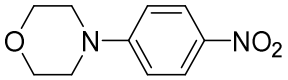

4-(4-Nitrophenyl)morpholine (**3.21**):[e] General procedure C was followed with reaction of 4-fluoronitrobenzene and morpholine. Column chromatography (1:2 hexanes:EtOAc) yielded the pure product as a yellow solid (88 mg, 85% yield). Characterization data were in agreement with the literature.[31] ^{1}H NMR (400 MHz, $CDCl_3$): δ 8.15 (d, *J* = 9.4 Hz, 2H), 6.84 (d, *J* =9.4 Hz, 2H), 3.87 (t, *J* = 5.1 Hz, 4H), 3.37 (t, *J* = 5.2 Hz, 4H). ^{13}C{^{1}H} NMR (100 MHz, $CDCl_3$): δ 155.1, 139.2, 126.0, 112.8, 66.5, 47.3.

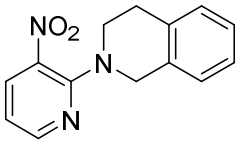

2-(3-Nitropyridin-2-yl)-1,2,3,4-tetrahydroisoquinoline (**3.22**):[a] General procedure C was followed with reaction of 2-chloro-3-nitro-pyridine and 1,2,3,4-tetrahydroisoquinoline. Column chromatography (3:1 hexanes:EtOAc) yielded the pure product as a yellow solid (151 mg, 85% yield). Characterization data were in agreement with the literature.[32] ^{1}H NMR (400 MHz, $CDCl_3$): δ 8.36 (dd, *J* = 4.5, 1.7 Hz, 1H), 8.17 (dd, *J* = 8.1, 1.8 Hz ,1H), 7.22-7.15 (m, 3H), 7.15-7.09 (m, 1H), 6.73 (q, *J* = 4.4 Hz,1H), 4.49 (s, 2H), 3.77 (t, *J* = 5.5 Hz, 2H), 3.02 (t, *J* = 5.8 Hz, 2H). ^{13}C{^{1}H} NMR (100 MHz, $CDCl_3$): δ 152.7, 151.9, 135.8, 135.2, 133.6, 132.4, 128.6, 126.9, 126.5, 126.4, 112.8, 50.4, 46.1, 28.7.

[a] Prepared by S. K. Kashani

General procedure D for SNAr reactions with O nucleophiles. General procedure C was followed with three modifications. First, the flow rates of the reagent pumps were set to 16.7 μL/min instead of 50 μL/min. Second, the 0.5 mL reactor coil was replaced with a 1.0 mL reactor coil. Third, the oil bath temperature was set to 130 °C instead of 115 °C. The first 75 min (2.5 residence volumes) of effluent was discarded to reach steady-state, then effluent was collected for 30 min. DCM (60 mL) was added to the collected effluent and the organic phase was washed with water (5 × 10 mL). The organic layer was dried over Na_2SO_4 and the solvent evaporated. The residue was chromatographed on silica gel to yield the pure product.

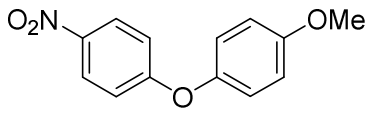

1-Methoxy-4-(4-nitrophenoxy)benzene (**3.23**):[a] General procedure D was followed with reaction of 4-fluoronitrobenzene and 4-methoxyphenol. Column chromatography (6:1 hexanes:EtOAc) yielded the pure product as an off-white solid (218 mg, 89% yield). Characterization data were in agreement with the literature.[33] ^{1}H NMR (400 MHz, CDCl3): δ 8.17 (d, *J* = 9.3 Hz, 2H), 7.03 (d, *J* = 9.1 Hz, 2H), 6.98-6.92 (m, 4H), 3.83 (s, 3H). ^{13}C{1H} NMR (100 MHz, CDCl3): δ 164.3, 157.3, 147.9, 142.4, 126.0, 122.0, 116.5, 115.4, 55.8.

General procedure E for SNAr reactions with S nucleophiles. Nucleophile (3.75 mmol) and base (3.75 mmol) were combined and made up to 3.00 ml with NMP to give a 1.25 M solution and loaded into a 5 mL Hamilton Gastight syringe. Electrophile (3.75 mmol) was made up to 3.00 mL with NMP to make a 1.25 M solution and loaded into a second 5 mL Hamilton Gastight syringe. The continuous flow reactor depicted in Figure 3.5 was used with flow rates of 10 μL/min for the electrophile solution and 15 μL/min for the nucleophile solution to give a residence time of 20 min and a 1:1.5:1.5 ratio of electrophile:nucleophile:base (MIm), through a 0.5 ml reactor submerged in a 90 °C oil bath. Two quench pumps, one delivering water at 37.5 μL/min and one delivering EtOAc at 37.5 μL/min prevented crystallization upon exiting the heated zone and a 5 psi back pressure regulator provided system pressure. The first 50 min (2.5 residence volumes) of effluent was discarded to reach steady state, then effluent was collected for 30 min. 1 M HCl (20 mL) was added to the collected effluent and the product was extracted with DCM (3 × 40 mL). The

[a] Prepared by S. K. Kashani

combined organic extracts were washed with 2 M NaOH (40 mL) and then distilled water multiple times to remove NMP from the solution, dried over Na_2SO_4 and the solvent evaporated. The residue was chromatographed on silica gel to yield the pure product.

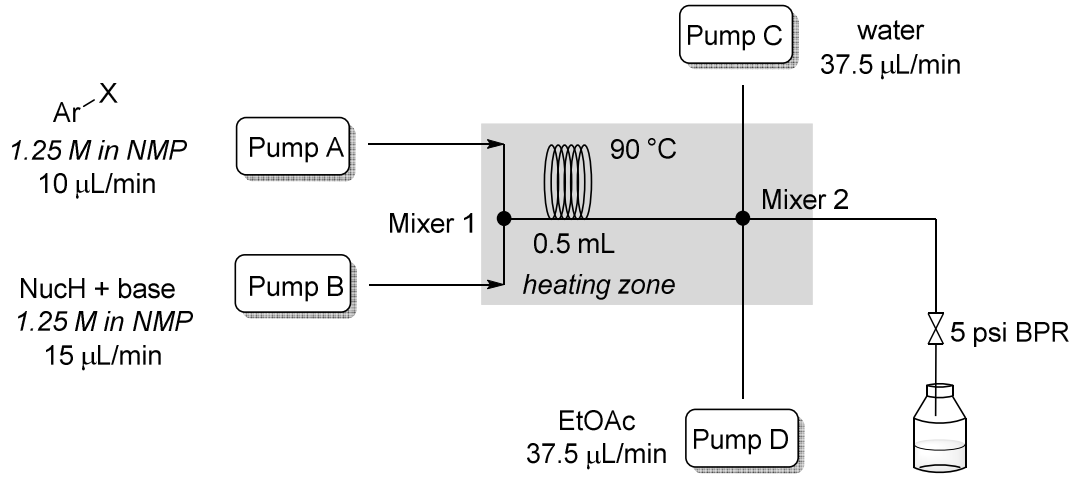

Figure 3.5. Schematic of flow reactor used for S_NAr reactions with S nucleophiles.

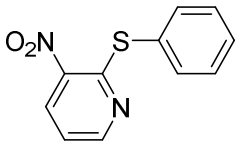

3-Nitro-2-(phenylthio)pyridine (**3.24**):[a] General procedure E was followed with reaction of 2-chloro-3-nitropyridine and thiophenol. Column chromatography (10:1 hexanes:EtOAc) yielded the pure product as a yellow solid (85 mg, 97% yield). Characterization data were in agreement with the literature.[34] ^{1}H NMR (400 MHz, $CDCl_3$) δ 8.51-8.47 (m, 2H), 7.58-7.53 (m, 2H), 7.48-7.42 (m, 3H), 7.19-7.15 (m, 1H). ^{13}C NMR (100 MHz, $CDCl_3$) 158.4, 153.5, 141.5, 136.1, 133.7, 129.7, 129.5, 129.3, 119.5.

General procedure F for S_N2 reactions with N and S nucleophiles. Nucleophile (10 mmol) and base (12.5 mmol) were combined neat and loaded into a 5 mL Hamilton Gastight syringe. Electrophile (12.5 mmol) was made up to 3.13 mL with NMP to make a 4.0 M solution and loaded into a second 5 mL Hamilton Gastight syringe. The continuous flow reactor depicted in Figure 3.6

[a] Prepared by S. K. Kashani

was used with flow rates set to give a residence time of 30 min and a 1:1.25:1.25 ratio of nucleophile:electrophile:base (Bu_3N for aniline or sulfur nucleophiles, DBU for aliphatic amine nucleophiles). Flow rates differed for each reaction based on density differences between different nucleophile-base solutions; specific flow rates used for each product are given below. Reaction concentration also varied, depending on nucleophile-base solution density. Concentrations within the reactor ranged from 1.7 M to 2.1 M. and are given below. The first 40 min (1.33 residence volumes) of effluent was discarded to reach steady state, then effluent was collected for 60 min. The material collected was partitioned between 0.1 M K_2CO_3 (50 mL) and 2:1 EtOAc:hexanes (20 mL). The aqueous phase was extracted with an additional 2 × 15 mL 2:1 EtOAc:hexanes and the combined organic extracts were then washed with 3 × 5 mL H_2O, dried over Na_2SO_4 and the solvent evaporated. The residue was chromatographed on silica gel to yield the pure product.

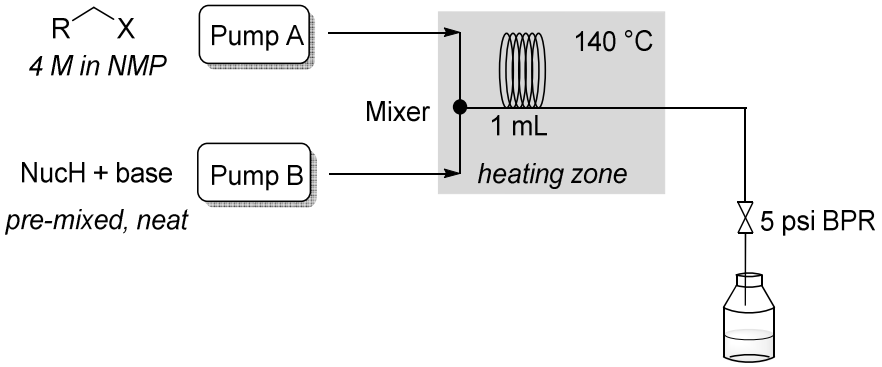

Figure 3.6. Schematic of flow reactor used for S_N2 reactions with N or S nucleophiles.

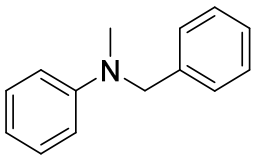

N-Benzyl-N-methylaniline (**3.25**): General procedure F was followed. Benzyl chloride solution flow rate was 14.3 µL/min and *N*-methylaniline/Bu_3N mixture flow rate was 19.0 µL/min giving a reaction concentration of 1.7 M. Column chromatography (hexanes→2.5% EtOAc in hexanes) yielded the pure product as a colourless oil (0.51 g, 96% yield). Characterization data were in agreement with the literature.[35] ^{1}H NMR (400 MHz, $CDCl_3$): δ 7.36–7.34 (m, 2H), 7.30–7.25 (m, 5H), 6.79 (d, J = 8.9 Hz, 2H), 6.76 (t, J = 7.3 Hz, 1H), 4.58 (s, 2H), 3.06 (s, 3H). ^{13}C{^{1}H} NMR (100 MHz, $CDCl_3$): δ 149.9, 139.2, 129.3, 128.7, 127.0, 126.9, 116.4, 112.5, 56.8, 38.6.

Alternatively, the reaction could be performed neat. A solution of *N*-methylaniline (1.07 g, 10 mmol), benzyl chloride (1.58 g, 12.5 mmol) and Bu_3N (2.31 g, 12.5 mmol) was prepared and loaded into a 5 mL Hamilton Gastight syringe. The reactor coil depicted in Figure 3.6 was used, fed via a single pump at 33.3 µL/min. The first 40 min of effluent were discarded then product was collected for 60 min. Work-up was the same as the experiment using general procedure F. Yield: 0.63 g, 90%.

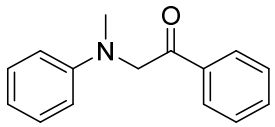

N-Methyl-N-phenacylaniline (**3.26**): General procedure F was followed. 2-Bromoacetophenone solution flow rate was 14.3 µL/min and *N*-methylaniline/Bu_3N mixture flow rate was 19.0 µL/min giving a reaction concentration of 1.7 M. Column chromatography (5%→17% EtOAc in hexanes) followed by recrystallization from hexanes yielded the pure product as yellow needles (0.43 g, 78% yield). Characterization data were in agreement with the literature.[36] ^{1}H NMR (400 MHz, $CDCl_3$): δ 8.01–7.99 (m, 2H), 7.61 (t, *J* = 7.4 Hz, 1H), 7.50 (t, *J* = 7.6 Hz, 2H), 7.23–7.20 (m, 2H), 6.73 (t, *J* = 7.3 Hz, 1H), 6.68 (d, *J* = 8.8 Hz, 2H), 4.78 (s, 2H), 3.11 (s, 3H). ^{13}C{1H} NMR (100 MHz, $CDCl_3$): δ 196.6, 149.3, 135.6, 133.7, 129.3, 128.9, 127.9, 117.2, 112.4, 59.1, 39.7.

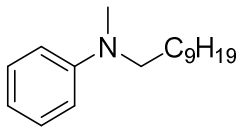

N-Decyl-N-methylaniline (**3.27**): General procedure F was followed. Iododecane solution flow rate was 14.3 µL/min and *N*-methylaniline/Bu_3N mixture flow rate was 19.0 µL/min giving a reaction concentration of 1.7 M. Column chromatography (hexanes→3% EtOAc in hexanes) yielded the pure product as colourless oil (0.60 g, 90% yield). Characterization data were in agreement with the literature.[37] ^{1}H NMR (400 MHz, $CDCl_3$): δ 7.25–7.21 (m, 2H), 6.72–6.66 (m, 3H), 3.30 (t, *J* = 7.5 Hz, 2H), 2.93 (s, 3H), 1.57 (pent, *J* = 7.3 Hz, 2H), 1.32–1.28 (m, 14H), 0.90 (t, *J* = 7.8 Hz, 3H). ^{13}C{^{1}H} NMR (100 MHz, $CDCl_3$): δ 149.5, 129.3, 115.9, 112.2, 53.0, 38.4, 32.0, 29.8, 29.71, 29.70, 29.5, 27.3, 26.8, 22.8, 14.3.

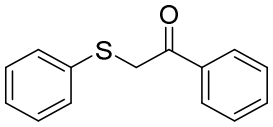

2-Phenylthioacetophenone (**3.28**): General procedure F was followed with two modifications. First, the nucleophile and base were separately dosed neat via syringe pumps equipped with 5 mL Hamilton Gastight syringes due to immiscibility. The three reagent streams: electrophile solution (4M in NMP), nucleophile and base were combined in a PEEK cross mixer and then entered the reaction coil as in Fig 3.6. 2-Bromoacetophenone solution flow rate was 14.6 µL/min, Bu_3N flow rate 13.9 µL/min, thiophenol flow rate 4.8 µL/min giving a reaction concentration of 1.8 M. Second, 1 M HCl was used in the place of 0.1 M K_2CO_3 during the work-up steps. Column chromatography (5%→10% Et_2O in hexanes) yielded the pure product as a white solid (0.53 g, 83% yield). Characterization data were in agreement with the literature.[38] ^{1}H NMR (400 MHz, $CDCl_3$): δ 7.96–7.94 (m, 2H), 7.58 (tt, *J* = 7.4, 1.3 Hz, 1H), 7.47 (t, *J* = 7.6 Hz, 2H), 7.41–7.38 (m, 2H), 7.31–7.26 (m, 2H), 7.25–7.23 (m, 1H), 4.28 (s, 2H). ^{13}C{^{1}H} NMR (100 MHz, $CDCl_3$): δ 191.2, 135.5, 134.9, 133.6, 130.6, 129.2, 128.8, 127.2, 41.3.

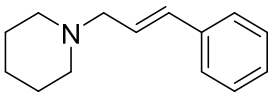

N-Cinnamylpiperidine (**3.29**): General procedure F was followed. Cinnamyl chloride solution flow rate was 17.6 µL/min and piperidine/DBU mixture flow rate was 15.7 µL/min giving a reaction concentration of 2.1 M. Column chromatography over silica deactivated with Et_3N (2:1 hexanes:EtOAc) yielded the pure product as a pale yellow oil (0.58 g, 84% yield). Characterization data were in agreement with the literature.[39] ^{1}H NMR (400 MHz, $CDCl_3$): δ 7.37 (d, *J* = 7.8 Hz, 2H), 7.30 (t, *J* = 7.5 Hz, 2H), 7.21 (t, *J* = 7.3 Hz, 1H), 6.49 (d, *J* = 15.8 Hz, 1H), 6.30 (dt, *J* = 15.8, 6.8 Hz, 1H), 3.12 (dd, *J* = 7.0, 1.2 Hz, 2H), 2.43 (br s, 4H), 1.61 (pent, *J* = 5.6 Hz, 4H), 1.45 (pent, *J* = 5.2 Hz, 2H). ^{13}C{^{1}H} NMR (100 MHz, $CDCl_3$): δ 137.2, 132.7, 128.7, 127.5, 127.4, 126.4, 62.1, 54.8, 26.2, 24.5.

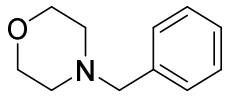

N-Benzylmorpholine (**3.30**): General procedure F was followed. Benzyl chloride solution flow rate was 17.8 μL/min and morpholine/DBU flow rate was 15.5 μL/min giving a reaction concentration of 2.1 M. Column chromatography (30%→50% EtOAc in hexanes) yielded the pure product as a pale yellow oil (0.63 g, 94% yield). Characterization data were in agreement with the literature.[40] ^{1}H NMR (400 MHz, $CDCl_3$): δ 7.33–7.26 (m, 5H), 3.71 (t, J = 4.6 Hz, 4H), 3.50 (s, 2H), 2.44 (t, J = 4.5 Hz, 4H). $^{13}C\{^{1}H\}$ NMR (100 MHz, $CDCl_3$): δ 137.9, 129.3, 128.4, 127.3, 67.2, 63.6, 53.8.

General procedure G for S_N2 reactions with O nucleophiles (silylations). TBSCl (5.75 mmol) was made up to 2.50 mL with DCM to give a 2.3 M solution and loaded into a 5 mL Hamilton Gastight syringe. Alcohol (5.0 mmol) and BuIm (10 mmol) were made up to 2.50 mL with DCM to give 2.0 M and 4.0 M concentrations respectively and loaded into another 5 mL Hamilton Gastight syringe. The continuous flow reactor and flow rates depicted in Figure 3.7 were used to give a residence time of 5 min and ratio of 1:1.15:2 alcohol:TBSCl:base (BuIm). The first 15 min (3 residence volumes) of effluent was discarded to reach steady state, then effluent was collected for 15 min. Work-up varied by compound and details for each compound are given below.

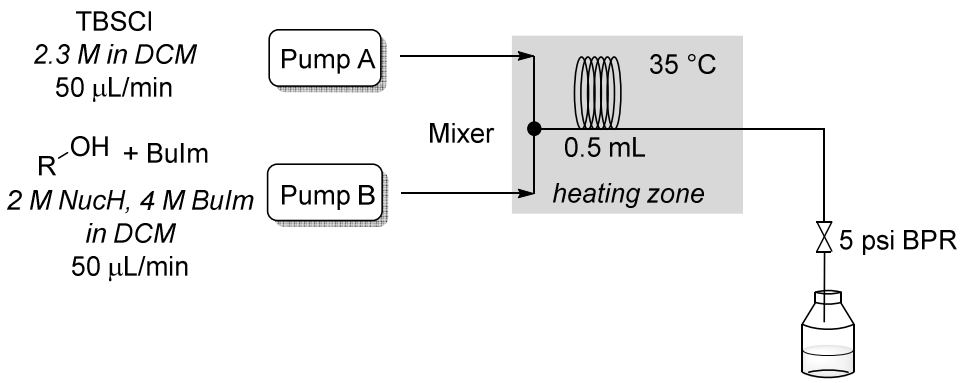

Figure 3.7. Schematic of flow reactor used for S_N2 reactions (silylations) with O nucleophiles.

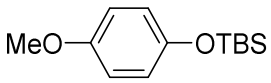

tert-Butyl(4-methoxyphenoxy)dimethylsilane (**3.33**):[a] General procedure G was followed with reaction of TBSCl and 4-methoxyphenol. A photograph of the biphasic effluent is shown in Figure 3.8 below. To the collected biphasic effluent, DCM (40 mL) was added and the mixture washed with 3 × 20 mL of 1 M HCl. The organic phase was then dried over Na_2SO_4, the solvent evaporated and the product purified on silica gel (6:1, hexanes:EtOAc) to yield the pure product as colourless oil (0.35 g, 97% yield). Characterization data were in agreement with the literature.[41] ^{1}H NMR (400 MHz, $CDCl_3$): δ 6.77 (s, 4H), 3.76 (s, 3H), 0.99 (s, 9H), 0.18 (s, 6H). $^{13}C\{^1H\}$ NMR (100 MHz, $CDCl_3$): δ 154.2, 149.5, 120.7, 114.6, 55.7, 25.9, 18.3, –4.3.

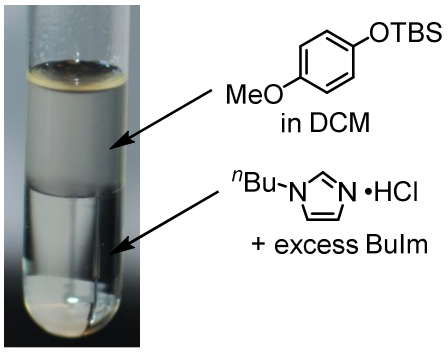

Figure 3.8. Photograph of the biphasic reaction mixture after production of silyl ether **3.33**.

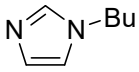

(recovered)

Recovered 1-butylimidazole (**3.32**):[e] The aqueous acidic extracts (combined 60 mL) from the work-up of **3.33** were basified by the addition of 2 M NaOH (60 mL) and extracted with 3 × 40 mL of DCM. The combined organic phases were dried over Na_2SO_4 and the solvent evaporated to yield 0.18 g of analytically pure BuIm (95%). Characterization data were in agreement with the literature.[42] ^{1}H NMR (400 MHz, $CDCl_3$): δ 7.41 (s, 1H), 6.99 (s, 1H), 6.85 (s, 1H), 3.88 (t, J = 7.1, 2H), 1.71 (m, 2H), 1.28 (m, 2H), 0.89 (t, J = 7.4, 3H). $^{13}C\{^1H\}$ NMR (100 MHz, $CDCl_3$): δ 137.1, 129.4, 118.8, 46.7, 33.1, 19.7, 13.5.

[a] Prepared by S. K. Kashani

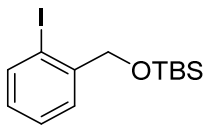

tert-Butyl((2-iodobenzyl)oxy)dimethylsilane (**3.34**): General procedure G was followed with reaction of TBSCl and 2-iodobenzyl alcohol. The biphasic effluent collected was partitioned between 1 M HCl (20 mL) and 2:1 EtOAc:hexanes (20 mL). The aqueous phase was extracted with an additional 2×15 mL 2:1 EtOAc:hexanes and the combined organic extracts were washed with 5 mL brine, dried over Na_2SO_4 and the solvent evaporated. The residue was chromatographed on silica gel (hexanes) to yield the pure product as colourless oil (0.50 g, 95% yield). Characterization data were in agreement with the literature.[43] ^{1}H NMR (400 MHz, $CDCl_3$): δ 7.77 (d, J = 7.8 Hz, 1H), 7.51 (d J = 7.7 Hz, 1H), 7.37 (t, J = 7.6 Hz, 1H), 6.96 (t, J = 7.8, 1H), 4.63 (s, 2H), 0.98 (s, 9H), 0.14 (s, 6H). ^{13}C{^{1}H} NMR (100 MHz, $CDCl_3$): δ 142.9, 138.6, 128.5, 128.2, 127.4, 95.8, 69.4, 26.0, 18.4, –5.3.

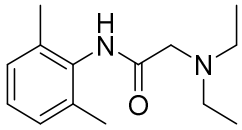

Lidocaine (**3.38**)**:** The conditions used were based on the literature batch procedure[18] with minimal modifications necessary to allow telescoping in flow. Specifically, toluene was used as the solvent for both reaction steps to facilitate telescoping without solvent switching, both reaction steps were performed at 90 °C in the same heated zone to prevent crystallization of the amide intermediate produced in the first acylation step, and Bu_3N and DBU respectively were used as acid scavengers to prevent precipitate formation during both reactions.

2,6-Dimethylaniline (0.61 g, 5.0 mmol) and Bu_3N (0.93 g, 5.0 mmol) were made up to 5.00 mL with toluene and loaded into a 5 mL Hamilton Gastight syringe. Chloroacetyl chloride (0.63 g, 5.5 mmol) was made up to 5.00 mL with toluene and loaded into another 5 mL Hamilton Gastight syringe. Et_2NH (1.01 g, 15 mmol) and DBU (1.51 g, 10 mmol) were combined neat and loaded into a third 5 mL Hamilton Gastight syringe. The continuous flow reactor depicted in Figure 3.9 was used to give a residence time of 1.25 min for the acylation and 9.5 min for the S_N2 reaction. Reaction stoichiometry was, with respect to 2,6-dimethylaniline, 1.1 eq. of chloroacetyl chloride

and 1 eq. of Bu_3N for the acylation reaction, then 3 eq. of Et_2NH and 2 eq. of DBU (1 eq. consumed by $Bu_3N{\cdot}HCl$ from the previous acylation step) for the S_N2 reaction.

The first 20 min (~2 residence volumes) of effluent was discarded to reach steady-state, then effluent was collected for 60 min. All material collected was partitioned between 1 M NaOH (20 mL) and 2:1 EtOAc:hexanes (20 mL). The aqueous phase was extracted with an additional 2 × 15 mL 2:1 EtOAc:hexanes and the combined organic extracts were washed with 3 × 5 mL water, then extracted with 5×5 mL 1M HCl. The combined aqueous extracts were washed with 5 mL Et_2O then the *p*H was raised to >14 by addition of 50% NaOH. The solution was extracted with 4 × 5 mL hexanes and the combined extracts were dried over Na_2SO_4. The solvent was evaporated and the residue chromatographed on Et_3N deactivated silica gel (25 × 150 mm column, 10%→30% EtOAc in hexanes eluent) to yield the pure product as a white powder (0.37 g, 66% yield). Characterization data were in agreement with the literature.[44] ^1H NMR (400 MHz, $CDCl_3$): δ 8.92 (s, 1H), 7.09 (m, 3H), 3.22 (s, 2H), 2.69 (q, J = 7.1 Hz, 4H), 2.23 (s, 6H), 1.14 (t, J = 7.1 Hz, 6H). $^{13}C\{^1H\}$ NMR (100 MHz, $CDCl_3$): δ 170.4, 135.2, 134.1, 128.3, 127.2, 57.6, 49.1, 18.7, 12.8.

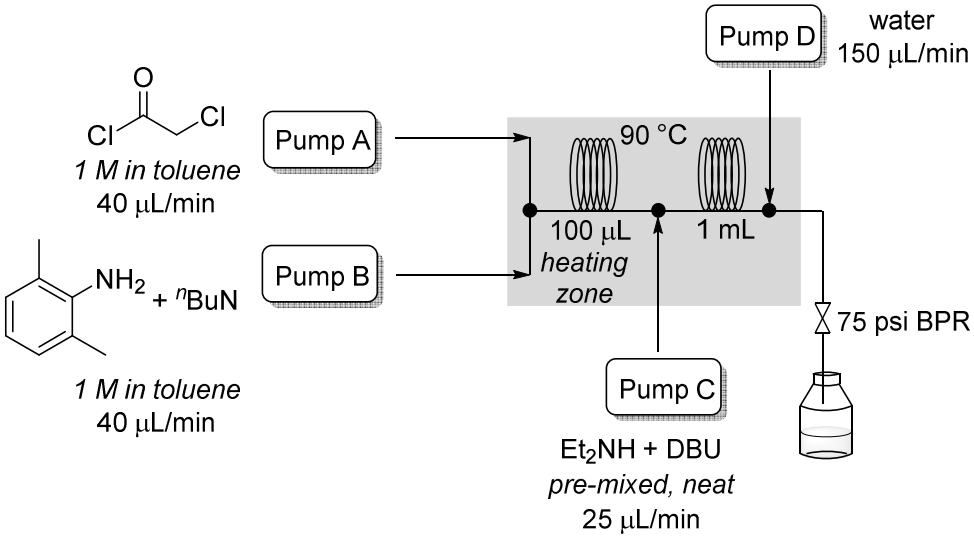

Figure 3.9. Schematic of flow reactor used for telescoped synthesis of Lidocaine.

3.5 References

[1] Jiménez-González, C.; Poechlauer, P.; Broxterman, Q. B.; Yang, B.-S.; am Ende, D.; Baird, J.; Bertsch, C.; Hannah, R. E.; Dell'Orco, P.; Noorman, H.; Yee, S.; Reintjens, R.; Wells, A.; Massonneau, V.; Manley, J. Key green engineering research areas for sustainable manufacturing: A perspective from pharmaceutical and fine chemicals manufacturers. *Org. Process Res. Dev.* **2011**, *15*, 900−911.

[2] a) Roughley, S. D.; Jordan, A. M. The medicinal chemist's toolbox: An analysis of reactions used in the pursuit of drug candidates. *J. Med. Chem.* **2011**, *54*, 3451−3479; b) Schneider, N.; Lowe, D. M.; Sayle, R. A.; Tarselli, M. A.; Landrum, G. A. Big data from pharmaceutical patents: A computational analysis of medicinal chemists' bread and butter. *J. Med. Chem.* **2016**, *59*, 4385−4402; c) Brown, D. G.; Boström, J. Analysis of past and present synthetic methodologies on medicinal chemistry: Where have all the new reactions gone? *J. Med. Chem.* **2016**, *59*, 4443−4458.

[3] Newman, S. G.; Jensen, K. F. The role of flow in green chemistry and engineering. *Green Chem.* **2013**, *15*, 1456−1472.

[4] a) Malet-Sanz, L.; Susanne, F. Continuous flow synthesis. A pharma perspective. *J. Med. Chem.* **2012**, *55*, 4062-4098; b) Rodrigues, T.; Schneider, P.; Schneider, G. Accessing new chemical entities through microfluidic systems. *Angew. Chem. Int. Ed.* **2014**, *53*, 5750−5758; c) Gutmann, B.; Cantillo, D.; Kappe, C. O. Continuous-flow technology — A tool for the safe manufacturing of active pharmaceutical ingredients. *Angew. Chem. Int. Ed.* **2015**, *54*, 6688−6728; d) Baumann, M.; Baxendale, I. R. The synthesis of active pharmaceutical ingredients (APIs) using continuous flow chemistry. *Beilstein Journal of Organic Chemistry* **2015**, *11*, 1194−1219; e) Porta, R.; Benaglia, M.; Puglisi, A. Flow chemistry: Recent developments in the synthesis of pharmaceutical products. *Org. Process Res. Dev.* **2016**, *20*, 2−25; f) Britton, J.; Raston, C. L. Multi-step continuous-flow synthesis. *Chem. Soc. Rev.* **2017**, *46*, 1250−1271.

[5] The benefits of conducting a flow process under high concentrations are rarely realized in practice due to solubility/precipitation issues, however for reactions that are not prone to precipitation they can be, e.g., Michael additions of amine nucleophiles. See: Löwe, H.; Hessel, V.; Löb, P.; Hubbard, S. Addition of secondary amines to α,β-unsaturated carbonyl compounds and nitriles by using microstructured reactors. *Org. Process Res. Dev.* **2006**, *10*, 1144−1152.

[6] For example: a) Hartman, R. L.; Naber, J. R.; Zaborenko, N.; Buchwald, S. L.; Jensen, K. F. Overcoming the challenges of solid bridging and constriction during Pd-catalyzed C−N bond formation in microreactors. *Org. Process Res. Dev.* **2010**, *14*, 1347−1357; b) Kuhn, S.; Noël, T.; Gu, L.; Heider, P. L.;

Jensen, K. F. A Teflon microreactor with integrated piezoelectric actuator to handle solid forming reactions. *Lab Chip* **2011**, *11*, 2488–2492.

[7] Mo, Y.; Jensen, K. F. A miniature CSTR cascade for continuous flow of reactions containing solids. *React. Chem. Eng.* **2016**, *1*, 501–507.

[8] Isoni, V.; Mendoza, K.; Lim, E.; Teoh, S. K. Screwing NaBH4 through a barrel without a bang: A kneaded alternative to fed-batch carbonyl reductions. *Org. Process Res. Dev.* **2017**, *21*, 992–1002.

[9] Giri, G.; Yang, L.; Mo, Y.; Jensen, K. F. Adding crystals to minimize clogging in continuous flow synthesis. *Cryst. Growth Des.* **2019**, *19*, 98–105.

[10] For reviews on engineering solutions to handles solids in continuous flow see: a) Wu, K.; Kuhn, S. Strategies for solids handling in microreactors. *Chemica Oggi* **2014**, *32*, 62–66; b) Schoenitz, M.; Grundemann, L.; Augustin, W.; Scholl, S. Fouling in microstructured devices: A review. *Chem. Commun.* **2015**, *51*, 8213–8228; c) Hartman, R. L. Managing solids in microreactors for the upstream continuous processing of fine chemicals. *Org. Process Res. Dev.* **2012**, *16*, 870–887.

[11] a) Seddon, K. R. A taste of the future. *Nature Materials* **2003**, *2*, 363–365; b) Maase, M.; Massonne, K. Biphasic acid scavenging utilizing ionic liquids: The first commercial process with ionic liquids. In *Ionic Liquids IIIB: Fundamentals, Progress, Challenges, and Opportunities*; American Chemical Society: 2005; ACS Symposisum series Vol. 902, p 126–132.

[12] a) Dean, J. A. *Lange's Handbook of Chemistry*, McGraw-Hill: New York, 1999; b) Maase, M.; Huttenloch, O. Neutralization and phase-separation method for isolating acids from chemical reaction mixtures using 1-alkylimidazoles. WO Patent 2005/061416 A1, 2005; c) Greaves, T. L.; Drummond, C. J. Protic ionic liquids: Properties and applications. *Chem. Rev.* **2008**, *108*, 206–237.

[13] See Appendix II and the following references: a) Riddick, J. A.; Bunger, W. B.; Sakano, T.; Wissberger, A. *Organic Solvents: Physical Properties and Methods of Purification*, Wiley VHC: New York, 1986; b) Reichenbach, J.; Ruddell, S. A.; González-Jiménez, M.; Lemes, J.; Turton, D. A.; France, D. J.; Wynne, K. Phonon-like hydrogen-bond modes in protic ionic liquids. *J. Am. Chem. Soc.* **2017**, *139*, 7160–7163.

[14] a) Yang, Z.-Z.; Li, Y.-N.; Wei, Y.-Y.; He, L.-N. Protic onium salts-catalyzed synthesis of 5-aryl-2-oxazolidinones from aziridines and CO_2 under mild conditions. *Green Chem.* **2011**, *13*, 2351–2353; b) Kaupmees, K.; Trummal, A.; Leito, I. Basicities of strong bases in water: A computational study. *Croat. Chem. Acta* **2014**, *87*, 385–395.

[15] During the original submission of this work, Roger and coworkers reported designer ionic liquid-forming bases that may be used in cross-coupling reactions. These bases were proposed but not demonstrated to enable continuous flow reactions. See: Choudhary, H.; Berton, P.; Gurau, G.; Myerson, A. S.; Rogers, R. D. Ionic liquids in cross-coupling reactions: "Liquid" solutions to a "solid" precipitation problem. *Chem. Commun.* **2018**, *54*, 2056–2059.

[16] a) Qian, Z.; Baxendale, I. R.; Ley, S. V. A flow process using microreactors for the preparation of a quinolone derivative as a potent 5HT1B antagonist. *Synlett* **2010**, *2010*, 505–508; b) Ahmed-Omer, B.; Sanderson, A. J. Preparation of fluoxetine by multiple flow processing steps. *Org. Biomol. Chem.* **2011**, *9*, 3854–3862; c) Hopkin, M. D.; Baxendale, I. R.; Ley, S. V. An expeditious synthesis of imatinib and analogues utilising flow chemistry methods. *Org. Biomol. Chem.* **2013**, *11*, 1822–1839; d) Hwang, Y.-J.; Coley, C. W.; Abolhasani, M.; Marzinzik, A. L.; Koch, G.; Spanka, C.; Lehmann, H.; Jensen, K. F. A segmented flow platform for on-demand medicinal chemistry and compound synthesis in oscillating droplets. *Chem. Commun.* **2017**, *53*, 6649–6652; e) Cole, K. P.; Groh, J. M.; Johnson, M. D.; Burcham, C. L.; Campbell, B. M.; Diseroad, W. D.; Heller, M. R.; Howell, J. R.; Kallman, N. J.; Koenig, T. M.; May, S. A.; Miller, R. D.; Mitchell, D.; Myers, D. P.; Myers, S. S.; Phillips, J. L.; Polster, C. S.; White, T. D.; Cashman, J.; Hurley, D.; Moylan, R.; Sheehan, P.; Spencer, R. D.; Desmond, K.; Desmond, P.; Gowran, O. Kilogram-scale prexasertib monolactate monohydrate synthesis under continuous-flow CGMP conditions. *Science* **2017**, *356*, 1144–1150; f) Bogdan, A. R.; Charaschanya, M.; Dombrowski, A. W.; Wang, Y.; Djuric, S. W. High-temperature boc deprotection in flow and its application in multistep reaction sequences. *Org. Lett.* **2016**, *18*, 1732–1735; g) Lin, H.; Dai, C.; Jamison, T. F.; Jensen, K. F. A rapid total synthesis of ciprofloxacin hydrochloride in continuous flow. *Angew. Chem. Int. Ed.* **2017**, *56*, 8870–8873.

[17] a) Corey, E. J.; Venkateswarlu, A. Protection of hydroxyl groups as *tert*-butyldimethylsilyl derivatives. *J. Am. Chem. Soc.* **1972**, *94*, 6190–6191; b) Patschinski, P.; Zhang, C.; Zipse, H. The Lewis base-catalyzed silylation of alcohols — A mechanistic analysis. *J. Org. Chem.* **2014**, *79*, 8348–8357.

[18] For typical batch conditions see: Reilly, T. J. The preparation of Lidocaine. *J. Chem. Educ.* **1999**, *76*, 1557.

[19] Britton, J.; Chalker, J. M.; Raston, C. L. Rapid vortex fluidics: Continuous flow synthesis of amides and local anesthetic lidocaine. *Chem. Eur. J.* **2015**, *21*, 10660–10665.

[20] Adamo, A.; Beingessner, R. L.; Behnam, M.; Chen, J.; Jamison, T. F.; Jensen, K. F.; Monbaliu, J.-C. M.; Myerson, A. S.; Revalor, E. M.; Snead, D. R.; Stelzer, T.; Weeranoppanant, N.; Wong, S. Y.; Zhang,

P. On-demand continuous-flow production of pharmaceuticals in a compact, reconfigurable system. *Science* **2016**, *352*, 61–67.

[21] Wang, Y.; Gu, M. The concept of spectral accuracy for MS. *Anal. Chem.* **2010**, *82*, 7055–7062.

22 Chun, S.; Chung, Y. K. Transition-metal-free poly(thiazolium) iodide/1,8-diazabicyclo[5.4.0]undec-7-ene/phenazine-catalyzed esterification of aldehydes with alcohols. *Org. Lett.* **2017**, *19*, 3787–3790.

23 Tu, Y.; Yuan, L.; Wang, T.; Wang, C.; Ke, J.; Zhao, J. Palladium-catalyzed oxidative carbonylation of aryl hydrazines with CO and O_2 at atmospheric pressure. *J. Org. Chem.* **2017**, *82*, 4970–4976.

24 Ilangovan, A.; Saravanakumar, S.; Malayappasamy, S.; Manickam, G. A convenient approach for the deprotection and scavenging of the PMB group using $POCl_3$. *RSC Adv.* **2013**, *3*, 14814–14828.

25 Rao, Y.; Li, X.; Danishefsky, S. J. Thio FCMA intermediates as strong acyl donors: A general solution to the formation of complex amide bonds. *J. Am. Chem. Soc.* **2009**, *131*, 12924–12926.

26 Goodman, C. A.; Eagles, J. B.; Rudahindwa, L.; Hamaker, C. G.; Hitchcock, S. R. Synthesis, X-ray crystallography, and reactions of *N*-acyl and *N*-carbamoyl succinimides. *Synth. Commun.* **2013**, *43*, 2155–2164.

27 Smedley, C. J.; Barrow, A. S.; Spiteri, C.; Giel, M.-C.; Sharma, P.; Moses, J. E. Sulfur–fluoride exchange (SuFEx)-mediated synthesis of sterically hindered and electron-deficient secondary and tertiary amides via acyl fluoride intermediates. *Chem. Eur. J.* **2017**, *23*, 9990–9995.

28 Smith, S. M.; Thacker, N. C.; Takacs, J. M. Efficient amide-directed catalytic asymmetric hydroboration. *J. Am. Chem. Soc.* **2008**, *130*, 3734–3735.

29 a) Al-Hiari, Y. M.; Bennett, S. J.; Davies, R. J.; Khalaf, A. I.; Waigh, R. D.; Worsley, A. J.; Cox, B. Steps towards a practical synthesis of macrocyclic bisbenzylisoquinolines. *J. Heterocycl. Chem.* **2005**, *42*, 647–659; b) Alonso, E.; Ramón, D. J.; Yus, M. Reductive deprotection of allyl, benzyl and sulfonyl substituted alcohols, amines and amides using a naphthalene-catalysed lithiation. *Tetrahedron* **1997**, *53*, 14355–14368.

30 Feng, Y.-S.; Mao, L.; Bu, X.-S.; Dai, J.-J.; Xu, H.-J. $Pd(OAc)_2$-catalyzed dinitration reaction of aromatic amines. *Tetrahedron* **2015**, *71*, 3827–3832.

31 Fang, W.; Jiang, J.; Xu, Y.; Zhou, J.; Tu, T. Novel robust benzimidazolylidene palladium complexes: Synthesis, structure, and catalytic applications in amination of chloroarenes. *Tetrahedron* **2013**, *69*, 673–679.

32 Hedley, K. A.; Stanforth, S. P. Ring-opening reactions of *N*-aryl-,1,2,3,4-tetrahydroisoquinoline derivatives. *Tetrahedron* **1992**, *48*, 743–750.

33 Zhang, Q.; Wang, D.; Wang, X.; Ding, K. (2-Pyridyl)acetone-promoted Cu-catalyzed *O*-arylation of phenols with aryl iodides, bromides, and chlorides. *J. Org. Chem.* **2009**, *74*, 7187–7190.

34 Xiang, J.; Zhang, Z.; Mu, Y.; Xu, X.; Guo, S.; Liu, Y.; Russo, D. P.; Zhu, H.; Yan, B.; Bai, X. Discovery of novel tricyclic thiazepine derivatives as anti-drug resistant cancer agents by combining diversity-oriented synthesis and converging screening approach. *ACS Comb. Sci.* **2016**, *18*, 230–235.

35 Liu, D.; Liu, C.; Li, H.; Lei, A. Direct functionalization of tetrahydrofuran and 1,4-dioxane: Nickel-catalyzed oxidative C(sp3)–H arylation. *Angew. Chem. Int. Ed.* **2013**, *52*, 4453–4456.

36 Shinde, M. H.; Kshirsagar, U. A. *N*-Bromosuccinimide promoted and base switchable one pot synthesis of α-imido and α-amino ketones from styrenes. *Org. Biomol. Chem.* **2016**, *14*, 858–861.

37 Zeng, M.; Herzon, S. B. Synthesis of 1,3-amino alcohols, 1,3-diols, amines, and carboxylic acids from terminal alkynes. *J. Org. Chem.* **2015**, *80*, 8604–8618.

38 Dias, R. M. P.; Burtoloso, A. C. B. Catalyst-free insertion of sulfoxonium ylides into aryl thiols. A direct preparation of β-keto thioethers. *Org. Lett.* **2016**, *18*, 3034–3037.

39 G. Hirata, G.; Satomura, H.; Kumagae, H.; Shimizu, A.; Onodera, G.; Kimura, M. Direct allylic amination of allylic alcohol catalyzed by palladium complex bearing phosphine–borane ligand. *Org. Lett.* **2017**, *19*, 6148–6151.

40 Kovalenko, O. O.; Volkov, A.; Adolfsson, H. Mild and selective Et_2Zn-catalyzed reduction of tertiary amides under hydrosilylation conditions. *Org. Lett.* **2015**, *17*, 446–449.

41 Shirley, H. J.; Bray, C. D. Spiroketal formation by cascade oxidative dearomatization: An approach to the phorbaketal skeleton. *Eur. J. Org. Chem.* **2016**, *2016*, 1504–1507.

42 Martínez, R.; Torregrosa, R.; Pastor, I. M.; Yus, M. Isoprene as lithiation mediator: Synthesis of 2-substituted 1-alkylimidazole derivatives. *Synthesis* **2012**, *44*, 2630–2638.

43 Sun, F.; Gu, Z. Decarboxylative alkynyl termination of palladium-catalyzed Catellani reaction: A facile synthesis of α-alkynyl anilines via *ortho* C–H amination and alkynylation. *Org. Lett.* **2015**, *17*, 2222–2225.

44 Badawi, H. M.; Förner, W.; Ali, S. A. The conformational stability, solvation and the assignments of the experimental infrared, Raman, 1H and 13C NMR spectra of the local anesthetic drug Lidocaine. *Spectrochim. Acta A Mol. Biomol. Spectrosc.* **2015**, *142*, 382–391.

Chapter 4 Overcoming Scope Limitations by Catalyst Resting State Manipulation[a]

4.1 Introduction

The development of cross-coupling reactions in the second half of the twentieth century revolutionized the field of synthetic organic chemistry and introduced a plethora of new bond disconnections for retrosynthetic analysis. Despite nearly 50 years of research and development in this area, new transformations are continually reported, ever expanding the range of applicable substrates and accessible transformations. A commonality shared by both newly reported and well-established transformations however is a propensity for reaction failure with changes to substrates or conditions from those reported in the literature. This is perhaps unsurprising considering the fact that catalytic reactions occur through a balance of multiple elementary steps — all occurring under the same set of conditions — and in competition with a plethora of catalyst deactivation pathways, including sequestration of the catalyst as inactive species, competitive inhibition by solvent or substrate molecules, decomposition of either the catalyst structure or loss of supporting ligand, precipitation of bulk metal, etc.[1] These various pathways leading to reaction failure manifest as 'scope limitations' — substrates for which a given catalyst is ineffective to enact a desired transformation.

The most common approach to overcome a scope limitation is to identify a different catalyst that can facilitate the desired transformation for a substrate that previously failed, and this is a major area of focus within both academic and industrial communities. However, there are situations where an alternative approach is equally effective or superior to expand reaction scope. This chapter focuses on situations where controlling the addition rate of one of the cross-coupling reagents is an effective strategy to overcome severe scope limitations. Initially development of a mechanistic understanding to explain the success of such a strategy in the context of historic Kumada-Corriu and Murahashi cross-coupling of aggressive organometallic cross-coupling

[a] Parts of this chapter have appeared in print: a) Hua, X.; Masson-Makdissi, J.; Sullivan, R. J.; Newman, S. G. Inherent vs. apparent chemoselectivity in the Kumada–Corriu cross-coupling reaction. *Org. Lett.* **2016**, *18*, 5312−5315; b) Sullivan, R. J.; Freure, G. P. R.; Newman, S. G. Overcoming scope limitations in cross-coupling of diazo nucleophiles by manipulating catalyst speciation and using flow diazo generation. *ACS Catal.* **2019**, *9*, 5623−5630. Excerpts from the results section are adapted with permission from Sullivan, R. J.; Freure, G. P. R.; Newman, S. G. *ACS Catal.* **2019**, *9*, 5623−5630. Copyright 2019 American Chemial Society.

nucleophiles will be explored. Subsequently, the application of the strategy to overcome limitations in a more modern transformation, the palladium catalyzed cross-coupling of aryl halides with diazo compounds will be described.

4.1.1 Kumada-Corriu cross-coupling

The Kumada-Corriu cross-coupling is one of the first catalytic cross-coupling reactions, forming a new C–C bond between an aryl or vinyl halide and a Grignard reagent.[2] First reported in 1972, this seminal work sparked the explosion of research efforts developing cross-coupling chemistry. While synthetically useful,[3] the aggressive nucleophilic nature of the Grignard reagents nonetheless imposes severe scope limitations if the aryl halide coupling partner is functionalized with an electrophilic group that is susceptible to direct attack by the Grignard reagent (Scheme 4.1). As a result, Kumada-Corriu reactions are seldomly used in complex molecule synthesis. Instead, cross-coupling reactions utilizing less aggressive nucleophiles such as organotin (Stille), organozinc (Negishi), organoboron (Suzuki-Miyaura) or organosilicon (Hiyama) reagents are preferred, with the Suzuki-Miyaura cross-coupling the most widely used variant.[4]

Scheme 4.1. A) Kumada-Corriu reactions fail in the presence of electrophilic functional groups. B) The mechanism of a Kumada-Corriu reaction.

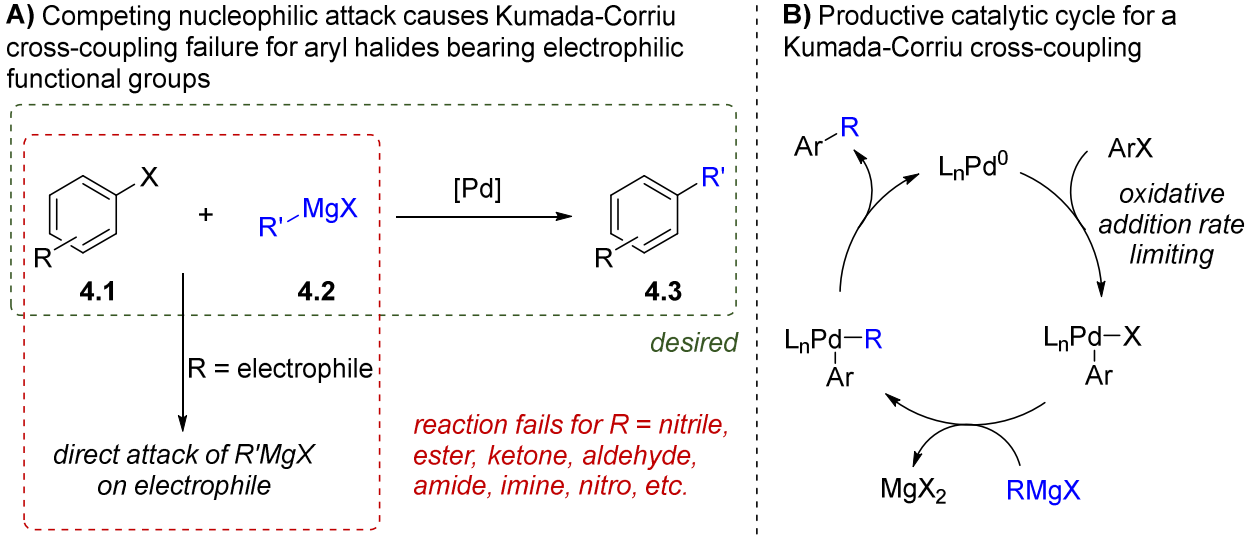

Recent work by Buchwald[5] and Knochel[6] however demonstrated that there was in fact potential to perform Kumada-Corriu couplings with aryl iodides or bromides bearing electrophilic

functional groups if the reaction was conducted under cryogenic temperatures or in the presence of *i*-PrI to facilitate a Pd(I)/Pd(III) mechanism (Scheme 4.2). Subsequently, colleagues in the Newman group demonstrated that slow addition of the Grignard reagent was a suitable strategy to facilitate cross couple with a wide variety of functionalized aryl chlorides and diverse heterocycles (Scheme 4.3).[7] The rate of Grignard reagent addition had a marked affect on cross-coupling product yield (Figure 4.1), and development of a mechanistic explanation to account for these observations is the focus of the first part of this chapter.

Scheme 4.2. Electrophilic functional group tolerance achieved by performing Kumada-Corriu reactions at cryogenic temperatures (A) or by inclusion of *i*-PrI as an additive (B).

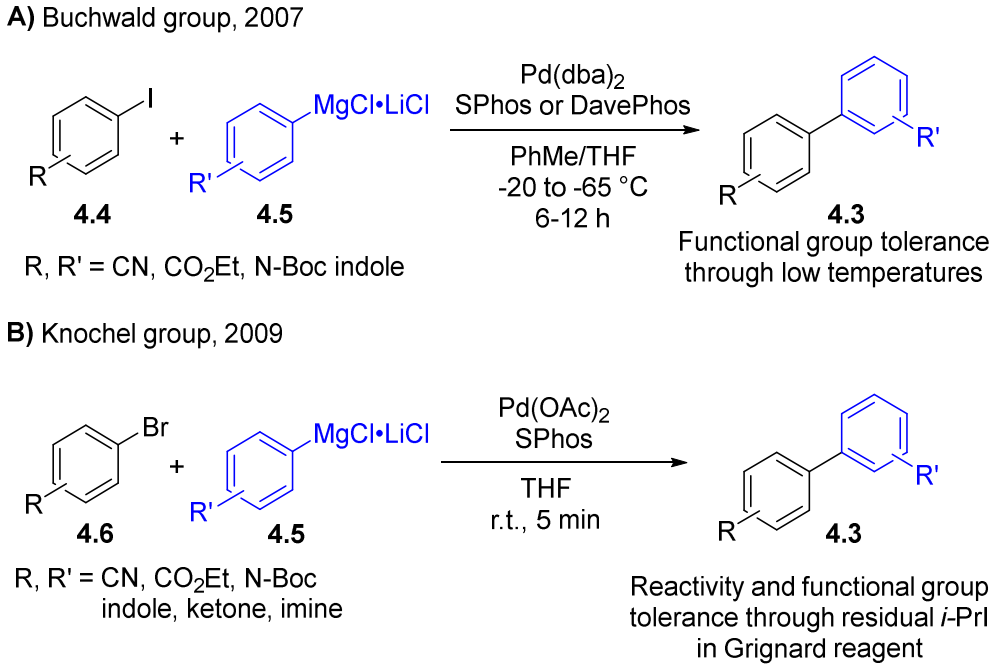

Scheme 4.3. Kumada-Corriu cross-coupling achieved by slow addition of the Grignard reagent.

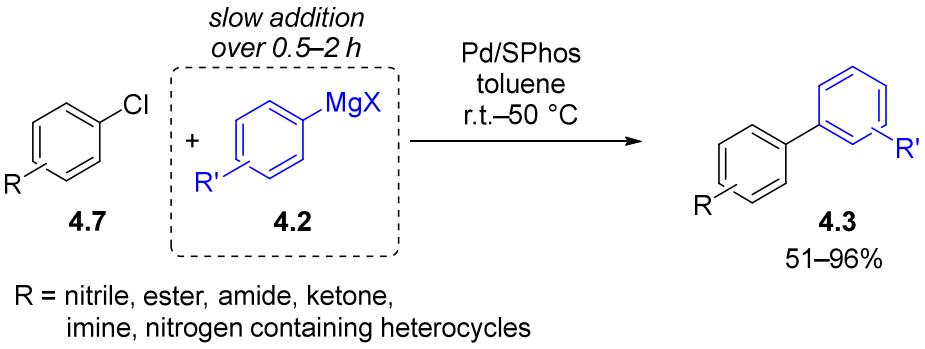

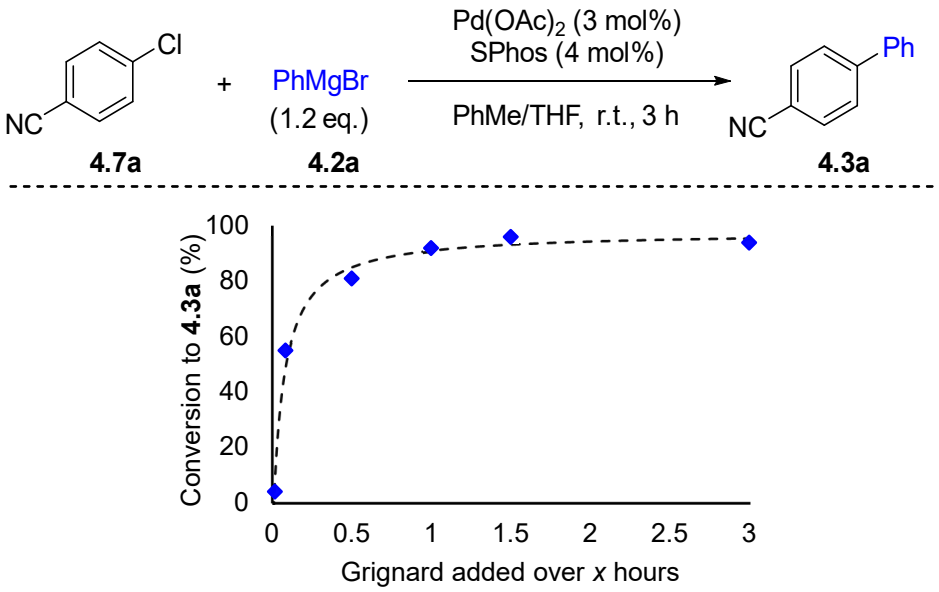

Figure 4.1. Influence of Grignard addition rate on reaction yield for the coupling of 4-chlorobenzonitrile (**4.7a**) and PhMgBr (**4.2a**).

4.1.2 Murahashi cross-coupling

The Murahashi cross-coupling is another seminal cross-coupling reaction. Reported in 1975, this reaction forms a new C–C bond between an aryl or vinyl halide and an organolithium reagent.[8] Unfortunately, this transformation has seen little synthetic use due to a very limited substrate scope. Because of the high reactivity of organolithium reagents, multiple, unproductive reaction pathways often compete with the desired catalytic cycle, including direct lithium halide exchange with the aryl halide, resulting in low yields and complex product mixtures (Scheme 4.4).

Recent work by Feringa and coworkers however demonstrated that by using bulky, electron rich ligands, in combination with slow addition of the organolithium reagent, high-yielding Murahashi cross-coupling products could be obtained from aryl bromides (RLi added over 1 h, Scheme 4.5) or chlorides (RLi added over 0.75–4 h, Scheme 4.6).[9] Furthermore, a correlation between necessary addition rate of the organolithium reagent and the propensity of the aryl chloride to undergo oxidative addition was observed, with activated aryl chlorides (i.e., aryl chlorides bearing electron withdrawing groups) being compatible with faster RLi addition rates than deactivated aryl chlorides (i.e., those bearing electron donating groups). While the reported functional group tolerance of this transformation was still rather limited, comprising only

alkanes/alkenes, ethers, amines, trifluoromethyl groups, and a few electron rich heterocycles, the ability to perform selective Murahashi cross-couplings at all represented marked progress.

Scheme 4.4. A) Murahashi cross-coupling results in low selectivity due to competing lithium-halide exchange. B) The operative catalytic cycle for a Murahashi cross-coupling reaction.

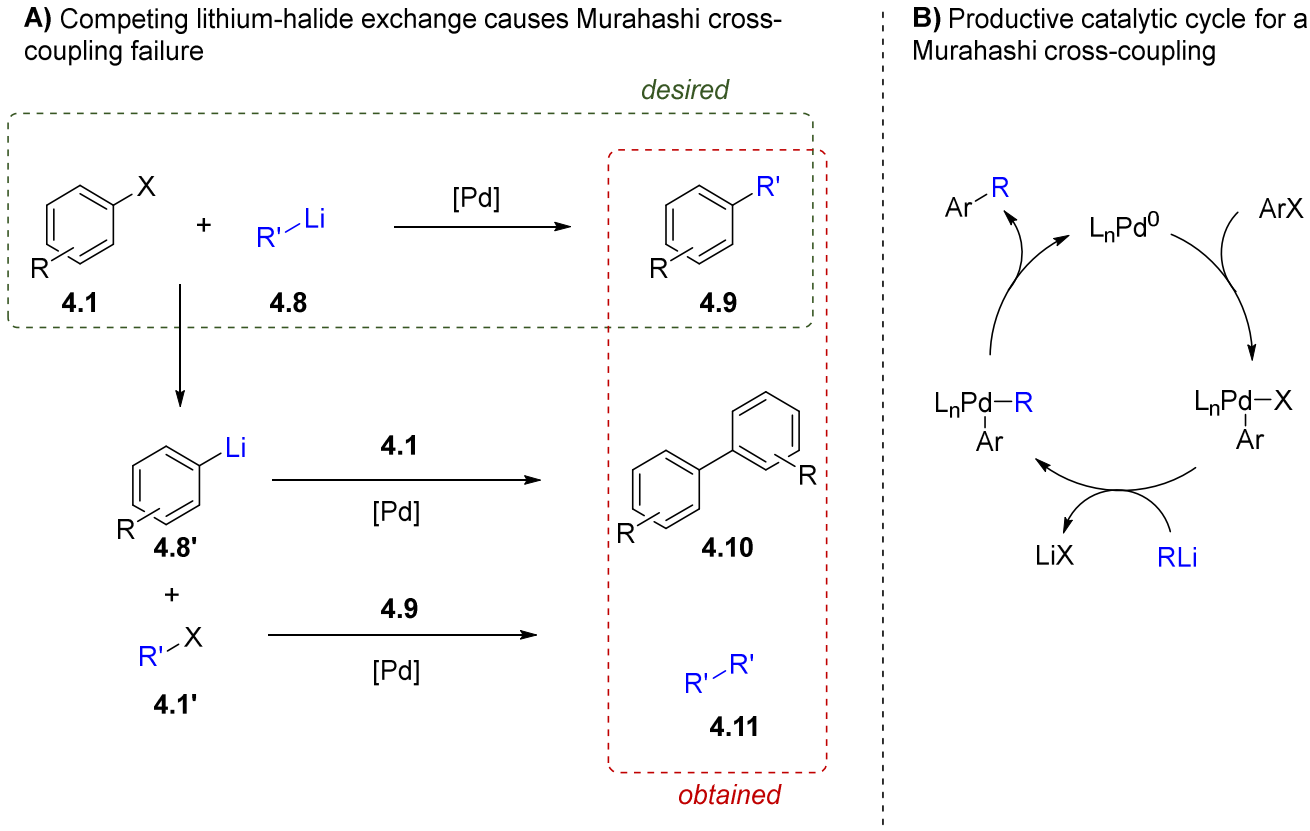

Scheme 4.5. Murahashi cross-coupling of aryl bromides enabled by slow addition of the organolithium reagent.

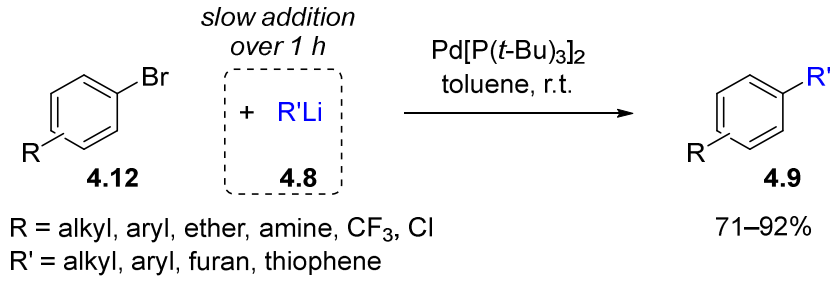

Scheme 4.6. Murahashi cross-coupling of aryl chlorides enabled by slow addition of the organolithium reagent.

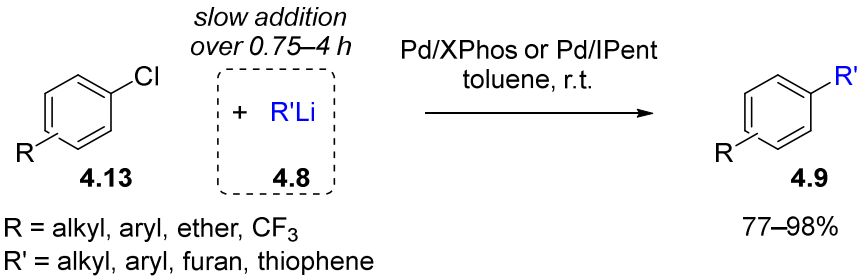

4.1.3 Controlling nucleophile addition rate manipulates catalyst resting state

The reports discussed above demonstrated that product distribution could be effectively controlled by modifying the addition rate of the organometallic reagent. But what underlying mechanism was responsible for this? We hypothesized that for a reaction under kinetic control — as is the case for cross-couplings with highly aggressive Grignard or organolithium reagents — the product distribution is a function of relative rates of competing reactions.[10] Using the reaction of 4-chlorobenzonitrile with PhMgCl as an example, the two steps in competition are transmetallation of Grignard **4.2a** with Pd(II) oxidative addition intermediate **II**, and direct nucleophilic attack of Grignard **4.2a** on the electrophilic nitrile group of either the starting material **4.7a** or product **4.3a** (Scheme 4.7). It follows that the rate of transmetallation is given by rate = $k_{t.m.}$[**4.2a**][**II**], while the rate of nucleophilic attack is rate = $k_{nuc.1}$[**4.2a**][**4.7a**] for attack on the starting material and rate = $k_{nuc.2}$[**4.2a**][**4.3a**] for attack on the product.

The fact that it is ever possible to achieve high selectivity for the desired cross-coupling product indicates that transmetallation is, in principle, kinetically competent to outcompete undesired nucleophilic attack (i.e., $k_{t.m.} > k_{nuc.1} \approx k_{nuc.2}$). However, in most cases the observed product selectivity does not reflect this because there is a very large difference in concentration of Pd(II) intermediate **II** and the other electrophilic species **4.7a** and **4.3a**. The reasons for this are twofold. First, the Pd(II) species **II** is an intermediate on a catalytic cycle, and the total amount of Pd distributed throughout the entire cycle is sub-stoichiometric, typically ≤5% compared to aryl halide **4.7a**. Secondly, for cross-coupling reactions with aggressive organometallic nucleophiles oxidative addition is generally the rate determining step, while transmetallation is facile.[2c] As a

result, Pd(II) intermediate **II** is slow to form but rapidly consumed, and therefore present in very low concentrations under typical conditions (i.e., all Grignard added at start of reaction).

Scheme 4.7. Transmetallation is in kinetic competition with direct nucleophilic attack of the Grignard reagent on electrophilic functional groups present on the aryl halide.

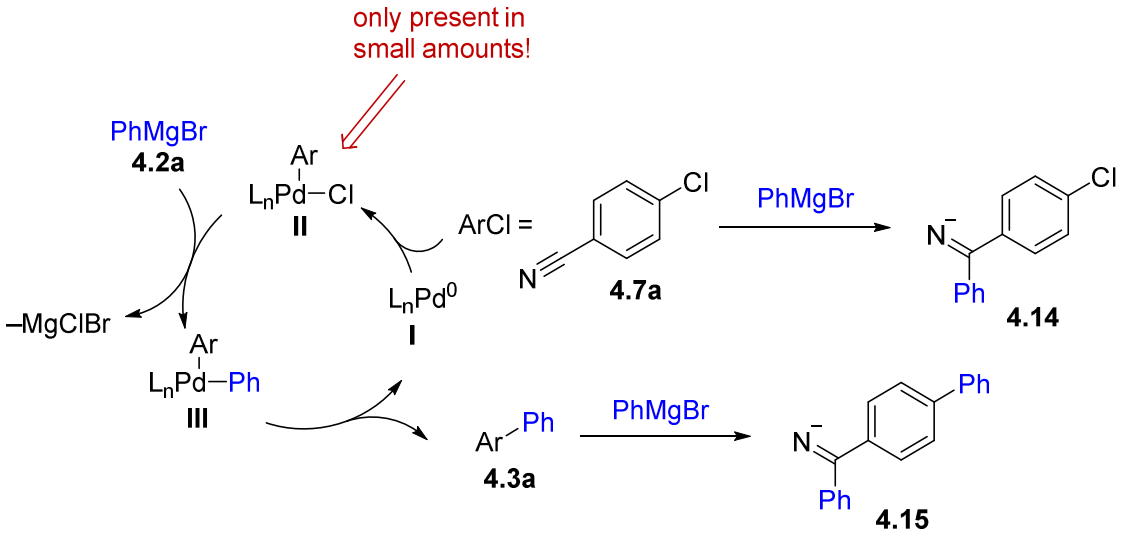

We hypothesized that when the Grignard reagent is added slower than the turnover of the catalytic cycle however, the concentration of Pd(II) intermediate **II** increases because there is insufficient organometallic reagent present to fully consume it. As a result, Pd(II) species **II** becomes the catalyst resting state, with its concentration maintained at a sufficient level to allow rate of transmetallation to exceed rate of undesired direct nucleophilic attack, providing high selectivity for the desired cross-coupling product. While the example used to introduce this hypothesis was a Grignard reagent, the analogous explanation for the cross-couplings of organolithium reagents facilitated by slow addition is proposed, where lithium-halogen exchange rather than direct nucleophilic attack is the undesired, competing reaction. To test these hypotheses, real-time ESI-MS experiments[11] were conducted to monitor the appearance and accumulation or depletion of Pd(II) oxidative addition intermediates as a function of organometallic nucleophile addition rate for the Kumada-Corriu and Murahashi reactions enabled by nucleophile slow addition.

4.1.4 Palladium catalyzed aryl halide–diazo cross-coupling

Competing side reactions that erode yield in a cross-coupling reaction are present in many more transformations than the earliest developed examples from the labs of Kumada, Corriu and Murahashi. We hypothesized that the strategy of manipulating catalyst resting state by controlling addition rate of the nucleophilic coupling partner might be a widely applicable strategy to solve similar problems faced in modern cross-coupling chemistry with more diverse coupling partners.

We were intrigued by the palladium catalyzed cross-couplings with diazo nucleophiles. This chemistry was first developed by Barluenga and coworkers in 2007, using *N*-tosylhydrazones in combination with strong base to form the diazos *in situ*.[12] The reaction leads selectively to 1,1-disubstituted olefins (Scheme 4.8), in contrast to Mizoroki-Heck reactions that favor 1,2-substitution patterns with e.g., styrene coupling partners.[13] Due to the importance of polysubstituted olefins,[14] this reaction with *N*-tosylhydrazones has been used for the synthesis of diverse heterocycles, natural products, and bioactive molecules.[15]

Scheme 4.8. Cross-coupling of *N*-tosylhydrazones developed by Barluenga and coworkers proceeds through a Pd-carbene intermediate.

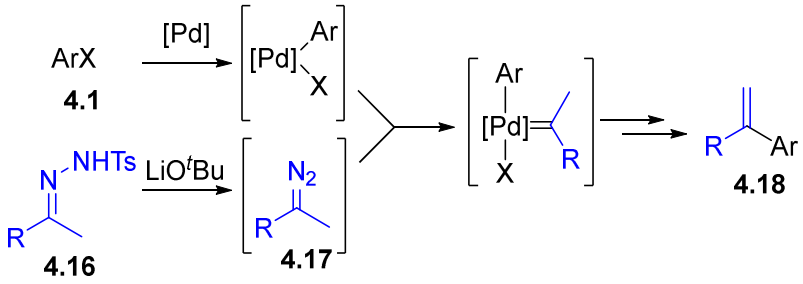

Seminal contributions from the groups of Van Vranken,[16] Wang,[17] and others have shown that diazo species can be used directly in Pd(0)-catalyzed cross-coupling reactions,[18] often in the absence of strong base and with shorter reaction times compared to analogous reactions of *N*-tosylhydrazones. However, these reactions suffer from two severe scope limitations. First, the diazo coupling partners have structural limitations due to the necessity to include a stabilizing electron withdrawing group for safety. And second, only specific organohalides, such as cis-vinyl iodides,[19] benzyl or allyl halides,[20] and, rarely, aryl iodides[21] have been successfully used. While the direct coupling of aryl halides and diazo compounds is perhaps the most obvious version of

the reaction, it wasn't reported until 2010 and only worked well for aryl iodides; extension to aryl bromides required high catalyst loadings and aryl chlorides were not reported.[22]

Previous mechanistic studies on the Pd-catalyzed coupling of aryl halides with diazo compounds suggested that oxidative addition may be the rate determining step,[22] which precedes reaction with the diazo. Diazos are known to undergo numerous other reactions, including unimolecular decomposition[23] and direct interaction with Pd(0).[24] Given the sparsity of aryl bromides and the absence of aryl chlorides, which under go slower oxidative addition,[25] we hypothesized that a conceptually similar problem of competing reaction pathways was causing the scope limitations. In this case, the desired reaction with the Pd(II)ArX intermediate is in competition with decomposition of the diazo reagent. When oxidative addition, and therefore catalyst turnover, is rapid (with e.g., aryl iodides) the entire cross-coupling reaction is complete before the diazo compound decomposes via other pathways. However, when the turnover limiting oxidative addition is slow (with e.g., aryl bromides and chlorides), the bulk of the diazo compound decomposes while waiting for catalyst turnover, leading to depletion of the diazo reagent and low yields of the desired cross-coupling product (Scheme 4.9A).

We hypothesized that a similar approach of manipulating catalyst resting state could be used to overcome these limitations. By adding the diazo reagent slower than catalyst turnover, the Pd(II) oxidative addition intermediate would accumulate such that as diazo is added there is always a sufficient concentration of Pd(II) present for reaction by the desired pathway.

In addition to addressing limitations with the aryl halide electrophiles, we envisioned also addressing the limitations with the diazo nucleophiles. As discussed in the general introduction, on-demand synthesis of diverse diazo compounds in continuous flow allows safe access to a wide variety of non-stabilized, functionalized diazo compounds by, for example, oxidation of hydrazones over MnO_2 (vide supra, Chapter 1, section 1.1.3).[26] Furthermore, continuous flow diazo synthesis is ideally compatible with reagent slow addition, by producing the diazo at the desired addition rate. The combination of these two strategies — on demand diazo synthesis and artificial manipulation of the catalyst resting state — provide a substantial expansion in the scope of this reaction, which is reported for the first time using diverse non-stabilized diazo reagents and with aryl bromides and chlorides (Scheme 4.9B).

Scheme 4.9. Hypothesis to explain previous reaction failure and strategy to unlock diverse organohalides & diazo reagents.

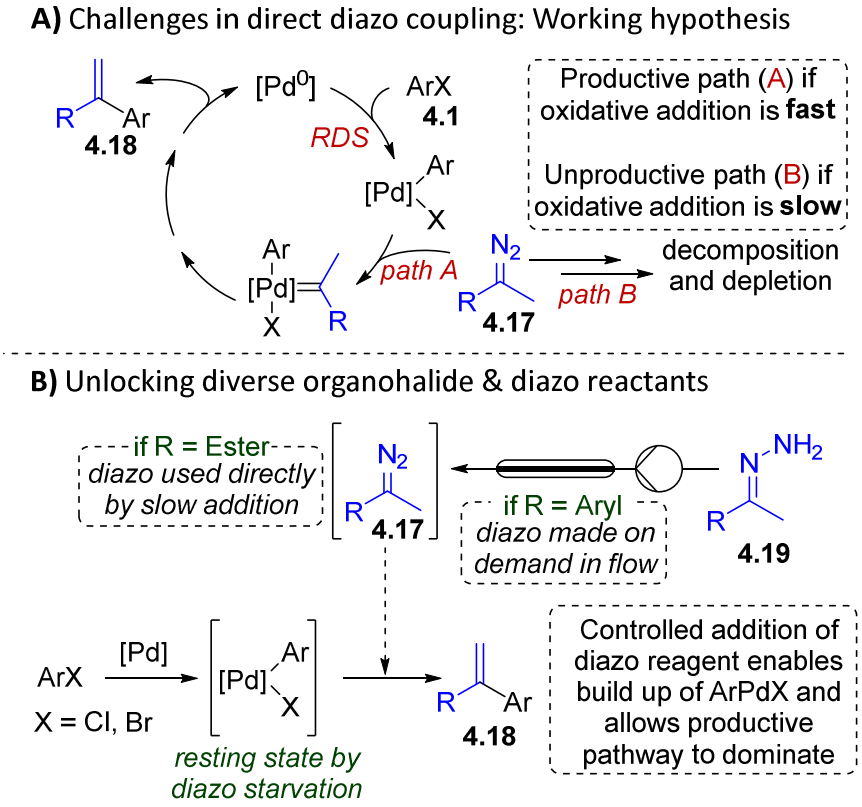

4.2 Results and Discussion

4.2.1 Real-time ESI-MS investigation into operative mechanism for success of slow addition strategy in Kumada-Corriu and Murahashi cross-couplings[a]

To provide support for the hypothesis that slow addition of the organometallic reagents allows productive cross-coupling chemistry by facilitating an accumulation of the Pd(II) oxidative addition intermediate, real-time direct infusion ESI-MS experiments[11] were conducted to monitor the appearance and accumulation or depletion of Pd(II) oxidative addition intermediate **II** (Figure 4.2B). When PhMgBr was added over the course of only 5 min a Pd-containing species was initially observed at *m/z* = 618, representing the loss of chloride from Pd(II) intermediate **II** (Figure

[a] This work was conducted in collaboration with X. Hau and J. Masson-Makdissi who assisted by preparing the starting materials and determining reaction yields as a function of addition organometallic rate.

4.2C). However, this signal rapidly depleted as the Grignard was added. Formation of imines **4.16** and **4.17** was observed, formed by nucleophilic attack of the Grignard on the nitrile group of the starting material and the desired cross-coupling product, respectively. In contrast, when the experiment was run with Grignard reagent slowly added over 1 h, Pd(II) intermediate **II** was present during the entire course of the reaction (Figure 4.2D). Small amounts of side product **4.16** were formed only during the initial induction period, providing further support for the hypothesis that this side reaction does not occur provided a sufficient concentration of **II** is present to achieve chemoselective transmetallation.

Since the 4-chlorobenzonitrile starting material and 4-phenylbenzonitirile product used in the initial ESI-MS investigation (Figure 4.2) could not be observed with the instrument parameters and experimental conditions that allowed detection of the Pd species of interest, the same slow and fast addition experiments with ESI-MS monitoring were repeated using 5-chloro-2-methylbenzoxazole (**4.7b**, Figure 4.3A) as the electrophile to confirm that starting material consumption and product formation were consistent with the observed presence or absence of active ArPdCl species. In these circumstances the identity of the side product(s) were unknown; however, the starting material **4.7b**, desired product **4.3b** and ArPdCl intermediate could all be observed simultaneously. The same observation of ArPdCl depletion when PhMgBr was added over only 5 min (Figure 4.3B) and pseudo-steady-state ArPdCl concentration when the Grignard was added over the optimal 1 h (Figure 4.3C) were observed as with the 4-chlorobenzonitrile substrate. As expected, the quantity of product **4.3b** increased only when the active ArPdCl intermediate was present. This occurred to a much greater extent during the slow Grignard addition experiment.

During the slow addition experiment, the starting material gradually decreased and desired product proportionately increased over the course of the Grignard addition. Due to the continuous withdrawal of solution from the mixture to enable the real-time monitoring, and the necessary withdrawal rate of 50−100 μL/min to prevent clogging of the PEEK tube leading from the reaction flask, the starting material became depleted at ~40 min, representing 2/3 of the total Grignard addition. At this point, precipitate formation in the reaction flask began and quickly resulted in clogging of the PEEK tubing leading to the MRA valve and therefore the end of data collection.

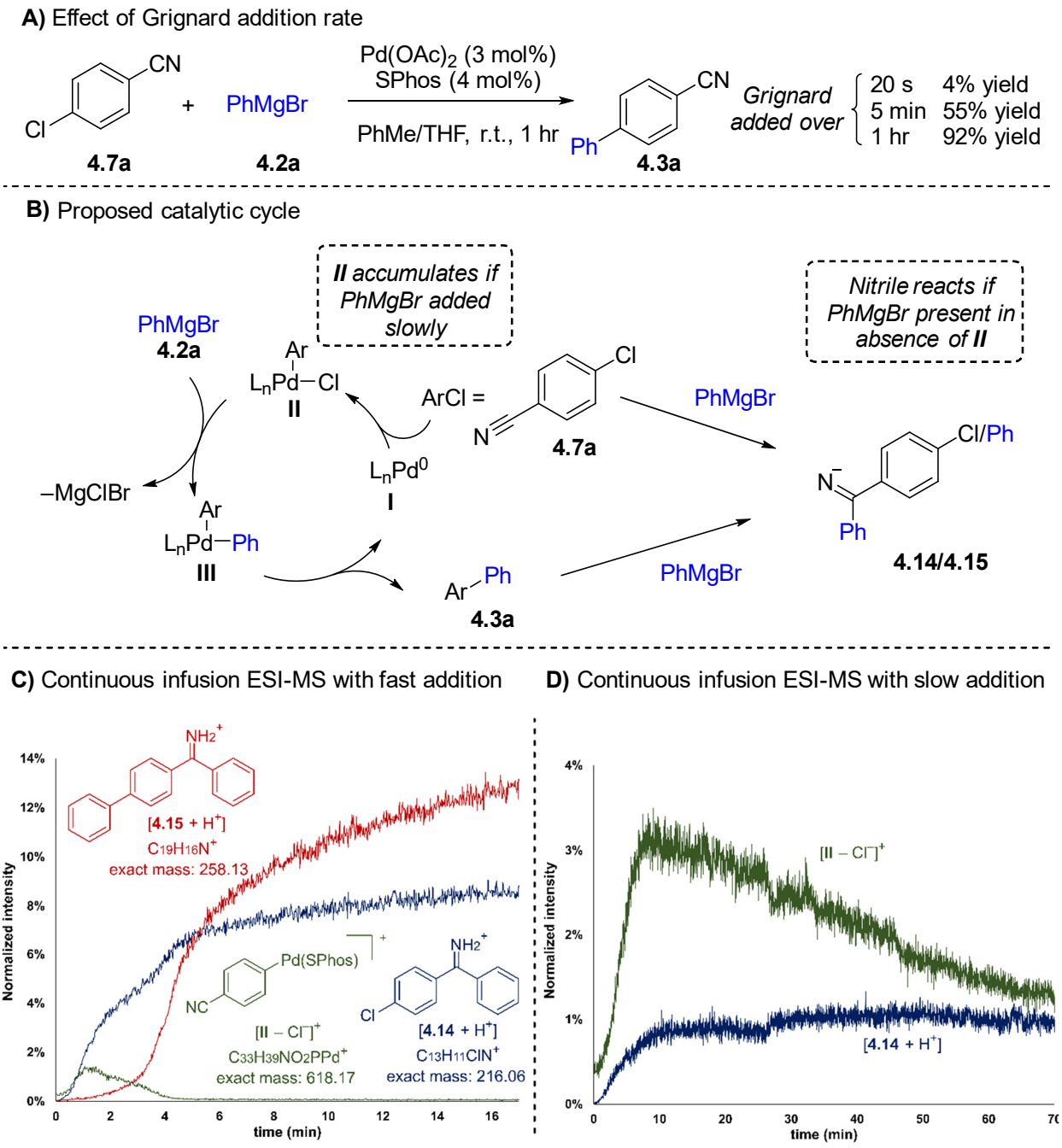

Figure 4.2. A) A substantial difference in yield is observed depending on how slowly the Grignard reagent is added over the duration of the reaction. B) Mechanistic interpretation of selectivity. C) Real time mass spectrometric monitoring with PhMgBr added over 5 minutes. Intensity represents the height of the most abundant isotope peak normalized to the total ion current from *m/z* = 100 to 800. D) PhMgBr added over 1 h.

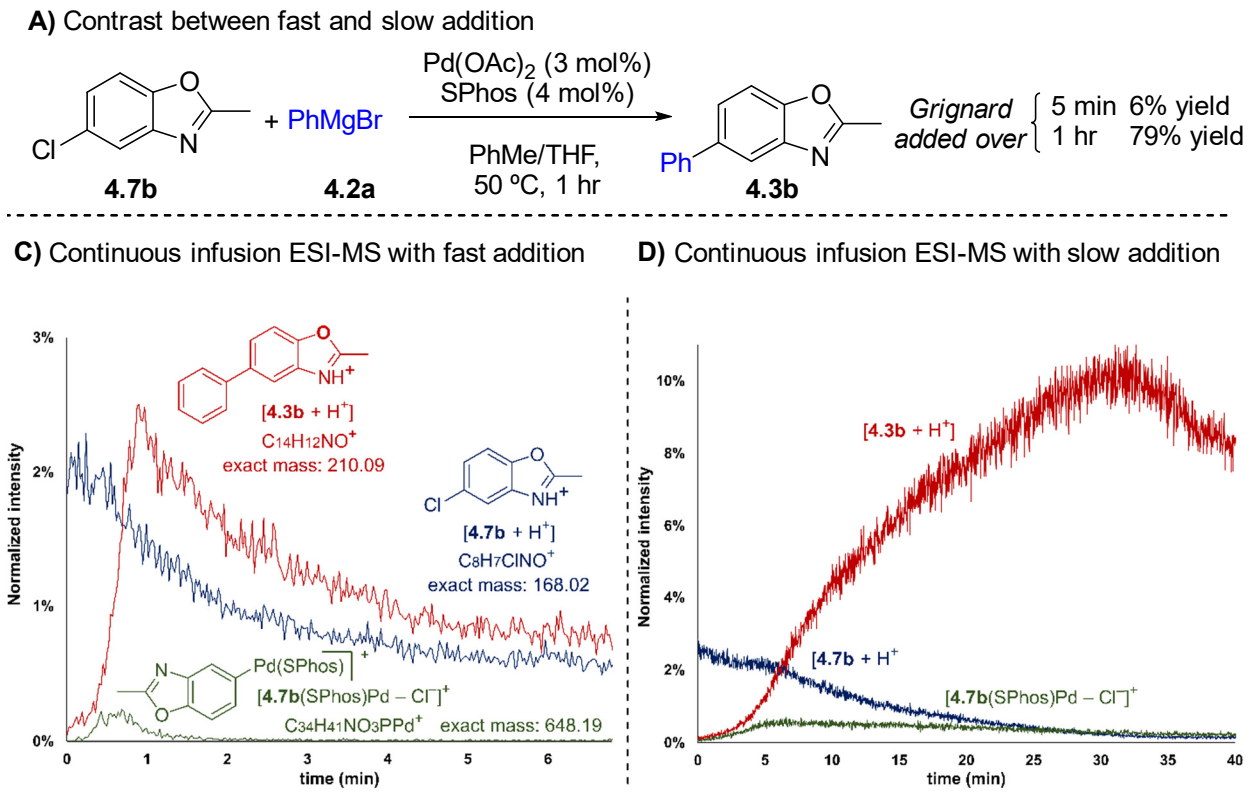

Figure 4.3. A) A substantial difference in yield is observed depending on the rate of Grignard addition. B) Real time mass spectrometric monitoring with PhMgBr added over 5 minutes. Intensity represents the height of the most abundant isotope peak normalized to the total ion current from *m/z* = 100 to 800. C) PhMgBr added over the course of 1 h.

Interestingly, between 30 and 40 min when the concentration of the starting material was nearing 0 and the concentration of product was high it was observed that the amount of product plateaued and then began to decline. This was likely an artifact of the early depletion of the starting material as a result of the reaction solution withdrawal leading to the presence of excess Grignard reagent at the end of the reaction and partial product decomposition as a result.

Pleased that the real-time ESI-MS experiments supported our initial hypothesis for the operative mechanism for the success of the slow addition strategy with the Kumada-Corriu cross-coupling, attention was turned to monitoring the ArPdCl oxidative addition intermediate in the Murahashi cross-coupling of chloronaphthalene (**4.13a**) with phenyllithium (**4.8a**) developed by Feringa and coworkers[9b] (Figure 4.4). Similar results were observed as with the Kumada-Corriu chemistry. When the organolithium nucleophile was added quickly the oxidative addition

intermediate initially appeared but was quickly depleted. In contrast, a pseudo steady-state concentration was observed when PhLi was added at the optimal, slow addition rate.

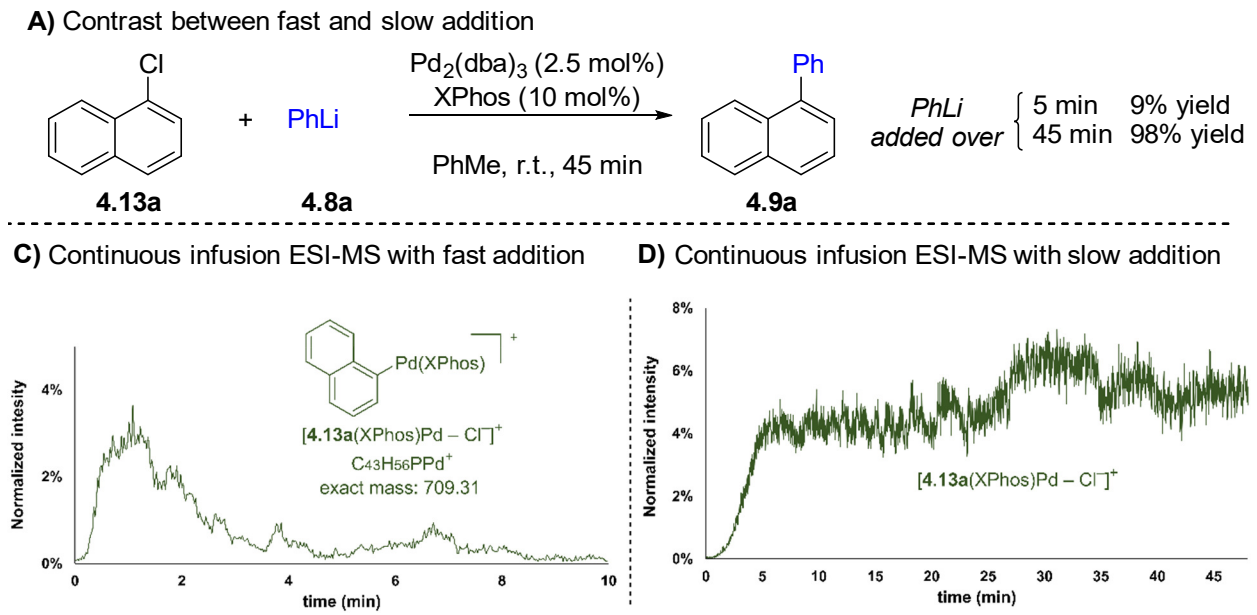

Figure 4.4. A) Direct coupling of organolithium reagents with aryl chlorides also requires slow addition of the nucleophile to obtain high yields. B) Real time mass spectrometric monitoring with PhLi added over 5 minutes. Intensity represents the height of the most abundant isotope peak normalized to the total ion current from *m/z* = 100 to 800. C) PhLi added over 45 min.

Together with the results from the Kumada-Corriu reactions, these data support the hypothesis that selectivity for transmetallation over undesired side reactions is achieved when using slow addition of the nucleophile by manipulating the catalyst resting state. The concentration of Pd(II) oxidative addition intermediate is increased by starvation of the nucleophilic coupling partner. As a result, chemoselective transmetallation occurs because the concentration of the Pd(II) oxidative addition intermediate is always sufficient for transmetallation to outcompete undesired side reactions. In other words, by manipulating the catalyst resting state, enough Pd(II) intermediate is always present to efficiently react with the organometallic reagent as it is added to the reaction medium.

4.2.1 Catalyst resting state manipulation and flow generation of non-stabilized diazos to enable aryl halide–diazo cross-coupling[a]

Attention was then turned to applying this strategy to overcome limitations in the cross-coupling with diazo nucleophiles. In this case, it was hypothesized that decomposition of the diazo compound was the competing side reaction that could be overcome by accelerating transmetallation through catalyst resting state manipulation. The cross-coupling of chlorobenzene (**4.20a**) with ethyl 2-diazopropanoate (**4.21**) was selected, catalyzed by the Pd/XPhos system previously reported for the analogous cross-coupling with aryl bromides.[22] Negligible yield of desired product **4.22a** was obtained if the diazo coupling partner was added in one dose at the start of the reaction, however when **21** was added by syringe pump, a strong correlation was observed between addition rate of diazo and yield of product **4.22a** (Figure 4.5) with 80% yield achieved when adding the diazo over the course of 3 h.

To further investigate the relationship between the diazo addition rate and yield, reactions between **4.21** and an electron-poor (4-chlorobenzonitrile, **4.20b**) and electron-rich (4-chloroanisole, **4.20c**) aryl chloride were investigated. As was the case with **4.20a**, both substrates exhibited an increase in yield with controlled diazo addition, with substantially different optimal rates depending on the electronic nature of the substituent on the aryl chloride. For **4.20b**, a 63% yield could already be achieved if the diazo reagent was added in one dose at the start of the reaction, whereas only trace product could be achieved in this manner when using **4.20c**. With diazo reagent added over a period of 30 min or longer ~90% yield was achieved for **4.20b**, while for **4.20c** only moderate yield was achieved even with diazo added over 5 h.

These results provided strong support for both initial hypotheses. Desired products could be produced from aryl chlorides if diazo was added slowly over the duration of the reaction, and the optimal addition rate may be approximating catalyst turnover rate, ensuring that the Pd(II) oxidative addition intermediate is always present to react with incoming diazo compound by maintaining it as the resting state. Secondly, substituents that accelerated oxidative addition allowed faster addition rates for the diazo reagent, consistent with oxidative addition being rate

[a] The work with aryl chlorides and stabilized diazo compounds was conducted by G. P. R. Freurre under my supervision. All other work with aryl bromides and flow-generated diazo, as well as computational work, compounds was performed by me.

limiting. Furthermore, addition rates slower than strictly necessary were not detrimental to product yield, providing support for the assertion that decomposition of the diazo compound in the absence of rapid catalyst turnover is indeed the problem previously preventing coupling with aryl chlorides.

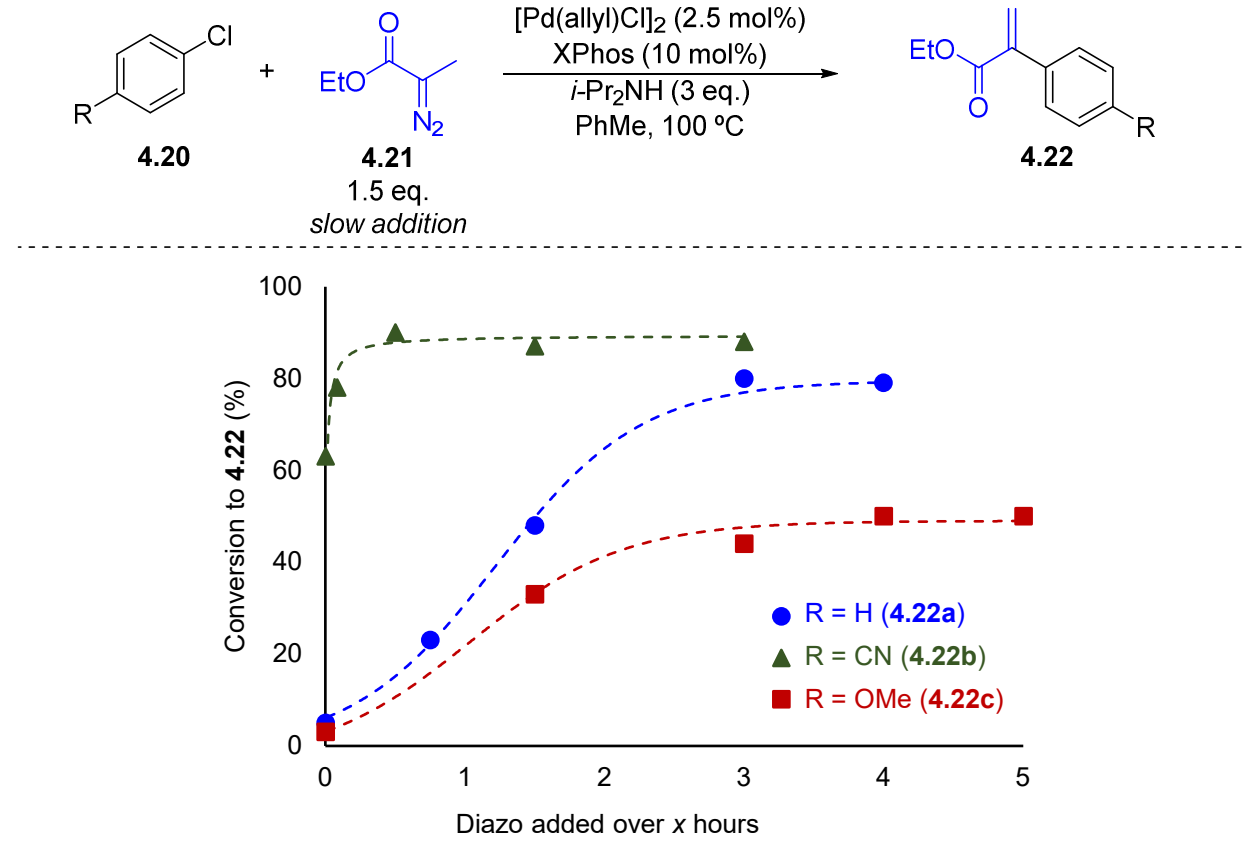

Figure 4.5. Effect of diazo addition rate on product yield for the cross-coupling of ethyl 2-diazopropanoate with aryl chlorides.[a]

[a] Conditions: 0.2 mmol of ArCl, 3 eq of *i*-Pr_2NH, $[Pd(allyl)Cl]_2$ (2.5 mol%), XPhos (10 mol%) in toluene (1 mL) at 100 °C, 1.5 eq of ethyl 2-diazopropanate in toluene (1 mL) added by syringe pump and stirred 15 additional min after addition was complete. Yield determined by proton NMR of crude mixture with 1,3,5-trimethoxybenzene as internal standard. Dotted lines are added for assistance with visualization only.

Since slower than necessary addition rates were not detrimental to product yield, a 3 h addition rate was selected to examine substrate scope (Table 4.1). A wide variety of electron withdrawing groups were tolerated including cyano (**4.22b**), acetyl (**4.22d**), aldehyde (**4.22e**) and chalcone (**4.22f**). Electron neutral phenyl (**4.22a**), styrene (**4.22g**) and thiomethyl (**4.22h**) groups were also compatible. An increase in catalyst loading allowed the presence of the strongly electron

donating 4-methoxy group (**4.22c**) to be tolerated as well. Relatively high steric hinderance from 2,6-dimethyl substitution was also compatible (**4.22i**), as were indole (**4.22j**) and benzodioxole (**4.22k**) heterocycles. The strategy of controlled diazo addition rate was also amenable to allow cross-coupling with aryl bromides at decreased catalyst loadings (**4.22a**).

Attention was next turned to expanding the scope of the diazo compounds with the use of non-stabilized diazo reagents. It is unsurprising that previous reports on these direct cross-coupling reactions are primarily limited to well-behaved α-diazo carbonyl compounds, since these species are isolable, less prone to decomposition, and, in many cases, commercial. Non-stabilized diazo reagents on the other hand present considerable safety risks during their preparation and isolation due to a tendency to (explosively) decompose.[27] For cross-coupling with aryl halides, these less stable diazo species should also be particularly challenging substrates due to faster background decomposition reactions than the stabilized analogues. Nonetheless, we believed that these challenges could be overcome with the combination of slow diazo addition and flow chemistry for safe, 'on-demand' diazo generation.

The strategy reported by Ley and coworkers for the generation of non-stabilized α-aryl diazo compounds by the continuous flow oxidation of hydrazones over MnO_2 was selected for this purpose.[26d–e] The literature protocol reported the production of diazo compounds in methylene chloride using short contact times (<1 s) with the oxidant. To be compatible with our cross-coupling chemistry, modifications were required to match the rate of diazo formation and consumption. To generate 2-diazoacetophenone (**4.24**) from acetophenone hydrazone (**4.23**) at required flow rates, a solution of **4.23** and 2 equivalents of *i*-Pr_2NH could be passed through a 5 cm × ¼" outer diameter, 3 mm inner diameter 316 stainless steel column packed with MnO_2 at 0.35 mL/min, providing ~75–80% yield (Scheme 4.10).

Scheme 4.10. Oxidation of acetophenone hydrazone to 2-diazoacetophenone over a packed bed of MnO_2.

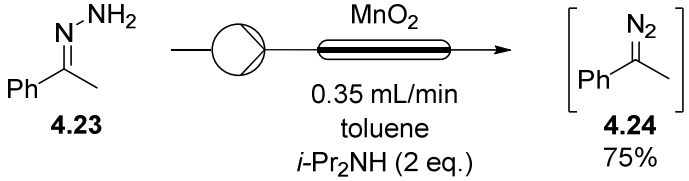

Table 4.1. Direct cross-coupling of aryl chlorides with diazo reactant.[a]

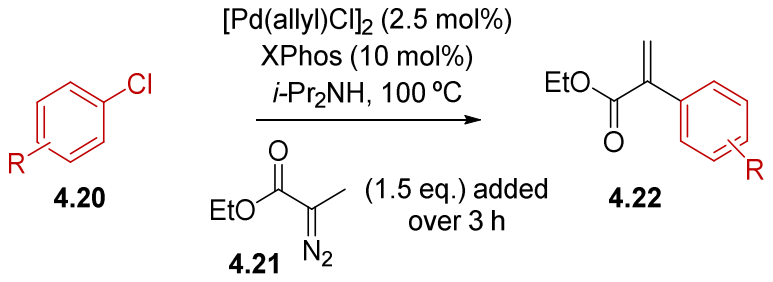

product	yield (%)	product	yield (%)	product	yield (%)
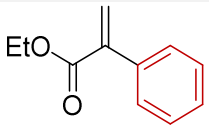 **4.22a**	75 (77[b])	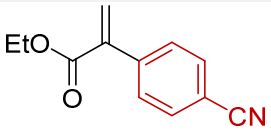 **4.22b**	77	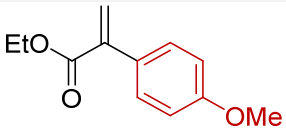 **4.22c**	66[c]
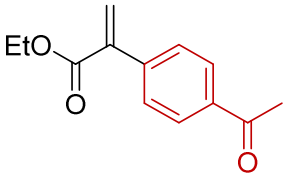 **4.22d**	84	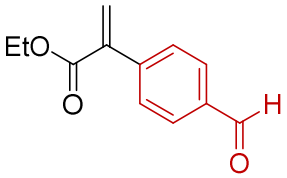 **4.22e**	65	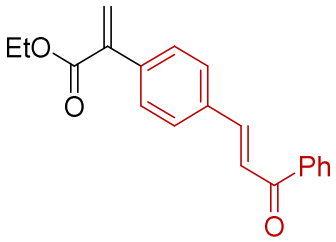 **4.22f**	91
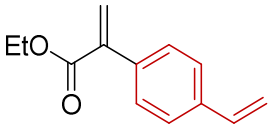 **4.22g**	73	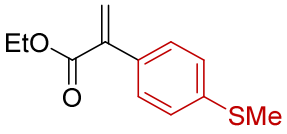 **4.22h**	62	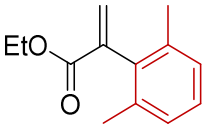 **4.22i**	52
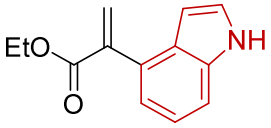 **4.22j**	73	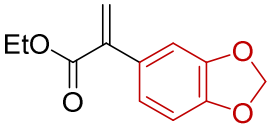 **4.22k**	50		

[a] Conditions: 0.2 mmol of ArCl, 3 eq of *i*-Pr$_2$NH, [Pd(allyl)Cl]$_2$ (2.5 mol%), XPhos (10 mol%) in toluene (1 mL) at 100 °C, 1.5 eq of ethyl 2-diazopropanate in toluene (1 mL) added over 3 h and stirred 15 additional min after addition complete. Isolated yield. [b] From bromobenzene; 15 min addition time at 80 °C with 3.5 mol% loading of Pd(XPhos)(allyl)Cl. [c] 5 mol% [Pd(allyl)Cl]$_2$, 20 mol% XPhos was used.

This was now compatible with our desired cross coupling chemistry, allowing diazo addition over a range of ~10–45 min at 0.2 mmol scale. We first demonstrated the application of these non-

stabilized, flow-generated diazo compounds to the cross-coupling with aryl bromides (Table 4.2). A 90% yield was achieved for the coupling of bromobenzene (**4.25a**) with 2-diazoacetophenone (**4.24**) after only a moderate increase in the stoichiometry of the non-stabilized diazo species to 2 eq. compared to 1.5 for ethyl 2-diazopropanoate (see Appendix III, Table AIII.1 for optimization data). The scope of suitable aryl bromides was very broad with little impact from electron withdrawing trifluoromethyl (**4.26b**), nitro (**4.26c**), or ketone (**4.26d**) groups, or electron donating methyl (**4.26e**), or methoxy (**4.26f**) groups. Steric hinderance at the 2-position of the aryl bromide was also tolerated (**4.26g**, **4.26h**), as was the presence of a benzylic alcohol (**4.26i**), free aniline (**4.26j**) or chloro group (**4.26k**). The electron rich heterocycles thiophene (**4.26l**), furan (**4.26m**), indole (**4.26n**) and oxindole (**4.26o**) were also readily prepared. Lewis basic, nitrogen containing heterocycles including pyridine, pyrimidine, and quinoline were incompatible substrates, presumably deactivating the catalyst by coordinative inhibition preventing interaction with the weak diazo nucleophile.

Next, attention was turned to the scope of α-aryl diazo compounds (Table 4.3). Again, electronics had a minor impact, with electron neutral naphthyl (**4.29a**), and electron withdrawing methyl ester (**4.29b**) groups equally tolerated, and only a slight decrease in yield from the presence of an electron donating methoxy group (**4.29c**) attributed to decreased stability of the diazo reagent. Steric hinderance at the 2-position of the aryl ring of the diazo was also not problematic (**4.29d**) nor was replacing the aryl group with thiophene (**4.29e**). The synthesis of tetra- (**4.29f**, **4.29g**) and tri-substituted (**4.29h**, **4.29i**) olefins was also possible, with an increase in the reaction temperature to 100 °C and catalyst load to 5%. *E*:*Z* selectivity was poor for the non-tethered tri-substituted olefin (**4.29i**), as expected based on previous results with stabilized diazo compounds.[22]

Lastly, the coupling of flow-generated, non-stabilized α-aryl diazo compounds with aryl chlorides was targeted. (2-Thiophenyl)-2-methyldiazomethane was successfully coupled with aryl chlorides (Table 4.4) bearing para-cyano (**4.31a**), ketone (**4.31b**), ester (**4.31c**), amide (**4.31d**) and nitro functional groups (**4.31e**), as well as an aryl chloride bearing a meta-nitro group (**4.31f**), all in reasonable yield with diazo addition over 20 min, highlighting the ability of a wide variety of electron withdrawing groups to accelerate oxidative addition and allow faster diazo addition rates.

Table 4.2. Scope of aryl bromides.[a]

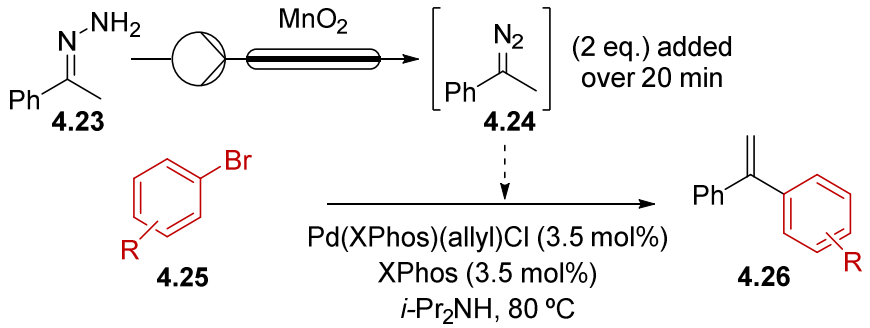

product	yield (%)	product	yield (%)	product	yield (%)
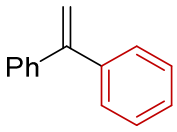 **4.26a**	90	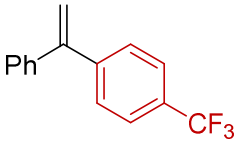 **4.26b**	88	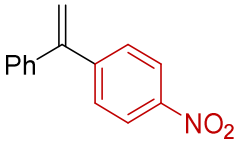 **4.26c**	82
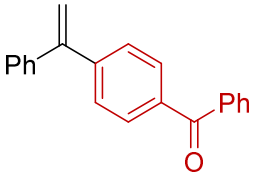 **4.26d**	87	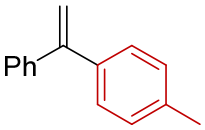 **4.26e**	84	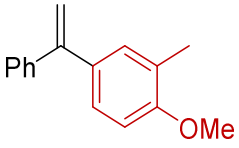 **4.26f**	87
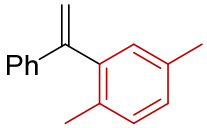 **4.26g**	87	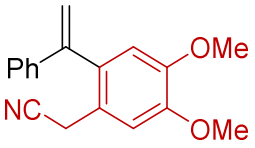 **4.26h**	98	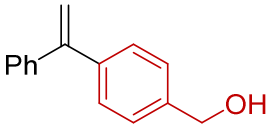 **4.26i**	91
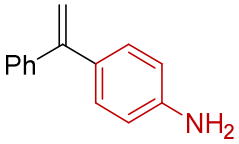 **4.26j**	73	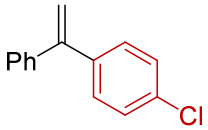 **4.26k**	88	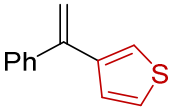 **4.26l**	70[b]
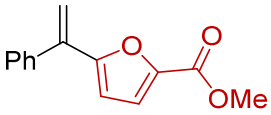 **4.26m**	71[b]	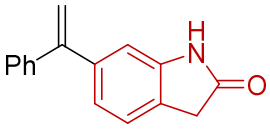 **4.26n**	87	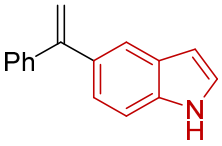 **4.26o**	88

[a] Conditions: 0.2 mmol of ArBr, 1 eq of *i*-Pr_2NH, Pd(XPhos)(allyl)Cl (3.5 mol%), XPhos (3.5 mol%) in toluene (1 mL) at 80 °C, 2 eq of flow-generated 2-diazoaceptophenone (~0.06 M solution in toluene with 0.15 M *i*-Pr_2NH, 7 mL) was added over 20 min and stirred 15 additional min after addition complete. Isolated yield. [b] 7 mol% catalyst was used.

Table 4.3. Scope of diazo compounds.[a]

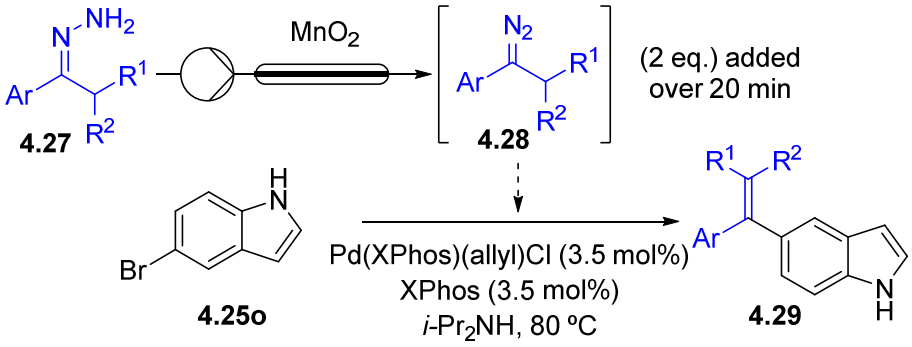

product	yield (%)	product	yield (%)
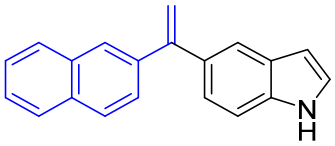 **4.29a**	88	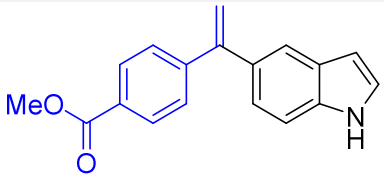 **4.29b**	80[b]
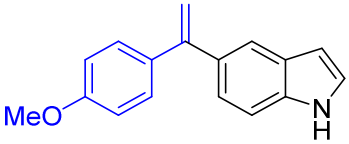 **4.29c**	91	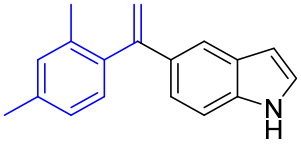 **4.29d**	85
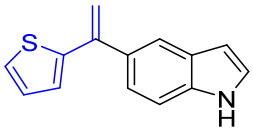 **4.29e**	77[c]	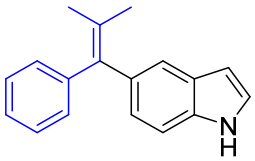 **4.29f**	73[d]
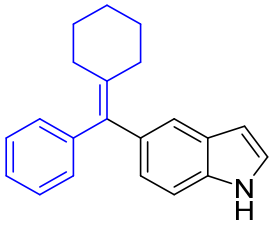 **4.29g**	47[d]	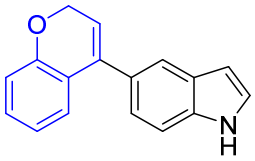 **4.29h**	43[c,d]
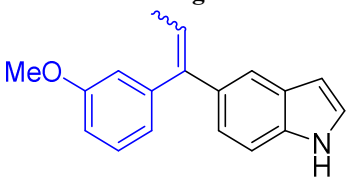 **4.29i**	87[d,e]		

[a] Conditions: 0.2 mmol of 5-bromoindole, 1 eq of *i*-Pr_2NH, Pd(XPhos)(allyl)Cl (3.5 mol%), XPhos (3.5 mol%) in toluene (1 mL) at 80 °C, 2 eq of flow-generated diazo (~0.06 M solution in toluene with 0.15 M *i*-Pr_2NH, 7 mL) was added over 20 min and stirred 15 additional min after addition complete. Isolated yield. [b] The hydrazone solution was prepared at ½ concentration and oxidized over MnO_2 at 2× flow rate due to solubility limitations. [c] The packed bed of

MnO_2 was cooled at 0 °C for generation of this diazo compound. [d] The reaction was conducted at 100 °C with 5% catalyst loading and diazo compound added over 30 min. [e] 2.3:1 mixture of *Z*:*E* isomers.

Table 4.4. Scope of activated aryl chlorides.[a]

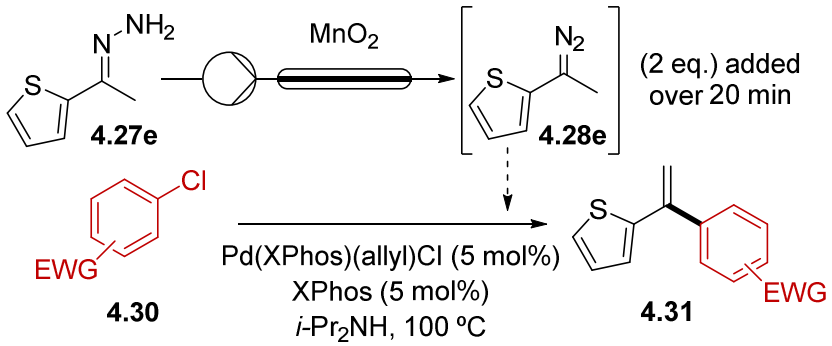

product	yield (%)	product	yield (%)	product	yield (%)
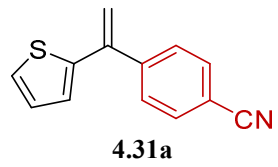 **4.31a**	69	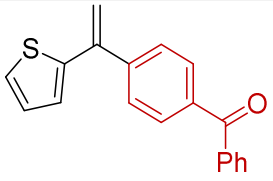 **4.31b**	72	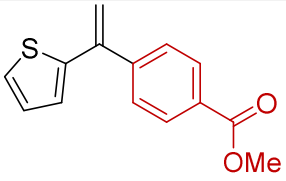 **4.31c**	62
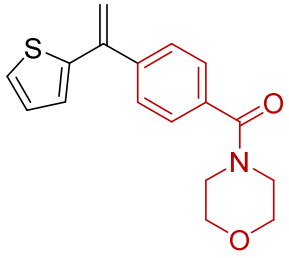 **4.31d**	68	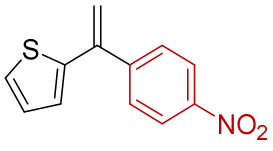 **4.31e**	82	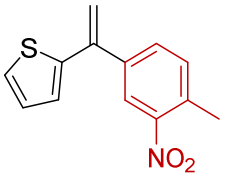 **4.31f**	89

[a] Conditions: 0.2 mmol of ArCl, 1 eq of *i*-Pr_2NH, Pd(XPhos)(allyl)Cl (5%), XPhos (5%) in toluene (1 mL) at 100 °C, 2 eq of flow-generated diazo (~0.06 M solution in toluene with 0.15 M *i*-Pr_2NH, 7 mL) was added over 20 min and stirred 5 additional min after addition complete. Isolated yield (0.2 mmol scale).

To provide further insight into the reaction mechanism DFT calculations were performed examining the reaction of chorobenzene (**4.20a**) with methyl 2-diazopropanoate (Figure 4.6, red). CyJohnPhos was used as a model ligand in the place of XPhos to reduce computational expense while maintaining similar ligand electronics. It was determined that oxidative addition of Pd(0) into PhCl (**TS1**) was the turnover frequency determining transition state (TDTS, i.e., the rate

determining step)[28] confirming what was previously hypothesized based on experimental observations for the analogous reaction with PhBr and PhI.[22] Oxidative addition (**I1→I2**) and N_2 loss followed by phenyl migratory insertion (**I3→I5**) are highly exergonic and therefore irreversible elementary steps, while β-hydride elimination coupled with product release (**I5→I7**) and base-assisted reduction to Pd(0) (**I7→I8**) are roughly energetically neutral (±5 kcal/mol) and therefore reversible. These results are in general agreement with previous computational studies with similar elementary steps for related systems.[29] Regeneration of **I1** from **I8** by release of *i*-$Pr_2NH{\cdot}HCl$ to complete catalyst turnover is thermodynamically uphill under standard conditions (i.e., 1 M in all species), but the low solubility of the *i*-$Pr_2NH{\cdot}HCl$ salt provides a driving force for this turnover in practice.

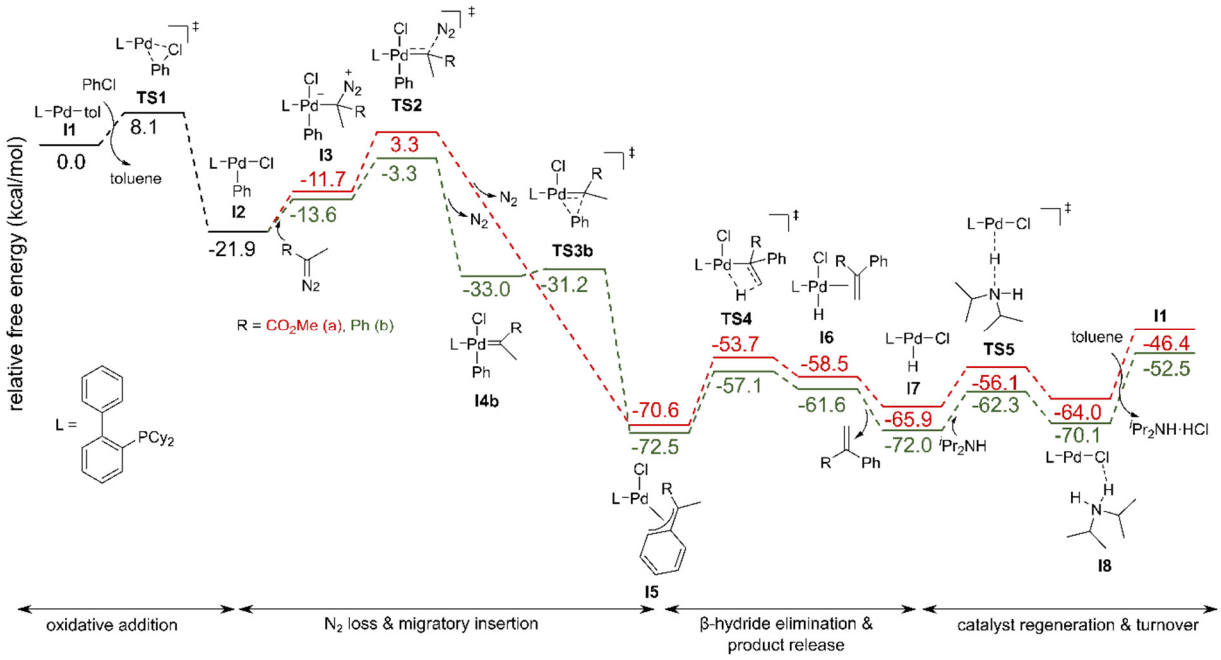

Figure 4.6. Energy profile of the catalytic cycle for the cross-coupling of chlorobenzene with methyl 2-diazopropanoate and 2-diazoacetophenone respectively; M06-L/def2-TZVP//M06-L/def2-SVP level of theory.

The reaction pathway was also calculated for the non-stabilized diazo compound 2-diazoacetophenone (**4.24**, Figure 4.6, green). In contrast to the reaction with methyl 2-diazo propanoate, a stable palladium carbene intermediate (**I4b**) was calculated. No reaction barrier for

phenyl group migration existed with the more stabilized diazo, which instead collapses to the benzyl Pd intermediate **I5a** directly following loss of nitrogen. [30]

In order to explain the success of the diazo slow addition strategy, speciation within the catalytic cycle was examined. Two consecutive turnovers in the cross-coupling of methyl 2-diazopropanoate with PhCl were analyzed (Figure 4.7), considering the energies relative to a forward cycle starting from the turnover frequency determining intermediate (TDI, i.e., the intermediate that maximizes the energetic span of the catalytic cycle)[28] **I5a**. This suggests that palladium speciation within the catalytic cycle will mainly be divided between intermediates **I5**, **I7**, **I8**, and **I2**, with **I5** contributing the largest amount under standard conditions, but potential for any of these 4 intermediates to become the resting state under relevant reaction conditions (concentrations ≠ 1 M). Further, it is clear that all reversible steps between **I5** and **I8** are fast due to low activation barriers, while irreversible oxidative addition (**I1→I2**) and nitrogen extrusion (**I3→I5**) are slow, mainly as a consequence of operating from the disfavored sides of chemical equilibria (between **I8**/**I1** and **I2**/**I3** respectively) rather than overly high activation barriers for the transition states relative to the immediately preceding intermediates.

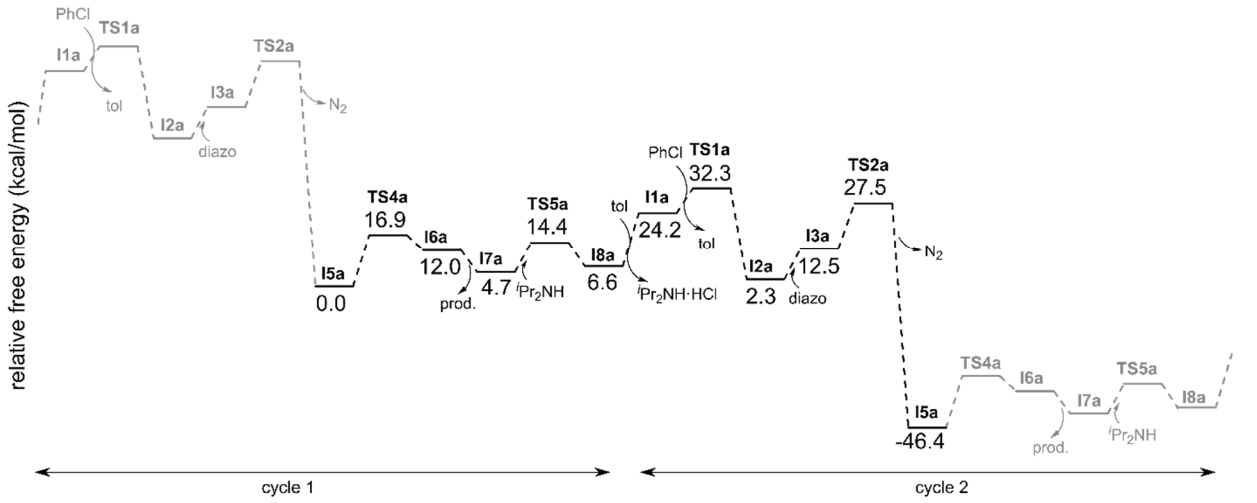

Figure 4.7. Energy profile for two consecutive catalytic cycles in the cross-coupling of chlorobenzene with methyl 2-diazopropanoate with energies relative to TDI **I5a**; M06-L/def2-TZVP//M06-L/def2-SVP level of theory.

Because **I2** is formed and consumed in slow, irreversible steps, the concentration of **I2** relative to the other palladium species can be manipulated by changing either rate of its formation

or consumption. Since the barrier for **I2** formation (**TS1**) is higher than the barrier for **I2** consumption (**TS2**), this species will be present at very low concentrations under standard conditions. However, by decreasing the concentration of diazo, the consumption reaction slows and allows **I2** to accumulate. Under these conditions, productive cross-coupling can occur because the necessary intermediate **I2** becomes the resting state, ensuring it is always present to react with diazo compound as it is added and avoiding the diazo decomposition that occurs in the absence of **I2**. It is only possible to achieve and maintain this situation when the addition rate of diazo compound does not exceed the rate of formation of **I2**, that is, when diazo addition rate is equal to or slower than oxidative addition.

Next, to rationalize the large variation in the optimal addition rate of diazo compound for different substituted aryl chlorides, key energies were calculated using chlorobenzene, 4-chlorobenonitrile, and 4-chloroanisole (Figure 4.8). Turnover frequencies (TOF) at standard conditions were calculated using the relative free energies of the net transformation (ΔG°) and the TDTS (**TS1**) and TDI (**I5**) using the energetic span model.[28] The ΔG and E_{TDI} (**I5a,c,d**) were largely unaffected by substitution on the aryl group. Only the E_{TDTS} (**TS1a,c,d**) exhibited significant energetic differences between the three substrates, indicating that it is solely the rate of oxidative addition that affects rate of catalyst turnover. The calculated TOFs were found to range over 4 orders of magnitude, consistent with the experimental observations of greatly different maximum diazo addition rates required for electron rich versus electron poor substrates.

4.3 Conclusions

Real-time ESI-MS reaction monitoring provided evidence to support the hypothesis that starving a reaction of the nucleophilic cross-coupling partner by using a slow addition strategy leads to accumulation of the Pd(II) oxidative addition intermediate, manipulating the catalyst resting state. The increase in concentration of this crucial Pd(II) intermediate accelerates the rate of transmetallation over undesired side reactions, facilitating chemoselective Kumada-Corriu or Murahashi cross-coupling reactions.

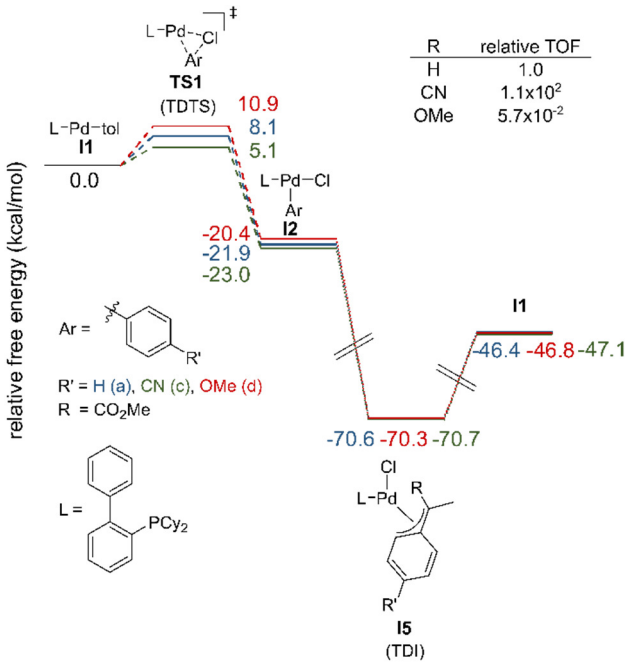

Figure 4.8. Relative free energies of TDTS and TDI in the cross-coupling of ethyl 2-diazopropanoate with 4-chlorobenzonitrile, chlorobenzene, or 4-chloroanisole; M06-L/def2-TZVP//M06-L/def2-SVP level of theory.

It was then demonstrated that a conceptually similar strategy of catalyst resting state manipulation was applicable to overcome severe scope limitations in the palladium catalyzed cross-coupling of aryl bromides and chlorides with diazo compounds. It is proposed that starving the reaction of diazo compound, by adding the diazo slower than the rate of catalyst turnover, shifts the rate determining step from oxidative addition to palladium(II) mediated nitrogen extrusion, making the oxidative addition Pd(II)ArCl intermediate the resting state of the catalytic cycle. This hypothesis is supported experimentally with observation of a clear trend between electronic substitution of the aryl chloride and necessary rate of diazo addition, and computationally with DFT calculations investigating the reaction mechanism.

Additionally, the expansion of the scope of diazo reagents applicable in this chemistry was also demonstrated to include non-stabilized α-aryl diazo compounds by the safe, continuous on-demand flow generation of the diazo species. The strategy of diazo slow addition should further be applicable to any diazo cross-coupling reaction suffering from poor yield due to background diazo decomposition rates faster than catalyst turnover, and therefore is anticipated to allow access

to a much greater range of aryl (pseudo)halides for a variety of diazo coupling reactions in the future.

4.4 Experimental

4.4.1 Real-time ESI-MS reaction monitoring experiments

4.4.1.1 Instrumentation

Real-time ESI-MS monitoring experiments were performed using an Advion ExpressION^S compact mass spectrometer in the positive ionization mode with capillary temperature 200 ºC, capillary voltage 120 V, source gas temperature 250 ºC, ESI voltage 3500 V and sweep rate of 2500 $m/z \cdot s^{-1}$. Data were smoothed using a five-point boxcar average.

4.4.1.2 Experimental details of real-time ESI-MS monitoring

The experimental setup shown in Figure 4.9 was used to dilute the reaction solutions by a factor of ~870 into the mobile phase before feeding into the mass spec. A two stage dilution with first 50 μL/min THF (Grignard experiments, Figures 4.2 and 4.3) or toluene (PhLi experiments, Figure 4.4) and then 200 μL/min mass spec mobile phase (0.1% acetic acid in 95:5 MeOH:H_2O) was necessary to prevent precipitation and clogging in the Rheodyne MRA 100-000 sampling valve. Slow addition experiments were scaled to an initial volume of 10 mL (before addition of the Grignard or PhLi solution) and fast addition experiments to an initial volume of 3 mL to ensure that the amount of solution removed over the course of the monitoring did not exceed ~30%.

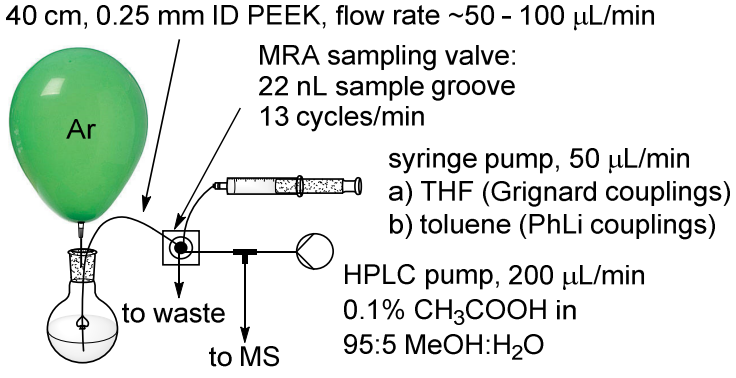

Figure 4.9. Experimental setup for real-time mass spectroscopic monitoring of cross-coupling reactions.

Experimental conditions for real-time ESI monitoring of Kumada-Corriu coupling reactions

Fast Grignard addition (Figures 4.2C and 4.3B). $Pd(OAc)_2$ (12 µmol, 3 mol%), SPhos (16 µmol, 4 mol%) and the aryl chloride (0.40 mmol, 1eq.) were added to an oven-dried, 25 mL round bottom flask equipped with a magnetic stir bar and Teflon septum. The flask was purged by an argon balloon and toluene (3 mL) was added. The reaction mixture was stirred, and Grignard reagent was added (0.48 mmol, 1.2 eq., 1 M in THF) over 5 min using a 1 mL HSW norm-ject plastic syringe in a NewEra NE-300 syringe pump with continuous withdrawal for MS monitoring using the setup shown in Figure 4.9.

To calculate yield for fast addition experiments (Figures 4.2B and 4.3A), the procedure was repeated at 0.20 mmol scale. After addition of the organometallic species was complete the reaction was allowed to stir for the remainder of the 1 h reaction time, then was quenched with $NH_4Cl_{(aq)}$, 1,3,5-timethoxybeneze (0.05 mmol) was added (internal standard) and the organic phase extracted with EtOAc and eluted though a plug of silica gel. Yield was determined from the crude ^{1}H-NMR.

Slow Grignard addition (Figures 4.2D and 4.3C). $Pd(OAc)_2$ (60 µmol, 3 mol%), SPhos (80 µmol, 4 mol%) and the aryl chloride (2.0 mmol, 1 eq.) were added to an oven-dried 25 mL flask equipped with a magnetic stir bar and Teflon septum. The flask was purged by an argon balloon and toluene (10 mL) was added. Separately, Grignard reagent (~3 mmol) was diluted to a final concentration of 0.32 M with toluene. The reaction mixture was stirred, and the Grignard reagent was added over 1 h using a 20 mL HSW norm-ject plastic syringe in a NewEra NE-300 syringe pump with continuous withdrawal for MS monitoring using the setup shown in Figure 4.9.

Experimental conditions for real-time ESI monitoring of Murahashi coupling reactions

Fast PhLi addition (Figure 4.4B). The general conditions reported by Feringa and coworkers[9] for their 'catalyst system B' were used with PhLi added over 5 minutes instead of 45 minutes on 3 mL scale with continuous withdrawal for MS monitoring using the setup shown in Figure 4.9. $Pd_2(dba)_3$ (10.3 mg, 0.011 mmol, 2.5 mol%) and XPhos (21.5 mg, 0.045 mmol, 10 mol%) were dissolved in toluene (3 mL). 1-Chloronaphthalene (73.2 mg, 0.45 mmol) was added, the solution was stirred at room temperature and PhLi diluted to 0.6 M in THF (1.0 mL, 0.6 mmol, 1.35 eq.) was added over 5 minutes with continuous withdrawal for MS monitoring.

To calculate the yield for fast addition (Figure 4.4A) the experiment was duplicated without MS monitoring and stirred for an additional 40 minutes after the addition was complete to give a total reaction time of 45 minutes. The reaction was quenched with $NH_4Cl_{(aq)}$, hexadecane was added as an internal standard and the mixture was extracted with EtOAc, diluted to an appropriate concentration and quantified by GC-FID with a 5-point calibration curve. A 9% yield of the product **4.9a** was observed.

Slow PhLi addition (Figure 4.4C). The general conditions reported by Feringa and coworkers[9] for their 'catalyst system B' were used on 10 mL scale with PhLi addition over 45 minutes and continuous withdrawal for MS monitoring as above. A 98% yield is reported for this reaction in their manuscript, which is consistent with the large amount of product and minimal amounts of by-products observed in our ESI monitoring experiment under these conditions.

4.4.2 Aryl halide–diazo cross-coupling

4.4.2.1 General experimental details

NMR spectra were collected on a Bruker Avance 400 MHz spectrometer. ^{1}H and ^{13}C were referenced to residual solvent signals and ^{31}P and ^{19}F were reference externally to 85% H_3PO_4 and neat CF_3COOH respectively. IR spectra of compounds were obtained using a Nicolet6700 FT-IR spectrometer with a diamond ATR crystal (ThermoScientific). IR spectra of diazo compounds were monitored using a Mettler Toledo FlowIR equipped with a silicon wafer ATR element. Accurate mass data was obtained from an Agilent 5977A GC/MS using MassWorks 4.0 from CERNO bioscience.[31] MnO_2, ≥90% activated, was obtained from Fluka (product number 63548), all other chemicals were obtained from commercial sources and used as received. Toluene was degassed with Ar and passed through a PureSolv solvent purification system before use. Cross-coupling reactions were carried out in oven-dried glassware under an Ar atmosphere. 5% $AgNO_3$ impregnated silica gel was prepared by adding a solution of $AgNO_3$ (7.5 g) in MeCN (100 mL) to a slurry of silica gel (150 g) in MeCN (500 mL) and evaporating the solvent. Ethyl 2-diazopropanoate,[32] and Pd(XPhos)(allyl)Cl[33] were prepared by literature procedures and their characterization data were in agreement with that reported by the authors.

4.4.2.2 General procedures

General procedure for ethyl 2-diazopropanoate-aryl chloride cross-coupling. $[Pd(allyl)Cl]_2$ (1.8 mg, 5.0 μmol), XPhos (9.5 mg, 20 μmol) and aryl chloride (if solid; 0.20 mmol) were placed in an 8 mL screw top tube and flushed with Ar. Toluene (1 mL) and aryl chloride (if liquid; 0.20 mmol) were added and the solution stirred at room temperature for 10 min. *i*-Pr_2NH (85 μL, 0.6 mmol) was added and the solution stirred an additional 3 min at room temperature. Separately a solution of ethyl 2-diazopropanoate (42 μL, 0.36 mmol) in toluene (1.2 mL) was prepared and taken up into a 1 mL plastic HSW syringe and placed on a NewEra NE-300 syringe pump. The aryl chloride solution was placed in a 100 °C oil bath and stirred for 3 min followed by addition of ethyl 2-diazopropanoate solution at a rate of 333 μL/h for 3 h (1 mL, 0.30 mmol diazo). The reaction was stirred an additional 15 min after addition was complete then cooled to room temperature and filtered through silica eluting with acetonitrile and purified by flash column chromatography immediately.

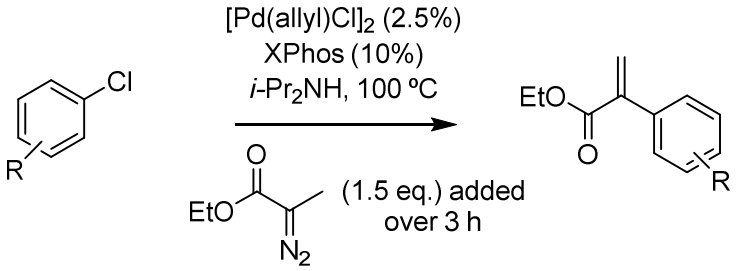

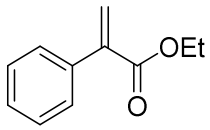

Ethyl 2-phenylacrylate (**4.22a**).[a] Prepared by the general procedure and purified on silica eluting with 5% EtOAc in hexanes. Yield 26.6 mg (75%) colourless oil. Characterization data were in agreement with the literature.[34] ^1H NMR (400 MHz, $CDCl_3$) 7.43 (m. 2H), 7.35 (m, 3H), 6.36 (d, J = 1.3 Hz, 1H), 5.89 (d, J = 1.3 Hz, 1H), 4.30 (q, J = 7.1 Hz, 2H), 1.34 (t, J = 7.1 Hz, 3H). $^{13}C\{^1H\}$ NMR (100 MHz, $CDCl_3$) 166.9, 141.7, 136.9, 128.4, 128.24, 128.21, 126.6, 61.2, 14.3.

[a] Prepared by G. P. R. Freure

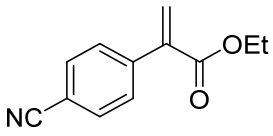

Ethyl 2-(4-cyanophenyl)acrylate (**4.22b**).[a] Prepared by the general procedure and purified on silica eluting with 10% EtOAc in hexanes. Yield 31.1 mg (77%) colourless oil. Characterization data were in agreement with the literature.[35] ^{1}H NMR (400 MHz, $CDCl_3$) 7.65 (d, J = 8.7 Hz, 2H), 7.53 (d, J = 8.1 Hz, 2H), 6.49 (d, J = 0.8 Hz, 1H), 5.97 (d, J = 0.9 H, 1H), 4.30 (q, J = 7.1 Hz, 2H), 1.35 (t, J = 7.1 Hz, 3H). ^{13}C{^{1}H} NMR (100 MHz, $CDCl_3$) 165.8, 141.4, 140.3, 132.0, 129.2, 129.0, 118.8, 112.0, 61.6, 14.3.

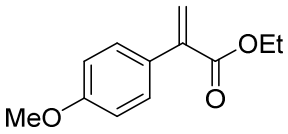

Ethyl 2-(4-methoxyphenyl)acrylate (**4.22c**).[a] Prepared by the general procedure with 2× catalyst load (10 μmol $[Pd(allyl)Cl]_2$, 40 μmol XPhos) and purified on silica eluting with 0.5→10% EtOAc in hexanes. Yield 27.4 mg (66%) pale yellow oil. Characterization data were in agreement with the literature.[36] ^{1}H NMR (400 MHz, $CDCl_3$) 7.37 (d, J = 8.8 Hz, 2H), 6.88 (d, J = 8.8 Hz, 2H), 6.25 (d, J = 1.0 Hz, 1H), 5.82 (d, J = 1.1 Hz, 1H), 4.29 (q, J = 7.1 Hz, 2H), 3.82 (s, 3H), 1.33 (t, J = 7.2 Hz, 3H). ^{13}C{^{1}H} NMR (100 MHz, $CDCl_3$) 167.3, 159.7, 141.1, 129.6, 129.4, 125.1, 113.7, 61.2, 55.4, 14.4.

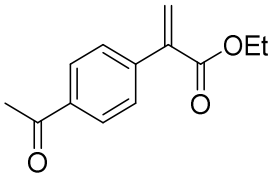

Ethyl 2-(4-acetylphenyl)acrylate (**4.22d**).[a] Prepared by the general procedure and purified on silica eluting with 3.5→10% EtOAc in hexanes. Yield 36.5 mg (84%) pale yellow oil. Characterization date were in agreement with the literature.[35] ^{1}H NMR (400 MHz, $CDCl_3$) 7.94 (d, J = 8.5 Hz, 2H), 7.52 (d, J = 8.5 Hz, 2H), 6.45 (d, J = 1.0 Hz, 1H), 5.97 (d, J = 1.0 Hz, 1H), 4.30 (q, J = 7.2 Hz,

[a] Prepared by G. P. R. Freure

2H), 2.61 (s, 3H), 1.34 (t, J = 7.2 Hz, 3H). $^{13}C\{^{1}H\}$ NMR (100 MHz, $CDCl_3$) 197.8, 166.3, 141.5, 140.9, 136.7, 128.7, 128.3, 128.2, 61.5, 26.8, 14.3.

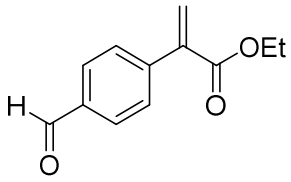

Ethyl 2-(4-formylphenyl)acrylate (**4.22e**).[a] Prepared by the general procedure and purified on silica eluting with 3.5% EtOAc in hexanes. Yield 26.5 mg (84%) pale yellow oil. ^{1}H NMR (400 MHz, $CDCl_3$) 10.03 (s, 1H), 7.87 (d, J = 8.4 Hz, 2H), 7.59 (d, J = 8.2 Hz, 2H), 6.48 (d, J = 0.8 Hz, 1H), 5.99 (d, J = 0.8 Hz, 1H), 4.30 (q, J = 7.1 Hz, 2H), 1.34 (t, J = 7.2 Hz, 3H). $^{13}C\{^{1}H\}$ NMR (100 MHz, $CDCl_3$) 192.0, 166.1, 142.9, 140.8, 136.0, 129.6, 129.2, 128.6, 61.6, 14.3. IR ν(C=O) 1698, 1725 cm^{-1}. HRMS calcd for $C_{12}H_{12}O_3$ 204.0786; found 204.0781, spectral accuracy 96.7%.

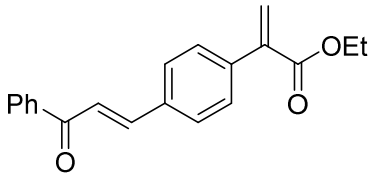

Ethyl 2-(chalcone-4-yl)acrylate (**4.22f**).[a] Prepared by the general procedure and purified on silica eluting with 3.5→10% EtOAc in hexanes. Yield 55.8 mg (91%) pale yellow oil. ^{1}H NMR (400 MHz, $CDCl_3$) 8.02 (d, J = 8.6 Hz, 2H), 7.82 (d, J = 15.7 Hz, 1H), 7.57 (m, 8H), 6.41 (d, J = 0.8 Hz, 1H), 5.96 (d, J = 0.9 Hz, 1H), 4.31 (q, J = 7.1 Hz, 2H), 1.33 (t, J = 7.1 Hz, 3H). $^{13}C\{^{1}H\}$ NMR (100 MHz, $CDCl_3$) 190.6, 166.5, 144.3, 141.0, 139.0, 138.3, 134.8, 133.0, 129.0, 128.8, 128.6, 128.3, 127.3, 122.5, 61.4, 14.3. IR ν(C=O) 1661, 1721 cm^{-1}. HRMS calcd for $C_{20}H_{18}O_3$ 306.1256; found 306.1250, spectral accuracy 98.1%.

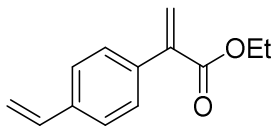

Ethyl 2-(4-styenyl)acyrlate (**4.22g**).[a] Prepared by the general procedure and purified on silica eluting with 3.5% EtOAc in hexanes. Yield 29.6 mg (73%) pale yellow oil. ^{1}H NMR (400 MHz, $CDCl_3$) 7.40 (s, 4H), 6.73 (dd, J = 17.6, 10.9 Hz, 1H), 6.33 (d, J = 1.2 Hz, 1H), 5.90 (d, J = 1.2

[a] Prepared by G. P. R. Freure

Hz, 1H), 5.77 (d, J = 17.6 Hz, 1H), 5.27 (d, J = 11.0 Hz, 1H), 4.30 (q, J = 7.1 Hz, 2H), 1.34 (t, J = 7.2 Hz, 3H). $^{13}C\{^1H\}$ NMR (100 MHz, $CDCl_3$) 166.9, 141.3, 137.6, 136.5, 136.3, 128.6, 126.3, 126.1, 114.4, 61.3, 14.4. IR ν(C=O) 1719 cm^{-1}. HRMS calcd for $C_{13}H_{14}O_2$ 202.0994; found 202.0998, spectral accuracy 99.4%.

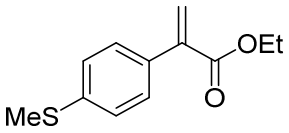

Ethyl 2-(4-methylthiophenyl)acrylate (**4.22h**).[a] Prepared by the general procedure and purified on silica eluting with 3.5% EtOAc in hexanes. Yield 27.3 mg (62%) pale yellow oil. Characterization data were in agreement with the literature.[37] ^1H NMR (400 MHz, $CDCl_3$) 7.36 (d, J = 8.4 Hz, 2H), 7.23 (d, J = 8.4 Hz, 2H), 6.31 (d, J = 1.0 Hz, 1H), 5.87 (d, J = 1.0 Hz, 1H), 4.29 (q, J = 7.1 Hz, 2H), 2.49 (s, 3H), 1.34 (t, J = 7.1 Hz, 3H). $^{13}C\{^1H\}$ NMR (100 MHz, $CDCl_3$) 166.9, 141.0, 138.8, 133.6, 128.8, 126.2, 126.0, 61.3, 15.8, 14.3.

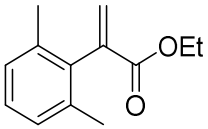

Ethyl 2-(2,6-dimethylphenyl)acrylate (**4.22i**).[a] Prepared by the general procedure and purified on silica eluting with 3.5% EtOAc in hexanes. Yield 21.2 mg (52%) pale yellow oil. ^1H NMR (400 MHz, $CDCl_3$) 7.13 (dd, J = 8.3, 6.7 Hz, 1H), 7.05 (d, J = 7.6 Hz, 2H), 6.65 (d, J = 1.8 Hz, 1H), 5.61 (d, J = 1.8 Hz, 1H), 4.23 (q, J = 7.1 Hz, 2H), 2.18 (s, 6H), 1.26 (t, J = 7.1 Hz, 3H). $^{13}C\{^1H\}$ NMR (100 MHz, $CDCl_3$) 166.6, 140.3, 137.0, 136.2, 129.1, 127.6, 127.3, 61.0, 20.4, 14.3. IR ν(C=O) 1716 cm^{-1}. HRMS calcd for $C_{13}H_{16}O_2$ 204.1150; found 204.1145, spectral accuracy 99.0%.

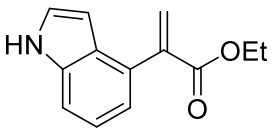

Ethyl 2-(indol-4-yl)acrylate (**4.22j**).[a] Prepared by the general procedure and purified on silica eluting with 4:1 hexanes:EtOAc. Yield 31.6 mg (73%) pale yellow oil. ^1H NMR (400 MHz,

[a] Prepared by G. P. R. Freure.

$CDCl_3$) 8.21 (br s, 1H), 7.38 (d, J = 8.1 Hz, 1H), 7.20 (m, 2H), 7.10 (d, J = 7.3 Hz, 1H), 6.53 (d, J = 1.6 Hz, 1H), 6.47 (m, 1H), 5.99 (d, J = 1.7 Hz, 1H), 4.29 (q, J = 7.1 Hz, 2H), 1.30 (t, J = 7.1 Hz, 3H). $^{13}C\{^1H\}$ NMR (100 MHz, $CDCl_3$) 167.5, 141.1, 136.0, 129.7, 127.6, 126.8, 124.4, 121.9, 120.5, 111.2, 102.1, 61.2, 14.4. IR ν(C=O) 1694 cm^{-1}. HRMS calcd for $C_{13}H_{13}NO_2$ 215.0946; found 215.0941, spectral accuracy 99.1%.

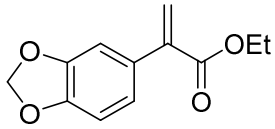

Ethyl 2-(1,3-benzodioxol-5-yl)acrylate (**4.22k**). Prepared by the general procedure and purified on silica eluting with 2→5% EtOAc in hexanes. Yield 22.0 mg (50%) orange oil. ^1H NMR (400 MHz, $CDCl_3$) 6.90 (m, 2H), 6.79 (d, J = 8.0 Hz, 1H), 6.25 (d, J = 1.3 Hz, 1H), 5.97 (s, 2H), 5.81 (d, J = 1.2 Hz, 1H), 4.28 (q, J = 7.2 Hz, 2H), 1.33 (t, J = 7.2 Hz, 3H). $^{13}C\{^1H\}$ NMR (100 MHz, $CDCl_3$) 167.0, 147.7, 147.5, 141.2, 130.9, 125.6, 122.2, 109.0, 108.1, 101.3, 61.3, 14.4. IR ν(C=O) 1714 cm^{-1}. HRMS calcd for $C_{12}H_{12}O_4$ 220.0736; found 220.0789, spectral accuracy 99.5%.

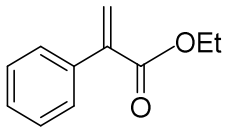

Ethyl 2-phenylacrylate (**4.22a** prepared from PhBr). Pd(XPhos)(allyl)Cl (4.6 mg, 7.0 μmol) and XPhos (3.3 mg, 7.0 μmol) were placed in a 25 mL round bottom flask and flushed with Ar. Toluene (1 mL), *i*-Pr_2NH (28 μL, 0.20 mmol) and bromobenzene (21 μL, 0.20 mmol) were added. Separately a solution of ethyl 2-diazopropanoate (42 μL, 0.36 mmol) in toluene (1.2 mL) was prepared and taken up into a 1 mL plastic HSW syringe and placed on a NewEra NE-300 syringe pump. The aryl chloride solution was placed in an 80 °C oil bath and stirred for ~3 min followed by addition of ethyl 2-diazopropoanate solution at a rate of 4 mL/h for 15 min (1 mL, 0.30 mmol diazo). The reaction was stirred an additional 15 min after addition was complete then cooled to room temperature and filtered through silica eluting with 2:1 EtOAc:hexanes and purified immediately by flash column chromatography on silica eluting with 3.5% EtOAc in hexanes. Yield 27.3 mg (77%) colourless oil. Characterization data were in agreement with the literature.[34]

Hydrazone synthesis. Hydrazones were prepared by the general procedure reported by Poh et. al. with modification to the isolation and purification protocols.[26e]

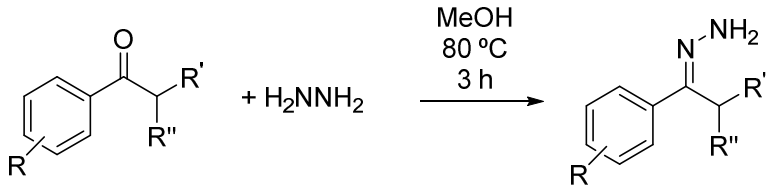

Isolation procedure A. The reaction mixture was partitioned between water (25 mL) and DCM (25 mL). The aqueous layer was extracted with an additional 2×10 mL DCM and the combined organic extracts were dried over Na_2SO_4 and the solvent removed *in vacuo.* The crude hydrazone was then recrystallized from 20:1 hexanes:EtOAc.

Isolation procedure B. The reaction mixture was diluted with water (25 mL) and the crystallized product was collected by filtration and washed with water (5 mL). The filter cake was taken up in DCM (25 mL), dried over Na_2SO_4 and the solvent removed *in vacuo*.

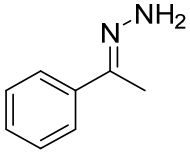

Acetophenone hydrazone (**4.23**). Prepared by the general procedure using isolation procedure A without recrystallization. Yield 1.24 g (93%) colourless oil, stored frozen at −20 °C. Characterization data were in agreement with the literature.[26e] ^{1}H NMR (400 MHz, $CDCl_3$) 7.65 (m, 2H), 7.32 (m, 3H), 5.37 (br s, 2H), 2.11 (s, 3H). $^{13}C\{^1H\}$ NMR (100 MHz, $CDCl_3$) 147.2, 139.4, 128.2, 128.0, 125.4, 11.6.

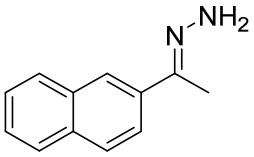

2-Acetonaphthone hydrazone (**4.27a**). Prepared by the general procedure using isolation procedure B. Yield 1.59 g (87%) white solid. Characterization data were in agreement with the literature.[38] ^{1}H NMR (400 MHz, $CDCl_3$) 7.97 (m, 2H), 7.82 (m, 3H), 7.47 (m, 2H), 5.44 (br s, 2H), 2.25 (s, 3H). $^{13}C\{^1H\}$ NMR (100 MHz, $CDCl_3$) 147.2, 139.8, 133.36, 133.28, 128.4, 128.0, 127.7, 126.23, 126.17, 124.7, 123.6, 11.5.

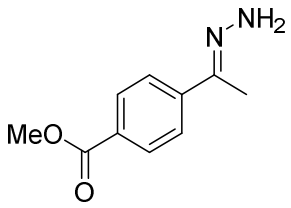

Methyl 4-acetylbenzoate hydrazone (**4.27b**). Prepared by the general procedure using isolation procedure B. Yield 0.96 g (50%) white solid. ^{1}H NMR (400 MHz, $CDCl_3$) 8.01 (d, J = 8.8 Hz, 2H), 7.71 (d, J = 8.8 Hz, 2H), 5.50 (br s, 2H), 3.91 (s, 3H), 2.14 (s, 3H). ^{13}C{^{1}H} NMR (100 MHz, $CDCl_3$) 167.1, 145.7, 143.6, 129.7, 129.4, 125.4, 52.2, 11.5. HRMS calcd for $C_{10}H_{12}N_2O_2$ 192.0899; found 192.0901, spectral accuracy 98.8%.

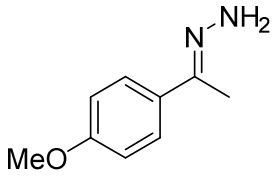

4'-Methoxyacetopheone hydrazone (**4.27c**). Prepared by the general procedure using isolation procedure B. Yield 1.23 g (75%) white solid. Characterization data were in agreement with the literature.[39] ^{1}H NMR (400 MHz, $CDCl_3$) 7.59 (d, J = 8.9 Hz, 2H), 6.88 (d, J = 8.9 Hz, 2H), 5.24 (br s, 2H), 3.82 (s, 3H), 2.12 (s, 3H). ^{13}C{^{1}H} NMR (100 MHz, $CDCl_3$) 159.8, 147.6, 132.3, 126.9, 113.8, 55.4, 11.8.

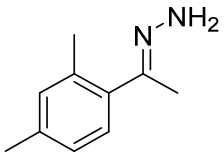

2',4'-dimethylacetophenone hydrazone (**4.27d**). Prepared by the general procedure using isolation procedure A. Yield 0.92 g (56%) white solid. ^{1}H NMR (400 MHz, $CDCl_3$) 7.11 (d, J = 7.7 Hz, 1H), 6.98 (m, 2H), 5.24 (br s, 2H), 2.31 (s, 6H), 2.09 (s, 3H). ^{13}C{^{1}H} NMR (100 MHz, $CDCl_3$) 150.2, 138.0, 137.5, 135.3, 131.5, 128.0, 126.5, 21.2, 20.3, 15.7. HRMS calcd for $C_{10}H_{14}N_2$ 162.1157; found 162.1175, spectral accuracy 97.4%.

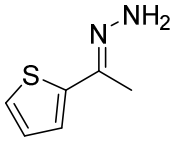

2-Acetylthiophene hydrazone (**4.27e**). Prepared by the general procedure using isolation procedure A. Yield 0.95 g (68%) white solid. Characterization data in agreement with the literature.[26f] ^{1}H NMR (400 MHz, $CDCl_3$) 7.20 (d, J = 5.1 Hz, 1H), 7.11 (d, J = 3.6 Hz, 1H), 6.98 (dd, J = 5.0, 3.8 Hz, 1H), 5.26 (br s, 2H), 2.14 (s, 3H). ^{13}C{^{1}H} NMR (100 MHz, $CDCl_3$) 145.0, 143.9, 127.1, 126.0, 124.1, 12.1.

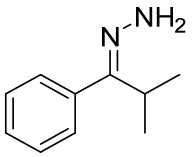

Isobutyrophenone hydrazone (**4.27f**). Prepared by the general procedure with the modification of 6 h reaction time at 80 °C and using isolation protocol A with Et_2O in the place of DCM and no recrystallization. Yield 1.49 g (90%) colourless oil, stored frozen at −20 °C. Characterization data were in agreement with the literature.[40] ^{1}H NMR (400 MHz, $CDCl_3$) 7.45 (t, J = 7.2 Hz, 2H), 7.36 (t, J = 7.4 Hz, 1H), 7.17 (m, 2H), 4.93 (br s, 2H), 2.72 (heptet, J = 6.9 Hz, 1H), 1.08 (d, J = 6.9 Hz, 6H). ^{13}C{^{1}H} NMR (100 MHz, $CDCl_3$) 157.5, 134.4, 129.1, 128.5, 127.9, 36.1, 20.4.

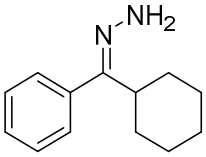

Cyclohexyl phenyl ketone hydrazone (**4.27g**). Prepared by the general procedure using isolation procedure A. Yield 0.79 g (39%) white solid. ^{1}H NMR (400 MHz, $CDCl_3$) 7.46 (t, J = 7.1 Hz, 2H), 7.37 (t, J = 7.4 Hz, 1H), 7.17 (d, J = 8.3 Hz, 2H), 4.92 (br s, 2H), 2.37 (m, 1H), 1.79 (m, 4H), 1.64 (m, 1H), 1.25 (m, 4H), 1.14 (m, 1H). ^{13}C{^{1}H} NMR (100 MHz, $CDCl_3$) 157.2, 134.7, 129.2, 128.5, 127.8, 46.0, 30.8, 26.4, 26.3. HRMS calcd for $C_{13}H_{18}N_2$ 202.1470; found 202.1508, spectral accuracy 90.8%.

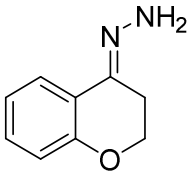

4-Chromanone hydrazone (**4.27h**). Prepared by the general procedure using isolation procedure A. Yield 1.60 g (98%) yellow solid. Characterization date were in agreement with the literature.[41] ^{1}H NMR (400 MHz, $CDCl_3$) 7.90 (dd, J = 7.9, 1.6 Hz, 1H), 7.19 (td, J = 7.8, 1.7, 1H), 6.95 (td, J = 7.6, 1.2 Hz, 1H), 6.88 (dd, J = 8.2, 0.9 Hz, 1H), 5.28 (br s, 2H), 4.28 (t, J = 6.1 Hz, 2H), 2.67 (t, J = 6.2 Hz, 2H). ^{13}C{^{1}H} NMR (100 MHz, $CDCl_3$) 156.2, 142.0, 129.8, 124.0, 121.74, 121.73, 117.5, 64.9, 23.6.

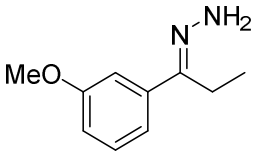

3'-Methoxyprophionone hydrazone (**4.27i**). Prepared by the general procedure using isolation procedure A with Et_2O in the place of DCM and no recrystallization. Yield 1.62 g (90%) pale yellow oil, stored at −20 °C. Characterization data were in agreement with the literature.[42] ^{1}H NMR (400 MHz, $CDCl_3$) 7.25 (m, 2H), 7.20 (dt, J = 8.0, 1.3, 1H), 6.85 (ddd, J = 8.0, 2.6, 1.2 Hz, 1H), 5.42 (br s, 2H), 3.83 (s, 3H), 2.62 (q, J = 7.8 Hz, 2H), 1.17 (t, J = 7.7 Hz, 3H). ^{13}C{^{1}H} NMR (100 MHz, $CDCl_3$) 159.8, 151.6, 139.9, 129.4, 118.2, 114.2, 110.8, 55.4, 18.7, 9.9.

General procedure for diazo-aryl bromide cross-coupling. Pd(XPhos)(allyl)Cl (4.6 mg, 7.0 μmol), XPhos (3.3 mg, 7.0 μmol) and aryl bromide (if solid; 0.20 mmol) were placed in a 25 mL round bottom flask and flushed with Ar. Toluene (1 mL), *i*-Pr_2NH (28 μL, 0.20 mmol) and aryl bromide (if liquid; 0.20 mmol) were added. Separately a 10.0 mL solution of hydrazone (0.76 mmol) and *i*-Pr_2NH (213 μL, 1.5 mmol) in toluene was prepared and loaded into a Hamilton air-tight® glass syringe and placed in a Nexus Fusion 200 syringe pump. The hydrazone solution was pumped at 0.5 mL/min through a 5 cm long, 3 mm ID, ¼" O.D. 316 stainless steel tubular reactor fitted with HPLC end frits and packed with MnO_2 (~370 mg, 4 mmol), with the effluent passing through the flow IR and then directed into an 50% aqueous acetic acid quench.[26e] Once the ν(C=N=N) vibration at ~2040 cm^{-1} began to appear (after ~90 s) the flow rate was decreased to 0.35 mL/min and the flask containing the ArBr solution was submerged in an 80 °C oil bath. After

allowing ~2 min for the diazo peak to stabilize and the reaction flask to heat to temperature, the diazo solution was directed into the reaction flask for the next 20 min (7 mL of diazo solution added, ~0.40 mmol given ~75% yield of diazo from hydrazone). Following the addition of the diazo reagent the reaction flask was stirred an additional 15 min, then cooled to room temperature and filtered through a plug of silica, eluting with 2:1 EtOAc:hexanes. The product was purified immediately by flash column chromatography.

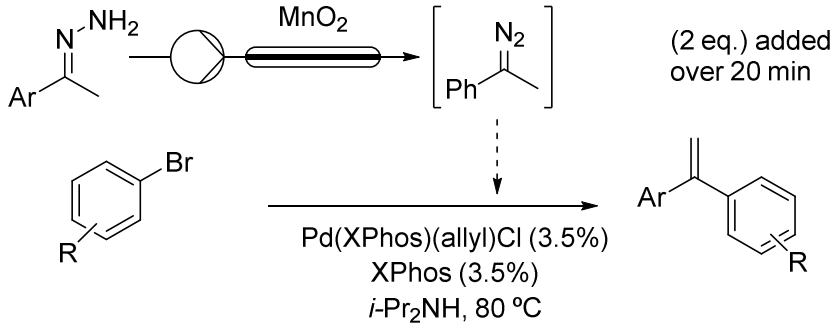

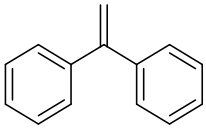

1,1-Diphenylethylene (**4.26a**). Prepared by the general procedure and purified on silica eluting with hexanes. Yield 32.7 mg (90%) colourless oil. Characterization data were in agreement with the literature.[43] ^{1}H NMR (400 MHz, $CDCl_3$) 7.36 (m, 5H), 5.49 (s, 2H). $^{13}C\{^{1}H\}$ NMR (100 MHz, $CDCl_3$) 150.2, 141.6, 128.4, 128.3, 127.8, 114.4.

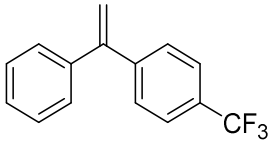

1-(4-Trifluoromethylphenly)-1-phenylethylene (**4.26b**). Prepared by the general procedure and purified on silica eluting with hexanes. Yield 43.5 mg (88%) white solid. Characterization data were in agreement with the literature.[44] ^{1}H NMR (400 MHz, $CDCl_3$) 7.61 (d, J = 8.7 Hz, 2H), 7.47 (d, J = 8.7 Hz, 2H), 7.35 (m, 5H), 5.58 (d, J = 1.0 Hz, 1H), 5.53 (d, J = 0.9 Hz, 1H). $^{13}C\{^{1}H\}$ NMR (100 MHz, $CDCl_3$) 149.1, 145.2 (q, J = 1.2 Hz), 140.8, 129.9 (q, J = 32.3 Hz), 128.7, 128.5, 128.3, 128.2, 125.3 (q, J = 3.8 Hz), 124.4 (q, J = 272.0 Hz), 116.0. $^{19}F\{^{1}H\}$ NMR (376 MHz, $CDCl_3$) -61.3.

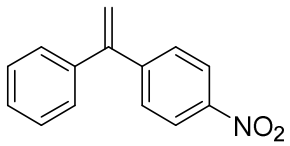

1-(4-Nitrophenyl)-1-phenylethylene (**4.26c**). Prepared by the general procedure and purified on 5% $AgNO_3$ impregnated silica eluting with 2% EtOAc in hexanes. Yield 37.0 mg (82%) colourless oil. Characterization data were in agreement with the literature.[45] ^{1}H NMR (400 MHz, $CDCl_3$) 8.20 (dt, J = 9.0, 2.2 Hz, 2H), 7.50 (dt, J = 8.9, 2.2 Hz, 2H), 7.37 (m, 3H), 7.29 (m, 2H), 5.64, (d, J = 0.7 Hz, 1H), 5.60 (d, J = 0.7 Hz, 1H). ^{13}C{^{1}H} NMR (100 MHz, $CDCl_3$) 148.5, 148.2, 147.4, 140.3, 129.1, 128.6, 128.5, 128.3, 123.7, 117.4.

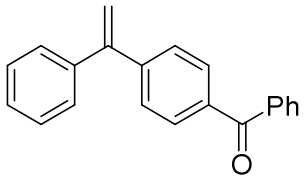

1-(Benzophenon-4-yl)-1-phenylethylene (**4.26d**). Prepared by the general procedure and purified on 5% $AgNO_3$ impregnated silica eluting with 2% EtOAc in hexanes. Yield 49.5 mg (87%) white solid. Characterization data were in agreement with the literature.[46] ^{1}H NMR (400 MHz, $CDCl_3$) 7.82 (m, 4H), 7.60 (tt, J = 7.4, 2.1 Hz, 1H), 7.48 (m, 4H), 7.36 (m, 5H), 5.58 (s, 2H). ^{13}C{^{1}H} NMR (100 MHz, $CDCl_3$) 196.4, 149.4, 145.7, 140.9, 137.8, 136.8, 132.5, 130.2, 130.1, 128.45, 128.41, 128.36, 128.2, 128.1, 116.1.

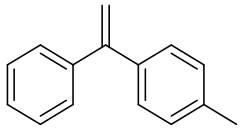

1-Phenyl-1-(tol-4-yl)ethylene (**4.26e**). Prepared by the general procedure and purified on silica eluting with hexanes. Yield 32.8 mg (84%) colourless oil. Characterization data were in agreement with the literature.[44] ^{1}H NMR (400 MHz, $CDCl_3$) 7.36 (m. 5H), 7.28 (d, J = 8.1 Hz, 2H), 7.18 (d, J = 8.2 Hz, 2H), 5.47 (d, J = 1.2 Hz, 1H), 5.44 (d, J = 1.2 Hz, 1H), 2.41 (s, 3H). ^{13}C{^{1}H} NMR (100 MHz, $CDCl_3$) 150.0, 141.8, 138.7, 137.6, 129.0, 128.4, 128.3, 12.8.2, 127.8, 113.7, 21.3.

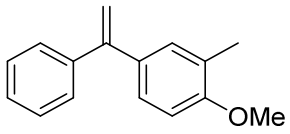

1-(4-Methoxy-3-methylphenyl)-1-phenylethylene (**4.26f**). Prepared by the general procedure and purified on 5% $AgNO_3$ impregnated silica eluting with 2% EtOAc in hexanes. Yield 39.0 mg (87%) white solid. ^{1}H NMR (400 MHz, $CDCl_3$) 7.37 (m, 5H), 7.17 (m, 2H), 6.81 (d, J = 8.9 Hz, 1H), 5.42 (d, J = 1.4 Hz, 1H), 5.38 (d, J = 1.4 Hz, 1H), 3.87 (s, 3H), 2.25 (d, 3H). ^{13}C{^{1}H} NMR (100 MHz, $CDCl_3$) 157.7, 149.8, 142.1, 133.7, 130.6, 128.5, 128.2, 127.7, 126.9, 126.3, 112.9, 109.6, 55.5, 16.4. HRMS calcd for $C_{16}H_{16}O$ 224.1201; found 224.1282, spectral accuracy 99.0%.

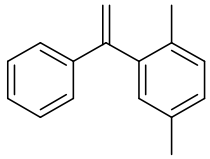

1-(2,5-dimethylphenyl)-1-phenylethylene (**4.26**g). Prepared by the general procedure and purified on silica eluting with hexanes. Yield 36.4 mg (87%) colourless oil. Characterization data were in agreement with the literature.[47] ^{1}H NMR (400 MHz, $CDCl_3$) 7.31 (m, 5H), 7.10 (m, 3H), 5.79 (d, J = 1.4 Hz, 1H), 5.22 (d, J = 1.4 Hz, 1H), 2.38 (s, 3H), 2.05 (s, 3H). ^{13}C{^{1}H} NMR (100 MHz, $CDCl_3$) 149.7, 141.6, 140.8, 135.2, 133.1, 130.8, 130.1, 128.4, 128.3, 127.6, 126.6, 114.8, 21.0, 19.7.

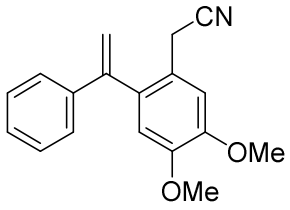

1-(2-Cyanomethyl-4,5-dimethoxy)-1-phenylethylene (**4.26h**). Prepared by the general procedure and purified on 5 silica eluting with 10:1→3:1 hexanes:EtOAc. Yield 54.8 mg (98%) pale yellow oil. ^{1}H NMR (400 MHz, $CDCl_3$) 7.28 (m, 5H), 6.96 (s, 1H), 6.78 (s, 1H), 5.86 (d, J = 1.1 Hz, 1H), 5.26 (d, J = 1.1 Hz, 1H), 3.94 (s, 3H), 3.87 (s, 3H), 3.42 (s, 2H). ^{13}C{^{1}H} NMR (100 MHz, $CDCl_3$) 148.9, 148.7, 147.3, 139.6, 133.7, 128.8, 128.4, 126.5, 120.2, 118.4, 116.5, 113.7, 111.7, 56.2, 56.1, 21.4. HRMS calcd for $C_{18}H_{17}NO_2$ 279.1259; found 279.1290, spectral accuracy 98.3%.

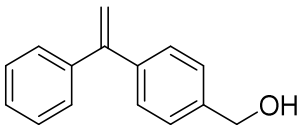

1-(4-Hydroxymethylphenyl)-1-phenylethylene (**4.26i**). Prepared by the general procedure and purified on silica eluting with 5:1→3:1 hexanes:EtOAc. Yield 38.4 mg (91%) white solid. Characterization data were in agreement with the literature.[48] ^{1}H NMR (400 MHz, $CDCl_3$) 7.34 (m, 9H), 5.48 (s, 2H), 4.71 (s, 2H), 2.01 (br s, 1H). $^{13}C\{^{1}H\}$ NMR (100 MHz, $CDCl_3$) 149.8, 141.5, 141.0, 140.4, 128.6, 128.4, 128.3, 127.7, 127.0, 114.4, 65.2.

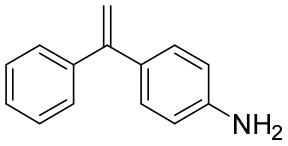

1-(4-Aminophenyl)-1-phenylethylene (**4.26j**). Prepared by the general procedure and purified on silica eluting with 10:1→4:1 hexanes:EtOAc. Yield 28.5 mg (73%) colourless oil. Characterization data were in agreement with the literature.[45] ^{1}H NMR (400 MHz, $CDCl_3$) 7.33 (m, 5H), 7.16 (dt, J = 8.6, 2.3 Hz, 2H), 6.65 (dt, J = 8.7, 2.4 H, 2H), 5.38 (d, J = 1.4 Hz, 1H), 5.28 (d, J = 1.4 Hz, 1H), 3.71 (br s, 2H). $^{13}C\{^{1}H\}$ NMR (100 MHz, $CDCl_3$) 149.9, 146.3, 142.2, 131.9, 129.4, 128.5, 128.2, 127.6, 114.7, 112.0.

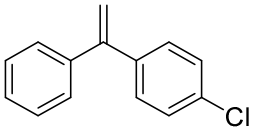

1-(4-Chlorophenyl)-1-phenylethylene (**4.26k**). Prepared by the general procedure and purified on silica eluting with hexanes. Yield 37.8 mg (88%) colourless oil. Characterization data were in agreement with the literature.[48] ^{1}H NMR (400 MHz, $CDCl_3$) 7.32 (m, 9H), 5.48 (d, J = 1.0 Hz, 1H), 5.46 (d, J = 1.0 Hz, 1H). $^{13}C\{^{1}H\}$ NMR (100 MHz, $CDCl_3$) 149.1, 141.1, 104.1, 133.7, 129.7, 128.5, 128.4, 128.3, 128.1, 114.8.

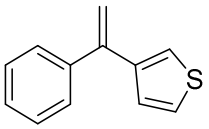

1-Phenyl-1-(thiophen-3-yl)ethylene (**4.26l**). Prepared by the general procedure with 2× catalyst load (0.014 mmol Pd(XPhos)(allyl)Cl, 0.014 mmol XPhos) and purified on 5% $AgNO_3$

impregnated silica eluting with 0.5% EtOAc in hexanes. Yield 26.3 mg (70%) colourless oil. Characterization data were in agreement with the literature.[45] ^{1}H NMR (400 MHz, $CDCl_3$) 7.38 (m, 5H), 7.31 (dd, J = 5.0, 3.0 Hz, 1H), 7.19 (dd, J = 5.0, 1.3 Hz, 1H), 7.14 (dd, J = 3.0, 1.3 Hz, 1H), 5.55 (d, J = 1.2 Hz, 1H), 5.35 (d, J = 1.2 Hz, 1H). ^{13}C{^{1}H} NMR (100 MHz, $CDCl_3$) 144.7, 142.7, 141.6, 128.3, 128.2, 127.9, 127.3, 125.6, 123.4, 113.6.

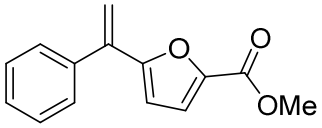

1-(5-Methoxycarbonylfuran-2-yl)-1-phenylethylene (**4.26m**). Prepared by the general procedure with 2× catalyst load (0.014 mmol Pd(XPhos)(allyl)Cl, 0.014 mmol XPhos) and purified on 5% $AgNO_3$ impregnated silica eluting with 4% EtOAc in hexanes. Yield 32.2 mg (71%) colourless oil. ^{1}H NMR (400 MHz, $CDCl_3$) 7.40 (m, 5H), 7.16 (d, J = 3.6 Hz, 1H), 6.27 (s, J = 3.6 Hz, 1H), 6.01 (d, J = 0.5 Hz, 1H), 5.42 (d, J = 0.7 Hz, 1H), 3.91 (s, 3H). ^{13}C{^{1}H} NMR (100 MHz, $CDCl_3$) 159.3, 157.5, 143.9, 138.7, 138.6, 128.25, 128.47, 128.4, 119.6, 116.0, 111.0, 52.0. IR ν(C=O) 1721 cm^{-1}. HRMS calcd for $C_{14}H_{12}O_3$ 228.0786; found 228.0791, spectral accuracy 99.6%.

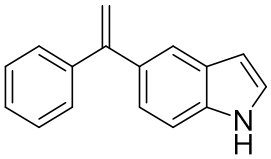

1-(Indol-5-yl)-1-phenylethylene (**4.26n**). Prepared by the general procedure and purified on silica eluting with 10:1→5:1 hexanes:EtOAc. Yield 38.6 mg (88%) white solid. ^{1}H NMR (400 MHz, $CDCl_3$) 8.12 (br s, 1H), 7.64 (m, 1H), 7.43 (m, 2H), 7.35 (m, 4H), 7.22 (m, 2H), 6.55 (m, 1H), 5.49 (d, J = 1.4 Hz, 1H), 5.44 (d, J = 1.4 Hz, 1H). ^{13}C{^{1}H} NMR (100 MHz, $CDCl_3$) 151.1, 142.6, 135.6, 133.7, 128.6, 128.2, 127.9, 127.6, 124.8, 123.0, 120.8, 113.1, 110.7, 103.1. HRMS calcd for $C_{16}H_{13}N$ 219.1048; found 219.1094, spectral accuracy 99.3%.

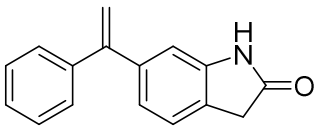

1-(2-Oxindol-6-y)-1-phenylethylene (**4.26o**). Prepared by the general procedure and purified on silica eluting with 2:1 hexanes:EtOAc. Yield 41.0 mg (87%) white solid. ^{1}H NMR (400 MHz,

$CDCl_3$) 8.21 (br s, 1H), 7.33 (m, 5H), 7.19 (d, J = 7.7 Hz, 1H), 7.02 (dd, J = 7.7, 1.3 Hz, 1H), 6.84 (d, J = 1.3 Hz), 5.45 (s, 2H), 3.55 (s, 2H). $^{13}C\{^1H\}$ NMR (100 MHz, $CDCl_3$) 177.5, 149.9, 142.5, 141.9, 141.4, 128.39, 128.38, 128.0, 124.9, 124.5, 122.7, 114.7, 109.7, 36.1. IR ν(C=O) 1693 cm^{-1}. HRMS calcd for $C_{16}H_{13}NO$ 235.0997; found 235.1003, spectral accuracy 99.4%.

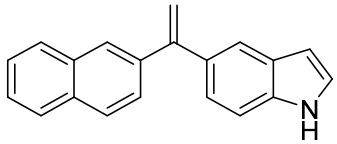

1-(Indol-5-yl)-1-(2-naphthyl)ethylene (**4.29a**). Prepared by the general procedure and purified on silica eluting with 10:1→5:1 hexanes:EtOAc. Yield 47.5 mg (88%) off-white solid. ^1H NMR (400 MHz, $CDCl_3$) 8.14 (br s, 1H), 7.80 (m, 4H), 7.65 (m, 1H), 7.52 (dd, J = 8.5, 1.7 Hz, 1H), 7.45 (m, 2H), 7.35 (d, J = 8.5 Hz, 1H), 7.24 (dd, J = 8.4, 1.7 Hz, 1H), 7.21 (m, 1H), 6.52 (m, 1H), 5.54 (d, J = 1.4 Hz, 1H), 5.53 (d, J = 1.4 Hz, 1H). $^{13}C\{^1H\}$ NMR (100 MHz, $CDCl_3$) 151.1, 140.1, 135.7, 133.8, 133.5, 133.1, 128.4, 127.9, 127.7, 127.6, 127.5, 126.9, 126.2, 126.0, 124.8, 123.1, 121.0, 113.7, 110.8, 103.2. HRMS calcd for $C_{20}H_{15}N$ 269.1204; found 269.1207, spectral accuracy 99.0%.

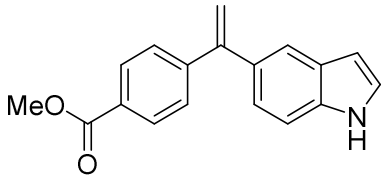

1-(Indol-5-yl)-1-(4-methoxycarbonyphenyl)ethylene (**4.29b**). Prepared by the general procedure with hydrazone solution prepared at ½ dilution (0.76 mmol in 20.0 mL solution) and pumped at 2× flow rate (0.7 mL/min) due to limited solubility. Purified on silica eluting with 5:1 hexanes:EtOAc→5% MeCN in 5:1 hexanes:EtOAc. Yield 44.3 mg (80%) white solid. ^1H NMR (400 MHz, $CDCl_3$) 8.21 (br s, 1H), 8.01 (d, J = 8.3 Hz, 2H), 7.58 (s, 1H), 7.46 (d, J = 8.3 Hz, 2H), 7.36 (d, J = 8.5 Hz, 1H), 7.23 (t, J = 2.9 Hz, 1H), 7.17 (dd, J = 8.5, 1.3 Hz, 1H), 6.54 (m, 1H), 5.55 (s, 1H), 5.49 (s, 1H), 3.93 (s, 3H). $^{13}C\{^1H\}$ NMR (100 MHz, $CDCl_3$) 167.2, 150.4, 147.3, 135.7, 133.0, 129.6, 129.2, 128.6, 127.9, 125.0, 122.9, 120.8, 114.7, 110.9, 103.2, 52.2. IR ν(C=O) 1691 cm^{-1}. HRMS calcd for $C_{18}H_{15}NO_2$ 277.1103; found 277.1206, spectral accuracy 99.5%.

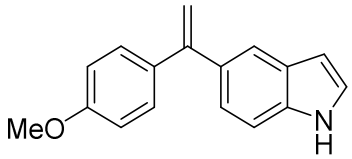

1-(Indol-5-yl)-1-(4-methoxyphenyl)ethylene (**4.29c**). Prepared by the general procedure and purified on 5% $AgNO_3$ impregnated silica eluting with 5:1→5:2 hexanes:EtOAc. Yield 30.3 mg (61%) white solid. ^{1}H NMR (400 MHz, $CDCl_3$) 8.15 (br s, 1H), 7.62 (m, 1H), 7.34 (m, 3H), 7.21 (m, 2H), 6.88 (m, 2H), 6.53 (m, 1H), 5.36 (d, J = 1.5 Hz, 1H), 5.35 (d, J = 1.5 Hz, 1H), 3.83 (s, 3H). ^{13}C{^{1}H} NMR (100 MHz, $CDCl_3$) 159.3, 150.5, 135.6, 135.2, 134.0, 129.7, 127.9, 124.7, 123.1, 120.8, 113.5, 111.8, 110.6, 103.1, 55.4. HRMS calcd for $C_{17}H_{15}NO$ 249.1154; found 249.1138, spectral accuracy 98.7%.

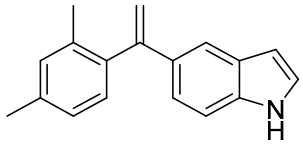

1-(Indol-5-yl)-1-(2,4-dimethylphenyl)ethylene (**4.29d**). Prepared by the general procedure with the packed column of MnO_2 cooled in an ice bath at 0 °C and purified on 5% $AgNO_3$ impregnated silica eluting with 10:1→5:1 hexanes:EtOAc. Yield 42.2 mg (85%) colourless oil. ^{1}H NMR (400 MHz, $CDCl_3$) 8.07 (br s, 1H), 7.49 (m, 1H), 7.27 (m, 2H), 7.20 (d, J = 7.5 Hz, 1H), 7.17 (dd, J = 3.1, 2.6 Hz, 1H), 7.06 (m, 2H), 6.49 (m, 1H), 5.75 (d, J = 1.7 Hz, 1H), 5.13 (d, J = 1.6 Hz, 1H), 2.40 (s, 3H), 2.07 (d, 3H). ^{13}C{^{1}H} NMR (100 MHz, $CDCl_3$) 150.3, 139.9, 137.0, 136.3, 135.5, 133.2, 131.0, 130.2, 128.0, 126.3, 124.7, 121.2, 119.2, 113.0, 110.9, 130.3, 21.3, 20.2. HRMS calcd for $C_{18}H_{17}N$ 247.1361; found 247.1387, spectral accuracy 99.4%.

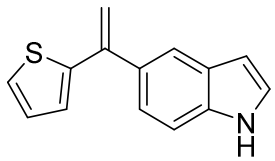

1-(Indol-5-yl)-1-(thiophen-2-yl)ethylene (**4.29e**). Prepared by the general procedure and purified on silica eluting with 8:1 hexanes:EtOAc. Yield 34.6 mg (77%) off-white solid. ^{1}H NMR (400 MHz, $CDCl_3$) 8.17 (br s, 1H), 7.74 (m, 1H), 7.38 (d, J = 8.4 Hz, 1H), 7.30 (dd, J = 8.4, 1.6 Hz, 1H), 7.24 (m, 2H), 6.98 (m, 2H), 6.56 (m, 1H), 5.57 (d, J = 1.0 Hz, 1H), 5.27 (d, J = 1.0 Hz, 1H). ^{13}C{^{1}H} NMR (100 MHz, $CDCl_3$) 146.0, 144.3, 135.8, 133.3, 127.8, 127.3, 126.6, 124.91, 124.87,

123.1, 120.8, 112.8, 110.7, 103.2. HRMS calcd for $C_{14}H_{11}NS$ 225.0612; found 225.0594, spectral accuracy 99.3%.

General procedure for the synthesis of tri- and tetra-substituted olefins. Pd(XPhos)(allyl)Cl (6.6 mg, 10 μmol), XPhos (4.8 mg, 10 μmol) and 5-bromoindole (39.2 mg, 0.20 mmol) were placed in a 25 mL round bottom flask and flushed with Ar. Toluene (1 mL) and *i*-Pr_2NH (28 μL, 0.20 mmol) were added. Separately a 10.0 mL solution of hydrazone (0.76 mmol) and *i*-Pr_2NH (213 μL, 1.5 mmol) in toluene was prepared and loaded into a Hamilton air-tight® glass syringe and placed in a Nexus Fusion 200 syringe pump. The hydrazone solution was pumped at 0.5 mL/min through the packed column of MnO_2 described previously, then the flow rate was decreased to 0.23 mL/min once the diazo IR peak began to appear at ~2040 cm^{-1}. The flask containing the 5-bromoindole solution was submerged in a 100 °C oil bath. After allowing ~2 min for the diazo peak to stabilize and the reaction flask to heat to temperature, the diazo solution was directed into the reaction flask for the next 30 min (10.5 mL of diazo solution, ~0.60 mmol given ~75% yield of diazo from hydrazone). Following the addition of the diazo reagent the reaction flask was stirred an additional 15 min, then cooled to room temperature and filtered through a plug of silica, eluting with 2:1 EtOAc:hexanes. The product was purified immediately by flash column chromatography.

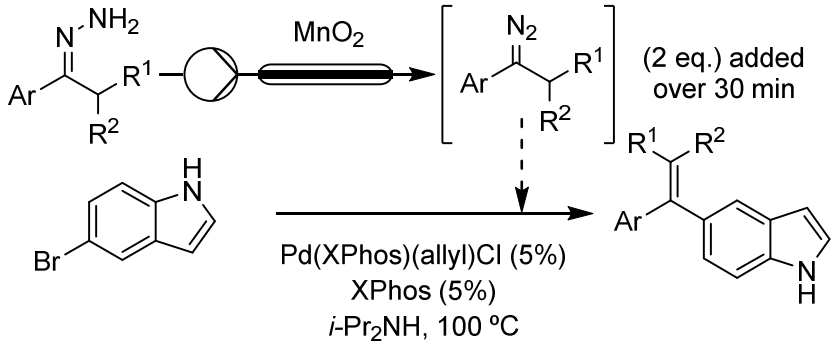

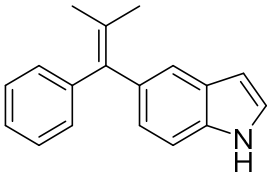

1-(Indol-5-yl)-2-methyl-1-phenylprop-1-ene (**4.29f**). Prepared by the general procedure and purified on 5% $AgNO_3$ impregnated silica eluting with 4:1→2:1 hexanes:EtOAc. Yield 35.9 mg (73%) colourless oil. ^1H NMR (400 MHz, $CDCl_3$) 8.07 (br s, 1H), 7.43 (s, 1H), 7.28 (m, 3H), 7.17

(m, 4H), 6.97 (dd, J = 8.4, 1.5 Hz, 1H), 6.50 (m, 1H), 1.85 (s, 3H), 1.84 (s, 3H). $^{13}C\{^{1}H\}$ NMR (100 MHz, $CDCl_3$) 144.3, 138.0, 135.4, 134.5, 130.2, 130.0, 127.9, 127.7, 125.9, 124.7, 124.4, 121.9, 110.5, 102.8, 22.8, 22.7. HRMS calcd for $C_{18}H_{17}N$ 247.1361; found 247.1350, spectral accuracy 98.8%.

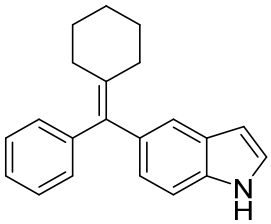

2-(Indol-5-yl)-2-phenylmethylenecyclohexane (**4.29g**). Prepared by the general procedure and purified on silica eluting with 6:1 hexanes:EtOAc. Yield 26.8 mg (47%) white solid. ^{1}H NMR (400 MHz, $CDCl_3$) 8.06 (br s, 1H), 7.41 (s, 1H), 7.27 (m, 3H), 7.16 (m, 4H), 6.96 (dd, J = 8.3, 1.6 Hz, 1H), 6.50 (m, 1H), 2.29 (m, 4H), 1.62 (m, 6H). $^{13}C\{^{1}H\}$ NMR (100 MHz, $CDCl_3$) 144.1, 138.4, 135.4, 135.1, 134.5, 130.0, 127.9, 127.7, 125.9, 124.7, 124.4, 121.8, 110.5, 102.8, 32.7, 32.6, 28.90, 28.86, 27.1. HRMS calcd for $C_{21}H_{21}N$ 287.1674; found 287.1661, spectral accuracy 98.9%.

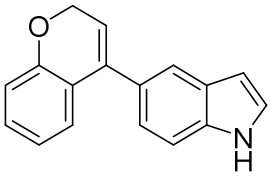

5-(2H-chromen-4-yl)indole (**4.29h**). Prepared by the general procedure and purified on silica eluting with 6:1 hexanes:EtOAc. Yield 21.3 mg (43%) off-white solid. ^{1}H NMR (400 MHz, $CDCl_3$) 8.20 (br s, 1H), 7.64 (s, 1H), 7.41 (d, J = 8.4 Hz, 1H), 7.26 (m, 1H), 7.17 (m, 2H), 7.09 (dd, J = 7.6, 1.5 Hz, 1H), 6.91 (dd, J = 8.0, 1.0 Hz, 1H), 6.85 (td, J = 7.5, 1.1 Hz, 1H), 6.58 (m, 1H), 5.83 (t, J = 3.9 Hz, 1H), 4.88 (d, J = 4.0 Hz, 2H). $^{13}C\{^{1}H\}$ NMR (100 MHz, $CDCl_3$) 155.0, 138.1, 135.6, 130.2, 129.1, 128.0, 126.4, 124.9, 124.7, 123.2, 121.2, 120.9, 119.4, 116.2, 110.9, 103.0, 65.6. HRMS calcd for $C_{17}H_{13}NO$ 247.0997; found 247.1006, spectral accuracy 98.9%.

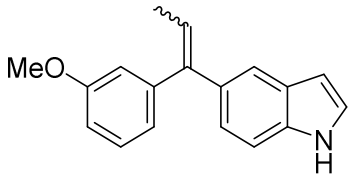

1-(Indol-5-yl)-1-(3-methoxyphenyl)prop-1-ene (**4.29i**). Prepared by the general procedure and purified on silica eluting with 6:1 hexanes:EtOAc. Yield 45.8 mg (87%) colourless oil as a mixture of 2.3:1 *Z*:*E* isomers (determined by ^{1}H NMR analysis of the mixture). HRMS calc for $C_{18}H_{17}NO$ 263.1310; found 263.1361, spectral accuracy 99.3%

Complete separation of the isomers was not possible, but partial separation on 5% $AgNO_3$ impregnated silica eluting with 2:1 hexanes:EtOAc allowed enrichment of each individual isomer to >10:1 purity for individual characterization.

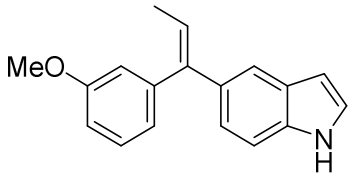

(Z)-1-(Indol-5-yl)-1-(3-methoxyphenyl)prop-1-ene. ^{1}H NMR (400 MHz, $CDCl_3$) 8.07 (br s, 1H), 7.46 (m, 1H), 7.29 (m, 2H), 7.15 (m, 2H), 6.83 (m, 3H), 6.48 (m, 1H), 6.14 (q, *J* = 7.0 Hz, 1H), 3.80 (s, 3H), 1.79 (d, *J* = 7.0 Hz, 3H). ^{13}C{^{1}H} NMR (100 MHz, $CDCl_3$) 159.5, 143.2, 142.6, 135.3, 135.1, 129.1, 127.9, 124.6, 122.9, 122.5, 122.0, 119.7, 115.7, 112.4, 110.6, 103.1, 55.3, 15.9.

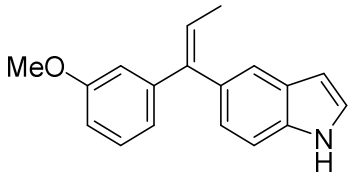

(E)-1-(Indol-5-yl)-1-(3-methoxyphenyl)prop-1-ene. ^{1}H NMR (400 MHz, $CDCl_3$) 8.15 (br s, 1H), 7.48 (m, 1H), 7.38 (d, *J* = 8.4 Hz, 1H), 7.23 (t, *J* = 2.7 Hz, 1H), 7.16 (t, *J* = 8.0 Hz, 1H), 6.99 (dd, *J* = 8.3, 1.6 Hz, 1H), 7.87 (m, 2H), 6.76 (ddd, *J* = 8.1, 2.6, 0.8 Hz, 1H), 6.54 (m, 1H), 6.19 (q, *J* = 7.0 Hz, 1H), 3.75 (s, 3H), 1.80 (d, *J* = 7.0 Hz, 3H). ^{13}C{^{1}H} NMR (100 MHz, $CDCl_3$) 159.5, 145.6, 143.3, 135.0, 131.6, 128.9, 127.9, 124.7, 124.4, 123.9, 122.3, 120.2, 113.3, 112.0, 110.8, 102.9, 55.3, 16.0.

General procedure for diazo-activated aryl chloride cross-coupling. Pd(XPhos)(allyl)Cl (6.6 mg, 10 μmol), XPhos (4.8 mg, 10 μmol) and aryl chloride (0.20 mmol) were placed in a 25 mL round bottom flask and flushed with Ar. Toluene (1 mL) and *i*-Pr_2NH (28 μL, 0.20 mmol) were added. Separately a 10.0 mL solution of 2-acetylthiophene hydrazone (106 mg, 0.76 mmol) and *i*-Pr_2NH (213 μL, 1.5 mmol) in toluene was prepared and loaded into a Hamilton air-tight® glass syringe and placed in a Nexus Fusion 200 syringe pump. The hydrazone solution was pumped at 0.5 mL/min through the packed column of MnO_2 described previously and cooled at 0 °C, then the flow rate was decreased to 0.35 mL/min once the diazo IR peak began to appear at ~2040 cm^{-1}. The flask containing the 5-bromoindole solution was submerged in a 100 °C oil bath. After allowing ~2 min for the diazo peak to stabilize and the reaction flask to heat to temperature, the diazo solution was directed into the reaction flask for the next 20 min (7 mL of diazo solution, ~0.40 mmol given ~75% yield of diazo from hydrazone). Following the addition of the diazo reagent the reaction flask was stirred an additional 5 min, then cooled to room temperature and filtered through a plug of silica, eluting with 2:1 EtOAc:hexanes. The product was purified immediately by flash column chromatography.

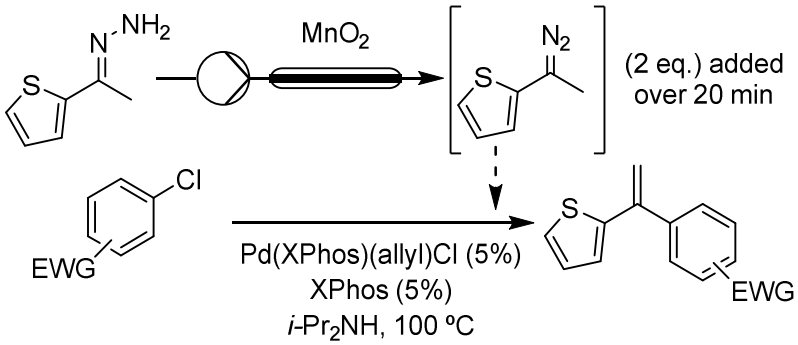

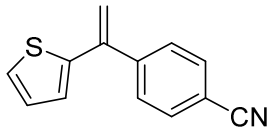

1-(4-Cyanophenyl)-1-(thiphen-2-yl)ethylene (**4.31a**). Prepared by the general procedure and purified on 5% $AgNO_3$ impregnated silica eluting with 5% EtOAc in hexanes→1% MeCN, 10% EtOAc in hexanes. Yield 29.3 mg (69%) bright yellow oil. ^1H NMR (400 MHz, $CDCl_3$) 7.66 (dt, J = 8.6, 2.0 Hz, 2H), 7.54 (dt, J = 8.6, 2.0 Hz, 2H), 7.27 (dd, J = 5.1, 1.1 Hz, 1H), 6.99 (dd, J = 5.1, 3.6 Hz, 1H), 6.85 (dd, J = 3.6, 1.1 Hz, 1H), 5.68 (s, 1H), 5.32 (s, 1H). $^{13}C\{^1H\}$ NMR (100 MHz, $CDCl_3$) 145.7, 143.4, 142.2, 132.2, 129.1, 127.6, 126.9, 125.9, 118.9, 115.8, 112.0. IR

ν(C≡N) 2267 cm^{-1}. HRMS calcd for $C_{13}H_9NS$ 211.0456; found 211.0507, spectral accuracy 99.1%.

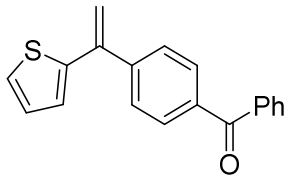

1-(Benzophenon-4-yl)-1-(thiophen-2-yl)ethylene (**4.31b**). Prepared by the general procedure and purified on 5% $AgNO_3$ impregnated silica eluting with 2→3% EtOAc in hexanes. Yield 42.0 mg (72%) off-white solid. ^{1}H NMR (400 MHz, $CDCl_3$) 7.85 (m, 4Hz), 7.55 (m, 5H), 7.27 (dd, *J* = 5.2, 1.0 Hz, 1H), 7.00 (dd, *J* = 5.1, 3.6 Hz, 1H), 6.93 (dd, *J* = 3.6, 1.1 Hz, 1H), 5.68 (s, 1H), 5.35 (s, 1H). ^{13}C{^{1}H} NMR (100 MHz, $CDCl_3$) 196.4, 145.2, 144.0, 142.7, 137.7, 137.3, 132.6, 130.22, 130.15, 128.4, 128.3, 127.5, 126.8, 125.5, 115.1. IR ν(C=O) 1652 cm^{-1}. HRMS calcd for $C_{19}H_{14}OS$ 290.0765; found 290.0784, spectral accuracy 98.7%.

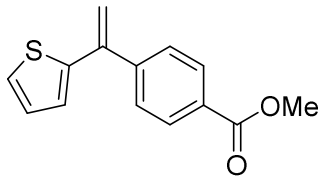

1-(4-Methoxycarbonylphenyl)-1-(thiophen-2-yl)ethylene (**4.31c**). Prepared by the general procedure and purified on 5% $AgNO_3$ impregnated silica gel eluting with 2→3% EtOAc in hexanes. Yield 30.4 mg (62%) pale yellow oil. ^{1}H NMR (400 MHz, $CDCl_3$) 8.04 (dt, *J* = 8.6, 1.9 Hz, 2H), 7.51 (dt, *J* = 8.6, 1.9 Hz, 2H), 7.26 (dd, *J* = 5.1, 1.1 Hz, 1H), 6.99 (dd, *J* = 5.1, 3.6 Hz, 1H), 6.88 (dd, *J* = 3.6, 1.1 Hz, 1H), 5.65 (s, 1H), 5.31 (s, 1H), 3.94 (s, 3H). ^{13}C{^{1}H} NMR (100 MHz, $CDCl_3$) 167.0, 145.7, 144.0, 142.8, 129.9, 129.7, 128.4, 127.5, 126.7, 125.5, 115.0, 52.3. IR ν(C=O) 1717 cm^{-1}. HRMS calcd for $C_{14}H_{12}O_2S$ 244.0558; found 244.0554, spectral accuracy 99.7%.

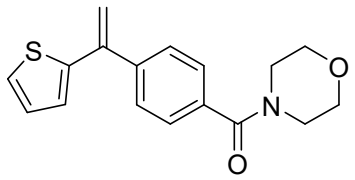

1-(4-Morpholinylcarbonylphenyl)-1-(thiophen-2-yl)ethylene (**4.31d**). Prepared by the general procedure and purified on silica eluting with 5:1 hexanes:EtOAc→5% MeCN in 2:1 hexanes:EtOAc. Yield 40.7 mg (68%) off-white solid. ^{1}H NMR (400 MHz, $CDCl_3$) 8.37 (dt, J = 8.4, 1.9 Hz, 2H), 7.41 (dt, J – 8.4, 1.9 Hz, 2H), 7.26 (dd, J = 5.1, 1.1 Hz, 1H), 6.98 (dd, J = 5.1, 3.6 Hz, 1H), 6.89 (dd, J = 3.6, 1.3 Hz, 1H), 5.62 (s, 1H), 5.27 (s, 1H), 3.72 (br s, 8H). ^{13}C{^{1}H} NMR (100 MHz, $CDCl_3$) 170.3, 144.2, 142.85, 142.78, 135.1, 128.6, 127.5, 127.3, 126.8, 125.5, 114.6, 67.1, 48.4 (br). IR ν(C=O) 1623 cm^{-1}. HRMS calcd for $C_{17}H_{17}NO_2S$ 299.0980; found 299.1004, spectral accuracy 99.1%

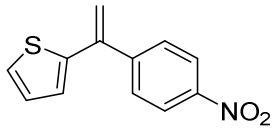

1-(4-Nitrophenyl)-1-(thiophen-2-yl)ethylene (**4.31e**). Prepared by the general procedure and purified on silica eluting with 10:1→3:1 hexanes:toluene. Yield 38.0 mg (82%) yellow oil. ^{1}H NMR (400 MHz, $CDCl_3$) 8.93 (dt, J = 8.9, 2.0 Hz, 2H), 7.60 (dt, J = 8.9, 2.1 Hz, 2H), 7.29 (dd, J = 5.1, 1.1 Hz, 1H), 7.01 (dd, J = 5.1, 3.6 Hz, 1H), 6.87 (dd, J = 3.6, 1.1 Hz, 1H), 5.72 (s, 1H), 5.36 (s, 1H). ^{13}C{^{1}H} NMR (100 MHz, $CDCl_3$) 147.7, 147.6, 143.3, 141.8, 129.3, 127.6, 126.9, 125.9, 123.7, 116.2. IR ν(NO_2) 1513, 1342 cm^{-1}. HRMS calcd for $C_{12}H_9NO_2S$ 231.0354; found 231.0380, spectral accuracy 99.4%.

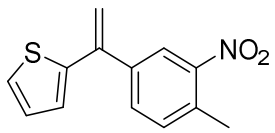

1-(4-Methyl-3-nitrophenyl)-1-(thiophen-2-yl)ethylene (**4.31f**). Prepared by the general procedure and purified on silica eluting with 10:1→3:1 hexanes:toluene. Yield 43.8 mg (89%) pale yellow oil. ^{1}H NMR (400 MHz, $CDCl_3$) 8.05 (d, J = 2.1 Hz, 1H), 7.57 (dd, J = 7.9, 1.9 Hz, 1H), 7.34 (d, J = 7.9 Hz, 1H), 7.28 (dd, J = 5.3, 1.1 Hz, 1H), 7.00 (dd, J = 5.1, 3.6 Hz, 1H), 6.88 (dd, J = 3.6, 1.1 Hz, 1H), 5.65 (s, 1H), 5.31 (s, 1H), 2.63 (s, 3H). ^{13}C{^{1}H} NMR (100 MHz, $CDCl_3$) 149.3,

143.6, 141.3, 140.3, 133.3, 132.78, 132.73, 127.6, 126.7, 125.8, 124.4, 115.1, 20.3. IR ν(NO_2) 1523, 1344 cm^{-1}. HRMS calcd for $C_{13}H_{11}NO_2S$ 245.0510; found 245.0529, spectral accuracy 98.9%.

Computational Methods. All calculations were performed using the Gaussian 09 software suite.[49] Structures were optimized at the M06-L[50]/def2-SVP[51] with associated ECP for Pd[52] level of theory and confirmed to be local minima or transition states by the presence of 0 or 1 imaginary frequencies respectively. For transition state structures the normal mode vibration corresponding to the imaginary frequency involved the motion of the correct atom(s) along the reaction coordinate in all cases. Energies were calculated at the M06-L/def2-TZVP[51] level of theory on the M06-L/def2-SVP optimized structures and incorporated solvation effects using the polarizable continuum model with toluene solvent[53]. Zero-point and thermal corrections were taken from the M06-L/def2-SVP frequency calculations.

4.5 References

[1] Crabtree, R. H. Deactivation in homogeneous transition metal catalysis: Causes, avoidance, and cure. *Chem. Rev.* **2015**, *115*, 127−150.

[2] a) Corriu, R. J. P.; Masse, J. P. Activation of Grignard reagents by transition-metal complexes. A new and simple synthesis of trans-stilbenes and polyphenyls. *J. Chem. Soc., Chem. Commun.* **1972**, 144a−144a; b) Tamao, K.; Sumitani, K.; Kumada, M. Selective carbon-carbon bond formation by cross-coupling of Grignard reagents with organic halides. Catalysis by nickel-phosphine complexes. *J. Am. Chem. Soc.* **1972**, *94*, 4374–4376; c) Knappke, C. E. I.; Jacobi von Wangelin, A. 35 years of palladium-catalyzed cross-coupling with Grignard reagents: How far have we come? *Chem. Soc. Rev.* **2011**, *40*, 4948−4962.

[3] For some recent examples of Kumada-Corriu cross-couplings see: a) Ishikawa, S.; Manabe, K. DHTP Ligands for the highly ortho-selective, palladium-catalyzed cross-coupling of dihaloarenes with Grignard reagents: A conformational approach for catalyst improvement. *Angew. Chem. Int. Ed.* **2010**, *49*, 772−775; b) Lou, S.; Fu, G. C. Nickel/bis(oxazoline)-catalyzed asymmetric Kumada reactions of alkyl electrophiles: Cross-couplings of racemic α-bromoketones. *J. Am. Chem. Soc.* **2010**, *132*, 1264−1266; c) Ackermann, L.; Potukuchi, H. K.; Kapdi, A. R.; Schulzke, C. Kumada–Corriu cross-couplings with 2-pyridyl Grignard reagents. *Chem. Eur. J.* **2010**, *16*, 3300−3303; d) Reeves, J. T.; Fandrick, D. R.; Tan, Z.; Song, J. J.; Lee, H.; Yee, N. K.; Senanayake, C. H. Room temperature palladium-catalyzed cross coupling of

aryltrimethylammonium triflates with aryl Grignard reagents. *Org. Lett.* **2010**, *12*, 4388−4391; e) Dai, W.; Xiao, J.; Jin, G.; Wu, J.; Cao, S. Palladium- and nickel-catalyzed Kumada cross-coupling reactions of gem-difluoroalkenes and monofluoroalkenes with Grignard reagents. *J. Org. Chem.* **2014**, *79*, 10537−10546; f) Krasovskiy, A. L.; Haley, S.; Voigtritter, K.; Lipshutz, B. H. Stereoretentive Pd-catalyzed Kumada–Corriu couplings of alkenyl halides at room temperature. *Org. Lett.* **2014**, *16*, 4066−4069; g) Bhattacharjya, A.; Klumphu, P.; Lipshutz, B. H. Kumada–Grignard-type biaryl couplings on water. *Nat. Commun.* **2015**, *6*, 7401−7406.

[4] A topic search on the Web of Science database for "Suzuki coupling" revealed over 14,000 publications from 2000–2019; more than three times the number of hits for Stille, Negishi, Kumada, and Hiyama coupling combined.

[5] Martin, R.; Buchwald, S. L. Pd-catalyzed Kumada−Corriu cross-coupling reactions at low temperatures allow the use of Knochel-type Grignard reagents. *J. Am. Chem. Soc.* **2007**, *129*, 3844−3845.

[6] Manolikakes, G.; Knochel, P. Radical catalysis of Kumada cross-coupling reactions using functionalized Grignard reagents. *Angew. Chem. Int. Ed.* **2009**, *48*, 205−209.

[7] Hua, X.; Masson-Makdissi, J.; Sullivan, R. J.; Newman, S. G. Inherent vs. apparent chemoselectivity in the Kumada–Corriu cross-coupling reaction. *Org. Lett.* **2016**, *18*, 5312−5315.

[8] Yamamura, M.; Moritani, I.; Murahashi, S.-I. The reaction of σ-vinylpalladium complexes with alkyllithiums. Stereospecific syntheses of olefins from vinyl halides and alkyllithiums. *J. Organomet. Chem.* **1975**, *91*, C39−C42.

[9] a) Giannerini, M.; Fañanás-Mastral, M.; Feringa, B. L. Direct catalytic cross-coupling of organolithium compounds. *Nat. Chem.* **2013**, *5*, 667–672; b) Hornillos, V.; Giannerini, M.; Vila, C.; Fañanás-Mastral, M.; Feringa, B. L. Catalytic direct cross-coupling of organolithium compounds with aryl chlorides. *Org. Lett.* **2013**, *15*, 5114–5117.

[10] For a discussion on product selectivity of competing reactions see Anslyn, E. V.; Dougherty, D. A. *Modern Physical Organic Chemistry*; University Science: Sausalito, 2006.

[11] a) Vikse, K. L.; Woods, M. P.; McIndoe, J. S. Pressurized sample infusion for the continuous analysis of air- and moisture-sensitive reactions using electrospray ionization mass spectrometry. *Organometallics* **2010**, *29*, 6615–6618; b) Hesketh, A. V.; Nowicki, S.; Baxter, K.; Stoddard, R. L.; McIndoe, J. S. Simplified real-time mass spectrometric analysis of reactions. *Organometallics* **2015**, *34*, 3816–3819; c) Yunker, L. P. E.; Ahmadi, Z.; Logan, J. R.; Wu, W.; Li, T.; Martindale, A.; Oliver, A. G.; McIndoe, J. S. Real-time mass

spectrometric investigations into the mechanism of the Suzuki–Miyaura reaction. *Organometallics* **2018**, *37*, 4297−4308.

[12] Barluenga, J.; Moriel, P.; Valdés, C.; Aznar, F. *N*-Tosylhydrazones as reagents for cross-coupling reactions: A route to polysubstituted olefins. *Angew. Chem. Int. Ed.* **2007**, *46*, 5587−5590.

[13] a) Beletskaya, I. P.; Cheprakov, A. V. The Heck reaction as a sharpening stone of palladium catalysis. *Chem. Rev.* **2000**, *100*, 3009−3066; b) Nilsson, P.; Olofsson, K.; Larhed, M. Focus on regioselectivity and product outcome in organic synthesis. In *The Mizoroki–Heck Reaction*; Oestreich, M., Ed.; John Wiley & Sons, Ltd.: West Sussex, 2009, p 133−157.

[14] a) Faulkner, D. J. Stereoselective synthesis of trisubstituted olefins. *Synthesis* **1971**, *1971*, 175−189; b) Reucroft, J.; Sammes, P. G. Stereoselective and stereospecific olefin synthesis. *Quart. Rev. Chem. Soc.* **1971**, *25*, 135−169; c) Flynn, A. B.; Ogilvie, W. W. Stereocontrolled synthesis of tetrasubstituted olefins. *Chem. Rev.* **2007**, *107*, 4698−4745; d) Kapat, A.; Sperger, T.; Guven, S.; Schoenebeck, F. *E*-Olefins through intramolecular radical relocation. *Science* **2019**, *363*, 391−396; e) Naret, T.; Khelifi, I.; Provot, O.; Bignon, J.; Levaique, H.; Dubois, J.; Souce, M.; Kasselouri, A.; Deroussent, A.; Paci, A.; Varela, P. F.; Gigant, B.; Alami, M.; Hamze, A. 1,1-Diheterocyclic ethylenes derived from quinaldine and carbazole as new tubulin-polymerization inhibitors: Synthesis, metabolism, and biological evaluation. *J. Med. Chem.* **2019**, *62*, 1902−1916.

[15] a) Florentino, L.; Aznar, F.; Valdés, C. Synthesis of (*Z*)-*N*-alkenylazoles and pyrroloisoquinolines from α-*N*-azoleketones through Pd-catalyzed tosylhydrazone cross-couplings. *Chem. Eur. J.* **2013**, *19*, 10506−10510; b) Peng, J.; Gao, Y.; Zhu, C.; Liu, B.; Gao, Y.; Hu, M.; Wu, W.; Jiang, H. Synthesis of polysubstituted 3-amino pyrroles via palladium-catalyzed multicomponent reaction. *J. Org. Chem.* **2017**, *82*, 3581−3588; c) Bzeih, T.; Zhang, K.; Khalaf, A.; Hachem, A.; Alami, M.; Hamze, A. One-pot reaction between *N*-tosylhydrazones and 2-nitrobenzyl bromide: Route to NH-free C2-arylindoles. *J. Org. Chem.* **2019**, *84*, 228−238; d) Messaoudi, S.; Tréguier, B.; Hamze, A.; Provot, O.; Peyrat, J.-F.; De Losada, J. R.; Liu, J.-M.; Bignon, J.; Wdzieczak-Bakala, J.; Thoret, S.; Dubois, J.; Brion, J.-D.; Alami, M. Isocombretastatins A versus Combretastatins A: The forgotten isoCA-4 isomer as a highly promising cytotoxic and antitubulin agent. *J. Med. Chem.* **2009**, *52*, 4538−4542; e) Rasolofonjatovo, E.; Provot, O.; Hamze, A.; Rodrigo, J.; Bignon, J.; Wdzieczak-Bakala, J.; Lenoir, C.; Desravines, D.; Dubois, J.; Brion, J.-D.; Alami, M. Design, synthesis and anticancer properties of 5-arylbenzoxepins as conformationally restricted isocombretastatin A-4 analogs. *Eur. J. Med. Chem.* **2013**, *62*, 28−39; f) Soussi, M. A.; Provot,

O.; Bernadat, G.; Bignon, J.; Desravines, D.; Dubois, J.; Brion, J. D.; Messaoudi, S.; Alami, M. IsoCombretaQuinazolines: Potent cytotoxic agents with antitubulin activity. *ChemMedChem* **2015**, *10*, 1392−1402; g) Wang, J.-L.; Li, H.-J.; Wu, Y.-C. Divergent synthesis of marine natural products Siphonodictyal B, Corallidictyals C/D, and Liphagal based on the early presence of an aldehyde group instead of a late-stage introduction. *J. Org. Chem.* **2018**, *83*, 8716−8723; h) Perez Encabo, A.; Turiel Hernandez, J. A.; Gallo Nieto, F. J.; Lorente Bonde-Larsen, A.; Sandoval Rodriguez, C. M. Synthesis of abiraterone and related compounds. WO Patent 2013/030410 A2, 2013.

[16] Greenman, K. L.; Carter, D. S.; Van Vranken, D. L. Palladium-catalyzed insertion reactions of trimethylsilyldiazomethane. *Tetrahedron* **2001**, *57*, 5219−5225.

[17] Peng, C.; Cheng, J.; Wang, J. Palladium-catalyzed cross-coupling of aryl or vinyl iodides with ethyl diazoacetate. *J. Am. Chem. Soc.* **2007**, *129*, 8708−8709.

[18] Zhang, Y.; Wang, J. Recent developments in Pd-catalyzed reactions of diazo compounds. *Eur. J. Org. Chem.* **2011**, *2011*, 1015−1026.

[19] Devine, S. K. J.; Van Vranken, D. L. Palladium-catalyzed carbene insertion into vinyl halides and trapping with amines. *Org. Lett.* **2007**, *9*, 2047−2049.

[20] a) Yu, W.-Y.; Tsoi, Y.-T.; Zhou, Z.; Chan, A. S. C. Palladium-catalyzed cross coupling reaction of benzyl bromides with diazoesters for stereoselective synthesis of (*E*)-α,β-diarylacrylates. *Org. Lett.* **2009**, *11*, 469−472; b) Chen, S.; Wang, J. Palladium-catalyzed reaction of allyl halides with α-diazocarbonyl compounds. *Chem. Commun.* **2008**, 4198−4200; c) Greenman, K. L.; Van Vranken, D. L. Palladium-catalyzed carbene insertion into benzyl bromides. *Tetrahedron* **2005**, *61*, 6438−6441.

[21] Zhang, Z.; Liu, Y.; Gong, M.; Zhao, X.; Zhang, Y.; Wang, J. Palladium-catalyzed carbonylation/acyl migratory insertion sequence. *Angew. Chem. Int. Ed.* **2010**, *49*, 1139−1142.

[22] Peng, C.; Yan, G.; Wang, Y.; Jiang, Y.; Zhang, Y.; Wang, J. Palladium-catalyzed coupling reaction of α-diazocarbonyl compounds with aromatic boronic acids or halides. *Synthesis* **2010**, *2010*, 4154–4168.

[23] a) Bamford, W. R.; Stevens, T. S. 924. The decomposition of toluene-p-sulphonylhydrazones by alkali. *J. Chem. Soc.* **1952**, 4735−4740; b) Shapiro, R. H.; Heath, M. J. Tosylhydrazones. V. Reaction of tosylhydrazones with alkyllithium reagents. A new olefin synthesis. *J. Am. Chem. Soc.* **1967**, *89*, 5734–5735; c) Adlington, R. M.; Barrett, A. G. M. Recent applications of the Shapiro reaction. *Acc. Chem. Res.* **1983**, *16*, 55–59.

[24] Berthon-Gelloz, G.; Marchant, M.; Straub, B. F.; Marko, I. E. Palladium-catalyzed cyclopropanation of alkenyl silanes by diazoalkanes: Evidence for a Pd^0 mechanism. *Chem. Eur. J.* **2009**, *15*, 2923–2931.

[25] Barrios-Landeros, F.; Hartwig, J. F. Distinct mechanisms for the oxidative addition of chloro-, bromo-, and iodoarenes to a bisphosphine palladium(0) complex with hindered ligands. *J. Am. Chem. Soc.* **2005**, *127*, 6944–6945.

[26] a) Müller, S. T. R.; Wirth, T. Diazo compounds in continuous-flow technology. *ChemSusChem* **2015**, *8*, 245–250; b) Deadman, B. J.; Collins, S. G.; Maguire, A. R. Taming hazardous chemistry in flow: The continuous processing of diazo and diazonium compounds. *Chem. Eur. J.* **2015**, *21*, 2298–2308; c) Movsisyan, M.; Delbeke, E. I. P.; Berton, J. K. E. T.; Battilocchio, C.; Ley, S. V.; Stevens, C. V. Taming hazardous chemistry by continuous flow technology. *Chem. Soc. Rev.* **2016**, *45*, 4892–4928; d) Tran, D. N.; Battilocchio, C.; Lou, S.-B.; Hawkins, J. M.; Ley, S. V. Flow chemistry as a discovery tool to access sp2–sp3 cross-coupling reactions via diazo compounds. *Chem. Sci.* **2015**, *6*, 1120–1125; e) Poh, J.-S.; Tran, D. N.; Battilocchio, C.; Hawkins, J. M.; Ley, S. V. A versatile room-temperature route to di- and trisubstituted allenes using flow-generated diazo compounds. *Angew. Chem. Int. Ed.* **2015**, *54*, 7920-7923; f) Rullière, P.; Benoit, G.; Allouche, E. M. D.; Charette, A. B. Safe and facile access to nonstabilized diazoalkanes using continuous flow technology. *Angew. Chem. Int. Ed.* **2018**, *57*, 5777–5782; g) Mastronardi, F.; Gutmann, B.; Kappe, C. O. Continuous flow generation and reactions of anhydrous diazomethane using a teflon AF-2400 tube-in-tube reactor. *Org. Lett.* **2013**, *15*, 5590–5593.

[27] a) Regitz, M.; Maas, G. *Diazo Compounds Properties and Synthesis*, Academic Press: Orlando, 1986; b) Sammakia, T. Phenyldiazomethane. In *Encyclopedia of Reagents for Organic Synthesis*, Wiley: 2001, doi: 10.1002/047084289X.rp060.

[28] Kozuch, S.; Shaik, S. How to Conceptualize Catalytic Cycles? The Energetic Span Model. *Acc. Chem. Res.* **2011**, *44*, 101–110.

[29] a) Ye, F.; Qu, S.; Zhou, L.; Peng, C.; Wang, C.; Cheng, J.; Hossain, M. L.; Liu, Y.; Zhang, Y.; Wang, Z.-X.; Wang, J. Palladium-catalyzed C–H functionalization of acyldiazomethane and tandem cross-coupling reactions. *J. Am. Chem. Soc.* **2015**, *137*, 4435–4444; b) Zhang, Z.; Liu, Y.; Ling, L.; Li, Y.; Dong, Y.; Gong, M.; Zhao, X.; Zhang, Y.; Wang, J. Pd-catalyzed carbonylation of diazo compounds at atmospheric pressure: A catalytic approach to ketenes. *J. Am. Chem. Soc.* **2011**, *133*, 4330–4341; c) Xia, Y.; Qu, S.; Xiao, Q.; Wang, Z.-X.; Qu, P.; Chen, L.; Liu, Z.; Tian, L.; Huang, Z.; Zhang, Y.; Wang, J. Palladium-catalyzed carbene migratory insertion using conjugated ene–yne–ketones as carbene precursors.

J. Am. Chem. Soc. **2013**, *135*, 13502−13511; d) Wang, H.; Yang, X.; Liu, Y.; Bi, S. Theoretical studies on a new class of C–C bond formation: Palladium-catalyzed reactions of α-diazocarbonyl compounds with allylic esters. *Organometallics* **2014**, *33*, 1404−1415; e) Yu, Y.; Lu, Q.; Chen, G.; Li, C.; Huang, X. Palladium-catalyzed intermolecular acylation of aryl diazoesters with ortho-bromobenzaldehydes. *Angew. Chem. Int. Ed.* **2018**, *57*, 319−323.

[30] While a palladium carbene intermediate alpha to an ester functional group has been found to be a stable intermediate with a bidentate ligand, similar results of direct group migration after N_2 loss without additional reaction barriers have also been obtained in other systems where Pd-carbene intermediates were initially postulated. See: a) Solé, D.; Mariani, F.; Bennasar, M.-L.; Fernández, I. Palladium-catalyzed intramolecular carbene insertion into C(sp3)−H bonds. *Angew. Chem. Int. Ed.* **2016**, *55*, 6467−6470; b) Ping, W.-W.; Jin, L.; Wu, Y.; Xue, X.-Y.; Zhao, X. On the mechanism of Pd(0)-catalyzed coupling of propargylic carbonates with *N*-tosylhydrazones: Density functional theory survey. *Tetrahedron* **2014**, *70*, 9373−9380.

[31] Wang, Y.; Gu, M. The oncept of spectral accuracy for MS. *Anal. Chem.* **2010**, *82*, 7055−7062.

[32] Yu, Z.; Pan, Y.; Wang, Z.; Wang, J.; Lin, Q. Genetically encoded cyclopropene directs rapid, photoclick-chemistry-mediated protein labeling in mammalian cells. *Angew. Chem. Int. Ed.* **2012**, *51*, 10600−10604.

[33] DeAngelis, A. J.; Gildner, P. G.; Chow, R.; Colacot, T. J. Generating active "L-Pd(0)" via neutral or cationic π-allylpalladium complexes featuring biaryl/bipyrazolylphosphines: Synthetic, mechanistic, and structure–activity studies in challenging cross-coupling reactions. *J. Org. Chem.* **2015**, *80*, 6794−6813.

[34] Sandoval, B. A.; Meichan, A. J.; Hyster, T. K. Enantioselective hydrogen atom transfer: Discovery of catalytic promiscuity in flavin-dependent 'ene'-reductases. *J. Am. Chem. Soc.* **2017**, *139*, 11313−11316.

[35] Jalil, A. A.; Kurono, N.; Tokuda, M. Facile synthesis of ethyl 2-arylpropenoates by cross-coupling reaction using electrogenerated highly reactive zinc. *Tetrahedron* **2002**, *58*, 7477−7484.

[36] Hu, X.-H.; Zhang, J.; Yang, X.-F.; Xu, Y.-H.; Loh, T.-P. Stereo- and chemoselective cross-coupling between two electron-deficient acrylates: An efficient route to (*Z*,*E*)-muconate derivatives. *J. Am. Chem. Soc.* **2015**, *137*, 3169−3172.

[37] Barluenga, J.; Tomás-Gamasa, M.; Aznar, F.; Valdés, C. Synthesis of 2-arylacrylates from pyruvate by tosylhydrazide-promoted Pd-catalyzed coupling with aryl halides. *Chem. Eur. J.* **2010**, *16*, 12801−12803.

[38] Chua, C. K.; Pumera, M. The reduction of graphene oxide with hydrazine: Elucidating its reductive capability based on a reaction-model approach. *Chem. Commun.* **2016**, *52*, 72−75.

[39] Mendoza-Espinosa, D.; Rendón-Nava, D.; Alvarez-Hernández, A.; Angeles-Beltrán, D.; Negrón-Silva, G. E.; Suárez-Castillo, O. R. Visible-light-promoted AuI to AuIII oxidation in triazol-5-ylidene complexes. *Chem. Asian J.* **2017**, *12*, 203−207.

[40] Campbell, J. R.; Pross, A.; Sternhel, S. Preparation and chemistry of some 1-iodo-1-phenylpropenes. *Aust. J. Chem.* **1971**, *24*, 1425−1436.

[41] Dota, K.; Sugita, Y.; Akioka, Y.; Maehata, N.; Arimori, S. Preparation of tetrazolinone compounds as pest control agents. WO Patent 2018/097318 A1, 2018.

[42] McHardy, S. F.; Liras, S.; Heck, S. D. 3-Azabicyclo[3.1.0]hexane derivatives as ppioid receptor antagonists. WO Patent 2003/035622 A1, 2003.

[43] Xu, L.; Li, B.-J.; Wu, Z.-H.; Lu, X.-Y.; Guan, B.-T.; Wang, B.-Q.; Zhao, K.-Q.; Shi, Z.-J. Nickel-catalyzed efficient and practical Suzuki−Miyaura coupling of alkenyl and aryl carbamates with aryl boroxines. *Org. Lett.* **2010**, *12*, 884−887.

[44] Tan, H.; Houpis, I.; Liu, R.; Wang, Y.; Chen, Z. Olefin preparation via palladium-catalyzed oxidative de-azotative and de-sulfitative internal cross-coupling of sulfonylhydrazones. *Org. Lett.* **2015**, *17*, 3548−3551.

[45] Lei, C.; Yip, Y. J.; Zhou, J. S. Nickel-catalyzed direct synthesis of aryl olefins from ketones and organoboron reagents under neutral conditions. *J. Am. Chem. Soc.* **2017**, *139*, 6086−6089.

[46] Tang, J.; Hackenberger, D.; Goossen, L. J. Branched arylalkenes from cinnamates: Selectivity inversion in Heck reactions by carboxylates as deciduous directing groups. *Angew. Chem. Int. Ed.* **2016**, *55*, 11296−11299.

[47] Li, R.; Wang, S. R.; Lu, W. FeCl3-Catalyzed alkenylation of simple arenes with aryl-substituted alkynes. *Org. Lett.* **2007**, *9*, 2219−2222.

[48] Zou, Y.; Qin, L.; Ren, X.; Lu, Y.; Li, Y.; Zhou, J. Selective arylation and vinylation at the α-position of vinylarenes. *Chem. Eur. J.* **2013**, *19*, 3504−3511.

[49] Frisch, M. J.; Trucks, G. W.; Schlegel, H. B.; Scuseria, G. E.; Robb, M. A.; Cheeseman, J. R.; Scalmani, G.; Barone, V.; Mennucci, B.; Petersson, G. A.; Nakatsuji, H.; Caricato, M.; Li, X.; Hratchian, H. P.; Izmaylov, A. F.; Bloino, J.; Zheng, G.; Sonnenberg, J. L.; Hada, M.; Ehara, M.; Toyota, K.; Fukuda, R.; Hasegawa, J.; Ishida, M.; Nakajima, T.; Honda, Y.; Kitao, O.; Nakai, H.; Vreven, T.; Montgomery Jr.,

J. A.; Peralta, J. E.; Ogliaro, F.; Bearpark, M. J.; Heyd, J.; Brothers, E. N.; Kudin, K. N.; Staroverov, V. N.; Kobayashi, R.; Normand, J.; Raghavachari, K.; Rendell, A. P.; Burant, J. C.; Iyengar, S. S.; Tomasi, J.; Cossi, M.; Rega, N.; Millam, N. J.; Klene, M.; Knox, J. E.; Cross, J. B.; Bakken, V.; Adamo, C.; Jaramillo, J.; Gomperts, R.; Stratmann, R. E.; Yazyev, O.; Austin, A. J.; Cammi, R.; Pomelli, C.; Ochterski, J. W.; Martin, R. L.; Morokuma, K.; Zakrzewski, V. G.; Voth, G. A.; Salvador, P.; Dannenberg, J. J.; Dapprich, S.; Daniels, A. D.; Farkas, Ö.; Foresman, J. B.; Ortiz, J. V.; Cioslowski, J.; Fox, D. J. *Gaussian 09, Rev. c.0.1*; Gaussian, Inc.: Wallingford, CT, USA, 2009.

[50] a) Zhao, Y.; Truhlar, D. G. A new local density functional for main-group thermochemistry, transition metal bonding, thermochemical kinetics, and noncovalent interactions. *J. Chem. Phys.* **2006**, *125*, 194101-1−194101-18; b) Zhao, Y.; Truhlar, D. G. The M06 suite of density functionals for main group thermochemistry, thermochemical kinetics, noncovalent interactions, excited states, and transition elements: Two new functionals and systematic testing of four M06-class functionals and 12 other functionals. *Theor. Chem. Acc.* **2008**, *120*, 215−241.

[51] Weigend, F.; Ahlrichs, R. Balanced basis sets of split valence, triple zeta valence and quadruple zeta valence quality for H to Rn: Design and assesment of accuracy. *PCCP* **2005**, *7*, 3297−3305.

[52] Andrae, D.; Haussermann, U.; Dolg, M.; Stoll, H.; Preuss, H. Energy-adjusted ab initio pseudopotentials for the 2nd and 3rd row transition-elements. *Theor. Chim. Acta* **1990**, *77*, 123−141.

[53] a) Miertus, S.; Scrocco, E.; Tomasi, J. Electrostatic interaction of a solute with a continuum - a direct utilization of ab initio molecular potentials for the prevision of solvent effects. *Chem. Phys.* **1981**, *55*, 117−129; b) Miertus, S.; Tomasi, J. Approximate evaluations of the electrostatic free-energy and internal energy changes in solution processes. *Chem. Phys.* **1982**, *65*, 239−245; c) Barone, V.; Cossi, M.; Tomasi, J. Geometry optimization of molecular structures in solution by the polarizable continuum model. *J. Comput. Chem.* **1998**, *19*, 404−417; d) Cossi, M.; Scalmani, G.; Rega, N.; Barone, V. New developments in the polarizable continuum model for quantum mechanical and classical calculations on molecules in solution. *J. Chem. Phys.* **2002**, *117*, 43−54.

Chapter 5 Efficient Kinetics in Flow by Cycling a Reaction Slug[a]

5.1 Introduction

Measuring reaction kinetics is an important and powerful tool for reaction optimization, mechanistic investigation, and scale-up.[1] Several different strategies for data treatment are available for determination of reaction orders, rate constants, and/or activation parameters. The use of robust, historical methods such as pseudo-first order conditions, the method of initial rates, the Michaelis-Menten equation, and Arrhenius and Eyring relationships is common,[2] while newer data treatment strategies including reaction progress kinetic analysis[1c,d] and variable time normalization analysis[3] have also been developed in an attempt to make data acquisition easier and require fewer experiments.

5.1.1 Pseudo-first order kinetics

Integrated rate laws provide simple mathematical relationships to determine reactant concentration as a function of time for reactions that are zeroth, first, second, or even n^{th} order in a single reagent (Table 5.1, entries 1–4). These allows simply graphical evaluation of reaction order by monitoring reagent concentration over the course of several half lives for reactions involving a single reagent, A. If the reaction order in A is zeroth, then a plot of [A] vs. time will be linear; if the reaction order in A is first a plot of ln[A] vs. time will be linear; and if the reaction order in A is second then a plot of $\frac{1}{[A]}$ vs. time will be linear.[2]

However, most reactions do not exhibit rate equations that are dependent on only a single reagent. While integrated rate laws can be derived for reactions that are non-zero order in multiple reagents, the relationships quickly become complicated and unwieldy to work with (entry 5). However, the method of pseudo-first order kinetics is a strategy to make reactions behave as if they are only dependent on a single reagent and therefore allow use of the simple integrated rate laws discussed above. This is accomplished by using a large (≥10 fold) excess of all reagents

[a] Parts of this chapter have appeared in print: Sullivan, R. J.; Newman, S. G. Reaction cycling for kinetic analysis in flow. *J. Org. Chem*, **2020**, ASAP, doi. 10.1021/acs.joc.0c00216. Excerpts from the results section and Figures 5.2, 5.3, and 5.7 are adapted with permission from Sullivan, R. J.; Newman, S. G. *J. Org. Chem.* **2020**, ASAP, doi. 10.1021/acs.joc.0c00216. Copyright 2020 American Chemial Society.

except one. As a result, the concentration of the reagents in excess doesn't change significantly as the reaction proceeds (less than 10%) while the disappearance of the limiting reagent can be followed over several half lives. This takes the overall rate equation Eq. 5.1 and simplifies it to Eq. 5.2 where $k_{obs} = k[B]^b[C]^c\ldots[n]^n$ which is constant when A is the limiting reagent and all others are in large excess. [2]

Table 5.1. Integrated rate laws for the various reaction orders in the generic rate equation rate = $k[A]^a[B]^b$.

Entry	Order in A	Order in B	Rate equation	Integrated rate law
1	0	0	$\text{rate} = k$	$[A] = [A]_0 - kt$
2	1	0	$\text{rate} = k[A]$	$\ln[A] = \ln[A]_0 - kt$
3	2	0	$\text{rate} = k[A]^2$	$\frac{1}{[A]} = \frac{1}{[A]_0} + kt$
4	n^{th}	0	$\text{rate} = k[A]^n$	$\frac{1}{[A]^{n-1}} = \frac{1}{[A]_0^{n-1}} + (n-1)kt$
5	1	1	$\text{rate} = k[A][B]$	$\left(\frac{1}{[B]_0 - [A]_0}\right)\ln\left(\frac{[A]_0[B]}{[B]_0[A]}\right) = kt$

$$\text{rate} = k[A]^a[B]^b[C]^c\ldots[n]^n \qquad \text{(Eq. 5.1)}$$

$$\text{rate} = k_{obs}[A]^a \qquad \text{(Eq. 5.2)}$$

While an elegant approach, this strategy does have some limitations. It is not capable of handling fractional or negative rate orders that can be encountered in complex mechanisms, it is not capable of determining the reaction order of catalytic species since catalysts are not consumed as the reaction progresses, and the method necessarily requires non-realistic reaction conditions by requiring large excesses of the other reagents.[2]

5.1.2 The method of initial rates

To address these limitations the method of initial rates is applicable. This method is based on approximating the instantaneous rate at the start of the reaction (when the concentrations of all species are known) by measuring average rate up to low conversion (typically less than 5 or 10%). By changing the concentration of each reagent, the impact on the initial rate can be determined, and from that the reaction order can be elucidated. For example, if doubling the concentration of one reagent has no effect on the initial rate, the reaction order for that reagent is zero. Similarly, if

doubling the concentration doubles the initial rate, the order for that reagent is one, and so forth. While this type of analysis can be performed by inspection of tabulated initial rate data as a function of reagent concentrations, a graphical approach that is less impacted by random experimental error is also available.[2]

The graphical approach derives from taking the logarithm of both sides of the rate equation (Eq. 5.1) to derive Eq. 5.3. It follows that measuring initial rates at various concentrations of a single reagent (e.g., A) while all else is held constant generates a linear relationship in the form: $\ln(\text{rate}) = a \cdot \ln[A] + \text{const.}$ with a slope equal to the reaction order. In contrast to the pseudo-first order approach, this method allows determination of reaction orders under realistic conditions and is also applicable to negative and non-integer reaction orders, as well as determining reaction order in catalyst. Furthermore, this method is also suitable for reactions that only proceed to partial conversion or suffer from competing side reactions that become dominant as the reaction progresses.[2]

$$\ln(\text{rate}) = a \cdot \ln[A] + b \cdot \ln[B] + c \cdot \ln[C] + \ldots + n \cdot \ln[n] + \ln(k) \qquad \text{(Eq. 5.3)}$$

5.1.3 Michaelis-Menten kinetics and Lineweaver-Burk plots

So far in the discussion it has been assumed that reaction orders are constant — that is the reaction order is independent of the reagent concentration. However, situations where the observed reaction order decreases with increasing reagent concentration are common. These are cases of saturation kinetics, a phenomenon that arises when the reagent concentration appears in both the numerator and denominator of the rate equation. This results when reaction mechanisms feature pre-equilibria steps before the elementary step involving the reagent in question. For example, the S_N1 reaction between *tert*-butyl bromide (**5.1**) and a metal cyanide salt (Scheme 5.1) has the complete rate law given in Eq. 5.4. However, under synthetically relevant conditions $k_2[CN^-] >> k_{-1}[Br^-]$, and therefore the rate law simplifies to Eq. 5.5. The observed reaction order in CN^- is zero, but if the kinetics were measured at very low concentration of CN^-, a positive reaction order would be found. In more complex systems however, such as those encountered in many catalytic reactions, the denominator is not dominated by a single term and therefore partial, fractional orders are often observed for the substrate(s).[2]

Scheme 5.1. Elementary steps in the S_N1 reaction between *tert*-butyl bromide and CN^-.

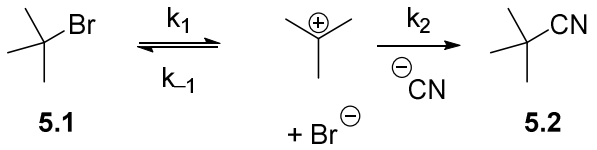

$$\text{rate} = \frac{k_1 k_2[\mathbf{5.1}][CN^-]}{k_{-1}[Br^-] + k_2[CN^-]} \quad \text{(Eq. 5.4)}$$

$$\text{rate} = k_1[\mathbf{5.1}] \quad \text{(Eq. 5.5)}$$

To mathematically treat situations such as these, Michaelis-Menten kinetics can be used. The Michaelis-Menten model was developed to describe enzyme kinetics that follow the general reaction mechanism shown in Scheme 5.2, where association with the enzyme is in pre-equilibrium (k_1/k_{-1}) and the rate limiting step is conversion of substrate to product (k_2). With these assumptions, release of the product from the enzyme (k_3/k_{-3}) has no bearing on the rate equation since it follows the rate determining step. Using the steady-state assumption for [E–S] (Eq. 5.6), the rate law for the reaction is Eq. 5.7. By combining the constants this simplifies to Eq. 5.8, where $v_{max}=k_1k_2[E]_0$ and $K_M = \frac{k_{-1}+k_2}{k_1}$. The constant v_{max} represents the maximum reaction rate that could be obtained at infinite [S], and therefore provides information about the efficiency of the enzyme to convert substrate to product in the active site. K_M on the other hand is the concentration of S that would achieve half v_{max} and provides information about the efficiency of substrate binding. Smaller K_M values signify larger enzyme-substrate binding equilibrium constants, and therefore greater enzyme-substrate affinity. While originally derived in the context of enzyme kinetics, the Michaelis-Menten relationship is widely applicable to model saturation kinetics in other situations as well.[2]

Scheme 5.2. The mechanism assumed for the derivation of the Michaelis-Menten model to describe enzyme kinetics.

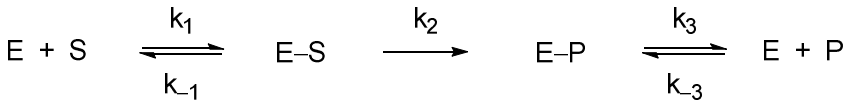

$$\frac{d[E-S]}{dt} = k_1([E]_0 - [E-S])[S] - k_{-1}[E-S] - k_2[E-S] = 0 \qquad \text{(Eq. 5.6)}$$

$$\text{rate} = \frac{k_1 k_2 [E]_0 [S]}{k_{-1} + k_2 + k_1[S]} \qquad \text{(Eq. 5.7)}$$

$$\text{rate} = \frac{v_{max}[S]}{K_M + [S]} \qquad \text{(Eq. 5.8)}$$

Because the Michaelis-Menten relationship is hyperbolic, it was historically challenging to fit data. To overcome this challenge, the Lineweaver-Burk plot was devised. This derives from taking the reciprocal of the Michaelis-Menten equation to give Eq. 5.9. It follows that a plot of 1/rate versus 1/[S] yields a linear relationship with a slope of K_M/v_{max} and y-intercept of $1/v_{max}$. While the Lineweaver-Burk plot was historically important, the determination of v_{max} and K_M relies on extrapolation to the y-axis and is therefore less accurate than directly fitting data to the Michaelis-Menten relationship using commercially available curve fitting software that is now widely available.[2]

$$\frac{1}{\text{rate}} = \frac{K_M}{v_{max}} \frac{1}{[S]} + \frac{1}{v_{max}} \qquad \text{(Eq. 5.9)}$$

5.1.4 Arrhenius and Eyring analyses

Determining the activation energy of a reaction is also desirable. This is accomplished by measuring the effect of temperature on the rate constant, k. The Arrhenius relationship, Eq. 5.10, describes the temperature dependence of the rate constant, and taking the natural logarithm of both sides provides the linear function Eq. 5.11. Therefore, a plot of $\ln(k)$ as a function of $\frac{1}{T}$ yields a straight line with a slope equal to $\frac{-E_a}{R}$, allowing determination of the activation energy (E_a). The concept of activation energy is equally relevant to single- and multi-step reaction mechanisms, and is simply the height of the highest energetic barrier that must be overcome to form the final products. [2]

$$k = Ae^{\frac{-E_a}{RT}} \qquad \text{(Eq. 5.10)}$$

$$\ln(k) = \frac{-E_a}{R}\left(\frac{1}{T}\right) + \ln(A). \qquad \text{(Eq. 5.11)}$$

The activation energy can be further broken down into enthalpic and entropic contributions for single step reactions. This derives from transition state theory which is built on the conceptual approximation of considering the reactants and activated complex as being in equilibrium and therefore described by an equilibrium constant, $K^{\ddagger}$. the development of transition state theory allowed the derivation of the Eyring equation (Eq. 5.12) which relates the rate constant, k, to this equilibrium constant, $K^{\ddagger}$, and temperature, T. The constants in the Eyring equation are κ, the transmission coefficient (the proportion of reagents achieving the transition state that actually proceed to form products; typically $\kappa \approx 1$), k_B, the Boltzmann constant, and h, Plank's constant which come from statistical thermodynamics.[2]

$$k = \kappa\left(\frac{k_B T}{h}\right) K^{\ddagger} \qquad \text{(Eq. 5.12)}$$

Since equilibria constants are related to Gibbs free energy by Eq. 5.13, the Eyring equation can be rewritten in terms of the Gibbs free energy of activation (Eq. 5.14) and subsequently expanded into the separate contributions from the enthalpy and entropy of activation (Eq. 5.15). Lastly, rearrangement and taking the natural logarithm of both sides yields the linear relationship Eq. 5.16, and it follows that a plot of $\ln\left(\frac{kh}{\kappa k_B T}\right)$ as a function of $\frac{1}{T}$ yields a straight line with a slope of $\frac{-\Delta H^{\ddagger}}{R}$ and y-intercept of $\frac{\Delta S^{\ddagger}}{R}$ to allow determination of the enthalpy and entropy of activation.[2]

$$\Delta G = -RT\ln(K) \qquad \text{(Eq. 5.13)}$$

$$k = \kappa\left(\frac{k_B T}{h}\right) e^{\frac{-\Delta G^{\ddagger}}{RT}} \qquad \text{(Eq. 5.14)}$$

$$k = \kappa\left(\frac{k_B T}{h}\right) e^{\frac{-\Delta H^{\ddagger}}{RT}} e^{\frac{\Delta S^{\ddagger}}{R}} \qquad \text{(Eq. 5.15)}$$

$$\ln\left(\frac{kh}{\kappa k_B T}\right) = \frac{-\Delta H^{\ddagger}}{R}\left(\frac{1}{T}\right) + \frac{\Delta S^{\ddagger}}{R} \qquad \text{(Eq. 5.16)}$$

5.1.5 Reaction Progress Kinetic Analysis (RPKA)

The experimental techniques discussed so far require many experiments to collect all necessary data. To address this laborious burden Blackmond and coworkers developed the method of reaction progress kinetic analysis (RPKA) that allows determination of reaction orders and other

kinetic information from a minimal number of experiments. Use of RPKA rests on the ability to determine the instantaneous reaction rate at all points during a reaction. This can be accomplished in one of two ways. The first option is to continuously monitor reagent concentration, by for example using *in situ* reactIR, and then take the derivative of the conversion over time data to calculate the instantaneous rate at each time point. The second option is to measure the instantaneous reaction rate directly as the reaction proceeds, by for example using reaction calorimetry.[1c,d]

The underlying principle of the RPKA method is that determining instantaneous rate at all points as a reaction proceeds generates data equivalent to performing hundreds of separate initial rate experiments. For reactions involving only a single reagent, the shape of a plot of instantaneous rate as a function of reagent concentration therefore directly informs on reaction order. If this plot results in a horizontal line the reaction is zeroth order (i.e., the reaction rate is unaffected by changing reagent concentration) while a line with a positive slope implies first order (i.e., rate is directly proportional to concentration), and a hyperbolic relationship demonstrates saturation kinetics (i.e. an increase in concentration provides a less than proportional increase in rate).[1c,d]

Most reactions involve more than one reagent however, and therefore data interpretation is slightly more involved in these cases. Rather than a single experiment, a small handful of experiments are required, using different values of "excess" of one reagent and various graphical manipulation strategies to elucidate the reaction orders. RPKA methods are also ideally suited to probe for the presence of catalyst deactivation by performing experiments with the same "excess" but different initial concentrations. While the RPKA method is efficient and powerful, it requires the ability to continuously monitoring instantaneous rate, and therefore can be challenging to implement in practise. Furthermore, the data analysis method cannot handle multiple reagents exhibiting fractional reaction orders, so for systems with multiple species exhibiting saturation kinetics the method cannot provide insight.[1c,d]

5.1.6 Variable Time Normalization Analysis (VTNA)

To address the limitations of RPKA, the method of Variable Time Normalization Analysis (VTNA) was developed. Whereas RPKA is best-designed for continuous monitoring of instantaneous reaction rate, VTNA utilizes (non-continuous) conversion over time data which is

generally easier to obtain. Furthermore, the data analysis used in VTNA does not suffer from limitations preventing determination of multiple fractional or negative reaction orders and can therefore provide insight even with complex systems. The mathematical basis of the VTNA method lies in comparing the conversion over time profiles of two reactions where the initial concentration of a single reagent differs, but all other conditions are the same. For example, in the generic reaction A + B → P, two reactions are conducted where $[A]_0$ is unchanged but $[B]_0$ is doubled (Figure 5.1). The conversion over time profiles differ because the reaction with higher $[B]_0$ is faster. However, if the x-axis is normalized to exclude the effect of [B], then the data for both reactions overlay. The function to achieve normalization is approximated by the trapezoid rule (Eq. 5.20), and only when the correct value for the exponent (β) is used will the data overlay. β is of course the reaction order with respect to B that one wishes to determine. The same method is applied for each reagent, so in total the number of experiments required is n+1 to determine the reaction orders of n reagents.[3]

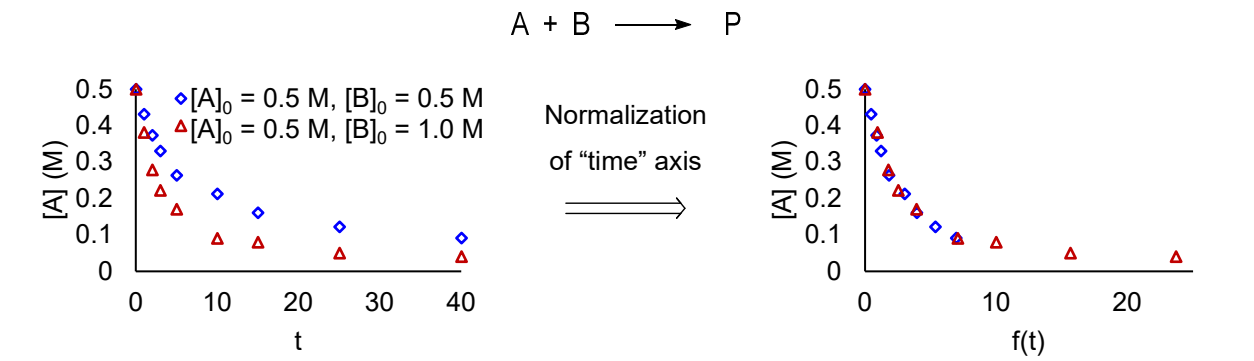

$$-\frac{d[A]}{dt} = k[A]^{\alpha}[B]^{\beta} \qquad \text{(Eq. 5.17)}$$

$$-\frac{d[A]}{df(t)} = k[A]^{\alpha} \qquad \text{(Eq. 5.18)}$$

$$df(t) = [B]^{\beta}dt \qquad \text{(Eq. 5.19)}$$

$$f(t) = \int_0^t [B]^{\beta}dt \approx \sum_{i=1}^{n} \left(\frac{[B]_i + [B]_{i-1}}{2}\right)^{\beta} (t_i - t_{i-1}) \qquad \text{(Eq. 5.20)}$$

Figure 5.1. Derivation of the "time" axis normalization to remove the effect of [B].

5.1.7 Kinetics in flow

Common to all kinetic methods discussed above is that monitoring of reaction progress (or instantaneous rate) over time is required to obtain kinetic data. Even with newer RPKA and VTNA methods this is still laborious, and therefore routine collection of kinetic data at the reaction discovery and early development stage is not commonplace. While automation of batch experiments using liquid-handling robotics can alleviate this burden, access to robotic systems capable of this work is limited, and the ability to interface with online analytics is more restricted in batch systems.[4]

Continuous flow systems offer much more flexibility to incorporate automation and online analytics, in addition to other benefits stemming from efficient mixing and access to wider ranges of temperatures and pressures.[5] However, a major inefficiency hinders acquiring kinetic data in flow, and as result batch is usually preferred for kinetics.[6] This is a consequence of the coupling of time and space in flow, where 'reaction time' is a consequence of flow rate and reactor volume. As a result, while it is trivial to acquire a kinetic profile in batch by taking aliquot samples as the reaction proceeds (Figure 5.2A), in flow a new experiment is needed for each and every data point in the conversion over time profile (Figure 5.2B).[7] While performing *n* experiments for *n* data points is effective, it is also wasteful of time and materials. For example, Blackmond and coworkers compared batch and flow for the monitoring of an aldol reaction taking 40 min to reach completion.[6] The requirement to perform a new steady-state experiment for each data point in flow resulted in a 5-fold increase in experiment time and material consumption.

Solutions to this problem have so far focused on using stepped or gradient flow rates and complex model fitting software to circumvent the need to collect steady-state samples.[8] However these approaches are limited by the complicated mathematics required, and applications have thus far been restricted to relatively simple reactions. Furthermore, the application of these model fitting approaches is targeted towards elucidating rate constants when the reaction order in each reagent is known. A failure to unambiguously determine reaction orders without relying on chemical intuition is a feature of these model fitting strategies and therefore precludes their usefulness for mechanistic investigations.[8f]

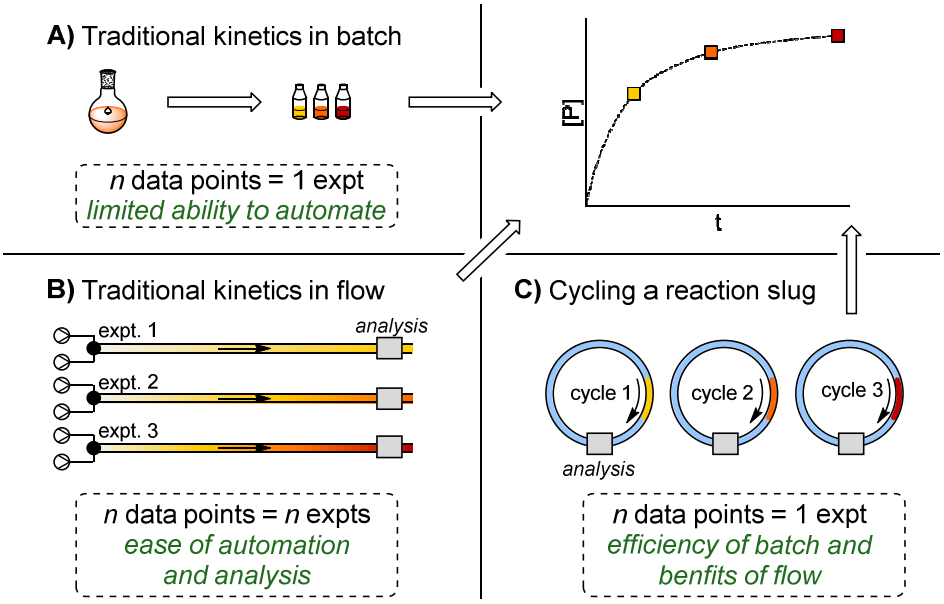

Figure 5.2. A) Generation of reaction profiles in batch is accomplished by aliquot sampling over time. B) Generation of reaction profiles in flow is accomplished by running a new steady-state experiment for each data point. C) An envisioned flow reactor capable of analysing progress over time by cycling a reaction slug.[a]

Conceptually, the shortcoming of using a flow reactor for kinetics is that the reaction is 'thrown out' after analysis. Inspired by the ability to incorporate cycles to recover and reuse reagents such as catalysts or auxiliaries,[9] we envisioned that recovery and cycling of an entire reaction solution should be possible with an appropriately designed flow reactor by performing the reaction as a discrete slug pushed by an inert carrier fluid (Figure 5.2C).[10] Analyzing the reaction once every 'cycle' provides conversion over time data. Given the growing number, diversity, and utility of advanced flow systems[11] and the expanding scope of reactions that can be performed equally well or better in flow,[12] it was believed that development of a simple and reliable method to obtain kinetic data from continuous systems would be highly valuable.

The focus of this chapter is the design and implementation of this reactor to enable straightforward acquisition of kinetic data. The versatility of the system is demonstrated through the study of a range of reactions using varied solvents, temperatures, and methods of kinetic

[a] Adapted with permission from Sullivan, R. J.; Newman, S. G. *J. Org. Chem.* **2020**, ASAP, doi. 10.1021/acs.joc.0c00216. Copyright 2020 American Chemial Society.

analysis. The value of routinely performing kinetics is additionally highlighted by the observation of non-intuitive rate behavior for some seemingly simple transformations. The setup is assembled from commercially available components, and data quality was comparable or superior to batch sampling in all cases.

5.2 Results and Discussion

Moving a reaction slug through a reactor requires an inlet and outlet for the carrier stream to continuously enter and exit while somehow retaining the slug. In order to provide these essential features, we focused on developing a valve arrangement that facilitated 'cycling' a reaction slug along a looping figure eight path. This was accomplished by repurposing a commercially available 6-port, two-way injection valve and an 11-port, 10-position selector valve[13] by altering the fluid connectivity at the port connections and designing a custom rotor for the selector valve (see Figure 5.8 in the Experimental section for full details). The modifications necessary are inexpensive[14] and easy to implement. The principle of operation to 'cycle' the reaction slug is that when the reaction slug is in coil A it is directed to coil B and when in coil B it is directed back to coil A (Figure 5.3). Each time the slug is passed back and forth between the two reaction coils it travels through an intermediate zone where analysis is performed. While a range of online analysis tools can be envisioned,[15] we elected to use a sampling valve that removes a small aliquot for off-line analysis, keeping the system cost and complexity low.

While small droplets have been widely used as reaction 'slugs' in automated screening and optimization platforms,[10] we selected to use large slugs (>50 cm in length) to avoid problems with rate acceleration occurring at droplet/carrier stream interfaces[10a] or reaction solvent/reagent bleed/carryover into the carrier stream or subsequent slugs.[16] The immiscible carrier stream used can be either gaseous (e.g., N_2) or liquid (e.g., aqueous, fluorous, etc.) depending on the desired application; we demonstrate both options using N_2 and water respectively as carrier streams in different examples. The residence coils and remaining reactor materials can be selected for compatibility with the chemistry and conditions of interest; we opted for 0.5 mm I.D. PFA tubing for simplicity and optical transparency.

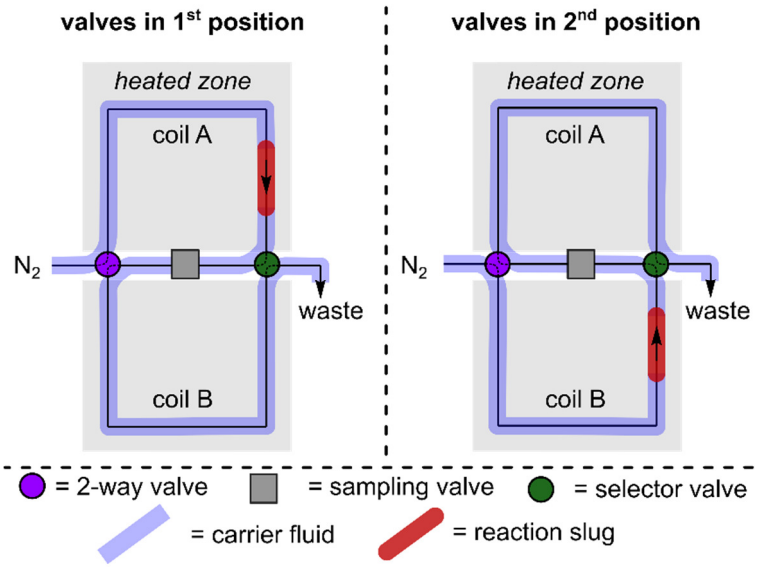

Figure 5.3. A schematic of the reactor coils and valves used to cycle a single reaction slug through a sampling valve multiple times, facilitating sequential sampling for reaction progress monitoring.[a]

The ability to cycle slugs of solvent using the reactor was first examined. Solvent slugs with varying viscosity (H_2O, EtOH, toluene, $CHCl_3$) could be cycled using N_2 as the carrier stream without slug break up to provide a range of sampling intervals (~1.5–10 min between sample collections) over various temperatures (0–90 °C or ~5 °C below the atmospheric solvent boiling point of solvent). Above a certain limit, excessively high flow rates resulted in slug break up due to shear forces with the reactor walls, but the accessible sampling intervals were more than sufficient to study the kinetics for the majority of reactions.[17] When using H_2O as the carrier stream, temperatures above solvent atmospheric boiling points could be used in combination with the application of system back pressure.

With the ability to cycle a solvent slug confirmed, we next turned to the room-temperature acylation reaction between benzoyl chloride (**5.3**) and benzyl alcohol (**5.4**) as a well understood transformation to confirm that reactions performed in the cycling flow reactor exhibited the same kinetic behaviour as under typical batch conditions. We selected Bu_3N (**5.5**) as the organic base to avoid solid handling issues,[12e] N_2 as the inert carrier stream to move the reaction slug[18] through the reactor, and the method of variable time normalization analysis (VTNA)[3] to analyze the data

[a] Adapted with permission from Sullivan, R. J.; Newman, S. G. *J. Org. Chem.* **2020**, ASAP, doi. 10.1021/acs.joc.0c00216. Copyright 2020 American Chemial Society.

(Figure 5.4). In addition to performing experiments with the cycling flow reactor, all experiments were repeated using a traditional batch set-up (i.e., a round-bottom flask) for reactor validation.

Identical results were obtained in both cases, finding first order behavior for both **5.3** (Figure 5.4A) and **5.4** (Figure 5.4B) and a partial reaction order of ~0.5 for **5.5** (Figure 5.4C). Related tertiary amine mediated acylation reactions are known to proceed by a nucleophilic catalyzed mechanism,[19] although the partial order suggests a complex mechanism may be operative. By normalizing to all reaction components, a straight line was obtained with a slope equal to the rate constant (Figure 5.4D). Replication of experiments in batch showed indistinguishable kinetic profiles (e.g., Figure 5.4E) and found a value for the rate constant in excellent agreement with the value found using the flow reactor (2% difference), confirming the validity and transferability of the collected data.

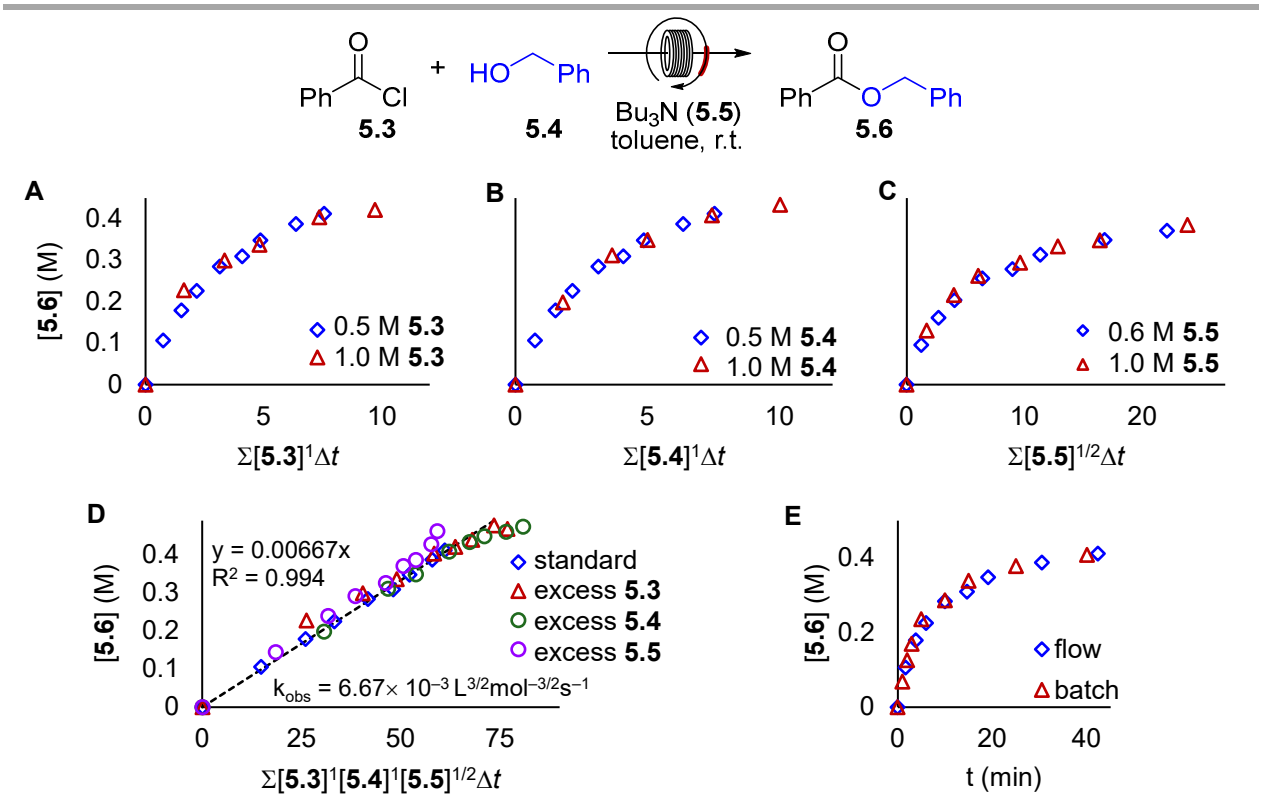

Figure 5.4. Kinetic data obtained using the cycling flow reactor. A) VTNA plot showing 1st order in **5.3**. B) VTNA plot showing 1st order in **5.4**. C) VTNA plot showing ~0.5 order in **5.5**. D) VTNA plot to calculate rate constant. E) Overlay of data collected using flow reactor and batch data. Standard conditions: 0.5 M **5.3**, 0.5 M **5.4**, 0.6 M **5.5** in toluene, room temperature.

Satisfied that the reactor operated as desired, we next explored the ability to rapidly obtain kinetic data for a variety of reactions (Table 5.2). An S_NAr reaction at 80 °C (entry 1) and a silylation at 0 °C (entry 2) were examined to assess the reactor performance over a range of temperatures. The flow reactor performed well in both cases, providing either equivalent or slightly superior data quality (less noise) compared to parallel experiments in batch. The solvolysis of a secondary alkyl halide was probed using a pseudo-first order approach to distinguish between an S_N1 or S_N2 mechanism, as well as demonstrate the ability to perform an Eyring analysis by varying the reaction temperature (entry 3). A Pd catalyzed C–S cross-coupling reaction was examined using the method of initial rates to show the applicability towards air- and moisture-sensitive chemistry and complex, multi-step reaction mechanisms (entry 4). Lastly, the ability to perform all necessary reactions simultaneously as consecutive slugs to maximize data collection efficiency was demonstrated with the analysis of a Diels-Alder cycloaddition (entry 5). The carrier fluid was also changed from N_2 to H_2O for this example to demonstrate the flexibility in choice of carrier solvent and the ability to conduct experiments above the atmospheric boiling point of the solvent ($CHCl_3$).

Table 5.2. Reactions investigated using the flow reactor.

Entry	Reaction		
	Analysis method	Demonstrating	Rate equation found
1	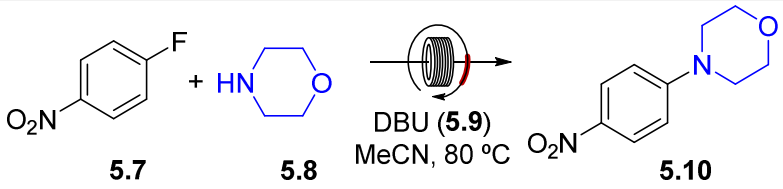 **5.7** **5.8** **5.10**		
	VTNA	Elevated temperature	$\text{rate} = k[\mathbf{5.7}][\mathbf{5.8}]$ 0^{th} order in **5.9**
2	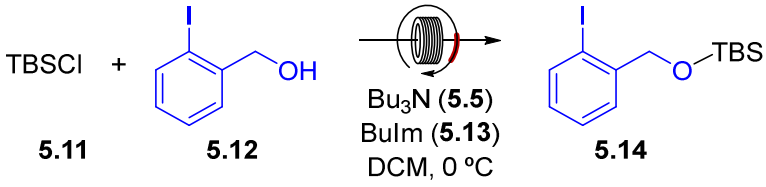 **5.11** **5.12** **5.14**		
	VTNA	Lowered temperature	$\text{rate} = \frac{k[\mathbf{5.11}][\mathbf{5.12}][\mathbf{5.13}]^2}{[\mathbf{5.5}]}$

3	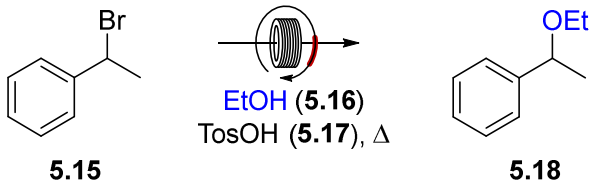 **5.15** **5.18**		
	pseudo-first order	Distinguish S_N1/S_N2; Temperature variation (Eyring analysis)	rate = k[**5.15**][**5.16**] 0th order in **5.17**
4	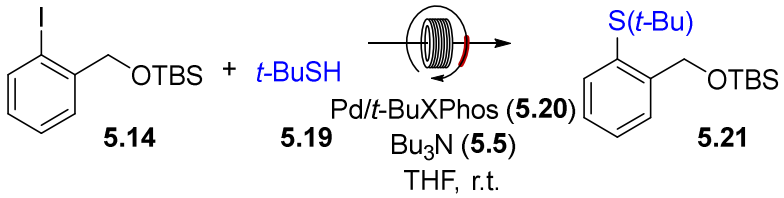 **5.14** **5.19** **5.21**		
	method of initial rates	O_2/H_2O free reaction; Complex mechanism	rate= k[**5.20**][**5.19**]^x[**5.5**]^y $0 < x,y < 1$ 0th order in **5.14** *saturation kinetics*
5	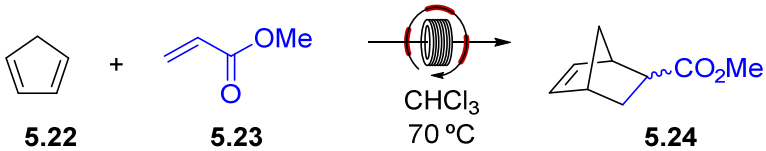 **5.22** **5.23** **5.24**		
	VTNA	Simultaneous reactions; Exceeding solvent b.p.; H_2O carrier phase	rate = k[**5.22**][**5.23**]

The observed rate equation for the S_NAr reaction at elevated temperature was as expected, with first order behavior observed for both electrophile **5.7** and nucleophile **5.8**, and 0th order for base **5.9**. Data obtained with the cycling flow reactor was in excellent agreement with the parallel data collected in batch, confirming that the choice of large slugs prevented appreciable loss of solvent to the gaseous carrier phase even when operating just below the atmospheric boiling point of the solvent. Investigating the silylation of alcohol **5.12** at lowered temperature provided further support that the kinetics obtained using the cycling flow reactor provide an accurate representation of the chemistry, with excellent agreement between the flow generated- and parallel batch generated-data.

In addition, a non-intuitive second order behaviour for the nucleophilic catalyst **5.13** and negative order with respect to base **5.5** were observed in this reaction highlighting the value of performing routine kinetic experiments. A plausible reaction mechanism that accounts for the observed reaction orders is given in Scheme 5.3. Neither steady-state nor rapid-preequilibrium approximations are consistent with the observed rate orders. However, if both attack of 1-butylimidazole (**5.13**) on TBSCl (**5.11**) to form TBS-BuIm$^+$ intermediate **5.25** and attack of 2-iodobenzyl alcohol (**5.12**) on intermediate **5.25** to lead to the product are comparably slow, while in between these steps a rapid equilibrium with the stoichiometric base (**5.5**) depletes the concentration of **5.25**, the observed rate orders would be obtained. The rate behavior observed with these substrates contrasts with previous studies of the TBS protection of naphthalen-1-ylmethanol using DMAP or 1-methylimidazole as nucleophilic catalysts and Et_3N as the base.[20] In these cases first order in catalyst and no inhibitory effect of base was observed, suggesting nucleophilic attack of the catalyst on TBSCl was the sole limiting step for these substrates.

Scheme 5.3. Postulated mechanism for the TBS protection of **5.12** mediated by **5.5** and **5.13**.

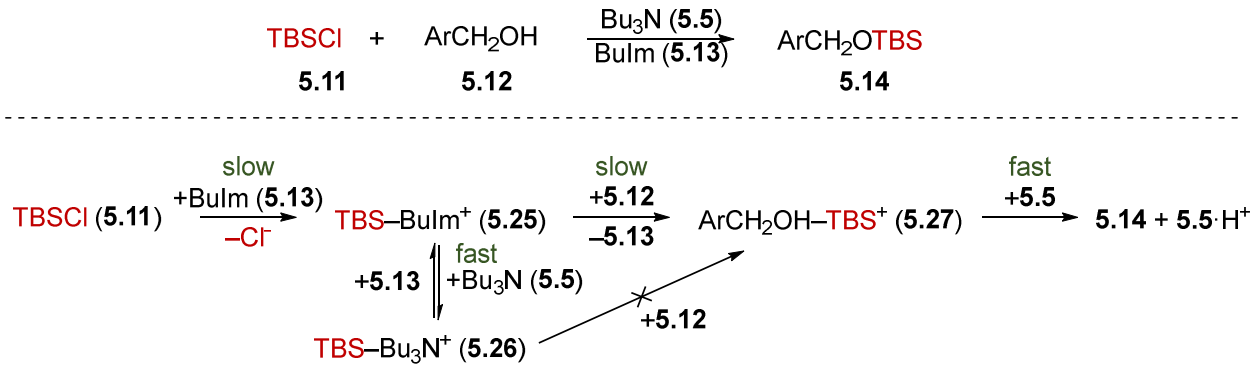

For the solvolysis of alkyl bromide **5.15**, selected to demonstrate the ability to distinguish between potential reaction mechanisms and determine activation parameters, an S_N2 mechanism was found to be operative. First order behavior for **5.15** was found using integrated rate laws under pseudo-first order conditions, to demonstrate the applicability of the reactor for other methods of kinetic analysis (Figure 5.5A). First order behavior in EtOH (**5.16**) and zeroth order in acid **5.17** were determined by examining the effect of changing concentration on the observed rate constant (Table 5.3). Observing the effect of changing temperature on the rate constant allowed activation parameters to be calculated. An Eyring analysis of the data (Figure 5.5B, $k = k_{obs}/[EtOH]$) yielded

values for the enthalpy (18.9 kcal/mol) and entropy (−15.2 cal/(mol·K)) of activation that were also consistent with an S_N2 mechanism.[21]

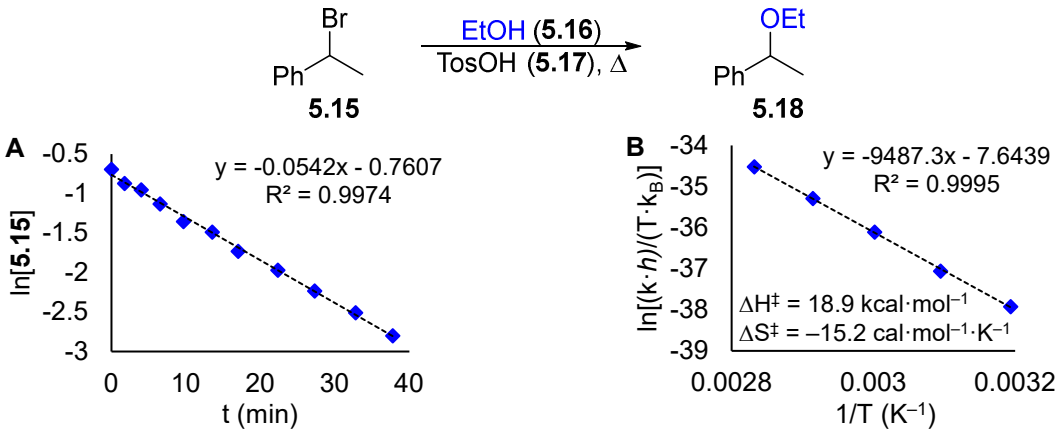

Figure 5.5. A) Linear integrated rate law plot showing first order in electrophile **5.15.** B) Eyring plot. Standard conditions: 0.5 M **5.15**, 0.125 M **5.17** in EtOH, 70 °C.

Table 5.3. k_{obs} values for the ethanolysis of **5.15**.[a]

Entry	[**5.17**] (M)	[**5.16**] (M)	k_{obs}
1	0.125	16.0	0.0542
2	0.0250	16.0	0.0599
3	0.125	14.5[b]	0.0484
4	0.125	12.7[c]	0.0384

[a] All reactions 0.5 M in **5.15**. [b] 10:1 EtOH:*t*-BuOH as solvent. [c] 4:1 EtOH:*t*-BuOH as solvent.

To demonstrate the applicability towards O_2 and H_2O sensitive chemistries and complex reaction mechanisms, a palladium catalyzed C–S cross-coupling recently reported by Buchwald and coworkers was investigated. [22] First order behavior was found for catalyst **5.20** (Figure 5.6A) and zeroth order for aryl halide **5.14** (Figure 5.6B), consistent with the previously identified $LPd^{II}ArX$ resting state,[22] by using the method of initial rates which is best suited for reactions that may not reach full conversion or exhibit complex rate equations. The reaction orders for thiol **5.19** and base **5.5** proved to be more complex, yielding curving log-log plots of initial rate vs. concentration (Figure 5.6C and D). Both **5.19** and **5.5** exhibited saturation kinetics and Michaelis-Menten plots of the data fit well yielding v_{max} and K_M values for each reagent (Figure 5.6E and F).

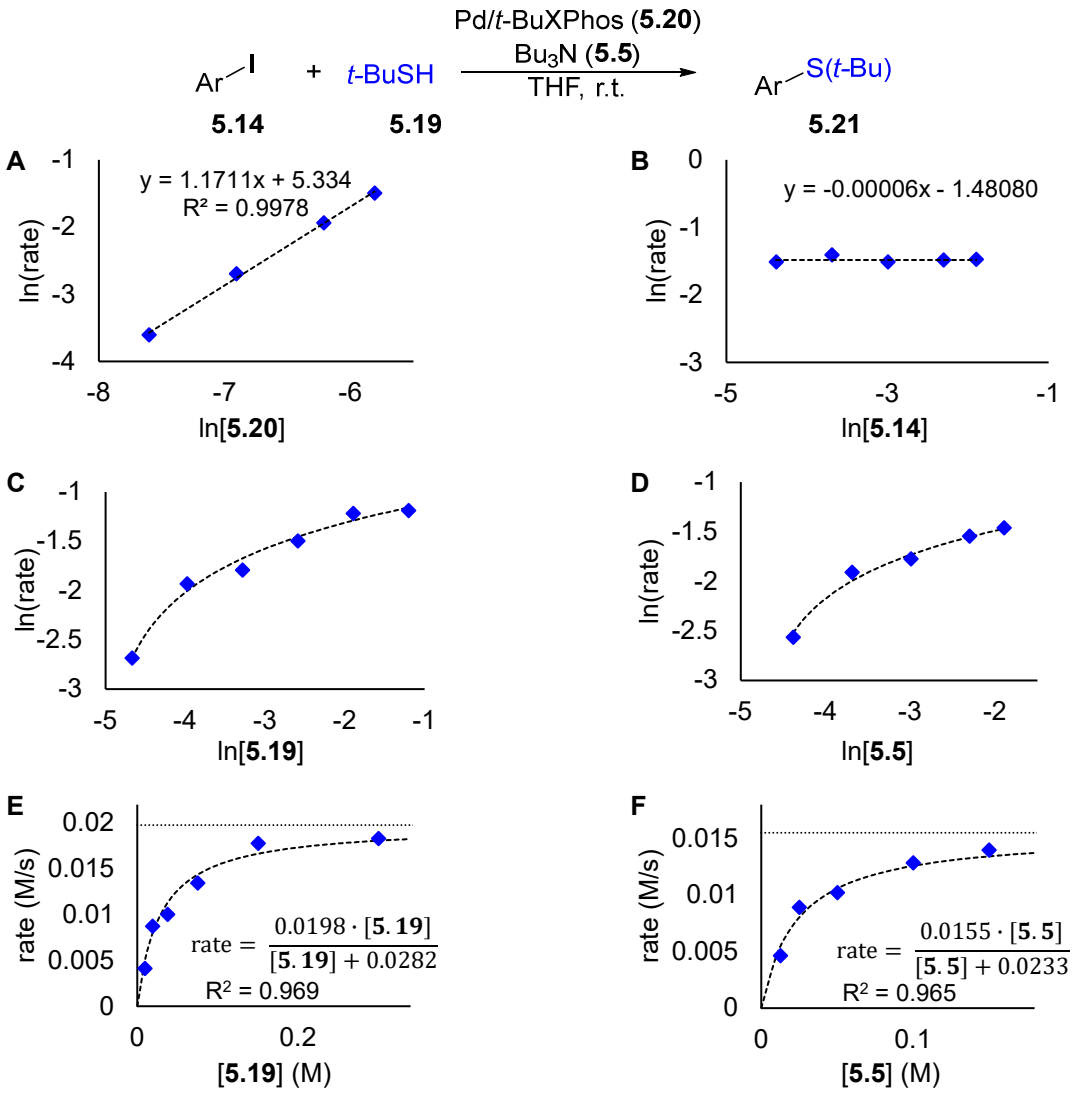

Figure 5.6. Initial rate kinetics for C–S cross coupling of ArI **5.14** and thiol **5.19** catalyzed by a Pd/*t*-BuXPhos system. A) log-log plot of initial rate vs. [**5.20**], B) log-log plot of initial rate vs. [**5.14**], C) log-log plot of initial rate vs. [**5.19**], D) log-log plot of initial rate vs. [**5.5**], E) Michaelis-Menten plot of initial rate vs. [**5.19**], F) Michaelis-Menten plot of initial rate vs. [**5.5**]. Standard conditions: 50 mM **5.14**, 75 mM **5.19**, 100 mM **5.5**, 3 mM **5.20** in THF, room temperature.

These data are consistent with a rate determining step of either deprotonation of the palladium bound thiol intermediate **III** or reductive elimination of the product from intermediate **IV** (see Scheme 5.4). Subsequent DFT calculations concluded that reductive elimination is the rate limiting step (Figures AIV.15–17 in Appendix IV). Not only was it possible to obtain high quality data for this air- and moisture-sensitive reaction using the cycling flow reactor, it was operationally

simpler compared to the analogous batch experiments that would require sampling from a flask kept under inert atmosphere.

Scheme 5.4. Putative catalytic cycle for the Pd catalyzed C–S bond formation. L = *t*-BuXPhos, ArI = **5.14**.

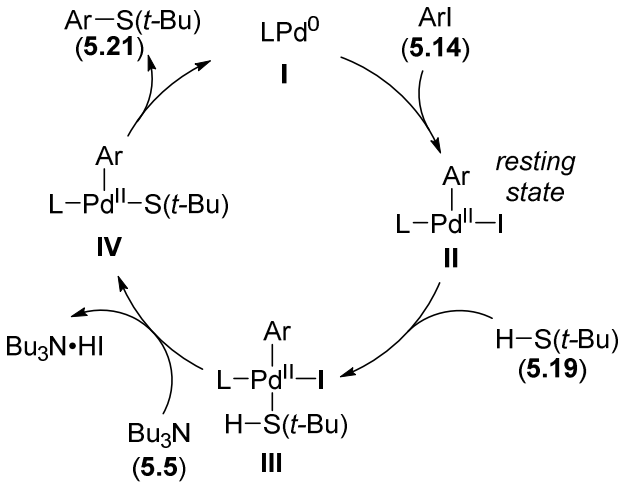

While experiments discussed thus far featured single reaction slugs cycled and analyzed over time, the ability to perform multiple reactions simultaneously, and therefore generate all data necessary for kinetic analysis at the same time, was envisioned. This is especially appealing for slow reactions, where the time required to collect all data is particularly tedious. The Diels-Alder reaction between cyclopentadiene (**5.22**) and methyl acrylate (**5.23**) required ~3 h to reach >80% conversion at 70 °C, making it an ideal candidate to demonstrate this ability. The volume of the residence coils was increased and the three necessary reactions (i.e., "standard conditions", and excess in each reagent) were injected as sequential slugs in a way that allowed the flow path to be altered each time all slugs were in the same residence coil (Figure 5.7).[23] The carrier phase was also changed from N_2 to water to allow the reaction to be conducted above the boiling point of the solvent through application of backpressure, highlighting another benefit of using a flow reactor over a batch setup.[24] In this way, all necessary data for kinetic analysis was collected in ~3 h, as opposed to the ~9 h that would have been required if running each reaction consecutively with this flow reactor, or the ~60 h that would be required to collect equivalent data using the traditional steady-state approach of changing the flow rate to change residence time for each data point.

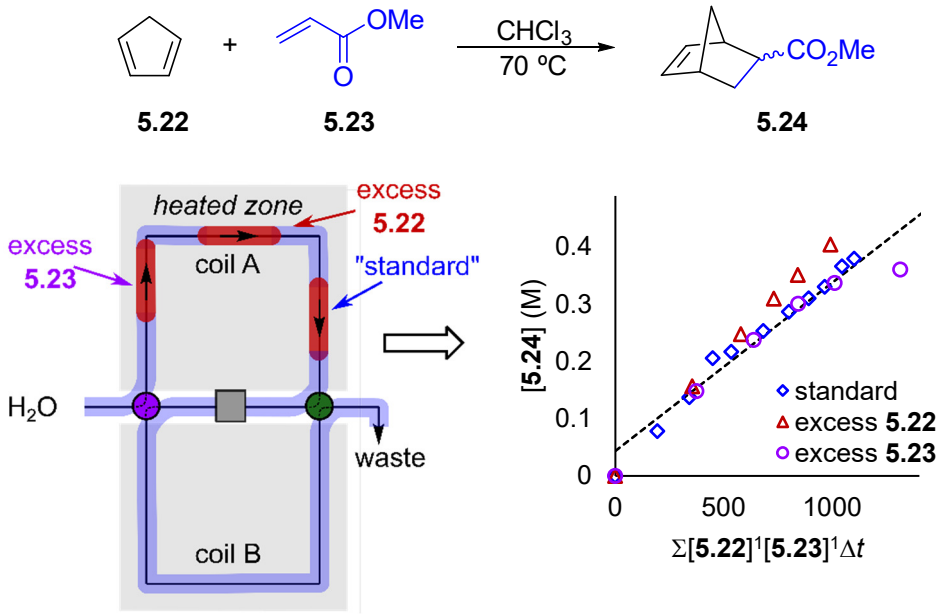

Figure 5.7. Operating with multiple sequential reaction slugs allows monitoring of multiple reactions simultaneously.[a]

While the system has some limitations, in e.g., handling multi-phasic or extremely fast reactions, the ability to efficiently collect reaction progress data in flow, and applicability to a wide range of reactions and conditions holds promise for wide applicability.

5.3 Conclusions

A reactor that allows reaction progress to be monitored over time from a continuously cycling reaction slug has been developed. The reactor performance was assessed over a wide range of temperatures (0–80 °C), solvents (toluene, MeCN, DCM, EtOH, THF, $CHCl_3$) and reactions (acylation, S_NAr, silylation, ethanolysis, C–S cross-coupling, Diels-Alder). The ability to use the reactor to distinguish between potential reaction mechanisms and determine activation parameters was demonstrated. Lastly, the ability to perform multiple reactions simultaneously as consecutive reaction slugs was shown with the kinetic analysis of a Diels-Alder reaction.

[a] Adapted with permission from Sullivan, R. J.; Newman, S. G. *J. Org. Chem.* **2020**, ASAP, doi. 10.1021/acs.joc.0c00216. Copyright 2020 American Chemial Society.

The application of the reactor to collect data for a variety of different methods of kinetic analysis was also demonstrated, including variable time normalization analysis, pseudo-first order kinetics, Eyring plots and the method of initial rates. We believe the development of this reactor marks the first true equivalent in flow to the generation of reaction progress data in batch, where analysis over time from a single reaction solution is the most efficient strategy with regards to both time and material consumption. Therefore, since this reactor combines both the efficiency of the traditional batch sampling strategy with the benefits of flow, we believe this platform will lower the impediment to routine kinetic analysis, through both stand-alone operation and in combination with reaction platforms to automate kinetic experiments and data generation.

5.4 Experimental

5.4.1 General experimental details

Benzoyl chloride (**5.3**), benzyl alcohol (**5.4**), Bu_3N (**5.5**), TBSCl (**5.11**), cyclopentadiene (**5.22**) and methyl acrylate (**5.23**) were distilled before use. All other chemicals were obtained from commercial sources and used as received. THF was degassed with Ar and passed through a PureSolv solvent purification system before use. Solutions for thiol cross-coupling reactions were prepared in oven-dried glassware under an Ar atmosphere.

NMR spectra were collected on a Bruker Avance 400 MHz spectrometer. ^{1}H and ^{13}C were referenced to residual solvent signals. GC yields for all kinetic studies were obtained via 5 or 6-point calibration curves using FID analysis on an Agilent Technologies 7890B GC with 30 m × 0.25 mm HP-5 column. For all reactions analyzed using VTNA or the method of initial rates the concentration of the product was determined by GC-FID using 5-point calibration curves and the remaining reagent concentrations were calculated through mass balance assertion (i.e., stoichiometry). For the ethanolysis reaction the concentration of starting material (1-bromoethylbenzene) was monitored. For quantification of the C–S cross-coupling product **5.21**, the GC response factor (i.e., calibration curve slope) was determined by quantifying the disappearance of aryl iodide **5.14** and monitoring the appearance of the product peak for a reaction where conversion of **5.14** was taken to completion. For calculation of the unreacted cyclopentadiene concentration, both the methyl 5-norbornen-2-carboxylate product and the dicyclopentadiene by-product were quantified and taken into account.

Calculations were performed using the Gaussian 09 software suite.[25] Structures were optimized at the M06-L[26]/def2-SVP[27] level of theory with associated ECP for Pd and I,[28] and confirmed to be local minima or transition states by the presence of 0 or 1 imaginary frequencies respectively. For transition state structures the normal mode vibration corresponding to the imaginary frequency involved the motion of the correct atom(s) along the reaction coordinate in all cases. Energies were calculated at the M06-L/def2-TZVP[27] level of theory on the M06-L/def2-SVP optimized structures and incorporated solvation effects using the polarizable continuum model with THF solvent[29]. Zero-point and thermal corrections were taken from the M06-L/def2-SVP frequency calculations. Et_3N and PhI were used as model substrates for Bu_3N and aryl iodide **5.14** respectively.

5.4.2 Details of flow reactor and equipment

Flow reactor set up for acylation, S_NAr, silylation and ethanolysis experiments

A detailed description of the fluid paths through the valves to achieve cycling of a reaction slug is given in Figure 5.8. A schematic of the entire reactor is shown in Figure 5.9 and a detailed schematic of the tubing connections and volumes is provided in Figure 5.10. All tubing in the reactor was 1/16" O.D., 0.5 mm I.D. PFA with the exception of the N_2 line from the mass flow controller to the reactor which was 1/16" O.D., 0.75 mm I.D. 316 stainless steel (316 SS). PEEK fittings were used for all connections. The cross mixers and two-way valve were made of PEEK. The 6-port, 2-position valves and the 11-port, 10-position selector valve were ChemInert valves from Vici Valco, controlled electronically with both rotational directions operative for the selector valve. All internal channels were 0.4 mm bore (analytical HPLC dimension).

The 11-port, 10-position valve was fitted with a custom rotor, providing the port connectivity shown in Figure 5.11. The use of a 10-position valve is not necessary. This valve was selected based on availability; only six-positions are required so any selector valve with ≥ 6 positions and a suitably fabricated custom rotor to provide the same fluid connectivity would be sufficient.

PEEK fittings and parts were purchased from UpChurch Scientific. Stainless steel fittings and parts were purchased from VICI Valco or Swagelok. Back pressure was provided by using as the receiving flask a 100 mL solvent reservoir equipped with a PTFE cap (Vapourtec) that seals around 1/16" O.D. tubing and connects to a gas supply via a Luer connection. 10 psi of dynamic

pressure was provided by down-regulation of the house compressed air. Photographs of the reactor are provided in Appendix IV (Figures AIV.1–2). A Chemxy fusion 200 dual channel syringe pump equipped with 2.5 mL glass syringes (Hamilton, air-tight) was used for formation of the reaction slug.

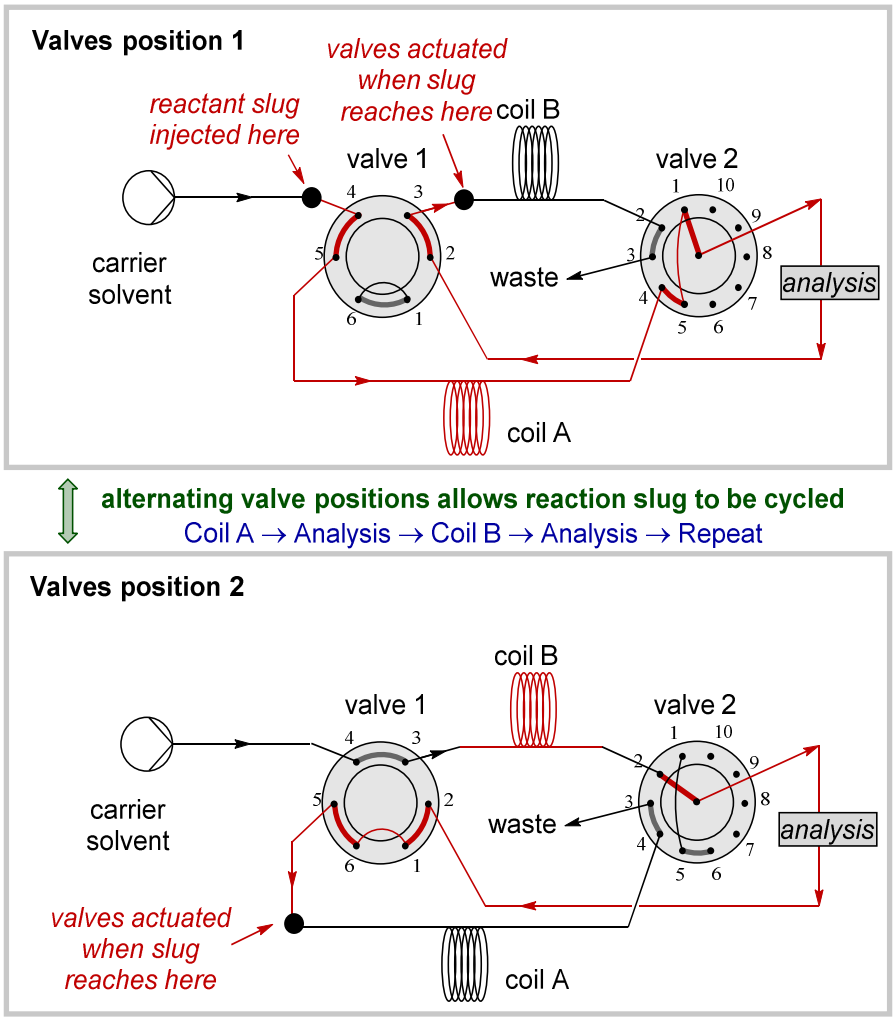

Figure 5.8. Principle of valve operation to cycle reaction slug.

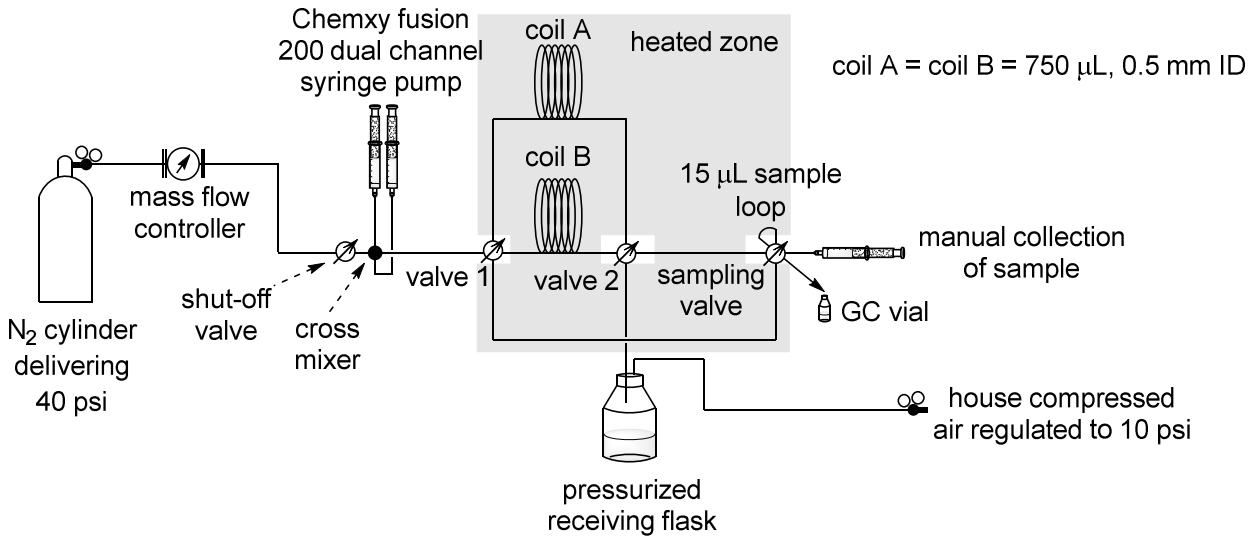

Figure 5.9. Schematic of flow reactor used for the collection of kinetic data for acylation, S_NAr, silylation and ethanolysis reactions.

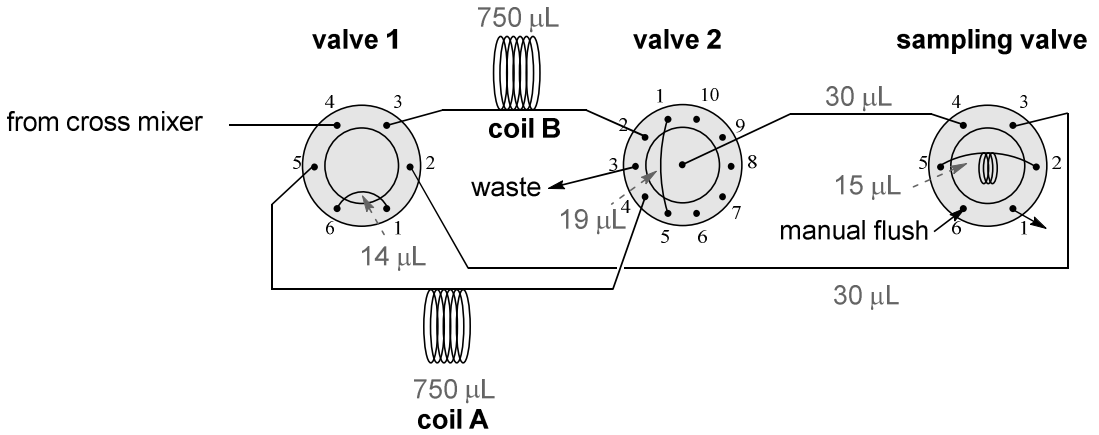

Figure 5.10. Tubing connectivity at the three valves. Ports 7 through 10 of the selector valve are unused and port 6 is plugged.

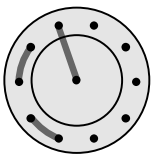

Figure 5.11. Port connectivity of custom rotor used in the 11-port, 10-position valve.

Flow reactor set up for palladium catalyzed thiol etherification experiments

Minimal changes were required to perform the palladium catalyzed reactions under inert atmosphere (Figure 5.12). Specifically, the receiving flask was pressurized with N_2 instead of compressed air and the apparatus was purged with N_2 at 0.8 mL/min for 1 h before experiments were conducted. Additionally, due to the lower concentrations used for the cross-coupling experiments the sampling loop volume was increased from 15 μL to 20 μL to allow collection of larger aliquots.

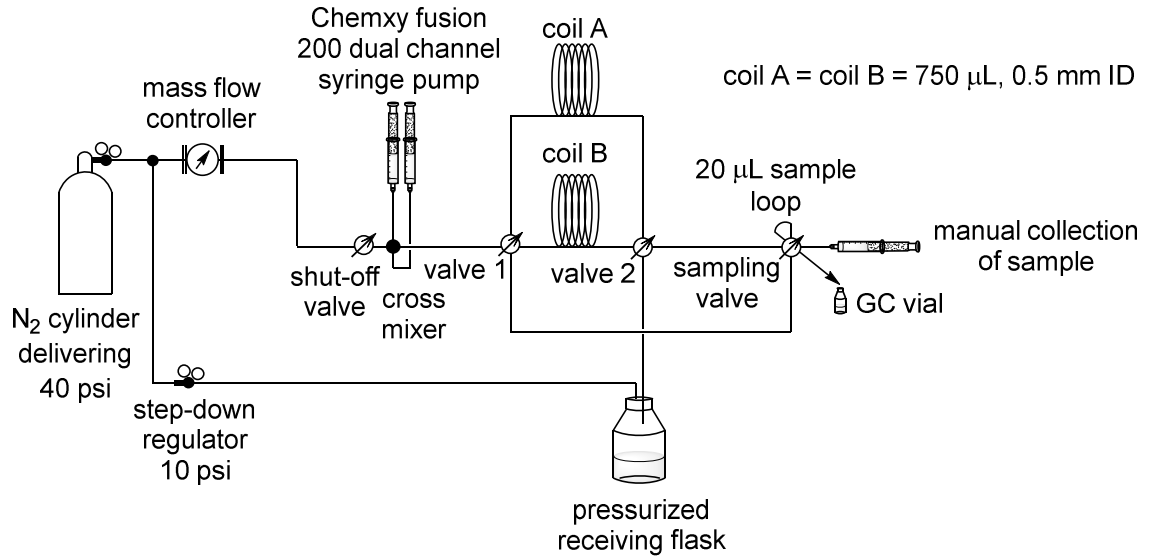

Figure 5.12. Schematic of flow reactor used for the collection of kinetic data for the palladium catalyzed thiol etherification reaction.

Flow reactor set up for cycloaddition experiments

Modifications required for the collection of kinetic data for the cycloaddition reaction were as follows (Figure 5.13–14): The aqueous carrier solvent was delivered by a Hitec-Zang SyrDos 2 continuous dual syringe pump equipped with 0.5 mL glass syringes. A 1.25 mL, 1/16" O.D., 1.0 mm I.D. PFA loading coil with tee mixers before and after was added before the reactor valves to facilitate formation of sequential reaction slugs and initiate the reactions. The two reactor coils (A and B) were changed to 2.0 mL, 1/16" O.D., 1.0 mm I.D. PFA, and a spring-loaded 75 psi back pressure regulator was installed at the reactor exit. PEEK tee-mixers, check valves and back

pressure regulators were purchased from UpChurch Scientific. Photographs of the reactor setup are provided in Figures AIV.3–4 in Appendix IV.

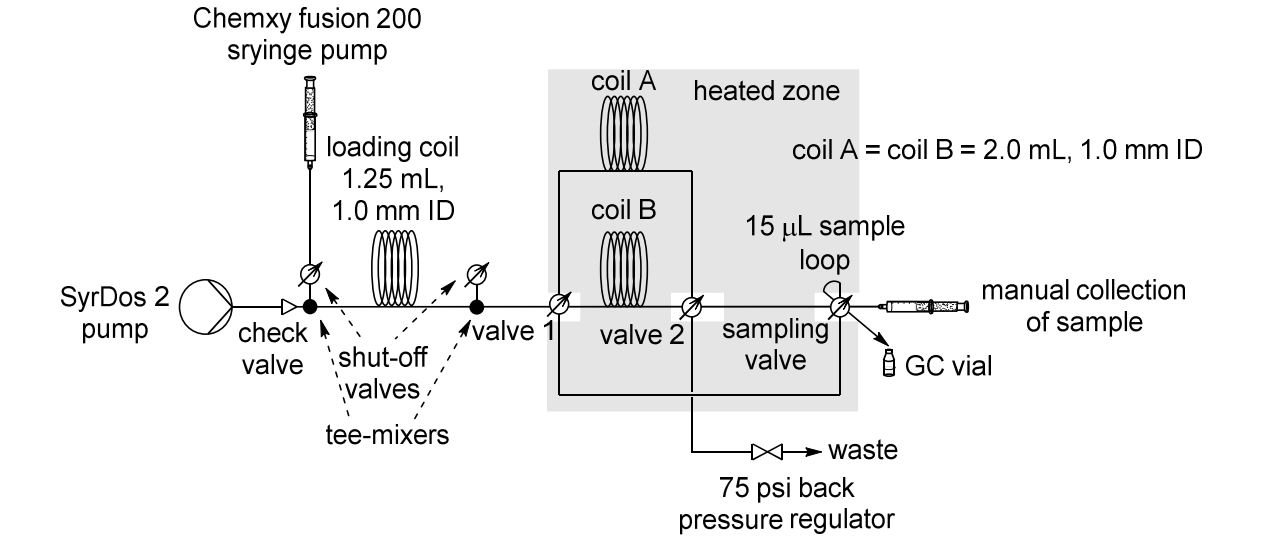

Figure 5.13. Schematic of flow reactor used for the collection of kinetic data for the cycloaddition reaction: Connectivity to load slugs into loading coil.

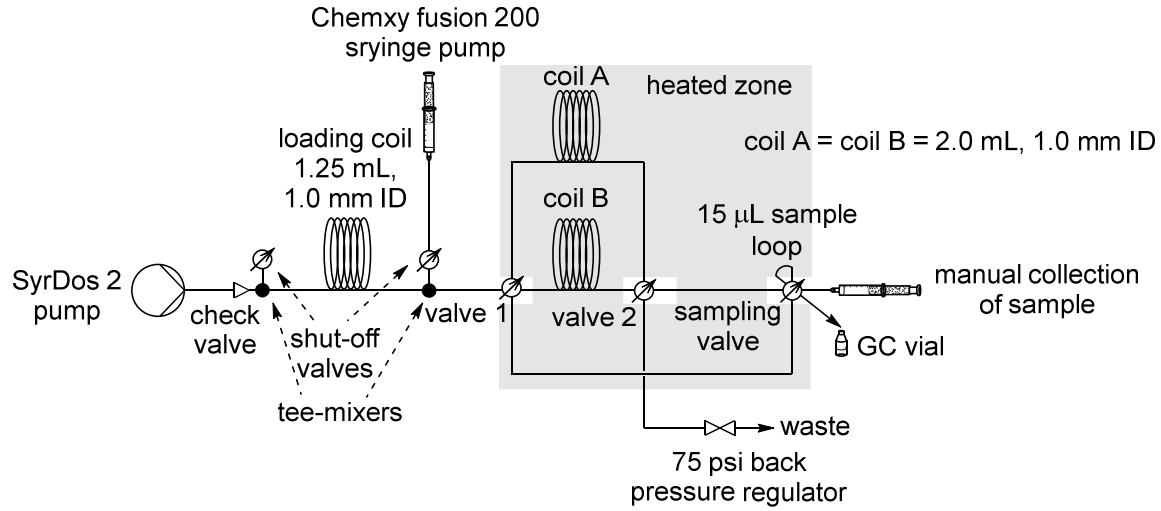

Figure 5.14. Schematic of flow reactor used for the collection of kinetic data for the cycloaddition reaction: Connectivity to initiate reactions and obtain kinetic data.

5.4.3 Preparation of starting and reference materials.

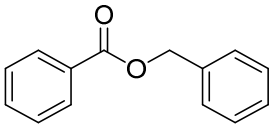

Benzyl benzoate (**5.6**). To a solution of benzoyl chloride (0.56 g, 4.0 mmol) in toluene (5 mL) was added benzyl alcohol (0.47 g, 4.4 mmol) and Et_3N (0.44 g, 4.4 mmol) and stirred 15 min at 40 °C. The resulting suspension was then washed with 1 M HCl (5 mL) and the organic phase dried over Na_2SO_4. Evaporation of the solvent and purification on silica gel (25 × 100 mm, hexanes→5% EtOAc in hexanes eluent) yielded the pure product as a colourless oil. Yield 0.57 g (67%). Characterization data were in agreement with the literature.[30] ^{1}H NMR (400 MHz, $CDCl_3$) 8.09 (d, J = 7.9 Hz, 2H), 7.57 (t, J = 7.3 Hz, 1H), 7.40 (m, 7H), 5.38 (s, 2H). $^{13}C\{^1H\}$ NMR (100 MHz, $CDCl_3$) 166.6, 136.2, 133.2, 130.3, 1298, 128.7, 128.5, 128.4, 128.3, 66.8.

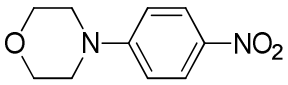

4-(4-Nitrophenyl)morpholine (**5.10**). The reaction solutions used for the generation of the batch kinetic data were combined, EtOAc (20 mL) was added and the organics washed with 2 × 10 mL 1 M HCl then dried over Na_2SO_4. The solvent was evaporated and the residue chromatographed on silica gel (25 × 100 mm, 5:1 hexanes:EtOAc eluent) to provide 0.30 g of the pure product as an orange powder. Characterization data were in agreement with the literature.[12e] ^{1}H NMR (400 MHz, $CDCl_3$) 8.15 (d, J = 9.4 Hz, 2H), 6.84 (d, J =9.4 Hz, 2H), 3.87 (t, J = 5.1 Hz, 4H), 3.37 (t, J = 5.2 Hz, 4H). $^{13}C\{^1H\}$ NMR (100 MHz, $CDCl_3$) 155.1, 139.2, 126.0, 112.8, 66.5, 47.3.

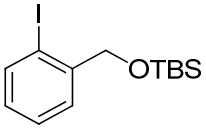

tert-Butyl((2-iodobenzyl)oxy)dimethylsilane (**5.14**). 2-Iodobenzyl alcohol (1.2 g, 5.1 mmol) and TBSCl (0.9 g, 6.0 mmol) were dissolved in 1-methylimidazole (5 mL, 63 mmol) and stirred 10 min at room temperature then 10 min at 35 °C. The solution was diluted with 50 mL 2:1 EtOAc:hexanes and washed with 15 mL 5 M HCl then 2 × 15 mL 1 M HCl and the organic phase dried over Na_2SO_4. The solvent was evaporated and the residue chromatographed on silica gel (25

× 100 mm, hexanes → 5% EtOAc in hexanes eluent) to yield the pure product as a colourless oil. Yield 1.60 g (90%). Characterization data were in agreement with the literature.[12e] ^{1}H NMR (400 MHz, $CDCl_3$): δ 7.77 (d, *J* = 7.8 Hz, 1H), 7.51 (d *J* = 7.7 Hz, 1H), 7.37 (t, *J* = 7.6 Hz, 1H), 6.96 (t, *J* = 7.8, 1H), 4.63 (s, 2H), 0.98 (s, 9H), 0.14 (s, 6H). ^{13}C{^{1}H} NMR (100 MHz, $CDCl_3$): δ 142.9, 138.6, 128.5, 128.2, 127.4, 95.8, 69.4, 26.0, 18.4, –5.3.

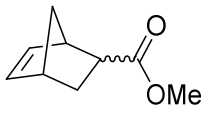

Methyl 5-norbornene-2-carboxylate (**5.24**). Cyclopentadiene (0.93 mL, 11 mmol) and methyl acrylate (0.90 mL, 10 mmol) were combined in $CHCl_3$ (20 mL) and refluxed 4 h. The solvent was evaporated and the residue chromatographed on silica gel to yield the pure product as a colourless oil in ~3:1 mixture of isomers. Yield 0.93 g (61%). Characterization data were in agreement with the literature.[31] ^{1}H NMR (400 MHz, $CDCl_3$) *endo* isomer: 6.18 (dd, *J* = 5.6, 3.0 Hz, 1H), 5.92 (dd, *J* = 5.6, 2.8 Hz, 1H), 3.62 (s, 3H), 3.19 (br s, 1H), 2.94 (m, 1H), 2.90 (br s, 1H), 1.90 (m, 1H), 1.39 (m, 2H), 1.26 (d, *J* = 8.1 Hz, 1H), *exo* isomer: 6.13 (dd, *J* = 5.6, 2.9 Hz, 1H), 6.10 (dd, *J* = 5.6, 3.1 Hz, 1H), 3.68 (s, 3H), 3.03 (br s, 1H), 2.92 (br s, 1H), 2.21 (dd, *J* = 10.3, 4.6 Hz, 1H), 1.90 (m, 1H), 1.52 (d, 8.4 Hz, 1H), 1.39 (m, 2H). ^{13}C{^{1}H} NMR (100 MHz, $CDCl_3$) *endo* isomer: 175.4, 137.9, 132.5, 51.6, 49.7, 45.8, 43.3, 42.6, 29.4, *exo* isomer: 176.9, 138.2, 135.9, 51.8, 46.7, 46.5, 43.1, 41.7, 30.5.

5.4.4 Procedures for flow kinetic experiments

Exemplary procedure: Benzoyl chloride + benzyl alcohol

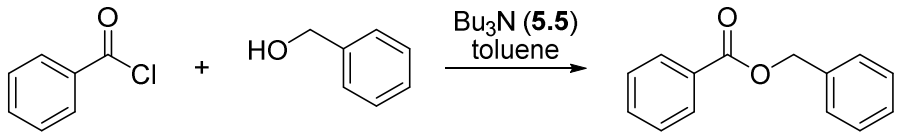

5.3 **5.4** **5.6**

General procedure. Solutions of benzoyl chloride (**5.3**) with hexadecane were prepared in toluene ("electrophile solutions"). Solutions of benzyl alcohol (**5.4**) with Bu_3N (**5.5**) were prepared in toluene ("nucleophile solutions"). For each reaction, 0.5 mL of desired electrophile solution and 0.5 mL of desired nucleophile solution were separately loaded into two 2.5 mL Hamilton glass

syringes, installed onto the Chemxy fusion 200 dual channel syringe pump and primed, then connected cross-mixer of the flow reactor (Figure 5.9).

The N_2 flow was set to 3 mL/min for 2 min (to quickly establish pressure equilibration with the back pressure) then set to 0.8 mL/min. Valve 1 was set to position 1, valve 2 was set to position 1 (see Figure 5.8) and the sampling valve was set to collect a sample. The 2-way valve was closed (to interrupt the N_2 flow) and 0.15 mL of each solution was dispensed by the syringe pump at a rate of 1.5 mL/min to form a 0.30 mL the reaction slug (~5 s). The 2-way valve was opened to let the reaction slug travel through coil A to valve 2 to the sampling valve.

Once ~50 µL of the slug passed through the sampling valve, the valve was actuated and a 15 µL aliquot sample was eluted with 600 µL EtOAc into a GC vial containing 100 µL MeOH to quench. Once the remainder of the reaction slug had exited the sampling valve and fully passed through valve 1 to coil B, valve 1 was set to position 2, valve 2 was set to position 2 (clockwise rotation) and the sampling valve was set to collect a sample again.

Notes: 1) Valve 1 is actuated before valve 2 to maintain N_2 pressure behind the reaction slug. If valves are actuated in reverse order, pressure is released behind the reaction slug causing interruptions to the flow. 2) The sampling valve is actuated at this time to empty the sample loop before the reaction slug returns to the valve and prevent contamination/dilution of the reaction slug with the solvent used to flush the sample loop by sending the contents of the sample loop through the other reactor coil to waste.

The reaction slug travelled through coil B, passing through valve 2 to the sampling valve. As with the first sample, once the first ~50 µL of the reaction slug had passed through the sampling valve it was actuated to collect the second sample which was quenched into a new GC vial in the same manner as the first sample. Again, after the reaction slug had fully passed though the sampling valve and valve 1, the valves were actuated: valve 1 to position 1, valve 2 to position 1 (counter-clockwise rotation), and the sampling valve to collect a new sample.

This sequence of sample collection + valve actuation was repeated to collect subsequent samples. To increase the time increment between samples, the flow rate of N_2 was decreased to 0.4 mL/min after the 3rd sample was collected and to 0.2 mL/min after the 6th sample was collected. This procedure allowed the collection of aliquots at approximately 1:45, 4:15, 6:30, 10:15, 14:45,

19:00, 29:30 and 40:45 min (the exact collection time of each sample was recorded and used for the subsequent data analysis).

Electrophile solution 1: **5.3** (116 µL, 1.0 mmol), hexadecane (59 µL, 0.20 mmol) made up to 1.00 mL with toluene.

Electrophile solution 2: **5.3** (232 µL, 2.0 mmol), hexadecane (59 µL, 0.20 mmol) made up to 1.00 mL with toluene.

Nucleophile solution 1: **5.4** (103 µL, 1.0 mmol), **5.5** (286 µL, 1.2 mmol) made up to 1.00 mL with toluene.

Nucleophile solution 2: **5.4** (207 µL, 2.0 mmol), **5.5** (286 µL, 1.2 mmol) made up to 1.00 mL with toluene.

Nucleophile solution 3: **5.4** (103 µL, 1.0 mmol), **5.5** (572 µL, 2.0 mmol) made up to 1.00 mL with toluene.

Reaction 1. Electrophile solution 1 + nucleophile solution 1: 0.50 M **5.3**, 0.50 M **5.4**, 0.60 M **5.5**.

Reaction 2. Electrophile solution 2 + nucleophile solution 1: 1.0 M **5.3**, 0.50 M **5.4**, 0.60 M **5.5**.

Reaction 3. Electrophile solution 1 + nucleophile solution 2: 0.50 M **5.3**, 1.0 M **5.4**, 0.60 M **5.5**.

Reaction 4. Electrophile solution 1 + nucleophile solution 3: 0.50 M **5.3**, 0.50 M **5.4**, 1.0 M **5.5**.

1-Fluoro-4-nitrobenzene + morpholine

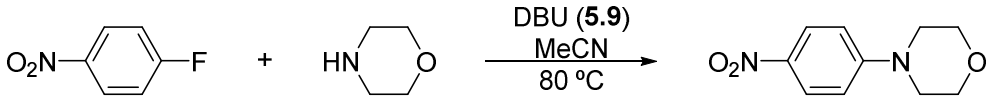

5.7 **5.8** **5.10**

General procedure. Solutions of **5.7** with hexadecane were prepared in MeCN ("electrophile solutions"). Solutions of **5.8** with **5.9** were prepared in MeCN ("nucleophile solutions"). For each reaction, 0.5 mL of the desired electrophile solution and 0.5 mL of the desired nucleophile solution were separately loaded into two 2.5 mL Hamilton glass syringes, installed onto the Chemxy fusion 200 dual channel syringe pump, primed, and connected to the cross-mixer of the flow reactor (see Figure 5.9). The reactor coils were submerged in an 80 °C water bath. The valves were not submerged but placed just above the surface of the water.

Reaction slugs were formed as in the exemplary procedure and the initial N_2 flow rate was the same at 0.8 mL/min. Valve operation was identical. Samples were manually collected into GC vials using 600 μL of MeCN to elute from the sample loop, quenching by dilution and cooling. After the first two samples had been collected the N_2 flow was set to 0.5 mL/min, then after two more samples had been collected N_2 flow was set to 0.2 mL/min and 4 more samples were collected. This allowed collection of reaction aliquots at approximately 1:20, 3:00, 5:30, 8:15, 16:15, 25:00, 35:00 and 44:00 min (the exact collection time of each sample was recorded and used for the subsequent data analysis).

Electrophile solution 1: **5.7** (106 μL, 1.0 mmol), 1,3,5-trimethoxybenzene (134 mg, 0.80 mmol) made up to 1.00 mL with MeCN.

Electrophile solution 2: **5.7** (212 μL, 2.0 mmol), 1,3,5-trimethoxybenzene (135 mg, 0.80 mmol) made up to 1.00 mL with MeCN.

Nucleophile solution 1: **5.8** (87 μL, 1.0 mmol), **5.9** (150 μL, 1.0 mmol) made up to 1.00 mL with MeCN.

Nucleophile solution 2: **5.8** (174 μL, 2.0 mmol), **5.9** (150 μL, 1.0 mmol) made up to 1.00 mL with MeCN.

Nucleophile solution 3: **5.8** (87 μL, 1.0 mmol), **5.9** (300 μL, 2.0 mmol) made up to 1.00 mL with MeCN.

Reaction 1. Electrophile solution 1 + nucleophile solution 1: 0.50 M **5.7**, 0.50 M **5.8**, 0.50 M **5.9**.

Reaction 2. Electrophile solution 2 + nucleophile solution 1: 1.0 M **5.7**, 0.50 M **5.8**, 0.50 M **5.9**.

Reaction 3. Electrophile solution 1 + nucleophile solution 2: 0.50 M **5.7**, 1.0 M **5.8**, 0.50 M **5.9**.

Reaction 4. Electrophile solution 1 + nucleophile solution 3: 0.50 M **5.7**, 0.50 M **5.8**, 1.0 M **5.9**.

TBSCl and 2-iodobenzyl alcohol

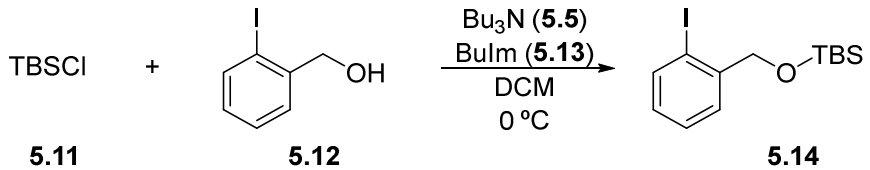

5.11 **5.12** **5.14**

General procedure. Solutions of TBSCl (**5.11**) with hexadecane were prepared in DCM (electrophile solutions). Solutions of alcohol **5.12** with Bu_3N (**5.5**) and BuIm (**5.13**) were prepared in DCM (nucleophile solutions). For each reaction 0.5 mL of desired electrophile solution and 0.5 mL of desired nucleophile solution were separately loaded into two 2.5 mL Hamilton glass syringes, installed onto the Chemxy fusion 200 dual channel syringe pump and primed, then connected cross-mixer of the flow reactor (Figure 5.9). The reactor coils were submerged in a 0 °C ice-water bath. The valves were not submerged but placed just above the surface of the bath.

Reaction slugs were formed as in the exemplary procedure and the initial N_2 flow rate was the same at 0.8 mL/min. Valve operation was identical. Samples were manually collected into GC vials containing 100 μL MeOH for quench using 600 μL of EtOAc to elute from the sample loop. After the first three samples had been collected the N_2 flow was set to 0.4 mL/min and an additional 5 samples were collected. This allowed collection of reaction aliquots at approximately 1:40, 3:40, 5:50, 9:40, 14:20, 18:40, 23:20 and 27:40 min (the exact collection time of each sample was recorded and used for the subsequent data analysis).

Electrophile solution 1: **5.11** (1.50 g, 10 mmol) and hexadecane (586 μL, 2.0 mmol) was made up to 10.00 mL with DCM.

Electrophile solution 2: 0.55 mL of electrophile solution 1 and hexadecane (264 μL, 0.090 mmol) was made up to 10.00 mL with DCM.

Nucleophile solution 1: **5.12** (116 mg, 0.50 mmol), **5.5** (143 μL, 0.60 mmol), **5.13** (6.6 μL, 0.050 mmol) made up to 0.50 mL with DCM.

Nucleophile solution 2: **5.12** (117 mg, 0.50 mmol), **5.5** (143 μL, 0.60 mmol), **5.13** (3.3 μL, 0.025 mmol) made up to 0.50 mL with DCM.

Nucleophile solution 3: **5.12** (176 mg, 0.75 mmol), **5.5** (143 μL, 0.60 mmol), **5.13** (6.6 μL, 0.050 mmol) made up to 0.50 mL with DCM.

Nucleophile solution 4: **5.12** (117 mg, 0.50 mmol), **5.5** (238 μL, 1.0 mmol), **5.13** (6.6 μL, 0.050 mmol) made up to 0.50 mL with DCM.

Reaction 1. Electrophile solution 2 + nucleophile solution 1: 0.28 M **5.11**, 0.25 M **5.12**, 0.30 M **5.5**, 0.025 M **5.13**.

Reaction 2. Electrophile solution 2 + nucleophile solution 2: 0.28 M **5.11**, 0.25 M **5.12**, 0.30 M **5.5**, 0.013 M **5.13**.

Reaction 3. Electrophile solution 2 + nucleophile solution 3: 0.28 M **5.11**, 0.38 M **5.12**, 0.30 M **5.5**, 0.025 M **5.13**.

Reaction 4. Electrophile solution 2 + nucleophile solution 4: 0.28 M **5.11**, 0.25 M **5.12**, 0.50 M **5.5**, 0.025 M **5.13**.

Reaction 5. Electrophile solution 1 + nucleophile solution 4: 0.50 M **5.11**, 0.25 M **5.12**, 0.50 M **5.5**, 0.025 M **5.13**.

1-Bromoethylbenzene and EtOH

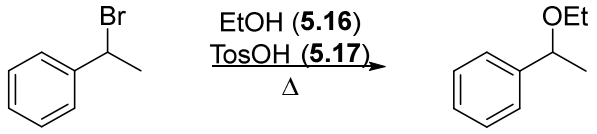

5.15 **5.18**

General procedure. A 1.0 M solution of 1-bromoethylbezene (**5.15**) was prepared in EtOH or EtOH:*t*-BuOH mixture ("electrophile solutions") and loaded into a 2.5 mL Hamilton glass syringe (no background reaction was observed at room temperature over several hours). Solutions of TosOH (**5.17**) in EtOH or EtOH:*t*-BuOH mixture were prepared and loaded into a second 2.5 mL Hamilton glass syringe. The two syringes were installed onto the Chemxy fusion 200 dual channel syringe pump, primed, and connected to the cross-mixer of the flow reactor (Figure 5.9). The reactor coils were submerged in the water bath at desired reaction temperature. The valves were placed just above the surface of the water bath.

Reaction slugs were formed as in the exemplary procedure. The initial N_2 flow rate was varied depending on the reaction temperature used and are given below for each reaction temperature. Valve operation was identical. Samples were manually collected into GC vials using 600 μL of MeCN to elute from the sample loop, quenching by dilution and cooling.

Electrophile solution 1: **5.15** (273 μL, 2.0 mmol), 1,3,5-trimethoxybenzene (269 mg, 1.6 mmol) made up to 2.00 mL with EtOH.

Electrophile solution 2: **5.15** (136 μL, 1.0 mmol), 1,3,5-trimethoxybenzene (135 mg, 0.80 mmol) made up to 1.00 mL with 4:1 EtOH:*t*-BuOH.

Electrophile solution 3: **5.15** (136 μL, 1.0 mmol), 1,3,5-trimethoxybenzene (137 mg, 0.80 mmol) made up to 1.00 mL with 10:1 EtOH:t-BuOH.

TosOH solution 1: **5.17** (95 mg, 0.50 mmol) made up to 2.00 mL with EtOH.

TosOH solution 2: **5.17** (96 mg, 0.50 mmol) made up to 10.00 mL with EtOH.

TosOH solution 3: **5.17** (47 mg, 0.25 mmol) made up to 1.00 mL with 4:1 EtOH:*t*-BuOH.

TosOH solution 4: **5.17** (46 mg, 0.25 mmol) made up to 1.00 mL with 10:1 EtOH:*t*-BuOH.

Reaction 1. Electrophile solution 1 + TosOH solution 1, 40 °C. N_2 flow 0.5 mL/min, samples collected at 3:30, 6:20, 9:30 min then N_2 flow decreased to 0.2 mL/min, samples collected at 17:45, 29:00, 40:00, 51:00 min.

Reaction 2. Electrophile solution 1 + TosOH solution 1, 50 °C. N_2 flow 0.5 mL/min, samples collected at 2:15, 5:15, 8:15, 11:15 min then N_2 flow decreased to 0.2 mL/min, samples collected at 16:20, 23:10, 29:00, 34:45, 40:20, 46:00 min.

Reaction 3. Electrophile solution 1 + TosOH solution 1, 60 °C. N_2 flow 0.6 mL/min, samples collected at 2:00, 4:15, 6:40 min then N_2 flow decreased to 0.4 mL/min, samples collected at 10:00, 14:00, 17:45 min then N_2 flow decreased to 0.3 mL/min, samples collected at 23:00, 28:30, 34:10, 39:30, 45:10 min.

Reaction 4. Electrophile solution 1 + TosOH solution 1, 70 °C. N_2 flow 0.6 mL/min, samples collected at 1:45, 4:00, 6:30 min then N_2 flow decreased to 0.4 mL/min, samples collected at 9:40, 13:30, 17:00 min then N_2 flow decreased to 0.3 mL/min, samples collected at 22:20, 27:15, 32:45, 37:45 min.

Reaction 5. Electrophile solution 1 + TosOH solution 1, 80 °C. N_2 flow 0.7 mL/min, samples collected at 1:30, 3:30, 5:30 min then N_2 flow decreased to 0.5 mL/min, samples collected at 7:45, 10:30, 13:15 min then N_2 flow decreased to 0.3 mL/min, samples collected at 18:00, 23:15, 28:15 min.

Reaction 6. Electrophile solution 1 + TosOH solution 2, 70 °C. N_2 flow 0.6 mL/min, samples collected at 1:45, 4:15, 6:50 min then N_2 flow decreased to 0.4 mL/min, samples collected at 10:30, 14:45, 19:00 min then N_2 flow decreased to 0.3 mL/min, samples collected at 24:10, 30:15, 36:30 min.

Reaction 7. Electrophile solution 2 + TosOH solution 3, 70 °C. N_2 flow 0.6 mL/min, samples collected at 1:45, 4:10, 6:35 min then N_2 flow decreased to 0.4 mL/min, samples collected at 10:00, 14:20, 18:15 min then N_2 flow decreased to 0.3 mL/min, samples collected at 23:30, 29:00, 34:30, 29:50 min.

Reaction 8. Electrophile solution 3 + TosOH solution 4, 70 °C. N_2 flow 0.6 mL/min, samples collected at 1:50, 4:15, 6:45 min then N_2 flow decreased to 0.4 mL/min, samples collected at 9:50, 14:00, 17:40 min then N_2 flow decreased to 0.3 mL/min, samples collected at 23:00, 28:20, 33:50, 39:50 min.

TBS protected 2-iodobenzyl alcohol and *t*-BuSH

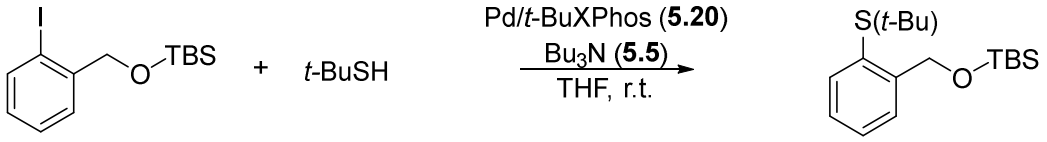

5.14 **5.19** **5.21**

General procedure. Solutions were prepared under Ar in oven dried glassware. A stock solution of Pd(*t*-BuXPhos)(allyl)Cl was prepared by combining $[PdCl(allyl)]_2$ (**5.28**) and *t*-BuXPhos (**5.29**) in THF and aging 10 min ("catalyst solution"). Solutions of TBS protected 2-iodobenzyl alcohol (**5.14**), *t*-BuSH (**5.19**), Bu_3N (**5.5**) and hexadecane were prepared in THF ("substrate solutions"). The reactor was purged with N_2 at 0.8 mL/min for 1 h before experiments were conducted. For each reaction, 0.5 mL of desired catalyst solution and 0.5 mL of desired substrate solution were separately loaded into two 2.5 mL Hamilton glass syringes, installed onto the Chemxy fusion 200 dual channel syringe pump, primed, and connected to the cross-mixer of the flow reactor (Figure 5.12).

Reaction slugs were formed as in the exemplary procedure and the initial N_2 flow rate was the same at 0.8 mL/min. Valve operation was identical. Samples were manually collected into GC vials using 600 μL of EtOAc to elute from the sample loop, quenching by dilution. Five samples were collected at approximately 1:30, 3:25, 5:25, 7:20 and 9:10 min (the exact collection time of each sample was recorded and used for the subsequent data analysis).

Order in catalyst experiments:

Catalyst solution 1: $[PdCl(allyl)]_2$ (**5.28**, 5.7 mg, 0.016 mmol) and *t*-BuXPhos (**5.29**,13.6 mg, 0.032 mmol) were made up to 4.00 mL with THF.

Catalyst solution 2: 0.75 mL of catalyst solution 1 was diluted to 1.00 mL with THF.

Catalyst solution 3: 0.50 mL of catalyst solution 1 was diluted to 1.00 mL with THF.

Catalyst solution 4: 0.50 mL of catalyst solution 1 was diluted to 2.00 mL with THF.

Catalyst solution 5: 0.50 mL of catalyst solution 4 was diluted to 1.00 mL with THF.

Substrate solution 1: **5.14** (52 μL, 70 mg, 0.20 mmol), **5.19** (34 μL, 0.30 mmol), **5.5** (95 μL, 0.40 mmol), hexadecane (58 μL, 0.20 mmol) made up to 2.00 mL with THF.

Reaction 1. Catalyst solution 2 + substrate solution 1: 0.050 M **5.14**, 0.075 M **5.19**, 0.10 M **5.5**, 0.0030 M Pd(*t*-BuXPhos)(allyl)Cl (6%).

Reaction 2. Catalyst solution 3 + substrate solution 1: 0.050 M **5.14**, 0.075 M **5.19**, 0.10 M **5.5**, 0.0020 M Pd(*t*-BuXPhos)(allyl)Cl (4%).

Reaction 3. Catalyst solution 4 + substrate solution 1: 0.050 M **5.14**, 0.075 M **5.19**, 0.10 M **5.5**, 0.0010 M Pd(*t*-BuXPhos)(allyl)Cl (2%).

Reaction 4. Catalyst solution 5 + substrate solution 1: 0.050 M **5.14**, 0.075 M **5.19**, 0.10 M **5.5**, 0.00050 M Pd(*t*-BuXPhos)(allyl)Cl (1%).

Order in ArI experiments:

Catalyst solution 1: **5.28** (4.3 mg, 0.012 mmol) and **5.29** (10.1 mg, 0.024 mmol) were made up to 4.00 mL with THF.

Substrate solution 1: **5.14** (39 μL, 52 mg, 0.15 mmol), **5.19** (8.4 μL, 0.075 mmol), **5.5** (24 μL, 0.10 mmol), hexadecane (15 μL, 0.05 mmol) made up to 0.50 mL with THF.

Substrate solution 2: **5.14** (26 μL, 35 mg, 0.10 mmol), **5.19** (8.4 μL, 0.075 mmol), **5.5** (24 μL, 0.10 mmol), hexadecane (15 μL, 0.05 mmol) made up to 0.50 mL with THF.

Substrate solution 3: **5.14** (13 μL, 17 mg, 0.050 mmol), **5.19** (8.4 μL, 0.075 mmol), **5.5** (24 μL, 0.10 mmol), hexadecane (15 μL, 0.050 mmol) made up to 0.50 mL with THF.

Substrate solution 4: **5.14** (6.5 μL, 9 mg, 0.025 mmol), **5.19** (8.4 μL, 0.075 mmol), **5.5** (24 μL, 0.10 mmol), hexadecane (15 μL, 0.050 mmol) made up to 0.50 mL with THF.

Substrate solution 5: **5.14** (3.2 μL, 4 mg, 0.013 mmol), **5.19** (8.4 μL, 0.075 mmol), **5.5** (24 μL, 0.10 mmol), hexadecane (15 μL, 0.050 mmol) made up to 0.50 mL with THF.

Reaction 1. Catalyst solution 1 + substrate solution 1: 0.15 M **5.14**, 0.075 M **5.19**, 0.10 M **5.5**, 0.0030 M Pd(*t*-BuXPhos)(allyl)Cl.

Reaction 2. Catalyst solution 1 + substrate solution 2: 0.10 M **5.14**, 0.075 M **5.19**, 0.10 M **5.5**, 0.0030 M Pd(*t*-BuXPhos)(allyl)Cl.

Reaction 3. Catalyst solution 1 + substrate solution 3: 0.050 M **5.14**, 0.075 M **5.19**, 0.10 M **5.5**, 0.0030 M Pd(*t*-BuXPhos)(allyl)Cl.

Reaction 4. Catalyst solution 1 + substrate solution 4: 0.025 M **5.14**, 0.075 M **5.19**, 0.10 M **5.5**, 0.0030 M Pd(*t*-BuXPhos)(allyl)Cl.

Reaction 5. Catalyst solution 1 + substrate solution 5: 0.013 M **5.14**, 0.075 M **5.19**, 0.10 M **5.5**, 0.0030 M Pd(*t*-BuXPhos)(allyl)Cl.

Order in *t*-BuSH experiments:

Catalyst solution 1: **5.28** (4.3 mg, 0.012 mmol) and **5.29** (10.2 mg, 0.024 mmol) were made up to 4.00 mL with THF.

Substrate solution 1: **5.14** (13 μL, 17 mg, 0.050 mmol), **5.19** (34 μL, 0.30 mmol), **5.5** (24 μL, 0.10 mmol), hexadecane (15 μL, 0.050 mmol) made up to 0.50 mL with THF.

Substrate solution 2: **5.14** (13 μL, 17 mg, 0.050 mmol), **5.19** (17 μL, 0.15 mmol), **5.5** (24 μL, 0.10 mmol), hexadecane (15 μL, 0.050 mmol) made up to 0.50 mL with THF.

Substrate solution 3: **5.14** (13 μL, 17 mg, 0.050 mmol), **5.19** (8.4 μL, 0.075 mmol), **5.5** (24 μL, 0.10 mmol), hexadecane (15 μL, 0.050 mmol) made up to 0.50 mL with THF.

Substrate solution 4: **5.14** (13 μL, 17 mg, 0.050 mmol), **5.19** (4.2 μL, 0.038 mmol), **5.5** (24 μL, 0.10 mmol), hexadecane (15 μL, 0.050 mmol) made up to 0.50 mL with THF.

Substrate solution 5: **5.14** (13 μL, 17 mg, 0.050 mmol), **5.19** (2.1 μL, 0.019 mmol), **5.5** (24 μL, 0.10 mmol), hexadecane (15 μL, 0.050 mmol) made up to 0.50 mL with THF.

Substrate solution 6: **5.14** (13 μL, 17 mg, 0.050 mmol), **5.19** (1.0 μL, 0.0094 mmol), **5.5** (24 μL, 0.10 mmol), hexadecane (15 μL, 0.050 mmol) made up to 0.50 mL with THF.

Reaction 1. Catalyst solution 1 + substrate solution 1: 0.050 M **5.14**, 0.30 M **5.19**, 0.10 M **5.5**, 0.0030 M Pd(*t*-BuXPhos)(allyl)Cl.

Reaction 2. Catalyst solution 1 + substrate solution 2: 0.050 M **5.14**, 0.15 M **5.19**, 0.10 M **5.5**, 0.0030 M Pd(*t*-BuXPhos)(allyl)Cl.

Reaction 3. Catalyst solution 1 + substrate solution 3: 0.050 M **5.14**, 0.075 M **5.19**, 0.10 M **5.5**, 0.0030 M Pd(*t*-BuXPhos)(allyl)Cl.

Reaction 4. Catalyst solution 1 + substrate solution 4: 0.050 M **5.14**, 0.038 M **5.19**, 0.10 M **5.5**, 0.0030 M Pd(*t*-BuXPhos)(allyl)Cl.

Reaction 5. Catalyst solution 1 + substrate solution 5: 0.050 M **5.14**, 0.019 M **5.19**, 0.10 M **5.5**, 0.0030 M Pd(*t*-BuXPhos)(allyl)Cl.

Reaction 6. Catalyst solution 1 + substrate solution 6: 0.050 M **5.14**, 0.0094 M **5.19**, 0.10 M **5.5**, 0.0030 M Pd(*t*-BuXPhos)(allyl)Cl.

Order in Bu_3N experiments:

Catalyst solution 1: **5.28** (4.2 mg, 0.012 mmol) and **5.29** (10.0 mg, 0.024 mmol) were made up to 4.00 mL with THF.

Substrate solution 1: **5.14** (13 μL, 17 mg, 0.050 mmol), **5.19** (8.4 μL, 0.075 mmol), **5.5** (36 μL, 0.15 mmol), hexadecane (15 μL, 0.050 mmol) made up to 0.50 mL with THF.

Substrate solution 2: **5.14** (13 μL, 17 mg, 0.050 mmol), **5.19** (8.4 μL, 0.075 mmol), **5.5** (24 μL, 0.10 mmol), hexadecane (15 μL, 0.050 mmol) made up to 0.50 mL with THF.

Substrate solution 3: **5.14** (13 μL, 17 mg, 0.050 mmol), **5.19** (8.4 μL, 0.075 mmol), **5.5** (12 μL, 0.050 mmol), hexadecane (15 μL, 0.050 mmol) made up to 0.50 mL with THF.

Substrate solution 4: **5.14** (13 μL, 17 mg, 0.050 mmol), **5.19** (8.4 μL, 0.075 mmol), **5.5** (6 μL, 0.025 mmol), hexadecane (15 μL, 0.050 mmol) made up to 0.50 mL with THF.

Substrate solution 5: **5.14** (13 μL, 17 mg, 0.050 mmol), **5.19** (8.4 μL, 0.075 mmol), **5.5** (3 μL, 0.013 mmol), hexadecane (15 μL, 0.050 mmol) made up to 0.50 mL with THF.

Reaction 1. Catalyst solution 1 + substrate solution 1: 0.050 M **5.14**, 0.075 M **5.19**, 0.15 M **5.5**, 0.0030 M Pd(*t*-BuXPhos)(allyl)Cl.

Reaction 2. Catalyst solution 1 + substrate solution 2: 0.050 M **5.14**, 0.075 M **5.19**, 0.10 M **5.5**, 0.0030 M Pd(*t*-BuXPhos)(allyl)Cl.

Reaction 3. Catalyst solution 1 + substrate solution 3: 0.050 M **5.14**, 0.075 M **5.19**, 0.050 M **5.5**, 0.0030 M Pd(*t*-BuXPhos)(allyl)Cl.

Reaction 4. Catalyst solution 1 + substrate solution 4: 0.050 M **5.14**, 0.075 M **5.19**, 0.025 M **5.5**, 0.0030 M Pd(*t*-BuXPhos)(allyl)Cl.

Reaction 5. Catalyst solution 1 + substrate solution 5: 0.050 M **5.14**, 0.075 M **5.19**, 0.013 M **5.5**, 0.0030 M Pd(*t*-BuXPhos)(allyl)Cl.

Cyclopentadiene and methyl acrylate

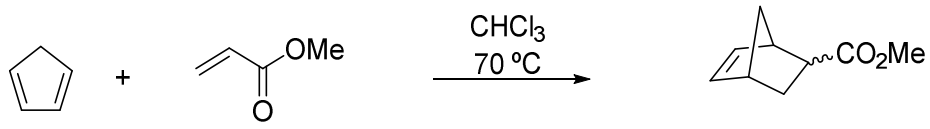

5.22 **5.23** **5.24**

Solutions of methyl acrylate (**5.23**) with hexadecane were prepared in $CHCl_3$ ("acrylate solutions"). A 2.25 M solution of cyclopentadiene (**5.22**) in $CHCl_3$ was prepared by diluting freshly distilled **5.22** (189 µL, 2.25 mmol) up to 1.00 mL with $CHCl_3$ ("diene solution").

Acrylate solution 1: **5.23** (34 µL, 0.38 mmol), hexadecane (22 µL, 0.075 mmol) up to 0.50 mL with $CHCl_3$.

Acrylate solution 2: **5.23** (68 µL, 0.75 mmol), hexadecane (22 µL, 0.075 mmol) up to 0.50 mL with $CHCl_3$.

Acrylate solution 3: **5.23** (68 µL, 0.75 mmol), hexadecane (44 µL, 0.15 mmol) up to 0.50 mL with $CHCl_3$.

Slugs were loaded into the loading coil by taking the desired acrylate solution into a 2.5 mL Hamilton glass syringe, installing on the Fusion 200 syringe pump, priming and then connecting to the first tee-mixer (Figure 5.13). The slugs were loaded as follows: 333 µL of

acrylate solution 1, 150 μL of H_2O, 333 μL of acrylate solution 2, 150 μL of H_2O, 167 μL of acrylate solution 3, 50 μL of H_2O.

The diene solution was then loaded into a 2.5 mL Hamilton glass syringe, installed on the Fusion 200 syringe pump and primed. The syringe was then connected to the second tee-mixer (Figure 5.14) and 50 μL was eluted to prime the tubing.

Reactor valves were set to the following positions: Valve 1, position 1; valve 2, position 1; sampling valve set to collect sample and the reactor coils were lowered into a 70 °C water bath.

The SyrDos pump was started at 200 μL/min until the dienophile solution 1 slug approached the second tee-mixer. The SyrDos flow rate was then decreased to 133 μL/min and the diene solution was delivered at 67 μL/min to give a 0.5 mL reaction slug 0.50 M in **5.23** and 0.75 M in **5.22**. After the dienophile solution 1 slug completely exited the loading coil the SyrDos flow rate was set to 200 μL/min again and the diene pump was stopped.

Once the dienophile solution 2 slug approached the second tee-mixer the SyrDos flow rate was again set to 133 μL/min and the diene solution was delivered at a rate of 67 μL/min, initiating the second 0.5 mL reaction slug that was 1.0 M in **5.23** and 0.75 M in **5.22**. After the dienophile solution 2 slug completely exited the loading coil the SyrDos flow rate was set back to 200 μL/min again and the diene pump was stopped.

As the last slug (dienophile solution 3) approached the second tee-mixer, the SyrDos flow rate was decreased to 67 μL/min and the diene solution was delivered at 133 μL/min, initiating the last 0.5 mL reaction slug that was 0.50 M in **5.23** and 1.5 M in **5.22**. After the dienophile solution 3 slug completely exited the loading coil the SyrDos pump was set to 200 μL/min again and the diene solution pump was stopped.

All three reaction slugs were now formed and travelling inside coil A. Once the first reaction slug entered the sampling valve, and ~50 μL had passed through, the sampling valve was actuated and a 15 μL aliquot sample was eluted with 600 μL EtOAc into a GC vial. The sample removal line was then flushed with H_2O. Once the remainder of the reaction slug had exited the sampling valve, the sampling valve was set back to the position to collect a new sample, and the sample removal line was then flushed with EtOAc.

Once the second reaction slug entered the sampling valve, and ~50 µL had passed through, the sampling valve was again actuated and a 15 µL aliquot sample was eluted with 600 µL EtOAc into a GC vial. The sample removal line was then flushed with H_2O. Once the remainder of the reaction slug had exited the sampling valve, the sampling valve was set back to the position to collect a new sample, and the sample removal line was then flushed with EtOAc.

Once the third reaction slug entered the sampling valve, and ~50 µL had passed through, the sampling valve was again actuated and a 15 µL aliquot sample was eluted with 600 µL EtOAc into a GC vial. The sample removal line was then flushed with H_2O. Once the remainder of the reaction slug had exited the sampling valve, and fully passed through valve 1 to coil B, valve 1 was set to position 2, valve 2 was set to position 2 (clockwise rotation) and the sampling valve was set to collect a sample again and flushed with EtOAc.

All three reaction slugs were now travelling through coil B. Sampling was continued in the same manner as each reaction slug again passed through the sampling valve. After all three reaction slugs had passed back into coil A, the reactor valves were again actuated: valve 1 to position 1, valve 2 to position 1 (counter-clockwise rotation), and the sampling valve to collection. Sampling and valve actuation were repeated to collect desired samples.

Note. In experiments using N_2 as the carrier fluid the entire reaction slug was formed very quickly (~5 s) to facilitate the ability to increase the sample interval as the reaction progressed by decreasing the N_2 flow rate without needing to consider residence time discrepancies between the front and back of the reaction slug. In these experiments however, the use of residence time was necessary to facilitate multiple consecutive reaction slugs and therefore reactions were initiated at the same flow rate as the carrier flow rate for the entire reaction progress. In order to increase the interval between sample collection as the reaction progressed therefore the carrier flow rate was unchanged and sample collection was simply skipped at 50, 1:10, 1:30, 1:50, 2:10, 2:20, 2:40 and 2:50 min. To skip sample collection, the sampling valve was simply not actuated as the reaction slugs travelled through, and only reactor valves 1 and 2 were actuated after all three reaction slugs had passed from one reactor coil into the other.

5.5 References

[1] a) Moore, J. W.; Pearson, R. G. *Kinetics and Mechanism*; 3 ed.; Wiley: New York, 1981; b) Masel, R. I. *Chemical Kinetics and Catalysis*; Wiley: New York, 2001; c) Blackmond, D. G. Reaction progress kinetic analysis: A powerful methodology for mechanistic studies of complex atalytic reactions. *Angew. Chem. Int. Ed.* **2005**, *44*, 4302–4320; d) Blackmond, D. G. Kinetic profiling of catalytic organic reactions as a mechanistic tool. *J. Am. Chem. Soc.* **2015**, *137*, 10852−10866.

[2] Anslyn, E. V.; Dougherty, D. A. *Modern Physical Organic Chemistry*; University Science: Sausalito, 2006.

[3] a) Burés, J. A simple graphical method to determine the order in catalyst. *Angew. Chem. Int. Ed.* **2016**, *55*, 2028−2031; b) Burés, J. Variable time normalization analysis: General graphical elucidation of reaction orders from concentration profiles. *Angew. Chem. Int. Ed.* **2016**, *55*, 16084−16087; c) Martínez-Carrión, A.; Howlett, M. G.; Alamillo-Ferrer, C.; Clayton, A. D.; Bourne, R. A.; Codina, A.; Vidal-Ferran, A.; Adams, R. W.; Burés, J. Kinetic treatments for catalyst activation and deactivation processes based on variable time normalization analysis. *Angew. Chem. Int. Ed.* **2019**, *58*, 10189−10193.

[4] a) Fermier, A. M.; Oyler, A. R.; Armstrong, B. L.; Weber, B. A.; Rodriguez, R. L.; Weber, J. V.; Nalasco, J. A. Automation of chemical reaction kinetics and product distribution studies in pharmaceutical development. *J. Assoc. Lab. Automation* **2002**, *7*, 83−88; b) Chung, R.; Yu, D.; Thai, V. T.; Jones, A. F.; Veits, G. K.; Read de Alaniz, J.; Hein, J. E. Tandem reaction progress analysis as a means for dissecting catalytic reactions: Application to the aza-piancatelli rearrangement. *ACS Catal.* **2015**, *5*, 4579–4585; c) Rougeot, C.; Situ, H.; Cao, B. H.; Vlachos, V.; Hein, J. E. Automated reaction progress monitoring of heterogeneous reactions: Crystallization-induced stereoselectivity in amine-catalyzed Aldol reactions. *React. Chem. Eng.* **2017**, *2*, 226–231; d) Malig, T. C.; Koenig, J. D. B.; Situ, H.; Chehal, N. K.; Hultin, P. G.; Hein, J. E. Real-time HPLC-MS reaction progress monitoring using an automated analytical platform. *React. Chem. Eng.* **2017**, *2*, 309–314; e) Fermier, A. M.; Oyler, A. R.; Armstrong, B. L.; Weber, J. V.; Nalasco, J. Apparatus for the automation of chemical reaction kinetics studies. WO patent 2002/077614 A2, 2002.

[5] a) McMullen, J. P.; Jensen, K. F. Integrated microreactors for reaction automation: New approaches to reaction development. *Annu. Rev. Anal. Chem.* **2010**, *3*, 19–42; b) Hartman, R. L.; McMullen, J. P.; Jensen, K. F. Deciding whether to go with the flow: Evaluating the merits of flow reactors for synthesis. *Angew. Chem. Int. Ed.* **2011**, *50*, 7502−7519; c) Newman, S. G.; Jensen, K. F. The role of flow in green

chemistry and engineering. *Green Chem.* **2013**, *15*, 1456−1472; d) Ley, S. V.; Fitzpatrick, D. E.; Ingham, R. J.; Myers, R. M. Organic synthesis: March of the machines. *Angew. Chem. Int. Ed.* **2015**, *54*, 3449−3464.

[6] Valera, F. E.; Quaranta, M.; Moran, A.; Blacker, J.; Armstrong, A.; Cabral, J. T.; Blackmond, D. G. The flow's the thing…Or is it? Assessing the merits of homogeneous reactions in flask and flow. *Angew. Chem. Int. Ed.* **2010**, *49*, 2478−2485.

[7] For example: a) McMullen, J. P.; Jensen, K. F. Rapid determination of reaction kinetics with an automated microfluidic system. *Org. Process Res. Dev.* **2011**, *15*, 398−407; b) Gholamipour-Shirazi, A.; Rolando, C. Alkylation of substituted benzoic acids in a continuous flow microfluidic microreactor: Kinetics and linear free energy relationships. *Org. Process Res. Dev.* **2012**, *16*, 811−818; c) Roberge, D. M.; Noti, C.; Irle, E.; Eyholzer, M.; Rittiner, B.; Penn, G.; Sedelmeier, G.; Schenkel, B. Control of hazardous processes in flow: Synthesis of 2-nitroethanol. *J. Flow Chem.* **2014**, *4*, 26−34; d) Hone, C. A.; Boyd, A.; O'Kearney-McMullan, A.; Bourne, R. A.; Muller, F. L. Definitive screening designs for multistep kinetic models in flow. *React. Chem. Eng.* **2019**, *4*, 1565−1570.

[8] a) Mozharov, S.; Nordon, A.; Littlejohn, D.; Wiles, C.; Watts, P.; Dallin, P.; Girkin, J. M. Improved method for kinetic studies in microreactors using flow manipulation and noninvasive Raman spectrometry. *J. Am. Chem. Soc.* **2011**, *133*, 3601−3608; b) Moore, J. S.; Jensen, K. F. "Batch" kinetics in flow: Online IR analysis and continuous control. *Angew. Chem. Int. Ed.* **2014**, *53*, 470−473; c) Schwolow, S.; Braun, F.; Rädle, M.; Kockmann, N.; Röder, T. Fast and efficient acquisition of kinetic data in microreactors using in-line Raman analysis. *Org. Process Res. Dev.* **2015**, *19*, 1286−1292; d) Durand, T.; Henry, C.; Bolien, D.; Harrowven, D. C.; Bloodworth, S.; Franck, X.; Whitby, R. J. Thermolysis of 1,3-dioxin-4-ones: Fast generation of kinetic data using in-line analysis under flow. *React. Chem. Eng.* **2016**, *1*, 82−89; e) Hone, C. A.; Holmes, N.; Akien, G. R.; Bourne, R. A.; Muller, F. L. Rapid multistep kinetic model generation from transient flow data. *React. Chem. Eng.* **2017**, *2*, 103−108; f) Aroh, K. C.; Jensen, K. F. Efficient kinetic experiments in continuous flow microreactors. *React. Chem. Eng.* **2018**, *3*, 94−101.

[9] a) Vural Gursel, I.; Noel, T.; Wang, Q.; Hessel, V. Separation/recycling methods for homogeneous transition metal catalysts in continuous flow. *Green Chem.* **2015**, *17*, 2012−2026; b) Sullivan, R. J.; Newman, S. G. Chiral auxiliary recycling in continuous flow: Automated recovery and reuse of Oppolzer's sultam. *Chem. Sci.* **2018**, *9*, 2130−2134.

[10] For examples of reaction performed in discrete slugs or droplets see: a) Song, H.; Chen, D. L.; Ismagilov, R. F. Reactions in droplets in microfluidic channels. *Angew. Chem. Int. Ed.* **2006**, *45*,

7336−7356; b) Sesen, M.; Alan, T.; Neild, A. Droplet control technologies for microfluidic high throughput screening (μHTS). *Lab Chip* **2017**, *17*, 2372−2394; c) Kaminski, T. S.; Garstecki, P. Controlled droplet microfluidic systems for multistep chemical and biological assays. *Chem. Soc. Rev.* **2017**, *46*, 6210−6226; d) Isbrandt, E. S.; Sullivan, R. J.; Newman, S. G. High throughput strategies for the discovery and optimization of catalytic reactions. *Angew. Chem. Int. Ed.* **2019**, *58*, 7180−7191; e) Candoni, N.; Grossier, R.; Lagaize, M.; Veesler, S. Advances in the use of microfluidics to study crystallization fundamentals. *Annu. Rev. Chem. Biomol.* **2019**, *10*, 59−83; f) Reizman, B. J.; Jensen, K. F. Simultaneous solvent screening and reaction optimization in microliter slugs. *Chem. Commun.* **2015**, *51*, 13290−13293; g) Hwang, Y.-J.; Coley, C. W.; Abolhasani, M.; Marzinzik, A. L.; Koch, G.; Spanka, C.; Lehmann, H.; Jensen, K. F. A segmented flow platform for on-demand medicinal chemistry and compound synthesis in oscillating droplets. *Chem. Commun.* **2017**, *53*, 6649−6652.

[11] a) Reizman, B. J.; Jensen, K. F. Feedback in flow for accelerated reaction development. *Acc. Chem. Res.* **2016**, *49*, 1786−1796; b) Mascia, S.; Heider, P. L.; Zhang, H.; Lakerveld, R.; Benyahia, B.; Barton, P. I.; Braatz, R. D.; Cooney, C. L.; Evans, J. M. B.; Jamison, T. F.; Jensen, K. F.; Myerson, A. S.; Trout, B. L. End-to-end continuous manufacturing of pharmaceuticals: Integrated synthesis, purification, and final dosage formation. *Angew. Chem. Int. Ed.* **2013**, *52*, 12359−12363; c) Adamo, A.; Beingessner, R. L.; Behnam, M.; Chen, J.; Jamison, T. F.; Jensen, K. F.; Monbaliu, J.-C. M.; Myerson, A. S.; Revalor, E. M.; Snead, D. R.; Stelzer, T.; Weeranoppanant, N.; Wong, S. Y.; Zhang, P. On-demand continuous-flow production of pharmaceuticals in a compact, reconfigurable system. *Science* **2016**, *352*, 61−67; d) Perera, D.; Tucker, J. W.; Brahmbhatt, S.; Helal, C. J.; Chong, A.; Farrell, W.; Richardson, P.; Sach, N. W. A platform for automated nanomole-scale reaction screening and micromole-scale synthesis in flow. *Science* **2018**, *359*, 429-434; e) Coley, C. W.; Thomas, D. A.; Lummiss, J. A. M.; Jaworski, J. N.; Breen, C. P.; Schultz, V.; Hart, T.; Fishman, J. S.; Rogers, L.; Gao, H.; Hicklin, R. W.; Plehiers, P. P.; Byington, J.; Piotti, J. S.; Green, W. H.; Hart, A. J.; Jamison, T. F.; Jensen, K. F. A robotic platform for flow synthesis of organic compounds informed by AI planning. *Science* **2019**, *365*, eaax1566.

[12] a) Plutschack, M. B.; Pieber, B.; Gilmore, K.; Seeberger, P. H. The hitchhiker's guide to flow chemistry. *Chem. Rev.* **2017**, *117*, 11796−11893; b) Pastre, J. C.; Browne, D. L.; Ley, S. V. Flow chemistry syntheses of natural products. *Chem. Soc. Rev.* **2013**, *42*, 8849−8869; c) Newton, S.; Carter, C. F.; Pearson, C. M.; Alves, L. D.; Lange, H.; Thansandote, P.; Ley, S. V. Accelerating spirocyclic polyketide synthesis using flow chemistry. *Angew. Chem. Int. Ed.* **2014**, *53*, 4915−4920; d) Cole, K. P.; Groh, J. M.; Johnson, M. D.; Burcham, C. L.; Campbell, B. M.; Diseroad, W. D.; Heller, M. R.; Howell, J. R.; Kallman, N. J.;

Koenig, T. M.; May, S. A.; Miller, R. D.; Mitchell, D.; Myers, D. P.; Myers, S. S.; Phillips, J. L.; Polster, C. S.; White, T. D.; Cashman, J.; Hurley, D.; Moylan, R.; Sheehan, P.; Spencer, R. D.; Desmond, K.; Desmond, P.; Gowran, O. Kilogram-scale prexasertib monolactate monohydrate synthesis under continuous-flow CGMP conditions. *Science* **2017**, *356*, 1144–1150; e) K. Kashani, S.; Sullivan, R. J.; Andersen, M.; Newman, S. G. Overcoming solid handling issues in continuous flow substitution reactions through ionic liquid formation. *Green Chem.* **2018**, *20*, 1748–1753; f) Russell, M. G.; Jamison, T. F. Seven-step continuous flow synthesis of Linezolid without intermediate purification. *Angew. Chem. Int. Ed.* **2019**, *58*, 7678–7681.

[13] Only 7 ports and 6-positions are needed. We had access to an 11-port, 10-position selector valve rather than a 7-port, 6-position selector valve, but a 7-port, 6-position selector valve (or any other selector valve with >7-ports, 6-positions) could be substituted by fabrication of a suitable rotor. See Figure 5.11.

[14] A custom router for the selector valve was purchased from Vici Valco (~$100 USD).

[15] Price, G. A.; Mallik, D.; Organ, M. G. Process analytical tools for flow analysis: A perspective. *J. Flow Chem.* **2017**, *7*, 82–86.

[16] a) Zheng, B.; Ismagilov, R. F. A Microfluidic approach for screening submicroliter volumes against multiple reagents by using preformed arrays of nanoliter plugs in a three-phase liquid/liquid/gas flow. *Angew. Chem. Int. Ed.* **2005**, *44*, 2520–2523; b) Chen, D. L.; Ismagilov, R. F. Microfluidic cartridges preloaded with nanoliter plugs of reagents: An alternative to 96-well plates for screening. *Curr. Opin. Chem. Biol.* **2006**, *10*, 226–231.

[17] Extremely fast reactions are ideally suited for traditional steady-state flow kinetics experiments, since the time inefficiencies of that strategy are not problematic when investigating reactions with incredibly short timescales, and therefore we believe these are best considered complimentary tools.

[18] Reaction slugs used were 300 μL (≈ 1.5 m long in the 0.5 mm I.D. reaction coils) and were sampled from the center of the slug, such that concerns over solvent loss to the gasseous carrier phase or reaction acceleration at droplet interfaces were not relevant.

[19] a) Hubbard, P.; Brittain, W. J. Mechanism of amine-catalyzed ester formation from an acid chloride and alcohol. *J. Org. Chem.* **1998**, *63*, 677–683; b) Oosthoek-de Vries, A. J.; Nieuwland, P. J.; Bart, J.; Koch, K.; Janssen, J. W. G.; van Bentum, P. J. M.; Rutjes, F. P. J. T.; Gardeniers, H. J. G. E.; Kentgens, A. P. M. Inline reaction monitoring of amine-catalyzed acetylation of benzyl alcohol using a microfluidic stripline nuclear magnetic resonance setup. *J. Am. Chem. Soc.* **2019**, *141*, 5369–5380.

[20] Patschinski, P.; Zhang, C.; Zipse, H. The Lewis base-catalyzed silylation of alcohols — A mechanistic analysis. *J. Org. Chem.* **2014**, *79*, 8348−8357.

[21] For a discussion of typical values for activation enthalpies and entropies see ref 2.

[22] Xu, J.; Liu, R. Y.; Yeung, C. S.; Buchwald, S. L. Monophosphine ligands promote Pd-catalyzed C–S cross-coupling reactions at room temperature with soluble bases. *ACS Catal.* **2019**, *9*, 6461−6466.

[23] When using sequential droplets in microfuidic screening platforms it is sometimes necessary to include "blank" droplets between reactions to prevent bleed through of materials (for an example see ref 11f). This was found to be unnecessary in this case, likely due to the fact that this reactor uses large reaction slugs (450 μL ≈ 60 cm long slugs in the 1.0 mm I.D. reaction coils) rather than droplets making small amounts of bleed through inconsequential.

[24] Obtaining kinetic data from (near-)refluxing solutions in batch is hampered by unknown partitioning of volatile components (e.g., cyclopentadiene) between the reaction solution and headspace (see ref 5b) while sampling from batch vessels under pressure requires specialized autoclaves equipped with dip tubes for sample removal. In flow however, the combination of back pressure to prevent boiling and no headspace facilitates collection of high-quality kinetic data above the atmospheric boiling of reaction components.

[25] Frisch, M. J.; Trucks, G. W.; Schlegel, H. B.; Scuseria, G. E.; Robb, M. A.; Cheeseman, J. R.; Scalmani, G.; Barone, V.; Mennucci, B.; Petersson, G. A.; Nakatsuji, H.; Caricato, M.; Li, X.; Hratchian, H. P.; Izmaylov, A. F.; Bloino, J.; Zheng, G.; Sonnenberg, J. L.; Hada, M.; Ehara, M.; Toyota, K.; Fukuda, R.; Hasegawa, J.; Ishida, M.; Nakajima, T.; Honda, Y.; Kitao, O.; Nakai, H.; Vreven, T.; Montgomery Jr., J. A.; Peralta, J. E.; Ogliaro, F.; Bearpark, M. J.; Heyd, J.; Brothers, E. N.; Kudin, K. N.; Staroverov, V. N.; Kobayashi, R.; Normand, J.; Raghavachari, K.; Rendell, A. P.; Burant, J. C.; Iyengar, S. S.; Tomasi, J.; Cossi, M.; Rega, N.; Millam, N. J.; Klene, M.; Knox, J. E.; Cross, J. B.; Bakken, V.; Adamo, C.; Jaramillo, J.; Gomperts, R.; Stratmann, R. E.; Yazyev, O.; Austin, A. J.; Cammi, R.; Pomelli, C.; Ochterski, J. W.; Martin, R. L.; Morokuma, K.; Zakrzewski, V. G.; Voth, G. A.; Salvador, P.; Dannenberg, J. J.; Dapprich, S.; Daniels, A. D.; Farkas, Ö.; Foresman, J. B.; Ortiz, J. V.; Cioslowski, J.; Fox, D. J. *Gaussian 09, Rev. c.0.1*; Gaussian, Inc.: Wallingford, CT, USA, 2009.

[26] a) Zhao, Y.; Truhlar, D. G. A new local density functional for main-group thermochemistry, transition metal bonding, thermochemical kinetics, and noncovalent interactions. *J. Chem. Phys.* **2006**, *125*, 194101-1−194101-18; b) Zhao, Y.; Truhlar, D. G. The M06 suite of density functionals for main group thermochemistry, thermochemical kinetics, noncovalent interactions, excited states, and transition

elements: Two new functionals and systematic testing of four M06-class functionals and 12 other functionals. *Theor. Chem. Acc.* **2008**, *120*, 215–241.

[27] Weigend, F.; Ahlrichs, R. Balanced basis sets of split valence, triple zeta valence and quadruple zeta valence quality for H to Rn: Design and assesment of accuracy. *PCCP* **2005**, *7*, 3297–3305.

[28] Andrae, D.; Haussermann, U.; Dolg, M.; Stoll, H.; Preuss, H. Energy-adjusted ab initio pseudopotentials for the 2nd and 3rd row transition-elements. *Theor. Chim. Acta* **1990**, *77*, 123–141.

[29] a) Miertus, S.; Scrocco, E.; Tomasi, J. Electrostatic interaction of a solute with a continuum - a direct utilization of ab initio smolecular potentials for the prevision of solvent effects. *Chem. Phys.* **1981**, *55*, 117–129; b) Miertus, S.; Tomasi, J. Approximate evaluations of the electrostatic free-energy and internal energy changes in solution processes. *Chem. Phys.* **1982**, *65*, 239–245; c) Barone, V.; Cossi, M.; Tomasi, J. Geometry optimization of molecular structures in solution by the polarizable continuum model. *J. Comput. Chem.* **1998**, *19*, 404–417; d) Cossi, M.; Scalmani, G.; Rega, N.; Barone, V. New developments in the polarizable continuum model for quantum mechanical and classical calculations on molecules in solution. *J. Chem. Phys.* **2002**, *117*, 43–54.

[30] Feng, J.; Liang, S.; Chen, S.-Y.; Zhang, J.; Fu, S.-S.; Yu, X.-Q. A metal-free oxidative esterification of the benzyl C-H bond. *Adv. Synth. Catal.* **2012**, *354*, 1287–1292.

[31] Meng, D.; Li, D.; Ollevier, T. Recyclable Iron(II) Caffeine-derived ionic salt catalyst in the Diels–Alder reaction of cyclopentadiene and α,β-unsaturated N-acyl-oxazolidinones in dimethyl carbonate. *RSC Advances* **2019**, *9*, 21956–21963.

Chapter 6 Conclusions and Suggestions for Future Work

6.1 Conclusions

At the heart of synthetic chemistry is a drive to maximize efficiency — developing new transformations to allow shorter synthetic routes, designing new reagents to give more atom economical reactions, optimizing reactions to maximize yield and selectivity — and this thesis continued along these lines with the presentation of new conceptual strategies to improve efficiency in chemical processes by using the tools and techniques of flow chemistry to implement or facilitate closed cycles that allow reagent/catalyst turnover.

As the ninth principle of Green Chemistry,[1] catalysis is the conventional form in which chemists encounter the concept of reagent 'turnover' and can easily appreciate the efficiency improvements that result from using a sub-stoichiometric reagent to enable a transformation. From a conceptual standpoint catalyst turnover is simply the implementation of a closed loop, cycling in time as the reaction progresses, that allows the catalyst to be repeatedly recovered and reused. We envisioned that any strategy to implement an analogous 'cycle' could achieve the same efficiency improvements and developed two new conceptual strategies to implement or facilitate turnover.

The first strategy focused on implementing closed cycles through the physical motion of materials in looping paths. This was applied to achieve 'turnover' of stoichiometric reagents, introducing the 'pseudo-catalytic cycle in space' concept, as well as cycle entire reaction solutions to efficiently obtain conversion over time profiles in flow. The second conceptual approach to facilitate cycles was a strategy to 'turn on' catalysis in situations where a functional catalyst should exist in principle (on the basis of the kinetical feasibility of all individual elementary steps) but is not operational in practise due to dominating undesired background reactions under typical reaction conditions. A strategy to manipulate the catalyst resting state by starvation of the 'reactive' stoichiometric reagent was developed that allows the catalytic cycle to become operational and provides high yields of desired products.

The 'pseudo-catalytic cycle in space' concept was introduced and developed in Chapter two where a telescoped continuous flow process incorporating recovery and recycling of a stoichiometric chiral auxiliary was designed to achieve 'turnover' of this reagent. A chiral auxiliary mediated hydrogenation was used for the proof of concept work, addressing the

traditional inefficiencies of auxiliary mediated transformations by achieving formal sub-stoichiometric loading of the auxiliary with all reaction steps combined into a single process.

In order to implement a 'pseudo-catalytic cycle in space' it is necessary to operate under continuous flow conditions. For many reactions the conversion from traditional batch to continuous flow is non-trivial, and in Chapter 3 we focused on providing a solution to a common problem that can hinder this transition, namely problems with solid handling/formation due to need to quench acidic by-products with a stoichiometric base and the concomitant formation of insoluble base·HX salts. A general strategy to avoid this problem was developed using acid scavenging organic bases that form low-melting ionic liquids upon protonation, and demonstrated to facilitate acylation, S_NAr, and S_N2 chemistry in continuous flow with minimal additional modifications to published batch conditions beyond substitution of the amine base to an appropriate, ionic-liquid forming option. The ease of transitioning from batch to continuous flow therefore lowers the impediment toward implementing a strategy such as a 'pseudo-catalytic cycle in space'.

In Chapter 4 the second strategy of catalyst resting state manipulation was developed and demonstrated. Reactions where oxidative addition is rate determining and subsequent transmetallation is in kinetic competition with undesired background reaction(s) were explored. It was hypothesized that by depriving the reaction of the nucleophile via slow addition of this reagent, the Pd(II) oxidative addition intermediate would be allowed to accumulate. As a result, when the nucleophile was added dropwise this necessary Pd(II) species would be present in sufficient concentration for transmetallation to outcompete the undesired background reaction(s) that would otherwise consume the nucleophile via unproductive pathways.

This hypothesis was supported by direct infusion ESI-MS studies of Kumada-Corriu and Murahashi cross-coupling reactions for which the yield is sensitive to organometallic reagent addition rate. Then Pd catalyzed aryl halide–diazo cross-coupling reactions with aryl chlorides and bromides were enabled using an analogous diazo slow-addition strategy. Subsequently, combining diazo slow addition with on-demand, continuous flow synthesis of diverse diazo reagents substantially broadened the accessible substrate scope of this interesting palladium-catalyzed transformation.

The last topic that was explored, in Chapter 5, returned to cycling materials in space to provide 'turnover', but this time the ability to cycle an entire reaction solution was targeted. This was needed to allow efficient collection of conversion over time data in flow, a previously outstanding problem making it inefficient to collect kinetic data using a flow reactor. A reactor was designed that could cycle an entire reaction slug, enabling efficient collection of conversion over time data by sampling/analyzing the reaction once each 'cycle'. The reactor was demonstrated by investigating the kinetics of six different reactions with widely ranging conditions and using various methods of data analysis.

In summary, the work in this thesis demonstrated new conceptual strategies to increase reaction or process efficiency. It was shown that the tools of continuous flow chemistry could be used to construct closed cycles operative in space to 'turnover' reagents or whole reaction solutions, or to facilitate operative catalytic cycles to turnover catalysts by manipulating catalyst resting state. These two strategies are both general conceptual approaches that should be widely applicable in a variety of situations, and it is our hope that this work will inspire continued research in these areas of non-conventional strategies to improve efficiency by implementing or facilitating closed cycles to enable 'turnover'.

6.2 Suggested Future Work

6.2.1 Future directions for the pseudo-catalytic cycle in space work

For the concept of a 'pseudo-catalytic cycle in space' we demonstrated the application to improve efficiency of chiral auxiliary mediated transformations. Another class of transformations that could substantially benefit from such an approach is oxidation chemistry. Many oxidation reactions do not have catalytic variants, and instead use of stoichiometric oxidants is relied on.[2] Furthermore, many of the most important, highly selective oxidants result in transformations with low atom efficiency due to the high molar masses of by-products produced. For example, hypervalent iodine mediate oxidations such as the Dess-Martin variant (Scheme 6.1) are heavily used in complex product synthesis and produce significant amounts of iodine(III) by-product **6.4** as stoichiometric waste.[3] The conceptual framework of the pseudo-catalytic cycle in space could be used to address this issue, by coupling the alcohol oxidation with hypervalent iodine reagent regeneration (Figure 6.1).

Scheme 6.1. Dess-Martin oxidation of alcohols to ketones/aldehydes.

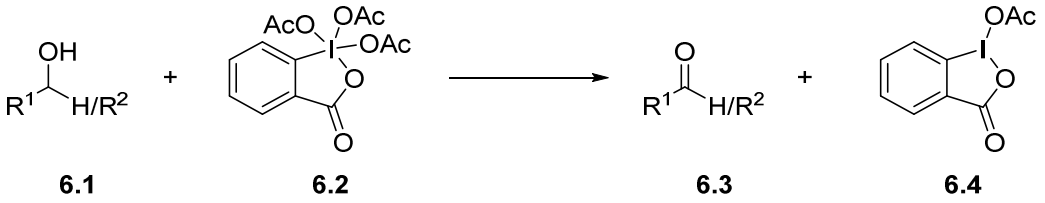

6.1 **6.2** **6.3** **6.4**

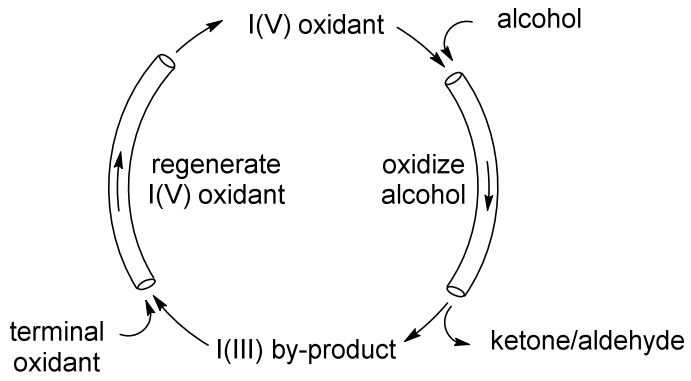

Figure 6.1. Application of a pseudo-catalytic cycle in space to address the low atom economy of hypervalent iodine mediated oxidation chemistry.

Use of the Dess-Martin Periodinane (DMP, **6.2**) directly will likely be problematic due to the low solubilities of both the I(III) by-product **6.4** and 2-iodoxybenzoic acid (IBX, **6.5**) produced as an intermediate during DMP regeneration (Scheme 6.2). However, various IBX analogues have been developed with enhanced solubility and demonstrated efficiency as oxidants for alcohols analogous to DMP (Chart 6.1),[3a,c] and these oxidants therefore have potential to be applied in conjunction with the pseudo-catalytic cycle in space concept to improve the efficiency of hypervalent iodine mediated oxidations.

Scheme 6.2. Regeneration of DMP proceeds via oxidation to IBX, an intermediate with very low solubility.

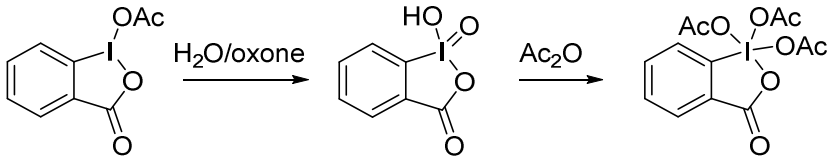

6.4 **6.5** **6.2**

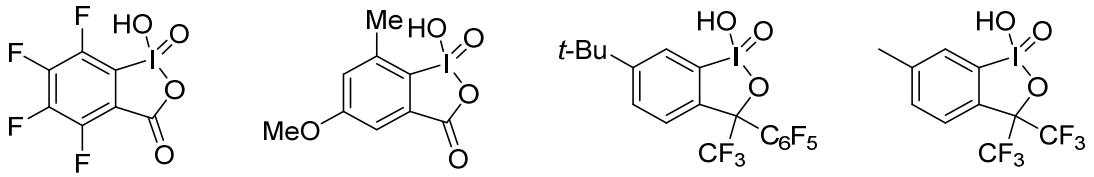

Chart 6.1. Soluble IBX analogues.

6.2.2 Future directions for the catalyst resting state manipulation work

The concept of manipulating catalyst resting state combined with flow generation of cross-coupling nucleophiles should also be widely applicable. An interesting research area where this strategy should be impactful is iron catalyzed cross-coupling reactions. Unlike traditional palladium and nickel catalysts that are generally ineffective for sp^3 hybridized electrophiles/nucleophiles, iron catalysts enable sp^2–sp^3 and sp^3–sp^3 bond formation. This is particularly attractive due to the ability to incorporate chirality in the products and access molecules with diverse 3-dimensional shapes. For the more established sp^2–sp^3 variant, functional group tolerance is fairly good at high catalyst loadings (5–10%),[4] but at lower loadings (≤1%) — that are desirable for large scale, industrial application — this tolerance quickly erodes.[5] In addition to tolerating functional groups on the electrophilic coupling partner, functionalization of the nucleophilic Grignard reagent also remains a challenge. Although densely functionalized Grignard reagents can be prepared by rapid transmetallation with, for example, *i*-PrMgBr·LiCl,[6] the Grignard reagents formed need to be handled under cryogenic conditions to prevent decomposition, hindering their use in cross-coupling chemistry. The combination of on-demand flow generation to make these functionalized Grignard reagents and slow addition to the iron-catalyst/aryl halide solution should overcome these challenges and open the scope of this transformation (Scheme 6.3).

Scheme 6.3. Proposed use of on-demand, flow synthesis of functionalized Grignard reagents combined with controlled Grignard addition rate to manipulate catalyst resting state and overcome scope limitations in iron catalyzed sp^2–sp^3 cross-coupling.

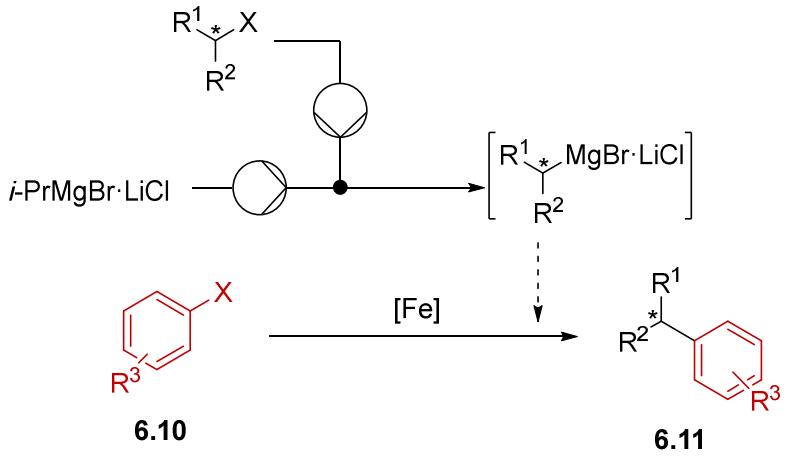

It would also be interesting to investigate if the concept of resting state manipulation by reagent slow addition can be applied in asymmetric catalysis to improve ee. For transformations where an uncatalyzed background reaction is competitive with the catalyzed process it is challenging to obtain high ee since the uncatalyzed process produces both the desired and undesired enantiomer indiscriminately. However, if moderate enantioselectivity is observable this implies that the catalyzed process is, in principle, kinetically competent to outcompete the background reaction if the catalyst resting state could be manipulated. A promising transformation for investigation of this hypothesis is the chiral Lewis base catalyzed aldol reaction between trichlorosilyl protected enolates and aldehydes developed by Denmark and coworkers.[7] While excellent enantioselectivities are achieved in the reaction of ketone derive trichlorosilyl enolates **6.12** with aldehydes catalyzed by chiral phosphoramide catalysts (e.g., **6.17**) (Scheme 6.4A),[7,8] low ee is obtained in the analogous reaction with more electron rich, acetate derived trichlorosilyl enolates **6.15** (Scheme 6.4B).[7a] It has been confirmed that this is due to the competitive, uncatalyzed background reaction being operative even at –80 °C with these more reactive silyl enolates.[7a]

Scheme 6.4. Chiral phosphoramide catalyzed aldol reactions developed by Denmark and coworkers work well for ketone derived trichlorosilyl enolates (A) but poorly for acetate derived trichlorosilyl enolates (B) due to competitive, uncatalyzed background reactivity with these substrates.

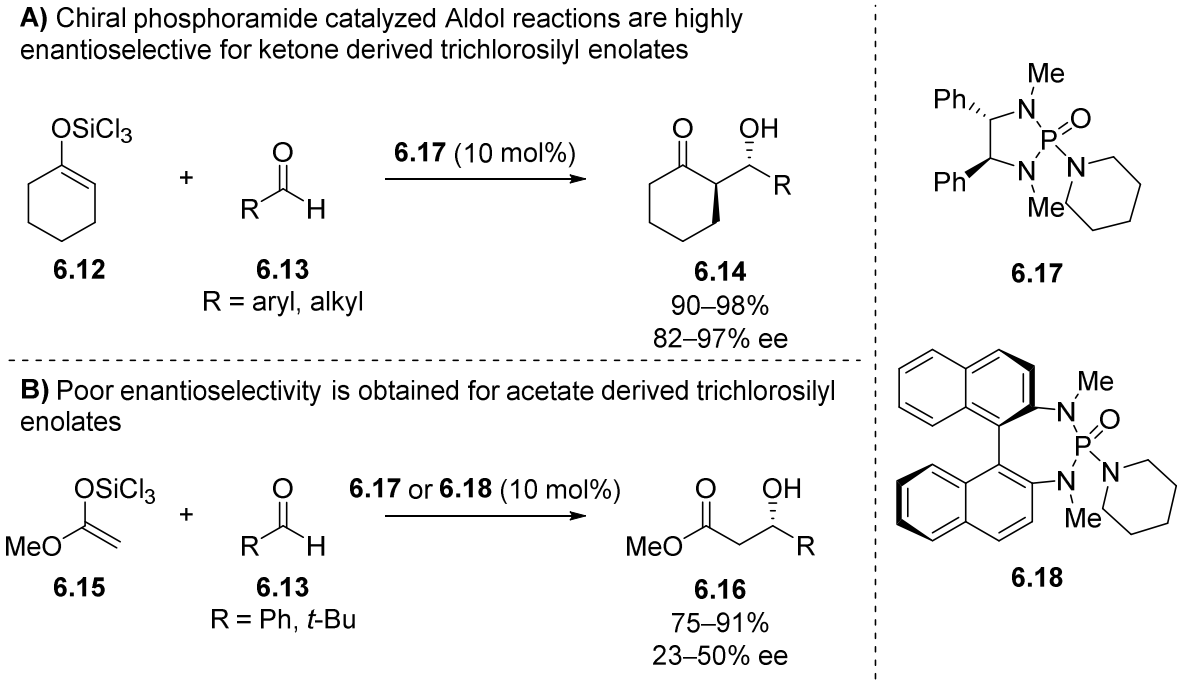

A putative catalytic cycle for this transformation is shown in Scheme 6.5. Under typical conditions (i.e., stoichiometric aldehyde present at the beginning of the reaction) the concentration of species **6.19** is expected to be very low since it is rapidly consumed by reaction with the aldehyde and therefore the catalyst resting state is likely to be **6.20**. However, if the reaction mixture was starved of aldehyde by slow addition of that reagent the relative concentrations of **6.19** and **6.20** should approach a statistical distribution. As a result, the concentration of **6.19** would be significant rather than minute and this necessary intermediate would be present to react with incoming aldehyde as it is added, theoretically allowing all aldehyde to be consumed by the catalyzed pathway and therefore leading to high ee.

Scheme 6.5. A putative catalytic cycle for the phosphoramide catalyzed aldol reaction.

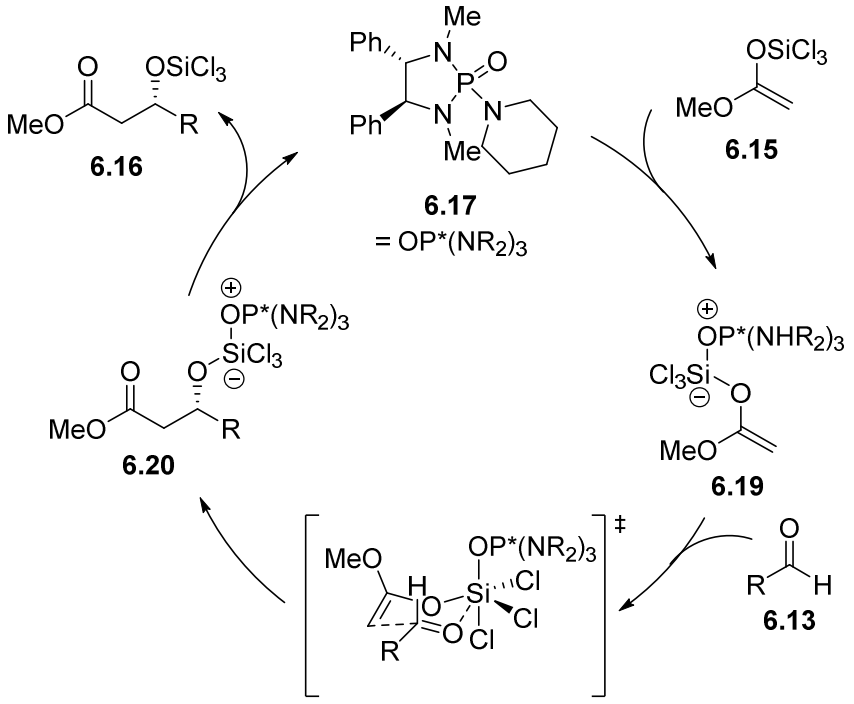

6.2.3 Future directions for the acid scavenging using ionic liquid-forming bases work and the cycling reactor for kinetic analysis

The acid scavenging by forming ionic liquids project has already led to future work applying this solution to cross-coupling reactions.[9] Future directions for the flow kinetics reactor involve increasing the level of automation. Valve actuation and sample collection and analysis could be fully automated by increasing the level of computer control and interfacing directly with a liquid handling robot or HPLC to automate the analysis of samples in addition to collection. This would realize the end goal of providing an automated platform to perform routine kinetic analysis and ideally lead towards a commercialized instrument.

6.3 References

[1] Anastas, P.; Eghbali, N. Green Chemistry: Principles and practice. *Chem. Soc. Rev.* **2010**, *39*, 301–312.

[2] Carey, F. A.; Sundberg, R. J. *Advanced Organic Chemistry Part B: Reactions and Synthesis*; 5 ed.; Springer: New York, 2007.

[3] a) Tohma, H.; Kita, Y. Hypervalent iodine reagents for the oxidation of alcohols and their application to complex molecule synthesis. *Adv. Synth. Catal.* **2004**, *346*, 111–124; b) Zhdankin, V. V.; Stang, P. J. Chemistry of polyvalent iodine. *Chem. Rev.* **2008**, *108*, 5299–5358; c) Uyanik, M.; Ishihara, K. Hypervalent iodine-mediated oxidation of alcohols. *Chem. Commun.* **2009**, 2086–2099; d) Yoshimura, A.; Zhdankin, V. V. Advances in synthetic applications of hypervalent iodine compounds. *Chem. Rev.* **2016**, *116*, 3328–3435.

[4] a) Sherry, B. D.; Fürstner, A. The promise and challenge of iron-catalyzed cross coupling. *Acc. Chem. Res.* **2008**, *41*, 1500–1511; b) Czaplik, W. M.; Mayer, M.; Cvengroš, J.; von Wangelin, A. J. Coming of age: Sustainable iron-catalyzed cross-coupling reactions. *ChemSusChem* **2009**, *2*, 396–417; c) Mako, T. L.; Byers, J. A. Recent advances in iron-catalysed cross coupling reactions and their mechanistic underpinning. *Inorganic Chemistry Frontiers* **2016**, *3*, 766–790; d) Guérinot, A.; Cossy, J. Iron-catalyzed C–C cross-couplings using organometallics. *Top. Curr. Chem.* **2016**, *374*, 49.

[5] Bisz, E.; Kardela, M.; Piontek, A.; Szostak, M. Iron-catalyzed $C(sp^2)$–$C(sp^3)$ cross-coupling at low catalyst loading. *Catal. Sci. Technol.* **2019**, *9*, 1092–1097.

[6] a) Knochel, P.; Dohle, W.; Gommermann, N.; Kneisel, F. F.; Kopp, F.; Korn, T.; Sapountzis, I.; Vu, V. A. Highly functionalized organomagnesium reagents prepared through halogen–metal exchange. *Angew. Chem. Int. Ed.* **2003**, *42*, 4302–4320; b) Ziegler, D. S.; Wei, B.; Knochel, P. Improving the halogen–magnesium exchange by using new turbo-Grignard reagents. *Chem. Eur. J.* **2019**, *25*, 2695–270.

[7] a) Denmark, S. E.; Winter, S. B. D.; Su, X.; Wong, K.-T. Chemistry of trichlorosilyl enolates. 1. New reagents for catalytic, asymmetric aldol additions. *J. Am. Chem. Soc.* **1996**, *118*, 7404–7405; b) Denmark, S. E.; Stavenger, R. A. Asymmetric catalysis of aldol reactions with chiral Lewis bases. *Acc. Chem. Res.* **2000**, *33*, 432–440.

[8] a) Denmark, S. E.; Wong, K.-T.; Stavenger, R. A. The chemistry of trichlorosilyl enolates. 2. Highly-selective asymmetric aldol additions of ketone enolates. *J. Am. Chem. Soc.* **1997**, *119*, 2333–2334; b) Denmark, S. E.; Winter, S. B. D. The chemistry of chlorosilyl enolates 3.: Variation of the silyl group and the effect on rate and enantiomeric excess of acetate aldol additions. *Synlett* **1997**, *1997*, 1087–1089; c) Denmark, S. E.; Stavenger, R. A.; Wong, K.-T. Asymmetric aldol additions catalyzed by chiral phosphoramides: Electronic effects of the aldehyde component. *Tetrahedron* **1998**, *54*, 10389–10402; d)

Denmark, S. E.; Stavenger, R. A. Highly 1,4-Syn Diastereoselective, phosphoramide-catalyzed aldol additions of chiral methyl ketone enolates. *J. Org. Chem.* **1998**, *63*, 9524–9527; e) Denmark, S. E.; Stavenger, R. A.; Wong, K.-T. Lewis base-catalyzed, asymmetric aldol additions of methyl ketone enolates. *J. Org. Chem.* **1998**, *63*, 918–919; f) Denmark, S. E.; Stavenger, R. A.; Wong, K.-T.; Su, X. Chiral phosphoramide-catalyzed aldol additions of ketone enolates. Preparative aspects. *J. Am. Chem. Soc.* **1999**, *121*, 4982–4991; g) Denmark, S. E.; Pham, S. M. Kinetic analysis of the divergence of reaction pathways in the chiral Lewis base promoted aldol additions of trichlorosilyl enol ethers: A rapid-injection NMR study. *Helv. Chim. Acta* **2000**, *83*, 1846–1853; h) Denmark, S. E.; Stavenger, R. A. The chemistry of trichlorosilyl enolates. Aldol addition reactions of methyl ketones. *J. Am. Chem. Soc.* **2000**, *122*, 8837–8847; i) Denmark, S. E.; Fujimori, S. The effects of a remote stereogenic center in the Lewis base catalyzed aldol additions of chiral trichlorosilyl enolates. *Org. Lett.* **2002**, *4*, 3477–3480; j) Denmark, S. E.; Pham, S. M.; Stavenger, R. A.; Su, X.; Wong, K.-T.; Nishigaichi, Y. Chiral phosphoramide-catalyzed aldol additions of ketone trichlorosilyl enolates. Mechanistic aspects. *J. Org. Chem.* **2006**, *71*, 3904–3922.

[9] K. Kashani, S.; Jessiman, J. E.; Newman, S. G. Exploring homogeneous conditions for mild Buchwald-Hartwig amination in batch and flow. *Org. Process Res. Dev.*, **2020**, ASAP, doi : 10.1021/acs.oprd.0c00018.

Appendix I. Supporting Information for Chapter 2

AI.1 Additional equipment details for the flow reactor

AI.1.1 Active mixer reactor for acylation

R1 in Figure 2.2. The series of mixers was constructed by making active mixer units as reported by Ley and co-workers.[1] Three 1.00 mL plastic HSW syringes with the plungers removed were heated at the open end until soft and then a thread was cut using 1/4-28 PEEK male nuts. Four 3×10 mm PTFE coated stir bars were inserted in the mixer and PTFE tape was used to improve the seal between the PEEK fitting and the cut thread. The mixers were connected together with 10 cm of PFA tubing (1/16" O.D., 0.5 mm I.D., 20 µL). 100 cm PFA tubing (1/16" O.D., 0.5 mm I.D. 100 µL volume) was connected after last chamber to allow the emulsion to settle into slugs before entering the gravity liquid-liquid separator. The agitators were operated by a magnetic stir plate set at maximum (1400 rpm). A ~7.5 mm air gap between the stir plate surface and the mixers was maintained through use of cardboard spacers to prevent heat transfer from the stir plate surface that became warm to the touch with extended hours of operation.

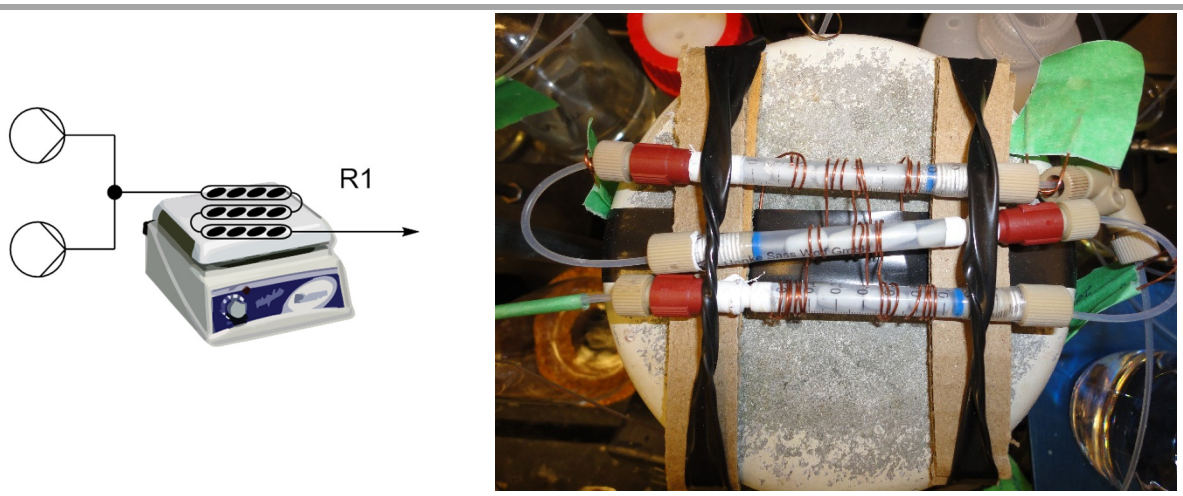

Figure AI.1. Schematic and photo of continuous stirred tubular reactor used for acylation.

[1] O'Brien, M.; Koos, P.; Browne, D. L.; Ley, S. V. A prototype continuous-flow liquid-liquid extraction system using open-source technology. *Org. Biomol. Chem.* **2012**, *10*, 7031–7036.

AI.1.2 Gravity liquid-liquid separators

AI.1.2.1 Gravity liquid-liquid separator with active withdrawal of both organic and aqueous phases (type 1)

S1 and S3 in Figure 2.2. A 2.5 mL glass Hamilton syringe was used for the body of the separator. The biphasic mixture was introduced at ~1 cm distance from bottom of chamber. The aqueous (lower) phase was withdrawn by pump from the luer joint at the bottom of syringe. The organic (upper) phase was withdrawn by pump through a tube ~1.5 cm from bottom of chamber. The phase boundary was maintained at ~0.75 cm from bottom of chamber by manually setting the pump withdrawal rates.

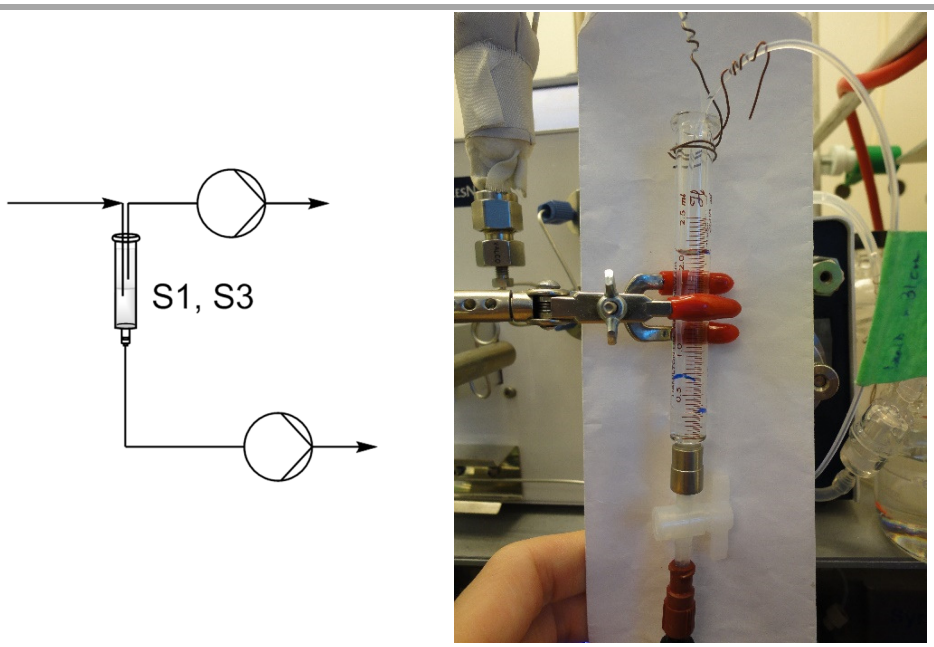

Figure AI.2. Schematic and photo of type 1 gravity liquid-liquid separator.

AI.1.2.2 Gravity liquid-liquid separators with active withdrawal of aqueous phase and passive withdrawal of organic phase (type 2)

S4 in Figure 2.2. An 8 mm O.D. 6 mm I.D. glass tube was cut to 12 cm length. Male luer joints were attached at the bottom and at 10 cm up the side by a glassblower. The biphasic mixture was introduced at ~3 cm distance from bottom of chamber. The aqueous (lower) phase was withdrawn by pump P12 from the luer joint at the bottom and the organic (upper) phase flowed

out through the upper luer joint and was collected in a flask. The phase boundary was maintained at ~2.5 cm from the bottom by manually setting the pump withdrawal rate.

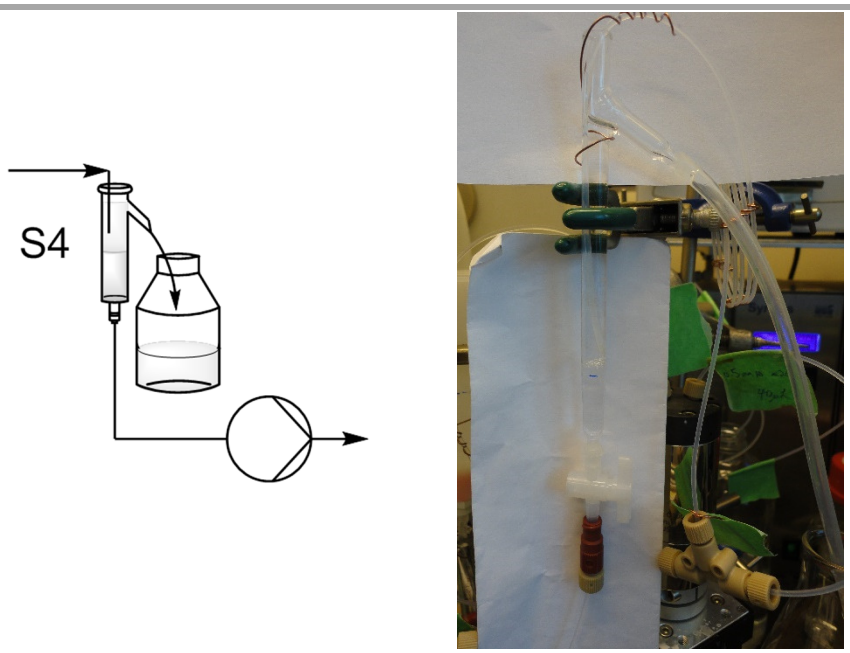

Figure AI.3. Schematic and photo of type 2 gravity liquid-liquid separator.

AI.1.3 Modifications to Biotage Universal Phase Separator

S2 in Figure 2.2. The membrane material of the Biotage Universal Phase Separator (product number 120-1930-V) was well suited for the separation after the hydrogenation, but the physical design of the unit required slight modification to adapt to the low flow rate of our scale. The membrane was cut to height of 4 cm to lower the volume of solvent retained in the membrane to ~1 mL, and the barrel of a 25 mL HSW syringe (with the end cut off to give an open cylinder) was placed around the membrane. The biphasic solution was introduced between the membrane and the syringe barrel. This kept the small volume of floating organic phase always in close contact with the membrane. The organic phase diffused through the membrane and was collected in a 2.5 mL glass Hamilton syringe body equipped with a closed two-way valve at the luer end, used as a solution reservoir for pump P6. The lower aqueous phase filled the entire reservoir both inside and outside the syringe barrel, allowing accumulation of the aqueous phase which was removed by Pasteur pipette approximately once per hour.

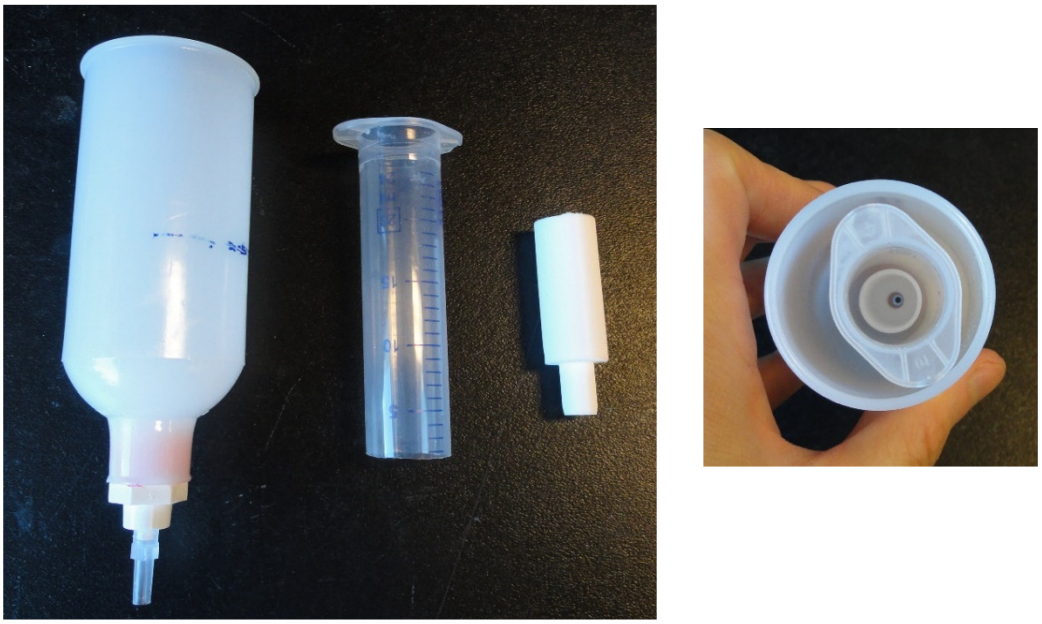

Figure AI.4. Photo of modified Biotage Universal Phase Separator components (left, outer reservoir, syringe body and shortened membrane) and assembled (right).

AI.1.4 Packed bed reactor (PBR)

R2 in Figure 2.2. The packed bed reactor was fabricated from 30 cm of 1/4" O.D., 3.0 mm I.D. 316 stainless steel fitted with fritted HPLC column end fittings (Valco ECEF413.0F). A thermocouple was attached to the centre of the PBR and then a heating cable (McMaster Carr 3641K23) was wrapped the length of the column. The PBR was then wrapped in vinyl backed fibreglass insulation. The temperature of the PBR reactor was controlled by a J-Kem model 210 temperature controller. A 6.5 bar (100 psi) Upchurch back pressure regulator was placed after the PBR.

The packed bed reactor was interfaced with the commercially available H-Cube Mini from ThalesNano to provide *in situ* generated hydrogen. The decision to use an in-house fabricated PBR rather than purchasing catcarts was solely financially driven. Our PBR was re-packed after each experiment with a mixture of commercially available Pd/C (110 mg) and 150–212 μm glass beads (3.0 g, product G9018 from Sigma Aldrich) to limit pressure drop.[2]

[2] Jensen, R. K.; Thykier, N.; Enevoldsen, M. V.; Lindhardt, A. T. A high mobility reactor unit for R&D continuous flow rransfer hydrogenations. *Org. Process Res. Dev.* **2017**, *21*, 370–376.

Liquid volume of the packed bed was determined to be 1.0 mL by subtracting the mass once filled with water from the dry mass of the freshly backed PBR. Estimating equal occupancies of each of the 3 fluid phases (organic, aqueous and gaseous) gives a very rough estimate of residence time for the organic phase of 1.3 min. Measuring the time until breakthrough when introducing substrate through the clean packed bed was in rough agreement with this estimate.

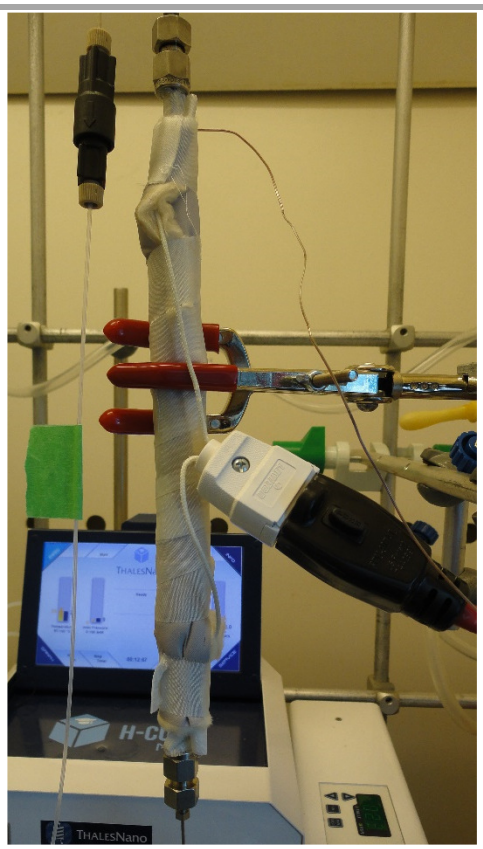

Figure AI.5. Photo of the in-house fabricated packed bed reactor.

AI.1.5 Tube-in-tee mixer

M1 in Figure 2.2. A tube-in-tee mixer[3] was used for the acid wash after the methanolysis due to problems with inefficient mixing in an ordinary tee mixer. This was fabricated by taking an ordinary PFA tee mixer with 1.0 mm I.D. through-holes and enlarging the straight bore to 1/16"

[3] Ingham, R. J.; Battilocchio, C.; Fitzpatrick, D. E.; Sliwinski, E.; Hawkins, J. M.; Ley, S. V. A aystems approach towards an intelligent and self-controlling platform for integrated continuous reaction sequences. *Angew. Chem. Int. Ed.* **2015**, *54*, 144–148.

all the way through with a 1/16” drill bit, then further boring out one half of the straight bore to 2.0 mm I.D. as show in Figure AI.6.

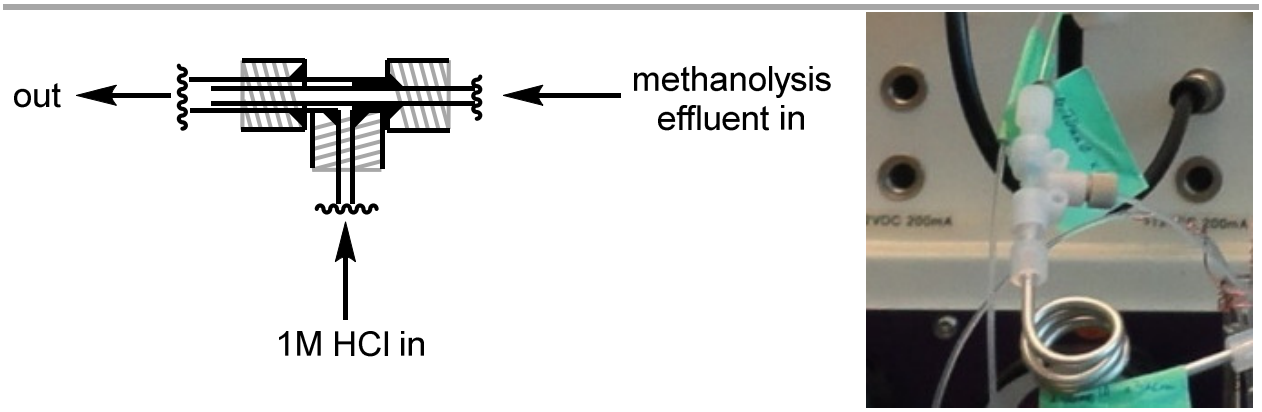

Figure AI.6. Schematic and photo of the in-house fabricated tube-in-tee mixer.

AI.1.6 Photograph of flow reactor setup

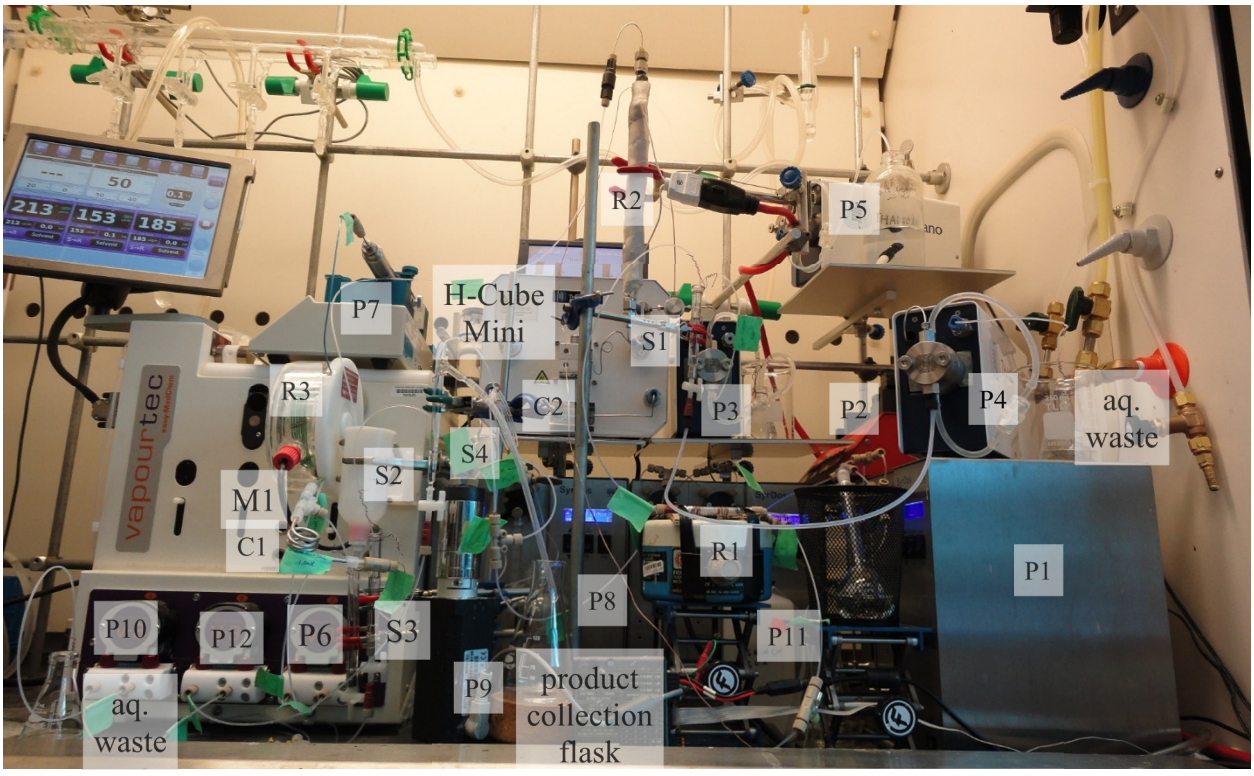

Figure AI.7. Photograph of complete flow reactor set up.

AI.2 Spectra of substrates and products

Spectra of substrates and products are freely available in the supporting information for: Sullivan, R. J.; Newman, S. G. Chiral auxiliary recycling in continuous flow: Automated recovery and reuse of Oppolzer's sultam. *Chem. Sci.* **2018**, *9*, 2130–2134. Content may be accessed at the following link: http://dx.doi.org/10.1039/C7SC05192A.

AI.3 Example GC traces of diastereomers following hydrogenation

```
File       :D:\MassHunter\GCMS\1\data\Ryan S\FID\RS-III-59\isothermal\hy
...         drog 1.D
Operator   :
Instrument :    5975B GCMS
Acquired   : 13 Jul 2017  11:14     using AcqMethod isotherm 250.M
Sample Name:
Misc Info  :
```

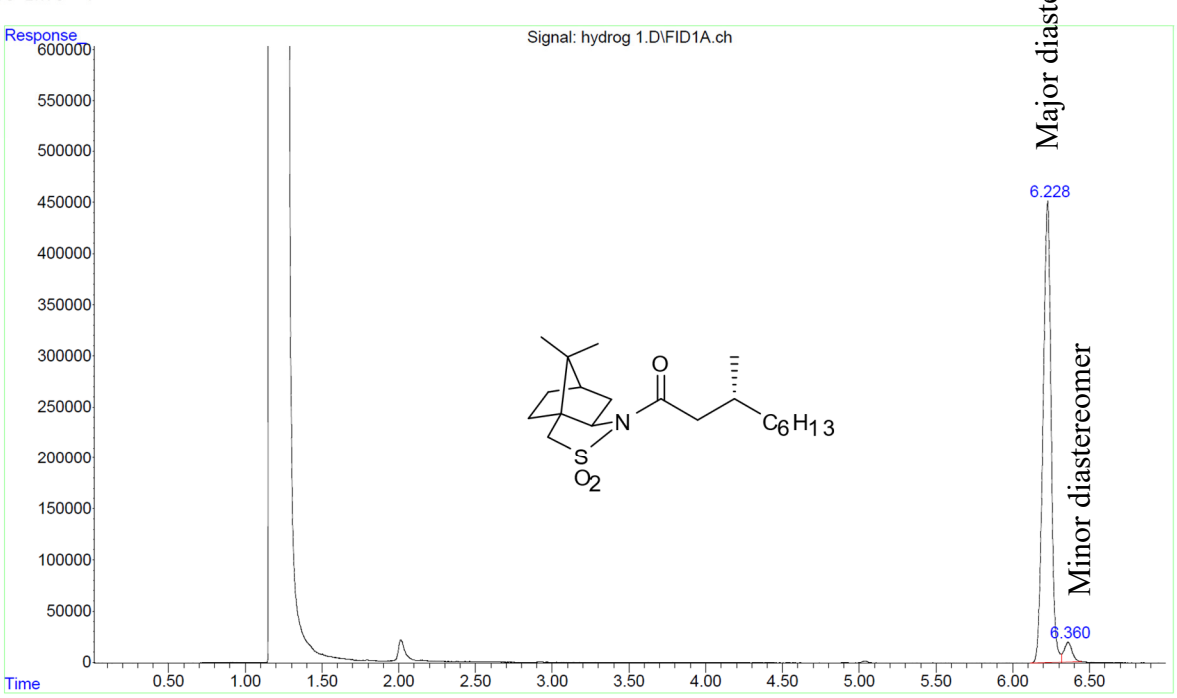

Area Percent Report

```
D ata Path : D:\MassHunter\GCMS\1\data\Ryan S\FID\RS-III-59\isothermal\
D ata File : hydrog 1.D
  Signal(s) : FID1A.ch
A cq On :    13 Jul 2017 1 1:14
S ample :
  Misc      :
  ALS Vial  : 3   Sample Multiplier: 1

I ntegration File: autoint1.e

M ethod :    D:\MassHunter\GCMS\1\methods\MS.m
T itle :

  Signal    : FID1A.ch

peak R .T. S  tart E    nd P  K p eak p     eak p    eak %    of
#   m  in m    in m     in T  Y height a    rea %    max. t  otal
--- - ---- -  ---- -   --- - -- ------- -  ------ - ----- - -----
1   6 .228 6  .115 6  .317 B V 4  51761 1 6336302 100.00% 95.861%
2   6 .360 6  .317 6  .447 V B 1   9178 7   05294 4  .32% 4 .139%
S                      um of corrected areas: 1   7041596


MS.m Fri Oct 13 11:20:15 2017
```

File :D:\MassHunter\GCMS\1\data\Ryan S\FID\RS-III-60\isothermal\hy
... dog 1.D
Operator :
Instrument : 5975B GCMS
Acquired : 25 Jul 2017 12:33 using AcqMethod isotherm 225.M
Sample Name:
Misc Info :

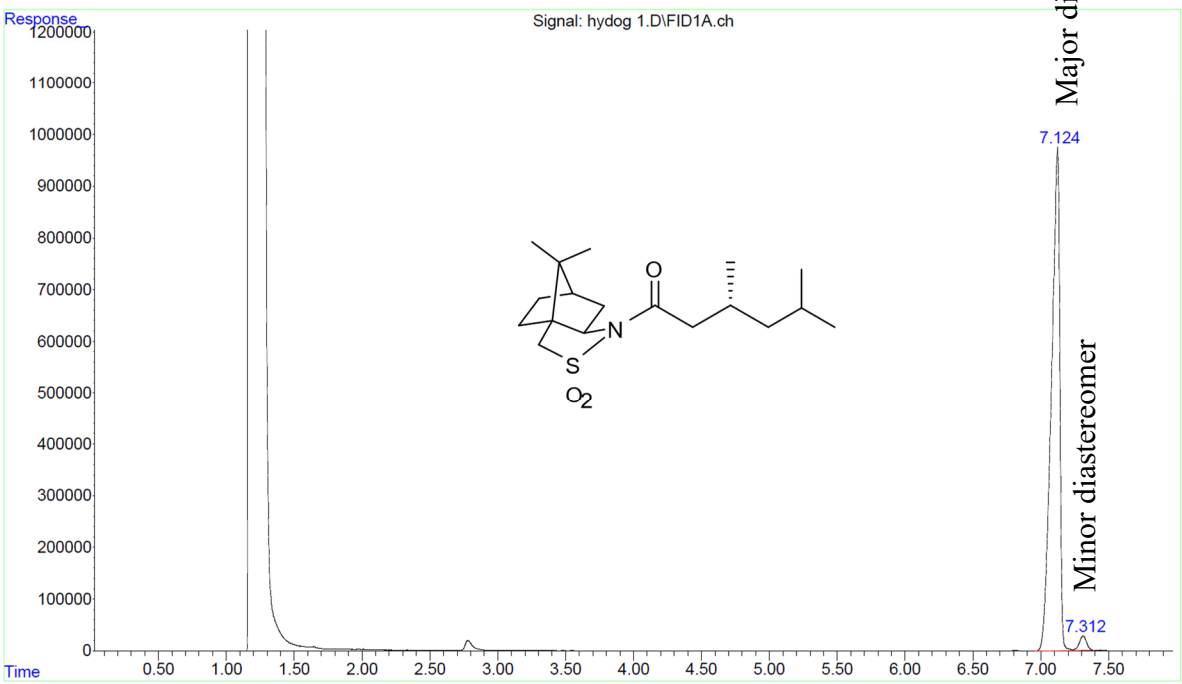

Area Percent Report

D ata Path : D:\MassHunter\GCMS\1\data\Ryan S\FID\RS-III-60\isothermal\
D ata File : hydog 1.D
Signal(s) : FID1A.ch
A cq On : 25 Jul 2017 1 2:33
S ample :
Misc :
ALS Vial : 3 Sample Multiplier: 1

I ntegration File: autoint1.e

M ethod : D:\MassHunter\GCMS\1\methods\MS.m
T itle :

Signal : FID1A.ch

peak #	R .T. m	S tart in m	E nd in m	P K T	p eak Y	p eak height	a rea	p eak rea %	eak % max.	of t otal
1	7 .124	6 .957	7 .234	B V	9 74472	4 1865966		100.00%		97.548%
2	7 .312	7 .234	7 .394	V B	2 7948	1 052414		2 .51%		2 .452%

S um of corrected areas: 4 2918380

MS.m Fri Oct 13 11:19:32 2017

```
File       :D:\MassHunter\GCMS\1\data\Ryan S\FID\RS-IV-8\isotherm\hydrog
...          1.D
Operator   :
Instrument :    5975B GCMS
Acquired   : 21 Sep 2017  11:10     using AcqMethod isotherm 275.M
Sample Name:
Misc Info  :
```

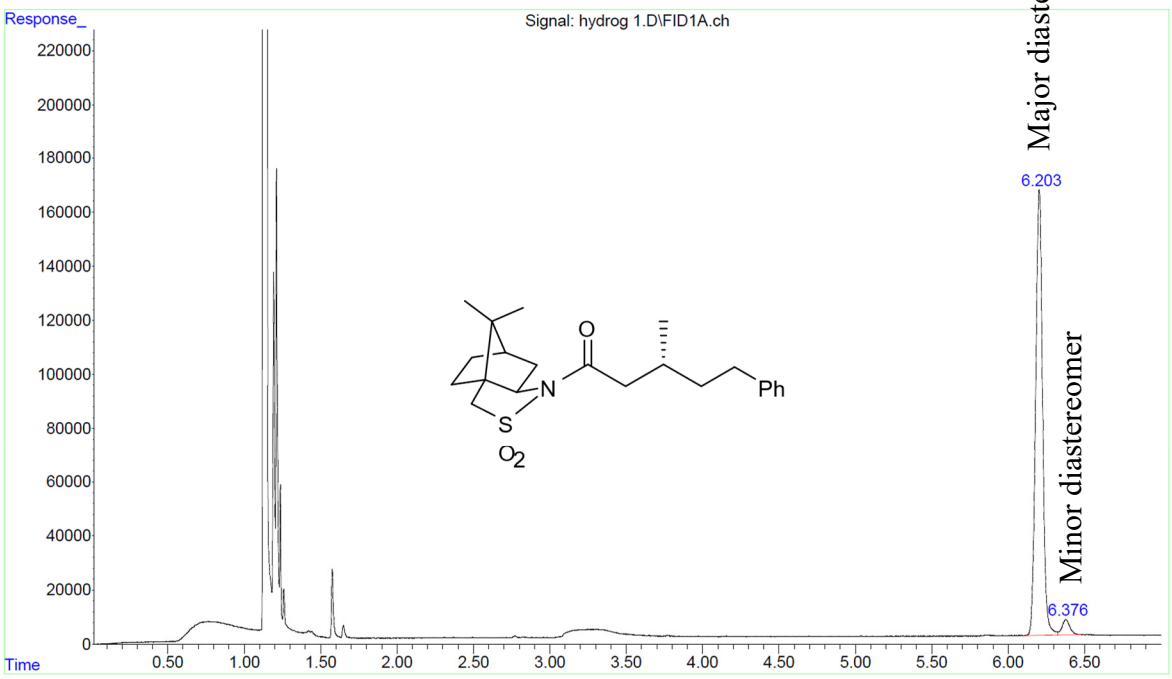

Area Percent Report

```
D ata Path : D:\MassHunter\GCMS\1\data\Ryan S\FID\RS-IV-8\isotherm\
D ata File : hydrog 1.D
  Signal(s) : FID1A.ch
A cq On :    21 Sep 2017 1 1:10
S ample :
  Misc      :
  ALS Vial  : 17   Sample Multiplier: 1

I ntegration File: autoint1.e

M ethod :    D:\MassHunter\GCMS\1\methods\MS.m
T itle :

  Signal    : FID1A.ch

peak R .T. S  tart E    nd P  K p eak p     eak p    eak %    of
#    m  in m    in m     in T  Y height a    rea %    max. t  otal
--- - ---- -  ---- -   --- - -- ------- -  ------ - ----- - -----
1    6 .203 6  .104 6  .323 B V 1  64854 5  201757 100.00% 96.258%
2    6 .376 6  .323 6  .475 V B 5    698 2   02215 3  .89% 3 .742%
S                      um of corrected areas: 5    403972


MS.m Fri Oct 13 11:22:25 2017
```

```
File       :D:\MassHunter\GCMS\1\data\Ryan S\FID\RS-III-64\hydrog 1.D
Operator   :
Acquired   : 31 Jul 2017  12:08     using AcqMethod FID_long.M
Instrument :    5975B GCMS
Sample Name:
Misc Info  :
Vial Number: 6
```

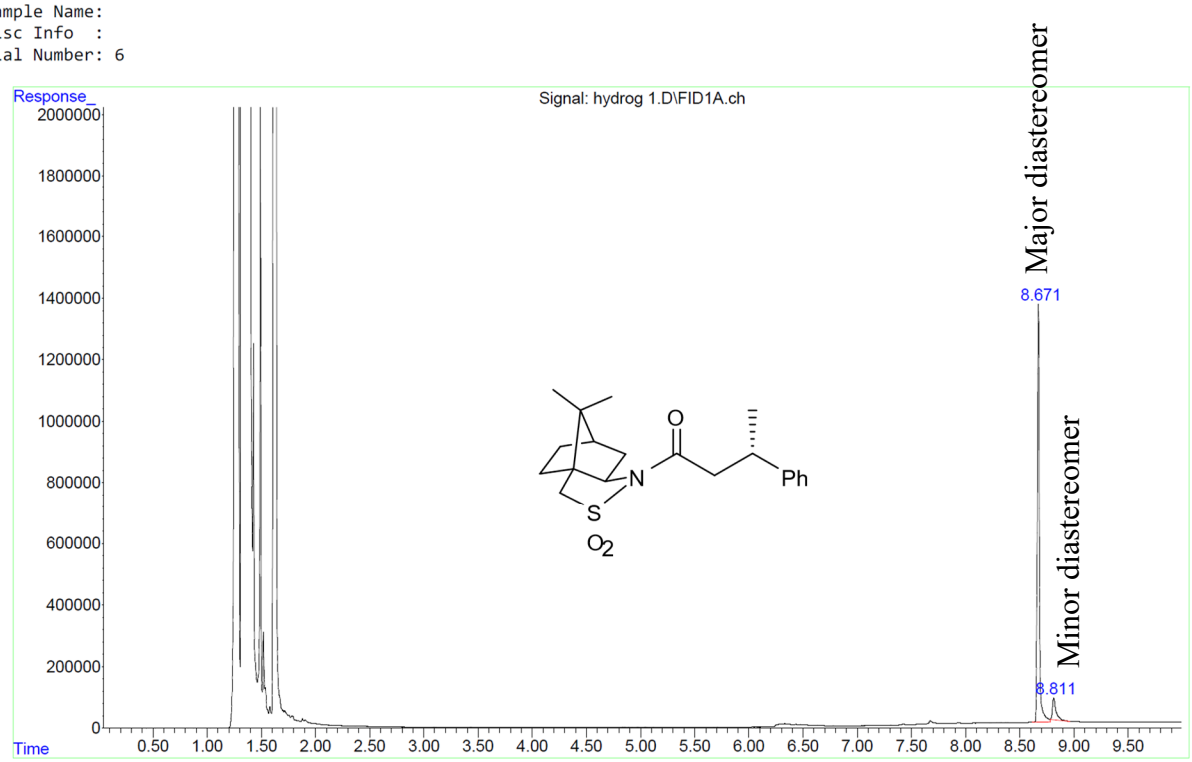

Area Percent Report

```
D ata Path : D:\MassHunter\GCMS\1\data\Ryan S\FID\RS-III-64\
D ata File : hydrog 1.D
  Signal(s) : FID1A.ch
A cq On :    31 Jul 2017 1 2:08
S ample :
  Misc      :
  ALS Vial  : 6   Sample Multiplier: 1

I ntegration File: autoint1.e

M ethod :    D:\MassHunter\GCMS\1\methods\MS.m
T itle :

  Signal    : FID1A.ch

peak R .T. S  tart E    nd P  K p eak p     eak p    eak %    of
#   m  in m    in m     in T  Y height a    rea %    max. t  otal
--- - ---- -  ---- -   --- - -- ------- -  ------ - ----- - -----
1   8 .671 8  .616 8  .783 B V 1 361159 1 7790937 100.00% 91.578%
2   8 .811 8  .784 8  .961 M     7 1846 1  636124 9  .20% 8 .422%
S                      um of corrected areas: 1   9427061


MS.m Fri Oct 13 11:25:28 2017
```

AI.4 Diastereoselective excess monitoring of hydrogenation

Diastereoselectivity over the hydrogenation stage was monitorred by withdrawing a ~25 μL aliquot from the post-hydrogenation organic phase and submitting to GC analysis every 30 min during telescoped flow experiments. Plots of d.e. over time for each substrate are provided below:

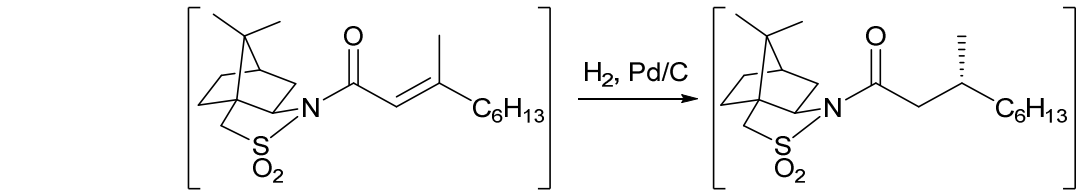

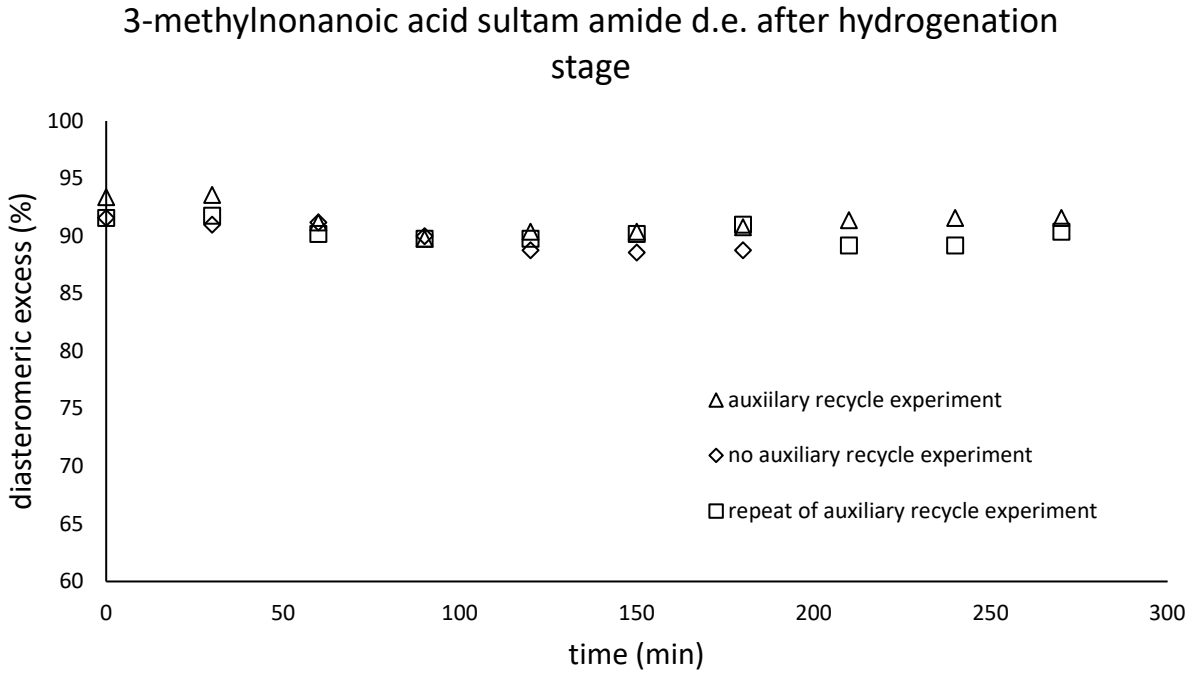

Figure AI.8. Diastereoselectivity over hydrogenation step of experiments with (*E*)-3-methylnon-2-eneoic acid chloride substrate.

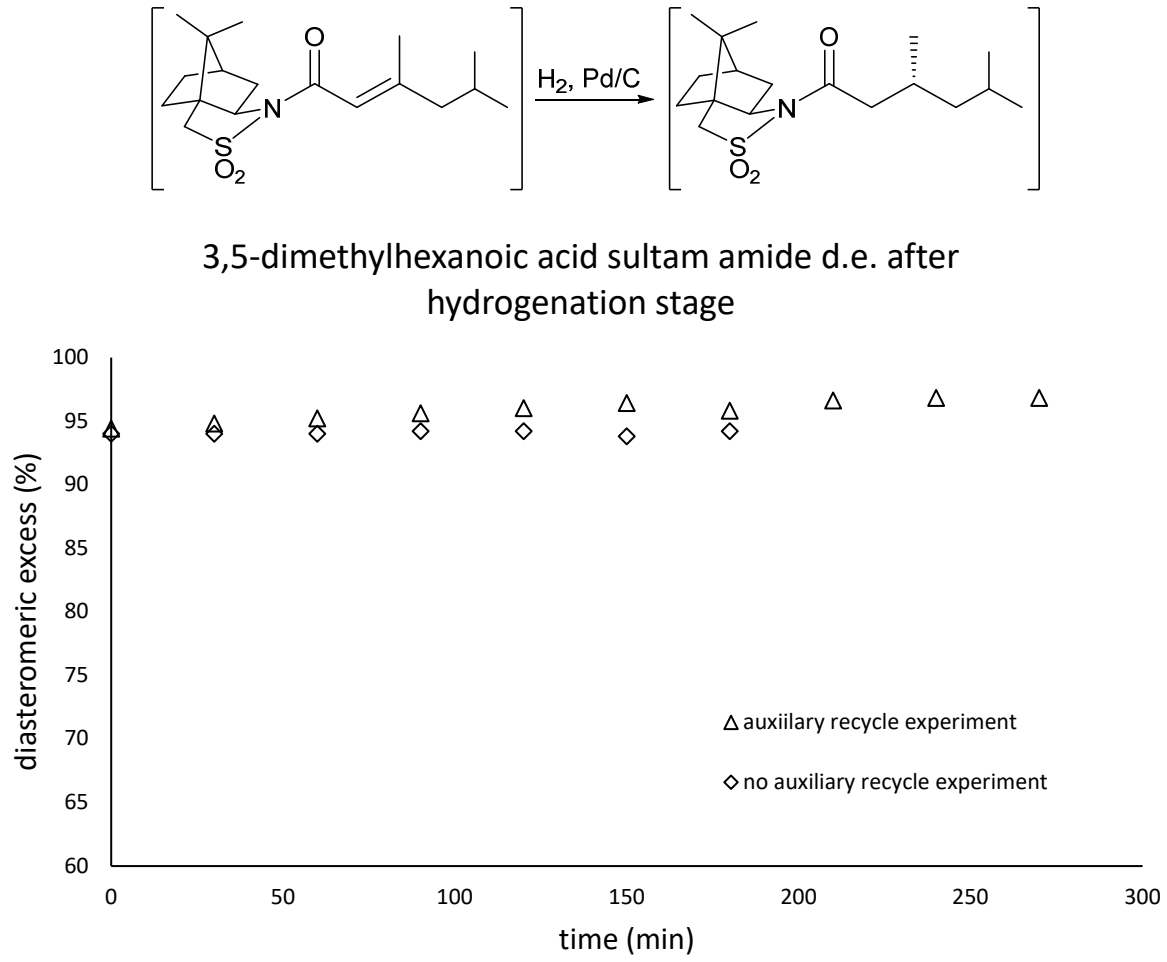

Figure AI.9. Diastereoselectivity over hydrogenation step of experiments with (*E*)-3,5-dimethylhex-2-eneoic acid chloride substrate.

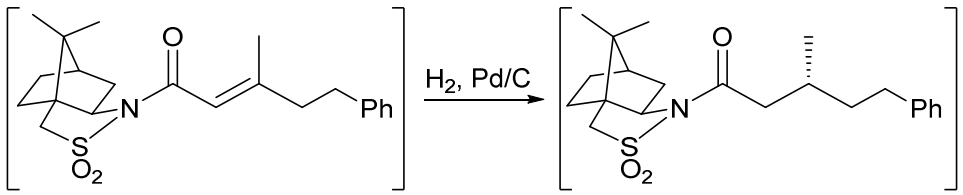

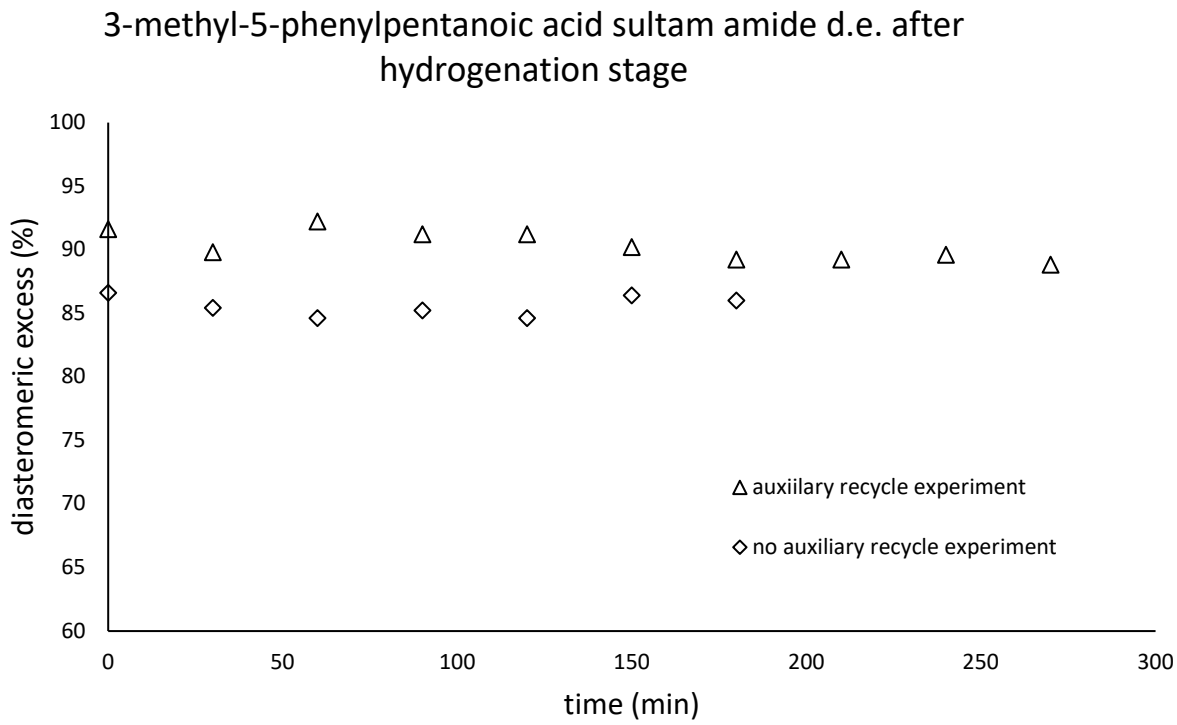

Figure AI.10. Diastereoselectivity over hydrogenation step of experiments with (*E*)-3-methyl-5-phenylpent-2-eneoic acid chloride substrate.

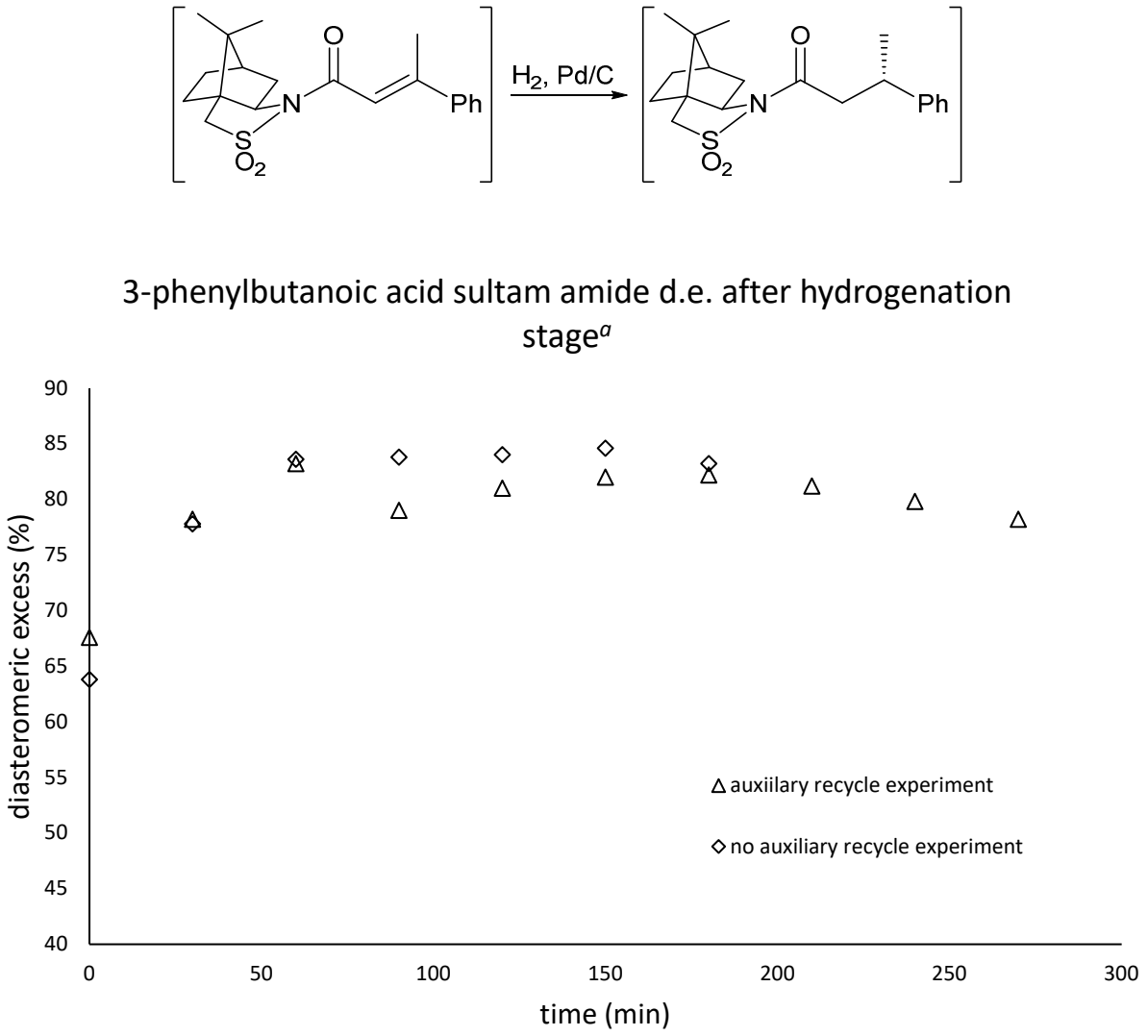

Figure AI.11. Diastereoselectivity over hydrogenation step of experiments with (*E*)-3-phenylbut-2-eneoic acid chloride substrate.

[a] The d.r. of the 3,3-dialkyl substrates over the hydrogenation was steady from the first elution of product from the PBR, but the 3,3-aryl,alkyl substrate exhibited an initially lower d.r. of 80:20 that increased over the first 60 min of operation to 92:8 (auxiliary recovery experiment) or 90:10 (auxiliary recycle experiment) and then remained steady at this selectivity for the remainder of the experiment. This was attributed to chromatography effects within the PBR and represents a longer time to attain true steady-state operation with this substrate.

AI.5 Chiral HPLC trace of (*R*)-3-methyl-5-phenylbutanoic acid methyl ester

```
Data File C:\CHEM32\1\DATA\NEWMAN\RS OCT 05 17 2017-10-05 15-58-00\072-0401.D
Sample Name: RS3 Oct 05 17

    ======================================================================
    Acq. Operator   : Beauchemin                    Seq. Line :   4
    Acq. Instrument : Instrument 1                  Location : Vial 72
    Injection Date  : 10/5/2017 7:01:22 PM             Inj :   1
                                                   Inj Volume : 5 µl
    Acq. Method     : C:\Chem32\1\DATA\NEWMAN\RS OCT 05 17 2017-10-05 15-58-00\COL4-0_25PC-IPROH-
                      75MIN.M
    Last changed    : 10/5/2017 3:56:24 PM by Beauchemin
    Analysis Method : C:\CHEM32\1\DATA\NEWMAN\RS OCT 05 17 2017-10-05 15-58-00\072-0401.D\DA.M (
                      COL4-0_25PC-IPROH-75MIN.M)
    Last changed    : 10/11/2017 5:00:43 PM by Beauchemin
                      (modified after loading)
```

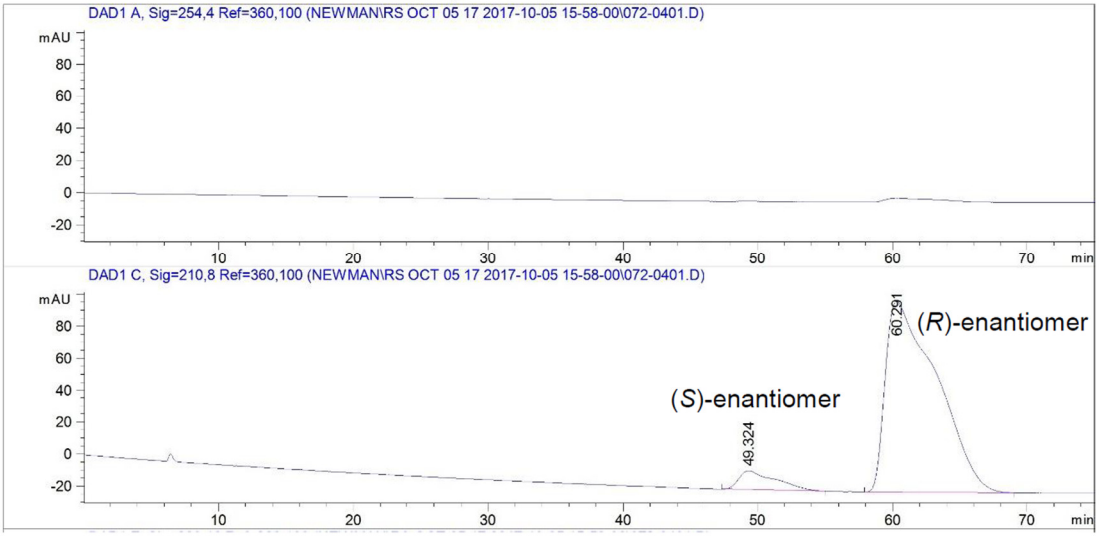


```
Data File C:\CHEM32\1\DATA\NEWMAN\RS OCT 05 17 2017-10-05 15-58-00\072-0401.D
Sample Name: RS3 Oct 05 17

   ======================================================================
                          Area Percent Report
   ======================================================================

   Sorted By             :      Signal
   Multiplier            :      1.0000
   Dilution              :      1.0000
   Use Multiplier & Dilution Factor with ISTDs


   Signal 1: DAD1 A, Sig=254,4 Ref=360,100


   Signal 2: DAD1 C, Sig=210,8 Ref=360,100

   Peak RetTime Type  Width     Area      Height     Area
     #   [min]       [min]   [mAU*s]     [mAU]       %
   ----|-------|----|-------|----------|----------|--------|
      1  49.324 BV    2.5198 2238.77808   11.83050   6.6108
      2  60.291 BB    3.5475 3.16264e4   119.34978  93.3892

   Totals :                  3.38652e4   131.18029
```

Appendix II. Supporting Information for Chapter 3

AII.1 Solubility studies of triethylammonium halide salts

Since the conjugate acids of organic bases are usually sparingly soluble in non-polar solvents, clogging is common even at dilute concentrations for substitution reactions that are performed with, e.g., triethylamine in toluene. When using more polar solvents, as is common for S_NAr and S_N2 reactions however, it can be difficult to predict whether or not precipitation of the conjugate acid will be problematic in a flow reaction. The likelihood of clogging depends on the choice of solvent, temperature, concentration, base, and leaving group. These things are often optimized empirically when converting a batch procedure into flow. Because bases such as 1-methylimidazole, tributylamine, and DBU form ionic liquids upon protonation, use of these species as bases should overcome the need to perform extensive optimization. Nonetheless, there are particular combinations of base, concentration, and temperature where-in the use of these ionic-liquid scavengers would be unnecessary.

To obtain some data to understand when the use of triethylamine would allow substitution reactions to occur in flow with NMP as a solvent, some crude solubility experiments were carried out (Table AII.1). For instance, when slowly heating a 0.50 M solution of triethylammonium chloride in NMP, the mixture became homogeneous at an external bath temperature of 112 °C (entry 1). A 1.0 M solution became homogeneous at 135 °C (entry 2), whereas a 2.0 M solution did not become homogeneous at 150 °C (entry 3), the maximum temperature tested. This information allowed us to focus our studies of S_NAr and S_N2 reactions at concentrations and temperatures that would otherwise lead to clogging if, e.g., triethylamine was used as a base.

However, even in cases where a reaction is carried out under conditions where the triethylammonium salt does not immediately precipitate, clogging issues can still occur upon exiting the reactor or during quench. In contrast, reactions performed herein with ionic liquid-forming bases were observed to be exceptionally robust. Furthermore, control reactions in batch with triethylamine as the base for each S_N2 reaction studied led to precipitate formation during the course of the reaction, demonstrating that clogging issues would be present with the conditions investigated in the absence of the ionic liquid-forming acid scavenger.

Table AII.1. Solubility studies of triethylammonium halide salts in NMP.

entry	compound	Concentration (M)	Temperature to dissolve on heating (°C)
1	$Et_3N{\cdot}HCl$	0.50	112
2	$Et_3N{\cdot}HCl$	1.0	135
3	$Et_3N{\cdot}HCl$	2.0	not fully dissolved at 150
4	$Et_3N{\cdot}HBr$	0.50	78
5	$Et_3N{\cdot}HBr$	1.0	120
6	$Et_3N{\cdot}HBr$	2.0	not fully dissolved at 150

AII.2 Determination of tributylammonium chloride melting point

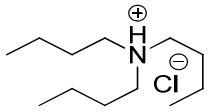

Tributylammonium chloride.[1] 4 M HCl (8 mmol) in dioxane was added dropwise to tributylamine (8 mmol) in diethyl ether and stirred for 20 minutes in room temperature. Removing volatile chemicals under reduced pressure and recrystallizing from mixture of hexane and ethyl acetate gave tributylammonium chloride as white needles. Characterization data were in agreement with the literature.[2] mp: 58–62 °C. ^{1}H NMR (400 MHz, $(CD_3)_2SO$): δ 10.43 (br s, 1H), 3.02–2.93 (m, 6H), 1.68–1.57 (m, 6H), 1.36–1.25 (m, 6H), 0.91 (t, J = 7.3 Hz, 9H).

AII.3 Spectra of products

Spectra of products are freely available in the supporting information for: K. Kashani, S.; Sullivan, R. J.; Andersen, M.; Newman, S. G. Overcoming solid handling issues in continuous flow substitution reactions through ionic liquid formation. *Green Chem.* **2018**, *20*, 1748–1753. Content may be accessed at the following link: http://dx.doi.org/10.1039/C8GC00618K.

[1] Prepared by S. K. Kashani.
[2] Reichenbach, J.; Ruddell, S. A.; González-Jiménez, M.; Lemes, J.; Turton, D. A.; France, D. J.; Wynne, K. Phonon-like hydrogen-bond modes in protic ionic liquids. *J. Am. Chem. Soc.* **2017**, *139*, 7160–7163.

Appendix III. Supporting information for Chapter 4

AIII.1 Isotope patterns of observed species.

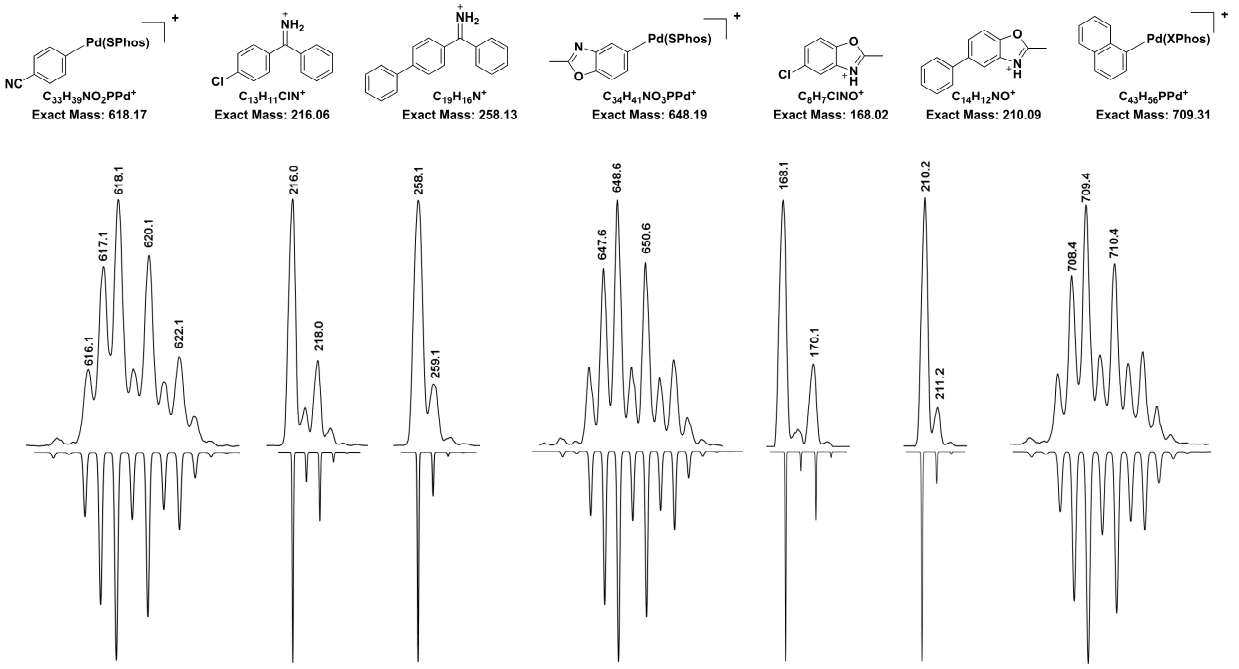

Figure AIII.1. Observed and calculated isotope patterns for the species monitored by ESI-MS.

AIII.2 Aryl bromide-diazo cross-coupling optimization

Initial optimization was performed using stabilized ethyl 2-diazopropoanate (Table AIII.1). Decreasing the palladium loading relative to the literature report had detrimental affect (entry 2). Changing between XPhos and SPhos had little effect (entry 3). Switching from $[Pd(allyl)Cl]_2$ to $Pd(OAc)_2$ resulted in marginal improvement (entry 4). Addition of the diazo over 3 (entry 6) or 15 min (entry 4) further improved yields but not to satisfactory levels, although allowing a further decrease the palladium loading to 2.5% (entry 8) with negligible impact relative to 5% loading. Examination of pre-ligated precatalysts showed the Buchwald G2 type precatalysts were ineffective (entry 9), but Pd(XPhos)(allyl)Cl (entry 10) and Pd(XPhos)(cinnamyl)Cl (entry 11) were active precatalysts. Inclusion of one additional equivalent of ligand was necessary for high yield (entry 13) and had greater impact that doubling the precatalyst loading (entry 12), suggesting that ligand destruction is the most significant source of catalyst death. Finally, increasing to 3.5%

from 2.5% catalyst loading led to near quantitative yield (entry 14) for the reaction with the stabilized diazo compound. When changing to the less stable, α-aryl diazo reagent, a decrease in yield was observed (entry 15), requiring an increase in the equivalency from 1.5 to 2.0 eq. to maintain high yield for reactions with the non-stabilized diazo reagents (entry 16).

Table AIII.1. Optimization of the aryl bromide-diazo cross-coupling reactions.

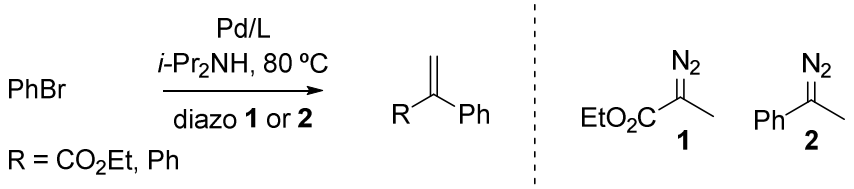

entry	Pd precatalyst	% Pd	ligand (%)	diazo	diazo eq.	addition time (min)	yield[a]
1	$[Pd(allyl)Cl]_2$	10	XPhos (10%)	**1**	1.5	n/a	86[1]
2	$[Pd(allyl)Cl]_2$	5	XPhos (10%)	**1**	1.5	n/a	53
3	$[Pd(allyl)Cl]_2$	5	SPhos (10%)	**1**	1.5	n/a	47
4	$Pd(OAc)_2$	5	XPhos (10%)	**1**	1.5	n/a	66
5	$Pd(OAc)_2$	5	XPhos (10%)	**1**	1.25	3	69
6	$Pd(OAc)_2$	5	XPhos (10%)	**1**	1.25	15	74
7	$Pd(OAc)_2$	5	XPhos (10%)	**1**	1.5	15	76
8	$Pd(OAc)_2$	2.5	XPhos (5%)	**1**	1.5	15	63
9	Pd-XPhos G2 precat.	2.5	n/a	**1**	1.5	15	27
10	Pd(XPhos)(allyl)Cl	2.5	n/a	**1**	1.5	15	54
11	Pd(XPhos)(cinnamyl)Cl	2.5	n/a	**1**	1.5	15	46
12	Pd(XPhos)(allyl)Cl	5	n/a	**1**	1.5	15	70
13	Pd(XPhos)(allyl)Cl	2.5	XPhos (2.5%)	**1**	1.5	15	77
14	Pd(XPhos)(allyl)Cl	3.5	XPhos (3.5%)	**1**	1.5	15	>95, (77[b])
15	Pd(XPhos)(allyl)Cl	3.5	XPhos (3.5%)	**2**	1.5	15	64[b]
16	Pd(XPhos)(allyl)Cl	3.5	XPhos (3.5%)	**2**	2	20	90[b]

[a] Conditions: 0.2 mmol of PhBr, 3 eq of *i*-Pr_2NH, toluene, 80 °C, diazo added all at once and stirred for 1 h or over *x* min and stirred 15 additional min after addition complete. Yield determined by proton NMR of crude mixture with 1,3,5-trimethoxybenzene as internal standard. [b] Isolated yield.

[1] Peng, C.; Yan, G.; Wang, Y.; Jiang, Y.; Zhang, Y.; Wang, J. Palladium-catalyzed coupling reaction of α-diazocarbonyl compounds with aromatic boronic acids or halides. *Synthesis* **2010**, *2010*, 4154–4168.

AIII.3 Robustness of diazo generation over MnO_2

The literature conditions for oxidation of hydrazones to diazo compounds over MnO_2 used flow rates of 0.5 mL/min and DCM as solvent, with DIPEA as the organic base.[2] To enable compatibility with the conditions needed for the diazo-aryl halide cross coupling (toluene, *i*-Pr_2NH, slower flow rate) the robustness of the generation of 2-diazoacetophenone from acetophenone hydrazone was investigated using an esterification quench with benzoic acid for quantification of diazo 'yield' (Scheme AIII.1).

Scheme AIII.1. Examination of diazo generation from acetophenone hydrazone using a quench with benzoic acid for quantification of diazo 'yield'.

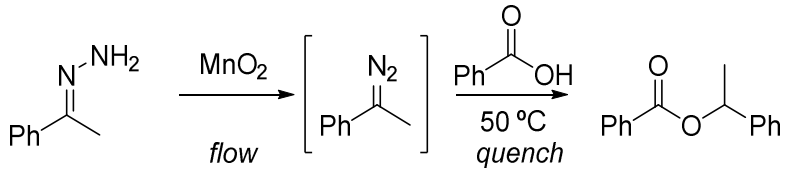

A Design of Experiments (DoE) 3 factor, 2-level factorial design was executed examining the effect of hydrazone concentration (0.05–0.1 M), flow rate through the MnO_2 packed bed (0.15–0.35 mL/min) and equivalence of *i*-Pr_2NH (1–2 eq). The affect of increased base always improved diazo yield, so 2 eq. of *i*-Pr_2NH was selected and additional experiments to complete a central composite design in order to generate a response surface for the factors of hydrazone concentration and flow rate were completed. The response surface is shown in Figure AIII.2. The effect of hydrazone concentration was relatively minor, while the effect of increased flow rate resulted in a slight increase in diazo yield. Flow rates of 0.35 mL/min were therefore selected and hydrazone concentration was modified to achieve desired molar addition rates for cross-coupling reactions.

[2] Poh, J.-S.; Tran, D. N.; Battilocchio, C.; Hawkins, J. M.; Ley, S. V. A versatile room-temperature route to di- and trisubstituted allenes using flow-generated diazo compounds. *Angew. Chem. Int. Ed.* **2015**, *54*, 7920–7923.

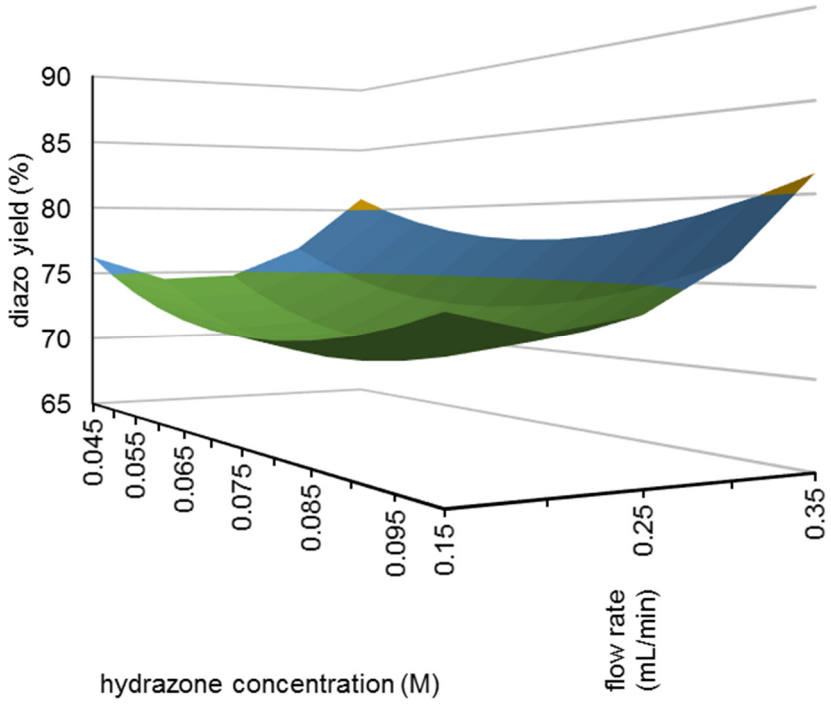

Figure AIII.2. Response surface of 2-diazoacetophenone yield as a function of acetophenone hydrazone concentration in toluene and flow rate through a 3×50 mm packed bed of MnO_2 in the presence of 2 eq. of *i*-Pr_2NH.

AIII.4 Calculation of TOF from computed energy profiles

In order to calculate turn over frequency (TOF) from an energy diagram, the energetic span model was applied. In this model, the energy separation between the turnover frequency determining transition state (TDTS, lowest energy intermediate) and turnover frequency determining intermediate (TDI, transition state that maximizes the energetic span) corrected for the free energy of the net process if the TDTS precedes the TDI according to Eq. AIII.1 is used.[3]

$$\mathrm{TOF} = \frac{k_\mathrm{B}T}{h}\mathrm{e}^{-\delta E/RT} \qquad \text{(Eq. AIII.1)}$$

$$\delta E = \begin{Bmatrix} T_\mathrm{TDTS} - I_\mathrm{TDI} & \text{if TDTS follows TDI} \\ T_\mathrm{TDTS} - I_\mathrm{TDI} + \Delta G_\mathrm{rxn} & \text{if TDTS proceeds TDI} \end{Bmatrix}$$

[3] Kozuch, S.; Shaik, S. How to conceptualize catalytic cycles? The energetic span model. *Acc. Chem. Res.* **2011**, *44*, 101–110.

For this transformation it was found that the TDTS was oxidative addition of Pd(0) into the aryl chloride and the TDI was the intermediate following aryl group migration into the Pd-carbene. The energies used and calculated TOF for the three substrates are summarized in Table AIII.2.

Table AIII.2. Calculated energies of ΔG, E_{TDTS}, E_{TDI} and δE used for the calculation of relative TOF presented in Figure 4.8.

ArCl	ΔG (kcal/mol)	E_{TDTS} (kcal/mol)	E_{TDI} (kcal/mol)	δE (kcal/mol)	TOF at T = 373 K (h^{-1})	relative TOF
PhCl	-46.402	8.128	-70.557	32.283	3.46×10^{-3}	1.0
4-CN-PhCl	-47.051	5.119	-70.719	28.787	3.86×10^{-1}	1.1×10^{2}
4-OMe-PhCl	-46.806	10.915	-70.297	34.406	1.97×10^{-4}	5.7×10^{-2}

AIII.5 Supplemental computational results

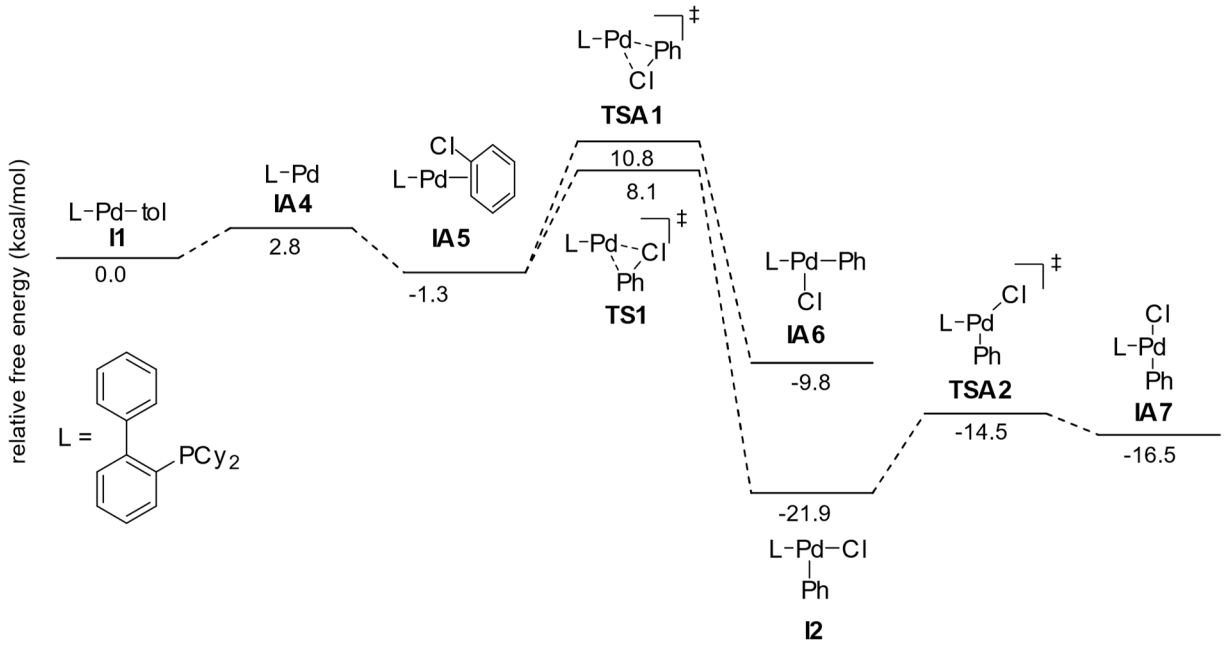

Figure AIII.3. Additional details of the oxidative addition; M06-L/def2-TZVP//M06-L/def2-SVP level of theory.

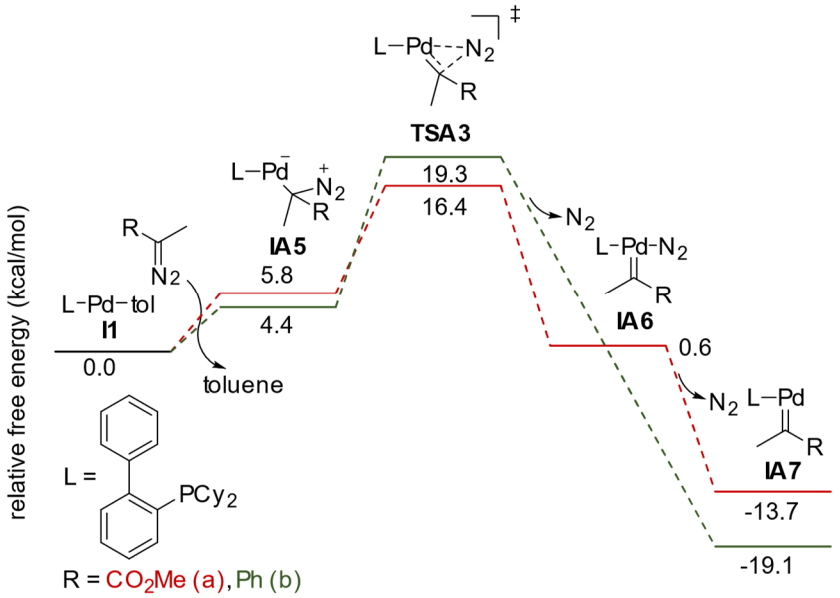

Figure AIII.4. Energy profile for the direct reaction of diazo compound with Pd(0); M06-L/def2-TZVP//M06-L/def2-SVP level of theory.

AIII.6 Spectra of substrates and products

Spectra of substrates and products are freely available in the supporting information for: Sullivan, R. J.; Freure, G. P. R.; Newman, S. G. Overcoming scope limitations in cross-coupling of diazo nucleophiles by manipulating catalyst speciation and using flow diazo generation. *ACS Catal.* **2019**, *9*, 5623–5630. Content may be accessed at the following link: http://dx.doi.org/10.1021/acs.orglett.6b02631.

AIII.7 Energies of calculated structures

Table AIII.3. Energies (in Hartree) for all organic and organometallic compounds and transition states. E_{DZ} and thermal corrections were calculated at the M06-L/def2-SVP level of theory; E_{TZ} single point energy calculations were performed on the M06-L/def2-SVP geometries at the M06-L/def2-TZVP level of theory with incorporation of solvation energy using the continuous polarization model for toluene.

	Energies		Thermal Corrections (T = 298.15 K, p = 1 atm)		
Structure	E_{TZ}	E_{DZ}	E_{zpe}	H	G
Organic molecules					
N_2	-109.55816665	-109.42719129	0.005618	0.008923	-0.012830
PhCl	-691.90314419	-691.50908577	0.091114	0.097511	0.062044
4-CN-PhCl	-784.17370038	-783.67374057	0.089743	0.097897	0.057361
4-OMe-PhCl	-806.45683059	-805.93269845	0.124025	0.132922	0.090862
toluene	-271.61989932	-271.33230639	0.127886	0.134964	0.097854
methyl 2-diazopropanoate	-416.06634552	-415.59652189	0.104973	0.114874	0.070240
2-diazoacetophenone	-419.22197190	-418.77047223	0.143246	0.152955	0.109315
Me 2-Ph-acrylate	-537.64882099	-537.06480304	0.177023	0.188758	0.139898
Me 2-(4'-CN-Ph)acrylate	-629.92095090	-629.23110151	0.175654	0.189197	0.135754
Me 2-(4'-OMe-Ph)acrylate	-652.20399742	-651.49008535	0.209903	0.224088	0.169563
1,1-diphenylethylene	-540.81203671	-540.24512970	0.214441	0.226436	0.176792
i-Pr2NH	-292.48458393	-292.16815112	0.205386	0.215626	0.172352
i-Pr_2NH·HCl	-753.32372048	-752.85519750	0.216316	0.228261	0.180256
Organometallic compounds (L = CyJohnPhos) PhCl + methyl 2-diazopropaoate (R = CO_2Me)					
L–Pd–tol **I1**	-1674.48021970	-1673.07013584	0.623360	0.656730	0.558172
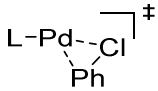 **TS1a**	-2094.74936770	-2093.23242448	0.585415	0.618070	0.521218
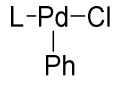 **I2a**	-2094.80190957	-2093.28180634	0.588455	0.620949	0.525970

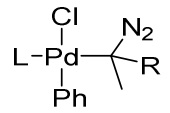 **I3a**	-2510.87488453	-2508.89215461	0.694777	0.737652	0.619059
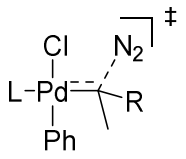 **TS2a**	-2510.84761272	-2508.86453662	0.691563	0.734378	0.615657
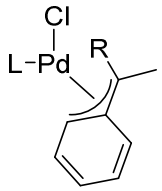 **I5a**	-2401.39413321	-2399.53768870	0.687239	0.727112	0.615482
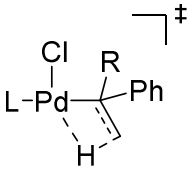 **TS4a**	-2401.36344740	-2399.50588228	0.683382	0.722655	0.611709
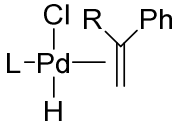 **I6a**	-2401.36923457	-2399.51139551	0.682935	0.723065	0.609757
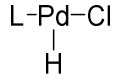 **I7**	-1863.70907575	-1862.42700161	0.504904	0.532865	0.446834
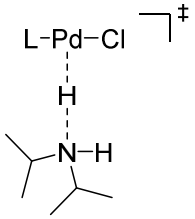 **TS5**	-2156.20319330	-2154.61122866	0.712039	0.749459	0.644229

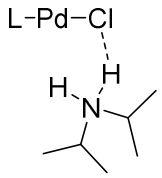 **I8**	-2156.21786769	-2154.62398231	0.716220	0.754504	0.646374
PhCl + 2-diazoacetophenone (R = Ph)					
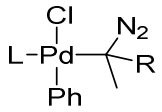 **I3b**	-2514.03175530	-2512.06570916	0.732370	0.775410	0.656273
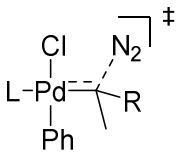 **TS2b**	-2514.01482815	-2512.04883080	0.730328	0.772935	0.655845
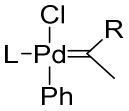 **I4b**	-2404.48268226	-2402.64105596	0.722004	0.763096	0.647291
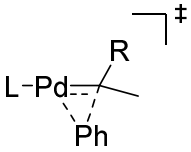 **TS3b**	-2404.48207734	-2402.63835704	0.722108	0.762297	0.649636
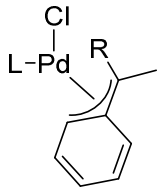 **I5b**	-2404.55217182	-2402.71200115	0.725583	0.765551	0.653925
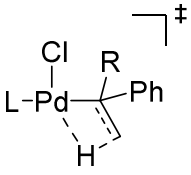 **TS4b**	-2404.52278717	-2402.68152806	0.721318	0.760973	0.649024

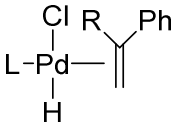 **I6b**	-2404.52942256	-2402.68628906	0.721851	0.762116	0.648525
4-CN-PhCl + methyl 2-diazopropaoate (R = CO_2Me, Ar = 4-CN-phenyl, R' = CN)					
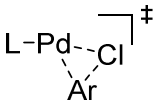 **TS1c**	-2187.02669185	-2185.40448543	0.584539	0.618792	0.518508
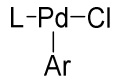 **I2c**	-2187.07690950	-2185.45143601	0.588032	0.622060	0.523936
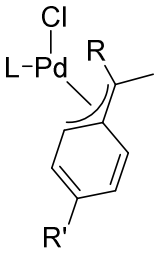 **I5c**	-2493.66518403	-2491.70459816	0.685358	0.727208	0.611036
4-OMe-PhCl + methyl 2-diazopropaoate (R = CO_2Me, Ar = 4-OMeN-phenyl, R' = OMe)					
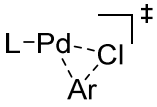 **TS1d**	-2209.30234571	-2207.65579782	0.619270	0.654021	0.553769
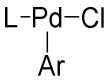 **I2d**	-2209.35531064	-2207.70566322	0.621923	0.656728	0.556782
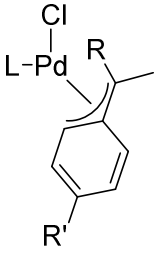 **I5d**	-2515.94927897	-2513.96352920	0.720342	0.762719	0.646173
Additional oxidative addition details					
 **IA1**	-1402.83660417	-1401.71056490	0.494978	0.520379	0.441043

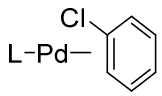 **IA2**	-2094.76450199	-2093.24977263	0.585854	0.618842	0.521268
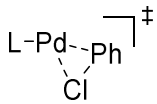 **TSA1**	-2094.74586445	-2093.22934160	0.586196	0.618738	0.522023
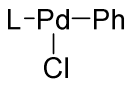 **IA3**	-2094.78013769	-2093.26313144	0.587559	0.620504	0.523390
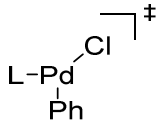 **TSA2**	-2094.78843398	-2093.26523179	0.587954	0.620092	0.524206
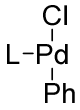 **IA4**	-2094.79157142	-2093.26770446	0.588408	0.621168	0.524207
Direct reaction of Pd(0) with methyl 2-diazopropanoate (R = CO_2Me)					
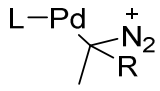 **IA5a**	-1818.92094126	-1817.33166099	0.600532	0.636355	0.534048
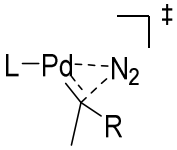 **TSA3a**	-1818.90406327	-1817.30922707	0.598741	0.634493	0.531430
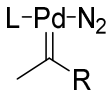 **IA6a**	-1818.92631534	-1817.32765456	0.599115	0.635618	0.531145
 **IA7a**	-1709.37754394	-1707.90912365	0.591879	0.625221	0.528243

Direct reaction of Pd(0) with 2-diazoacetophenone (R = Ph)					
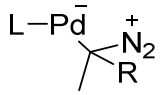 **IA5b**	-1822.07643815	-1820.50385805	0.638229	0.674257	0.570759
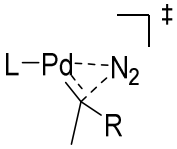 **TSA3b**	-1822.05289864	-1820.47683463	0.637299	0.672919	0.570959
 **IA7b**	-1712.53531954	-1711.08271800	0.628499	0.66232	0.563160

AIII.8 Cartesian coordinates of calculated structures

Cartesian coordinates of calculated structures are freely available in the supporting information for: Sullivan, R. J.; Freure, G. P. R.; Newman, S. G. Overcoming scope limitations in cross-coupling of diazo nucleophiles by manipulating catalyst speciation and using flow diazo generation. *ACS Catal.* **2019**, *9*, 5623−5630. Content may be accessed at the following link: http://dx.doi.org/10.1021/acs.orglett.6b02631.

Appendix IV. Supporting information for Chapter 5

AIV.1 Photographs of experimental setup

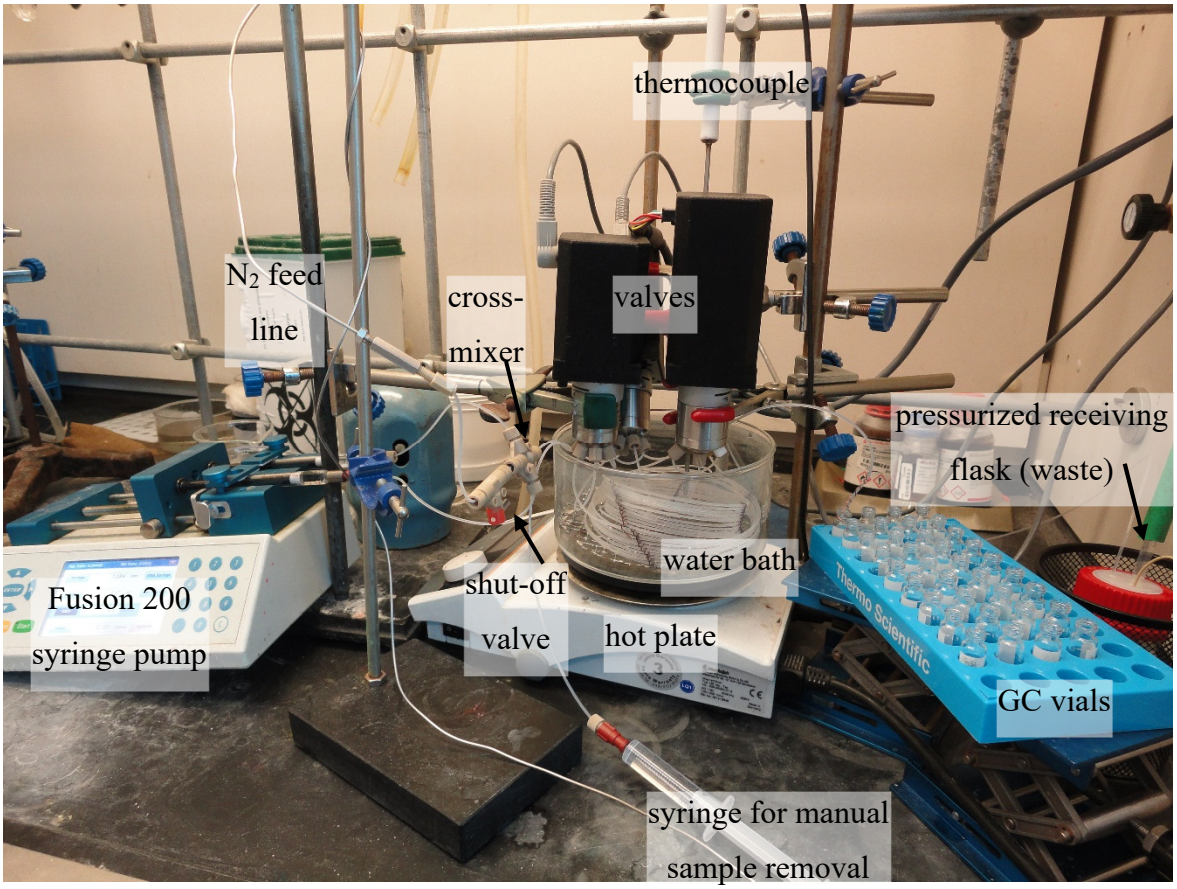

Figure AIV.1. Photograph of reactor used for acylation, S_NAr, TBS protection, and solvolysis kinetics; water is drained from the bath for clarity. Out of view: N_2 cylinder and mass flow controller, step-down regulator for compressed air, computer to control valves.

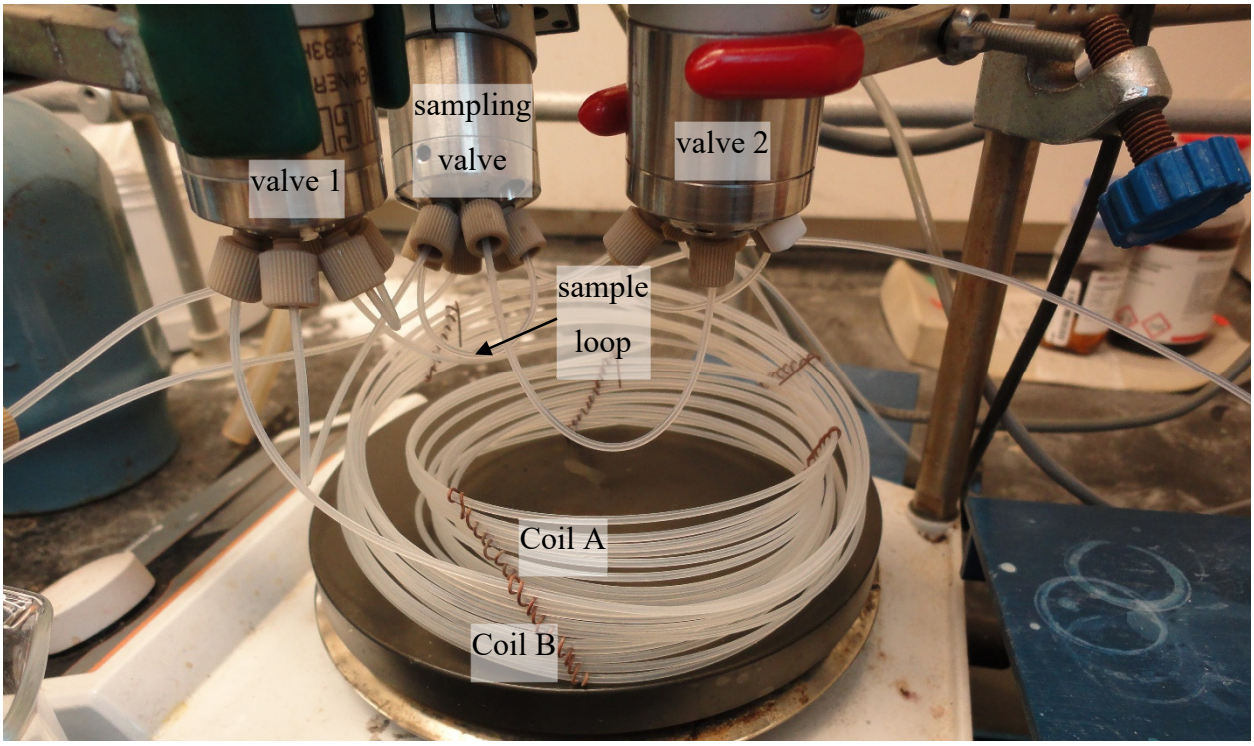

Figure AIV.2. Close-up photograph of reactor coils.

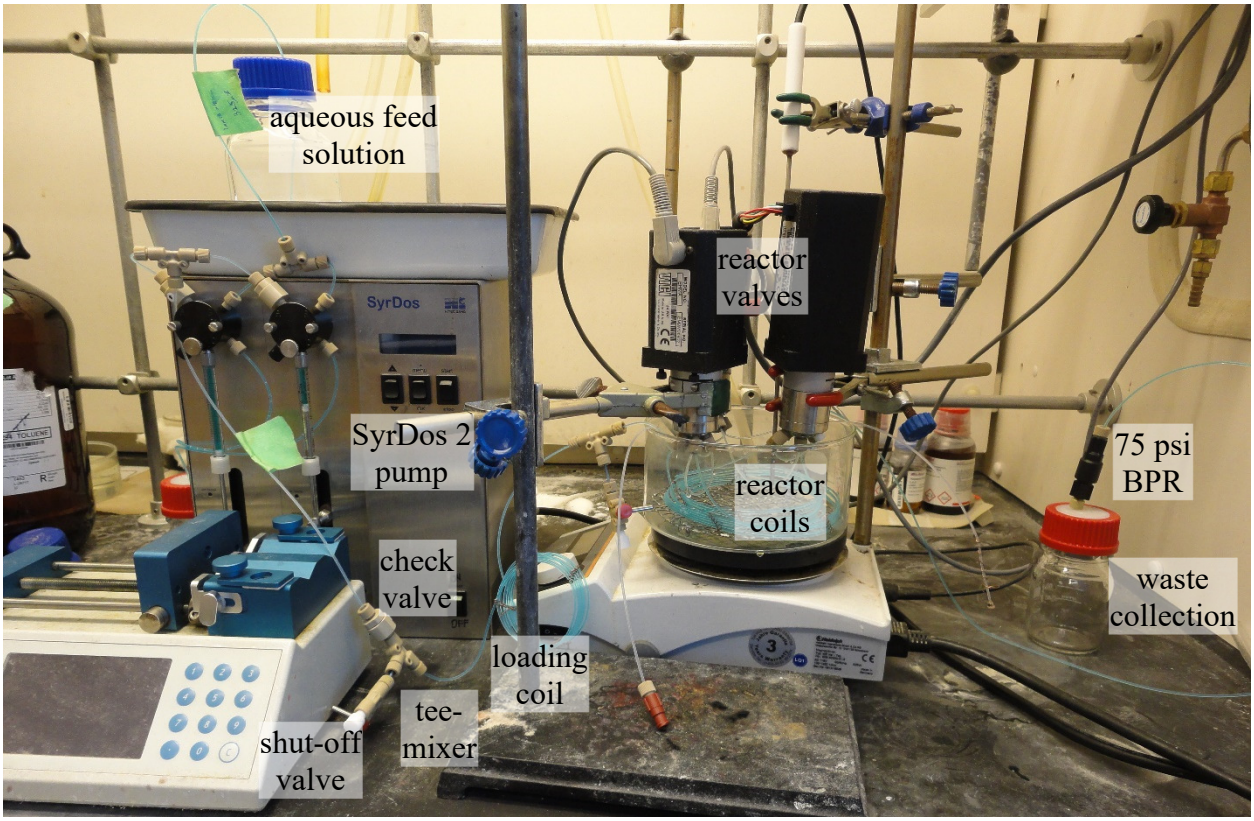

Figure AIV.3. Photograph of reactor setup used for cycloaddition kinetics. Blue dye (Brilliant blue) added to aqueous solution for visual contrast. Omitted from image: GC vials and syringes used for reaction initiation/manual sample collection.

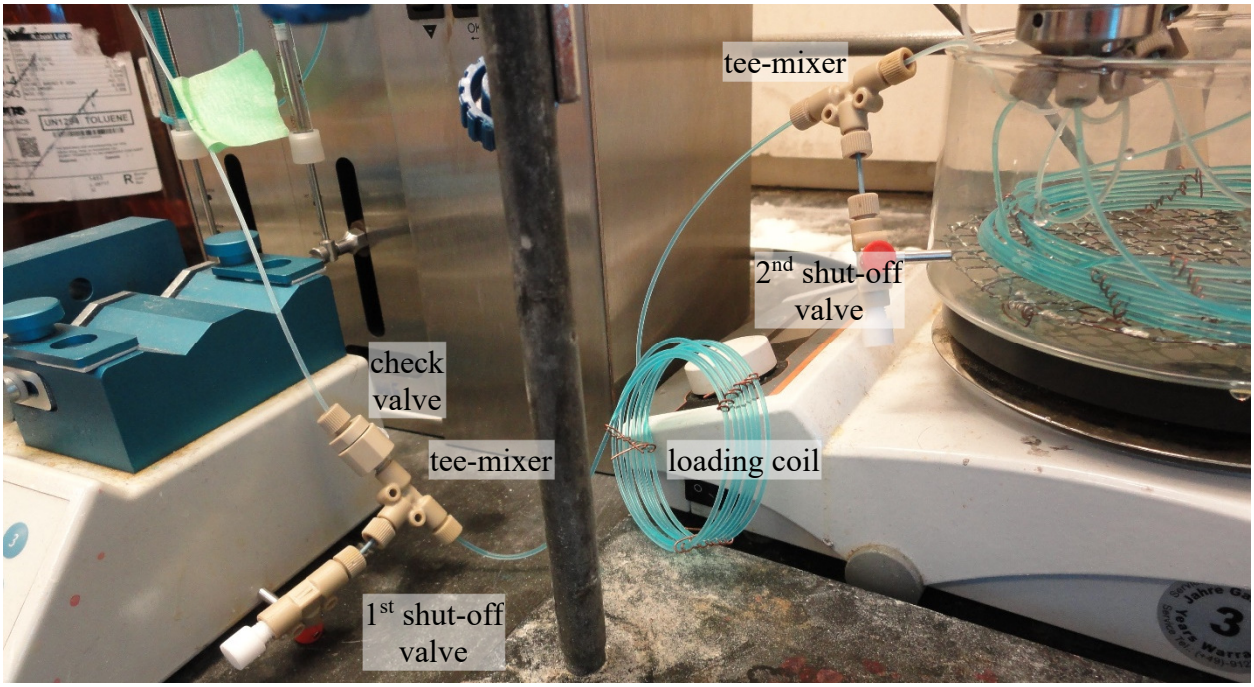

Figure AIV.4. Close-up photograph of loading coil. Syringe pump connected to 1st shut-off valve to load slugs then connected to 2nd shut off valve to initiate reactions.

AIV.2 Procedures for batch kinetic experiments

Benzoyl chloride + benzyl alcohol

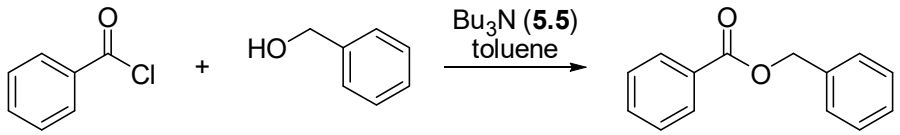

5.3 **5.4** **5.6**

General procedure. Benzoyl chloride (**5.3**) and hexadecane (59 µL, 0.20 mmol) were made up to 1.00 mL with toluene. Benzyl alcohol (**5.4**) and Bu_3N (**5.5**) were made up to 1.00 mL with toluene. The two solutions were combined at room temperature and stirred. 15 µL aliquots were taken at 1, 2, 3, 5, 10, 15, 25 and 40 min which were quenched with 600 µL of 5:1 EtOAc:MeOH and analyzed by GC-FID.

Reaction 1. 0.50 M **5.3** (116 µL, 1.0 mmol), 0.50 M **5.4** (103 µL, 1.0 mmol), 0.60 M **5.5** (286 µL, 1.2 mmol).

Reaction 2. 0.50 M **5.3** (116 µL, 1.0 mmol), 1.0 M **5.4** (207 µL, 2.0 mmol), 0.60 M **5.5** (286 µL, 1.2 mmol).

Reaction 3. 0.50 M **5.3** (116 µL, 1.0 mmol), 0.50 M **5.4** (103 µL, 1.0 mmol), 1.0 M **5.5** (572 µL, 2.0 mmol).

Reaction 4. 1.0 M **5.3** (232 µL, 2.0 mmol), 0.50 M **5.4** (103 µL, 1.0 mmol), 0.60 M **5.5** (286 µL, 1.2 mmol).

1-Fluoro-4-nitrobenzene + morpholine

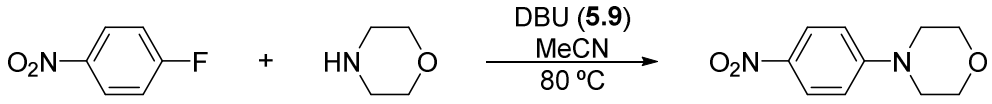

5.7 **5.8** **5.10**

General procedure. 1-Fluoro-4-nitrobenzene (**5.7**) and 1,3,5-trimethoxybenzene (134 mg, 0.80 mmol) were made up to 1.00 mL with MeCN. Morpholine (**5.8**) and DBU (**5.9**) were made up to 1.00 mL with MeCN. The two solutions were combined and stirred at 80 °C. 15 µL aliquots were taken at 2, 4, 6, 10, 15, 30 and 45 min which were quenched by dilution with 700 µL MeCN and analyzed by GC-FID.

Reaction 1. 0.50 M **5.7** (106 µL, 1.0 mmol), 0.50 M **5.8** (87 µL, 1.0 mmol), 0.50 M **5.9** (150 µL, 1.0 mmol).

Reaction 2. 1.0 M **5.7** (212 µL, 2.0 mmol), 0.50 M **5.8** (87 µL, 1.0 mmol), 0.50 M **5.9** (150 µL, 1.0 mmol).

Reaction 3. 0.50 M **5.7** (106 µL, 1.0 mmol), 1.0 M **5.8** (174 µL, 2.0 mmol), 0.50 M **5.9** (150 µL, 1.0 mmol).

Reaction 4. 0.50 M **5.7** (106 µL, 1.0 mmol), 0.50 M **5.8** (87 µL, 1.0 mmol), 1.0 M **5.9** (300 µL, 2.0 mmol).

TBSCl + 2-iodobenzyl alcohol

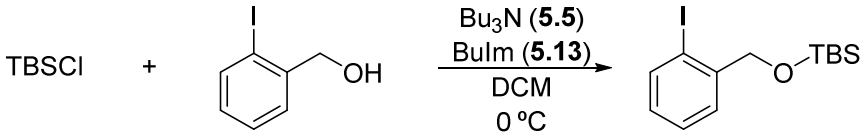

5.11 **5.12** **5.14**

General procedure. Solutions of TBSCl (**5.11**) and hexadecane were prepared in DCM (electrophile solution). Solutions of alcohol **5.12**, Bu_3N (**5.5**) and BuIm (**5.13**) were prepared in DCM (nucleophile solution). For each reaction 250 µL of electrophile solution was combined with 250 µL of nucleophile solution and the reaction stirred at 0 °C. 15 µL aliquots were taken at 2, 4,

6, 10, 15, 25, 35 and 45 min which were quenched with 600 μL of 5:1 EtOAc:MeOH and analyzed by GC-FID. It was essential to use a single stock solution of **5.11** to prepare all subsequent electrophile solutions to obtain best results.

Electrophile solution 1: **5.11** (1.50 g, 10 mmol) and hexadecane (586 μL, 2.0 mmol) was diluted to 10.00 mL with DCM.

Electrophile solution 2: 0.55 mL of electrophile solution 1 and hexadecane (264 μL, 0.090 mmol) was diluted to 10.00 mL with DCM.

Nucleophile solution 1: **5.12** (116 mg, 0.50 mmol), **5.5** (143 μL, 0.60 mmol), **5.13** (6.6 μL, 0.050 mmol).

Nucleophile solution 2: **5.12** (117 mg, 0.50 mmol), **5.5** (143 μL, 0.60 mmol), **5.13** (3.3 μL, 0.025 mmol).

Nucleophile solution 3: **5.12** (176 mg, 0.75 mmol), **5.5** (143 μL, 0.60 mmol), **5.13** (6.6 μL, 0.050 mmol).

Nucleophile solution 4: **5.12** (117 mg, 0.50 mmol), **5.5** (238 μL, 1.0 mmol), **5.13** (6.6 μL, 0.050 mmol).

Reaction 1. 0.28 M **5.11**, 0.25 M **5.12**, 0.30 M **5.5**, 0.025 M **5.13**: 250 μL of electrophile solution 2 + 250 μL of nucleophile solution 1.

Reaction 2. 0.28 M **5.11**, 0.25 M **5.12**, 0.30 M **5.5**, 0.013 M **5.13**: 250 μL of electrophile solution 2 + 250 μL of nucleophile solution 2.

Reaction 3. 0.28 M **5.11**, 0.38 M **5.12**, 0.30 M **5.5**, 0.025 M **5.13**: 250 μL of electrophile solution 2 + 250 μL of nucleophile solution 3.

Reaction 4. 0.28 M **5.11**, 0.25 M **5.12**, 0.50 M **5.5**, 0.025 M **5.13**: 250 μL of electrophile solution 2 + 250 μL of nucleophile solution 4.

Reaction 5. 0.5 M **5.11**, 0.25 M **5.12**, 0.50 M **5.5**, 0.025 M **5.13**: 250 μL of electrophile solution 1 + 250 μL of nucleophile solution 4.

AIV.3 Batch kinetics data

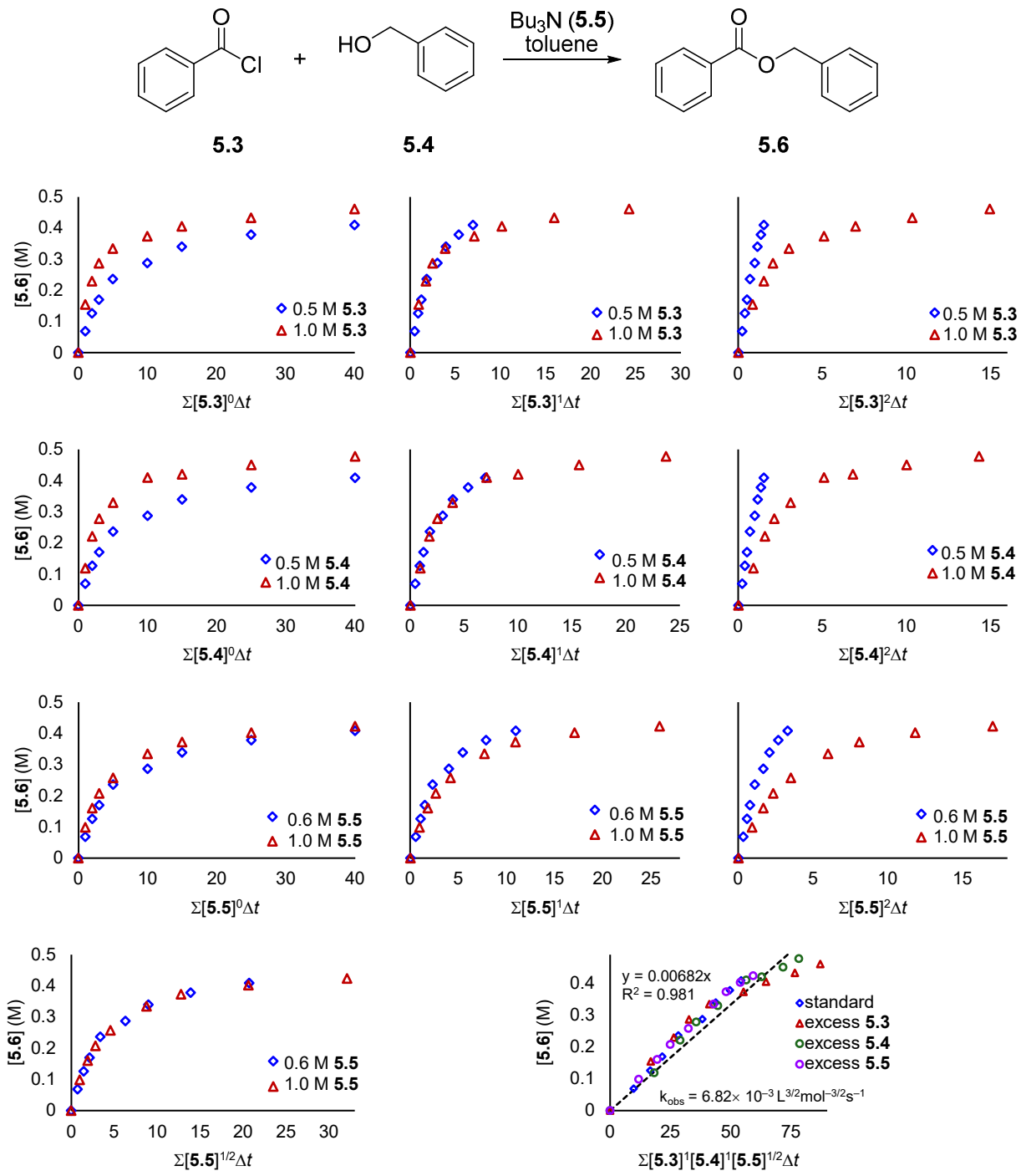

Figure AIV.5. Variable time normalization plots for reaction of **5.3** and **5.4**. Standard conditions: 0.5 M **5.3**, 0.5 M **5.4**, 0.6 M **5.5** in toluene, room temperature.

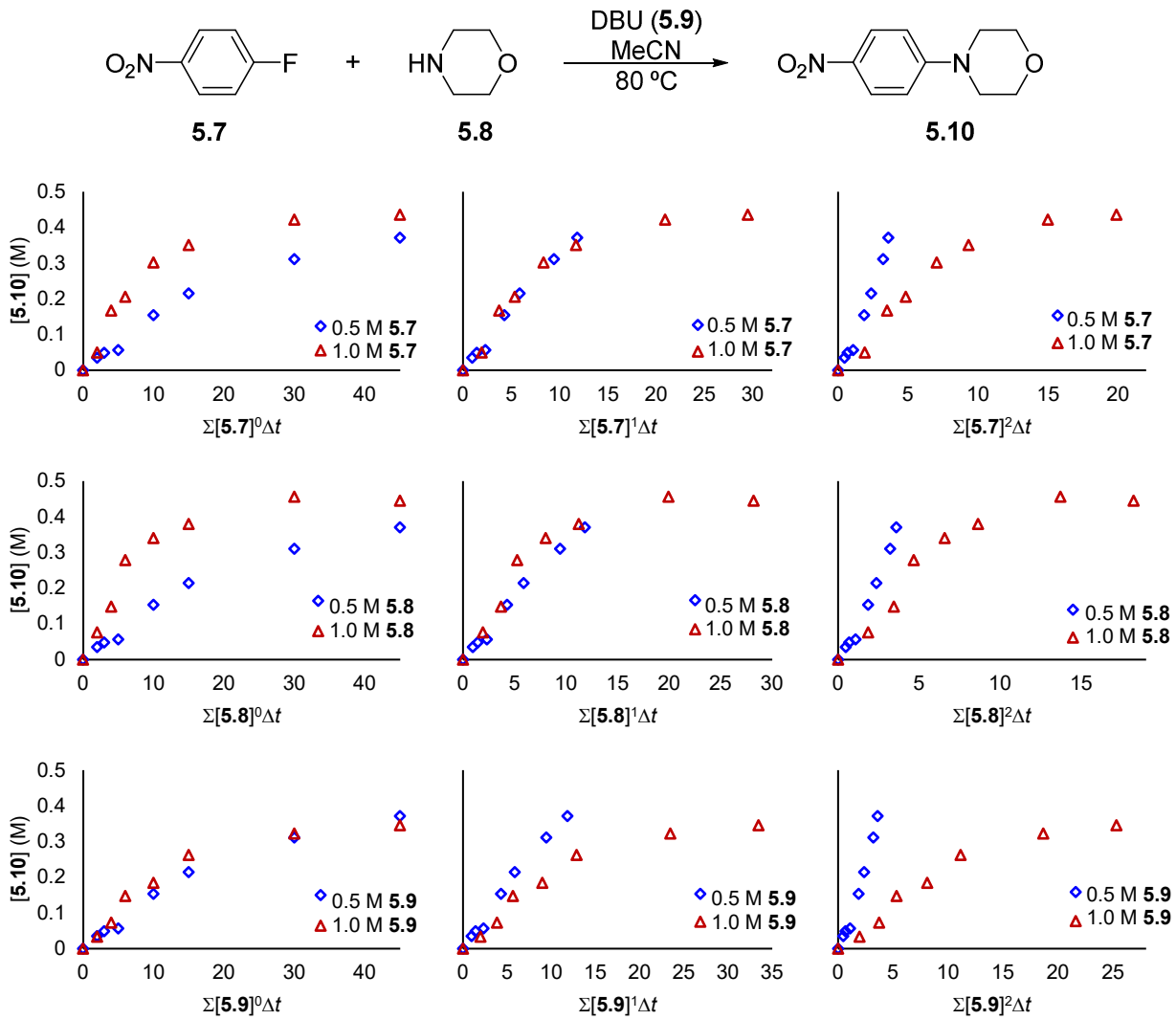

Figure AIV.6. Variable time normalization plots for reaction of **5.7** and **5.8.** Standard conditions: 0.5 M **5.7**, 0.5 M **5.8**, 0.5 M **5.9** in MeCN, 80 °C.

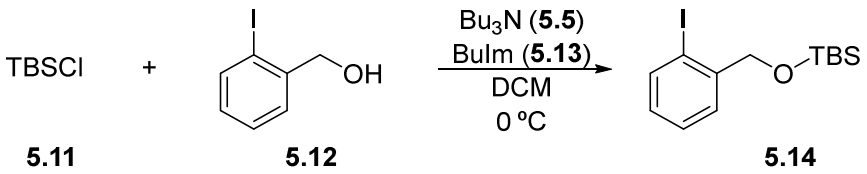
TBSCl
+
OH
Bu3N (5.5)
BuIm (5.13)
DCM
0 °C
O
TBS

5.11 **5.12** **5.14**

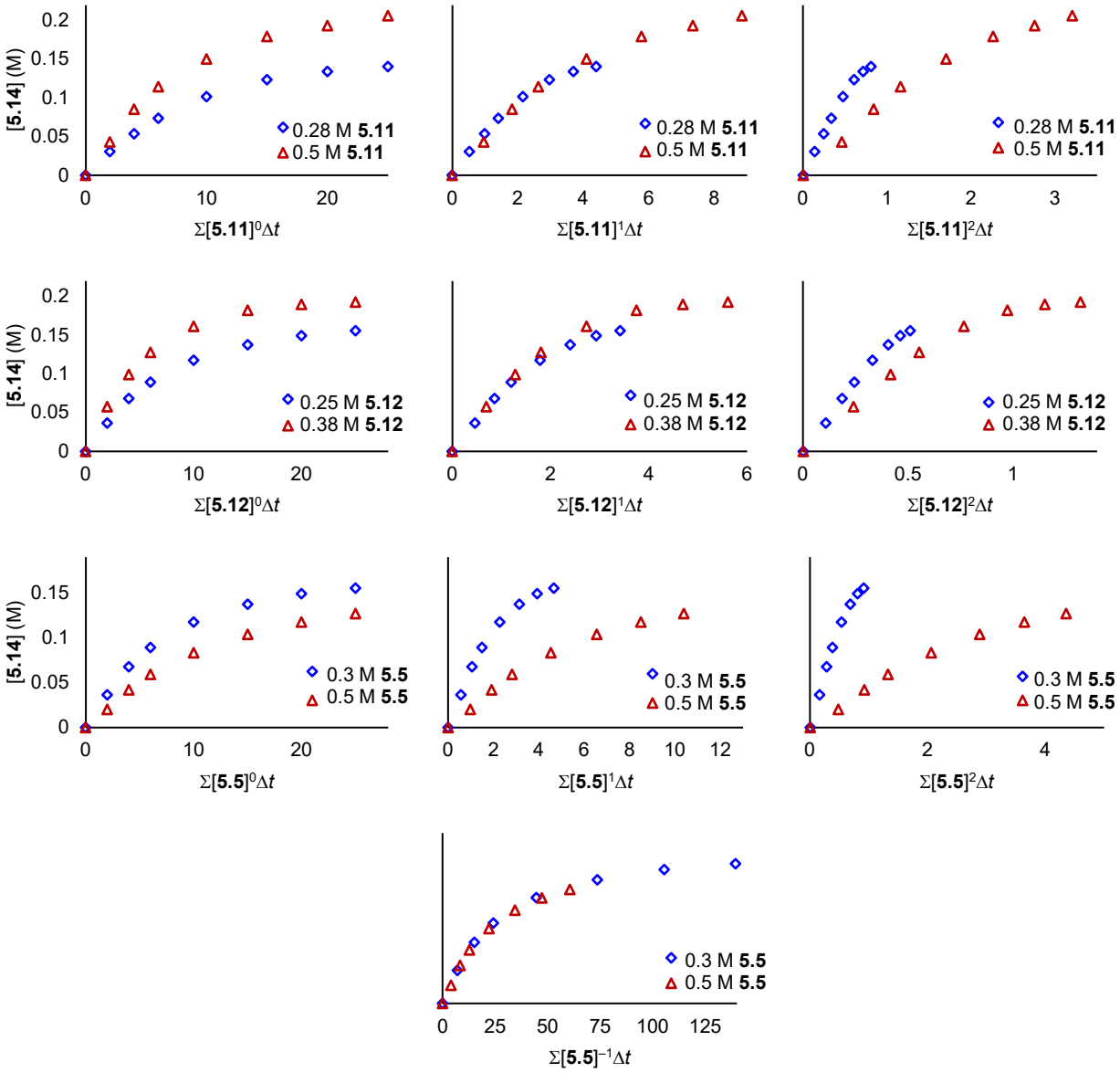
[5.14] (M)
0.28 M 5.11
0.5 M 5.11
Σ[5.11]⁰Δt
Σ[5.11]¹Δt
Σ[5.11]²Δt
0.25 M 5.12
0.38 M 5.12
Σ[5.12]⁰Δt
Σ[5.12]¹Δt
Σ[5.12]²Δt
0.3 M 5.5
0.5 M 5.5
Σ[5.5]⁰Δt
Σ[5.5]¹Δt
Σ[5.5]²Δt
Σ[5.5]⁻¹Δt

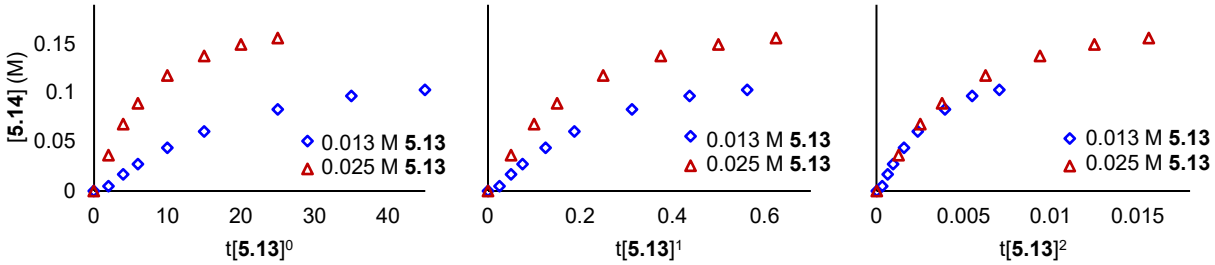

Figure AIV.7. Variable time normalization plots for reaction of **5.11** and **5.12**. Standard conditions: 0.28 M **5.11**, 0.25 M **5.12**, 0.5 M **5.5**, 0.025 M **5.13**, DCM, 0 °C.

AIV.4 Flow kinetic data used to determine reaction orders

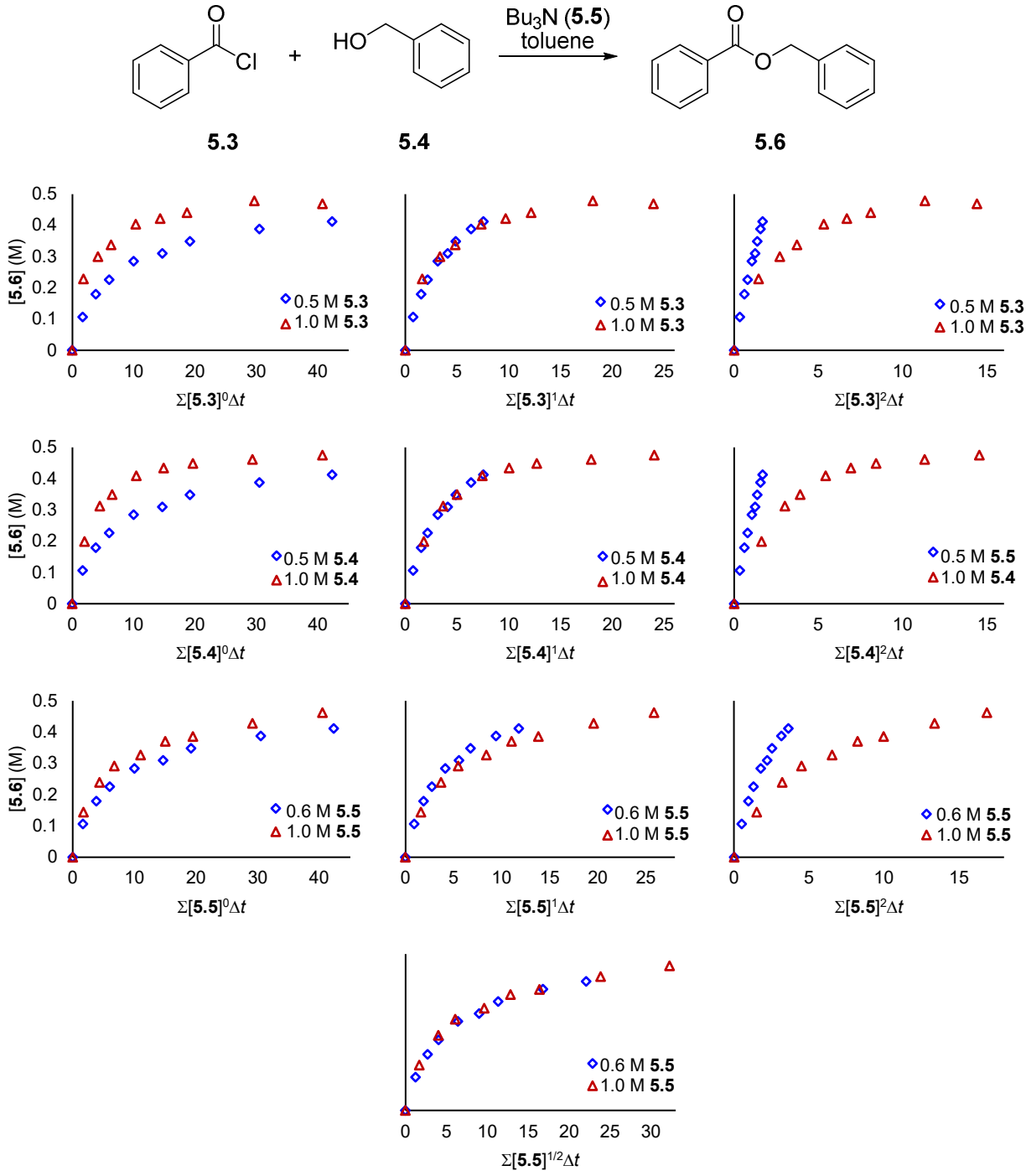

Figure AIV.8. Variable time normalization plots for reaction of **5.3** and **5.4**. Standard conditions: 0.5 M **5.3**, 0.5 M **5.4**, 0.6 M **5.5** in toluene, room temperature.

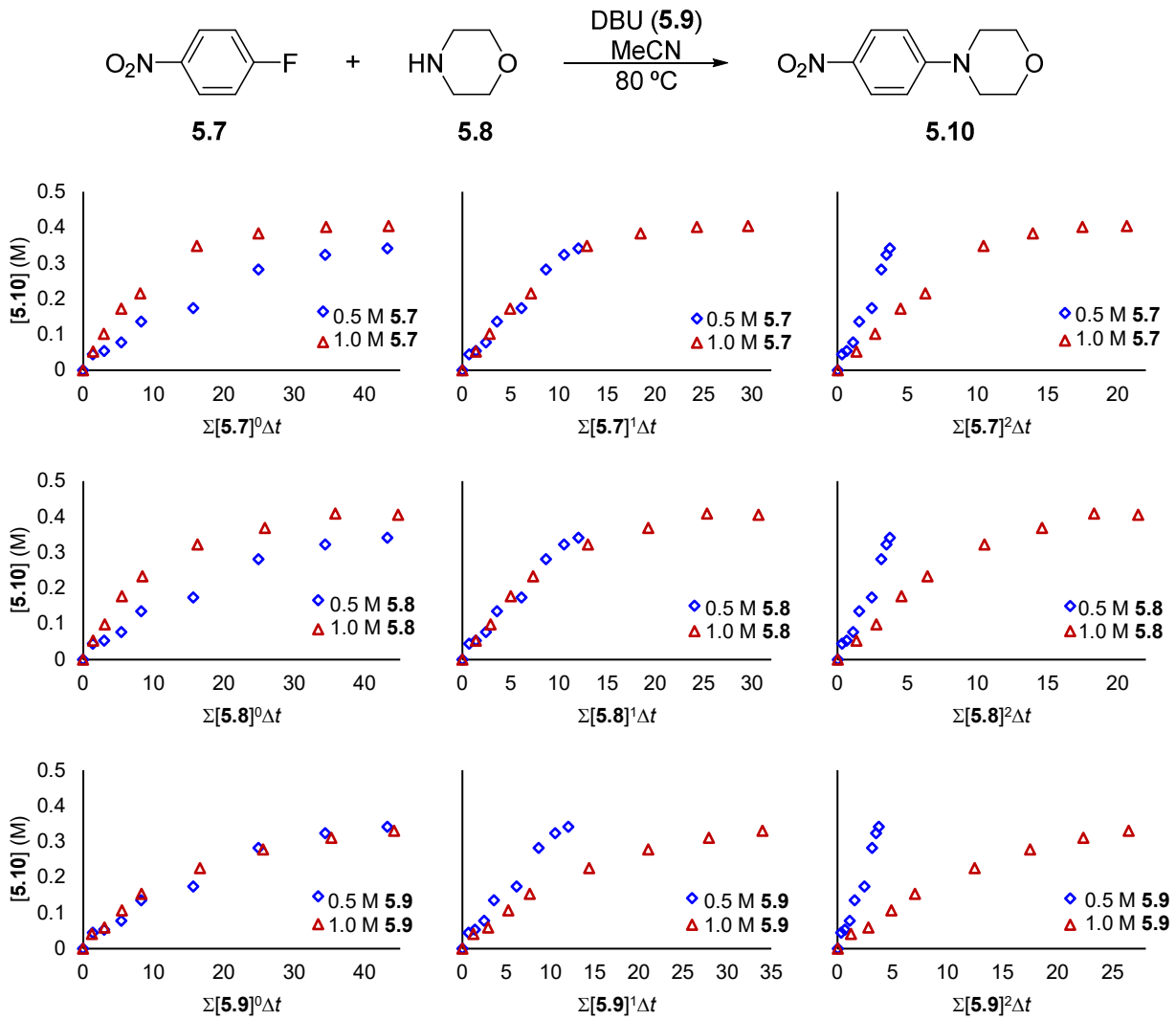

Figure AIV.9. Variable time normalization plots for reaction of **5.7** and **5.8**. Standard conditions: 0.5 M **5.7**, 0.5 M **5.8**, 0.5 M **5.9** in MeCN, 80 °C.

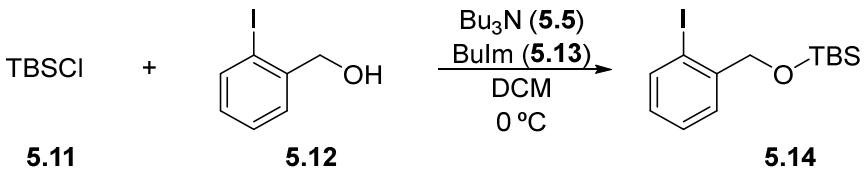
TBSCl
+
OH
Bu3N (5.5)
BuIm (5.13)
DCM
0 °C
TBS
O

5.11 **5.12** **5.14**

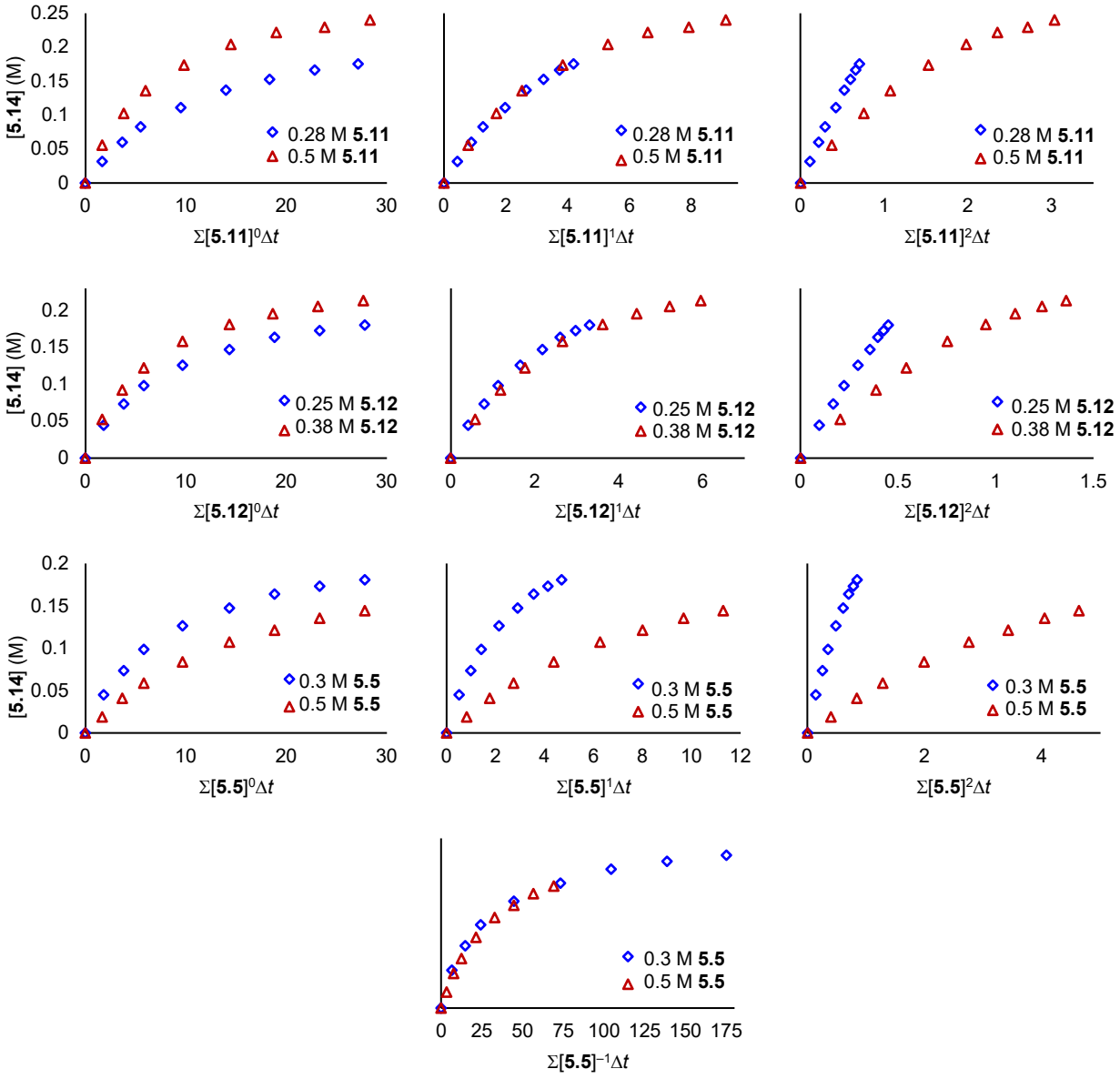
[5.14] (M)
0.28 M 5.11
0.5 M 5.11
Σ[5.11]⁰Δt
Σ[5.11]¹Δt
Σ[5.11]²Δt
0.25 M 5.12
0.38 M 5.12
Σ[5.12]⁰Δt
Σ[5.12]¹Δt
Σ[5.12]²Δt
0.3 M 5.5
0.5 M 5.5
Σ[5.5]⁰Δt
Σ[5.5]¹Δt
Σ[5.5]²Δt
Σ[5.5]⁻¹Δt

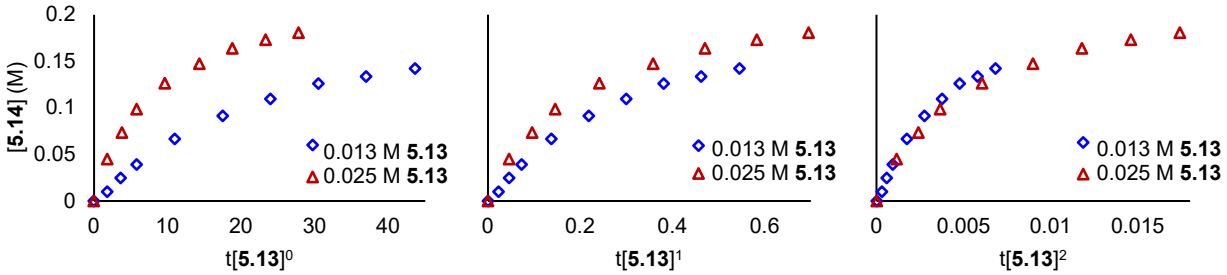

Figure AIV.10. Variable time normalization plots for reaction of **5.11** and **5.12**. Standard conditions: 0.28 M **5.11**, 0.25 M **5.12**, 0.5 M **5.5**, 0.025 M **5.13** in DCM, 0 °C.

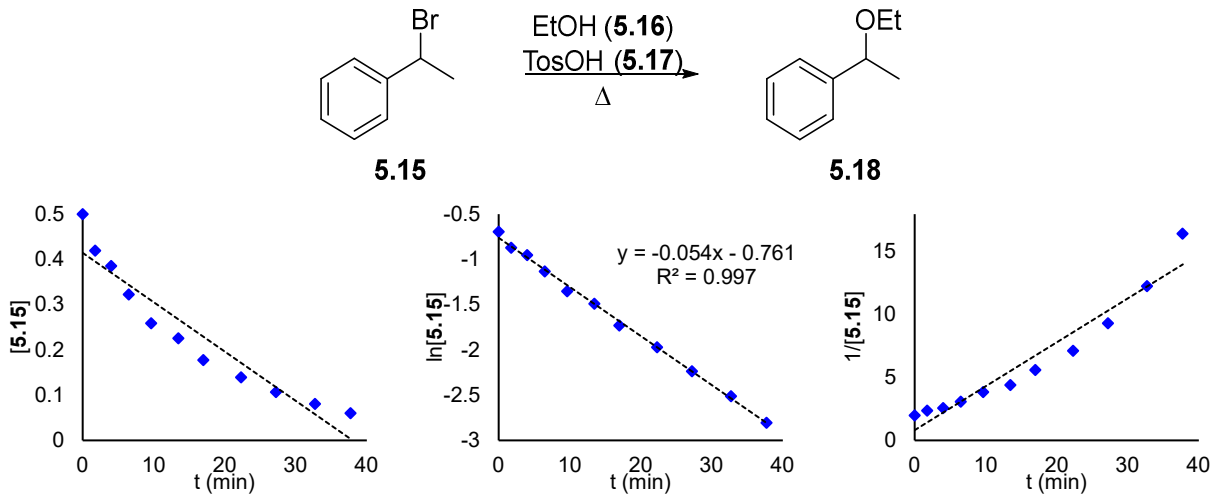

Figure AIV.11. Integrated rate law plots for the pseudo-first order ethanolysis of **5.15**. Conditions: 0.5 M **5.15**, 0.125 M **5.17** in EtOH, 70 °C.

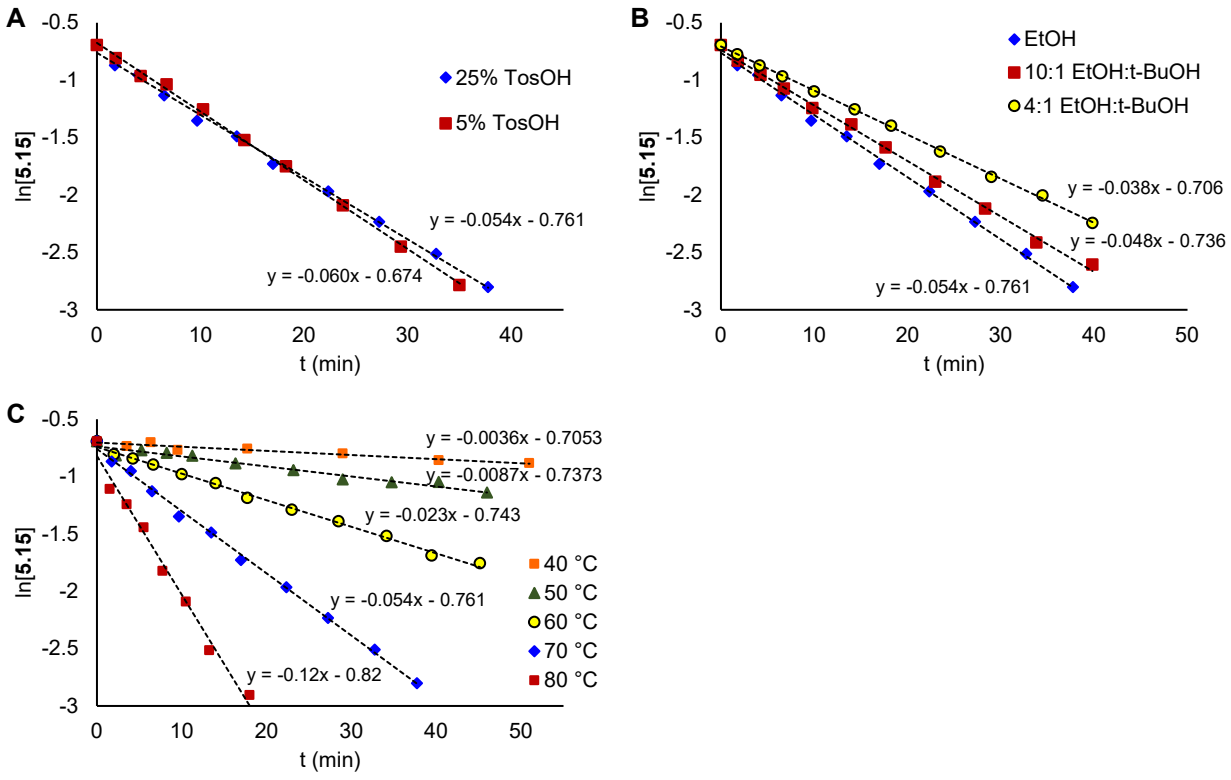

Figure AIV.12. Plots of ln[**5.15**] vs. time. A) Varying [**5.17**], B) varying [**5.16**], C) varying T.

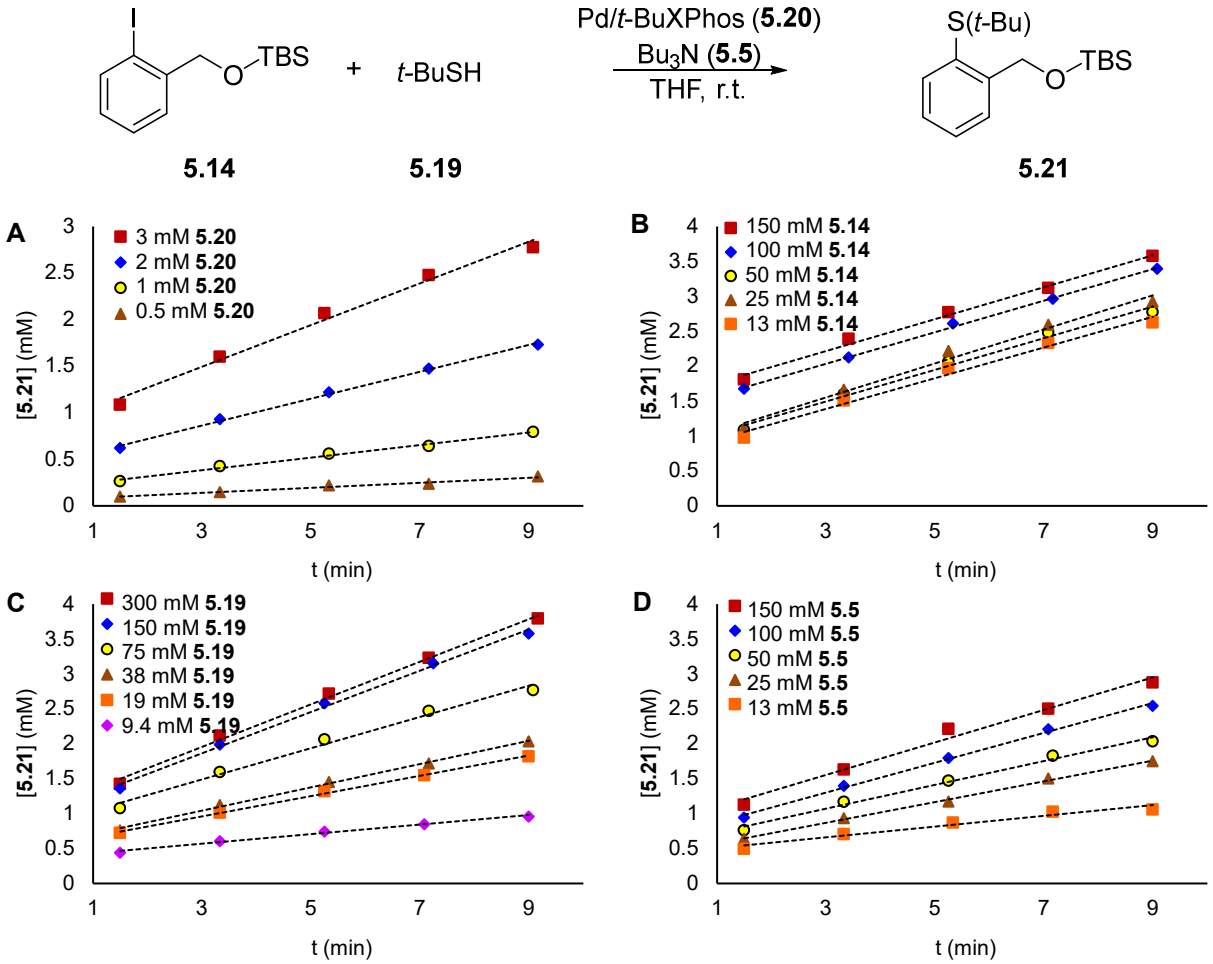

Figure AIV.13. Initial rate plots. A) Varying concentration of **5.20**, B) varying concentration of **5.14**, C) varying concentration of **5.19**, D) varying concentration of **5.5**. Standard conditions: 50 mM **5.14**, 75 mM **5.19**, 100 mM **5.5**, 3mM **5.20** (prepared from 1.5 mM **5.28**, 3 mM **5.29**) in THF, room temperature.

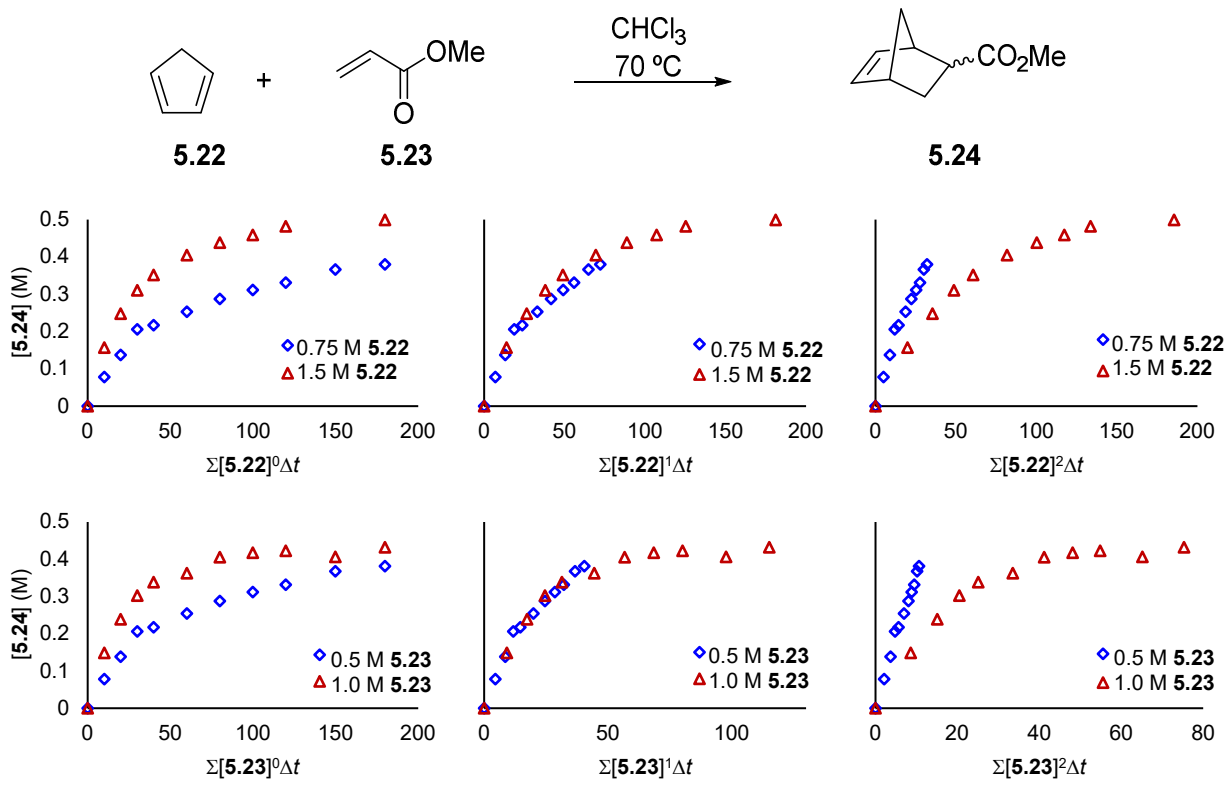

Figure AIV.14. Variable time normalization plots for reaction of **5.22** and **5.23**. Standard conditions: 0.75 M **5.22**, 0.5 M **5.23** in $CHCl_3$, 70 °C.

AIV.5 Calculated reaction pathway for the C–S cross-coupling reaction

Kinetic experiments identified either thiol deprotonation or reductive elimination as the rate determining steps of the catalytic cycle. To provide further insight, the reaction pathway for the cross-coupling of PhI with *t*-BuSH was calculated (Figure AIV.15). All individual elementary steps exhibited small activation barriers (< 10 kcal/mol). Only oxidative addition (**I2** to **I3**) and reductive elimination (**I8** to **I10**) were exergonic enough to be considered irreversible, with all other elementary steps occurring as rapid, reversible equilibria.

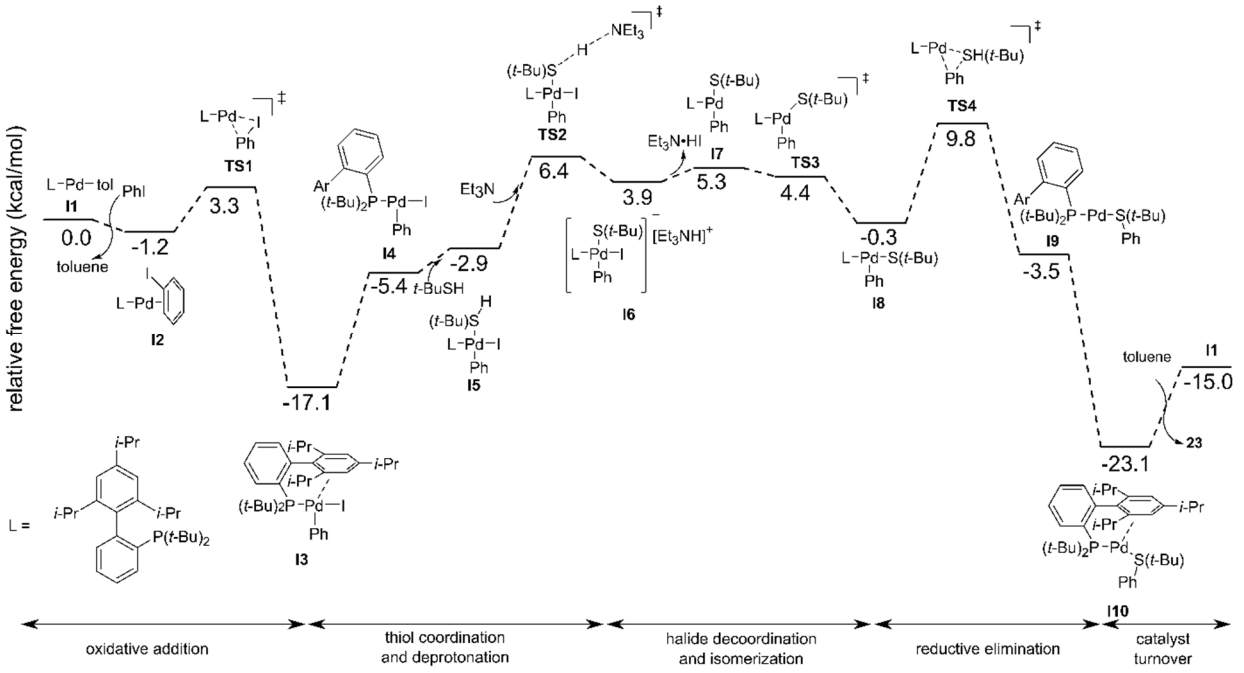

Figure AIV.15. Energy profile of one catalytic cycle for the cross-coupling of PhI with *t*-BuSH; M06-L/def2-TZVP//M06-L/def2-SVP level of theory. Only the lowest energy pathway is shown.

The oxidative addition intermediate **I3** was found to be the turnover frequency determining intermediate[1] (TDI, i.e., the catalyst resting state), in agreement with the previous ^{31}P NMR experiments[2] and the reaction order of 0 observed for aryl iodide **5.12**. Interestingly, it was found that *cis*-*trans* isomerization of **I4** to a *trans* species after oxidative addition was not favorable, (no stable *trans* intermediate could be located) presumably due to the steric bulk of the *t*-Bu groups on the phosphine in close proximity to the metal centre even after rotation of the biaryl group to reveal a vacant coordination site in **I4**. Exchange of I^- for *t*-BuS^- by coordination of *t*-BuSH, deprotonation and isomerization was slightly uphill by ~5 kcal/mol, with low activation barriers throughout. Reductive elimination (**TS4**) was found to the be turnover frequency limiting transition state (TDTS, i.e., the rate limiting step). The activation energy (energy separating TDI **I3** and TSTS **TS4**) is illustrated by placing two catalytic cycles consecutively in Figure AIV.16. For the reductive elimination, it could be envisioned to occur with the ligand in the open

[1] Kozuch, S.; Shaik, S. How to conceptualize catalytic cycles? The energetic span model. *Acc. Chem. Res*. **2011**, *44*, 101−110.

[2] Xu, J.; Liu, R. Y.; Yeung, C. S.; Buchwald, S. L. Monophosphine ligands promote Pd-catalyzed C–S cross-coupling reactions at room temperature with soluble bases. *ACS Catal.* **2019**, *9*, 6461−6466.

configuration **TS4**, or after rotation of the biaryl group to stabilize the vacant coordination site on Pd (**TS6,** Figure AIV.17). The activation barrier for ligand rotation was estimated by performing a potential energy scan of the ligand dihedral angle and was found to be ~13 kcal/mol. This was greater than the energy barrier for the reductive elimination with the ligand in an 'open' configuration (~10 kcal/mol), suggesting that reductive elimination occurs immediately following *cis-trans* isomerization of the thiol group to **I8** and then ligand rotation occurs from **I9** to give **I10**.

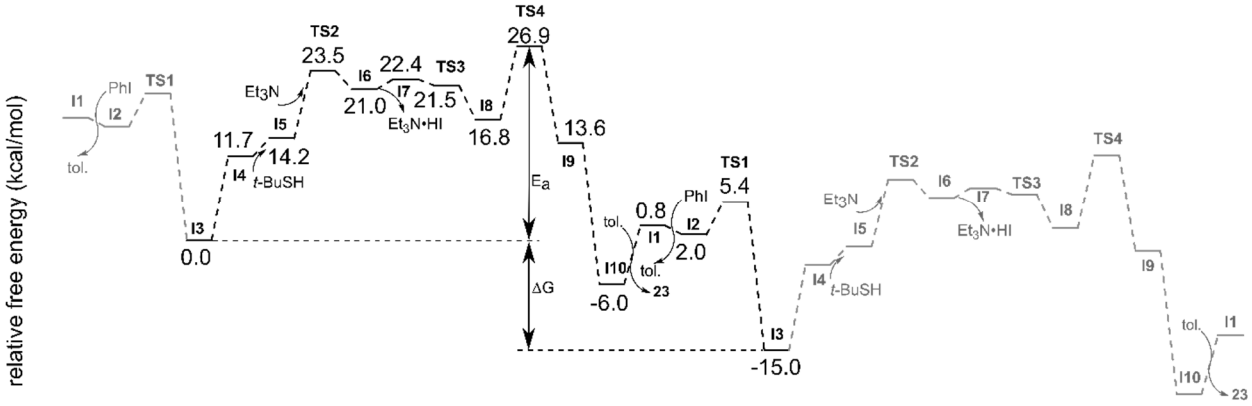

Figure AIV.16. Energy profile for two consecutive catalytic cycles in the cross-coupling of PhI with *t*-BuSH with energies relative to TDI **I3**; M06-L/def2-TZVP//M06-L/def2-SVP level of theory.

AIV.6 Troubleshooting and limitations

The main limitation of the flow reactor is an inability to handle heterogeneous reaction mixtures. Solid handling is an inherent limitation of flow in general, although obtaining good kinetics from heterogeneous liquid-solid mixtures is also problematic in batch since mass transport plays a significant role in reaction rate and factors such as particle shape and size, agitation, etc. can change over the course of the reaction.

Liquid-liquid or gas-liquid biphasic reactions also present a challenging due to inability to control which phase gets sampled. This could be addressed by incorporating a liquid-liquid or gas-liquid separator respectively before the sampling valve to send only the desired liquid stream for sampling, then recombining the two phases after the sampling valve before returning to the residence coil.

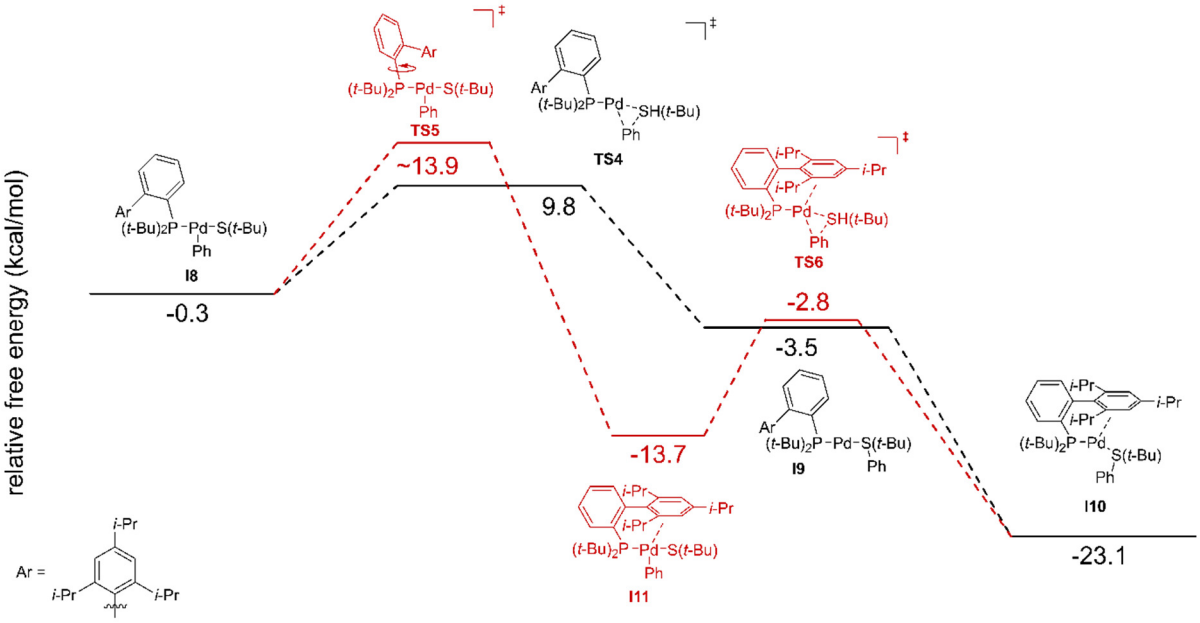

Figure AIV.17. Additional computation details regarding the ligand orientation during reductive elimination; M06-L/def2-TZVP//M06-L/def2-SVP level of theory. The energy of **TS5** was estimated from the maximum of a potential energy surface scan of the ligand dihedral angle.

Reactions generating gaseous bi-products are also currently a challenge to handle, again due to lack of control over which phase gets sampled. A gas-liquid separator installed before the sampling valve to off-gas the solution before sampling on each cycle could address this problem (no recombination after the sampling valve needed in this case).

There is also an upper limit to the carrier fluid flow rate in order to maintain integrity of the reaction slug which sets an upper limit on sampling frequency. This was empirically observed to be ~0.8 mL/min with the current reactor design. Higher flow rates of N_2 carrier gas resulted in excessive breaking of the reaction slug due to shear forces along the coil walls and gave a upper limit of ~1 sample every 90s. Faster sampling could be achieved by decreasing the volumes of the residence coils, but this would also begin to set a limit on the volume of the reaction slug, and therefore the number of samples that could be taken. Regardless, achieving sampling rates above ~1 sample / minute would be a challenge and therefore this reactor design is likely not amenable to extremely fast chemistries. However, extremely fast reactions are ideally suited for steady-state

flow kinetics experiments, since the time inefficiencies of that strategy are not problematic when investigating reactions with incredibly short timescales, and therefore we believe these are best considered complimentary tools.

AIV.7 Calibration curves

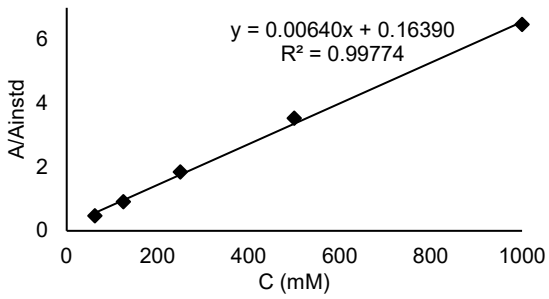

Figure AIV.18. Calibration curve for benzyl benzoate (**5.6**); 0.1 M hexadecane as internal standard.

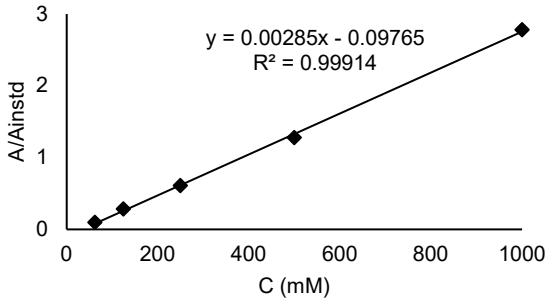

Figure AIV.19. Calibration curve for 4-(4-nitrophenyl) morpholine (**5.10**); 0.4 M 1,3,5-trimethoxybenzene as internal standard.

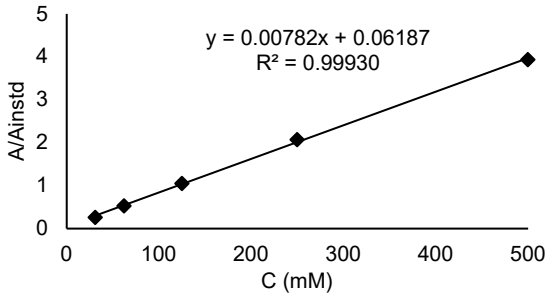

Figure AIV.20. Calibration curve for *tert*-butyl((2-iodobenzyl)oxy)dimethylsilane (**5.14**); 0.1 M hexadecane as internal standard.

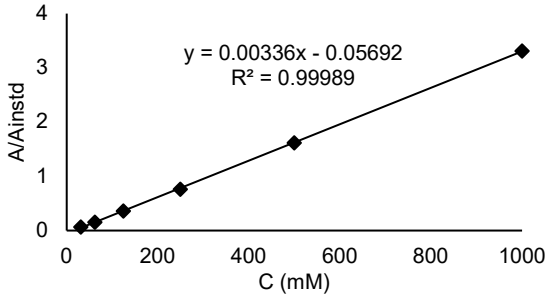

Figure AIV.21. Calibration curve for 1-bromoethylbenzene (**5.15**); 0.4 M 1,3,5-trimethoxybenzene as internal standard.

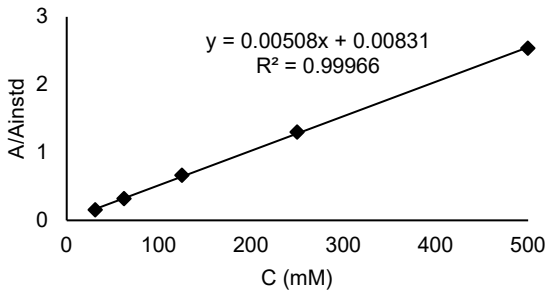

Figure AIV.22. Calibration curve for methyl 5-norbornene-2-carboxylate (**5.24**); 0.1 M hexadecane as internal standard.

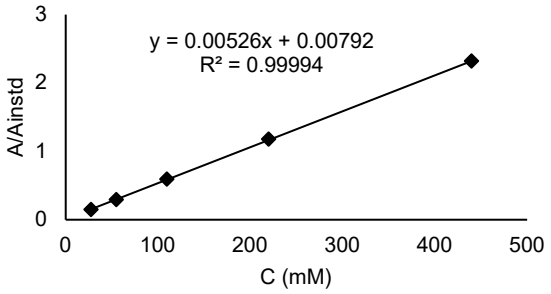

Figure AIV.23. Calibration curve for dicyclopentadiene; 0.1 M hexadecane as internal standard.

AIV.8 Spectra of starting and reference materials

Spectra of starting and reference materials are freely available in the supporting information for: Sullivan, R. J.; Newman, S. G. Reaction cycling for kinetic analysis in flow. *J. Org. Chem*, **2020**, ASAP, doi: 10.1021/acs.joc.0c00216. Content may be accessed at the following link: https://doi.org/10.1021/acs.joc.0c00216.

AIV.9 Energies of calculated structures

Table AIV.1. Energies (in Hartree) for all organic and organometallic compounds and transition states: E_{DZ} and thermal corrections were calculated at the M06-L/def2-SVP level of theory; E_{TZ} single point energy calculations were performed on the M06-L/def2-SVP geometries at the M06-L/def2-TZVP level of theory with incorporation of solvation energy using the continuous polarization model for THF.

	Energies		Thermal Corrections (T = 298.15 K, p = 1 atm)		
Structure	E_{TZ}	E_{DZ}	E_{zpe}	H	G
Organic molecules					
toluene	-271.6206739	-271.3323151	0.127719	0.134944	0.096017
PhI	-529.5707398	-529.3137692	0.089870	0.096724	0.058092
t-BuSH	-556.6856135	-556.3831547	0.130282	0.137790	0.100779
Et_3N	-292.4725907	-292.1551786	0.205427	0.215722	0.171732
$Et_3N{\cdot}HI$	-590.9958862	-590.6486939	0.219175	0.231623	0.179688
t-BuSPh	-787.7821525	-787.2365297	0.213448	0.225934	0.176048

Organometallic compounds (L = *t*-BuXPhos)					
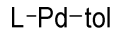 **I1**	-1873.509479	-1871.877435	0.798618	0.843669	0.724982
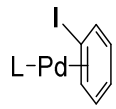 **I2**	-2131.462221	-2129.862899	0.761501	0.806118	0.687807
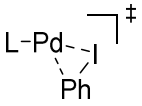 **TS1**	-2131.452934	-2129.849546	0.760883	0.805454	0.685721
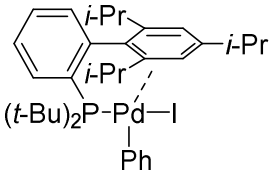 **I3**	-2131.490235	-2129.885513	0.763967	0.808442	0.690533
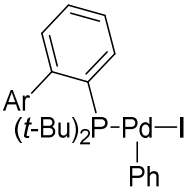 **I4**	-2131.466468	-2129.858705	0.762367	0.685409	0.685409
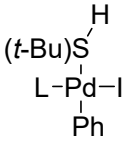 **I5**	-2688.171684	-2686.26779	0.895288	0.948866	0.80977
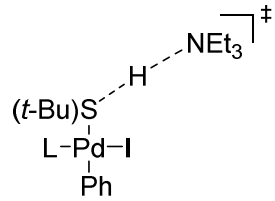 **TS2**	-2980.657771	-2978.437885	1.102390	1.164991	1.009864
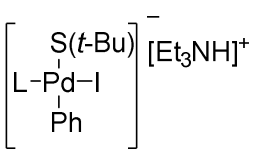 **I6**	-2980.666403	-2978.441724	1.107991	1.170922	1.014437

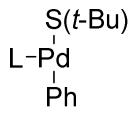 **I7**	-2389.639849	-2387.747795	0.885954	0.936322	0.806276
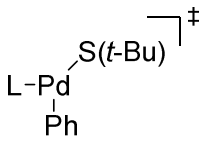 **TS3**	-2389.641901	-2387.747156	0.885561	0.935170	0.806939
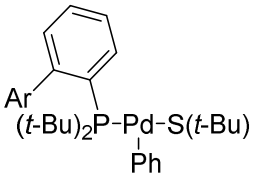 **I8**	-2389.647233	-2387.751497	0.884953	0.935526	0.804754
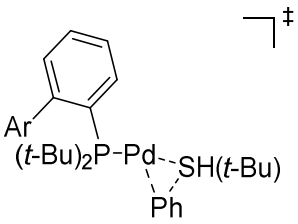 **TS4**	-2389.629697	-2387.736489	0.883936	0.934310	0.803382
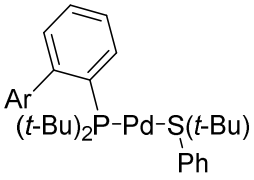 **I9**	-2389.650521	-2387.755725	0.885993	0.936883	0.802996
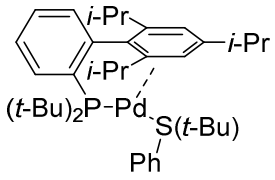 **I10**	-2389.68188	-2387.78978	0.884109	0.934892	0.803088
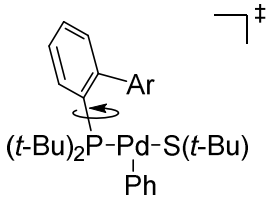 **TS5**[a]	-2389.625743	-2387.734902	0.886347	0.936484	0.807342

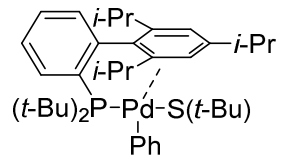 **I11**	-2389.669625	-2387.778985	0.885753	0.936207	0.805858
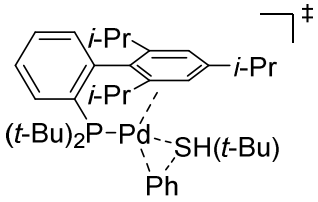 **TS6**	-2389.656562	-2387.766682	0.885903	0.935078	0.810177

[a] Transition state energy estimated from the maximum of a potential energy surface scan of the ligand dihedral angle.

AIV.10 Cartesian coordinates of calculated structures

Cartesian coordinates of calculated structures are freely available in the supporting information for: Sullivan, R. J.; Newman, S. G. Reaction cycling for kinetic analysis in flow. *J. Org. Chem*, **2020**, ASAP, doi: 10.1021/acs.joc.0c00216. Content may be accessed at the following link: https://doi.org/10.1021/acs.joc.0c00216.